STRUCTURAL STUDIES OF FLAVONOIDS AND THEIR INTERACTION WITH DUPLEX AND QUADRUPLEX DNA
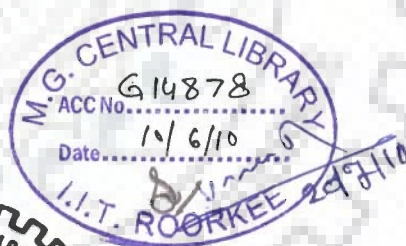
A THESIS

*Submitted in partial fulfilment of the
requirements for the award of the degree*

of

DOCTOR OF PHILOSOPHY

in

BIOTECHNOLOGY

by

AMIT KUMAR

DEPARTMENT OF BIOTECHNOLOGY
INDIAN INSTITUTE OF TECHNOLOGY ROORKEE
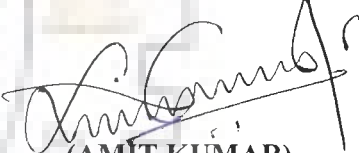ROORKEE - 247 667 (INDIA)
JULY, 2009

INDIAN INSTITUTE OF TECHNOLOGY ROORKEE
ROORKEE

CANDIDATE'S DECLARATION

I hereby certify that the work which is being presented in the thesis entitled **STRUCTURAL STUDIES OF FLAVONOIDS AND THEIR INTERACTION WITH DUPLEX AND QUADRUPLEX DNA** in partial fulfilment of the requirements for the award of the Degree of Doctor of Philosophy and submitted in the Department of Biotechnology of the Indian Institute of Technology Roorkee, Roorkee is an authentic record of my own work carried out during a period from January 2004 to July 2009 under the supervision of Prof. Ritu Barthwal, Professor & Head, Department of Biotechnology, Indian Institute of Technology Roorkee, Roorkee, India.

The matter embodied in this thesis has not been submitted by me for the award of any other degree of this or any other Institute.

(AMIT KUMAR)

This is to certify that the above statement made by the candidate is correct to the best of my knowledge.

(Ritu Barthwal)
Supervisor

Date: 14·07·2009

The Ph.D. Viva-Voce examination of **Mr. Amit Kumar**, Research Scholar, has been held on ...11/11/09...

Signature of Supervisor

11- 11- 9

Signature of External Examiner

CONTENTS

CHAPTER 3

CHAPTER 4

CHAPTER 5

ABSTRACT

Over the last two decades many strategies have been planned to design specific drugs for rare diseases like cancer to target their action at the DNA level. Advancements in our understanding of the interaction of small molecules with DNA have opened the doors for "rational" drug design. Special methods have now been developed to give accurate account of the precise location of ligand-DNA adducts on target DNA. We are now in a position to think of designing or explore ligands of our choice that recognize particular sequences of base pairs. Plants have evolved a diverse set of molecules/ligands that bind to DNA in a variety of ways, but with the common ability to act as potent inhibitors of DNA transcription and replication. As a consequence, plant products like flavonoids have been of considerable interest as potential anti cancer agents. Many compounds have been added to this list in the search for more potent drugs for use in chemotherapy in view of pronounced cytotoxicity of other synthetic drugs, resistance towards tumor cell lines and difference in their neoplastic potency. This work will allow us to enter into a new era of cancer therapy using ligand of the natural origin, available in our daily diets and flavonoids are one of them. A substantial body of research has been directed towards understanding the molecular basis of action and DNA sequence specificity for binding, by identifying the preferred binding sequences of many key drugs with DNA. Structural tools such as X-ray crystallography and NMR spectroscopy, coupled with molecular modeling techniques have considerable impact in advancing our understanding of the microscopic structural homogeneity of DNA and the molecular basis for drug-DNA interactions. In present work, UV-Visible and fluorescence spectroscopy, Nuclear Magnetic Resonance Spectroscopy (NMR) followed by restrained Molecular Dynamics (rMD) simulations and theoretical studies using Density Functional method (DFT) by Gaussian 98 and 03 have been used. These studies are supported by Diffusion Ordered Spectroscopy (DOSY), Electron Spray Ionization Mass Spectrometry (ESI-MS) and Fluorescence Life-Time Measurements to investigate about the binding mode of flavonoids with different duplex and quadruplex DNA sequences.

The Ph.D. thesis work has been reported in the form of seven chapters.

Chapter 1 contains introduction of the subject, a comprehensive review of the literature and scope of thesis.

Chapter 2 deals with the materials and methods used. The methods of detailed competition dialysis, UV-Visible, fluorescence spectroscopy and Electron Spray Ionization Mass Spectrometry (ESI-MS) to reveal DNA binding for their sequence specificity and selectivity, Nuclear Magnetic Resonance Spectroscopy- 1D NMR, DQF COSY, TOCSY, ^{1}H - ^{1}H NOESY for the proton assignment; HSQC (^{1}H–^{13}C) and HMBC (^{1}H–^{13}C) for the carbon assignment; ^{1}H - ^{31}P HMBC for the phosphorus assignment, ^{31}P - ^{31}P NOESY; UV-Visible and Fluorescence spectroscopy studies are done as a function of drug to DNA ratio; Diffusion Ordered Spectroscopy (DOSY) and Electron Spray Ionization Mass Spectrometry (ESI-MS) are done to understand the self-association; Fluorescence Life-Time Measurements are explained. The strategies used for restrained energy minimization, restrained Molecular Dynamics simulations and quantum mechanical calculations involving GIAO method (for chemical shift calculation) and DFT method (for optimization) are also discussed.

Chapter 3 deals with the calculation of chemical shift of ^{1}H and ^{13}C resonances in Nuclear Magnetic Resonances (NMR) spectra of representative molecules of flavone (Crysin, Apigenin, Luteolin and Acacetin), flavanol (Galangin, Kaemferol, Quercetin and Myricetin) and flavanone (Hesperetin and Naringenin) members of flavonoid group using the Gauge-Invariant Atomic Orbital (GIAO) method as implemented in Gaussian 98 for gas phase and Gaussian 03 for solvent phase, using Density Functional Theory (DFT) employing B3LYP exchange correlation at 6-311G** level of basis set. Molecular properties like electronic charges, dipole and energies and structural parameters like bond length, bond angles and torsional angles were calculated for all the hydroxyl substituted flavonoids in gas phase and in solvent DMSO, using the same basis set. These properties were correlated with their functional aspects. Based on the results, it was ascertained that acacetin (5,7-Dihydroxy-4′-methoxyflavone) and galangin (3,5,7-trihydroxy flavone) is non intercalator with DNA and other flavones like apigenin, luteolin and flavanols like kaemferol, quercetin and myricetin are found to be capable of both intercalation and topoisomerase poisoning. None of the flavanone derivatives, which have a saturated 2,3-bond, are active. It may be proposed that a minimal flavone structure for DNA intercalation and topoisomerase poisoning is required to be 3′, 4′-dihydroxy flavone.

Chapter 4 deals with the NMR chemical shift, rMD simulations and quantum mechanical calculations of luteolin, quercetin, rutin and genistein (Fig. 1). In this chapter, the structural and electronic properties of these flavonoids have been studied using Density Functional Theory (DFT) employing B3LYP exchange correlation. The chemical shift of ^1H and ^{13}C resonances in Nuclear Magnetic Resonance spectra have been calculated using Gauge–Invariant Atomic Orbital (GIAO) method as implemented in Gaussian 98 for gas phase and Gaussian 03 for solvent DMSO and compared with experimental data. The optimized solution structure of drugs was obtained by rMD simulation using inter-proton distance constraints obtained from 2D ROESY spectra. It was observed that A and C ring are planar in these flavonoids and the B ring of the quercetin and rutin rotate around C2'-C1'-C2 -O1 torsional angle to go in to two different conformation, *anti* and *syn*. The presence of *anti* and *syn* conformers have also been confirmed by solid state NMR and DFT studies. Similar effect has been also observed in case of genistein but around C6'-C1'-C3 –C4 torsional angle. A variation in flexibility of adopting two different conformations in these flavonoids may be related to a differential efficacy in biological activity and hence antioxidant or anticancer action.

Chapter 5 deals with the studies on self-association of luteolin, quercetin, rutin and genistein by rMD approach using one and two dimensional Nuclear Magnetic Resonance Spectroscopy supported by Absorption, Fluorescence, Diffusion Ordered Spectroscopy and Mass Spectrometry. Self association is a process which competes with binding to DNA and in formation of hetero-complexes. Concentration (1-10 μM) as well temperature (278-353 K) dependent one-dimensional proton NMR experiments are done and the change in chemical shift shows the presence of self association in all the four molecules. The two-dimensional NOESY studies show several intra-molecular and inter-molecular inter-proton connectivities suggesting specific dimer patterns involving hydrogen bonding. Absorption, emission and diffusion ordered spectroscopy demonstrate formation of self aggregates and accordingly association constant (K_a) is calculated. From DOSY experiment, it has been found that the apparent diffusion rate is fastest for luteolin and least for rutin. ESI-MS studies also prove the presence of dimer and higher aggregates which is also confirmed by isolation and fragmentation of dimer species by

MS-MS analysis. The structural differences between these molecules have been correlated to biological action.

Chapter 6 reports our attempt to investigate the interaction of four flavonoids, viz. luteolin, quercetin, genistein and rutin, having a similar structure but differing only in number and /or distribution of OH groups, with different duplex and telomeric G-quadruplex DNA sequences. Duplex DNA viz. calf thymus DNA, poly d(A-T), poly d(G-C), poly d(A .T) and quadruplex DNA d-(TTAGGG)$_4$, d-(TTAGGGT)$_4$, d-(TTGGGGT)$_4$ are used for titration with all these four flavonoids using competition dialysis assay, UV- visible and fluorescence spectroscopy. The life time fluorescence and mass spectrometric experiments also substantiate the effective binding of these four flavonoids with the G-quadruplex DNA. Competitive binding assay results show that relative affinity with different duplex and quadruplex DNA. The flavonoids shows maximum binding with calf thymus DNA and the trend for binding is quercetin > rutin > genistein > luteolin. Further, flavonoids prefer to bind with poly d-(A-T) rather to bind with poly d-(G-C). Similarly, with quadruplex DNA d-(TTAGGG)$_4$, these flavonoids show binding in the order of quercetin > rutin > luteolin > genistein while for other two sequences not much difference was found. Further, in absorption spectroscopic studies, the % hyperchromicity of these flavonoids with calf thymus DNA decreases in the following order: Luteolin > Genistein > Rutin > Quercetin; with poly d (A-T): Genistein > Rutin > Luteolin > Quercetin; while with poly d(A) it decreases in the order: Genistein > Rutin > Luteolin > Quercetin; with poly d(G-C) it decreases in the order: Genistein >Rutin > Luteolin > Quercetin; with (TTAGGGT)$_4$ it decreases in the order: Luteolin > Rutin > Genistein > Quercetin ands with (TTGGGGT)$_4$ decreases in the order: Rutin > Luteolin > Genistein > Quercetin. In the negative-ion ESI-MS spectra, peaks corresponding to the quadruplex DNA alone as well as with potassium adducts and with different flavonoids having stoichiometries (1:1) and (1:2) are clearly observed.

Chapter 7 deals with a detailed phosphorus and proton NMR study of binding of quercetin with human telomeric G-quadruplex sequence d–(TTAGGGT)$_4$. Titration studies are performed upto drug to DNA duplex ratio of 2.0 at 283, 298 and 318 K. In ^{31}P NMR, the 6 phosphate group resonances are observed in d–(TTAGGGT)$_4$, and further addition of quercetin up to 1:1 complex induces significant upfield shift with appearance of new set of resonance showing change in phosphodiester backbone. In proton experiments, 2D NOESY 1:1, 1.5:1 and 2.0:1 flavonoids-G-quadruplex complex yields several intra-molecular and inter-molecular contacts. We do not see evidence of thymine imino protons even at 283 K, indicating that quercetin binding does not stabilize or

induce T-tetrad formation. Further, absence of most of the sequential connectivities and the intra-base pair contacts show that DNA quadruplex is not intact. The drug is intercalated into the base pair of DNA, placed close to T1 and T2 base pairs. Further, large change in proton chemical shift of T7H6 and presence of sequential connectivity between G6H1'- T7H6 shows the binding of another molecule of quercetin below T7 base. A model was built using the inter-proton distances obtained from NOESY cross peaks by rMD simulations on complex. The torsional angles and inter-proton distances obtained from proton NMR experiments, exchange of bound and free drug by ^{31}P NMR experiments, along with the rMD simulations of the structure of drug–DNA complex show that these flavonoids intercalate between T1pT2 base pairs and end stack G6pT7 of DNA and stabilize the G-quadruplex complex. Diffusion Ordered Spectroscopy (DOSY) studies provide evidence of done to see the formation of intercalated complex and the spectra show two different populations of bound and free DNA as compared to that alone DNA.

Chapter 8 summarizes the results obtained and their implications in understanding the arrangement/ substitution of hydroxyl group on flavonoids and their molecular basis of action for targeting DNA for anti cancer therapy.

ACKNOWLEDGEMENT

This piece of work will never be accomplished without the God Almighty with His blessings and His power that work within me and also without the people behind my life for inspiring, guiding and accompanying me through thick and thin. It is a pleasure to convey my gratitude to all of them in my humble acknowledgment.

I would like to express my gratitude to my advisor, Professor Ritu Barthwal, Head, Department of Biotechnology for her support, patience, and encouragement throughout my Ph.D studies. It is not often that one finds an advisor that always finds the time for listening to the little problems and roadblocks that unavoidably crop up in the course of performing research. Her technical and editorial advice was essential to the completion of this thesis and has taught me innumerable lessons and insights on the workings of academic research in general. Her truly scientist intuition has made her as a constant oasis of ideas and passions in science, which exceptionally inspire and enrich my growth as a student, a researcher and a scientist want to be. I am indebted to her more than she knows.

Token of deep regards is being rendered to Prof. A. N. Tripathi, for taking intense interest in this study as well as providing his valuable suggestions that has improved the quality of this study.

I would also like to gratefully acknowledge my labmates Kushuma, lata, Asif and Dr. Maya, for their cooperation and their pleasant company in the lab. Kushuma, thanks for your company especially for the tea and being there when I need someone to talk to. Thanks for supporting me in those days when no body was with me. I would like to thanks my dearest friend madhurima for her care, love and affection and giving me a reason to join IIT Roorkee.

Today I recall all my friends Manish, Parmindra, Mankesh, Suarabh, Nilesh, Vijay, Deepankar for their help and support during my stay at Roorkee. Thanks Nilesh, for lending me your money whenever I needed. I am also thankful to Ajay Thakur and Prashant Jambhulkar for showing me their brotherly care even from far distance.

Thanks will not be enough for my wife Amita and my son Shivi, the pillar of my life, all I can say is it would take another thesis to express my deep love for them. Their patience, love and encouragement have upheld me, particularly in those many days in which I spent more time in lab than with them. Amita, I am indebted for the many sacrifices you have made to support me in undertaking my research work. By providing your steadfast support in hard times, you have once again shown the true affection and dedication you have always had towards me.

The smile of shivi always encouraged me and gave me strength to accomplish this work as fast as possible. Shivi, I have put you away from the day since you started observing the world. I promise I will never do this again from now onwards and will be with you forever.

Words fail me to express my regards to my mummy and papa whose love, persistent confidence in me and many years of support that provided the foundation for this work. It's only due to you and your constant silent prayers which gave me blessing to reach upto this level. I would also like to extend my sincere thanks to my Bhaiya Bhabhi and Didi Jiju ji for their confidence on me and their constant support to make this journey so congenial and easy. I thank them for their memorable concern, affection and constant care. I am lucky to have such a nice family and I wish to have the same in all my births.

July 2009
Dated

(Amit Kumar)

LIST OF PUBLICATIONS

To be communicated:

1. **Amit Kumar,** A. N. Tripathi and Ritu Barthwal. 2008. DFT Studies on Molecular Properties and Electronic Structure of bioflavonoids

2. **Amit Kumar,** A. N. Tripathi and Ritu Barthwal. 2008. Quantum Chemical and Nuclear Magnetic Resonance Spectral Studies on Molecular Properties and Electronic Structure of bioflavonoids.

3. **Amit Kumar** and Ritu Barthwal. 2009. Molecular association of flavonoids luteolin, quercetin and rutin using Nuclear Magnetic Resonance Spectroscopy supported by other physico-chemical techniques.

4. **Amit Kumar** and Ritu Barthwal. 2009. Recognition and stabilization of human telomeric G-Quadruplex by flavanoid Quercetin.

5. **Amit Kumar** and Ritu Barthwal. Studies of sequence specificity of bioflavonoids binding to DNA using biophysical techniques.

6. **Amit Kumar** and Ritu Barthwal. Binding of bioflavonoids to different G-quadruplex of telomeric sequences using different mass spectrometric methods.

Papers in Conferences/ Worshop/Symposium

1. **Amit Kumar** and Ritu Barthwal. 2009. Molecular association of flavonoids luteolin, quercetin and rutin using Nuclear Magnetic Resonance Spectroscopy supported by other physico-chemical techniques. National Magnetic Resonance Society NMRS, IICT, Hyderabad, Feb 2-6, 2009.

2. Ritu Barthwal, A. N. Tripathi and **Amit Kumar**. 2008. Quantum Chemical and Nuclear Magnetic Resonance Spectral Studies on Molecular Properties and Electronic Structure of flavonoids, Luteolin and Quercetin. International

Conference on Magnetic resonance in Biological Systems XXIIIrd ICMRBS San Diego, California, USA, August 24-29, 2008.

3. **Amit Kumar,** A. N. Tripathi and Ritu Barthwal. 2008. Quantum Chemical and Nuclear Magnetic Resonance Spectral Studies on Molecular Properties and Electronic Structure of bioflavonoids, National Magnetic Resonance Society NMRS, INMAS, New Delhi, Jan16-22, 2008.

4. Santosh Kumari, **Amit kumar**, S. K. Barthwal and Ritu Barthwal. 2005. Solution structure of anticancerous drugs Sanguinarine and Luteolin. International Conference on Magnetic resonance in Biological Systems ICMRBS 16 Jan-21 Jan 2005, Hyderabad, India.

Introduction

1.1 General

Over the last two decades many strategies have been planned to design specific drugs for rare diseases to target their action at the DNA level. Advancements in our understanding of the interactions of small molecules with DNA have opened the doors for "rational" drug design. Special methods have now been developed to give accurate account of the precise location of ligand-DNA adducts on target DNA. We are now in a position to think of designing or explore ligands of our choice that recognize particular sequences of base pairs. Nature has evolved a diverse set of molecules/ligands that bind to DNA in a variety of ways, but with the common ability to act as potent inhibitors of DNA transcription and replication. As a consequence, these natural products have been of considerable interest as potential anti cancer agents. Many synthetic compounds have been added to this list in the search for more potent drugs for use in chemotherapy in view of pronounced cytotoxicity of these drugs, resistance towards tumour cell lines and difference in their neoplastic potency. This work will allow us to enter into a new era of cancer therapy using ligands of the natural origin which have similar potency as chemosynthetic drugs but may have least side effects as these are available in our daily diets. These ligands can also be employed in the treatment of various types of cancers. They may also be useful as highly specific probes to locate particular sequences in the genomic DNA of cancerous cells. There are certain molecules that are shown to effect the very vital functions of living organisms, such as nucleic acid replication, protein biosynthesis and gene expression. Over the past 20 years, enormous advancement has been made

in our understanding of the interaction of these small molecules (ligands) with DNA of cancerous cells.

Cancer is a class of diseases in which a group of cells display *uncontrolled growth* (division beyond the normal limits), *invasion* (intrusion on and destruction of adjacent tissues), and sometimes *metastasis* (spread to other locations in the body via lymph or blood). Cancer causes about 13% of all deaths (WHO, 2006). According to the American Cancer Society, 7.6 million people died from cancer in the world during 2007 (American Cancer Society, 2007). Cell division is essential for growth, repair and reproduction. It is tightly controlled by genes inside the cell. Special genes, called oncogenes, stimulate the production of growth-stimulating chemicals that trigger cell division. If an oncogene is irreversibly switched on, it can cause uncontrolled cell division and lead to the formation of a cancer. Cancer-promoting *oncogenes* are typically activated in cancer cells, giving those cells new properties, such as hyperactive growth and division, protection against programmed cell death, loss of respect for normal tissue boundaries, and the ability to become established in diverse tissue environments. *Tumor suppressor genes* are then inactivated in cancer cells, resulting in the loss of normal functions in those cells, such as accurate DNA replication, control over the cell cycle, orientation and adhesion within tissues, and interaction with protective cells of the immune system. The p53 gene, found on chromosome 17, is a tumor-suppressor gene. In the cell, the p53 protein binds DNA at specific locations and stimulates another gene to produce a protein called p21. In turn, p21 suppresses a division-stimulating protein (cdk2) to prevent the cell from passing through to the next stage of cell division. When p53 is mutated and can no longer bind DNA effectively, the p21 protein is not available to act as the "stop signal" for cell division. Thus cells may divide uncontrollably and form tumors. Further, another control for cell division involves human telomeres which consist of 3'-TTAGGG

2

repetitive sequences overhang at the ends of chromosomes that prevent chromosomal degradation upon each cycle of replication. Since DNA polymerase cannot replicate the end of the lagging strand of linear chromosomes, approximately 50-200 nucleotides are lost each cell cycle. This normally results in senescence after 50-70 population doublings. Telomeres, therefore, serve as a protective end-cap that prevents double strand break (DSB) response, end-to-end chromosomal fusion, and other DNA- damage signal-cascades until telomeres reach a critically short length at which point senescence and cell death occur. Various protective structures are assumed by telomeres, such as the t-loop and the G-quadruplex (formed by the G-rich 3'- strand) composed of stacked tetrads known as G-tetrads with the aid of multiple telomere capping proteins. The enzyme telomerase, also a telomere capping protein, consists of both a reverse transcriptase subunit (hTERT) and an RNA component (hTERC), and serves to lengthen the G-rich, 3'-repeats of telomeres by using the RNA component as a primer. An important distinction between healthy cells and cancer cells is the ability of cancer cells to replicate indefinitely without undergoing cellular senescence or apoptosis. The immortality of cancer cells is due in part to constitutive expression of telomerase, while somatic cells either lack telomerase entirely or express exceptionally low levels. Telomerase activity is upregulated in 85-90% of tumor cells and in general, telomere length is also much shorter. By inhibiting telomerase, telomeres become susceptible to natural replicative degradation and the cells subsequently experience growth arrest. Several small molecule compounds are being developed that exploit these differences between normal cells and tumor cells. Therefore, molecules which could stabilize this conformation are thought to be protective telomerase inhibitors.

Such abnormal cancerous cell division can be checked by preventing the DNA replication process of cell cycle which is prerequisite for cell to enter in to mitosis.

This can be possible by three principally different ways of ligand binding to DNA are: first, through control of transcription factors and polymerases. Here, the drugs interact with the proteins that bind to DNA. Secondly, through RNA binding to DNA, forming DNA-RNA hybrids, which may interfere with transcriptional activity. Third, small ligand molecules that bind to DNA double helical structures by (i) intercalating between stacked base pairs thereby distorting the DNA backbone conformation and interfering with DNA-protein interaction or (ii) the groove binders. Both work through non-covalent interactions but the latter cause little distortion of the DNA backbone. For this purpose, synthetic chemical agents are employed in treatment of cancer. Thus, DNA as carrier of genetic information can be targeted for chemotherapy because of the ability to interfere with transcription and replication, major steps in cell growth and division. However, synthetic compound generally exhibit toxic side effects, such as cardiotoxicity, nausea, vomiting etc. limits their further application. Looking for non toxic or less toxic compounds with similar property is necessary to reveal. One may expect that natural compounds which are usually available in our diets would be an ideal goal. In this regard, flavonoids can solve our problem for not only the reason that these compounds are equally effective as their synthetic counterparts but for not posing problems like synthetic drugs. Thus, flavonoids are found to be less toxic to normal cells than conventional chemotherapeutic agents and therefore offer an opportunity for more successful treatment of cancer.

1.2 Structure of Nucleic Acids

1.2.1 Nucleotide Bases

1.2.1.1 Purines: Adenine and Guanine

Two different heterocyclic aromatic bases with a purine ring (composed of carbon and nitrogen) are found in DNA (Fig. 1.1a). Adenine has an amino group ($-NH_2$) on the C6 position of the purine ring. Guanine has an amino group at the C2

4

position and a carbonyl group at the C6 position. Besides these, minor bases like inosine, 7–methyl guanosine, etc. are also found as components of nucleic acids.

1.2.1.2 Pyrimidines: Thymine, Cytosine and Uracil

Thymine contains a methyl group at the C5 position with the carbonyl group at C4 and C2 positions. Cytosine contains a hydrogen atom at the C5 position and an amino group at C4 (Fig. 1.1b). In RNA thymine is replaced by uracil.

(a) Purines
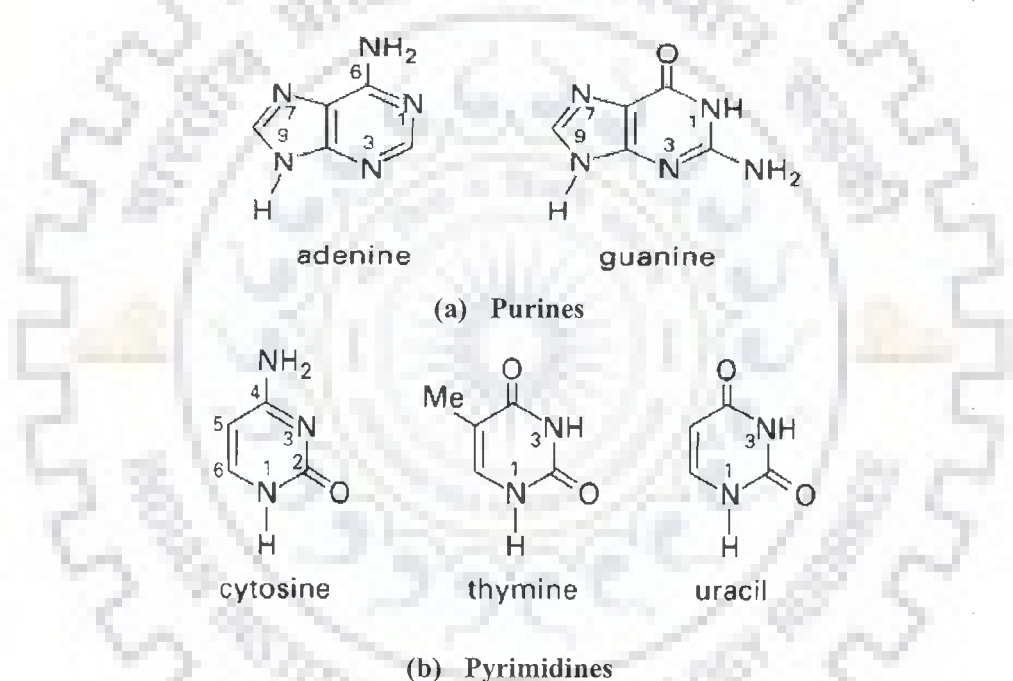
(b) Pyrimidines

Fig. 1.2: Molecular structure of (a) purines and (b) pyrimidines.

1.2.2 Sugar Ring

Ribose sugar is found in all RNA molecules while a slightly different sugar, β-D-2-deoxyribose is found in DNA. This is a derivative of β–D–ribose in which the hydroxyl (–OH) the 2' position is replaced by hydrogen (–H) (Fig. 1.2). The sugar moiety of DNA is one of the more flexible and dynamic parts of the molecule. The sugar base combination is called nucleoside unit. A nucleotide is a nucleoside phosphorylated at one of the free sugar hydroxyls.

Ribose (RNA)   2-Deoxyribose (DNA)
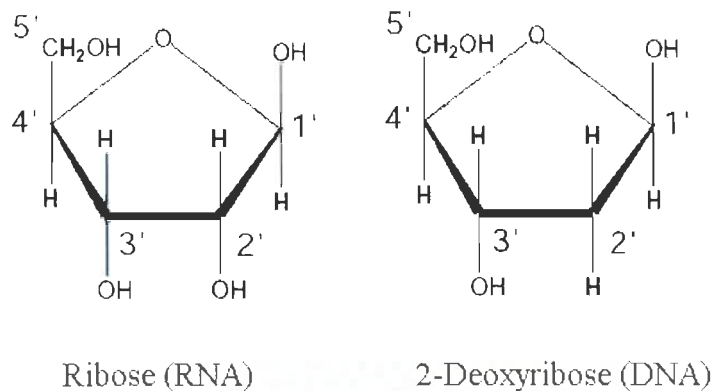
Fig. 1.2: Five membered furanose ring of ribose and deoxyribose sugar

1.2.3 Sugar Pucker

The five-membered ring is generally non planar and its conformation is designated as follows. If four atoms lie in the pane, this plane is chosen as reference plane and the conformation is designated as envelope (E) and if they do not, the reference plane is then, that of the three atoms that are closest to the five-atom, least-squares plane, and the conformation is described as twist (T).

a) The present E and T notations for puckered forms of the sugar ring confirm to those recommended for the conformational nomenclature of five and six-membered rings of monosaccharide and their derivatives.

b) The E/T notation has superseded the *endo/exo* description in which atoms now designated by superscripts were called *endo*, and those now designated by subscripts were called *exo*. They are shown by both systems of designation (Fig. 1.3a). Examples: C3'-*endo*/C2'-*exo* has become $^3T_2$ and C3'-*endo* has become ^3E.

c) Symmetrical twist conformations, in which both atoms exhibit equal displacements with respect to the five-atom plane are denoted by placing the superscript and subscript on the same side of the letter T, e.g. $_2^3T$, $_4^3T$, etc.

6

N-puckered
P = 0° - 18°

S-puckered
P = 144° - 162°

Ribose: $^3J_{H1'-H2'} \approx 1$ Hz

Ribose: $^3J_{H1'-H2'} \approx 7.9$ Hz

Deoxyribose: $^3J_{H1'-H2'} \approx 1.8$ Hz

Deoxyribose: $^3J_{H1'-H2'} \approx 10$ Hz
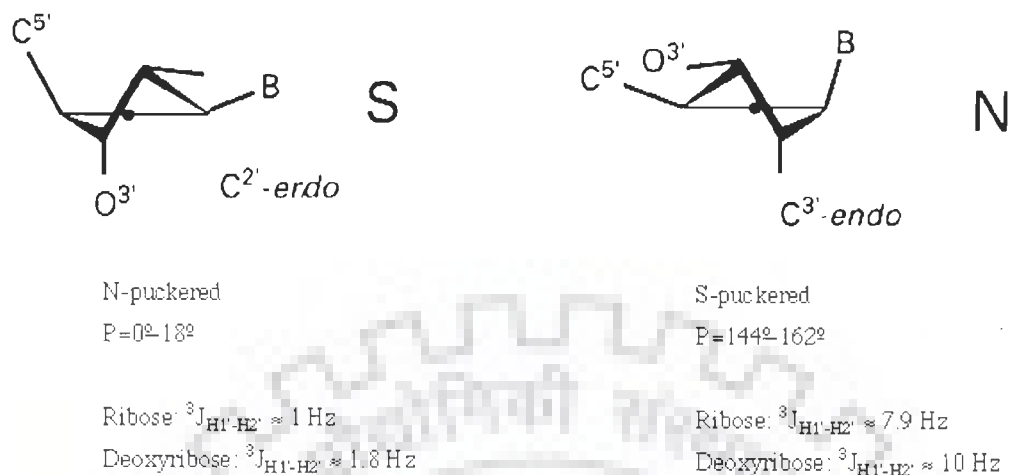
Fig. 1.3(a): Preferred conformation of sugar pucker C2' endo and C3' endo of sugar

1.2.4 Endocyclic Torsional Angles: Furanose Sugar Ring

The sugar ring occupies a pivotal position in the nucleotide unit because it is part of both the backbone and the side chain. In order to provide a complete description of the ring conformation, it is necessary to specify the endocyclic torsion angles for the ring as well as the bond lengths and bond angles. The five endocyclic torsion angles (Fig. 1.4a) for the bonds O4'–C1', C1'–C2', C2'–C3', C3'–C4' and C4'–O4' are denoted by the symbols, ν_0, ν_1, ν_2, ν_3 and ν_4 respectively. The magnitudes of such angles are all interrelated and, therefore, the geometry of the ribose ring can be defined from two parameters: the pseudorotation phase angle (P) and the pucker amplitude. The ribose ring is not a planar and usually presents C2'-endo (South) or C3'-endo (North) conformation. For the sugar pucker conformation, homonuclear $^3J_{H-H}$ coupling constant serve as the most direct determinant. These constants can be measured in a qualitative way from 2D ^1H-^1H TOCSY, 2D ^1H-^{13}C TOCSY-HMQC or 2D ^1H-^{13}C TOCSY-HSQC experiments:

- Very weak $J_{H1'-H2'}$ and strong $J_{H3'-H4'}$ cross-peaks correspond to *pure N-type conformation* (preferred conformation in RNA).

- Strong $J_{H1'-H2'}$ and weak $J_{H3'-H4'}$ cross-peaks correspond to *pure S-type conformation.*

- $J_{H2'-H3'}$ is similar in both states.

- Intermediate intensities indicate equilibrium between N and S states.

1.2.5 The Phosphodiester Bond

In DNA and RNA the individual nucleotides are joined by a 3'–5' phosphodiester bond. The nucleotides are joined from the 3' sugar carbon of one nucleotide, through the phosphate to the 5' sugar carbon of adjacent nucleotide. This is termed as 3'–5'

$$v0 = C4'-O4'-C1'-C2'$$
$$v1 = O4'-C1'-C2'-C3'$$
$$v2 = C1'-C2'-C3'-C4'$$
$$v3 = C2'-C3'-C4'-O4'$$
$$v4 = C3'-C4'-O4'-C1'$$

(a)

$\alpha(i) = O3(i-1) - P(i) - O5'(i) - C5'(i)$

$\beta(i) = P(i) - O5'(i) - C5'(i) - C4'(i)$

$\gamma(i) = O5'(i) - C5'(i) - C4'(i) - C3'(i)$

$\delta(i) = C5'(i) - C4'(i) - C3'(i) - O3'(i)$

$\varepsilon(i) = C4'(i) - C3'(i) - O3'(i) - P(i+1)$

$\zeta(i) = C3'(i) - O3'(i) - P(i+1) - O5'(i+1)$

(b)
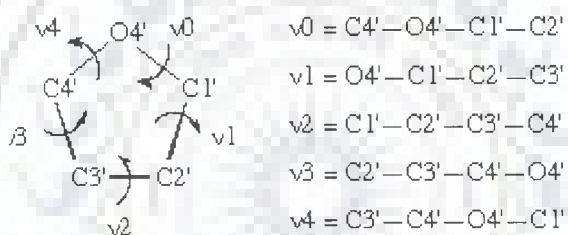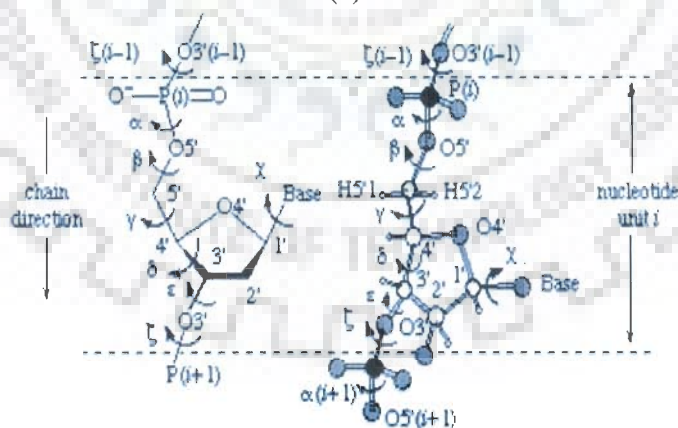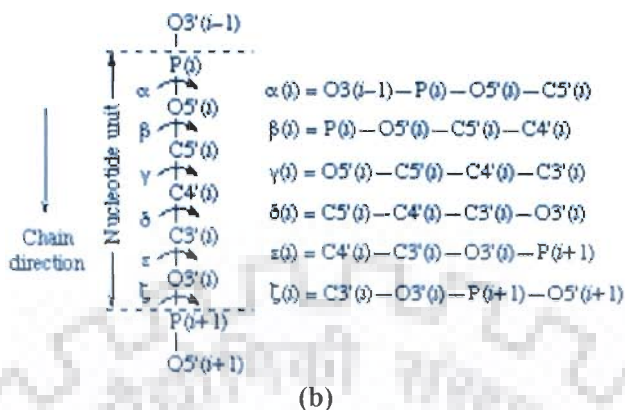
Fig. 1.4 : (a) A ribose unit showing atomic numbering and definition of torsion angles, v0, v1 , v2, v3 and v4 (b) Section of a polynucleotide backbone showing the atom numbering and the notation for torsion angles α, β, γ, δ, ε, and ζ.

phosphodiester bond (Fig. 1.5b). The primary sequence of nucleic acids is determined by the sequence of bases along the nucleotide chain and the function of acids namely replication, transcription and translation are governed by this sequence. The three–dimensional back bone conformation of nucleic acids is governed by a number of torsion. The sequential numbering of atoms $_{(n-1)}P$—O5'—C5'—C4'—C3'––O3'——P——O5'$_{(n+1)}$ is defined by torsion angles α, β, γ, ε and ζ as shown in Fig. 1.4b. Each conformation of the furanose ring can be unequivocally described by two pseudorotational parameters: the phase angle of pseudorotation, P, and the degree of pucker, ψ_{max}.

In nucleotides, the pseudorotation phase angle P is calculated from the endocyclic sugar torsion angles Fig. 1.5 (Altona et al, 1972).

$$\tan P = \frac{(v_4 + v_1) - (v_3 + v_0)}{2.v_2 (\sin 36° + \sin 72°)}$$

Given the phase angle P, the five torsional angles are related by

$$v_j = v_{max} \cdot \cos(P + j.\psi)$$

9

where j = 0 to 4 and $\psi = 720° / 5 = 144°$. The maximum torsion angle, v_{max} is derived by setting j = 0

$$v_{max} = v_0 / \cos P$$

At every phase angle P, the sum of the positive torsional angles is equal to the sum of the negative torsional angles, i.e. the sum of the five angles is zero.

$$v_0 + v_1 + v_2 + v_3 + v_4 = 0$$

Standard conformation ($P=0°$) is defined with a maximally positive C1'–C2'–C3'–C4' torsion angle [i.e. the symmetrical $^3T_2$ form], and P has value 0–360°. Conformations in the upper or northern half of the circle (P = 0–90°) are denoted N and those in the southern half of the circle (P = 180 / 90°) are denoted S conformation. The relationship between P and the *endo / exo* and T / E notations is illustrated in. It may be seen that the symmetrical twist (T) conformations arise at even multiples of 18° of P and the symmetrical envelope (E) conformations arise at odd multiples of 18° of P.
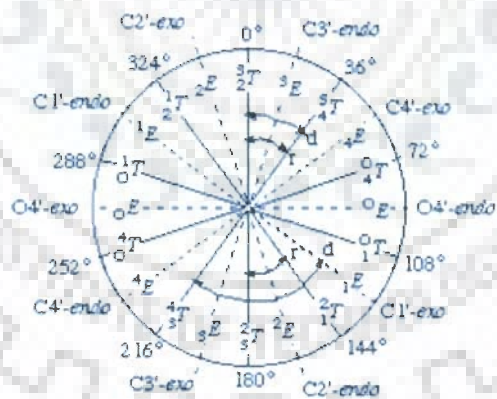
Fig. 1.5: Pseudorotation cycle of furanose ring in nucleosides (Altona et al, 1972)

The symbols 'r' and 'd' represent the usual range of P values for N and S conformations of ribo–(r) and 2'–deoxyribo–(d) furanose rings of –D–nucleosides and nucleotides. In B–DNA two ranges of pseudorotation phase angles are preferred C3' endo at $0° \le P \le 36°$ (N conformer) and C2' endo at $144° \le P \le 180°$ (S– conformer).

10

1.2.6 Glycosyl Torsion Angle (χ)

The glycosyl torsion (χ) angle define the orientation of the purine and pyrimidine bases relative to sugar ring. For pyrimidine nucleoside, χ is defined as torsion angle O4'–C1'–N1–C2 and for purines χ is O4'–C1'–N9–C4. Relative to the sugar moiety the base can adopt two main orientations about the glycosyl C1'–N link, called *syn* and *anti* (Fig. 1.8). Rotamers with *chi* values between -90° and +90° are called *syn* whereas *anti* refers to *chi* values from +90° to +270°. In Watson-Crick double helices both bases of base pairs are in *anti* conformation. Bases in *syn* conformation indicate a distortion of the double helix due to base pair opening or mismatched base pairs. The *syn* conformation is also found with guanines in left-handed Z–DNA (zig-zag helix).
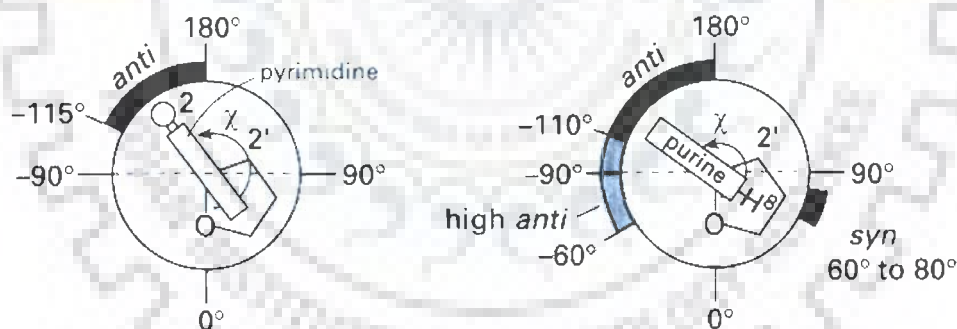
Fig. 1.6: Anti high, anti and syn orientations about the glycosidic bond in pyrimidine and purines.

In *anti*, the bulk of heterocyclic atoms i.e., the six-membered pyrimidine ring in purines and O_2 in pyrimidines is pointing away from the sugar, and in *syn*, pyrimidine is over and toward the sugar. An *anti* conformation is located near $\chi = 0°$, whereas in *syn* domain is around 210°. There is also a high *anti* which denotes a torsion angle lower than *anti*.

1.2.7 Duplex DNA

Duplex DNA is a right-handed helix formed by two individual DNA strands aligned in anti–parallel fashion. The two strands are held together by hydrogen bonds between individual bases as shown in Fig. 1.7. The bases are stacked near the center of the cylindrical helix. The hydrophobic interactions provide stability to the helix. A common feature of all the double helices is base stacking. Although the geometry of adjacent base pair varies, in each case the distance between neighboring base pair plane is about 3.4 Å. This is equal to Van der Waals radius of planar aromatic compound. It was shown that purines cause large upfield chemical shift due to stacking as compared to pyrimidines. The sugar and phosphate groups are at the outer side of the helix and forms a backbone of the helix.
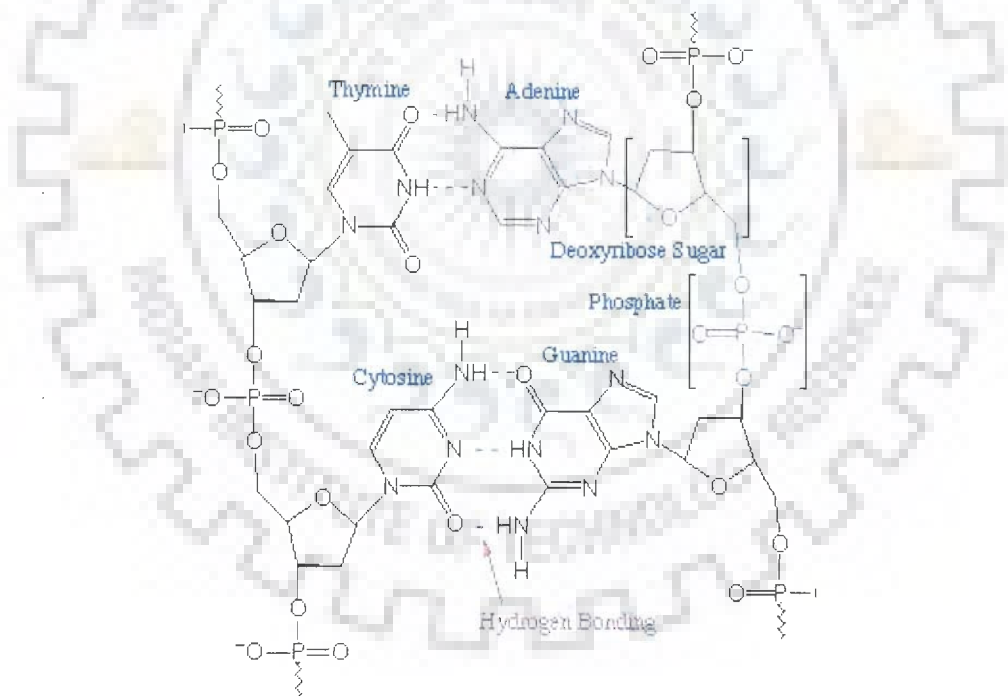
Fig. 1.7: Watson and Crick base pairs showing the hydrogen bonding arrangements in the double helical DNA

In a double helix, complementary base pairing connects the two-polynucleotide chains. Adenine always forms base pair with thymine and cytosine

forms base pair with guanine according to Watson and Crick base pairing scheme (Fig. 1.7). Although right handed DNA is presumed to be the predominant conformation *in vivo* but under different conditions of salt and humidity DNA shows structural polymorphism i.e. it exists in alternative conformations like A and Z DNA. The main features of A, B and Z–DNA are listed in Table 1.1. The structure of DNA can be described by number of helicoidal parameters like rise, pitch, tilt, roll, twist, no. of bases per turn, etc. These different types of DNA differ from each other in their helicoidal parameters, which define the helix of DNA. At high temperature, the secondary structure of DNA is lost and random coils are generated.

Table 1.1: Structural characteristics of A, B and Z type of double helices

Characteristics	A	B	Z
Helix sense	Right handed	Right-handed	Left handed
Repeating unit	1 bp	1bp	2 bp
Rotation/bp	33.6°	35.9°	60°/ 2
Mean bp/turn	10.7	10.0	12
Inclination of bp to axis	+19°	-1.2°	-9°
Rise/bp along axis	2.3Å	3.32Å	3.8Å
Pitch/turn of helix	24.6Å	33.2Å	45.6Å
Mean propeller twist	+18°	+16°	0°
Glycosyl angle	Anti	anti	C: anti, G: syn
Sugar pucker	C3'–endo	C2'–endo	C: C2–endo, G: C2'–exo
Diameter	26 Å	20 Å	18 Å

1.2.8 Quadruplex DNA

Nucleic acids can adopt a wide range of different conformations other than the well established A and B duplex forms. Telomeric DNA, gene promoter regions and immunoglobulin switch regions have been the focus of attention because they contain continuous repeats of G-rich sequences that have the ability to form G-quadruplex structures. In addition, a number of proteins have been identified that exhibit specific recognition of G-quadruplexes or promote G-quadruplex formation. Of particular interest are the telomeric DNA sequences found at the ends of chromosomes. These contain tandem repeats of guanine-rich DNA sequences of several kilobases that protect the ends from recombination, nuclease degradation and end-to-end fusions. Examples of such sequence repeats are TTAGGG, TTGGGG, TTTTGGGG, TTTAGGG and TTTTAGGG, which are found in telomeres of human, *Tetrahymena*, *Oxytricha*, *Arabidopsis*, *Chrorella* and *Chlamydomonas*, respectively. Telomeric sequences have the potential to form structures held together by guanine tetrads by either the intramolecular folding of a repetitive sequence, formation of a hairpin dimer or association of single strands to form a tetramer. Recent studies suggest that the G–quadruplex structure plays a role in interfering with telomerase action suggesting it as a potential therapeutic target for telomerase inhibition in cancer therapy. The basic unit of the G-quadruplex is the G-tetrad (Fig. 1.8a), which consists of a square planar arrangement of guanines hydrogen-bonded through their Watson-Crick and Hoogsteen edges. The O6 carbonyl groups are directed towards the interior of the G-tetrad and require the presence of a monovalent cation such as Na^+ or K^- to stabilize the structure.

The human telomeric sequence d[AGGG(TTAGGG)] forms an intramolecular quadruplex structure in Na^+ solution, with each strand having one antiparallel and one parallel neighbouring strand and *syn–syn–anti–anti* glycosidic torsion angles in each

14

G-tetrad. A more recent X-ray structure has shown that the same sequence is able to fold in the presence of K^+ to form a quite different parallel-stranded conformation with the A–T-rich loops on the outside of the core G-tetrad region (Parkinson *et al.* 2008). A number of parallel and anti-parallel stranded intermolecular G-quadruplex structures have now been studied in solution by a combined NMR and molecular dynamics approach (Wang and Patel 1993, Wang and Patel 1994; Marathias and Bolton, 2000; Gupta *et al.*, 1993; Aboulela *et al.*, 1994). A detailed list of literature for G-quadruplex structure by x ray crystallographic data and NMR are mentioned in the Table 1.3 at the end of this chapter. These structures consist of right-handed helices with all the residues adopting *anti* glycosidic torsion angles and predominantly C2'*endo* sugar pucker conformations. Each G-tetrad is well defined, adopting a coplanar alignment with strong stacking between adjacent G-tetrads. However, the terminal thymine residues are more dynamic, sampling multiple conformations in solution with little evidence to suggest formation of a stable T-tetrad. Stacking interactions with guanine tetrads by the neighbouring nucleotides in parallel-stranded quadruplexes has been explored with the NMR quadruplex structures of d(AGGGT)$_4$ and d(TAGGGT)$_4$ in the presence of K^+ ions. This comparison study revealed that although the G3 segments in the quadruplexes have largely similar structures, only the adenine residues in the d(AGGGT)$_4$ structure appear to form an A-tetrad (Fig. 1.8b) and have good stacking with the adjacent G-tetrad. Surprisingly, thymine and adenine residues in the d(TAGGGT)$_4$ quadruplex structure appear to sample a range of conformations resulting in poor stacking. Thus, DNA is capable of forming complex three-dimensional structures. These higher-ordered nucleic acid structures are often associated with important biological functions. Some other structural motifs, e.g., bulges and hairpins, are ubiquitous components of the complex folded assembly.
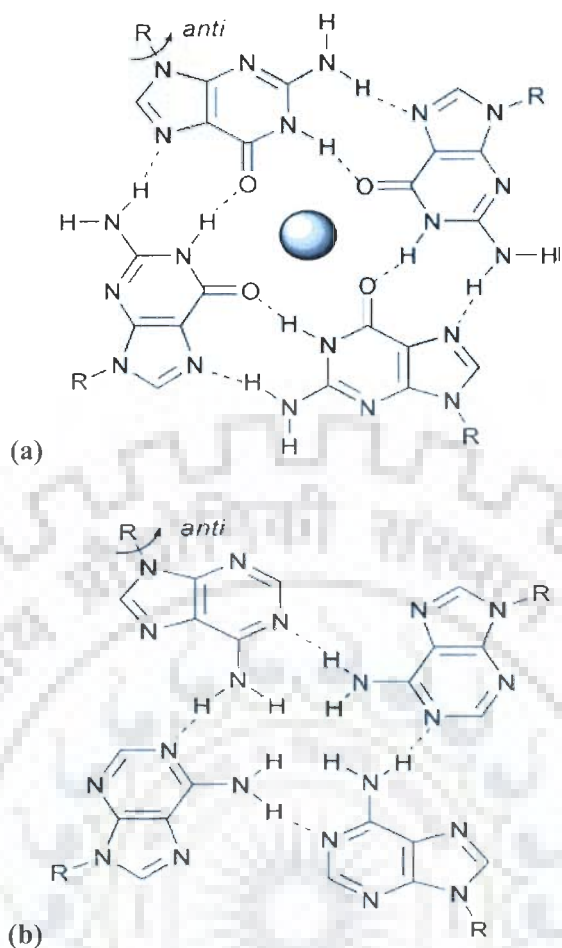
Fig. 1.8: Schematic drawing of the G-tetrad (a) with a bound K⁺ in the central channel, and (b) the A-tetrad with the hydrogen bonding pattern.

The properties of these DNA structures can be influenced by binding of drug molecules. Current effort of this thesis is to investigate how DNA-binding anticancer drug affect the structure and dynamics of those higher-ordered structures. Vise versa, the interactions between DNA-binding anticancer drugs and unusual structures can be recognized for understanding the mode of action of those molecules in cancerous cells.

1.3 Drug-DNA Interaction

DNA is an extremely important target for drug action, with a wide range of biological activities (anti-tumor, antiviral and antimicrobial) arising from the ability

16

of compounds to bind sequence specifically to DNA and interfere with DNA topoisomerases or with transcription binding factor (Singh *et al.*, 1992). The mode of action of some drugs for the treatment of cancer, genetic disorders, and viral diseases is thought to be based on their binding to DNA and their modification of DNA activity. The activity of the drug is often linked to the binding geometry. Thus, the potential activity of a drug could be assessed by detecting the DNA binding location and fit of the drug candidate.

The design and evaluation of molecules that can recognize DNA in a sequence selective manner requires a multi-disciplinary approach to evaluate preferred binding sequences, a thermodynamic description of the interaction to measure complex stability, and high resolution structural data to define precisely the molecular basis for sequence recognition. In combination this data can be used predicatively in further rational design. The current research effort focuses on the application of a range of biophysical techniques, high resolution structural analysis by NMR spectroscopy, together with state-of-the-art computational methods to investigate the molecular basis for drug-DNA recognition, the role of solvent in mediating weak interactions, and co-operative interactions between adjacent binding sites. All this will lead to 'rational drug design'- a deterministic approach to combat disease or an infectious pathogen. For "rational" design, the first necessary step is the identification of a molecular target critical to a disease like cancer. Then the important prerequisite of "drug design" is the determination of the molecular structure of target, which makes sense of the word "rational". Thus the mode of DNA/drug interaction could be important for the design of advanced drugs. There are several modes of DNA binding are found for anticancerous drugs.

1.3.1 Covalent DNA Binding

Drugs that interfere with DNA function by chemically modifying specific nucleotides. These drugs damage DNA. There are two types of alkylating agents: mono–functional (one reactive group) which cause single–strand breaks in DNA or damage bases and bi–functional (two reactive groups) which form cross–links. A large number of first generations of anti– cancer drugs were designed to combine a simple alkylating function. Their common feature is that they form an initial physical complex with DNA before covalently bonding to it. Many of them have also shown selective anti–tumor activity, this can be attributed to DNA binding specificity or to preferential metabolic activation by tumour cells. The mechanism of action of these anticancer agents is by alkyl group transfer and they cause alkylation of DNA at N7 or N2 position of guanine (other sites as well) and interaction may involve single strands or both strands. Anthramycin is an anti–tumor antibiotic that binds covalently to N–2 of guanine located in the minor groove of DNA. Cisplatin is a transition metal complex cis–diamine–dichloro–platinum and clinically used as anticancer drug. The effect of the drug is due to the ability to platinate the N–7 of guanine on the major groove site of DNA double helix. Other interactions involve the reaction of these drugs with amino, hydroxyl and phosphate groups of other cellular constituents. These drugs usually form a reactive intermediate ethyleneimonium ion.

Poly functional alkylating drugs offer resistance against cancer by increased ability to repair DNA defects, decreased cellular permeability to the drug, increased glutathione synthesis, which inactivates alkylating agents through conjugation reactions. Mitomycin C is a well characterized anti–tumor antibiotic, which forms a covalent interaction with DNA after enzymatic reductive activation of its quinone to alkylate DNA. The activated antibiotic forms a cross–linking structure between guanine bases

18

on adjacent strands of DNA thereby inhibiting single strand formation which is essential for m–RNA transcription and DNA replication.

1.3.2 Noncovalent DNA Binding

1.3.2.1 Intercalators

Intercalators are the most important group of compounds that interact reversibly with the DNA double helix. These are clinically useful anticancer antibiotics, which are primarily derived from *Streptomyces peucetius*. Some of them are valuable anticancer drugs currently used for the treatment of ovarian and breast cancers and acute leukemia, while many others are in different phases of clinical trials. Intercalating agents share common structural features such as the presence of planar polyaromatic systems, which bind by insertion between DNA base–pairs, termed as intercalation (Lerman, 1961). Binding of peptides to polynucleotides by intercalation are also reported (Rajeshwari, 1996).

Nowadays it is well accepted that the anti–tumor activity of intercalators is closely related to the ability of these compounds to stabilize the DNA–intercalator–topoisomerase II ternary complex. Majority of these drugs have shown marked preference for 5'–pyrimidine–purine–3' steps. The chromophores are linked to basic chains that might also play an important role in the affinity and selectivity shown by these compounds. Bis–intercalators have two potential intercalating ring systems connected by linkers, which can vary in length and rigidity. They also alter membrane fluidity and ion transport. One potential mechanism is based on the ability of these agents to participate in electron–transfer processes, with the subsequent generation of free radicals. The property results from the presence of two very different types of redox–active groups, namely the quinone and hydroquinone moieties as in daunomycin and adriamycin. Quinone moiety of daunomycin undergo one–electron reduction to a semiquinone radical, which in the presence of oxygen gives rise to

superoxide and other reactive oxygen species. The first crystal structure with a mono–intercalator and oligonucleotide was obtained by Wang and co–workers (Wang et al, 1987) for a complex of antibiotic daunomycin and d–(CGTACG)$_2$.

1.3.2.2 Groove Binding

The major and minor groove differs significantly in electrostatic potential, hydrogen bonding characteristics, steric effects and hydration. Typically minor groove binding molecules have several simple aromatic rings connected by bond with torsional freedom. This creates compounds, which with the appropriate twist, can fit into the helical curve of the minor groove with displacement of water from the groove and forming Van der Waalls contacts with the helical chains which define the walls of the groove. Additional specificity in the binding comes from contacts between the bound molecule and the edges of the base pairs on the 'floor' of the groove. Thus, the aromatic rings of many groove binding molecules form close contact with AH2 protons in the minor grooves of DNA. Pullman and coworkers have shown that the negative electrostatic potential is greater in the A.T minor groove than G.C rich regions, and this provides an additional important source for A.T specific minor groove binding of cations. Examples of minor groove binding drugs are netropsin and distamycin.

1.3.3 Other Anticancer Agents

1.3.3.1 Antimetabolites - Nucleic Acid Synthesis Inhibition

Purine antagonists like mercaptopurine act by hypoxanthine–guanine phosphoribosyl transferase (HGPRT) to form 6–thioinosinic acid, which inhibits enzymes involved in purine metabolism. Thioguanine which acts as inhibitor of purine nucleotide pathway is an enzyme which decreases intracellular concentration of guanine nucleotides and inhibit glycoprotein synthesis, finally blocking DNA / RNA synthesis.

20

1.3.3.2 Topoisomerase Targeting Drugs

Chromosomal DNA is extensively twisted and topoisomerases permit selected regions of DNA to untangle so as to allow transcription and replication. These enzymes temporarily break DNA, allowing for topological changes, and then reseal the breaks. Topoisomerase targeting drugs like etoposide stabilizes the topoisomerase II–DNA complex preventing it from making a topological change. This results in an irreversible double strand break, which is lethal to cells in S and G2 phases. Six anti–neoplastic drugs targeting topoisomerase II, i.e. doxorubicin, daunorubicin, idarubicin, mitoxantrone, etoposide and teniposide are currently approved for clinical use in the United States. Synthetic topoisomerase inhibitory analogs are also stuidied (Singh, *et al.*, 1992).

DNA topoisomerase II is a ubiquitous enzyme that is essential for the survival of all eukaryotic organisms and plays critical roles in virtually every aspect of DNA metabolism. The enzyme unknots and untangles DNA by passing an intact helix through a transient double–stranded break that it generates in a separate helix. Beyond its physiological functions, topoisomerase II is the target for some of the most active and widely prescribed anticancer drugs currently utilized for the treatment of human cancers. DNA is an extremely important target for drug action, with a wide range of biological activities (anti-tumor, antiviral and antimicrobial) arising from the ability of compounds to bind sequence specifically to DNA and interfere with DNA topoisomerases or with transcription binding factor (Lancelot et al, 2003). These antibiotics act by intercalating between base pairs of DNA causing lengthening of the double helix and a decrease in the helical twist on unwinding, inducing mediated strand scission. These drugs act in an insidious fashion and kill cells by increasing levels of covalent topoisomerase II–cleaved DNA complexes that are normally fleeting intermediates in the catalytic cycle of the enzyme.
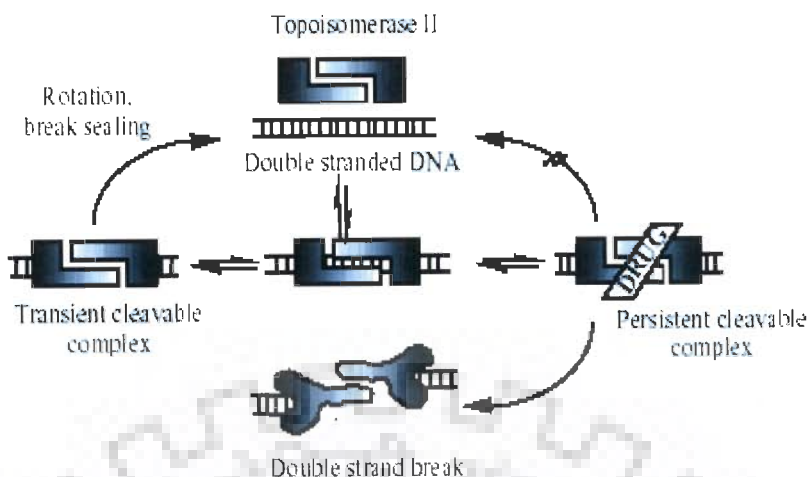
Fig. 1.9: DNA damage induced by inhibition of Topoisomerase II.

The anti–tumor topoisomerase II inhibitors presently used in the clinic, poison the enzyme by stabilizing cleavable complexes, presumably by increasing the rate of forwards reaction i.e. more rate of DNA cleavage or by decreasing the rate of backward reaction i.e. slow rate of religation of cleaved DNA (Fig. 1.9). Thus synthesis of DNA and RNA is blocked.

1.3.3.3 Microtubule Inhibitors

Microtubules are protein polymers involved in cellular movement and morphology. Microtubules occur in equilibrium between polymerized and free tubulin dimers. Inhibitor drugs disrupt this equilibrium. Vinca alkaloids (vinblastine, vincristine) are examples of this type of drugs.

1.3.3.4 Telomere and Telomerase Targeting Drugs

Most of these ligands have similar feature: extended planar aromatic electron deficient chromophore with cationic substituents, enabling them intercalate into G-quadruplex easily and improve its stability, such as anthraquinones, quinoacridines, phenanthrolines, acridines and carbocyanine dyes. GRN163/GRN163L and BIBR1532 are other small molecules that inhibit telomerase directly resulting in

22

telomere attrition over successive cycles of replication. RHPS4 and BRACO19 also stabilize G-quadruplex structures formed by the guanine-rich strand of telomeres and inhibit telomere maintenance by telomerase.

1.4 Forces Involved in Drug-DNA Interaction

1.4.1 Hydrogen Bonding

The phosphate group, sugar, bases in nucleic acids and hydrophilic groups in drug participate in hydrogen bonding with water. Since all linear hydrogen bonds have similar free energies, they make little net contribution to the favorable free energy change when drug and nucleic acid interact in solution. By contrast, formation of poorly aligned hydrogen bonds, or absence of some of them on the complex formation, carries a free energy penalty of about 4 KJ mol^{-1}. Thus hydrogen bonds are one of the most important means of making sequence specific interaction of nucleic acid with drug.

1.4.2 Electrostatic Forces: Salt Bridges

Salt bridges are electrostatic interactions between groups of opposite charge. They typically provide about 40 KJ mol^{-1} of stabilization per salt bridge. In drug–DNA complexes, strength of salt bridges decreases with the increase in concentration of the salt. They are much stronger when there are no water molecules between the ionized groups because water has a high dielectric constant. These are relatively long–range forces.

1.4.3 Entropic Forces: The Hydrophobic Effect

The hydrophobic effect is due to the behavior of water at an interface. Any molecule in water creates a sharply curved interface and so orders a layer of water molecules around itself. When molecules aggregate, the ordered water molecules at the interface are released and become part of the disordered bulk water, thus stabilizing the aggregate by increasing the entropy of the system.

Polar surfaces, where the enthalpy loss tends to offset the entropy gain or desolvation are less likely to aggregate than non–polar ones. Molecules of water left at the interface between the drug and the nucleic acid obviously decrease the entropy of the system. Therefore, the surface of the non–planar aromatic chromophore of drug tends to be exactly complementarily so that no unnecessary water molecules remain when the complex forms.

1.4.4 Base Stacking: Dispersion Forces

Base stacking is caused by two kinds of interaction: the hydrophobic effect mentioned above and dispersion forces. Molecules with no net dipole moment can attract each other by a transient dipole–induced–dipole interaction. Such dispersion forces decreases with the inverse sixth power of the distance separating the two dipoles, and so are very sensitive to the thermal motion of the molecules involved. Despite their extreme distance dependence, dispersion forces are clearly important in maintaining the structure of double stranded nucleic acids because they help to cause base stacking. Besides they allow aromatic ring of the drug to intercalate between bases and stabilize it by base stacking.

1.5 NMR Spectroscopy, UV-Vis and Fluorescence Spectroscopy Involved In Drug –DNA Interaction

NMR spectroscopy has enjoyed many advances recently, and the pace of development shows no signs of slowing. These advances are allowing NMR to help in solving important problems in the widespread manner in the field of drug discovery. NMR spectroscopy is now being used to determine protein structures, to monitor ligand-receptor binding, to study diffusion, to analyze mixtures using LC-NMR, to analyze solid-phase synthesis resins and to determine the structures of organic small molecules. Biomolecular NMR spectroscopy has expanded dramatically in recent years and is now a powerful tool for the study of structure, dynamics, and interactions

24

of biomolecules. NMR spectroscopy is already well-established as an efficient method for ligand screening. A number of recently developed techniques show promise as aids in structure-based drug design. An advantage of the method is that all these interactions can be studied in solution-time-consuming crystallization is not necessary. Being in solution form, even structural and biochemical changes in intact cells (in vivo NMR) can be monitored. Nuclear Magnetic Resonance (NMR) spectroscopy uses radiation to induce nuclear spin state changes which are unique for different atoms and their local environment. From the 1D and 2D NMR spectrum acquired on solid or liquid samples, the structure of molecules can be deduced. NMR can observe static as well as dynamic interactions between molecules. It requires that the sample to be dissolved in a deuterated solvent. The most commonly used resonances in NMR studies are ^{1}H, ^{13}C, ^{31}P and ^{15}N. ^{1}H NMR gives rise to a series of absorption lines in the region 0-15 ppm. A larger spectral dispersion of chemical shifts is observed in ^{13}C NMR. In ^{15}N NMR, chemical shifts are sensitive to primary structure as well as molecular conformation. But it has low sensitivity due to low natural abundance (0.36%) which causes difficulties in its detection hence offers limited applications of ^{15}N NMR. ^{31}P NMR has developed as a powerful probe of the structure and dynamics of DNA due to existence of spin ½, 100% natural abundance, moderate relaxation times, wide range of chemical shifts and non-interference from solvent peaks. In ^{31}P NMR, chemical shifts are sensitive to molecular conformation of the phosphate group. Thus it becomes very informative in case of nucleic acid structure elucidation since backbone of DNA and RNA contains phosphorus nuclei. NMR spectroscopy can provide both qualitative and quantitative information. This information can benefit numerous disciplines in drug discovery, including natural products research, synthetic medicinal chemistry, metabolism studies, drug production, quality control, rational drug design and combinatorial chemistry. This

focuses on how they might be of value in removing some of the current "bottlenecks" in structure-based drug discovery.

Fluorescence spectroscopy provides structural information on the basis of emission and excitation wavelength. The fluorophore has different emission and excitation wavelengths which gives different spectra ranging from 200-800nm. UV-Vis spectroscopy uses the wavelengths of light in the spectrum ranges of 120 to 800 nm. DNA typically absorbs in the region of 160 to 300 nm due to the electronic transitions regions of the bases. These techniques are conducted in solution and are simple to conduct, but average the results across molecules in different states.

1.6 Molecular Modeling Study Involved In Drug-DNA Interaction

Molecular modeling is a broad term that encompasses *ab initio* quantum mechanical calculations, semi-empirical calculations, and empirical calculations (charge-dependent molecular mechanics force fields). These techniques can be used to study the three-dimensional structure, dynamics, and properties of a molecule of interest. Molecular modeling can identify and define the possible key details of the molecular interaction and, using the graphics/computational approach, decide on optimal structural modifications likely to enhance either general binding affinity or recognition of a particular nucleotide-binding site. A number of studies have revealed the converse, with the discovery that particular patterns of chemical modification on a given drug (e.g., PIPER) with G-quadruplex can result in both change in biological activity and interaction energy.

The molecular modeling, particularly molecular mechanics and dynamics, are highly complementary to macromolecular NMR and X-ray crystallography. Molecular dynamics simulation can, in principle, provide a complete theoretical description of DNA structure and motions, and are thus a valuable independent means of developing models and interpreting experimental data. A combined approach is

26

desirable and, where the parent experimental structure is available, the simulation can be partially validated by reproducing the structure, thus paving the way for 'rational drug-designing'. For "rational" drug design, choice of a target, the evaluation of a structure of that target, the pivotal questions to consider in choosing a method for drug lead discovery, and evaluation of the drug leads.

1.7 Flavonoids

Flavonoids are a large family of compounds synthesized by plants that have a common chemical structure (Beecher, 2003). The basic structure of a flavonoid is shown in Fig. 1.10a. The diveristy of flavonoids based on the distribution of hydroxyl group on flavonoid ring yield different structure and function (Fig. 1.10 a, b). Flavonoids may be further divided into subclasses (see Table 1.2). Over the past decade, scientists have become increasingly interested in the potential for various dietary flavonoids to explain some of the health benefits like cancer prevention etc. associated with fruit- and vegetable-rich diets.

1.7.1 Metabolism and Bioavailability

Flavonoids connected to one or more sugar molecules are known as flavonoid glycosides, while those that are not connected to a sugar molecule are called aglycones. With the exception of flavanols (catechins and proanthocyanidins), flavonoids occur in plants and most foods as glycosides (Williamson, 2004). Even after cooking, most flavonoid glycosides reach the small intestine intact. Only flavonoid aglycones and flavonoid glucosides (bound to glucose) are absorbed in the small intestine, where they are rapidly metabolized to form methylated, glucuronidated, or sulfated metabolites (Manach *et al.*, 2004). Bacteria that normally
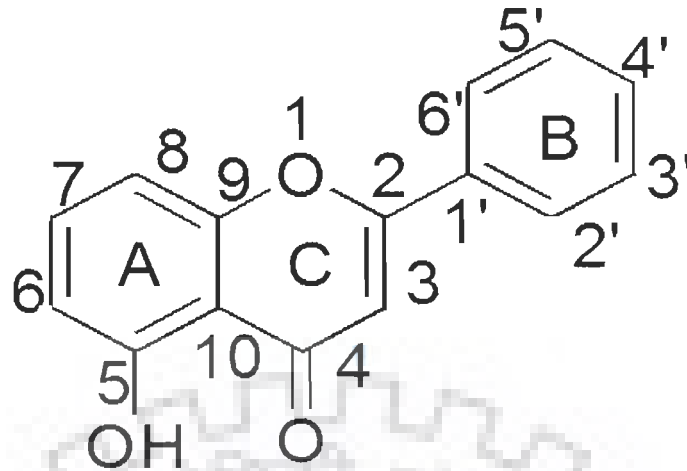
Fig. 1.10 (a) Molecular structure of flavanoid ring, (b) Different types of flavonoids based on substitution of hydrogen and hydroxyl group and (c) molecular structure of flavanones.
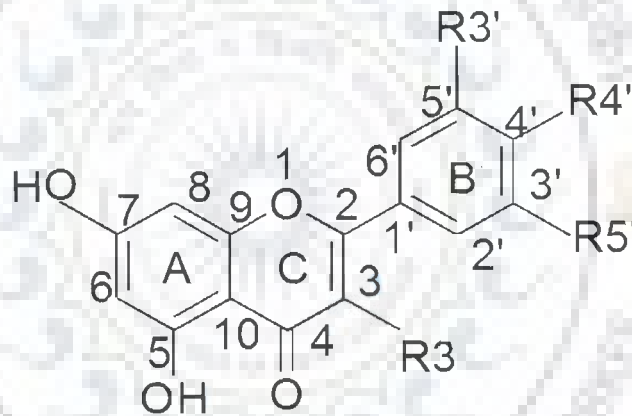
	R3	R3'	R4'	R5'
Chrysin	H	H	H	H
Apigenin	H	H	OH	H
Luteolin	H	OH	OH	H
Acacetin	H	H	OCH3	H
Galangin	OH	H	H	H
Kaemferol	OH	H	OH	H
Quercetin	OH	OH	OH	H
Myricetin	OH	OH	OH	OH

Fig. 1.10 (b)
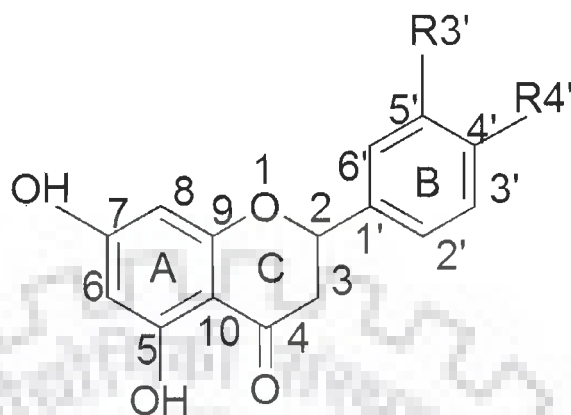
	R3'	R4'
Naringenin	H	OH
Hesperetin	OH	OCH3

Fig. 1.10 (c)

Table 1.2: Classification of bioflavonoids with their dietary source

Flavonoid Subclass	Dietary Flavonoids	Some Common Food Sources
Anthocyanidins	Cyanidin, Delphinidin, Malvidin, Pelargonidin, Peonidin, Petunidin	Red, blue, and purple berries; red and purple grapes; red wine
Flavanols	Monomers (Catechins): Catechin, Epicatechin, Epigallocatechin Epicatechin gallate, Epigallocatechin gallate Dimers and Polymers: Theaflavins, Thearubigins, Proanthocyanidins	Catechins: Teas (particularly green and white), chocolate, grapes, berries, apples Theaflavins, Thearubigins: Teas (particularly black and oolong) Proanthocyanidins: Chocolate, apples, berries, red grapes, red wine
Flavanones	Hesperetin, Naringenin, Eriodictyol	Citrus fruits and juices, e.g., oranges, grapefruits, lemons
Flavonols	Quercetin, Kaempferol, Myricetin, Isorhamnetin	Widely distributed: yellow onions, scallions, kale, broccoli, apples, berries, teas
Flavones	Apigenin, Luteolin	Parsley, thyme, celery, hot peppers,
Isoflavones	Daidzein, Genistein, Glycitein	Soybeans, soy foods, legumes

colonize the colon also play an important role in flavonoid metabolism and absorption. Flavonoids or flavonoids metabolites that reach the colon may be further metabolized by bacterial enzymes, and then absorbed. A person's ability to produce specific flavonoid metabolites may vary and depends on the milieu of the colonic microflora (Setchell *et al.*, 2002; Yuan *et al.*, 2007). In general, the bioavailability of flavonoids is relatively low due to limited absorption and rapid elimination. Bioavailability differs for the various flavonoids: isoflavones are the most bioavailable group of flavonoids, while flavanols (proanthocyanidins and tea catechins) and anthocyanins are very poorly absorbed (Manach *et al.*, 2005). Since flavonoids are rapidly and extensively metabolized, the biological activities of flavonoid metabolites are not always the same as those of the parent compound (reviewed in Williams *et al.*, 2004). When evaluating the data from flavonoid research in cultured cells, it is important to consider whether the flavonoid concentrations and metabolites used are physiologically relevant (Kroon *et al.*, 2004). In humans, peak plasma concentrations of soy isoflavones and citrus flavanones have not been found to exceed 10micromoles/liter after oral consumption. Peak plasma concentrations measured after the consumption of anthocyanins, flavanols and flavonols (including those from tea) are generally less than 1 micromole/liter (Manach *et al.*, 2004). Flavonoids are effective scavengers of free radicals in vitro (Heijnen *et al.* 2001; Chun *et al.* 2003). However, even with very high flavonoid intakes, plasma and intracellular flavonoid concentrations in humans are likely to be 100-1,000 times lower than concentrations of other antioxidants, such as ascorbate (vitamin C), uric acid, or glutathione. Moreover, most circulating flavonoids are actually flavonoid metabolites, some of which have lower antioxidant activity than the parent flavonoid. For these reasons, the relative contribution of dietary flavonoids to plasma and tissue

30

antioxidant function in vivo is likely to be very small or negligible (Frei and Higdon, 2003; Lotito and Frei, 2006; Williams *et al.* 2004).

1.7.2 Flavonoids and cancer

Although it is unclear how flavonoids work to protect against cancer, many of their biological actions have been attributed to their antioxidant activity. Of all the antioxidants found in fruits and vegetables, it is the flavonoids that people consume in greatest amounts, sometimes up to 1 gram per day. Flavonoids scavenge free radicals in the test tube; but, even with high flavonoid intakes, concentrations in humans are probably 100 to 1,000 times lower than concentrations of other antioxidants. Flavonoid metabolites have even lower antioxidant activity than the parent flavonoid. Thus, antioxidant activity is not considered the only mechanism at play. Many in vitro and animal model studies suggest flavonoids influence important cellular and molecular mechanisms related to carcinogenesis, but it is still unclear how high flavonoid intake can help prevent cancer in humans. Flavonoids inhibit the development of induced lung, esophageal, stomach, colon, skin, prostate and breast cancers in animals. Yet, epidemiological studies do not support a link between high intakes of dietary flavonoids and significant decreases in human cancer risk.

1.8 Literature Review

1.8.1 Structure and Conformation of flavonoids

Prior to the determination of the structure-activity correlations for its antioxidant potentials, DNA binding and other activities, it is important to understand their overall structural parameters, conformational preferences and intra- and interamolecular interactions of the molecule alone. It has been found that their function can be changed by means of various degrees of hydroxylated substitution and the number of hydroxyl groups; for instance 3OH of quercetin is very important for its antioxidant activities (Trouillas *et al.* 2006), luteolin inhibits fatty acid synthetase

31

(Lupu and Menendez, 2006) and apigenin induces apoptosis in tumour cells. Beside this, the potency of these flavonoids in binding with DNA and topoisomerase inhibition is different which is revealed and correlated with its structure (Webb and Ebeler, 2004). Further, flavonoids have been found from natural sources and whenever they were isolated, they have been identified by instrument analysis. Very few X-ray data on flavonoids including quercetin dihydrate (Jin *et al.* 1990), rutin (Chen *et al.* 2007), morin hydrate (Cody *et al.* 1994), luteolin (Cox *et al.* 2003) and the complexes of myricetin with triphenyl phosphine are available according to the Cambridge Structural database. Geometric data including hydrogen atom positions are usually obtained by X-ray analysis of crystals. Unfortunately, it is not an easy task to grow a crystal for X -ray diffraction studies. Flavonoids are difficult to crystallize and X-ray diffraction data are lacking for most of the members of this family. Thus, NMR provides us an alternative to study their structure and conformation. However, the solution structure for flavonoids is rare in literature. Further, the substitution of hydroxyl group caused changes of the ^{1}H and ^{13}C chemical shifts, the complete ^{1}H and ^{13}C NMR spectral assignments of hydroxylated flavonoids can be possible and these may lead us to identify these flavonoids without further experiments.

Recently ^{1}H and ^{13}C NMR spectral assignments were also presented for six hydroxyl flavones, compared with fourteen different additional hydroxyl flavones (Park *et al.* 2007). Based on ^{1}H and ^{13}C NMR data, quercetin has been isolated from *Tanacetum balsamita* (Nickavar *et al.*, 2003) and similar for, flavonol methyl esters from *Solanum pubescens* were characterized (Kumari *et al.*, 1986). It has been investigated for the bioactivity of the *in vivo* metabolites of quercetin (Spencer *et al.* 2003). ^{13}C CP/MAS NMR data were also reported to characterize the solid state conformation of flavonoids based on their NMR shielding data (Wawer and Zielinska, 2003). In solid phase, quercetin crystallizes as the dihydrate in a fairly planar

32

conformation and in solid state NMR and theoretical DFT studies showed a second conformer of quercetin with a planar conformation of the aromatic rings and the opposite arrangement of B-ring (Olejniczak and Potrzebowski, 2004).

Although in literature there exist several works on ^1H and ^{13}C NMR data for luteolin, quercetin and rutin (Markham, 1977; Markham and Chari, 1982; Lallemand and Duteil, 1977; Xioa *et al.*, 2005) but no systematic studies are carried out both experimentally and theoretically to compare the structural parameters and chemical shift. As it is well known that the structural parameters play very crucial role in different conformations in these compounds which are needed to correlate the differential efficacy in biological activity in solution.

Though experimental NMR chemical shifts for most of the flavonoids are available but there are doubts and ambiguities in proton and carbon chemical shifts assignments. Therefore, DFT can be an important source of structural information and can also remove all the ambiguities in chemical shift assignments which can be worth important to get the sound information regarding NMR chemical shifts, molecular properties and electronic structural parameters of these bioflavonoids without generating crystal for these molecules. Solid-state conformations of nine anthocyanidins were studied and the solid-state chemical shifts were found different from those obtained for solutions, indicating differences in conformation and intermolecular interactions. (Wolniak *et al.* 2008). DFT approach also shed light on the reactivity of two flavonoids, quercetin and taxifolin. particularly focus on the 3-OH site and the role played by the 2,3-double bond in the reactivity of that site for their antioxidant potential (Trouillas *et al.* 2006). A series of *ab initio* and DFT calculations have been performed to study a polyphenol namely theamide of caffeic acid: 3-(3,4-dihydroxyphenyl)-2-propen-amide (ACA). Several molecular properties have been computed for this amide, such as potential energy profiles for internal

rotation about different bonds, minimal conformer structures and corresponding vibrational frequencies. Twelve possible unlike conformations were found for caffeic acid, adopting the amide group in all of them a non co-planar conformation (Rincon *et al.*, 2007). Similarly, the structural and electronic characters of four types of hydroxyl group-substituted anthocyanidins (pelargonidin, cyanidin, delphinidin, and aurantinidin) were examined using quantum chemical calculations. For these cationic molecules, both the planar and nonplanar structures in the electronic ground state were determined and revealed that the planar structure is slightly more stable than the non-planar structure for each molecule (Sakata *et al.* 2006).

The structural properties of luteolin, apigenin and of all their possible mono-deprotonated species are studied with *ab initio* methods *in vacuo* and in solution. Molecular structures have been optimized by MP2 and DFT using different functionals and basis sets (Leopoldini *et al.*, 2004). An interesting behavior for the torsional potential between phenyl B ring and the 1,4-benzopyrone skeleton has been detected. Therefore, potential energy profiles along this coordinate have been characterized and analyzed in terms of conjugative and steric interactions through the evaluation of the coefficients fitted with an eight-term Fourier expansion (Amat *et al.*, 2008). Further, quercetin is known that it exerts its antioxidant activity through the capacity to donate protons and electrons to inhibit reactive oxygen species (ROS) that act like free radicals and it has been found that it is a relatively polar molecule, soluble in water, and which presents diamagnetic properties in its basal state, in addition to an aromatic character. It presents a greater tendency to give electrons than to attract them, which confirms its antioxidant capacity. The more important reactive sites that can be related to the antioxidant properties are located mainly in rings B and C. Electronic and vibrational spectroscopy investigations were also performed to characterize the Al(III) complexes: stoichiometry, stability constants and involved

34

groups in multi-site ligands. Quantum chemical calculations have been carried out in order to know the structural modifications generated to the ligand by complexation. Which showed that capacity of different studied functions to chelate Al(III) is the same when they are in competition and when they are individually taken. (Cornard and Merlin 2003; Cornard and Merlin 2002). Similarly, The ground and low-lying excited electronic states of the 1:1 complex of Zn with 3-hydroxyflavone (3HF) in methanol solution were studied using DFT approach (Cornard *et al.*, 2006). Similar studies were performed in 5, 7 dihydroxy flavone with Al (III) complex (Castro and Blanco, 2006).

High-level good *ab initio* calculations have been also performed on a chemical model of Rutin and the absolute reduction potential has been calculated (Namazian *et al.*, 2008). Similarly, a theoretical calculation based on the density functional theory (DFT) has been performed to understand the antioxidant activity of rosmarinic acid in view of a molecular structure. According to the geometry of the ground state molecule and its free radical, the HOMO and LUMO, the O–H bond dissociation energy (BDE), and the single electron density distribution of the radicals, were interpreted to determine the capacity of scavenging the radicals for rosmarinic acid by its structure. Compared with flavonoids, the higher antioxidant activity of rosmarinic acid may be from the abstraction of hydrogen atoms of the ortho-position hydroxyls on the rings A and B. This abstraction can occur continuously to form a semiquinone structure, or even to form a quinone structure. The activity of the ring A is similar with the ring B. However, the ring B is a stronger electron donor than the ring A, and, the radical formed from the H-abstraction of the ring A is more stable than that of the ring B. This shows that there is a good relationship between the BDE, which is used to show the stability of the parent molecule and the unpaired electron delocalization correlated to the stability of the free radical. These theoretical researches will be helpful to the

development for the antioxidant compounds (Cao *et al.*, 2005). The calculations based on the density functional theory (DFT) have been used further, to study the structure–activity of resveratrol in the chain reaction of auto oxidation. According to the geometry obtained by using same approach, the single electron distribution of the 4'- and 5-radical of resveratrol were calculated and it was found that resveratrol is a potential antioxidant. The 4'-hydroxyl group of resveratrol is more reactive than 3- and 5-positions because of the resonance effects. The dominant structure of the resveratrol radicals is a semiquinone structure which determines the stability of radicals, and the unpaired electron is mainly distributed to the O-atom and its ortho and para positions. The antioxidant activity of resveratrol is related to the spin density and the unpaired electron distribution of the O-atom. (Cao *et al.* 2003).

In this regard, structural and electronic characteristics of four flavonoids, namely quercetin, luteolin, catechin and taxifolin were done and deprotonation and hydrogen abstraction energies of the 3OH and 4OH hydroxyl groups were compared and analyzed with the help of an electronic description for each structure. The results showed significant role of p-delocalization upon stabilization but have also shown that inductive effects play a major role in the stabilization of deprotonated forms. Inspection of the charge transfer together with analysis of a simple model of catechol was also demonstrated the relative independence of each structural motif when hydrogen abstraction processes are considered (Antonczak, 2008).

^{13}C CP MAS NMR spectra of the flavonoids: morin, kaempferol, 3,7-dihydroxyflavone, tricin and isoflavones: genistein and formononetin were recorded to characterize solid-state conformations. Intramolecular hydrogen bonds forming five-, six- and seven-membered rings are present in the two morin molecules in the crystals – their ^{13}C resonances have been assigned with the aid of the calculated shielding constants. Linear relationships between the calculated shielding constants

rDFT (ppm) and chemical shifts (CPMAS, ppm) were obtained for all studied compounds. Higher correlation coefficients suggest that the conformation with "clockwise" orientation of both OH groups is more probable in the solid 3,7-dihydroxyflavone, whereas in the solid formononetin the OH and OCH3 substituents are directed "anticlockwise". The barrier to the rotation of phenyl ring B decreases in the order: morin (20-OH, 3-OH) > kaempferol (3- OH) > tricin (Zielinska *et al.* 2008).

1.8.2 Biological Activities

1.8.2.1 Antioxidant Activity

Antioxidants are compounds that protect cells against the damaging effects of reactive oxygen species, such as singlet oxygen, superoxide, peroxyl radicals, hydroxyl radicals and peroxynitrite. An imbalance between antioxidants and reactive oxygen species results in oxidative stress, leading to cellular damage. Oxidative stress has been linked to cancer, aging, atherosclerosis, ischemic injury, inflammation and neurodegenerative diseases (Parkinson's and Alzheimer's). Flavonoids may help provide protection against these diseases by contributing, along with antioxidant vitamins and enzymes, to the total antioxidant defense system of the human body. Epidemiological studies have shown that flavonoid intake is inversely related to mortality from coronary heart disease and to the incidence of heart attacks (Salvayre *et al.*, 2006; Papas, 1999; Wu and Simin, 1999).

1.8.2.2 Metal Chelation

Metal ions, such as iron and copper, can catalyze the production of free radicals. The ability of flavonoids to chelate (bind) metal ions appears to contribute to their antioxidant activity in vitro (Mira *et al.* 2002; Cheng and Breen, 2000). In living organisms, most iron and copper are bound to proteins, limiting their participation in reactions that produce free radicals. Although the metal-chelating activities of flavonoids may be beneficial in pathological conditions of iron or copper excess, it is

not known whether flavonoids or their metabolites function as effective metal chelators *in vivo* (Frei and Higdon, 2003).

1.8.2.3 Disease Prevention

1.8.2.3.1 Cardiac Disease

Several prospective cohort studies conducted in the U.S. and Europe have examined the relationship between some measure of dietary flavonoid intake and coronary heart disease (CHD) risk (Geleijnse *et al.* 2002; Hertog *et al.* 1997; Hirvonen *et al.* 2001; Knekt *et al.* 2002; Yochum *et al.* 1999; Hertog *et al.* 1997; Rimm *et al.* 1996; Sesso *et al.* 2003). Some studies have found that higher flavonoid intakes to be associated with significant reductions in CHD risk (Geleijnse *et al.* 2002; Hertog *et al.* 1997; Hirvonen *et al.* 2001; Knekt *et al.* 2002; Yochum *et al.* 1999; Mink *et al.* 2007), while others have reported no significant relationship (Sesso *et al.* 2003; Lin *et al.* 2007). In general, the foods that contributed most to total flavonoid intake in these cohorts were black tea, apples, and onions. One study in the Netherlands also found cocoa to be a significant source of dietary flavonoids. Of seven prospective cohort studies that examined relationships between dietary flavonoid intake and the risk of stroke, only two studies found that higher flavonoid intakes were associated with significant reductions in the risk of stroke (Keli *et al.* 1996; Knekt *et al.* 2002), while five found no relationship (Yochum *et al.* 1999; Mink *et al.* 2007; Sesso *et al.* 2003; Hirvonen *et al.* 2000; Knekt *et al.* 2000). Although data from prospective cohort studies suggest that higher intakes of flavonoid-rich foods may help protect against CHD, it cannot be determined whether such protection is conferred by flavonoids, other nutrients and phytochemicals in flavonoid-rich foods, or the whole foods themselves (Liu, 2003).

38

1.8.2.3.2 Vascular diseases

Vascular endothelial cells play an important role in maintaining cardiovascular health by producing nitric oxide, a compound that promotes arterial relaxation (vasodilation) (Vita, 2003). Arterial vasodilation resulting from endothelial production of nitric oxide is termed endothelium-dependent vasodilation. Several clinical trials have examined the effect of flavonoid-rich foods and beverages on endothelium-dependent vasodilation. Two controlled clinical trials found that daily consumption of 4-5 cups (900-1,250 ml) of black tea for four weeks significantly improved endothelium-dependent vasodilation in patients with coronary artery disease (Duffy *et al.*, 2001) and in patients with mildly elevated serum cholesterol levels (Hodgson *et al.* 2002) compared with the equivalent amount of caffeine alone or hot water. Other small clinical trials found similar improvements in endothelium-dependent vasodilation in response to daily consumption of about 3 cups (640 ml) of purple grape juice (Stein *et al.*, 1999) or a high-flavonoid dark chocolate bar for two weeks (Engler *et al.*, 2004). More recently, a 6-week cocoa intervention trial in 32 postmenopausal women with high cholesterol levels found significant improvements in endothelial function with daily cocoa supplementation (Wang-Polagruto *et al.*, 2006). Improvements in endothelial function were also noted in conventionally medicated type 2 diabetics following flavanol-rich cocoa supplementation for 30 days (Balzer *et al.*, 2008). The flavanol epicatechin appears to be one of the compounds in flavanol-rich cocoa responsible for its vasodilatory effects (Schroeter *et al.*, 2006). Interestingly, a recent randomized controlled trial in 44 older adults found that low doses of flavonoid-rich dark chocolate (6.3 grams/day for 18 weeks; equivalent to 30 calories) increased levels of plasma S-nitrosoglutathione, an indicator of nitric oxide production, compared to flavonoid-devoid white chocolate (Taubert *et al.*, 2007).

Endothelial nitric oxide production also inhibits the adhesion and aggregation of platelets, one of the first steps in blood clot formation (Vita, 2003). A number of clinical trials have examined the potential for high flavonoid intakes to decrease various measures of platelet aggregation outside of the body (ex vivo); such trials have reported mixed results. In general, increasing flavonoid intakes by increasing fruit and/or vegetable intake did not significantly affect ex vivo platelet aggregation (Cheng and Breen, 2000; Freese *et al.*, 2004; Janssen *et al.*, 1998) nor did increasing black tea consumption (Duffy *et al.* 2001; Hodgson *et al.*, 2002). However, several small clinical trials in healthy adults have reported significant decreases in ex vivo measures of platelet aggregation after consumption of grape juice (~500 ml/day) for 7-14 days (Polagruto *et al.*, 2003) Similar inhibition of platelet aggregation has been reported following acute or short-term consumption of dark chocolate (Innes *et al.*, 2003) and following acute consumption of a flavonoid-rich cocoa beverage (Rein *et al.*, 2000; Rein *et al.*, 2000). In addition, a placebo-controlled trial in 32 healthy adults found that 4-week supplementation with flavanols and procyanidins from cocoa inhibited platelet aggregation and function (Murphy *et al.*, 2003). The results of some controlled clinical trials suggest that relatively high intakes of some flavonoid-rich foods and beverages, including black tea, purple grape juice, and cocoa, may improve vascular endothelial function, but it is not known whether these short-term improvements will result in long-term reductions in cardiovascular disease risk.

1.8.2.3.3 Neurodegenerative Disease

Inflammation, oxidative stress, and transition metal accumulation appear to play a role in the pathology of several neurodegenerative diseases, including Parkinson's disease and Alzheimer's disease (Ramassamy, 2006). Because flavonoids have anti-inflammatory, antioxidant, and metal-chelating properties, scientists are interested in the neuroprotective potential of flavonoid-rich diets or individual

40

flavonoids. At present, the extent to which various dietary flavonoids and flavonoid metabolites cross the blood brain barrier in humans is not known (Youdim *et al.*, 2004; Schmitt-Schillig *et al.*, 2005). Although flavonoid-rich diets and flavonoid administration have been found to prevent cognitive impairment associated with aging and inflammation in some animal studies (Goyarzu *et al.*, 2004; Joseph *et al.*, 2003; Joseph *et al.*, 1999; Patil *et al.*, 2003), prospective cohort studies have not found consistent inverse associations between flavonoid intake and the risk of dementia or neurodegenerative disease in humans (Laurin *et al.*, 2004; White *et al.*, 2004; De-Rijk *et al.*, 1997; Engelhart *et al.*, 2002; Commenges *et al.*, 2000). In a cohort of Japanese-American men followed for 25-30 years, flavonoid intake from tea during midlife was not associated with the risk of Alzheimer's or other types of dementia in late life (Laurin *et al.*, 2004). Surprisingly, higher intakes of isoflavone-rich tofu during midlife were associated with cognitive impairment and brain atrophy in late life (White *et al.*, 2000). A prospective study of Dutch adults found that total dietary flavonoid intake was not associated with the risk of developing Parkinson's disease (De-Rijk *et al.*, 1997) or Alzheimer's disease (Engelhart *et al.*, 2002), except in current smokers whose risk of Alzheimer's disease decreased by 50% for every 12 mg increase in daily flavonoid intake. In contrast, a study of elderly French men and women found that those with the lowest flavonoid intakes had a risk of developing dementia over the next five years that was 50% higher than those with the highest intakes (Commenges *et al.*, 2000). More recently, a study in 1,640 elderly men and women found that those with higher dietary flavonoid intake (>13.6 mg/day) had better cognitive performance at baseline and experienced significantly less age-related cognitive decline over a 10-year period than those with a lower flavonoid intake (0-10.4 mg/day) (Letenneur *et al.*, 2007). Additionally, a randomized, double-blind, placebo-controlled clinical trial in 202 postmenopausal women reported that daily

supplementation with 25.6 g of soy protein (containing 99 mg of isoflavones) for one year did not improve cognitive function (Kreijkamp-Kaspers *et al.*, 2004). However, a randomized, double-blind, placebo-controlled, cross-over trial in 77 postmenopausal women found that 6-month supplementation with 60 mg/day of isoflavones improved some measures of cognitive performance (Casini *et al.*, 2006). Although scientists are interested in the potential of flavonoids to protect the aging brain, it is not yet clear how flavonoid consumption affects neurodegenerative disease risk in humans.

1.8.2.3.4 Cancer

Although various flavonoids have been found to inhibit the development of chemically-induced cancers in animal models of lung (Yang *et al.*, 1998), oral (Balasubramanian *et al.*, 1996), esophageal (Li *et al.*, 2002), stomach (Yamane *et al.*, 1996), colon (Guo *et al.*, 2004), skin (Huang *et al.*, 1997), prostate (Gupta *et al.*, 2001, Haddad *et al.*, 2006), and mammary (breast) cancer (Yamagishi *et al.*, 2002), epidemiological studies do not provide convincing evidence that high intakes of dietary flavonoids are associated with substantial reductions in human cancer risk. Most prospective cohort studies that have assessed dietary flavonoid intake using food frequency questionnaires have not found flavonoid intake to be inversely associated with cancer risk (Ross and Kasum, 2002). Two prospective cohort studies in Europe found no relationship between the risk of various cancers and dietary intakes of flavones and flavonols (Goldbohm *et al.*, 1995; Hertog *et al.*, 1994), catechins (Arts *et al.*, 2001), or tea (Goldbohm *et al.*, 1996). In a cohort of postmenopausal women in the U.S., catechin intake from tea, but not fruits and vegetables, was inversely associated with the risk of rectal cancer, but not other cancers (Arts *et al.*, 2002). Two prospective cohort studies in Finland, where average flavonoid intakes are relatively low, found that men with the highest dietary intakes of flavonols and flavones had a significantly lower risk of developing lung cancer than those with the lowest intakes

42

(Hirvonen et al, 2001; Knekt *et al.*, 2002). When individual dietary flavonoids were analyzed, dietary quercetin intake, mainly from apples, was inversely associated with the risk of lung cancer; myricetin intake was inversely associated with the risk of prostate cancer (Knekt *et al.*, 2002). Tea is an important source of flavonoids (flavanols and flavonols) in some populations, but most prospective cohort studies have not found tea consumption to be inversely associated with cancer risk (reviewed in Higdon *et al.*, 2003). The results of case-control studies, which are more likely to be influenced by recall bias, are mixed. While some studies have observed lower flavonoid intakes in people diagnosed with lung (De Stefani *et al.*, 1999), stomach (Garcia-Closas *et al.*, 1999; Lagiou *et al.*, 2004), and breast (Peterson *et al.*, 2003) cancer, many others have found no significant differences in flavonoid intake between cancer cases and controls (Garcia *et al.*, 1999; Garcia-Closas *et al.*, 1998). There is limited evidence that low intakes of flavonoids from food are associated with increased risk of certain cancers. Clinical trials will be necessary to determine if specific flavonoids are beneficial in the prevention or treatment of cancer; a few clinical trials are currently under way. However, in animal studies, administration of flavonoids has been shown to prevent the development and growth of various types of chemical carcinogen-induced or transplanted tumors (Buchler *et al.*, 2003; Kohno *et al.*, 2002; Rice *et al.*, 2002). The proposed mechanisms for these cancer prevention effects are multifaceted, including their anti-oxidant activities, their effects on signal transduction pathways involved in cell proliferation and angiogenesis, as well as their modulation of aromatase activity, a key enzyme involved in estrogen biosynthesis, and the enzymes required for metabolic activation of procarcinogens and the detoxification of carcinogens (Kellis and Vickery, 1984; Middleton *et al.*, 2000).

1.8.2.3.4.1 Effects on Cell-Signaling Pathways

Cells are capable of responding to a variety of different stresses or signals by increasing or decreasing the availability of specific proteins. The complex cascades of events that lead to changes in the expression of specific genes are known as cell-signaling pathways or signal transduction pathways. These pathways regulate numerous cell processes, including growth, proliferation, and death (apoptosis). Although it was initially hypothesized that the biological effects of flavonoids would be related to their antioxidant activity, available evidence from cell culture experiments suggests that many of the biological effects of flavonoids are related to their ability to modulate cell-signaling pathways (Williams *et al.*, 2004). Intracellular concentrations of flavonoids required to affect cell-signaling pathways are considerably lower than those required to affect cellular antioxidant capacity. Flavonoid metabolites may retain their ability to interact with cell-signaling proteins even if their antioxidant activity is diminished (Spencer *et al.*, 2001; 2003). Effective signal transduction requires proteins known as kinases that catalyze the phosphorylation of target proteins at specific sites. Cascades involving specific phosphorylations or dephosphorylations of signal transduction proteins ultimately affect the activity of transcription factors-proteins that bind to specific response elements on DNA and promote or inhibit the transcription of various genes. The results of numerous studies in cell culture suggest that flavonoids may affect chronic disease by selectively inhibiting kinases (william *et al.*, 2004; Hou *et al.*, 2004). Cell growth and proliferation are also regulated by growth factors that initiate cell-signaling cascades by binding to specific receptors in cell membranes. Flavonoids may alter growth factor signaling by inhibiting receptor phosphorylation or blocking receptor binding by growth factors (Lambert and Yang, 2003).

Modulation of cell-signaling pathways by flavonoids could help prevent cancer by:

44

Stimulating phase II detoxification enzyme activity (Kong *et al.*, 2001; Walle and Walle, 2002): Phase II detoxification enzymes catalyze reactions that promote the excretion of potentially toxic or carcinogenic chemicals.

Preserving normal cell cycle regulation (Chen et al, 2004; Wang *et al.*, 2004): Once a cell divides, it passes through a sequence of stages collectively known as the cell cycle before it divides again. Following DNA damage, the cell cycle can be transiently arrested at damage checkpoints, which allows for DNA repair or activation of pathways leading to cell death (apoptosis) if the damage is irreparable (Stewart *et al.*, 2003). Defective cell cycle regulation may result in the propagation of mutations that contribute to the development of cancer.

Inhibiting proliferation and inducing apoptosis (Kavanagh *et al.*, 2001; Shah *et al.*, 2004; Ramos *et al.*, 2007): Unlike normal cells, cancer cells proliferate rapidly and lose the ability to respond to cell death signals that initiate apoptosis.

Inhibiting tumor invasion and angiogenesis (Kim *et al.*, 2003; Bagli *et al.*, 2004): Cancerous cells invade normal tissue aided by enzymes called matrix-metalloproteinases. To fuel their rapid growth, invasive tumors must develop new blood vessels by a process known as angiogenesis.

Decreasing inflammation (Sakata *et al.* 2003; Cho *et al.*, 2003; O'Leary *et al.*, 2004): Inflammation can result in locally increased production of free radicals by inflammatory enzymes, as well as the release of inflammatory mediators that promote cell proliferation and angiogenesis and inhibit apoptosis (Steele *et al.*, 2003).

1.8.2.3.2 Effect on DNA interaction

Deoxyribonucleic acid (DNA) is an important genetic substance in organism. In recent years, the interactions of drugs with DNA and the investigation of new effective DNA probes have been the focus on the study of small molecules interacting with DNA. The areas of DNA involved in vital processes such as gene expression,

gene transcription, mutagenesis, carcinogenesis and cell death, etc., are of particular interest as targets for a wide range of anticancer and antibiotic drugs (Wadkins *et al.* 1998; Robinson *et al.* 1997; Lin and Patel, 1995; Hurley, 2002; Cao and He, 1998; Krishna *et al.* 1998; Radi *et al.*, 2003). Many organic dyes have already proven sensitive probes of DNA, such as ethidium bromide (EB) (Reinhardt, and Krugh, 1978; Vergani *et al.* 1997; Sutherla and Sutherla, 1970), acridine orange (AO) (Cao *et al.*, 1999), oxazide yellow homodimers (Rye *et al.*, 1993), nile blue (Chen *et al.*, 1993), diphenylamine blue (Lancker and Gheyssens, 1986) and neutral red (Huang and Feng, 2001).

The difference spectrum of the quercetin-DNA complex versus quercetin alone was characterized by a peak at 395 run. An increase in the magnitude of difference spectrum was seen with increased ionic strength. Spectrophotometric changes in absorbance and fluorescence of quercetin showed that ethidium bromide is able to displace quercetin from the quercetin-DNA complex. These results indicated that the binding of quercetin to DNA does not involve electrostatic interactions but may be intercalative in nature. Experiments using DNase I footprinting technique showed that the flavonoid does not possess any preferred sites of binding in DNA. Strand scission in DNA by the quercetin-Cu(II) system gave a generally uniform cutting pattern of internucleotide bonds. This led to the observation that the quercetin-Cu(II) cleavage reaction has the potential of being used as preferred DNA footprinting reagent (Ahmad *et al.* 1994).

The ability of luteolin to interact with DNA was investigated by fluorescence titration with CT DNA. Addition of CT DNA causes a slight shift of the maximum peak from 525 to 519 nm with a concomitant increase in fluorescence intensity. A progressive change in the fluorescence spectra of luteolin on addition of different

concentrations of DNA indicated an association between them (Choudhary *et al.* 2002).

It has also been reported that flavonoids can interact with DNA *in vitro* (Kanakis *et al.*, 2005), where polyphenol different binding modes were discussed. The aim of this study was to examine the interaction of transfer RNA with quercetin, kaempferol, and delphinidin in aqueous solution at physiological conditions and to make a comparison with the corresponding pigment–DNA adducts. FT-IR and UV-visible difference spectroscopic methods have been applied to determine the drug binding mode, the binding constants, and the effects of drug complexation on the stability and conformation of tRNA duplex. Both intercalative and external binding modes were observed. Structural analysis showed que, kae, and a del intercalate tRNA duplex with minor external binding to the major or minor groove and the backbone phosphate group. The stability of adduct formation is in the order of del > que > kae. A comparison with flavonoids–DNA adducts showed both intercalation and external bindings with the stability order que > kae > del. Low flavonoid concentration induces helical stabilization, whereas high pigment content causes helix opening. A partial B to A–DNA transition occurs at high drug concentration, while tRNA remains in the A-family structure (Kanakis *et al.*, 2006).

The interactions of flavonoids, such as quercetin, kaempferide and luteolin, with fish sperm deoxyribonucleic acid (DNA) were explored by using acridine orange (AO) as a fluorescence probe. The variations in the spectroscopic characteristics of DNA–AO in an aqueous medium upon addition of the three drugs were observed. Measurements of ultraviolet absorption and fluorescence spectra, determination of binding constants for flavonoids–double stranded DNA (dsDNA) or flavonoids–single stranded DNA (ssDNA) were following the trend like kaempferide > quercetin > luteolin for ds-DNA and quercetin > kaempferide > luteolin for ss-DNA. The binding

47

mode of quercetin, kaempferide and luteolin with DNA was evaluated to be groove binding (Bi *et al.*, 2006).

It was evident that quercetin can bind DNA by intercalation (Solimani *et al.*, 1995) and a comparison with the flavanol dihydroquercetin indicated that the interaction is correlated to the planarity and hydrophobicity of the benzopyranic-4-one plane The interaction is most probably of a hydrophobic nature between the most hydrophobic segment of the quercetin (benzopyran-4-one) and the intercalation site, which allows the chromophore to penetrate the DNA helix and to arrange its planar structure more or less parallel to the adjacent planes of the nitrogenous bases. A comparison between the planar and hydrophobic flavonol quercetin, and the non-planar and hydrophilic flavanone dihydroquercetin, showed that the interaction of the latter with DNA was strongly limited. The notable biological activity of the quercetin compared to the 'weaker' activity of the dihydroquercetin could also be derived from the different planarity (and probably hydrophobicity) of the two flavonoids (Solimani, 1996). Similarly, Flow linear dichroism LD spectra of the hydrophobic quercetin were compared with hydrophilic aglycoside morin and 3-glycoside rutin in the same conditions. Morin and rutin in an aqueous environment showed the same behaviour as quercetin with their common benzopyranic-4-one part within the biopolymer. The LD^R values (LD normalised to the relative isotropic absorption). indicated a greater affinity of the quercetin for the DNA. Comparison of the LD^R of morin and rutin showed a ratio very close to unity and this suggests the localisation of the 3-rutinoside of morin rutin rutin outside the intercalation site (Solimani, 1997).

Differential scanning calorimetry (DSC) along with UV/Vis absorption and photon correlation spectroscopy (PCS), on normal and glycated human placenta DNA were used to explore the antioxidant property of the naturally occurring polyhydroxy flavone quercetin (3,3',4',5,7-pentahydroxyflavone) in preventing the glycation. The

48

decrease in the absorption intensity of DNA in presence of sugars clearly indicates the existence of sugar molecules between the two bases of a base pair in the duplex DNA molecule. The melting temperature of placenta DNA was decreased when glycated suggesting a decrease in the structural stability of the double-stranded glycated DNA. But the dramatic changes in the structural properties of glycated DNA can be prevented to a significant extent by adding quercetin (Sengupta *et al.* 2006).

Quercetin zinc (II) complex was investigated focusing on its hydrolytic activity towards DNA. The complex successfully promotes the cleavage of plasmid DNA, producing single and double DNA strand breaks. The amount of conversion of supercoiled form (SC) of plasmid to the nicked circular form (NC) was found to be dependent on the concentration of the complex as well as the duration of incubation of the complex with DNA. The hydrolytic cleavage of DNA by the complex is supported by the evidence from free radical quenching, thiobarbituric acid-reactive substances (TBARS) assay and T4 ligase ligation (Jun *et al.* 2007).

The interaction between DNA and a series of flavonoids: quercetin (the most active), morin, rutin, naringin, and 2,3- dihydroquercetin (inactive) was studied. The sensitivity of equilibrium binding analysis was carried out by the dextran-polyethylene glycol-H_2O biphase system was not high enough to reveal and evaluate the binding affinity of these flavonoids toward DNA. The much more sensitive flow linear dichroism technique provided evidence that they can bind DNA by intercalation and that their affinity for DNA increased following the same sequence of their biological activity (Solimani *et al.* 1995).

Interactions of quercetin (que), kaempferol (kae) and delphinidin (del) with calf-thymus DNA and transfer RNA in aqueous solution at physiological conditions, using constant DNA or RNA and various drug/polynucleotide (phosphate) ratios of 1/65 to 1 were studied. Structural analysis showed quercetin, kaempferol and

delphinidin intercalate RNA duplex with minor external binding to the major or minor groove and the backbone phosphate group with the stability of adduct formation is in the order of del>que>kae>. A comparison with flavonoids-DNA adducts showed both intercalation and external bindings with stability order $K_{que}=7.25 \times 10^4$ M^{-1}, $K_{kae}=3.60 \times 10^4$ M^{-1} and $K_{del}=1.66 \times 10^4$ M^{-1}. Low flavonoid concentration induces helical stabilization, whereas high pigment content causes helix opening. A partial B to A-DNA transition occurs at high drug concentration, while t RNA remains in A-family structure (Tajmir-Riahi *et al.* 2007).

The binding affinities of flavonoids, genistein and quercetin, to DNA oligomers d(GCGTACGC)2 have been established by means of studying by NMR the diffusion coefficients of these compounds with and without the presence of DNA. Genistein was found to bind very weakly as compared to quercetin and luteolin. In the case of genistein a hydrogen bond between the $NH^{F, B}$ cytidine protons of the edge base pair and a genistein hydroxyl was proposed, based on the shape of the DOSY spectrum. MP2 and DFT calculations of genistein show a 9 kcal/ mol excess energy of the planar conformation as compared with a twisted one. For this reason intercalation of the planar genistein into the base pairs is rather unlikely (Bocian *et al.* 2006).

Similarly, the observed reduction in NH band in FT-IR experiments of free nucleic acids upon complexation with resveratrol and genistein drugs is an indication of the involvement of the hydroxyl (OH) and imino (NH) group during the interaction of the drugs and nucleic acids (DNA/RNA) through H-bonded formation. The interaction of RES and GEN with bases appears in the order of G $\geq$ T>C>A and A>C$\geq$ T>G. Further interaction of these natural compounds with DNA and RNA was also supported by changes in the vibrational frequency (shift/intensity) in symmetrical and asymmetrical stretching of aromatic rings of drugs in the complex spectra. No

appreciable shift was observed in the DNA and RNA marker bands, indicating that the B-DNA form and A-family conformation of RNA are not altered during their interaction with RES and GEN (Usha *et al.* 2005). It was further found from TCSPC analysis that the higher lifetime component or constituent of intercalated dyes (τ_2, A_2) decreased with the subsequent increase in smaller component or constituent of free dye (τ_1, A_1) after the interaction of drugs with the intercalated DNA (Usha *et al.* 2006).

The interactions between rutin or the inclusion complex of rutin-β-cyclodextrin and DNA were investigated by means of cyclic voltammetry, UV-vis absorption spectroscopy and fluorescence emission spectroscopy which showed that the benzopyranic- 4-one plane of rutin mainly intercalated into DNA in the absence of β-cyclodextrin, while the catecholic portion of rutin was located in the double helix of DNA in the presence of β-cyclodextrin (Gong-Jun *et al.* 2004).

Further, the interaction modes of quercetins with monomeric and dimeric G-quadruplexes were studied by absorption, fluorescence, CD, and ^{1}H NMR spectroscopies. The ligands were found to be stacked with terminal tetrads of monomeric G-quadruplexes by intercalation and bound to dimeric G-quadruplexes by groove binding (Sun *et al.* 2006). Furthermore, rutin, showed different absorption and fluorescence spectral characteristics when bound to blunt-end stacked and interlocked extended G-quadruplexes. ^{1}H NMR spectra showed these two extended G-quadruplexes bound with rutins in different manners: after binding, the blunt-end stacked extended G-quadruplexes were decomposed to monomers, and the interlocked extended G-quadruplexes did not change (Sun *et al.* 2007).

Similarly, ESI-MS, CD and PAGE studies indicated that daidzin molecules interacted with G- quadruplex with the stoichiometric ratio of 1:1 and 1:2 which is assume to be stabilized the π- π conjugacy interactions and hydrogen bonding

51

between diadzin and the bases of G-quadruplex (Li *et al.* 20006) and evaluation of flavonoids binding to DNA duplexes (Wang *et al.*, 2008).

Recently, interactions of five flavonoids with dsRNA and single stranded ssRNA were studied by UV/vis titrations. The results obtained supported the intercalative binding mode as a dominant interaction of studied flavonoids with dsRNA as well as major interaction with ssRNA. The study also reveal about the role of the hydroxyl group in binding. Flavonoids with one- or two-OH groups on the phenyl part of the molecule (luteolin, fisetin, kaempferol) specifically differentiate between poly A, poly U which showed negligible changes while with poly G it was strong changes and with poly C the moderate changes in the UV/Vis spectra were observed (Piantanida *et al.* 2009).

Table 1.3: List of literature available on G-quadruplex structure and their ligand complex.

PDB ID	Sequence	Method		Author	Year
2GWE	5'-d(GGGGTTTTGGGG)-3'	X-Ray		Lee *et al.*	-
2GWQ	5'-d(GGGGTTTTGGGG)-3'	X-Ray		Lee *et al.*	-
2KAZ	5'-d(GGGACGTAGTGGG)-3'	NMR			-
3EM2	5'-d(GGGGTTTTGGGG)-3'	X-Ray	Ligand	Campbell *et al.*	-
3EQW	5'-d(GGGGTTTTGGGG)-3'	X-Ray	Ligand	Campbell *et al.*	-
3ERU	5'-d(GGGGTTTTGGGG)-3'	X-Ray	Ligand	Campbell *et al.*	-
3ES0	5'-d(GGGGTTTTGGGG)-3'	X-Ray	Ligand	Campbell *et al.*	-
ET8	5'-d(GGGGTTTTGGGG)-3'	X-Ray	Ligand	Campbell *et al.*	-
3EUI	5'-d(GGGGTTTTGGGG)-3'	X-Ray		Campbell *et al.*	-
3EUM	5'-d(GGGGTTTTGGGG)-3'	X-Ray	Ligand	Campbell *et al.*	-
3CCO	5'-d(TAGGGTTAGGGT)-3'	X-Ray		Parkinson *et al.* 2008.	2008
3CDM	5'-d(TAGGG(TTAGGG)3)-3'	X-Ray		Parkinson *et al.* 2008.	2008
3CE5	5'-d(TAGGGTTAGGGT)-3'	X-Ray	Ligand	Campbell *et al.* 2008.	2008
2E4I	5'-d(A(BGM)GGTTA(BGM) GGTTA(BGM)(BGM)GTTA(BGM)GG)-3'	NMR		Matsugami *et al.* 2007.	2007
2GW0	5'-d(TGGGGT)-3'	X-Ray		Lee *et al.* 2007.	2007
2HRI	5'-d(TAGGGTTAGGG)-3'	X-Ray	Ligand	Parkinson, *et al.* 2007	2007
2HY9	5'-d(AAAGGGTTAGGGTTAGGGTTAGGGAA)-3'	NMR		Dai *et al.* 2007.	2007
2JPZ	5'-d(TTAGGGTTAG GGTTAGGGTT AGGGTT)-3'	NMR		Dai *et al.* 2007.	2007
2JT7	5'-d(TGGGGT)-3'	NMR	Ligand	Martino *et al.*, 2007.	2007
2JWQ	5'-d(TTAGGGT)-3'	NMR	Ligand	Hounsou *et al.*, 2007.	2007
2GWE	5'-d(GGGGTTTTGGGG)-3'	X-Ray		Lee *et al.*	-
2HRI	5'-d(TAGGGTTAGGG)-3'	X-Ray	Ligand	Parkinson, *et al.* 2007	2007
2HY9	5'-d(AAAGGGTTAGGGTTAGGGTTAGGGAA)-3'	NMR		Dai *et al.* 2007.	2007
2JPZ	5'-d(TTAGGGTTAG GGTTAGGGTT AGGGTT)-3'	NMR		Dai *et al.* 2007.	2007
2JT7	5'-d(TGGGGT)-3'	NMR	Ligand	Martino *et al.*, 2007.	2007
2O3M	5'-d(AGGGAGGGCGCTGGGAGGAGGG)-3'	NMR		Phan *et al.*, 2007.	2007

53

2F8U	5'-d(GGGCGCGGGAGGAATTGGGCGGG)-3'	NMR		Dai *et al.*, 2006.	2006
2GKU	5'-d(TTGGGTTAGGGTTAGGGTTAGGGA)-3'	NMR		Luu *et al.*, 2006.	2006
2GRB	5'-r((U33)GIGGU)-3'	X-Ray	RNA	Pan *et al.*, 2006.	2006
2HBN	5'-d(GGGGTTTTGGGG)-3'	X-Ray		Gill *et al.*, 2006.	2006
2IDN	3'-d(GGT)-5'-5'-d(TGGTGTGGTTGG)-3'	NMR		Martino *et al.*, 2006	2006
1XAV	5'-d(TGAGGGTGGGTAGGGTGGGTAA)-3'	NMR		Ambrus, *et al.*, 2005	2005
1XCE	5'-d(GCGGTTGGAT)-3'	NMR		Webba *et al.*, 2005.	2005
1Y8D	5'-d(GGGGTGGGAGGAGGGT)-3'	NMR		Phan *et al.*, 2005.	2005
2A5P	5'-d(TGAGGGTGGIGAGGGTGGGGAAGG)-3'	NMR		Phan *et al.*, 2005.	2005
2A5R	5'-d(TGAGGGTGGIGAGGGTGGGGAAGG)-3'	NMR	Ligand	Phan *et al.*, 2005.	2005
2AKG	5'-d(GGGGTTTTGGGG)-3'	NMR		Gill *et al.*, 2005.	2005
2AQY	5'-d(G(OIP)GTTAGGGTTAGGGT)-3'/ 5'-d(TAGGG(U))-3'	NMR		Zhang *et al.*, 2005.	2005
1RDE	5'-d(GGTTGGTGTGGTTGG)-3'	NMR		Mao *et al.*, 2004.	2004
1S45	5'-d(TGGGGT)-3'	X-Ray		Caceres *et al.*, 2004.	2004
1S47	5'-d(TGGGGT)-3'	X-Ray		Caceres *et al.*, 2004.	2004
1S9L	5'-((TLN)(LCG)(LCG)(LCG)(TLN))-3'	NMR	LNA	Randazzo *et al.*, 2004.	2004
1U64	5'-d(GGGTTTTGGGG)-3'	NMR		Sket, *et al.* 2004	2004
1V3N	5'-d(G(CBR)GAGAGC)-3'	X-Ray		Kondo *et al.*, 2004.	2004
1V3O	5'-d(G(I5C)GAGAGC)-3'	X-Ray		Kondo *et al.*, 2004.	2004
1V3P	5'-d(G(I5C)GAGAGC)-3'	X-Ray		Kondo *et al.*, 2004.	2004
1J6S	5'-r((BRUGAGGU)-3'	X-Ray	RNA	Pan *et al.*, 2003	2003
1L1H	5'-d(GGGGTTTTGGGG)-3'	X-Ray	Ligand	Haider *et al.*, 2003.	2003
1NYD	5'-d(GCGGTGGAT)-3'	NMR		Webba da Silva *et al.*, 2003.	2003
1MDG	5'-r(U(BGM)GAGGU)-3'	X-Ray	RNA	Pan *et al.*, 2003	2003
1C34	5'-d(GGTTGGTGTGGTTGG)-3'	NMR		Marathias and Bolton, 2000	2000
1C35	5'-d(GGTTGGTGTGGTTGG)-3'	NMR		Marathias and Bolton, 2000	2000
1C38	5'-d(GGTTGGTGTGGTTGG)-3'	NMR		Marathias and Bolton, 2000	2000
1EEG	5'-d(GGAGGA)-3'	NMR		Kettani *et al.*, 2000.	2000
1EVO	5'-d(TGGGCGGT)-3'	NMR		Patel et al., 2000	2000
1F3S	5'-d(GGGTTCAGG)-3'	NMR		Kettani *et al.*, 2000.	2000
1EMQ	5'-d(TGGTGGC)-3'	NMR		Patel and Hosur, 1999	1999
1EVM	5'-d(AGGGT)-3'	NMR		Patel et al., 1999.	1999

1EVN	5'-d(AGGGT)-3'	NMR		Patel et al., 1999.	1999
1K4X	5'-d(GGGGTTTTGGGG)-3'	NMR		Schultze et al., 1999	1999
1A8N	5'-d(GGGCTTTTGGGC)-3'	NMR		Kettani et al. 1998	1998
1A8W	5'-d(GGGCTTTTGGGC)-3'	NMR		Bouaziz et al., 1998	1998
1AFF	5'-d(TAGG)-3'	NMR		Kettani et al., 1997	1997
352D	5'-d(TGGGGT)-3'	X-Ray		Phillips et al., 1997.	1997
1HAO	5'-d(GGTTGGTGTGGTTGG)-3'	X-Ray	Protein	Padmanabhan et al., 1996.	1996
1HAP	5'-d(GGTTGGTGTGGTTGG)-3'	X-Ray	Protein	Padmanabhan et al., 1996	1996
1QDF	5'-d(GGTTGGTGTGGTTGG)-3'	NMR		Marathias et al., 1996,	1996
1QDH	5'-d(GGTTGGTGTGGTTGG)-3'	NMR		Marathias et al., 1996	1996
1QDI	5'-d(GGGGTTTTGGGG)-3'	NMR		Marathias et al., 1996	1996
1QDK	5'-d(GGGGTTTTGGGG)-3'	NMR		Marathias et al., 1996	1996
1FQP	5'-d(GGGTTTTGGG)-3'	NMR		Keniry et al., 1995.	1995
230D	5'-d(GGGGTUTUGG GGTTTTGGGG UUTTGGGX)-3'	NMR		Smith et al., 1995.	1995
148D	5'-d(GGTTGGTGTGGTTGG)-3'	NMR		Schultze et al., 1994.	1994
156D	5'-d(GGGGTTTTGGGG)-3'	NMR		Schultze et al., 1994.	1994
244D	5'-d(TGGGGT)-3'	X-Ray		Laughlan et al., 1994.	1994
139D	5'-d(TTGGGGT)-3'	NMR		Wang and Patel, 1993.	1993
143D	5'-d(AGGGTTAGGGTTAGGGTTAGGG)-3'	NMR		Wang and Patel, 1993.	1993
1RAU	5'-r(UGGGGU)-3'	NMR	RNA	Cheong et al., 1992	1992

Materials and Methods

2.1 Materials

The calf thymus and herring sperm DNA were purchased from Sisco Research Laboratory, Mumbai and deoxyribonucleic acid sequences poly d(A.T), poly d(A-T), poly d(G-C), d-(TTAGGG), d-(TTAGGGT), d-(TTGGGGT), deuterium oxide, dimethyl sulphoxide (DMSO) with isotopic purity 99.96% and luteolin, quercetin, rutin and genistein were purchased from Sigma-Aldrich Chemicals Ltd. 3 - (Trimethylsilyl) propionic-2, 2, 3, 3-d_4 acid sodium salt (TSP) was added to sample as an internal NMR reference. HPLC grade solvents and reagents like K_2HPO_4 and KH_2PO_4 were used for buffer preparation and were purchased from Qualigens Fine Chemicals India Ltd. Synthetic oligo-/polynucleotide and flavonoid samples were used without further purification

2.2 Sample preparation for competition dialysis, UV-visible and fluorescence spectroscopic studies

2.2.1 Preparation of Buffer Solution

All experiments related to calf thymus DNA and poly deoxyribonucleotides [poly d(A.T), poly d(A-T), poly d(G-C)] were performed in the standard buffer solution containing 50 mM NaCl, 10mM phosphate buffer, pH 7.0 at 25 °C. For G-quadruplex formation 100 mM KCl has been added in 10 mM K_2HPO_4 at pH 7.0 for telomeric DNA sequences d-(TTAGGG)$_4$, d-(TTAGGGT)$_4$ and d-(TTGGGGT)$_4$.

2.2.2 Preparation of Sample

Solution of luteolin, quercetin, rutin and genistein were prepared by dissolving a known quantity of sample in DMSO The concentration of flavonoids in DMSO solution were determined spectro photometrically at the λ_{max} of 349 nm (ε = 20,417 $M^{-1}cm^{-1}$), 380 nm (ε

= 14,920 $M^{-1}cm^{-1}$), 368 nm (ε = 19,700 $M^{-1}cm^{-1}$) and 260 nm (ε = 37,260 $M^{-1}cm^{-1}$) for luteolin, quercetin, rutin and genistein, respectively. Similarly, calf thymus DNA, herring sperm DNA and polynucleotides sequences [poly d(A.T), poly d(A-T), poly d(G-C), d-(TTAGGG)$_4$, d-(TTAGGGT)$_4$ and d-(TTGGGGT)$_4$] were dissolved in the phosphate buffer (pH 7.0) and quantified spectro photometrically at their respective λ_{max} (Table 2.1).

Table 2.1 List of polynucleotide and oligonucleotide with their molar extinction coefficient

Name of DNA	ε Value (L mol^{-1} cm^{-1})
CT DNA	6600
Poly d(A-T)	6000
Poly d(A).d(T)	6000
Poly d(G-C)	7400
(TTAGGG)$_4$	61300
(TTAGGGT)$_4$	69800
(TTGGGGT)$_4$	65900

2.3 Sample preparation for ESI-MS studies

For analysis, solutions containing one quadruplex already dissolved in 10 mM K_2HPO_4 at pH 7.0 containing 100 mM KCl and one flavonoid with a 1:4 M ratio (20 and 80 μM, respectively) were prepared in 50 mM ammonium acetate and allowed to equilibrate at room temperature. Methanol (1:3, vol/vol) was added just before the injection of the sample in MS.

2.4 Sample preparation for NMR studies

Solution of deoxyoligonucleotide, d-(TTAGGGT)$_4$ (2.41 mM single concentration) was prepared by dissolving a known quantity of sample in 90% water and 10% D$_2$O phosphate buffer (20 mM) of pH = 7.0 having 100 mM K$^+$ salt and their concentrations were determined by absorbance measurements at 260 nm using the extinction coefficient (ε) value, 69800 M^{-1}cm^{-1} for d-(TTAGGGT)$_4$. Ethylene diamine tetra acetic acid (EDTA), 0.1 mM, was added to suppress paramagnetic impurity, which may cause line broadening during NMR measurements. Typically 1μl of 0.1 M solution of 3-(Trimethylsilyl) propionic-2, 2, 3, 3-d$_4$ acid sodium salt (TSP) was added to the samples as an internal reference.

(i) d-(TTAGGGT)$_4$ and quercetin complex: A complex of **d-(TTAGGGT)$_4$** and quercetin was prepared by titration. Total 43.34 μl of 200 mM quercetin was added in steps to 0.60 ml of 2.41 mM d-(TTAGGGT)$_4$ sample during titration in order to make 2:1 complex of quercetin: d-(TTAGGGT)$_4$. The concentration of d-(TTAGGGT)$_4$ (N$_1$) in total volume of 0.64 ml is determined as follows:

$$N_1V_1 = N_2V_2$$

$$N_1 \times 0.6415 = 2.41 \times 0.6000$$

$$N_1 = 2.40 \text{ mM}$$

The concentration of quercetin in this solution is determined as follows:

$$N_3V_3 = N_4V_4$$

$$N_3 \times 0.6415 = 200 \text{ mM} \times 0.00154$$

$$N_3 = 0.48 \text{ mM}$$

The concentration of quercetin (D), d-(TTAGGGT)$_4$ (N) and drug/ nucleotide (D/N) ratio are shown in Table 2.2.

Table 2.2: Various concentration ratios (D/N) for the complex formed between quercetin and d-(TTAGGGT)$_4$

Nucleotide Concentration (mM) = N	Drug Concentration (mM) = D	D/N
2.41	0.00	-
2.40	0.48	0.20
2.39	1.20	0.50
2.36	1.79	0.75
2.34	2.36	1.00
2.29	4.09	1.75
2.24	4.58	2.00

2.5 Methodology

2.5.1 Competition Dialysis Assay

Competition dialysis assay is a new, powerful and effective tool for the quantitative determination of structural and sequence selectivity of binding of small molecules to nucleic acids. The experiment was carried out following the procedure of Ren and Chaires (Ren and Chaires, 1999; Chaires, 2005). For each competition dialysis assay, 200 mL of the dialysate solution containing 1 μM flavonoid was placed into a beaker. A volume of 0.5 mL (at 75 μM monomeric unit) of each of the DNA samples was pipeted into a separate dialyzer unit. All dialyzer units were having different DNA and then placed in the beaker containing the dialysate solution. The beaker was covered with Parafilm and wrapped in foil, and its contents were allowed to equilibrate with continuous stirring for 24 h at room temperature (20-22 °C). At the end of the equilibration period, DNA samples were carefully removed to microfuge tubes, and were taken to a final concentration of 1% (w/v) sodium dodecyl sulfate (SDS) by the addition of appropriate volumes of a 10% (w/v) stock solution. The total concentration of drug (C_t) within each dialysis unit was then determined spectrophotometrically using wavelengths and extinction coefficients appropriate for each

ligand as mentioned above. An appropriate correction for the slight dilution of the sample resulting from the addition of the stock SDS solution was made. The free ligand concentration (C_f) was determined spectrophotometrically using an aliquot of the dialysate solution, although its concentration usually did not vary appreciably from the initial concentration of 1 μM. The amount of bound alkaloid was then determined by difference ($C_b = C_t - C_f$). Data were plotted as a bar graph using Origin 7.0 software (MicroCal, Inc.; Northampton, MA, USA). These data were then used to calculate the apparent binding constant (K_{app}) using the relation (Chaires, 2005).

$$K_{app} = C_b / (C_f)(S_{total} - C_b)$$

where $S_{total} = 75$ μM polynucleotide concentration (expressed in terms of nucleotide phosphate).

2.5.2 Absorption Spectroscopy

The measurement most frequently performed on biopolymers is the absorption of visible or ultraviolet light. This technique is used for purposes ranging from simple concentration determinations to resolution of complex structural questions. Any molecule absorbs light in some wavelength range. However for any selected wavelength certain types of chemical groups usually dominate the observed spectrum. These groups are called chromophores. Absorption spectrum depends on the conformation of the biopolymers. Generally the conformation of the polymer mainly determines deviations of the polymer absorption spectrum from that of a simple monomer. The absorption spectrum of biomolecules is also sensitive for local environmental effects. These can include the local pH, dielectric constants, and rigidity of the medium and the presence of nearby groups capable of specific chemical interactions. This sensitivity can be manifested as changes in intensity, band shape, or wavelength of the absorption.

2.5.2.1 Theory of Absorbance

The electronic energy levels of simple molecules are widely separated and usually only the absorption of a higher energy photon, that is one of very short wavelength can excite a molecule from one level to another. In complex molecules the energy levels are more closely spaced and photons of near ultraviolet and visible light can effect the transmission. These substances, therefore, will absorb light in some areas of the near Ultraviolet and visible region. The vibrational energy states of the various parts of a molecule are much closer together than the electronic energy levels and thus photons of lower energy (longer wavelength) are sufficient to bring about vibrational changes. In fact, each of the many vibrational levels associated with the electronic states also has a large number of rotational levels associated with it. Thus, a transition can consist of a large electronic component, a smaller vibrational element and even smaller rotational changes.

Although absorption process is extremely rapid (10^{-15} s), the sequence of events that return the excited molecule to its ground state is considerably slow. Return to the ground state via fluorescence is considerably slower (10^{-8} sec).
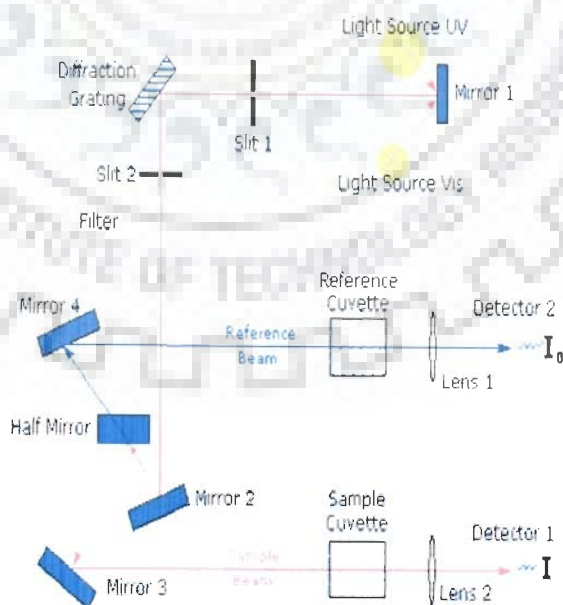
Fig. 2.1: Schematic diagram of absorbance spectroscopic experiments.

61

2.5.2.2 The Extinction Coefficient

If we consider a sample molecule in a layer perpendicular to the direction of light propagation and sufficient thin (dl) so that the light intensity within this layer is essentially constant. Then the fraction of light absorbed $(-dI/I)$ should be simply proportional to the number of absorbing molecules. The resulting equation is:

$$-dI/I = \varepsilon.c.dl$$

Where ε is a proportionality constant called molar extinction coefficient. It is independent of concentration for a set of non-interacting molecules and it contains the wavelength or frequency dependence of the absorption spectrum. If we integrate this equation over the entire sample, we obtain:

$$\ln (I_0/I) = \varepsilon \, cl$$

$$Or, \, A = \varepsilon \, cl$$

The quantity A is called absorbance or optical density.

The value of ε_{max} for typical single chromophore varies over a wide range from as little as $1 \, M^{-1} \, cm^{-1}$ to more than $10^{-5} \, M^{-1} \, cm^{-1}$. The most accurate measurement of A usually is obtained in the range of 0.1 - 2. Smaller values mean that only a tiny fraction of the incident light is absorbed; larger values means only small fraction of the incident light reaches to detector.

2.5.3 Fluorescence

Light emission can reveal properties of biological molecules quite different from the properties revealed by light absorption. Fluorescence process takes place on a slower time scale, therefore, wide range of interactions and perturbations influence the spectrum.

The common nucleic acid base has almost undetectably weak fluorescence. This is very useful for many studies. If a fluorescent probe binds at some specific site or it covalently attaches to DNA, then a variety of structural information can be obtained. Usually the probe is chosen so that it can be excited by light that only the probe can absorb and not the macromolecule. In this case the macromolecule is invisible and all information relates to the probe molecule. Fluorescence is much more sensitive to the environment of the chromophore than is light absorption. Therefore fluorescence is a most effective technique for following the binding of ligands or conformational changes. Because it is a slower process (10^{-9} to 10^{-8} sec) than absorption, during this period of time, all kinds of process can occur, including protonation or deprotonation reaction, local conformational changes.

2.5.3.1 Theory of Fluorescence

With fluorescence a photon is first absorbed and excites the molecule to a higher energy state ($S_o \longrightarrow S_1$) (Fig.2.2), the molecule does not remain in this excited state for long. In most cases the energy is lost by collisions between molecules (so called non radiative transition or quenching) the molecule falls back to the ground state (S_o) by re-emitting energy (the radiative transition known as Fluorescence).
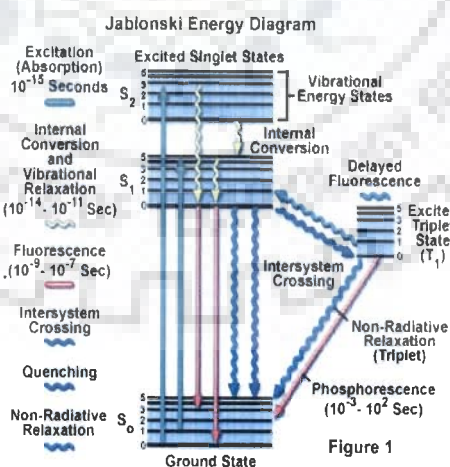
Fig.2.2: The process of fluorescence

63

As described above excitation of molecules does not involve electronic transitions but also vibrational and rotational changes. Fluorescence always occurs from the lowest vibrational level of S_1 to the lowest vibrational level of S_0. As we have seen absorption of energy involves the vibrational sub-levels, which are at a higher energy level (in S_1). In the excited state the molecule must first lose energy, to return to S_1, before fluorescence occurs. Energy is lost in going from V_3 to S_1 by molecular relaxation. The energy of emitted radiation during fluorescence is, therefore, smaller than originally absorbed less energy means longer wavelength, i.e., fluorescence emission occurs at longer wavelength than absorbance.

2.5.3.2 Quantitative fluorescence

The basic equation defining the relationship of fluorescence to concentration is:

$$F = \Phi . I_0 (1 - 10^{-\varepsilon CL})$$

Φ = Quantum efficiency

F = Total fluorescence intensity

I_0 = Intensity of exciting light

ε = Molar absorptivity (extinction coefficient)

C = Concentration

L = Path length of the cell

The basic fluorescence intensity-concentration equation indicates that there are three major factors other than concentration that affect the fluorescence intensity:

1. The Quantum efficiency Φ, the greater the value of Φ, the greater will be the fluorescence.

2. The intensity of exciting light I_0. Theoretically, a more intense source will yield a greater fluorescence. In actual practice a very intense-source can cause photochemical decomposition of the sample. Hence, one compromises on a source of moderate intensity.

3. The molar absorptivity of the compound ε. In order to emit radiation, a molecule must first absorb radiation. Hence, the higher the molar absorptivity, the better will be the fluorescence intensity of the compound. It is for this reason that saturated non aromatic compounds are non-fluorescent

For very dilute solutions the equation reduces to one, comparable to Beer's law in spectrophotometry.

$$F = K. \, \Phi.I_Q.\varepsilon.C.L$$

Thus a plot of fluorescence versus concentration should be linear at low concentrations and read a maximum at higher concentrations. The linearity of fluorescence as a function of concentration holds over a very wide range of concentration. Measurements from 10 μg/ml are possible and linearity extends up to 100 μg/ml or higher.

2.5.4 Life Time Measurement using Fluorescence Spectroscopy

Model FluoroLog®-TCSPC, make HORIBA Jobin Yvon Spex® was used for the life time measurement study. This is an ultra compact fluorescence lifetime spectrometer based on time correlated single photon counting (TCSPC) and ready to perform time-domain lifetime spectroscopy building up a histogram of the sample's fluorescence decay. This instrument has sub-ns pulsed LED. For our study, we used fixed-wavelength Nano LED of 470 nm. Standard optical pulse durations are <1.5 ns for LEDs. Resolution 0.2 nm, accuracy ± 0.5 nm, speed 150 nm/s, range 0-1300 nm, TAC range given is 50 nm, excitation wavelength is 350 nm for the experiment. 2:1 complex of flavonoids-G-quadruplex sequences was used for this study.

2.5.5 Circular Dichroism (CD) Spectroscopy

The CD spectra were obtained using a Applied Photophysics (Model Chirascan) spectropolarimeter equipped programmable Peltier junction temperature controlled cell holder. CD experiments were carried out on DNA samples at a concentration of 20 μM and

various flavonoids sample of 10 µM. The buffer used for the CD experiments was same as used in UV-Visible spectrophotometric experiments. The CD measurements used a 0.2 cm-path cell and were carried out at 298 K. The CD spectra were averaged over three scans and data was obtained with a 1 nm slit width from 350 to 200 nm at 0.1 nm intervals.

2.5.6 Electro Spray Ionization- Mass Spectrometer (ESI-MS)

Electro spray ionization mass spectrometry (ESI-MS) was utilized to investigate the binding stoichiometry of flavonoids to G-quadruplex. Mass spectra were performed on a Agilent esquire in the negative ion mode. The experimental conditions were optimized to avoid denaturation of the quadruplex species: the heated capillary temperature of the electrospray source was set to 100°C, and a voltage on the heated capillary of -11 V. Structures of four main flavonoids, including luteolin, quercetin, rutin and genistein, respectively. Full scan MS spectra were recorded in a m/z range from 800 to 2000, and 50 scans were summed for each spectrum. The relative intensities of the free and bound DNA in the mass spectra are assumed to be proportional to the relative abundances of these species in solution.

2.5.7 NMR Spectroscopy

Nuclear Magnetic Resonance (NMR) spectroscopy is a powerful spectroscopic technique that provides information about the structural and chemical properties of synthetic, biomolecules (Wuthrich, 1986), liquid crystals (Khetrapal, 1975), etc. NMR exploits the behaviour of certain atoms when they are placed in a very strong magnetic field and many of the spectral parameters can be interpreted directly in terms of conformation or dynamics. As ^1H, ^{13}C, ^{15}N and ^{31}P are all present in nucleic acids, there are large number of signals present that can report on structure, dynamics and the effect of ligand binding.

2.5.7.1 The Phenomenon of NMR

Subatomic particles (electrons, protons and neutrons) spin on their axis. A nucleus (of spin 1/2) when placed in a static magnetic field behaves like a small magnet. This nucleus is in the lower energy level (i.e. its magnetic moment does not oppose the applied field). In the absence of an external magnetic field, these orientations are of equal energy. Each level is given a magnetic quantum number, m, characterizing Z component of spin, I. On interaction with magnetic field, nuclei with spin I >1/2 distributes themselves among 2I + 1 energy level with the separation by:

$$\Delta E = h \, \gamma \, B_0$$

The overall spin, I, is important. A nucleus with spin 1/2 will have 2 possible orientations (Fig. 2.3a). These spins are capable of interacting with a beam of electromagnetic radiation. These energy levels correspond to the spins aligned along and against the applied magnetic field, B_0. The spin oriented to oppose B_0 has higher energy. These spin do not align perfectly along B_0 and this give rise to a permanent torque. The nucleus also has the property of angular momentum because of its spin and as a result the nuclei precess (Fig. 2.3b), with frequency of precession given by:

$$\omega_0 = \gamma B_0$$

where, γ is proportionality constant, ω_0 is the Larmor frequency in radians/second and B_0 is the magnitude of the applied magnetic field. When the frequency of the beam is same as that of precessing spin then absorption of energy takes place, which causes the nuclei to flip from a lower energy state to a higher energy state by a process termed

67

No field   Applied magnetic field

$m = -\frac{1}{2}$

$m = +\frac{1}{2}$

(a)

Applied magnetic field

Precessional orbit

Spinning nucleus

(b)

(c)
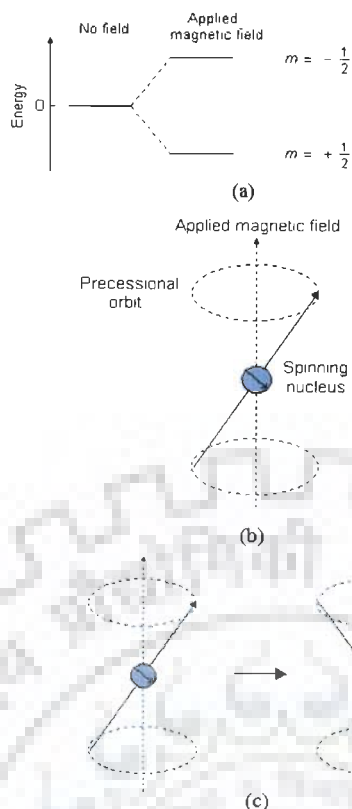
Fig. 2.3: (a) Energy levels for a nucleus with spin quantum number ½ (b) Precessional motion by the nucleus spinning on its axis in presence of the external magnetic field (c) Flipping of the magnetic moment on absorption of the radiations

resonance (Fig 2.3c). In an NMR sample there are many molecules, each with its spin precessing about B_0 at same frequency and result in a net magnetization of M_z oriented along the Z-axis. On application of a rotating radio frequency field with frequency at or near $\omega_0 = \gamma B_0$, the spins resonate giving rise to net M_{xy} component which is phase coherent. The following are the spectral parameters in NMR:

2.5.7.2 Chemical Shift

The magnetic field at the nucleus is not equal to the applied magnetic field, B_0; electrons around the nucleus shield it from the applied field. The difference between the applied magnetic field and the field at the nucleus is termed the nuclear shielding. The induced field is directly proportional to B_0.

This is represented by the equation:

68

$$B_{eff} = B_0 (1-\sigma)$$

where, σ is the shielding constant which depends on the nature of electrons around the nucleus. Chemical shift is a function of the nucleus and its environment. It is measured relative to a reference compound. For ^1H NMR, the reference is usually tetramethylsilane, $Si(CH_3)_4$. Chemical shift is expressed in parts per million (ppm) is given as:

$$\delta = 10^6 \ x \ \left(\frac{\delta_{ref} - \delta_{obs}}{\delta_{ref}} \right)$$

where, δ_{ref} is the position observed for a reference compound and δ_{obs} is the position of the signal of interest. There are useful general conclusions that can be drawn from specific chemical shift value, or changes due to the binding of the ligand.

2.5.7.3 Spin-Spin Coupling Constant (J)

Nuclei experiencing the same chemical environment or chemical shift are called equivalent. Those nuclei experiencing different environment or having different shifts are nonequivalent. Nuclei, which are close to one another, exert an influence on each effective magnetic field. This effect shows up in the NMR spectrum when the nuclei are nonequivalent. If the coupling between non-equivalent nuclei is less other's than or equal to three bond lengths, this effect is observable. This effect is called spin-spin coupling or J coupling and is expressed in Hertz (Hz). This coupling causes splitting of lines. The appearance of multiplet patterns depends on relative magnitude of δ and J for coupled nuclei. Vicinal couplings (^3J) display a characteristic dependence upon the involved dihedral angle (Fig. 2.4a) according to the relation dihedral couplings;

$$^3J = 8.5 \cos^2\theta - 2.8$$

$$^3J = 9.5 \cos^2\theta - 2.8$$
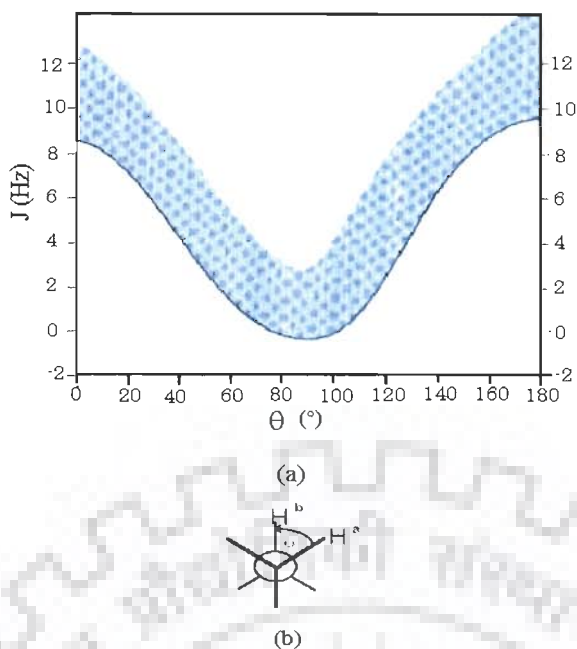
Fig. 2.4: (a) Karplus curve showing relationship between J couplings and dihedral angle (b) definition of the dihedral angle

This relationship is known as the Karplus relation. Fig. 2.4a and 2.4b shows the definition of dihedral angle and relationship between J couplings and dihedrals.

2.5.7.4 Relaxation Process

The magnetization does not precess infinitely in the transverse plane but turns back to the equilibrium state. This process is called relaxation. Two different time-constants describe this behaviour. The importance of these phenomena is in the Nuclear Overhauser Effect (NOE), which can be used to probe internuclear distances in a molecule. There are two major relaxation processes namely, spin-lattice (longitudinal) relaxation (T_1) and spin-spin (transverse) relaxation (T_2). The relaxation time T_1 represents the "lifetime" of the first order rate process that returns the magnetization to the Boltzman equilibrium along the +Z axis. The components of the lattice field can interact with nuclei in the higher energy state, and cause them to lose energy (returning to the lower state). The energy that a nucleus loses increases the amount of vibration and rotation within the lattice. The relaxation time,

T_1 depends on the motion of the molecule. As mobility increases, the vibrational and rotational frequencies increase, making it more likely for a component of the lattice field to be able to interact with excited nuclei. T_1 spin-lattice relaxation rate is then measured by plotting magnetization M as a function of τ:

$$M (\tau) = Mo \, (1 - 2\exp^{-(\tau/T1)})$$

T_2 represents the lifetime of the signal in the transverse plane (XY plane) and it is this relaxation time that is responsible for the line width. In solution NMR, very often T_2 and T_1 are equal. The very fast spin-spin relaxation time provides very broad signals. The transverse relaxation constant T_2 is related to the linewidth of the signals. The width of the signal at half height is given by:

$$(\Delta\omega)_{1/2} = 1 \, / \, \pi \, T_2$$

Fast decay leads to broad signals, slow decay to sharper lines. The transverse relaxation constant T_2 of spin $I=1/2$ nuclei is mainly governed by the homogeneity of the magnetic field and the strength of the dipolar interaction with other $I=1/2$ nuclei depending on the number and the distance of neighbouring nuclei and the overall tumbling time of the molecule, which is related to its size. Transverse relaxation (T_2) is faster than longitudinal relaxation. T_2 spin-spin relaxation rate is measured by plotting M as a function of τ:

$$M(\tau) = Mo^{(-\exp(\tau/T2))}$$

2.6 Two-dimensional (2D) NMR techniques

In one-dimensional pulsed Fourier transform NMR the signal is recorded as a function of one time variable and then Fourier transformed to give a spectrum, which is a function of one frequency variable. In two-dimensional NMR the signal is recorded as a function of two time variables, t_1 and t_2, and the resulting data Fourier transformed twice to yield a spectrum, which is a function of two frequency variables. The two-dimensional

71

signal is recorded in the following way. First, t_1 is set to zero, the pulse sequence is executed and the resulting free induction decay recorded. Then the nuclear spins are allowed to return to equilibrium, t_1 is then set to $\Delta 1$, the sampling interval in t_1, the sequence is repeated and free induction decay is recorded and stored separately from the first. Again the spins are allowed to equilibrate, t_1 is set to $2\Delta 1$, the pulse sequence repeated and a free induction decay recorded and stored. The free induction decay can be processed by tools like topspin and NMRLAB (Gunther, 2000). The whole process is repeated again for $t_1 = 3\Delta 1$, $4\Delta 1$ and so on until sufficient data is recorded, typically 50 to 500 increments of t_1. Thus recording a two-dimensional data set involves repeating a pulse sequence for increasing values of t_1 and recording free induction decay as a function of t_2 for each value of t_1. The general scheme for two-dimensional spectroscopy is shown in Fig. 2.5.
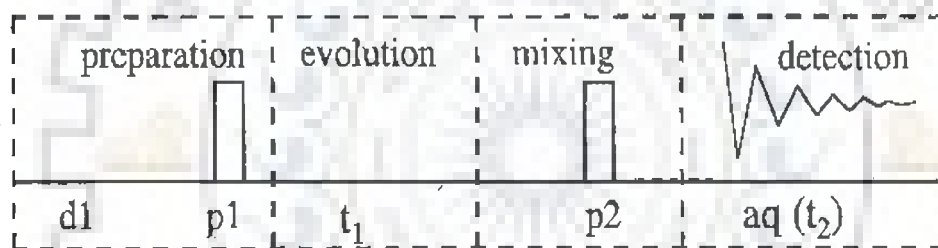
Fig. 2.5: Four different time segments of a 2D NMR experiment namely (i) preparation period (ii) evolution period (t_1) (iii) mixing period (τ_m) (iv) detection period (t_2)

Preparation time (d1): The sample is excited by one or more pulse. This consists of a delay time or a sequence of pulses separated by fixed time intervals saturation sequences. Thermal equilibrium is attained during this period.

Evolution Period (t1): The resulting magnetization is allowed to evolve for the first time period, t_1. The evolution period is the pulse sequence element that enables frequency labeling in the indirect dimension. Further, one or several radiofrequency pulses may be applied to create coherence.

Mixing time (τ_m): During this period coherence is transferred between spins. Mixing sequences utilize two mechanisms for magnetization transfer: scalar coupling or dipolar interaction (NOE). After the mixing period the signal is recorded as a function of the second time variable, t_2. This sequence of events is called a pulse sequence.

Detection Period (t2): The signal is recorded during the time t_2 at the end of the sequence, detection, often called direct evolution time; during this time the magnetization is labelled with the chemical shift of the second nucleus. The data is recorded at regularly spaced intervals in both t_1 and t_2.

Gradient enhanced NMR: It is a method for obtaining high resolution NMR spectra without the need for *phase cycling*. Gradient methodology is used extensively for two purposes, either rephasing (selection) or dephasing (elimination) of a particular magnetization transfer pathway. It includes the application of magnetic field gradient pulses to select specific coherences. By using actively shielded gradients, a gradient pulse is applied during the evolution period of the selected coherence to dephase the transverse magnetization and another gradient pulse refocuses the desired coherences remaining during the acquisition period.

2.6.1 Two – Dimensional Correlation Spectroscopy (2D-COSY)

The COSY experiment is used in determining those atoms which are connected through bonds. The basis of COSY experiment whose pulse sequence is shown in Fig. 2.6a is the classical Jeener sequence (Jeener, 1971). After the preparation period of 90° pulse constitutes brief mixing period whose effect is to mix single quantum coherence into a whole range of orders of coherence. However, only the single quantum coherence will give rise to any measurable signal during the detection period. The mixing process interchanges orders of coherence, mixes coherence among the transitions associated with a given spin and exchanges coherence between spins having a mutual scalar coupling. Thus a

magnetization, initially associated with the A spin of an A-X spin system, may be transferred to spin X through the scalar coupling, J_{ax}. Therefore the A magnetization in the X-Y plane will also depend upon the Larmor frequency ωx and the 2D COSY will show signals with frequency coordinates (ωA, ωX) and (ωX, ωA) as well as (ωA, ωA). The former are the characteristic cross peaks of COSY spectrum and the latter, the diagonal peaks, which corresponds to 1D spectrum. COSY experiment can be carried out with special phase cycling and data processing to change the 2D line shape into pure 2D absorption mode, allowing the use of phase-sensitive display. There are two different methods in use, the first requires the results of two complete COSY experiments with different phase cycling to be added (States et al, 1982) and the second known as TPPI (Time proportional phase incrementation) method uses a single experiment with phase cycling which changes with t_1 increment (Bodhenhausen et al, 1977; Keeler and Neuhaus, 1985; Marion and Wuthrich, 1983; Redfield et al, 1975). The phase sensitive COSY spectra have cross peaks in antiphase. The antiphase multiplet structure of a cross peak only occurs in the active coupling giving rise to cross peak. Extra splitting present in multiplet but which do not give rise to cross peaks are called passive couplings and appear in phase. Thus, the advantage of phase sensitive COSY is that the phase relation between peaks can be used for accurate assignment and calculation of coupling constants.

2.6.2 Phase Sensitive COSY: Double Quantum Filtered COSY (DQF-COSY)

The experiment uses a pulse sequence 90_ϕ-t_1-90_φ-90_ζ-t_2 where ϕ, φ and ζ are the appropriate phase cycles (Piantini et al, 1982). In double quantum filter COSY experiment, (Fig. 2.6a) the resonance from a COSY experiment is passed through a double quantum filter, thereby removing methyl and other singlets from the final spectrum. The short delays, Δ, immediately before and after the final pulse, are of order of microseconds. Twice as many transients are needed in these experiments to achieve the same signal to noise ratio

than in conventional COSY. Another advantage of DQF COSY is that it converts the phase of COSY diagonal signals from dispersive antiphase to absorptive antiphase. These signals then do not interfere with the cross peaks. So, the cross peaks lying close to diagonal can be observed in double quantum filtered phase-sensitive COSY. Double filter COSY can be used to determine the coupling constants (Celda et al, 1989; Gochin et al, 1990).

2.6.3 Total Correlated Spectroscopy (TOCSY)

During this pulse sequence, after the evolution period t_1, the magnetization is spin-locked. During this mixing time, the magnetization exchange through scalar coupling. During this spin-lock period, the magnetization behaves as a strongly coupled spin system and evolves under the influence of a "collective spin-mode". In that collective mode, coherence transfer is possible between all coupled nuclei in a spin system, (even if they are not directly coupled). This essentially gives the same information as that of COSY, except that COSY gives information only on the directly coupled spins, whereas TOCSY gives the complete spin-coupling network

COSY

Phase sensitive DQF COSY

75
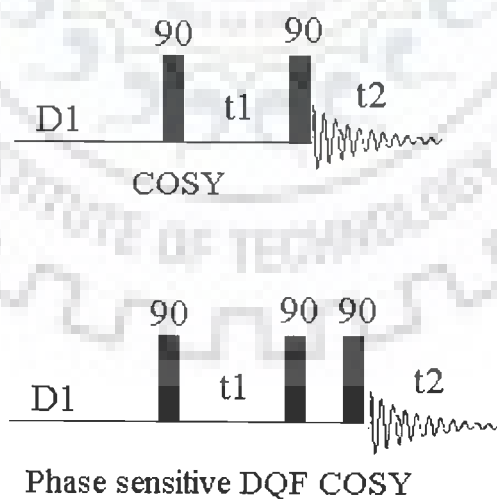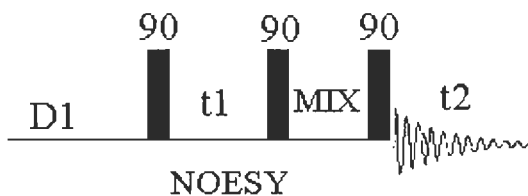
Fig. 2.6a: Pulse schemes of various 2D NMR techniques

2.6.4 Nuclear Overhauser Effect Spectroscopy (NOESY)

NOESY is one of the most useful techniques as it allows correlating nuclei through space (distance smaller than 5Å). By measuring cross peak intensity, distance information can be extracted. The pulse sequence starts as usual with a 90° pulse followed by an evolution time t_1 (Fig. 2.6a). This delay is varied systematically as usual to provide chemical shift information in the F1 domain. Then 90° pulse transmits some of the magnetization to the Z-axis and during the following mixing period, the non-equilibria Z component will exchange magnetization through relaxation (dipole-dipole mechanism). This exchange of magnetization is known as Nuclear Overhauser Effect (NOE). After some time (shorter than the relaxation time T1), the transverse magnetization is restored and detected. If relaxation exchange (or chemical exchange) has taken place during the mixing time, cross peaks will be observed in the spectra. The phase cycling ensures proper detection of NOESY signal.

2.6.5 Hetero – Nuclear Multiple Bonded Correlation Spectroscopy (HMBC)

Long-range hetero-nuclear correlation can yield signals for these nuclei while suppressing one-bond correlations. The most common application of this technique is for ^1H-^{13}C and ^1H-^{31}P. Δ_1 is set to 1/ (2J one-bond) and Δ_2 to 1/ (2J long- range). The phase is strongly dependent on the long range and hetero-nuclear proton coupling constant so each multiplet peak pattern has a different phase with an extreme first order component. The correlation experiment does not contain a diagonal. Each proton signal may be correlated

76

with one or more carbon signals. Those signals in the 1D spectrum that do not correlate with carbons do not appear in the 2D spectrum (Fig. 2.6 b).

Nucleus bound to H	Ratio of 1st and 3rd gradient	J (one-bond)
^{13}C	3.98	145 Hz
^{31}P	12.0	8 Hz
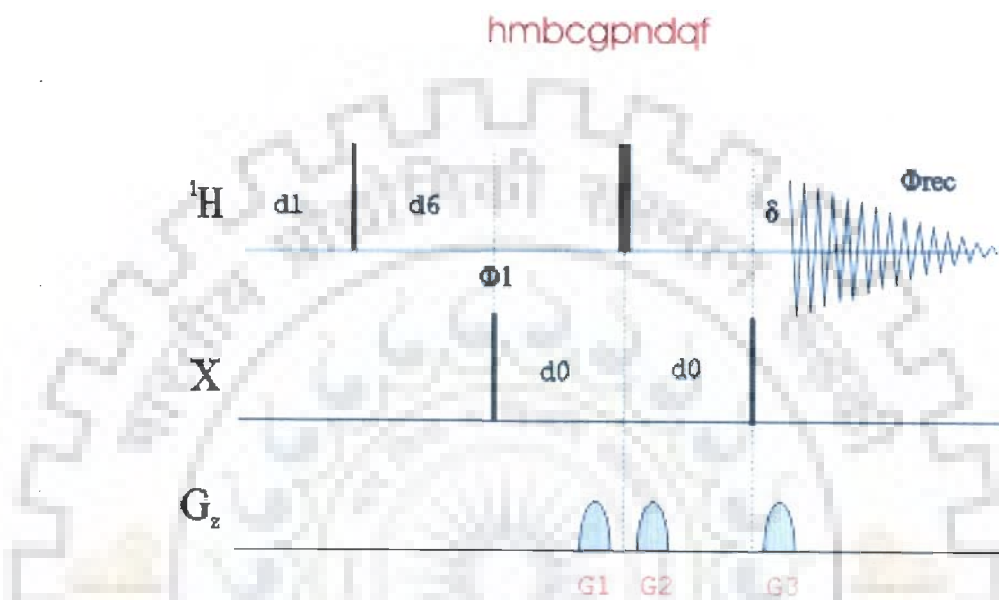
Fig. 2.6b: Pulse sequence for HMBC

2.6.6 Diffusion Ordered Spectroscopy (DOSY)

The DOSY experiment is the measure of diffusion coefficients by NMR. In DOSY spectra, chemical shift is detected along the F2 axis and diffusion coefficient is along the F1 axis. The method developed by Stejskal and Tanner which relies on two gradient pulses surrounding the 180° pulse in the spin echo was used. The first gradient dephases, the transverse magnetization in a spatially dependent manner along the z-axis and the second gradient then rephases the magnetization. The relation between translational self-diffusion and the measurable NMR parameters (Stejskal and Tanner, 1965) is:

$$A/A_0 = -\exp\left[D_t \gamma_H^2 \delta^2 G_z^{\,2}(\Delta - \delta/3)\right]$$

77

where A is the measured peak intensity (or volume), A_0 is the maximum peak intensity, D_t is the translational diffusion constant (in cm^2/s), γ_H is the gyromagnetic ratio of a proton (2.675197×10^4 G^{-1} s^{-1}), δ is the duration of the gradient, Δ is the time between gradients and G_z is the strength of the gradient (in G/cm). Data can be plotted as $-\ln(A/A_0)$ versus $\gamma_H^2 \delta^2 G_z^2 (\Delta - \delta/3)$. The slope of the line gives the value of D_t. The pulse program used is Pulsed gradient spin echo (stimulated echo sequence incorporating bipolar gradients) sequence modified with binomial water suppression (Fig: 2.6c). The gradient strengths were incremented as a square dependence in the range from 1 to 32 G cm^{-1}. It has been developed in order to facilitate the complex mixture analysis without physical separation. This experiment will monitor any modification of the solvent or of the solutes, and molecular events such as molecular interactions or associations.
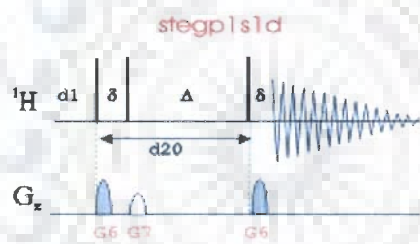
Fig. 2.6c: Pulse sequence for DOSY

2.7 Experimental parameters

All NMR experiments were recorded on Bruker Avance 500 MHz FT-NMR spectrometer at Central NMR Facility located at Indian Institute of Technology Roorkee.

2.7.1 Study of quercetin and human telomeric G-quadruplex DNA sequences d-(TTAGGGT)₄

^{31}P and ^{1}H NMR experiments were recorded for **d-(TTAGGG)₄** and its complexes with quercetin on successive addition of drug (Table 2.2) at 298 K in $H_2O + D_2O$ solvent. The parameters were as follows:

1D ^{1}H NMR experiments were acquired with 64 K data points; number of scans = 64–128 and digital resolution = 0.15–0.3 Hz / point. Receiver gain was optimized in each instance to obtain the best signal to noise ratio.

1D ^{31}P NMR experiments were acquired with 64 K data points, number of scan = 128 and digital resolution 0.12 Hz / point.

^{1}H – ^{31}P HMBC experiment were recorded with 2048 data points along t_2 dimension; 400 induction decays in t_1 dimension; no. of scans = 64 digital resolution 3.09 Hz / point in t_1 dimension and relaxation delay of 2.0 secs. τ value was optimized for 8 Hz coupling constants.

^{1}H – ^{1}H 2D NOESY *experiment* were recorded with variable mixing times (τ_m) 200, 300 and 350ms at 298 K. Number of data points = 2048 data points along t_2 dimension; 256 induction decays in t_1 dimension; no. of scans = 48-64 digital resolution 1.495 Hz / point in t_1 dimension and relaxation delay of 2.0 secs. Mixing time (τ_m) = 100, 200 and 300 ms were used for D / N= 0.5, 1.0, 1.5 and 2.0 complex.

^{31}P– ^{31}P 2D NOESY experiments for D / N = 0.2, 0.5, 1.0 and 2.0 at 298 K/ 318 K were recorded with mixing time of 150 / 200 ms; 4096 data points along t_2 dimension; 300 free–induction decays in t_1 dimension; no. of scans = 128; digital resolution 1.495 Hz / point in t_1 dimension and relaxation delay of 2.0 secs.

DOSY experiments were recorded with diffusion time (Δ) of 100 ms and the duration of the magnetic field gradients (δ) 6 ms, respectively in D_2O. Other parameters include a sweep width of 6000 Hz, 64 K data points, 16 transients, digital resolution 0.30 Hz / point and relaxation delay of 10 s.

2.7 Determination of three-dimensional structure

2.7.1 Resonance Assignments in Nucleic Acids

Resonance assignment is the first endeavour in the structural determination of DNA. From the NMR point of view, the protons can be grouped into four categories; (i) exchangeable NH and NH_2 protons of the bases and non-exchangeable base protons between 7-15 ppm (ii) non-exchangeable sugar protons between 2-6.5 ppm (iii) methyl protons of thymine between 0.5-2 ppm. In order to observe NH and NH_2, protons, experiments have been carried out in water whereas the other protons were observed in D_2O solution. The strategy for resonance assignment consists of two steps. In the first stage, the J correlated spectra are used to identify network of coupled spins. In the second stage, the spin systems so identified are assigned to particular nucleotides along the sequence of the molecule by making use of the NOESY spectrum as described below. The sugar protons H1', H2', H2", H3', H4', H5' and H5" form a complex J correlated network (Fig. 2.7). The various cross peaks observed in the 2D J-correlated between these protons was used in identification of spin system within individual nucleotide units. The H1' proton shows a cross peak with H2', H2" sugar protons. The H2' and H2" protons are further coupled to H3' proton. We have used phase sensitive DQF-COSY spectra to identify the various J-coupled cross peaks. In the second phase sequential assignment is carried out using NOESY spectrum. Short internucleotide distances between adjacent nucleotide units are used as shown in Figure 2.7. In right handed DNA with sugars in C3'-endo/C2'-endo/O1'-endo pucker and glycosidic angle in anti domain, a convenient strategy for sequential assignment is

$(H6/H8)_n \longrightarrow (H2', H2'')_{n-1}$

$(H6/H8)_n \longrightarrow (H1')_{n-1}$

$(H6/H8)_n \longrightarrow (H6/H8)_{n-1}$
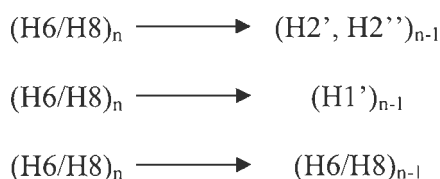
where, n stands for nth residue in 5'-3' oligonucleotide sequence. In case of Z-DNA, where the repeating unit is a dinucleotide, the internucleotide pathway is Base (2n–1) …. H5' (2n–1) …. Base (2n) …. H1' (2n) …. H2' (2n) and H2" (2n) …. Base (2n+1).
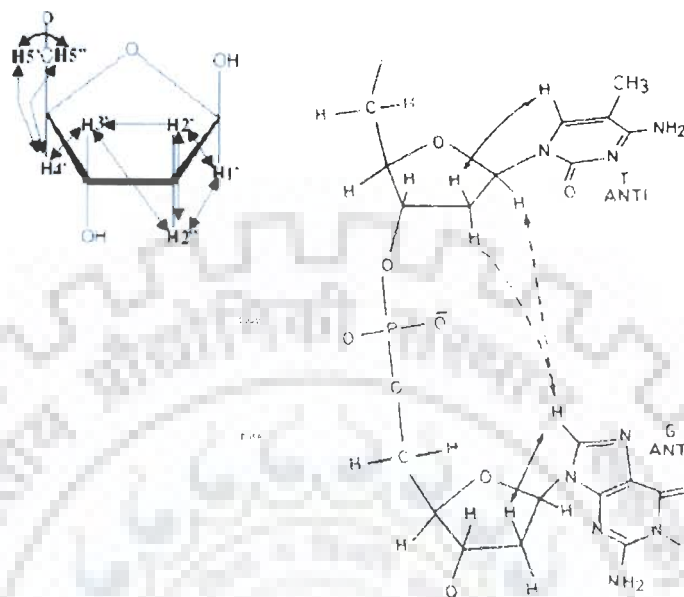
Fig. 2.7: Schematic representation of sugar J connectivities and short interproton distances between adjacent nucleotides units in right handed DNA.

2.7.2 Pseudorotation

Because of the r^{-6} dependence of the pre-steady state NOE, the relative magnitude of the NOEs provide a sensitive probe which can be used to obtain a qualitative view of the solution structures of short oligonucleotides. The glycosidic and sugar pucker conformations can be assessed qualitatively on the basis of the relative magnitudes of the intranucleotide sugar-base NOEs. The flexible five-membered sugar ring plays a pivotal role in nucleic acid structure and dynamic behaviour. In B-DNA family sugar responds to its surroundings (e.g. base stacking pattern) by an appropriate adaptation of its geometry. X-ray studies have now shown that P values usually occur in two distinct ranges. In a conformational wheel (Fig. 1.5 of Chapter 1) one range of form occupies the "Northern" half of the circle (N-type, P_N $0° \pm 90°$); the second range occupies the "Southern"

hemisphere (S-type, P_S 180 ± 90°). To a good approximation (0.4-0.7°) the torsion angles can be reproduced by a two-parameter pseudorotation equation:

$$\nu_j = \phi_m \cos [P + 0.8\pi (j-2)]$$

for j equals 0-4 and ϕ_m is amplitude of pucker. In crystal structures nucleotides usually a single pure N- or S-type conformer is found, but not necessarily the one that is predominant in aqueous solution. In some cases both N and S forms reside side by side in the same unit cell. Statistical analyses of X-ray data make it clear that details of sugar geometry of monomers are influenced by anisotropic crystal packing forces. The situation appears to be different in the helical oligomers, where stacking forces may play a more predominant role. NMR investigations in solution have demonstrated that N (C3'-endo) and S (C2'-endo) type conformations are in rapid equilibrium. If the interconversion rate between conformers is sufficiently rapid then observed couplings represent weighted average of couplings in individual conformers. Generally, in deoxyribose sugar, a trend to a larger proportions of C2'-endo pucker sugar is observed. A phase sensitive DQF-COSY spectrum allows J-coupling patterns to be delineated from the well-resolved cross peaks. In general, the relation between ^3J and φ takes the form of the semi empirical Karplus equation:

$$^3J = A \cos^2 (\varphi) + B \cos (\varphi) + C$$

The constants A, B and C have to be determined from ^3J values measured for compounds for which the value of φ, in solution, is known. There are five ^3J values in deoxyribose sugar, H1'-H2', H1'-H2", H2'-H3', H2"-H3' and H3'-H4', which are related to the relevant H-C-C-H dihedral angle, φ, according to the relation:

$$J = 10.2 \cos^2\varphi - 0.8 \cos \varphi$$

The above dihedral angles are inter-dependent and their values can be calculated in terms of the two pesudorotation parameters, P and φ_m, where φ_m is a constant for deoxyribose and thus various geometries can be expressed in terms of P. Fig. 2.8 (Hosur et

al, 1986) shows the plots of five coupling constants in a deoxyribose ring as a function of P, ($T_m = 38°$). It is clear from the curves that the value of coupling constants ^3J (H1'-H2") and ^3J (H2'-H3') vary within a narrow range of 6-10 Hz and are comparatively insensitive to the sugar geometry. On the other hand, values of ^3J (H2"-H3'), ^3J (H3'-H4') and ^3J (H1'-H2') coupling constants vary in the range 0-10 Hz and can be utilized with greater advantage in fixing the domains of sugar geometry. ^2J (H2'-H2") is a geminal coupling which does not show significant conformational dependent variation. ^3J (H1'-H2'), ^3J (H1'-H2"), ^3J (H2'-H3'), ^3J (H2"-H3') and ^3J (H3'-H4') are vicinal coupling which show a strong dependence on the conformation of the deoxyribose ring (Hosur et al, 1986). The approach used for determination of sugar geometry is based on interpretation of intra-sugar proton-proton distances.

2.7.3 Conformation about the Glycosidic Bond

A large body of crystallographic data for nucleotides clearly establishes that the torsional angle, χ_{CN}, defining the orientation of base ring falls into two relatively narrow ranges designated as syn and anti conformation (Sundaralignam, 1969).

$$\chi \begin{cases} \text{O4'-C1'-N9-C4 (Purines)} \\ \text{O4'-C1'-N1-C2 (Pyrimidines)} \end{cases}$$

The relative magnitudes of the intranucleotide and internucleotide (H8/H6)-H1' and (H8/H6)-(H2', H2") cross peaks in NOESY spectra at different mixing times can be used to establish the domains of glycosidic dihedral angles of individual nucleotide unit (Hosur et al, 1985; Roche et al, 1994). Below the spin diffusion limit, the intensity patterns of the cross peak look similar at all mixing times although the absolute intensity may vary with the mixing time. The expected intensity patterns for the above mentioned cross peaks for different glycosidic dihedral angles are given below:

1. For the syn conformation, a strong NOE between base H8/H6 and H1' protons should be observed. At the same time, the NOEs from base to H2' and H2" protons will be relatively weak and will have different intensities.
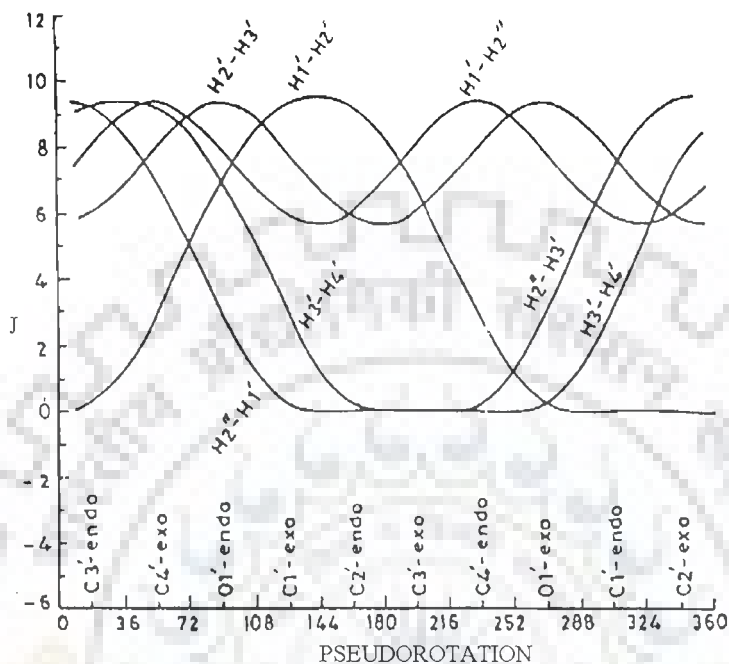
Fig. 2.8: Variation of the vicinal coupling constants in the deoxyribose ring as a function of the ring geometry.

2. In the anti conformation, the NOE from base H8/H6 to H2' is stronger than the NOE from base H8/H6 to H2". Also, for right handed structures the H2" proton shows a stronger NOE to the base proton of the next nucleotide.

3. In the high anti conformation, the (H8/H6)-H2' and (H8/H6)-H2" NOEs will have similar intensities for C2'-endo geometry.

The (H8/H6)-H1' distance depends only on χ while, other distances depend on both P and χ. Iso-distance contours have been calculated by Wuthrich (Wuthrich, 1986) in (P, χ) space for H8/H6-H2', H2", H3', H4' and H5' distances.

2.8 Estimation of interproton distances

If one resonance A is irradiated, an increase (positive NOE) or decrease (negative NOE) of signal intensity of other resonances such as resonance C is observed when spin C is close in space to spin A. This phenomenon is called Nuclear Overhauser Effect or NOE. The NOE effect is the method for elucidation of 3D structural features and stereochemistry using NMR together with information from scalar spin-spin couplings. The most important quantity derived from NOE cross peaks is the cross-relaxation rate between protons i and j. The cross relaxation rate σ_{ij} between two proton spins i and j is related to the distance between protons i and j in the following way:

$$\sigma_{ij} = <d_{ij}^{-6}> f(\tau_{ij}) \tag{1}$$

$<d_{ij}^{-6}>$ denotes an ensemble average of molecular structures interconverting in thermal equilibrium where $f(\tau_{ij})$ is a function of correlation time τ_{ij} for the vector connecting the two spins. This function accounts for the influence of motional averaging processes on the NOE. The cross relaxation rates can be measured from buildup rates of cross peaks in 2D NOE spectra at several mixing times. According to equation (1), the measured cross relaxation rates are a function of the ensemble average properties, which are dependent on the configurational space accessible to the molecular system at the temperature and time scale. If the interconversion between conformational equilibria in the oligonucleotide is fast on NMR time scale, NOEs from several equilibrium conformations will be observed simultaneously. This means that the derived set of distance constraints does not necessarily represent the average structure, and there may be no single conformation that is consistent with the data set. Initially the intensity of the cross peak in equation (1) varies linearly with mixing time, and therefore this condition is referred to as "linear regime", but on higher mixing times, this condition does not exist due to multispin relaxation. Interproton distances can be estimated by measuring the intensities of cross peaks in the "linear

regime". Two-spin approximation is used in NOE distance measurements in which only the rate of dipolar magnetization transfer between proximal spins i and j is monitored and all other spins are ignored. For two spin approximation, the intensity I_{ij} can be written as:

$$I_{ij} = \frac{\gamma^4 \hbar^2 \tau_c \tau_m}{10 r_{ij}^{-6}} \qquad \text{when } \omega \tau_c \gg 1$$

where γ is gyromagnetic ratio and $\hbar$, is Planck's constant divided by 2π. In order to determine the accurate value of τ_m for estimation of interproton distances, NOE build up curves should be obtained as a function of τ_m for several cross peaks, since spin diffusion can be different for different protons. Correlation times, τ_c, can be obtained from T2 and T1 measurements, according to the equation:

$$\tau_c = 2\omega^{-1}(3T_2/T_1)^{-1/2}$$

which holds good for $\omega \tau_c \gg 1$

If protons i, j, k, l have similar τ_c values and if r_{ij} is a known distance, then the unknown distance r_{kl} can be calculated by comparing the intensities I_{ij} and I_{kl} in a single spectrum. r_{ij}

$$\frac{I_{ij}}{I_{ij}} = \frac{r_{ij}^6}{r_{ij}^6}$$

The choice of known distance is important in the light of the mobility associated with different atoms in the nucleic acid. Gronenborn (Gronenborn and Clore, 1985) have expressed the opinion of using different yardsticks for NOEs involving different group of protons. The r(CH5-CH6) and r(H2'-H2") have different effective correlation times and can be used as reference depending on the cross peak being compared. The thymidine (H6-CH3) distance of 3.0 Å can be used as reference for all NOEs involving CH_3 protons, the sugar H2'-H2" protons and for the rest, cytidine H5-H6 distance of 2.45 Å can be used. Reid et al (Reid et al, 1989) examined H2'-H2" and H5-H6 cross relaxation at 15, 30, 60,

90 and 100 ms in dodecamer DNA duplexes. Results indicate that sugars and bases have the same correlation times, therefore all proton-proton distances in short DNA duplexes can be determined by scaling the initial NOE build up rate to the slope of cytosine H5-H6 cross peak, as H2'-H2" NOE cross peak are close to diagonal and are usually unresolved.

The characteristics of NMR data can be summarized as below:

1. NOEs cannot be translated into the precise distances. In practice this means that NOEs give only a number of approximate upper limits (e.g., 3 Å, 4 Å and 5 Å for strong, medium and weak NOEs). Sometimes it is not possible to make this division and only one single upper limit is used. For some proton pairs, corrections have to be applied to the upper limit value. This may arise due to stereo specific assignments (e.g., methyl group of thymine) or because of dynamic effects such as rotation of hydrogens in a methyl group and flipping of the aromatic rings.

2. Translating NOEs into reliable lower limit constraints is difficult, and it is preferable to take the sum of van der Waals radii as a lower limit to the distance. The absence of NOEs between two assigned protons may be translated into a minimum distance of proton pair.

3. NMR data contain contributions from different molecular conformations. Not all distance constraints need to be consistent with the single conformation.

4. NOE information is limited to short distance relative to the size of the drug-DNA complex. For some part of the molecule none or only a few NOEs are observed.

2.9 Restrained molecular dynamics and simulated annealing

When restrained energy minimization methods are used, inevitable local energy minima are encountered which can lead to inaccurate structures. To circumvent this, restrained molecular dynamics (rMD) are usually employed. This involves including NMR

restraints in one of the many molecular dynamics simulation programs. Molecular dynamics solve Newton's equation of motion,

$$F_i = m_i \, a_i \qquad (1)$$

Where F_i is the force, m_i is the mass and a_i is the acceleration of atom i. The force on atom i can be computed directly from the derivative of the potential energy V with respect to the coordinates r_i. The energy can be expressed in an explicitly differentiable form:

$$dV/dr_i = m_i \, d^2 r_i / dt^2 \qquad (2)$$

Therefore, with an adequate expression for the potential energy and the known masses, this differential equation can be solved for future positions in time t_i. In general, this can be solved only approximately, since V is usually a complex function of the coordinates of all (or many) of the atoms (i.e. $V = V \, (r_1, r_2, r_3, \ldots\ldots, r_N)$). The temperature can be calculated from the atomic velocities

$$3N/2 \, k_B \, T = \sum_{i=1}^{N} 1/2 \, m_i \, v_i^2 \qquad (3)$$

where, k_B is Boltzmann's constant, m_i and v_i are the mass and velocity of atom i, and N is the number of atoms (and 3N is the number of degrees of freedom). For a simulation at constant energy, the temperature fluctuates due to the interconversion of kinetic and potential energy. If the temperature is held constant then the atomic velocities can be adjusted accordingly. If the pressure is held constant, the volume is allowed to fluctuate by rescaling the interatomic distances.

The total potential energy V_{total} is usually defined as the sum of a number of terms:

$$V_{total} = V_{bond} + V_{angle} + V_{dihedr} + V_{vdw} + V_{coulomb} + V_{NMR} \qquad (4)$$

where, V_{bond}, V_{angle} and V_{dihedr} keep bond lengths, angles, and dihedral angles at their equilibrium values. The first five terms are empirical energy terms describing the

88

physical interactions between the atoms, whereas the last term is a means of including the NMR information, but does not correspond to any real physical force. They can be summarized as follows:

$$V_{bond} = \sum_{bond} \tfrac{1}{2}\, K_b(b-b_0)^2 \tag{5}$$

$$V_{angle} = \sum_{Angle} \tfrac{1}{2}\, K_\theta(\theta-\theta_0)^2 \tag{6}$$

$$V_{angle} = \sum_{dihedr} K_\Phi(1+\cos(n\phi-\delta)) \tag{7}$$

These are pseudo-harmonic potentials that constrain bond lengths (b), bond angles (θ), and the rotamer angles (ϕ, δ) for staggered and eclipsed conformations, and K is a constant. The van der Waals and electrostatic interactions are described by V_{vdw} and $V_{coulomb}$.

$$V_{vdw} = \sum_{Pairs\,(ij)} [C_{12}/\, r_{ij}^{12} - C_6/\, r_{ij}^6] \tag{8}$$

$$V_{coulomb} = \sum_{Pairs\,(ij)} qiqj\, /\, 4\pi\varepsilon_0\varepsilon_r\, r_{ij} \tag{9}$$

where equation (8) is the Lennard-Jones potential, containing repulsive and attractive terms (C is a constant), and equation (9) describes the coulombic interactions between two charged particles (i, j) with partial charges q that are at a distance r_{ij} apart in a dielectric medium described by $\varepsilon_0\varepsilon_r$ term. The potential V_{NMR} contains the NMR restraints, and has the effect of pulling the protons that show an NOE interaction closer to the measured distance r_{ij}. Similarly, these potentials are also pesudo-harmonic functions of similar forms to equations (5)-(7). Distance constraints which can be reasonably accurately determined may therefore be defined as follows:

$$V_{NOE} = \begin{cases} K_1(r_{ij}-r_{ij}^0)^2 & \text{if } r_{ij} > r_{ij}^0 \\ K_1(r_{ij}-r_{ij}^0)^2 & \text{if } r_{ij} < r_{ij}^0 \end{cases} \tag{10}$$

where, r_{ij} and r^0_{ij} are the calculated and experimental interproton distances, respectively, and K_1 and K_2 are force constants given by:

$$K_1 = k_B \, TS/ \, [2(\Delta^+_{ij})^2] \text{ and } K_2 = k_B \, TS/ \, [2(\Delta^-_{ij})^2] \tag{11}$$

Where k_B is Boltzmann's constant, T, absolute temperature of the simulation, S a scale factor, and Δ^+_{ij} and Δ^-_{ij} are the positive and negative error estimates, respectively, of r_{ij}. If, however, only ranges of distances can be specified, then the distance restraints are incorporated into a pseudo-square-well potential of the form:

$$V_{NOE} = \begin{cases} K_{NOE}(r_{ij}-r_{ij}^u)^2 & \text{if } r_{ij} > r_{ij}^u \\ 0 & \text{if } r_{ij}^l \leq r_{ij} \leq r_{ij}^u \\ K_{NOE}(r_{ij}-r_{ij}^l)^2 & \text{if } r_{ij} < r_{ij}^l \end{cases} \tag{12}$$

where r^u_{ij} and r^l_{ij} are the upper and lower limits, respectively, of the target distances obtained from the experimental, and K_{NOE} is the force constant, which is typically chosen to be the order of 1000 kJ mol^{-1} nm^{-1}.

To ensure that the experimental restraints are the dominating factor in determining the conformation of the molecule, it is very important that the force constants for the restraints are set sufficiently high that the experimental data are satisfied within the precision of the measurements. At the same time, the contribution from the empirical energy function should be such that in any individual rMD structure, the deviations from ideal geometry are small, and the non-bonded interactions are good (i.e. the Lennard-Jones potential is negative). Thus convergence on the structure is guided by the requirement to minimize NOE or other restraint violations. The number of distance restraint violations N_{viol} is counted when, for example, $r_{ij} \geq r_{ij}^0 + 1$, which would for 1 Å fluctuations. Another parameters which can be minimized in addition to N_{viol} is the sum of the distances in excess of the constraints $\sum \Delta r_{viol}$, which is defined as:

$$\sum \Delta r_{viol} = \sum_{K=1}^{N_{viol}} (r_{ij)k} - [(r_{ij}^0)_k + 1] \tag{13}$$

90

where the sum runs over all those interproton (or pseudoatom) distances for which N_{viol} is defined. Although an arbitrary structure may be used for restrained molecular dynamics calculation, in practice a starting structure obtained from distance geometry and energy minimization is often used. The rMD approach requires a relatively large amount of computation time compared to distance geometry methods. This problem can be overcome by using a simplified potential energy function, where all non-bonded contact interactions are described by a single van der Waals repulsion term. Also by using a cut off distance, in which non-bonded interactions for pairs of atoms that are separated by a distance greater than some reasonable value (e.g. 5-10 Å) are excluded, the number of non-bonded interactions is decreased considerably. Simulated annealing involves raising temperature of the system followed by slow cooling in order to overcome local minima and locate the global minimum region of the target function. It is computationally more efficient than rMD and yield structures of similar quality. The potentials are very similar to rMD and again Newton's laws of motion are solved as a function of time. However, in implementations found in commercial programs, the non-bonded interaction potential is modified so that there is a simple van der Waals repulsion term with a variable force constant K_{rep}:

$$V_{repel} = \begin{cases} 0 & \text{if } r \geq s. \ r_{min} \\ K_{rep} \ (s^2 r^2_{min} - r^2)^2 & \text{if } r < \ s. \ r_{min} \end{cases} \tag{14}$$

The values of r_{min} are given by the sum of the standard values of the van der Waals radii between two atoms as represented by the Lennard-Jones potential.

2.9.1 Strategy for Molecular Modeling

2.9.1.1 Restrained Molecular Dynamics (rMD) of Uncomplexed flavonoids

In Chapter 3, the conformational features of flavonoids viz. luteolin, quercetin, rutin and genistein obtained after rMD simulations are discussed. The structure of these flavonoids were made by using builder module in MOE (Molecular Operating Enviornment, CCG canada) module. H5'-H6' peak of these flavonoids was used as the reference using a distance = 2.45 Å. The initial structure of these flavonoids were energy minimized against NOE constraints using 1000 steps each of Steepest Descent and Conjugate Gradient using MMFF94 force field in MOE software. Conformational search was performed by using the following simulated annealing restrained molecular dynamics (rMD) protocol. The molecule was heated to a temperature of 800 K in steps of 100 K, Molecular dynamics was carried out for 25 ps at 900 K during which 25 structures were saved at regular intervals of 1 ps. Each of them was then slowly cooled to 300 K in steps of 100 K. The total number of distance restraints used in the calculations was mentioned in Chapter 3 for all four flavonoids including sugar moiety rutinoside of rutin. At the end of simulated annealing all the structures were minimized by 1000 steps of Conjugate gradient until a predefined convergence limit of root mean square derivative of < 0.01 Kcal mole^{-1} Å^{-1} was reached. The average structure obtained was examined in detail.

2.9.1.2 Restrained Molecular Dynamics (rMD) of quercetin complexed with human telomeric G-quadruplex DNA sequence d-(TTAGGGT)$_4$

In Chapter 7 we have discussed the conformational features of quercetin complexed with G-quadruplex DNA sequence d-(TTAGGGT)$_4$. Starting structure of the G-quadruplex d-(TTAGGGT)$_4$ was taken from the x-ray data available in protein data bank (PDB). The complex of quercetin-G- quadruplex was made using builder module in MOE. rMD studies were done using DISCOVER / MOE. The energy of the molecule was minimized using

1000 steps each of Steepest Descent and Conjugate Gradient Methods to remove any internal strain due to short contacts in starting structure using CFF91 (DISCOVER) or MMFF94 (MOE) force field. Dielectric constant was fixed as 1.0 * r (r=distance) for calculation of electro electrostatic interactions. Conformational search was performed by the following simulated annealing restrained molecular dynamics protocol: The molecule was heated to a temperature of 900K in steps of 100 K. Molecular Dynamics was carried out for 25 ps at 900K during which 25 structures were saved at regular intervals (1000 iterations steps of 1 fs each). Each of them was then slowly cooled to 300K in steps of 100 K. At each step of cooling the molecule was equilibrated for 1000 iterations steps of 1 fs each. At the end of simulated annealing, 1000 steps of Steepest Descent minimized all the structures until a predefined convergence limit of root mean square derivative of energy with respect to atomic coordinates of <0.01 kcal mol^{-1}Å^{-1} was reached. All molecular

3.0 Quantum mechanical calculations

The popularity of density functional methods and their applications to a broad range of problems and biochemical interest has been growing rapidly each year (Parr et al, 1989, Labauowski et al, 1991, Kohn et al, 1996). In chapter 3, the best known Hybrid B3LYP based on Becke's three parameters functional (Becke, 1993) and the correlation functional provided by Lee, Yang and Parr's correlation energy (LYP) which includes local and non-local terms (Lee et al, 1988) of density functional theory (DFT) was used. In all of these calculations, Cartesian Gaussian type orbitals (GTO's) were used as basis function for the molecular orbitals. Although the capability of the basis functions to describe bonding deformations of the electronic density can be enhanced by increasing the number of basis functions for each orbital or including higher angular functions, yet as a thumb rule it should be able to yield results which are comparable with larger basis set while remaining computationally manageable, and thus at least a basis set of the split-valence type with

polarization function should be employed. All calculations were done using the Gaussian 03 program package (Gaussian 03, 2004). Unconstrained geometry optimizations were performed using DFT with B3LYP functional methods. Basis sets 6-311G(d,p) was used for optimizing the geometry in DMSO solvents conditions. Although it does not include any solvent hydrogen bonding, van der Waals or anisotrophy contributions, yet it is found one of the most successful model for incorporating the solvent effects. The molecular properties and chemical shifts were computed using the optimized structure of the molecule. The chemical shifts were calculated both in gas phase and in solvent using the Gauge Independent Atomic Orbital (GIAO) approach. This approach allows the computation of the absolute chemical shielding due to the electronic environment of the individual nuclei.

Theoretical Studies on Molecular Properties and Electronic

Structure of Bioflavonoids: Flavones, Flavanones and Flavanols.

Prior to the determination of the structure-activity correlations for antioxidant potentials and DNA binding activities of flavonoids, it is important to first understand their overall structural parameters, conformational preferences and intra- and interamolecular interactions. Molecular palanarity is an important feature for DNA intercalation. Almost all the member of flavones and flavonols are planar but in case of flavanones (hesperetin and naringenin) this planarity is lost due to saturation of the C2-C3 bond. In this regard, it is worth important to study the NMR data with ^{1}H and ^{13}C chemical shifts and their structural parameters for hydroxyl substituted frequently encountered flavonoids, i.e. chrysin, apigenin, luteolin, acacetin, hesperetin, naringenin, galangin, kaemferol, quercetin, myricetin (Fig. 3.1a,b). Thus, the present chapter includes:

- Calculation of chemical shift of ^{1}H and ^{13}C resonances in Nuclear Magnetic Resonances (NMR) spectra of these molecules using the Gauge-Invariant Atomic Orbital (GIAO) method as implemented in Gaussian 98 for gas phase and Gaussian 03 for solvent phase, using Density Functional Theory (DFT) employing B3LYP exchange correlation at 6-311G** level of basis set.

- Molecular properties like electronic charges, dipole and energies and structural parameters like bond length, bond angles and torsional angles were calculated for all the hydroxyl substituted flavonoids in gas phase and in solvent DMSO, using the same basis set.

- Structure-function analysis was done for their functional efficacy for antioxidant and anticancer activities based on their molecular properties and structural parameters.
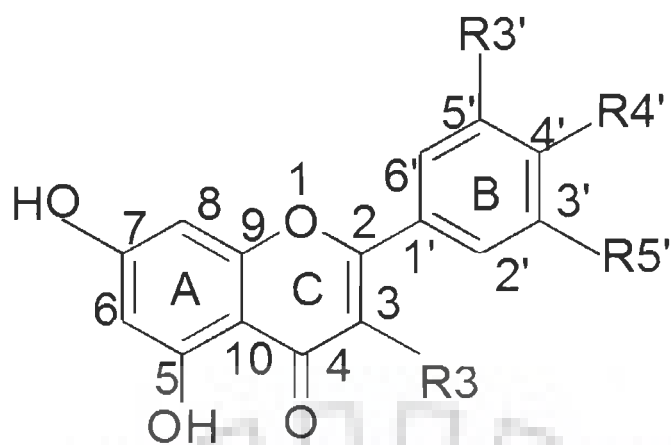
	R3	R3'	R4'	R5'
Chrysin	H	H	H	H
Apigenin	H	H	OH	H
Luteolin	H	OH	OH	H
Acacetin	H	H	OCH3	H
Galangin	OH	H	H	H
Kaemferol	OH	H	OH	H
Quercetin	OH	OH	OH	H
Myricetin	OH	OH	OH	OH

Fig. 3.1 (a): Molecular structure of flavones and flavanols.
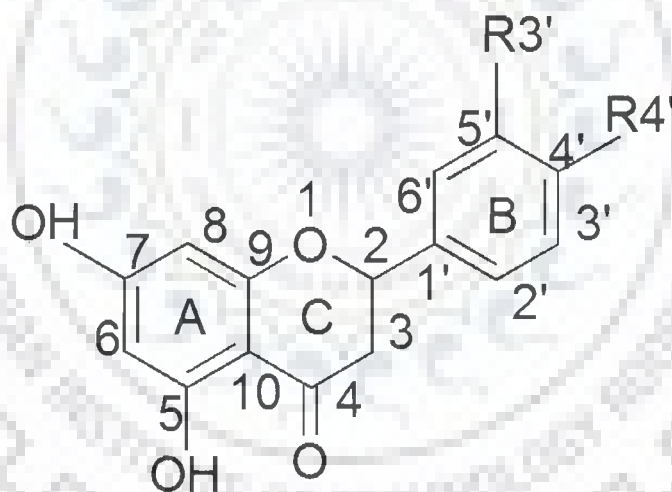
	R3'	R4'
Naringenin	H	OH
Hesperetin	OH	OCH3

Fig. 3.1 (b): Molecular structure of flavanones.

3.1   Results and Discussion

3.1.1 Proton and Carbon Chemical Shift of bioflavonoids

All the ^{1}H and ^{13}C chemical shifts were referenced to those of Tetra Methyl Silane (TMS). The absolute ^{1}H and ^{13}C shielding of TMS based on the B3LYP were calculated at the same level basis set used in the calculation to which they refer. The chemical shifts for each atom (^{1}H and ^{13}C) were computed by taking the difference between their value and the reference value for TMS. The calculated chemical shifts from 6-311G** with GIAO method are listed in Tables 3.1 and 3.2a-c. A quick look at the tables tells us that the calculated chemical shift range for ^{1}H are more sensitive to the variation of hydroxyl group position compared to that of ^{13}C. This can be rationalized by the fact that ^{1}H atom being the smallest of all atoms and being are mostly localized on periphery of the molecules, their chemical shifts would be more susceptible to intermolecular interactions in the aqueous solutions compared to that for other heavier atom. From the tabulated data, it can be easily seen that the variation of the difference between measured values and calculated results at B3LYP/6-311G** level of theory are quantitatively good and compare well with the experimental data. The largest difference in ^{13}C chemical shifts is observed for the carbon bonded to the hydroxyl group in compound. The value for chemical shifts of protons of hydroxyl group in gas and solvent phase differs significantly when compared. This may be due to the reason that solution and gas phase, the environment is quite different which results in to greater difference in chemical shift for hydroxyl proton. Beside this, other protons of hydroxyl group may also give several conformations in solvent as well and also involves intermolecular hydrogen bonding with the solvent. The large difference in carbon chemical shift is because the hydroxyl group attached to this carbon is free in the environment. The large difference of the chemical shifts for atoms (C4' and C3') on the side chain, may be due to higher structural flexibility of this part of molecule in

97

solution, whereas C5 atom being rigid in its position, involved in intra molecular hydrogen bonding within the molecule and is not showing such large difference. Furthermore, maximum deviation of around 10.0 ppm was observed in carbons C9 of chrysin, acacetin, naringenin, quercetin, 8.0 ppm in galangin and 6.2 ppm in kaemferol between theoretical chemical shift in solvent phase and experimental result.

Considering the fact that NMR chemical shifts are affected by the chemical environment i.e. molecular conformation and interaction with the solvent molecules, it is seen that the overall agreement between the calculated and measured values for ^{13}C chemical shift is satisfactory. It is of interest, however to see, how good the correlation between experimental and calculated results is? We therefore plot our experimental NMR results available in literatures versus theoretical calculation for carbon obtained with 6-311G** basis set as summarized in Tables 3.2a-c for flavonoids. A linear correlation between theoretical and experimental carbon chemical shift is clearly seen in Fig. 3.3(a-j). Here the correlation coefficient of experimental and calculated value in solvent DMSO for carbon of flavones, flavanones and flavanols were observed 0.99 whereas in CP/MAS and gas phase these values 0.97 for most of the flavonoids and 0.64 for myricetin. The correlation in solvent is good and approaching to 1. On the whole good correlation demonstrates that in general 6-311G** basis set predicts the best NMR parameters.

3.1.2. Structural Parameters

We have calculated values for bond length, bond angle and dihedral angles for 6-311G** in gas phase and solvent DMSO using DFT method with Becke's three parameter hybrid exchange functional (B3LYP).

Table 3.1: Comparison of proton chemical shift (ppm) of bioflavonoids with the experimental results reported in literature and with present observed chemical shift (ppm) with 6-311G wave function by GIAO method.**

Proton	Flavones								Flavanones				Flavanols							
	Chrysin		Apigenin		Luteolin		Acacetin		Hesperetin		Naringenin		Galangin		Kaemferol		Quercetin		Myricetin	
	Gas Phase	DMSO	Gas Phase	DMSO	Gas Phase	DMSO	Gas Phase	DMSO	Gas Phase	DMSO	Gas Phase	DMSO	Gas Phase	DMSO	Gas Phase	DMSO	Gas Phase	DMSO	Gas Phase	DMSO
H2'	8.24	8.48	7.94	8.29	7.08	7.49	7.88	8.39	6.30	7.34	7.82	7.97	8.34	8.56	8.27	8.45	7.47	7.84	7.46	7.52
H3'	7.65	8.04	7.14	7.40	3.60	6.32	7.07	7.51	3.45	3.80	7.14	7.33	7.64	8.04	7.16	7.44	3.47	6.35	4.94	6.37
H4'	7.58	8.02	4.04	6.82	5.32	6.55	-	-	-	-	3.67	6.27	7.49	7.89	3.84	6.57	5.12	6.28	1.43	4.21
H5'	7.60	8.00	6.68	7.30	7.16	7.25	6.59	7.16	7.28	7.33	6.49	7.06	7.60	7.96	6.64	7.22	7.13	7.35	4.84	6.29
H6'	7.95	8.28	8.17	8.41	7.89	7.87	7.68	8.33	7.31	7.66	7.09	7.54	9.00	8.95	8.86	8.79	8.52	8.35	8.17	8.01
H2	-	-	-	-	-	-	-	-	4.99	5.37	5.04	5.39	-	-	-	-	-	-	-	-
H3	6.50	6.80	6.51	6.88	6.33	6.66	7.71	6.73	2.19	2.24	2.19	2.23	7.63	7.59	7.46	7.34	7.44	7.3461	7.58	7.52
H3*	-	-	-	-	-	-	-	-	2.52	2.75	2.53	2.79	-	-	-	-	-	-	-	-
H5	4.11	6.83	13.02	12.68	12.97	13.27	4.07	6.79	4.22	6.04	4.01	6.75	4.31	7.05	4.27	6.99	4.28	12.97	4.30	7.04
H6	5.44	6.47	5.95	6.53	5.96	6.30	5.33	6.44	5.66	6.18	5.13	6.07	5.50	6.51	5.47	6.46	5.48	6.48	5.48	6.49
H7	3.78	6.75	4.04	6.85	4.05	6.77	3.83	6.69	3.89	5.84	3.72	6.66	3.88	6.83	3.83	6.67	3.84	6.77	3.86	6.80
H8	6.58	6.88	6.39	6.81	6.41	6.54	6.45	6.85	5.79	6.23	6.21	6.29	6.66	6.83	6.63	6.88	6.55	6.86	6.67	6.87
OCH$_3$	-	-	-	-	-	-	3.75	4.17	3.80	4.31	-	-	-	-	-	-	-	-	-	-

Table 3.2a. Comparison of carbon chemical shift (ppm) of bioflavonoids with the experimental results reported in literature and with present observed chemical shift (ppm) with 6-311G** wave function by GIAO method.

	Flavones				Flavanones							
	Acacetin				Hesperetin				Naringenin			
	Experimental*		Theoritical		Experimental*		Theoritical		Experimental*		Theoritical	
Atom	DMSO	CP/MAS	DMSO	Gas Phase	DMSO	CP/MAS	DMSO	Gas Phase	DMSO	CP/MAS	DMSO	Gas Phase
C-2	164.8	165.0	168.2	146.0	78.6	76.8	86.0	86.7	79.2	80.2	87.4	87.0
C-3	103.9	98.8	111.4	147.9	42.8	42.9	52.4	53.1	42.7	42.5	52.9	53.2
C-4	182.3	180.8	181.2	207.2	195.5	197.2	192.7	187.7	196.4	197.0	195.1	188.3
C-5	162.2	164.1	167.4	164.5	164.0	162.5	168.6	168.4	164.5	164.7	169.4	167.7
C-6	99.4	98.8	103.3	98.4	96.4	97.8	99.3	97.8	96.2	99.2	99.8	96.4
C-7	163.9	164.4	169.5	168.5	166.9	169.5	171.2	168.8	166.5	166.2	172.0	168.6
C-8	94.3	92.7	99.3	99.6	95.4	97.8	98.6	97.8	95.2	96.3	99.7	100.5
C-9	157.9	157.4	167.4	165.9	162.9	162.5	173.5	173.2	163.6	162.3	174.3	173.9
C-10	104.4	103.02	112.4	106.8	102.2	101.2	108.8	109.4	102.4	102.8	108.9	109.3
C-1'	123.5	119.2	129.5	137.1	131.3	133.1	139.9	144.0	130.0	130.0	138.94	139.5
C-2'	128.4	124.3	134.07	131.1	113.6	110.7	129.1	115.8	128.3	129.5	134.32	133.7
C-3'	114.8	119.2	123.9	123.0	146.6	145.4	151.8	157.6	115.4	117.0	120.93	120.8
C-4'	162.8	161.2	170.9	167.2	147.9	146.2	156.7	154.9	157.8	154.8	166.67	164.7
C-5'	114.8	111.1	115.1	112.0	111.5	110.7	124.1	130.7	115.4	115.2	118.68	116.0
C-6'	128.4	126.4	135.4	132.0	117.7	114.1	128.6	122.9	128.3	130.5	135.06	132.0
OCH3	56.1	55.5	57.9	56.2	-	54.0	63.7	60.5	-	-	-	-

* Wawer and Zielinska, 2001

Table 3.2b. Comparison of carbon chemical shift (ppm) of bioflavonoids with the experimental results reported in literature and with present observed chemical shift (ppm) with 6-311G** wave function by GIAO method.

	Flavones											
	Chrysin				Apigenin				Luteolin			
	Experimental*		Theoritical		Experimental*		Theoritical		Experimental*		Theoritical	
Atom	DMSO	CP/MAS	DMSO	Gas Phase	DMSO	CP/MAS	DMSO	Gas Phase	DMSO	CP/MAS	DMSO	Gas Phase
C-2	164.4	164.7	169.0	166.1	164.1	164.1	171.8	168.8	163.9	164.6	160.3	168.5
C-3	105.1	103.2	113.9	114.8	102.8	103.0	107.8	108.9	102.5	100.1	100.6	108.1
C-4	181.9	182.0	181.3	175.7	181.8	180.9	186.8	184.4	182.5	181.5	175.4	184.3
C-5	161.4	160.9	167.6	166.5	161.1	161.7	170.9	172.1	161.8	161.3	168.2	172.0
C-6	98.9	99.2	103.4	99.4	98.8	99.6	102.7	100.8	98.7	98.3	94.7	100.8
C-7	163.2	164.7	169.7	166.5	163.8	163.0	171.6	169.2	164.8	162.8	157.4	169.3
C-8	94.1	94.5	99.5	99.6	94.0	95.1	97.9	96.14	93.6	93.5	89.7	96.2
C-9	157.4	157.0	167.6	167.4	157.3	156.2	165.3	164.6	158.0	157.9	153.0	167.8
C-10	104.0	103.2	112.6	114.0	103.7	103.9	136.0	109.6	103.9	104.0	103.2	109.5
C-1'	130.7	129.9	138.7	139.4	121.3	120.6	128.0	129.9	122.3	122.3	118.5	128.7
C-2'	126.4	125.8	132.8	131.6	128.4	129.1	136.0	134.2	112.8	112.4	108.2	113.3
C-3'	129.1	129.9	136.0	134.2	116.0	115.5	121.7	120.8	145.6	145.9	139.8	149.6
C-4'	132.0	133.9	139.0	136.1	161.5	161.7	170.2	167.4	149.6	148.0	144.8	156.3
C-5'	129.1	129.9	135.9	134.0	116.0	114.0	120.4	117.4	115.4	116.8	111.4	120.5
C-6'	126.4	125.8	133.2	131.5	128.4	129.1	135.3	133.8	118.9	119.0	116.7	127.1

* Wawer and Zielinska, 2001

101

Table 3.2c. Comparison of carbon chemical shift (ppm) of bioflavonoids with the experimental results reported in literature and with present observed chemical shift (ppm) with 6-311G** wave function by GIAO method.

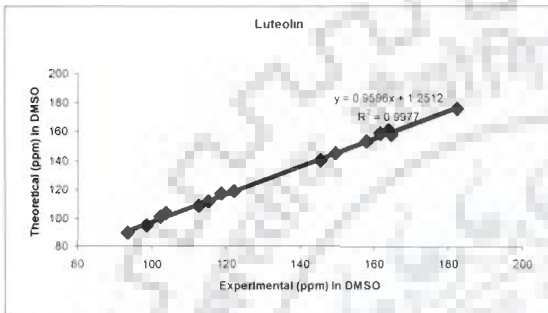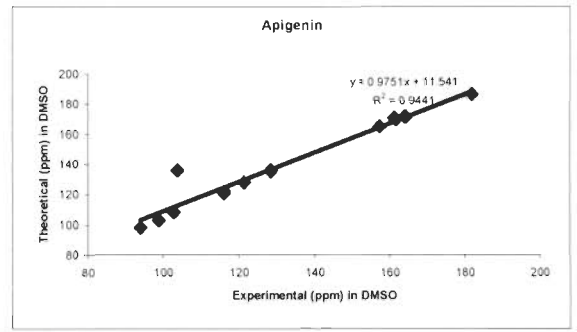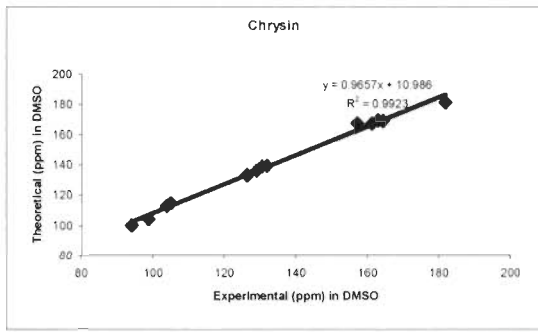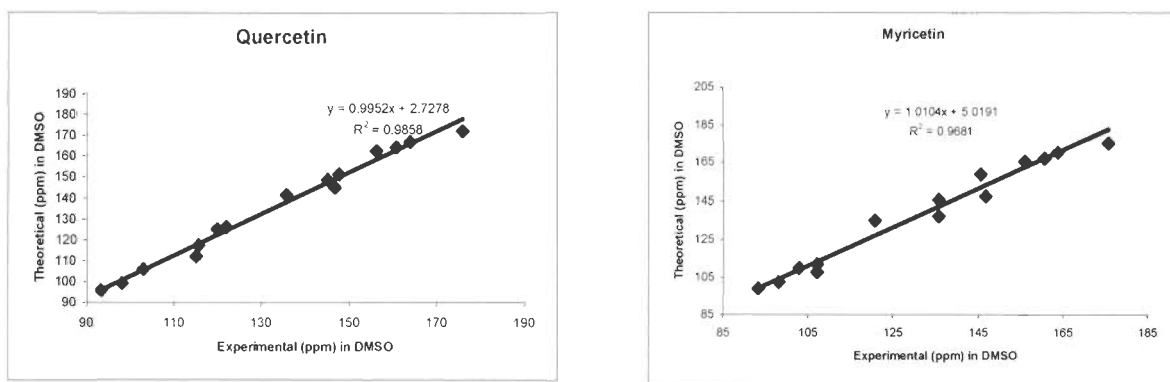| Atom	Flavanols															
	Galangin				Kaemferol				Quercetin				Myricetin			
	Experimental*		Theoritical		Experimental*		Theoritical		Experimental*		Theoritical		Experimental*		Theoritical	
	DMSO	CP/MAS	DMSO	Gas Phase	DMSO	CP/MAS	DMSO	Gas Phase	DMSO	CP/MAS	DMSO	Gas Phase	DMSO	CP/MAS	DMSO	Gas Phase
C-2	146.5	148.0	147.5	146.7	146.8	145.5	148.3	147.0	146.9	146.2	144.8	146.7	146.9	145.6	147.5	146.2
C-3	138.0	134.6	145.9	146.0	135.7	135.2	144.1	144.6	135.9	135.3	141.4	145.0	135.9	135.8	145.7	146.2
C-4	177.1	173.1	175.6	173.4	175.9	175.1	175.3	173.2	176.0	174.3	172.0	173.0	175.8	172.4	175.5	173.5
C-5	161.6	159.0	167.6	166.4	160.7	157.3	167.3	166.2	160.9	157.1	164.1	166.3	160.8	156.3	167.5	166.3
C-6	99.2	98.8	102.5	98.3	98.2	100.0	102.1	98.2	98.3	96.1	99.1	98.2	98.2	99.1	102.5	98.2
C-7	165.1	165.6	170.5	167.3	163.9	164.4	170.0	167.0	164.0	163.8	166.9	166.9	163.9	164.7	170.5	167.2
C-8	94.4	94.1	98.9	99.6	93.5	93.8	98.85	99.5	93.5	96.0	95.5	99.0	93.3	95.5	98..8	98.2
C-9	157.3	156.4	166	165.8	156.2	154.0	165.7	165.7	156.3	155.0	162.5	165.6	156.1	156.3	165.8	167.3
C-10	104.1	102.1	109.2	109.3	103.1	101.9	109.3	109.3	103.2	101.6	105.9	109.3	103.0	101.1	109.9	165.7
C-1'	130.7	130.0	138.4	138.2	121.7	121.6	129.4	130.0	122.2	125.0	126.2	129.3	120.8	120.4	135.0	136.8
C-2'	128.4	127.4	131.0	129.9	129.5	131.6	133.8	132.7	115.3	112.3	112.0	112.1	107.2	108.5	107.4	107.5
C-3'	129.3	129.0	135.4	133.2	115.5	115.0	121.0	119.5	145.2	141.6	148.6	149.3	145.8	142.5	159.1	157.3
C-4'	131.8	130.0	136.2	134.1	159.2	156.5	167.3	165.1	147.8	148.0	151.3	153.7	135.9	133.3	137.0	134.2
C-5'	129.3	129.0	135.4	133.9	115.5	114.9	119.7	117.1	115.8	115.7	117.4	120.5	145.8	142.3	158.9	157.7
C-6'	128.4	127.4	134.9	135.3	129.5	125.5	137.2	137.0	120.1	121.9	125.0	130.3	107.2	109.0	111.6	112.9

* Wawer and Zielinska, 2001

Chrysin
$y = 0.9657x + 10.986$
$R^2 = 0.9923$

Apigenin
$y = 0.9751x + 11.541$
$R^2 = 0.9441$

Luteolin
$y = 0.9596x + 12512$
$R^2 = 0.9977$

Acacetin
$y = 1.0006x + 5.2269$
$R^2 = 0.9921$

Hesperetin
$y = 0.9575x + 12.503$
$R^2 = 0.988$

Naringenin
$y = 0.9727x + 9.5683$
$R^2 = 0.9945$

Galangin
$y = 0.9841x + 7.0576$
$R^2 = 0.9873$

Kaemferol
$y = 0.9941x + 6.3152$
$R^2 = 0.9896$

103
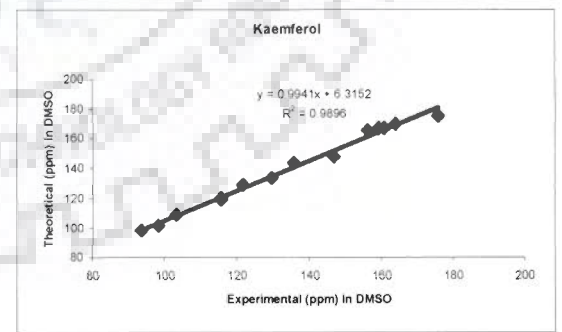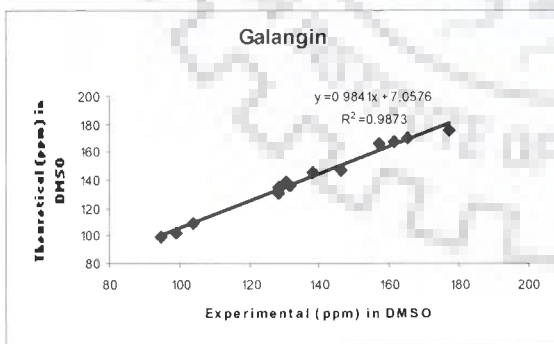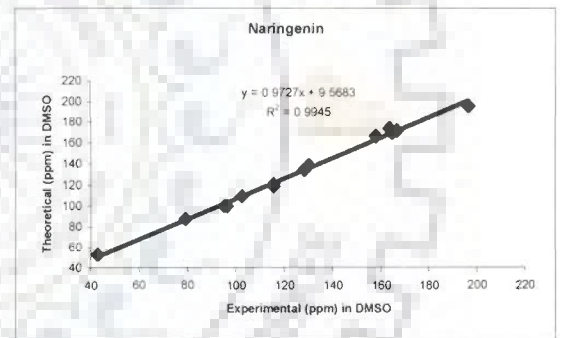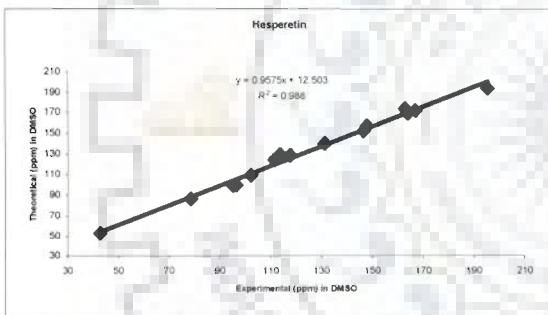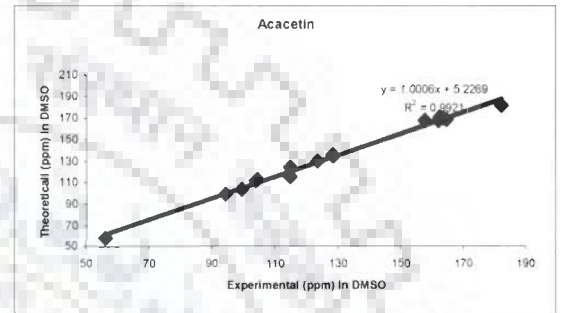
Fig. 3.3: Correlation of experimental and calculated carbon chemical shifts with B3LYP/ 6-311G**/GIAO method for flavones (a-d), flavanones (e-f) and flavanols (g-j) in solvent DMSO

The results of structural parameters for all these molecules of flavonoid family are shown in Table 3a-b. It may be noted that as we move towards a polarization function in basis set, the difference between the calculated and experimental results narrow down due to the fact that these functions are found to be very effective.

There are very few reports are available for x-ray data on some of the falvonoids viz. luteolin (Cox et al. 2003), quercetin (Jin et al. 1990), morin (Cody and Luft, 1994) flavonoids. For the luteolin and quercetin molecule, we found that all the calculated bond lengths are very close to the present data which compare reasonably well with the X-ray measurements reported in literature; the difference lies within a few hundredth of an angstrom.

The theoretical and experimental C–C and C–O bond distances present small differences, in the order of 0.01–0.02 Å, while the O–H bond distances show noticeable differences in a range of 0.01–0.7 Å. Experimentally, the RO–H bond distance is 0.97 Å (Dean, 1999), this value is very close to the theoretical results obtained in our study (0.95–0.99 Å). The large differences in the gas phase can be attributed to the fact that OH groups constituted the site for both intermolecular interactions among similar flavonoid molecules and hydrogen bonds with the DMSO of the lattice. Oppositely, in

104

the simulation in gas phase is modeled a single molecule free of intermolecular interactions, therefore the bond distances are almost not modified.

The theoretical bond angles between carbon atoms present differences about 2.5° among the members of flavone and flavanol, the presence of an oxygen atom diverted the bond angle values around 1–6° with respect to the theoretical bond angle among different members, and the presence of a OH group originates a great deviation of the angle in a range of 1–8°, such as the bond distances. Further, the maximum variation in the calculated and measured values for bond angle is less than 7° (gas phase), 2° (solvent) and 8.9° (gas phase), 2.5° (solvent) for luteolin and quercetin, respectively (Table 3.3b) when compared with the crystal data (Cox et al. 2003; Jin et al. 1990). For other members, it has been found that the bond length and bond angle values of the molecules of the same group in solvent DMSO are found to be consistent among other molecules of the same family of flavones, flavanones and flavonols. For example, the bond angle C1'-C2-O1, C1'-C2-C3 and C2-O1-C9 of the members of flavone and flavonol were found to be 112.4°, 126.5° and 120.9°, respectively in solvent due to the similar kind of planarity of A and C ring. But these values differ significantly for hesperetin and naringenin of flavanone with flavones and flavanol due the presence of saturated C1-C2 bond of C ring. Beside this, the presence of OH group originates a great deviation of the angle in a range of 1–8°, such as the bond distances.

From the bond length and bond angle analysis, we notice that such differences between theoretical values in gas and solvent phase arise due to the fact that structurally the molecule is in dynamic state in solution phase (i.e. Ring B attached to benzopyran ring) as compared to the gas phase optimized structure of the molecule. In the conformation of minimum energy of flavonoids (Fig. 3.2), the hydroxyl groups are oriented in such a way to maximize inter molecular hydrogen bond type interactions

Table 3.3a: Observed optimized structural parameters bond length with 6-311G** for bioflavonoids using DFT method.

	Flavones								Flavanones				Flavanols							
	Chrysin		Apigenin		Luteolin		Acacetin		Hesperetin		Naringenin		Galangin		Kaemferol		Quercetin		Myricetin	
	DMSO	Gas Phase	DMSO	Gas Phase	DMSO	Gas Phase	DMSO	Gas Phase	DMSO	Gas Phase	DMSO	Gas Phase	DMSO	Gas Phase	DMSO	Gas Phase	DMSO	Gas Phase	DMSO	Gas Phase
O4`-H4`	-	-	0.98	0.95	0.95	0.96	-	-	0.95	0.96	0.98	0.96	-	-	0.98	0.96	0.97	0.95	0.98	0.96
O4`-C4`	-	-	1.35	1.36	1.36	1.35	1.35	1.39	1.35	1.35	1.36	1.36	-	-	1.35	1.36	1.36	1.42	1.38	1.37
C1`-C2	1.47	1.53	1.46	1.44	1.44	1.46	1.46	1.54	1.51	1.53	1.51	1.54	1.46	1.56	1.46	1.56	1.46	1.53	1.46	1.54
C10-C5	1.42	1.40	1.42	1.41	1.42	1.42	1.42	1.40	1.42	1.42	1.42	1.40	1.42	1.40	1.42	1.40	1.42	1.40	1.42	1.40
C2-O1	1.36	1.41	1.36	1.38	1.37	1.36	1.36	1.42	1.36	1.36	1.45	1.46	1.37	1.42	1.37	1.42	1.37	1.39	1.37	1.43
C6`-C5`	1.39	1.39	1.39	1.40	1.40	1.38	1.39	1.39	1.39	1.39	1.39	1.39	1.39	1.39	1.38	1.39	1.40	1.40	1.39	1.38
C3`-O3`	-	-	-	-	1.36	1.37	-	-	-	-	-	-	-	-	-	-	1.37	1.42	1.35	1.36
O3`-H3`	-	-	-	-	0.96	0.96	-	-	-	-	-	-	-	-	-	-	0.98	0.96	0.97	0.95
O1-C9	1.37	1.41	1.37	1.38	1.37	1.37	1.37	1.41	1.36	1.36	1.36	1.40	1.35	1.40	1.35	1.40	1.37	1.40	1.35	1.40
O5-C5	1.35	1.37	1.34	1.36	1.36	1.33	1.34	1.37	1.35	1.35	1.35	1.37	1.34	1.37	1.34	1.37	1.34	1.42	1.34	1.37
O5-H5	0.98	0.96	0.99	0.95	0.95	0.99	0.98	0.96	0.98	0.96	0.98	0.96	0.98	0.95	0.98	0.96	0.98	0.96	0.98	0.95
O7-C7	1.35	1.37	1.35	1.36	1.36	1.35	1.35	1.36	1.35	1.35	1.35	1.36	1.34	1.36	1.35	1.36	1.36	1.42	1.35	1.36
C4-O4	1.23	1.23	1.25	1.22	1.23	1.24	1.23	1.25	1.23	1.22	1.22	1.23	1.24	1.23	1.24	1.23	1.25	1.42	1.24	1.24
C3-H3	1.08	1.091	1.08	1.07	1.08	1.08	1.08	1.09	1.08	1.08	1.10	1.11	-	-	-	-	-	-	-	-
C3-O3	-	-	-	-	-	-	-	-	-	-	-	-	1.35	1.37	1.35	1.37	1.40	1.42	1.35	1.38
O3-H3	-	-	-	-	-	-	-	-	-	-	-	-	0.98	0.96	0.98	0.96	0.95	0.96	0.98	0.96
C6-H6	1.08	1.08	1.08	1.08	1.08	1.08	1.08	1.07	1.08	1.08	1.08	1.08	1.08	1.08	1.08	1.07	1.08	1.08	1.08	1.08

which also play an important role in DNA binding. There are several reports which resolved the crystal structure of flavonoids and their derivatives (Cox et al. 2003; Jin et al. 1990). An X-ray structure determination of luteolin (Cox et al. 2003) and another flavonoid quercetin (Jin et al. 1990), showed that the benzopyran and phenyl ring are essentially planar. The dihedral angle between the two rings is 9° and that between the annellated rings is 6° (Wallet et al. 1988). However, from our study we assume that A and C annellated rings are planar while B ring is non planar as it rotate around the C2-C1' bond with torsional angle C1'-C2-O1-C9 in the solution for flavone and flavanol molecules ranges -157.5°-179.6° and in gas phase 155.5°-179.9°, while for flavanones, it was found 103 ° -177 ° in solvent and 168.6 ° - 175.2 ° in gas phase (Table 3.2b). This much variation in flavanones and its non planarity is found due to availability of saturated C2-C3 bond.

Beside this the bond lengths of the C10-C5 (~1.42 A°) and C4-O4 (~1.23 A°) are found to be longer and shorter, than the average bond length in all the flavonoids member. This further indicates the formation of similar kind of H-bond between –H5 and –O4 of ring A and C in all the molecules. The information about the orientation of substituents in luteolin and quercetin could be obtained from single crystal X-ray data. Although such structural data are available, but it can not explain much about the dynamic rotation of B ring with respect to A and C ring around C2-C1' bond. It is theoretical methods which can be used to search for explanation of the observed effects. A variable temperature gradient NMR experiment of flavonols and flavones in organic and aqueous mixtures have also revealed the presence of intramolecular hydrogen bonds in aqueous solution (Exarchou et al. 2004).

The planarities of these molecules manifest intercalation binding with DNA and allow inserting between two adjacent base pairs in a helix. Furthermore, the formation of inter

molecular hydrogen bonding due to the expanded orientation of hydroxyl group maximizes the chance of hydrogen bonding between -NH group of base pairs of DNA helix and stabilizes the binding. Comparison of calculated bond lengths and bond angles clearly show that hydroxyl groups of flavanols expand more than the respective hydroxyl groups of flavones which is needed relatively more for better binding with DNA. From the calculated optimized structure of this molecule, we saw that the pattern of variation of the bond lengths and bond angles in general are very similar to those of luteolin molecule. Further, we also notice that for members of flavanols, the value of the calculated dihedral angles at position C3 (C6'-C1'-C2-C3) are greater than 170°, whereas for flavones the value is less than 65° which clearly reflects the difference in structure on replacing -H by -OH group. Furthermore, as the number of hydroxyl groups increases by replacing the hydrogen atom among the members of flavonoids their overall energy increases. For the substitution of one –OH group the penalty for the energy is of 76 A.U, this trend of energy increment can be observed in the Table 3.3b.
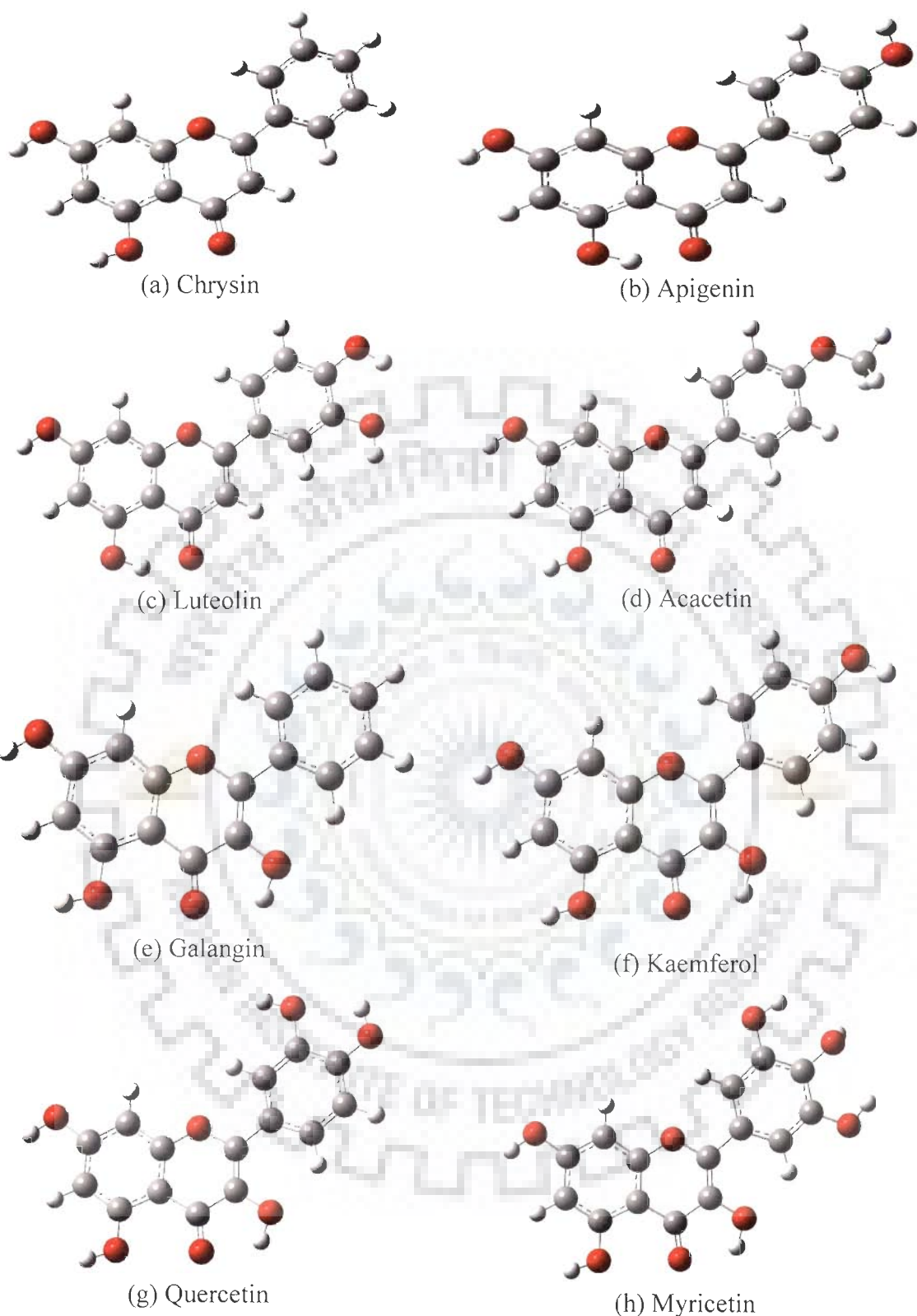
3.2. Structure-Function Relationship of Flavones, Flavanols and Flavanones

Polyphenolic flavonoids are among a wide variety of phytochemicals present in the human diet. Basic research, animal model, and human studies suggest flavonoid intake may reduce the risk of several chronic diseases. The vast number of flavonoids, including flavonols, flavones, and flavanones differ each other on the basis of position, number of hydroxyl groups and the saturation of C2- C3 bond. A number of in vitro studies have established the hierarchy of flavonoids in terms of their antioxidant activities (Cos et al. 1998; Rice-Evans et al. 1996), topoisomerase poisoning and DNA binding (Webb and Ebeler, 2004) for anti tumor activities.

Table3.3b: Observed optimized structural parameters bond angle and torsional angle with 6-311G** for bioflavonoids using DFT method.

| Angles	Flavones								Flavanones				Flavanols							
	Chrysin		Apigenin		Luteolin		Acacetin		Hesperetin		Naringenin		Galangin		Kaemferol		Quercetin		Myricetin	
	DMSO	Gas Phase	DMSO	Gas Phase	DMSO	Gas Phase	DMSO	Gas Phase	DMSO	Gas Phase	DMSO	Gas Phase	DMSO	Gas Phase	DMSO	Gas Phase	DMSO	Gas Phase	DMSO	Gas Phase
C4'-O4'-H4'	-	.	110.77	113.31	107.12	108.03	-	-	-	-	110.4	109.13	-	-	110.72	108.20	110.51	109.51	109.51	108.19
C4'-O4'-CH₃4'	-	-	-	-	-	-	118.74	123.29	115.44	116.57	-	-	-	-	-	-	-	-	-	-
C2'-C1'-C2	120.41	119.24	121.07	122.10	121.89	120.80	120.88	118.95	119.23	119.20	121.41	121.37	119.72	118.89	119.96	118.69	119.41	119.96	-119.25	118.87
C2-C1'-C6'	120.64	122.01	120.80	118.86	119.46	120.63	121.08	122.60	121.36	121.72	120.08	120.11	122.05	123.36	122.45	121.93	122.40	122.14	121.25	122.46
C1'-C2-O1	112.45	116.70	112.44	118.44	113.59	112.21	112.44	116.57	108.06	108.30	108.19	108.14	112.22	114.26	112.24	114.20	112.30	112.41	112.36	115.17
C1'-C2-C3	126.56	123.04	126.31	119.10	126.34	119.63	126.77	124.04	114.14	113.71	114.00	113.98	129.02	127.46	127.31	118.63	129.03	128.99	128.89	125.05
C3'-O3'-H3'	-	-	-	-	103.37	110.49	-	-	110.35	109.06	-	-	-	-	-	-	111.22	109.97	104.98	106.32
C2-O1-C9	120.98	123.16	121.11	112.63	120.91	116.96	121.05	123.63	116.41	116.92	116.93	117.11	122.86	124.62	122.87	124.70	120.00	118.40	122.84	123.61
C9-C10-C4	119.06	115.95	120.05	117.27	117.05	120.31	118.99	115.64	119.50	119.71	119.54	119.81	118.39	115.42	118.38	115.38	118.40	120.01	118.45	116.20
C5-O5-H5	110.03	108.61	106.21	115.24	107.65	106.40	110.03	110.50	109.97	108.59	110.04	108.81	110.24	110.04	110.17	110.31	110.31	109.46	110.23	110.40
C7-O7-H7	111.08	109.30	111.02	113.34	110.01	109.37	111.02	108.77	110.99	109.37	111.09	109.63	111.17	109.27	111.10	109.10	116.19	109.73	111.13	107.86
C3-O3-H3	-	-	-	-	-	-	-	-	-	-	-	-	-	-	-	-	102.10	102.72	104.98	107.10
Torsional angles																				
O4'-C4'-C3'-O3'	-	-	-	-	0.7	0.3	-	-	-1.5	2.0	-	-	-	-	-	-	-0.0	0.0	2.5	-0.6
C3'-C4'-O4'-CH₃4'	-	-	-	-	-	-	179.6	177.8	69.5	-65.0	-	-	-	-	-	-	-	-	-	-
H4'-O4'-C4'-C3'	-	-	-179.5	-179.5	-	-	-	-	-	-	-179.7	172.1	-	-	179.9	179.3	-0.0	0.0	-92.3	-158.9
C6'-C1'-C2-O1	-160.6	-145.7	-13.8	-32.6	-24.9	166.9	-166.1	-164.8	-163.5	-160.5	-135.7	-149.4	-179.9	172.9	-179.9	170.7	175.1	179.9	179.9	-147.4
C1'-C2-O1-C9	-179.1	177.6	179.5	155.2	-157.5	179.4	-179.4	-178.3	-177.0	-175.2	102.9	-168.6	-179.9	177.1	-179.9	177.9	179.6	179.9	179.8	-174.7
O1-C9-C10-C4	0.7	1.6	-0.5	-8.6	20.7	-0.5	0.5	1.7	5.8	5.0	5.0	1.7	-0.0	-0.3	-0.0	-1.6	-0.0	-1.6	-0.1	2.2
C6-C5-O5-H5	-0.1	0.7	179.8	155.1	153.6	-0.0	-0.1	-4.4	-0.6	-1.0	-0.7	-1.0	-0.0	-0.0	0.0	1.6	-0.0	-0.0	-0.0	-5.3
C2'-C1'-C2-O1	19.4	32.0	166.1	143.8	151.0	-13.2	14.4	15.3	-128.9	-147.4	46.2	39.5	0.0	0.0	-0.0	-9.3	-0.0	0.5	-0.4	
C2'-C1'-C2-C3	-160.3	-147.2	-14.3	-31.7	-36.0	166.1	-165.4	-164.4	-109.8	-90.9	-74.9	-82.0	-179.9	-179.9	-179.9	170.5	174.8	-179.9	-179.5	179.2
Total Energy (a.u)	-878.7	-878.7	-954.0	-953.9	-1029.0	-1029.2	-993.3	-993.2	-1069.7	-1069.7	-955.2	-955.1	-954.0	-953.9	-1029.2	-1029.2	1104.1	-1104.4	-1179.7	-1179.
Diploe moment μ (D)	5.87	3.66	2.27	5.03	2.55	2.60	3.88	2.62	6.35	4.48	4.31	2.47	6.72	4.47	4.34	2.99	6.45	6.49	5.74	3.79

(a) Chrysin

(b) Apigenin

(c) Luteolin

(d) Acacetin

(e) Galangin

(f) Kaemferol

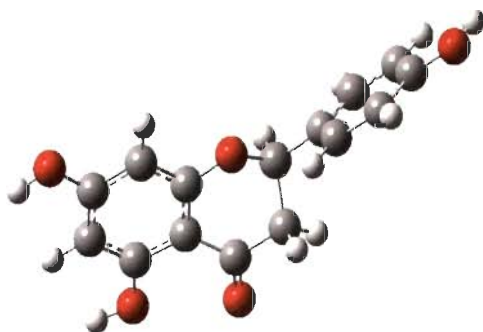(g) Quercetin

(h) Myricetin

Fig. 3.2: (i) Gaussian optimized structure of flavones and flavonols using B3LYP/6-311G** in solvent DMSO.
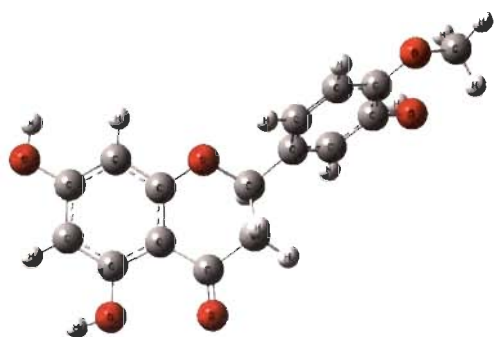
(i) Hesperetin

(j) Naringenin

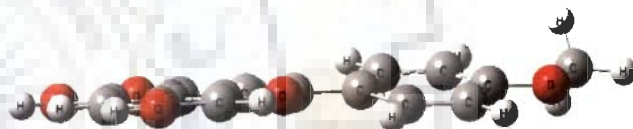**Fig. 3.2: (ii) Gaussian optimized structure of flavanones using B3LYP/6-311G** in solvent DMSO.**

(a) Chrysin

(b) Apigenin

(c) Luteolin

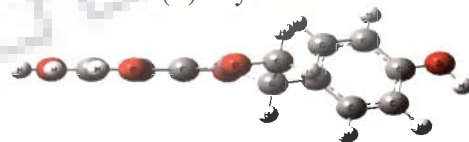

(d) Acacetin

(e) Galangin

(f) Kaemferol

(g) Quercetin

(h) Myricetin

(i) Hesperetin

(h) Naringenin

Fig. 3.3: Gaussian optimized structure of flavanones using B3LYP/6-311G in solvent DMSO showing planarity of the benzo pyran ring.**

111

3.2.1. Antioxidant activity

The antioxidant activity of flavonoids depends upon the arrangement of functional groups about the nuclear structure. The spatial arrangement of functional group is perhaps a greater determinant of antioxidant activity than the flavan backbone alone. Consistent with most polyphenolic antioxidants, both the configuration and total number of hydroxyl groups substantially influence several mechanisms of antioxidant activity (Cao et al. 1997; Pannala et al. 2001; Burda and Oleszek, 2001 and Haenen et al. 1997). Free radical scavenging capacity is primarily attributed to the high reactivities of hydroxyl substituents. The B-ring hydroxyl configuration is the most significant determinant of scavenging of Reactive Oxygen Species (ROS) (Cao et al. 1997; Haenen et al. 1997) and Reactive Nitrogen Species (RNS) (Pannala et al. 2001; Burda and Oleszek, 2001)Hydroxyl groups on the B-ring donate hydrogen and an electron to hydroxyl, peroxyl, and peroxynitrite radicals, stabilizing them and giving rise to a relatively stable flavonoid radical. Among structurally homologous flavones and flavanones, peroxyl and hydroxyl scavenging increases linearly and curvilinearly, respectively, according to the total number of OH groups (Cao et al, 1997).

A 3'4'-catechol structure in the B-ring strongly enhances lipid peroxidation inhibition (Mora et al. 1990; Ratti and Das, 1988 and Dugass et al. 2000). This arrangement is a salient feature of the most potent scavengers of peroxyl (Cao et al, 1997; Dugass et al. 2000), superoxide (Van Acker et al. 1996), and peroxynitrite radicals (Pannala et al. 2001). For example, the peroxyl radical scavenging ability of luteolin substantially exceeds kaempferol (Van Acker et al. 1996); both have identical hydroxyl configurations, but kaempferol lacks the B-ring catechol. Oxidation of a flavonoid occurs on the B-ring when the catechol is present (Van Acker et al. 1996), yielding a fairly stable *ortho*-semiquinone radical (Mora et al. 1990)

through facilitating electron delocalization (Arora et al. 1998). Flavones lacking catechol systems form relatively unstable radicals and are weak scavengers (Cao et al, 1997 Haenen et al. 1997). Chrysin, apigenin, acacetin flavones, galangin, kaemferol flavanol and naringenin, hesperetin flavanones lack these catechol systems, can be attributed under a group of unstable radicals and are weak scavengers. However, the significance of other hydroxyl configurations is less clear, but beyond increasing total number of hydroxyl groups, A-ring substitution correlates little with antioxidant activity. A 5-OH may also contribute to antioxidant effects and 5,7 -dihydroxy arrangement on A-ring of flavonoids increase this effect (Rice-Evans et al. 1996). Compared to the B-ring hydroxylation pattern, the impact of the A-ring arrangement on antioxidant activity is of questionable significance. Further, free radical scavenging by flavonoids is highly dependent on the presence of a free 3-OH (Haenen et al. 1997). Flavonoids with a 3-OH and 3',4'-catechol are reported to be 10- fold more potent than ebselen, a known RNS scavenger, against peroxynitrite (Pannala et al. 2001). The superiority of quercetin in inhibiting both metal- and nonmetal-induced oxidative damage is partially ascribed to its free 3-OH substituent (Ratti and Das, 1988; Arora et al. 1998), which is thought to increase the stability of the flavonoid radical. The torsion angle of the B-ring with respect to the rest of the molecule strongly influences free radical scavenging ability. Flavonols and flavanols with a 3-OH are planar, while the flavones and flavanones, lacking this feature, are slightly twisted (Van Acker et al. 1996). Planarity permits conjugation, electron dislocation, and a corresponding increase in flavonoid phenoxyl radical stability (Van Acker et al. 1996). Removal of a 3-OH abrogates coplanarity and conjugation, thereby compromising scavenging ability (Van Acker et al. 1996). Thus, the structural heterogeneity of flavonoids used to

evaluate their antioxidant activity pose challenges in assembling a collective hierarchy of structure function relationship.

3.2.2. Topoisomerase poisoning and DNA binding

The saturation of the C2-C3 double bond leads to a loss of benzopyran-4-one planarity which would evidently limit the interaction. It has been established that unlikely to flavonones only flavones and flavonols which have a double bond between the 2 and 3 carbons of the C-ring are capable of intercalative binding with DNA. The flavanonol analogue of quercetin and taxifolin lacks this double bond and loses all ability to intercalate. Similarly, flavonones like naringenin and hesperitin lack this double bonding between 2 and 3 carbon and these carbons are saturated which makes the annelated ring of A and C non planar. The double bond between C-2 and C-3 ensures a sufficiently planar structure to allow placement between adjacent bases of the DNA duplex (Van Acker et al., 1990). Further, it has been found that there is a requirement for at least one free hydroxyl group on the B-ring at 4'-position for intercalation to occur (Arora et al. 1998). One of flavonoids chrysin (5,7-dihydroxyflavone) which has B-ring completely lacking of hydroxyl group neither intercalates with DNA nor poison topoisomerases. The fact of hydrogen bond formation between 4' hydroxyl group of flavonoids and nitrogenous bases of DNA is supported by the inability of tamarixetin to intercalate with DNA. The 4'OH of B ring in tamarixetin is replaced by a methoxy group which is not capable of forming hydrogen bond. Further, luteolin 4'-O-glycoside is found to be a weak intecalator. This intercalation may be stabilized by the formation of hydrogen bonds by the hydroxyl groups of sugar moiety at 4'-C in B-ring.

Based on above facts, acacetin (5,7-Dihydroxy-4´-methoxyflavone) and galangin (3,5,7-trihydroxy flavone) can be ascertained as non intercalator with DNA and other flavones

114

like apigenin, luteolin and flavanols like kaemferol, quercetin and myricetin are found to be capable of intercalation and topoisomerase poisoning, both. None of the flavanone derivatives, which have a saturated 2,3-bond, are particularly active. So, it can be proposed a minimal flavone structure for DNA intercalation and topoisomerase poisoning is required to be 3', 4'-dihydroxy flavone.

3.3. Summary and Conclusions

The uses of DFT method have been demonstrated in the theoretical studies on molecular properties and electronic structure of representative molecules of flavone, flavanol and flavanone of flavonoid group. An overall analysis shows that B3LYP/6-311G** level of theory in solvent DMSO predicts sound results which are quantitatively good and compare well with the experimental data. Further, the structural analysis shows the role of inter and intra molecular hydrogen bonding in solution which is important for the flavonoids for their several functions like antioxidant properties and especially DNA binding for anti cancerous activity. Usually, it is not an easy task to grow a crystal for X -ray diffraction studies. Flavonoids are difficult to crystallize and X-ray diffraction data are lacking for most of the members of this family. The DFT studies yields enough information about the chemical shift and structural parameters of their best optimized conformation. Theoretical calculation of NMR parameter like chemical shift for different class of flavanoids compare well with the experimental data available in the literature. As the totality of the available evidence on different position of hydroxyl group and structural parameters for these flavonoids suggests a role in the prevention of cancer and for antioxidant properties, further research is warranted, particularly in their structure- function relationship studies.

Structural Elucidation of Luteolin, Quercetin, Rutin and Genistein by Nuclear Magnetic Resonance Spectroscopy, Quantum Mechanical and Restrained Molecular Dynamics Approach and Their Comparison

It has been found that the functional activities of flavonoids are changed by means of various degrees of functional group substitution and the number of hydroxyl groups; for instance 3-OH of quercetin is very important for its antioxidant activities and DNA binding potential. But this part is replaced by a glycoside moiety in rutin, a sugar derivative of quercetin and similarly by a phenyl group as in case of isoflavone genistein.. In this regard, it is worth important to study the NMR data with ^{1}H and ^{13}C chemical shifts and its structural parameters for 3-hydroxyl substituted flavonoid luteolin, 3-hydroxylated flavonoid quercetin and 3-glycosylated flavonoid rutin and isoflavone genistein. Thus, the present chapter includes:

• One- and two-dimensional NMR of luteolin, quercetin, rutin and genistein, i.e 1D, HSQC (^{1}H - ^{13}C), HMBC (^{1}H - ^{13}C) and ROESY (^{1}H - ^{1}H), in DMSO at 298 K for these four flavonoids.

• Restrained Molecular Dynamics (rMD) simulations of luteolin, quercetin, rutin and genistein were done using inter-proton distance constraints from 2D ROESY spectra.

• Structural and electronic properties of these flavonoids using Density Functional Theory (DFT) employing B3LYP exchange correlation and calculation of chemical shift of ^{1}H and ^{13}C resonances of these molecules using the Gauge–Invariant Atomic Orbital (GIAO) method as implemented in Gaussian 98 for gas phase and Gaussian 03 for DMSO.

• Comparison of NMR, quantum chemical properties and structural parameters and their structure-function relationship with respect to their OH3 substitution.

4.1 Results and Discussion

4.1.1 Resonance assignment of luteolin, quercetin, rutin and genistein

The structure and nomenclature of luteolin, quercetin, rutin and genistein are shown in Fig. 4.1. Peaks observed in ^{1}H NMR spectrum includes one doublet of doublet, four doublets and four singlet for luteolin, quercetin and genistein each and one doublet of doublet and two doublet apart from several singlet peaks in rutin (Fig. 4.2-4.5). Among the four singlet of hydroxyl protons, -OH (H5) group results in the most deshielded signal as this proton is closer to ketone group C4=O and is least mobile and accessible to the solvent, due to its participation in a strong intramolecular hydrogen bond of the C5-OH· · ·O4=C4 moiety. Similar pattern was followed in genistein for three hydroxyl groups. Accordingly chemical shift for -OH3', -OH4', -OH5, -OH7 are assigned to peaks at 8.52, 8.09, 12.98, 8.31 ppm for luteolin, 9.37, 9.59, 12.50, 10.78 ppm for quercetin and 7.70, 7.48, 12.54, 12.36 ppm for rutin, respectively. Similarly, 9.70 and 12.98 ppm peaks are assigned for -OH4' and -OH5 in genistein, respectively. No peak for as -OH7 was found as it may be due to fast exchange with solvent in genistein. One extra -OH at 3 positions in quercetin is assigned to the peak at 9.468. The one doublet of doublet due to ^{3}J coupling at 7.44 ppm in luteolin, 7.54 in quercetin, 7.54 in rutin and 7.38 in genistein are assigned to H6' due to the coupling of H5' protons having ^{3}J = 8.20 Hz, 8.60 Hz, 8.23 Hz and 8.58 Hz, respectively; H6' is shifted downfield with respect to H5' due to its proximity to O1 atom in both the molecules. Accordingly assignments has been made to singlet like H3, H6, H8 and H2' protons, listed in Table 4.1a. It was able to resolve all J_{HH} that are larger than 1.5 Hz, including a ^{5}J coupling between H5' and H2' in luteolin and quercetin. The complete

proton chemical shift with J couplings is summarized in Table 4.1a, b. Further, the ^{1}H–^{13}C Heteronuclear Single Quantum Coherence (HSQC) spectra (Fig. 4.6a-d) shows the coupling of 6 carbon atoms in luteolin, 5 carbon atoms in quercetin, 16 carbons in rutin and 7 carbons to protons in genistein to which they are directly bonded through a single bond. The other carbon atoms are assigned with the help of Heteronuclear Multiple Bond Correlation (HMBC) spectra (Fig. 4.7a-d) for both the molecules. There are several ambiguities in carbon chemical shift assignment for C2, C7, C5 and C9 (Park *et al.* 2007). The correct sequence of chemical shift value for these carbons were reported in order of C2 > C7 > C5> C9 (Park *et al.* 2007). But our results suggest the value in the order of C7 > C2 > C5> C9 which is also supported by our GIAO NMR calculation of DFT and other recent reports. The observed carbon chemical shifts and carbon-proton bond correlations are listed in Table 4.2a-b and 4.3, respectively. On comparison of our results with measurements of other groups (Lallemand and Duteil, 1977; Markham, 1977; Markham and Chari, 1982; Wawer and Zielinska, 2001; Owen *et al.* 2003; Nissler *et al.*2004; Olejniczak and Potrzebowski, 2004) we find it agrees better in the magnitude of the ppm values (Table 4.1a and 4.1b; 4.2a and 4.2b) for both carbon and proton. This was expected as the solvent was same i.e DMSO. Thus there were no significant change in shift positions observed which is generally quite sensitive to the molecular conformation and chemical environment. Fig. 4.8a-d shows the ROESY spectra of luteolin, quercetin, rutin and genistein in DMSO solution. We observed 6 cross peaks in genistein, 7 in luteolin, 8 in quercetin and 32 cross peaks in rutin and calculated the corresponding inter proton distances from integrals (Table 4.4a and 4.4b). Using these distance constraints restrained Molecular Dynamics (rMD) simulations was carried out to search for optimum conformation. The various structures at these time intervals differed only marginally from each other and hence indicate

(a) R= H   Luteolin
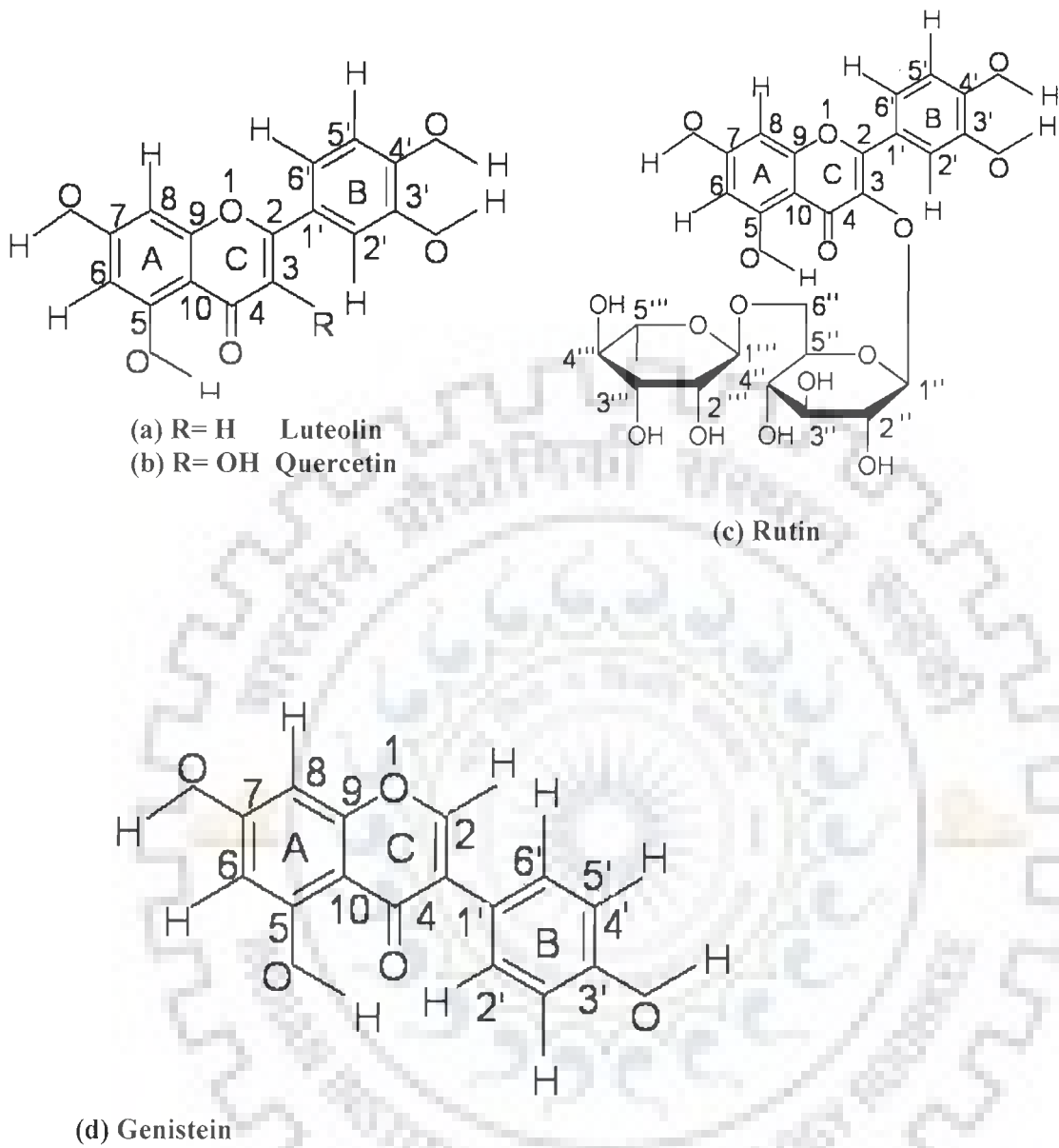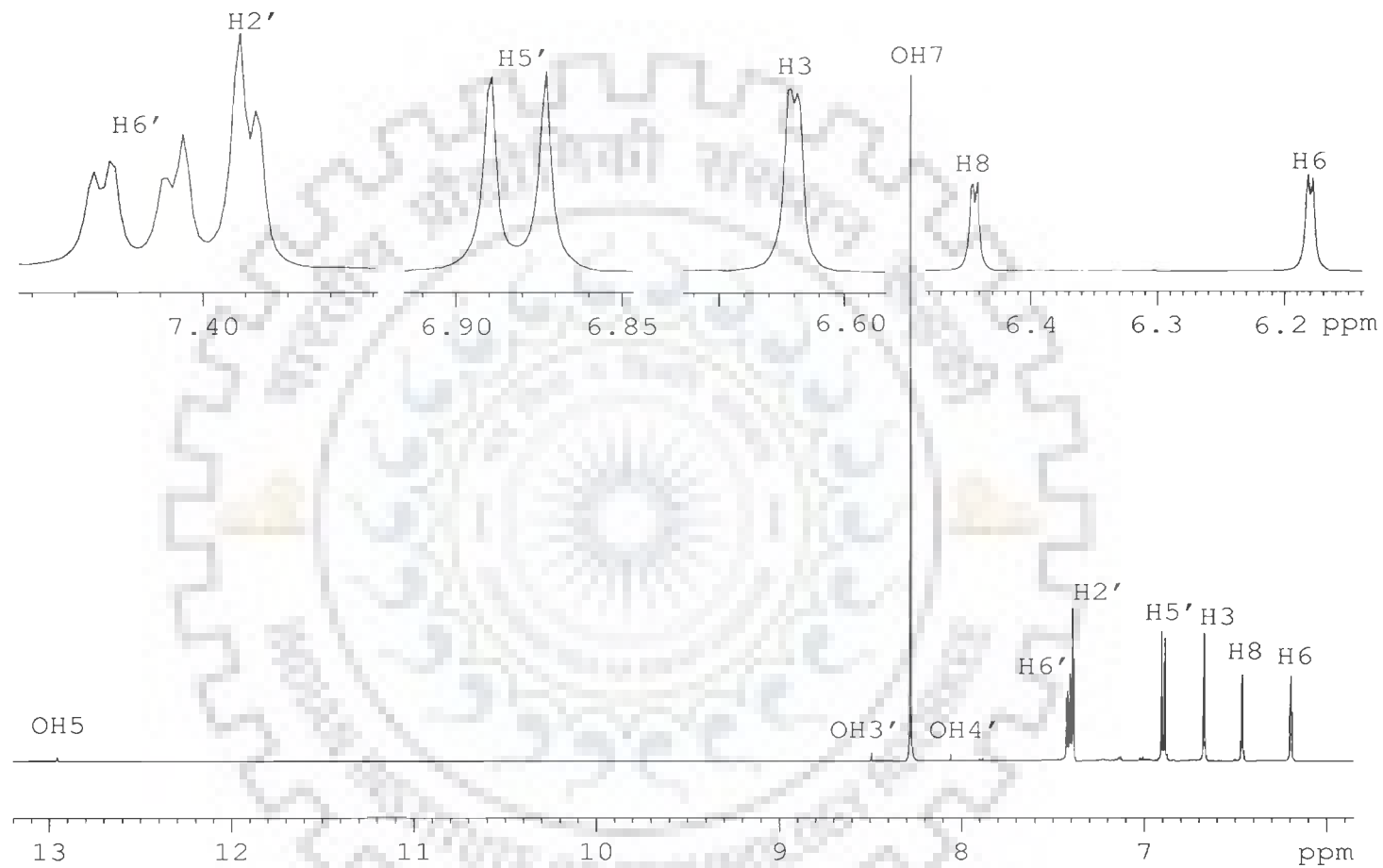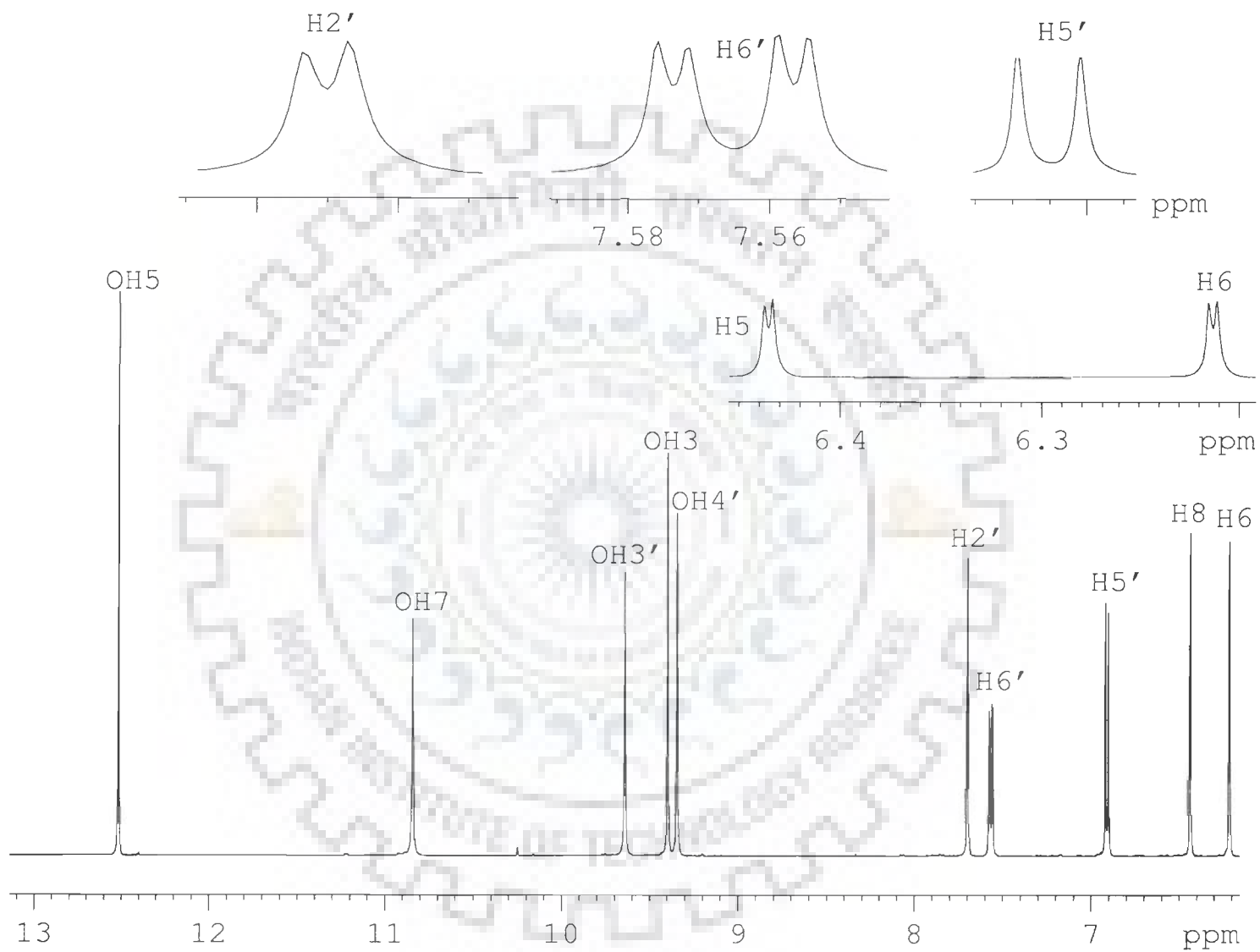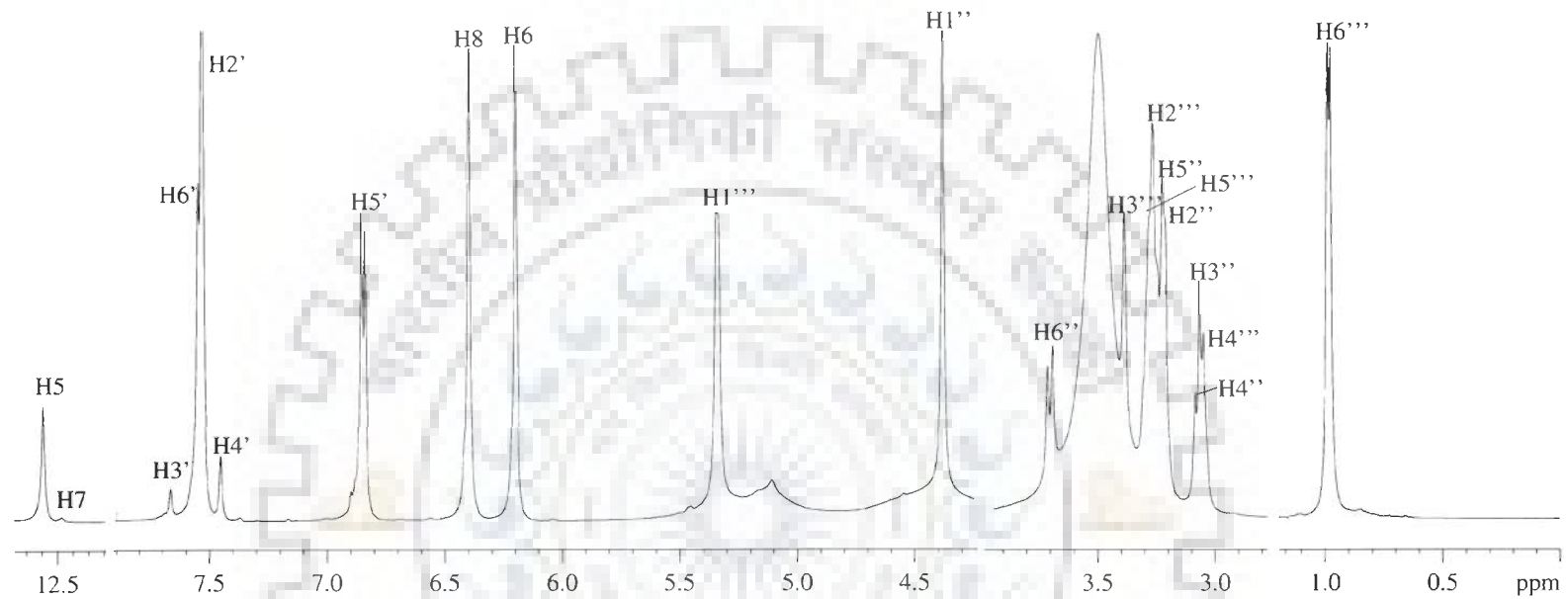(b) R= OH   Quercetin

(c) Rutin

(d) Genistein

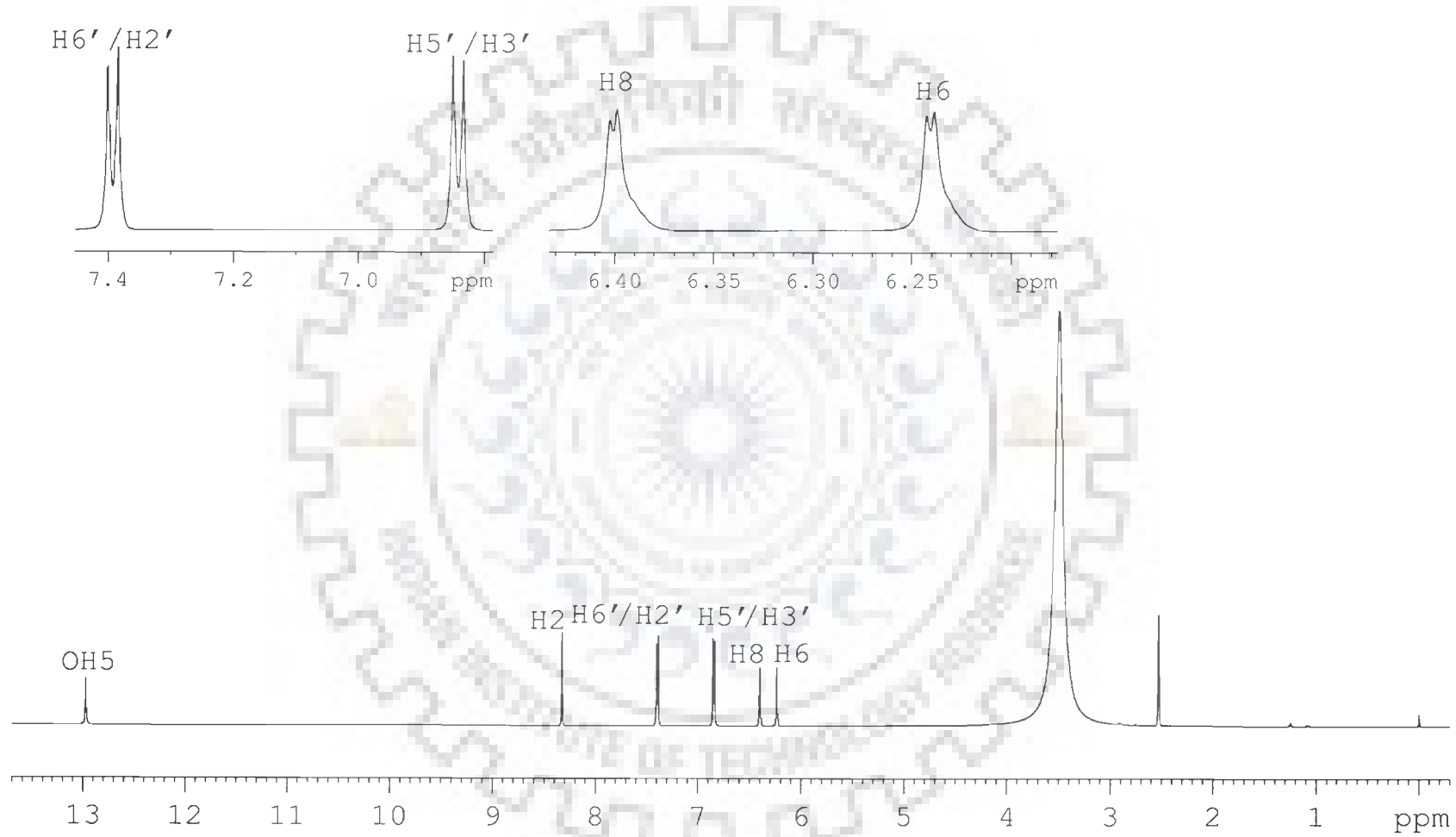Fig. 4.1: Molecular structure of (a) luteolin (b) quercetin (c) rutin and (d) genistein.

Fig. 4.2: Proton NMR spectra of luteolin in d-DMSO at 298 K.

Fig. 4.3: Proton NMR spectra of quercetin in d-DMSO at 298 K.

Fig. 4.4: Proton NMR spectra of rutin in d-DMSO at 298 K.

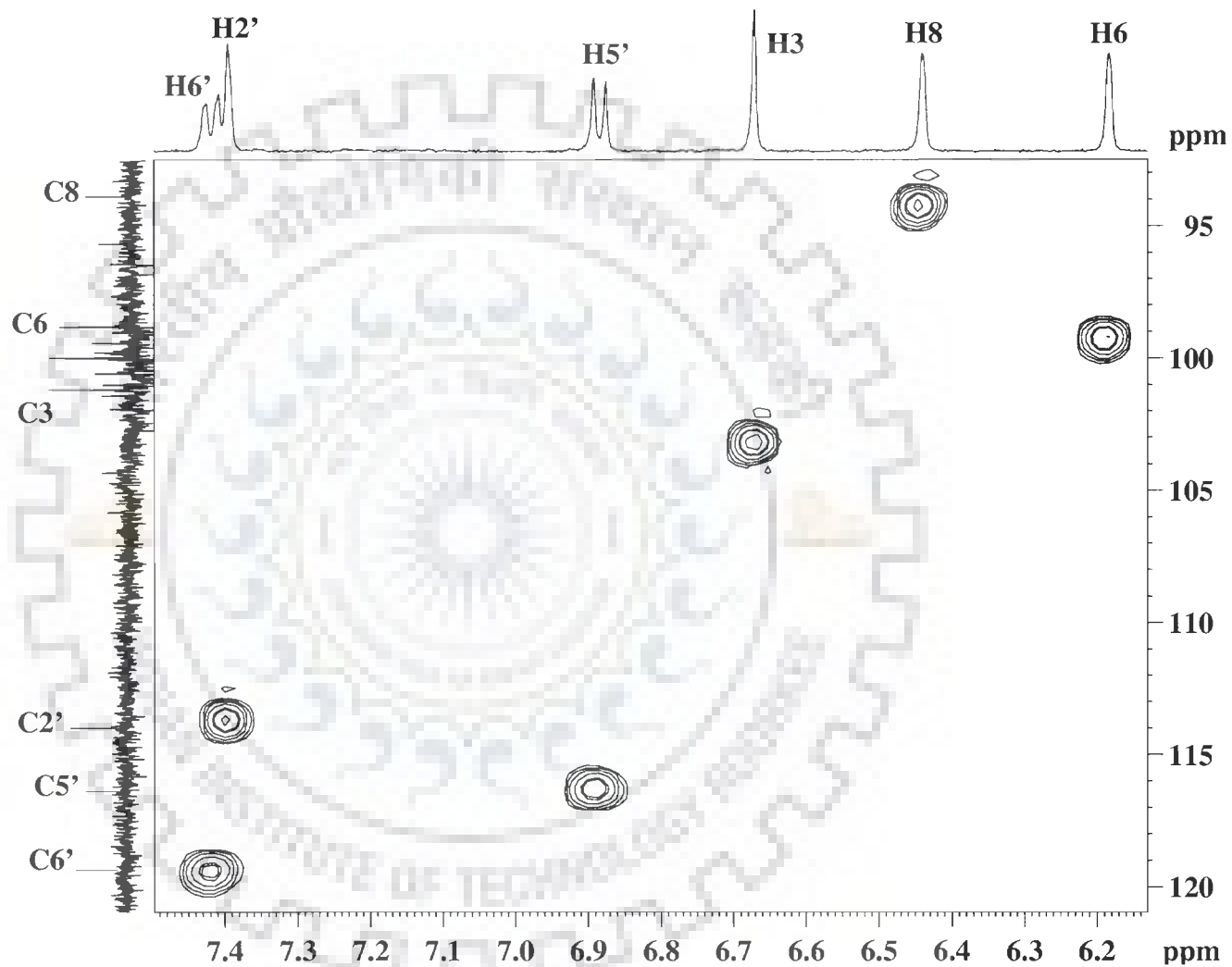**Fig. 4.5: Proton NMR spectra of genistein in d-DMSO at 298 K.**

Fig. 4.6a: HSQC spectra of luteolin in DMSO showing ^{1}H-^{13}C single bond correlations.

124
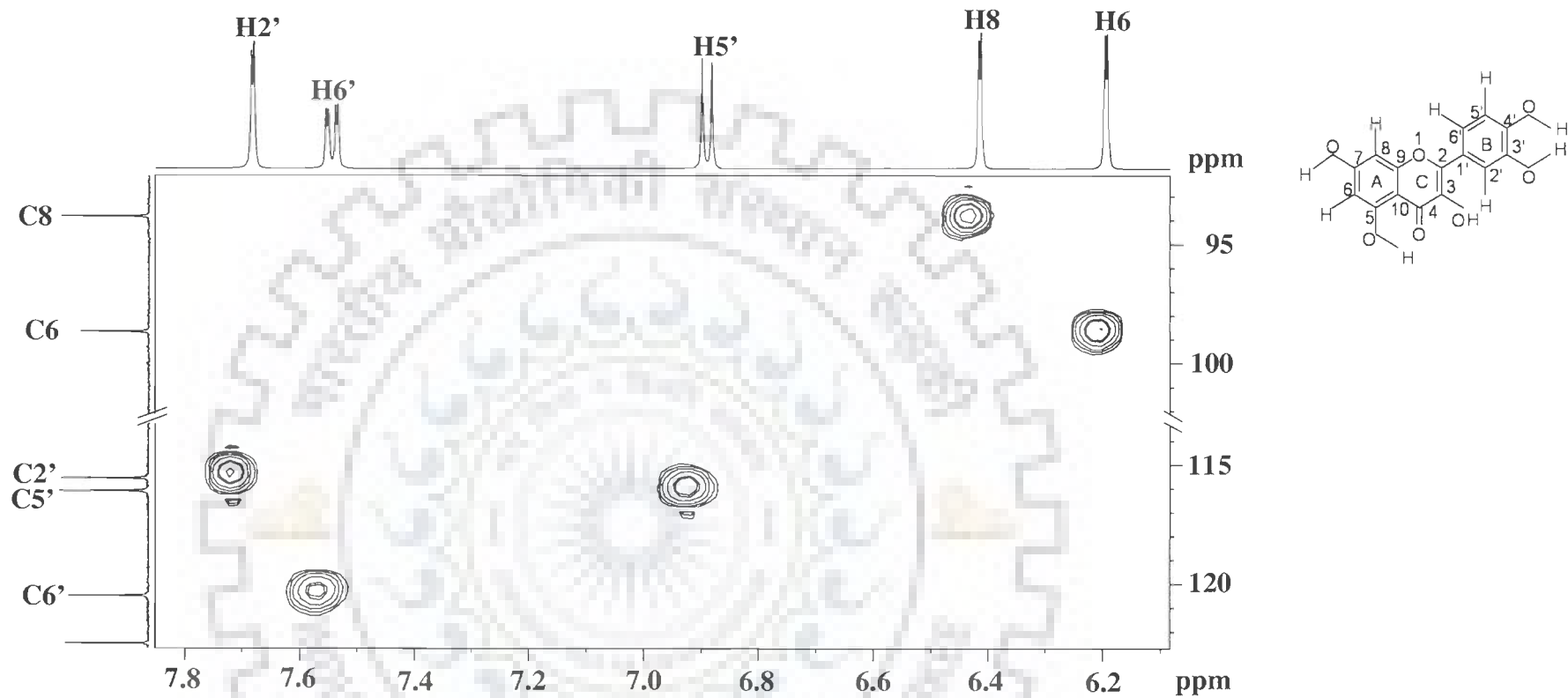
Fig. 4.6b: HSQC spectra of quercetin in DMSO showing ^1H-^{13}C single bond correlations.
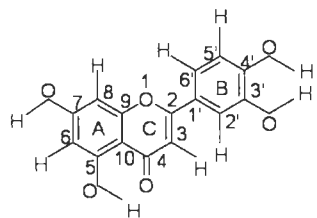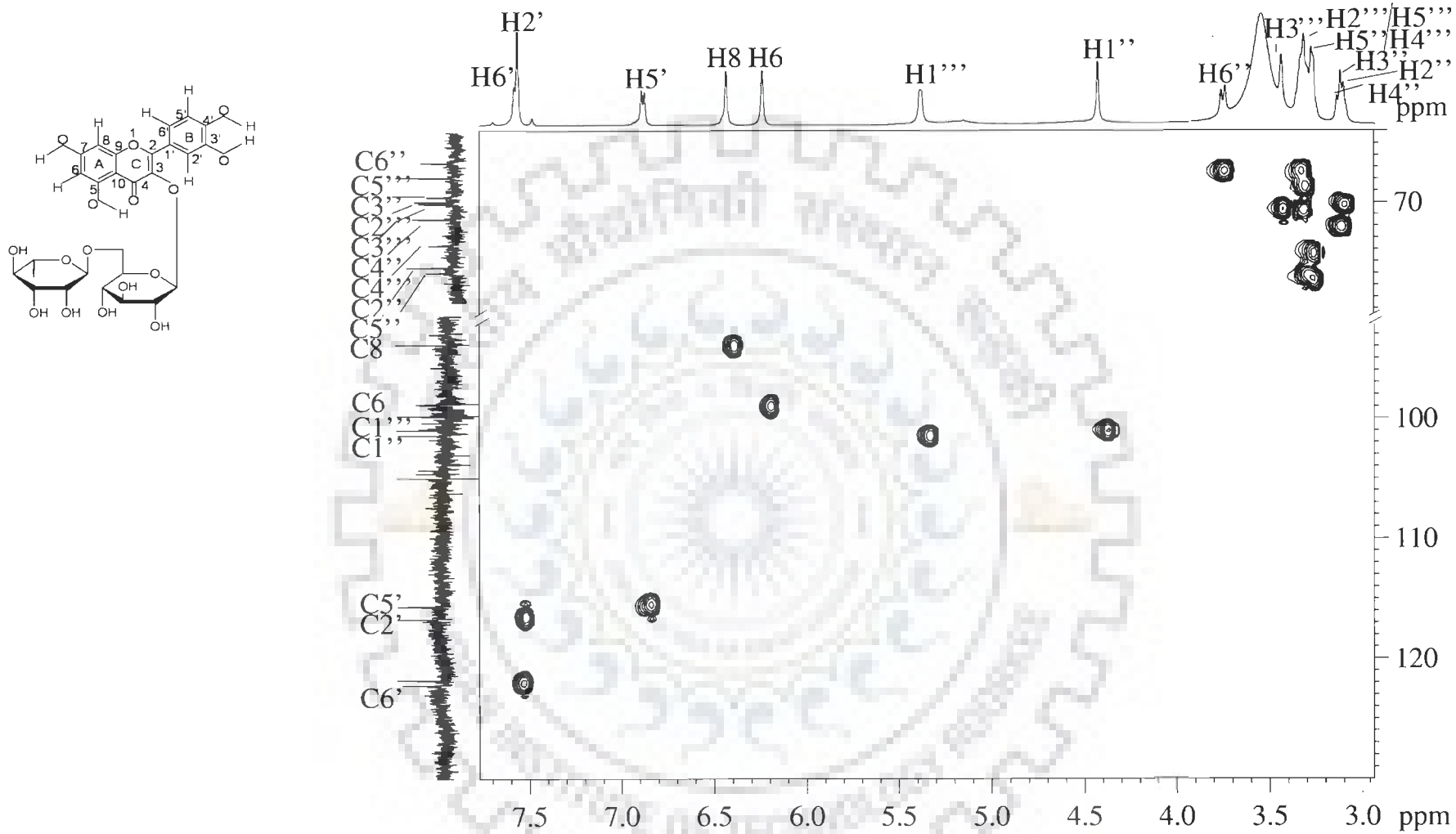
Fig. 4.6c: HSQC spectra of rutin in DMSO showing ^1H-^{13}C single bond correlations.
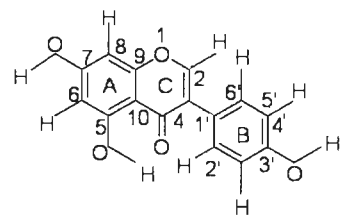
Fig. 4.6d: HSQC spectra of genistein in DMSO showing ^{1}H-^{13}C single bond correlations.

Fig. 4.7a: HMBC spectra of luteolin in DMSO showing ¹H-¹³C single bond correlations.

128

Fig. 4.7b: HMBC spectra of querectin in DMSO showing ^{1}H -^{13}C multiple bond correlations

Fig. 4.7c: (i) HMBC spectra of rutin in DMSO showing ^1H -^{13}C multiple bond correlations

Fig. 4.7c: (ii)
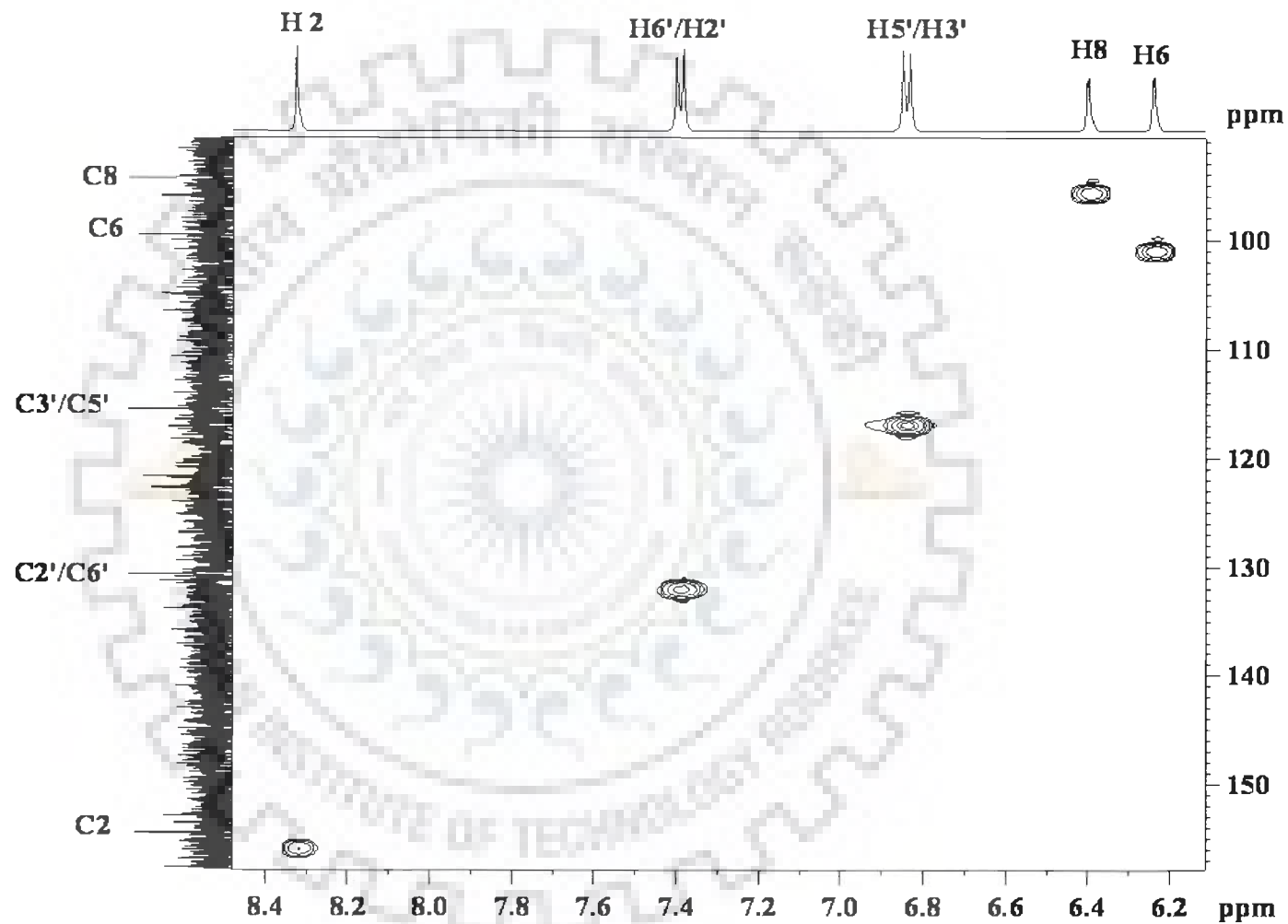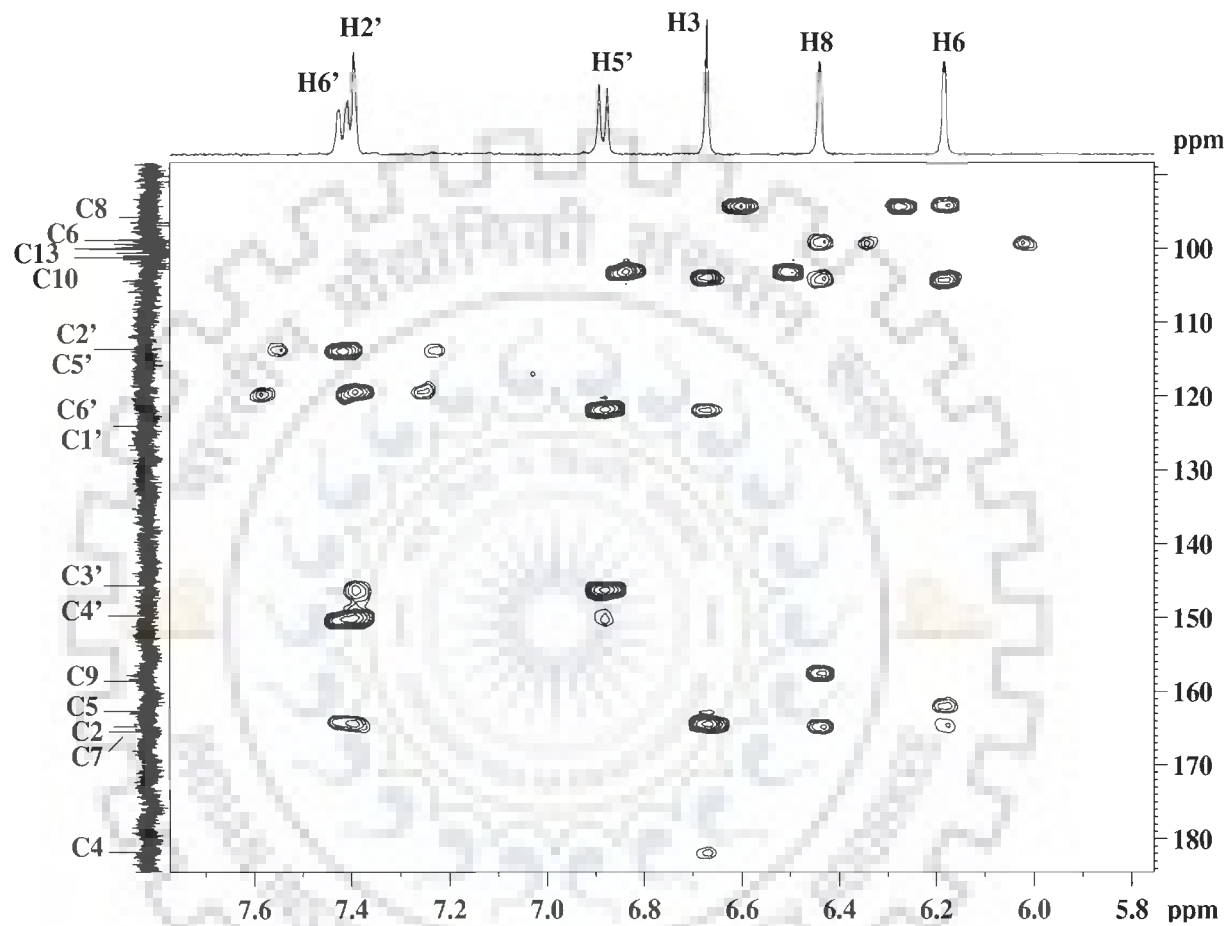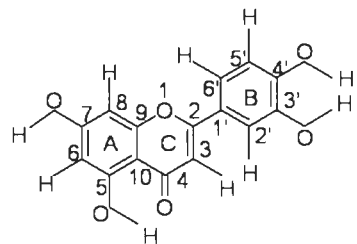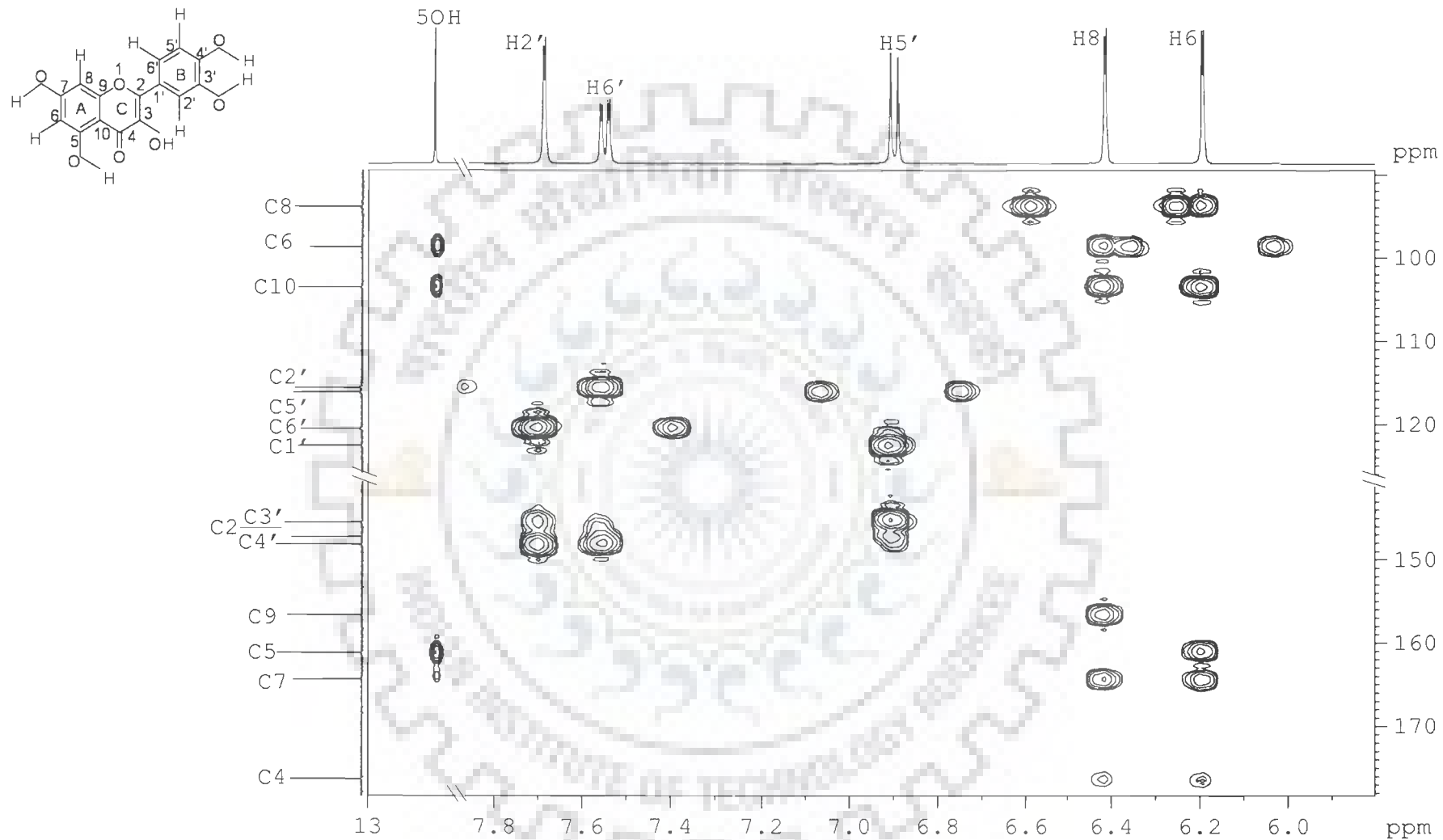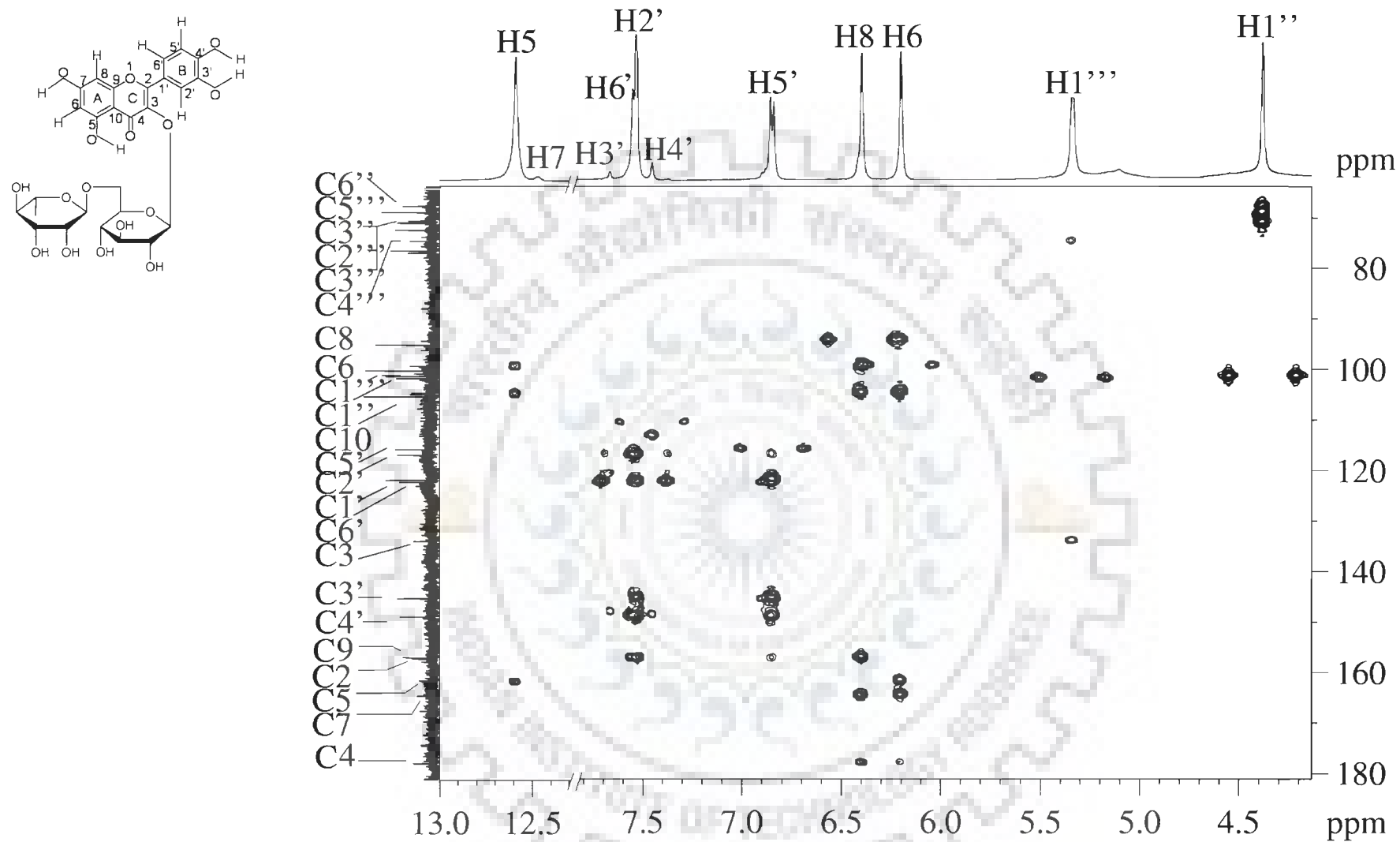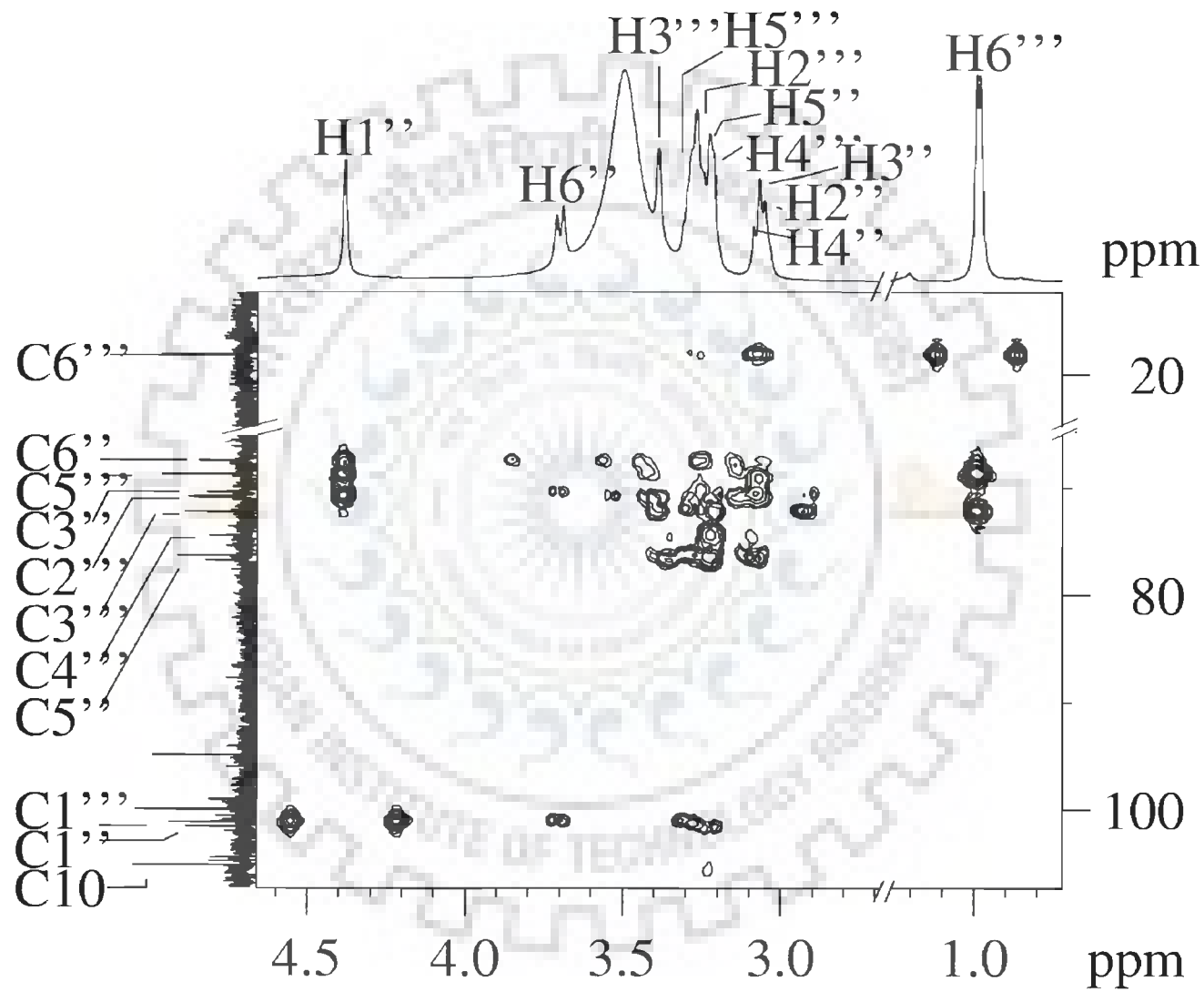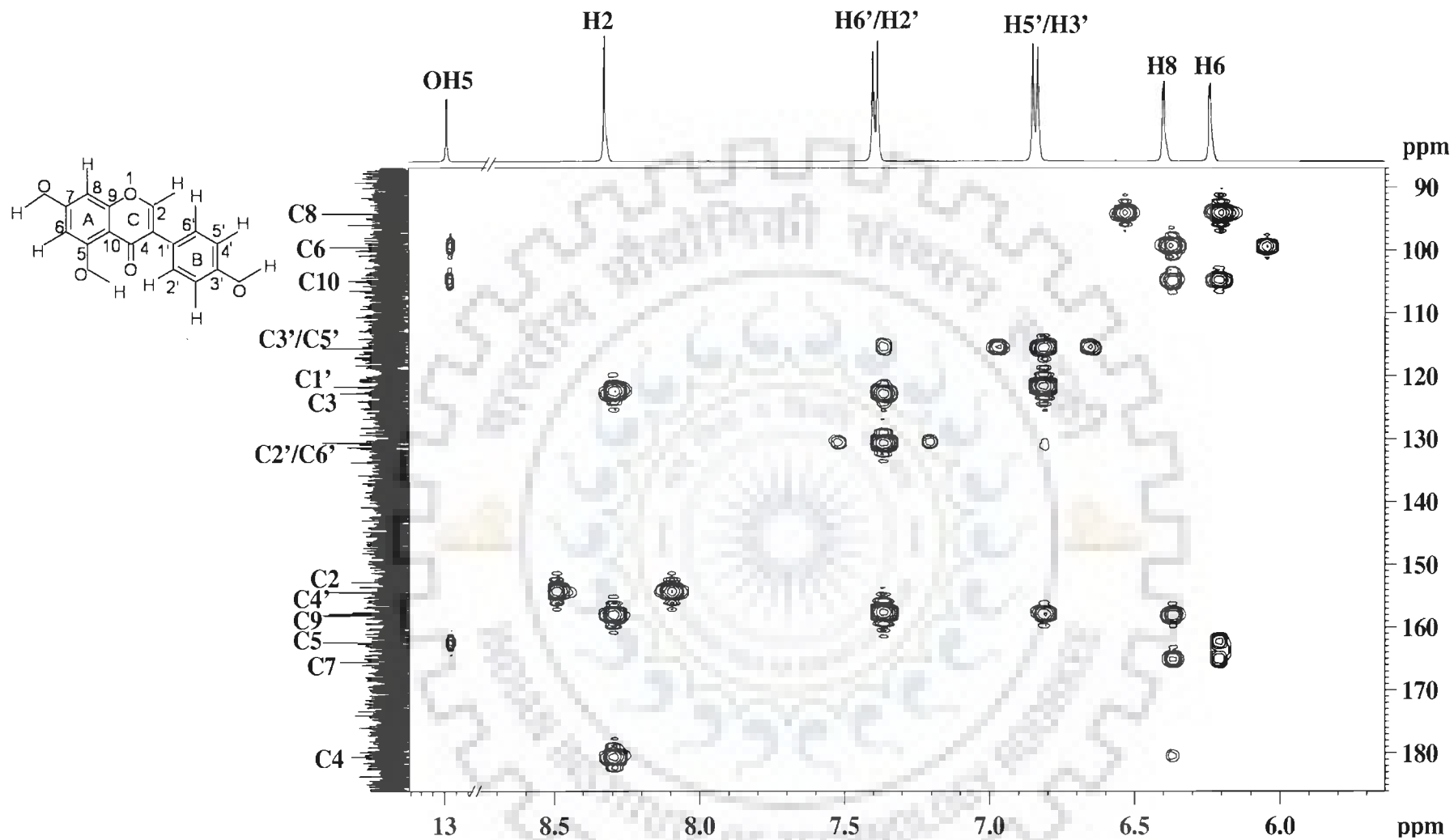
Fig. 4.7d: HMBC spectra of genistein in DMSO showing ^1H -^{13}C multiple bond correlations

Table 4.1a: Comparison of observed Proton chemical shift (ppm) of luteolin, quercetin, rutin and genistein with the experimental results reported in literature along with present calculated chemical shift (ppm) with 6-311G wave function by GIAO method**

Proton	Luteolin						Quercetin				
	Theoretical		Experimental				Theoretical		Experimental		
	B3LYP/ 6-311G** Gas Phase	B3LYP/ 6-311G** DMSO	Present NMR experiment DMSO	Nissler et al. 2004 DMSO	Owen et al. 2003 CD₃OD: DMSO (3:1)	Park et al. 2007 DMSO	B3LYP/ 6-311G** Gas Phase	B3LYP/ 6-311G** DMSO	Present NMR experiment DMSO	Nickavar et al. 2003	Spencer et al. 2003
H2'	7.081	7.496	7.423	7.38	7.392	7.39	7.473	7.846	7.685	7.78	7.715
H3'	3.603	6.329	8.527	-	-	9.90	3.479	6.3558	9.375	-	9.391
H4'	5.323	6.558	8.091	-	-	9.40	5.128	6.2845	9.596	-	9.625
H5'	7.166	7.254	6.929	6.88	6.919	6.89	7.139	7.3565	6.902	6.95	6.919
H6'	7.895	7.871	7.436	7.40	7.396	7.40	8.529	8.3586	7.543	7.65	7.575
H3	6.332	6.660	6.700	6.65	6.582	6.65	7.441	7.3461	-	-	9.337
H5	12.970	13.271	12.98	-	-	12.97	4.289	12.9777	12.504	-	12.509
H6	5.963	6.30	6.184	6.18	6.211	6.18	5.485	6.4826	6.192	6.26	-
H7	4.054	6.779	8.311	-	-	10.80	3.841	6.7706	10.788	-	10.813
H8	6.412	6.541	6.494	6.43	6.457	6.43	6.551	6.8641	6.417	6.41	-

Table 4.1b:

Proton	Rutin				Genistein			
	Theoretical		Experimental		Theoretical		Experimental	
	B3LYP/6-311G**	B3LYP/6-311G** DMSO	Present NMR experiment DMSO	Salvica et al. 2004	B3LYP/6-311G**	B3LYP/6-311G** DMSO	Present NMR experiment DMSO	Mazurek et al. 1998
H2	-	-	-	-	7.77	8.84	8.33	8.3
H2'	7.730	7.45	7.55	7.20	8.15	8.88	7.38	7.3
H3'	7.132	7.60	7.70	11.12	6.64	7.10	6.83	6.8
H4'	5.282	7.38	7.48	10.44	3.74	7.13	9.70	9.6
H5'	3.702	6.05	6.95	6.86	7.05	7.27	6.83	-
H6'	8.497	7.21	7.53	7.20	7.23	7.95	7.38	-
H5	12.91	12.54	12.75	12.91	13.03	12.33	12.98	12.9
H6	5.953	5.95	6.18	6.10	6.01	6.60	6.24	6.2
H7	4.036	12.36	12.50	12.73	4.11	7.09	-	10.9
H8	6.403	6.40	6.40	6.40	6.40	6.83	6.40	6.3

Table 4.1c: Comparison of J-coupling of protons of luteolin, quercetin, rutin and genistein with results reported in literature

Proton	Luteolin Our Result	Luteolin Owen *et al.* 2003 (21)	Quercetin Our Result	Rutin Our Result	Genistein Our Result
H6	6.18 (d, 1.91)	6.21 (dd, 2.13)	6.19 (d, 1.91)	-	6.24 (d, 2.01)
H8	6.49 (d, 1.98)	6.45 (d, 2.13)	6.41 (d, 1.91)	-	6.40 (d,2.05)
H2'	7.42 (d, 2.30)	7.39 (dd, 2.30)	7.68 (d, 2.20)	-	7.38 (d, 8.58)
H5'	6.93 (d, 8.21)	6.91 (dd, 8.91)	6.90 (d, 8.50)	6.90 (d, 8.13)	6.83 (d, 8.68)
H6'	7.44 (dd, 8.20, 2.51)	7.39 (dd, 8.91)	7.54 (dd,8.6, 2.09)	7.53 (dd, 8.23, 1.97)	7.38 (dd, 8.58, 1.95)
H3	6.67 (d, 1.83)	-	-	-	-
H1''	-	-	-	5.34 (d, 7.05)	-

Table 4.2a: Comparison of observed carbon chemical shift (ppm) of luteolin and quercetin with the experimental results reported in literature along with present calculated chemical shift (ppm) with 6-311G wave function by GIAO method**

Carbon	Luteolin Theoretical		Luteolin Experimental					Quercetin Theoretical			Quercetin Experimental			
	B3LYP/6-311G** Gas Phase	B3LYP/6-311G** DMSO	Present NMR experiment DMSO	Nissler et al. 2004 (20) DMSO	Owen et al. 2003 CD$_3$OD:DMSO 3:1	Wawer & Zielinska 2001 (25) DMSO	Kumari et al. 1986 DMSO	B3LYP 6-311G** Gas Phase	B3LYP 6-311G** DMSO	Olejniczak and Potrzebowski 2004 B3PW91/6-311G**	Present NMR experiment DMSO	Wawer & Zielinska 2001 DMSO	Markham, 1977 DMSO	Lallemand and Duteil 1977 DMSO
C2	168.549	160.36	164.0	164.4	165.44	163.9	163.9	146.71	144.89	144.1	147.23	146.9	146.9	123.0
C3	108.187	100.60	103.1	103.6	103.88	102.5	102.9	145.05	141.46	134.8	136.19	135.9	135.5	136.5
C4	184.397	175.47	182.1	182.4	183.11	182.5	181.7	173.05	172.06	172.3	176.28	176.0	175.8	176.5
C5	172.004	158.24	162.0	161.6	162.70	161.8	161.5	166.37	164.17	161.3	161.18	160.9	160.7	161.0
C6	100.880	94.76	99.2	100.0	99.74	98.7	98.9	98.21	99.14	88.9	98.66	98.3	98.2	99.5
C7	169.363	157.43	164.6	163.4	165.30	163.2	164.1	166.93	166.92	159.9	164.34	164.0	163.9	166.0
C8	96.278	89.75	94.5	95.2	94.75	93.6	93.9	99.07	95.54	88.8	93.83	93.5	93.3	94.5
C9	164.686	153.02	158.5	157.4	158.81	158.0	157.3	165.61	162.54	157.1	156.18	156.2	156.2	156.7
C10	109.549	103.21	104.0	105.8	104.98	103.9	103.8	109.38	105.90	101.8	103.48	103.2	103.1	104.0
C1'	128.779	118.54	122.0	121.8	123.22	122.3	121.6	129.31	126.28	121.9	122.47	122.2	122.1	123.0
C2'	113.340	108.27	113.5	105.8	114.04	112.8	113.4	112.16	112.08	108.0	115.55	115.3	115.3	116.5
C3'	149.682	139.81	146.0	146.3	146.65	145.6	145.8	149.33	148.61	146.8	145.49	145.2	145.0	145.7
C4'	156.310	144.81	150.0	150.4	150.51	149.6	149.7	153.76	151.33	148.7	148.13	147.8	147.6	148.1
C5'	120.540	111.48	115.5	116.5	114.04	115.4	116.1	120.50	117.48	109.6	116.08	115.8	115.6	116.1
C6'	127.133	116.76	120.0	119.7	119.96	118.9	119.0	130.37	125.04	116.0	120.48	120.1	120.0	121.0

Table 4.2b. Observed Carbon chemical shift (ppm) of rutin and genistein with the experimental results reported in literature and with present calculated chemical shift (ppm) with 6-311G wave function by GIAO method**

Rutin

Carbon	Theoretical		Experimental		
	B3LYP/ 6-311G**	B3LYP/ 6-311G** DMSO	Present NMR experiment (DMSO)	Xiao *et al.* 2005 (DMSO)	Lallemand & Duteil 1977 (DMSO)
C2	162.77	155.64	156.89	156.3	156.9
C3	142.24	132.98	133.78	133.2	133.9
C4	183.13	198.86	201.96	177.2	178.0
C5	171.95	168.50	161.00	156.5	161.4
C6	100.21	99.00	99.03	98.6	99.7
C7	169.28	165.14	164.75	164.0	166.3
C8	96.03	94.78	94.88	93.5	94.8
C9	163.7	172.21	178.25	161.1	156.7
C10	109.61	106.40	104.00	103.8	104.9
C1'	129.38	122.04	121.64	121.1	122.0
C2'	127.96	116.65	116.65	115.1	116.0
C3'	119.62	145.07	145.07	144.6	145.2
C4'	155.22	148.71	148.71	148.3	148.9
C5'	149.04	115.62	115.62	116.2	117.1
C6'	119.19	122.07	122.07	121.5	122.5
C1''	106.36	102.38	101.59	101.0	102.1
C2''	78.27	76.28	76.30	74.0	75.1
C3''	83.55	72.50	70.36	70.4	77.6
C4''	80.27	72.40	72.19	69.8	71.3
C5''	78.77	77.45	76.74	75.7	77.0
C6''	70.65	68.10	67.44	66.8	68.1
C1'''	107.43	102.13	101.16	100.6	101.7
C2'''	74.42	71.23	70.73	70.3	71.5
C3'''	82.45	71.34	70.89	70.4	71.5
C4'''	82.44	71.68	74.42	71.7	73.5
C5'''	78.78	67.54	68.67	68.4	69.4
C6'''	18.67	18.15	18.16	18.4	19.1

Genistein

Carbon	Theoretical			Experimental		
	B3LYP/ 6-311G** (Gas Phase)	B3LYP/ 6-311G** DMSO	Zielinska *et al.* 2008 B3LYP/ 6-31G** (Gas Phase)	Present NMR experiment (DMSO)	Kozerski *et al.*, 2003 (DMSO)	Mazurek *et al.* 1998 (DMSO)
C2	157.86	167.93	142.25	154.40	153.7	153.1
C3	131.16	136.08	109.72	122.72	124.6	121.3
C4	184.12	191.02	171.66	180.64	182.2	180.3
C5	172.69	178.85	158.44	162.65	160.4	162.2
C6	100.97	109.79	82.24	100.84	97.8	99.0
C7	169.45	178.48	157.29	164.20	161.2	164.3
C8	96.63	105.86	73.18	94.18	95.0	93.7
C9	164.83	171.16	151.58	157.83	157.3	157.7
C10	110.27	115.87	87.04	105.04	104.2	104.7
C1'	129.97	136.09	110.86	121.75	121.5	122.7
C2'	138.71	143.96	123.84	130.63	133.9	130.0
C3'	116.99	124.86	102.74	115.53	116.9	115.1
C4'	165.12	174.61	146.85	155.63	156.4	157.5
C5'	119.72	127.36	99.64	115.53	116.0	-
C6'	132.42	140.55	128.18	130.63	130.2	-

Table 4.3: Observed correlations of Carbon atoms with specific Protons in HSQC and HMBC spectra of luteolin, quercetin, rutin and genistein.

	Luteolin				Quercetin				Rutin				Genistein			
	Correlation with proton obtained from HSQC	Correlation with proton obtained from HMBC			Correlation with proton obtained from HSQC	Correlation with proton obtained from HMBC			Correlation with proton obtained from HSQC	Correlation with proton obtained from HMBC			Correlation with proton obtained from HSQC	Correlation with proton obtained from HMBC		
		ss*	m*	w*		ss*	m*	w*		ss*	m*	w*		ss*	m*	w*
C2	-	H4'	-	-	-	OH3	H6', H2'	-	-	H6', H8	H3'	-	H2	-	-	-
C3	H3	H3	-	H3	-	OH3	-	-	-	-	-	-	-	-	-	-
C4	-	-	-	-	-	-	OH3	H6, H8, H5	-	H1''	H6	-	-	H2	H8	H6
C5	-	-	H6	-	-	OH5, H6	-	-	-	H6	-	-	-	-	H5, H6	
C6	H6	-	H6	H6	H6	OH5	H8	OH7	H6	-	-	-	H6	-	H5	-
C7	-	-	-	-	-	H6, H8	-	OH5	-	H8, H6	-	-	-	-	H6, H8	-
C8	H8	H8	-	H8	H8	-	H6	OH7	H8	-	-	-	H8	-	-	-
C9	-	H8	-	-	-	H8	-	-	-	H8, H6	-	-	-	-		
C10	-	H3, H6	H8	-	-	OH5, H6, H8	-	-	-	H8, H6	-	-	-	OH5, H6, H8	-	-
C1'	-	H5'	-	H3'	-	H5'	-	-	-	H3'	-	-	-	H3'/H5'	-	-
C2'	H2'	H6'	H2'	-	H2'	H6', H5'	OH3'	-	H2'	H3' H6'	-	-	H2'	H6'		
C3'	-	H6'	H2'	-	-	H5'	OH3'	H2', OH4'	-	-	-	-	H3'	H5'	H2'/H6'	-
C4'	-	H2'	-	H3'	-	H2', H6'	H5', OH3', OH4'	-	-	H6', H3'	-	-	-	H2, H2'/H6'	H6, H8	-
C5'	H5'	H3'	H2'	-	H5'	-	-	-	H5'	H6', H3'	-	-	H5'	H3'	H2'/H6'	
C6'	H6'	H2'	H6'	-	H6'	H2'	H5'	-	H6'	H2'	H3'	-	H6'	H2'	-	
C1''	-	-	-	-	-	-	-	-	H1''	CH₃	-	-	-	-	-	-
C2''	-	-	-	-	-	-	-	-	-	-	H1''	-	-	-	-	-
C3''	-	-	-	-	-	-	-	-	H3''	-	H1''	-	-	-	-	-
C4''	-	-	-	-	-	-	-	-	H4''	-	H1''	-	-	-	-	-
C5''	-	-	-	-	-	-	-	-	H5''	-	-	-	-	-	-	-
C6''	-	-	-	-	-	-	-	-	H6''	-	H1''	-	-	-	-	-
C1'''	-	-	-	-	-	-	-	-	H1'''	-	H1''	-	-	-	-	-
C2'''	-	-	-	-	-	-	-	-	H2'''	-	H1''	-	-	-	-	-
C3'''	-	-	-	-	-	-	-	-	H3'''	-	H1''	-	-	-	-	-
C4'''	-	-	-	-	-	-	-	-	H4'''	-	-	-	-	-	-	-
C5'''	-	-	-	-	-	-	-	-	H5'''	-	H1''	-	-	-	-	-

* Intensity of cross peaks: ss - Very intense, m -Fairly intense, w -Weak intense
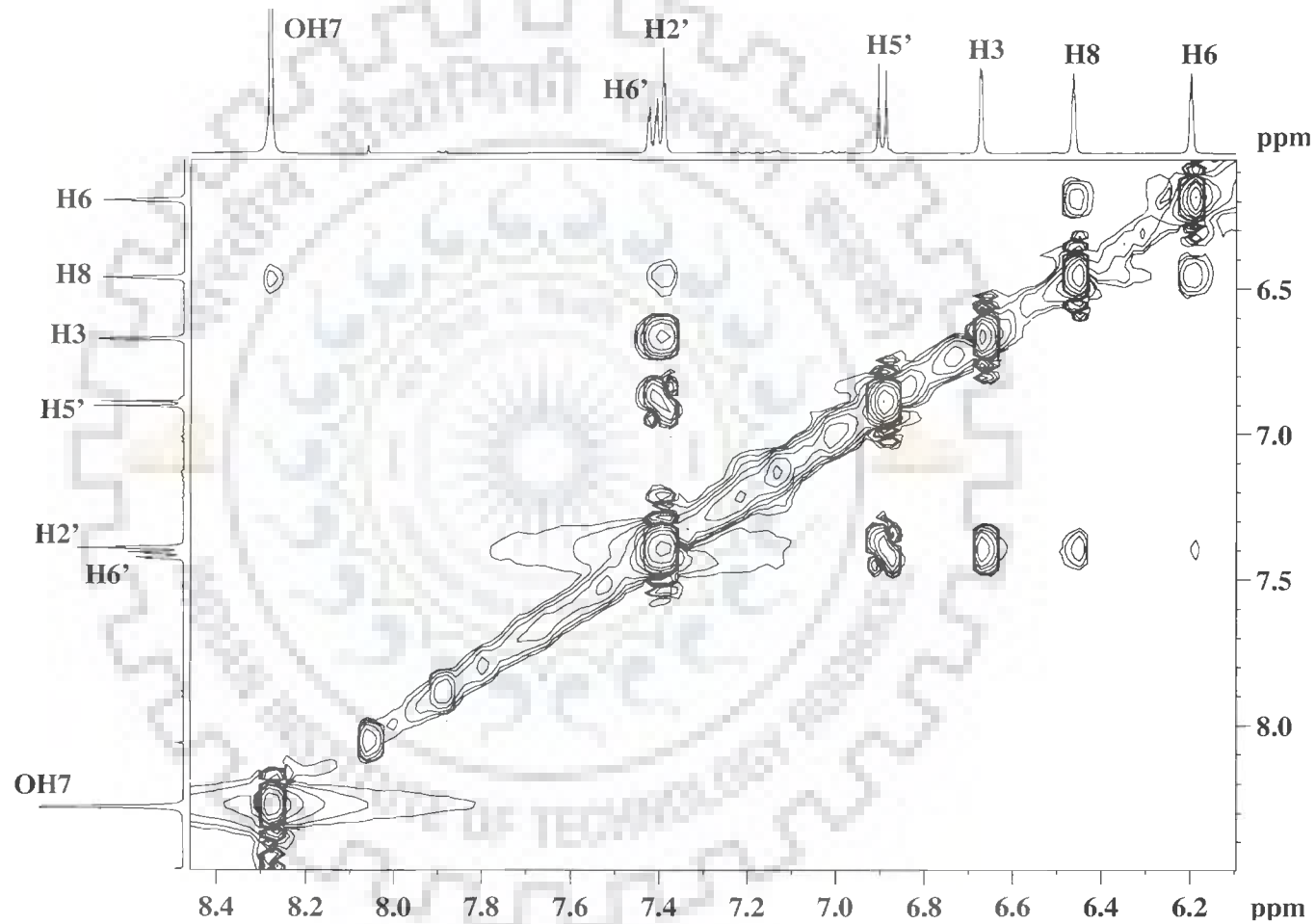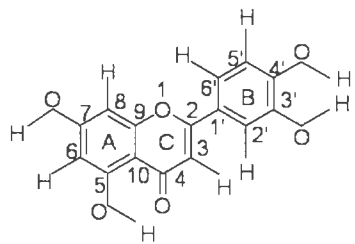
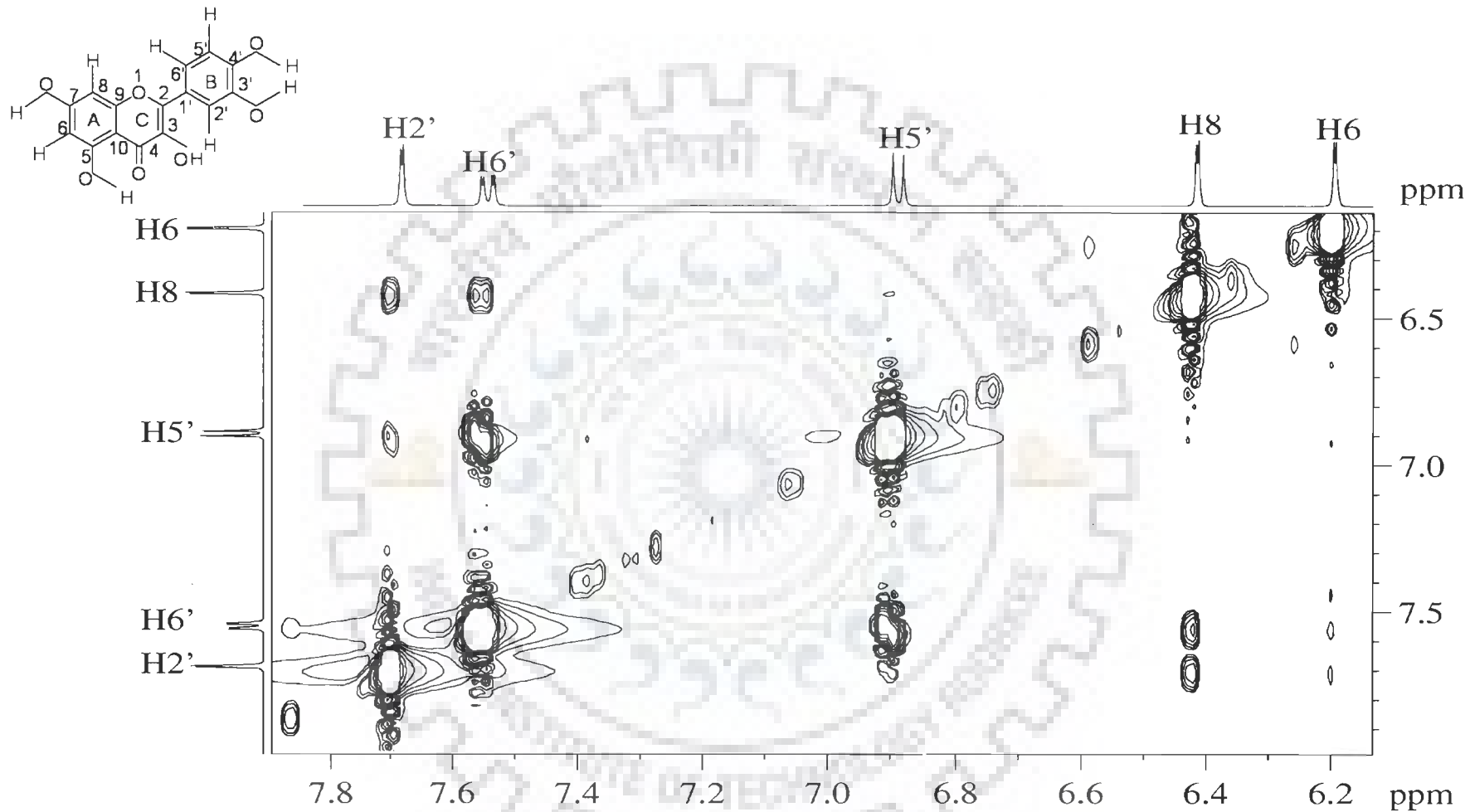Fig. 4.8(a): ROESY spectra of luteolin in DMSO showing interproton contacts.

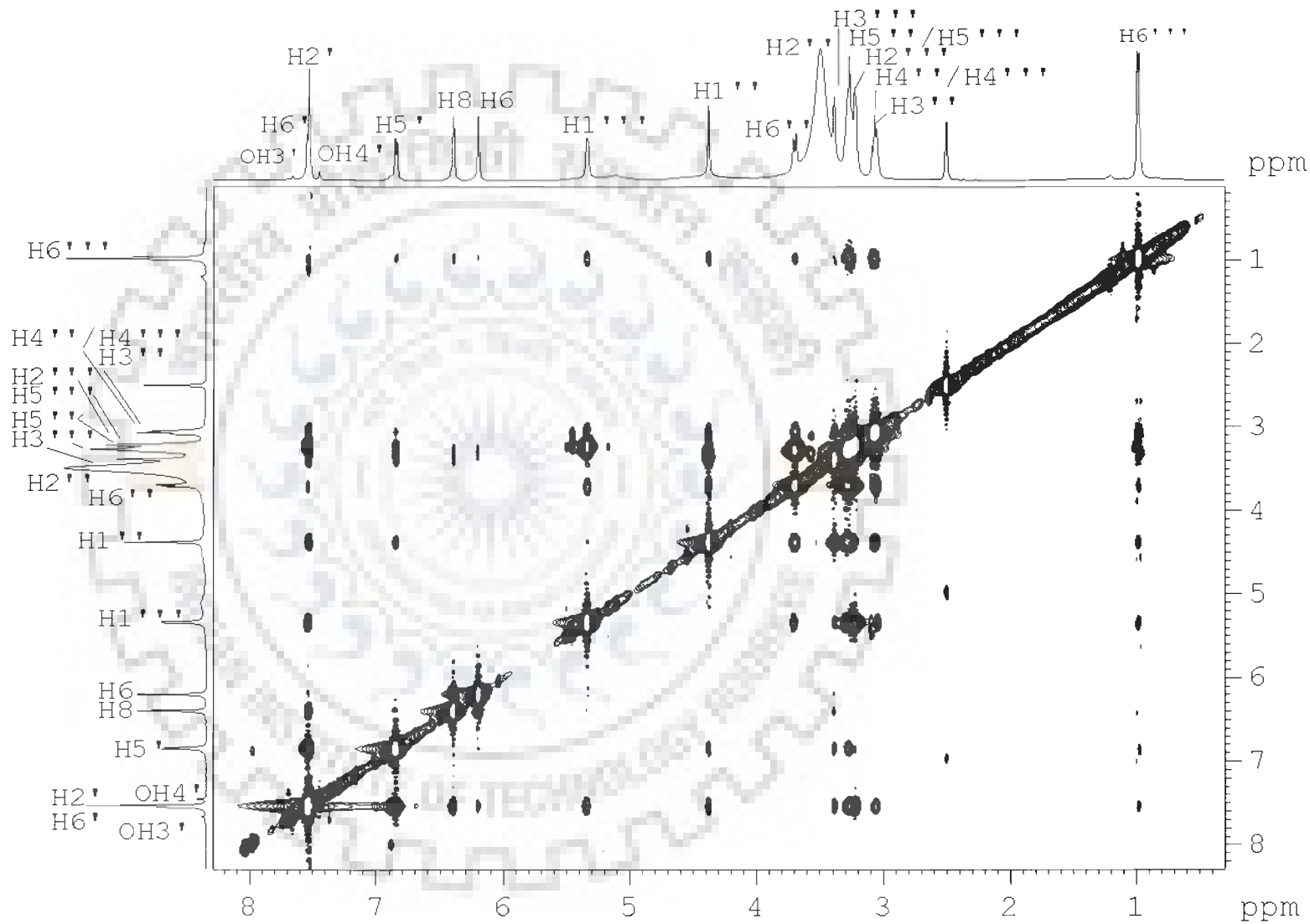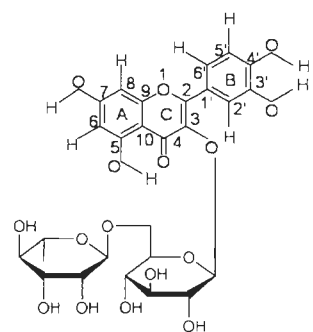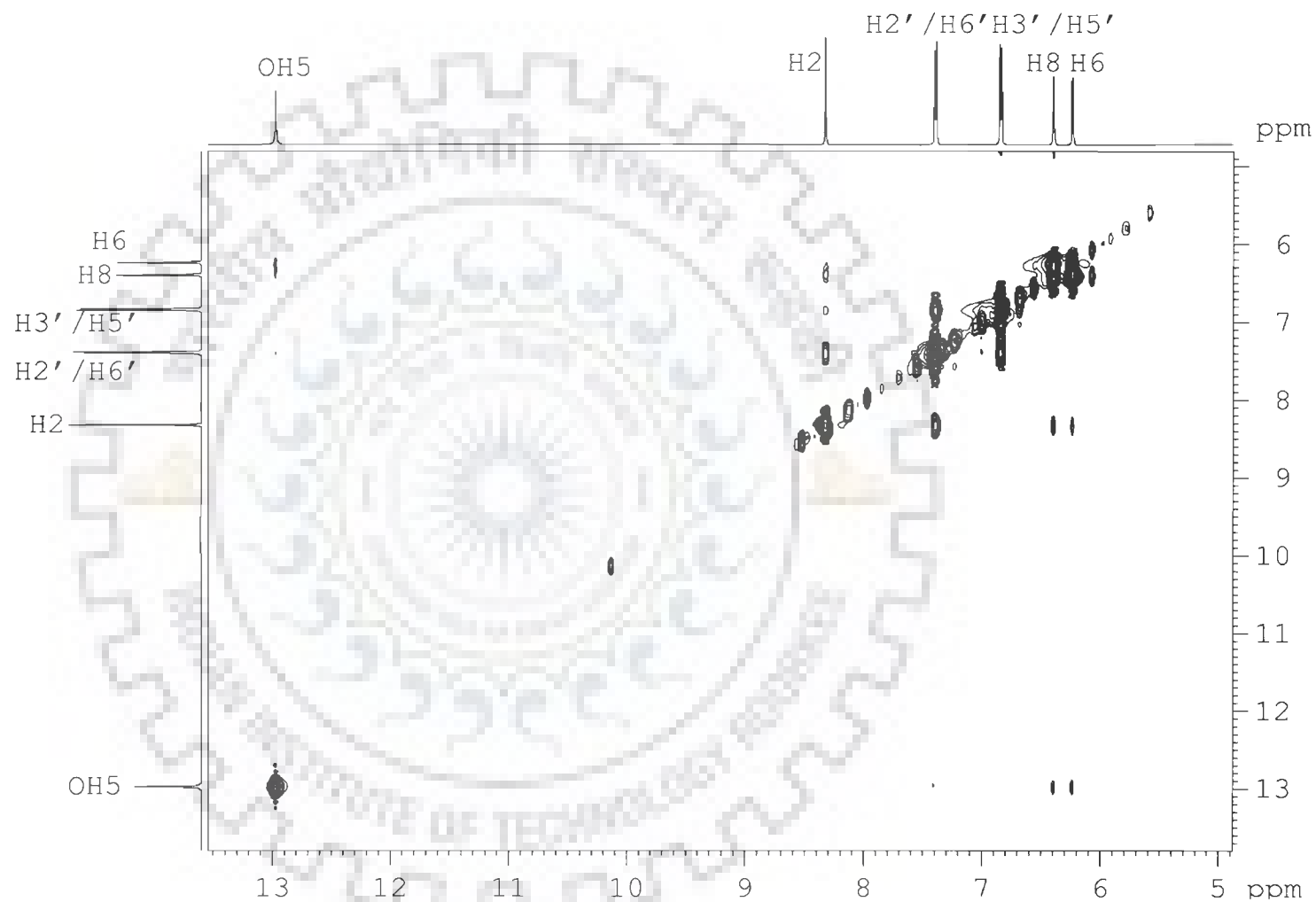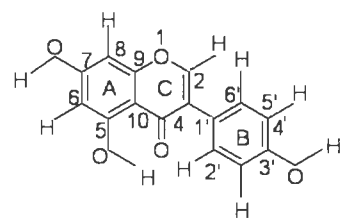Fig. 4.8(b): ROESY spectra of quercetin in DMSO showing interproton contacts.

Fig. 4.8(c) ROESY spectra of rutin in DMSO showing interproton contacts

Fig. 4.8(d): ROESY spectra of genistein in DMSO showing interproton contacts

Table 4.4a: Connectivities and interproton distances (Å) from ROESY spectra of luteolin and quercetin used in restrained molecular dynamics. The corresponding distances obtained from optimized rMD are also shown.

S. No.	Luteolin				Quercetin			
	Connectivities	Interproton distance (Å)	Distance in rMD structure (Å)		Connectivities	Interproton distance (Å)	Distance in rMD structure (Å)	
			Anti	Syn			Anti	Syn
1.	H2'-H8	3.92	4.19	6.35	H2'-H8	4.13	4.36	6.30
2.	H5'-H6'*	2.45	2.45	2.45	H5'-H6'*	2.45	2.45	2.45
3.	H5'-H2'	4.98	4.98	4.98	H5'-H2'	4.91	4.98	4.98
4.	H2'-H3	2.21	4.41	2.51	H6'-H8	3.97	6.24	4.28
5.	H6-H2'	7.60	7.55	8.38	H6-H8	4.26	4.31	4.31
6.	5OH-6H	3.99	3.51	3.51	H6-H2'	6.45	7.64	8.26
7.	5OH-3H	4.39	4.45	4.43	OH4'-H2'	5.20	5.29	5.29
8.	-	-	-	-	OH3'-H5'	4.30	4.50	4.50

Table 4.4b: Connectivities and interproton distances (Å) from ROESY spectra of rutin and genistein used in restrained molecular dynamics. The corresponding distances obtained from optimized rMD are also shown

S. No.	Rutin			S. No.	Connectivities	Interproton distance (Å)	Distance in rMD structure (Å)	S. No.	Genistein		
	Connectivities	Interproton distance (Å)	Distance in rMD structure (Å)						Connectivities	Interproton distance (Å)	Distance in rMD structure (Å)
1.	H6'-H6'''	5.8	5.84	14.	H6'''-H8	6.42	6.14	1.	H2-H8	4.82	4.51
2.	H6''-H2'	5.54	5.74	15.	H6'''-H6	5.65	5.83	2.	H2-H2'/H6'	2.92	2.67
3.	H1''-H2'	4.37	3.92	16.	H6'''-H1'''	4.52	4.59	3.	H3'/H5'-H2'/H6	2.45	2.46
4.	H1'''-H2'	3.93	5.73	17.	H6'''-H1''	4.86	5.15	4.	OH5-H8	5.78	6.24
5.	H1''-H5'	5.14	5.75	18.	H6'''-H6''	5.21	5.65	5.	OH5-H6	3.67	3.54
6.	H3'''-H5'	3.91	4.74	19.	H6'''-H5''	2.94	3.61	6.	H2-H6	6.50	7.07
7.	H3'''-H8	5.17	4.97	20.	H6'''-H4''	3.12	3.59				
8.	H5'''-H6	5.36	5.79	21.	H4''-H5'	5.89	7.06				
9.	H2'''-H1''	2.11	2.22	22.	H6''-H1''	3.37	4.08				
10.	H5'''-H6''	2.35	2.47	23.	H6-H6'	5.46	7.63				
11.	H8-H2'	4.20	6.24	24.	H4'''-H1'''	6.01	4.68				
12.	H5'-H6'*	2.45	2.47	25.	H4'''-H1'''	3.78	4.02				
13.	H6'''-H5'	5.47	5.15	26.	H3'''-H6''	2.13	3.78				

*Reference

that the structure obtained is a minimum energy conformer. The minimum energy conformer is shown in Fig. 4.9(i).

4.1.2 Structural Parameters

We have calculated values for bond length, bond angle and dihedral angles for five basis sets ranging from minimal basis set 3-21G (data not shown) to 6-311G** for gas phase and solvent DMSO using DFT method with Becke's three parameter hybrid exchange functional (B3LYP) and HF methods whereas for solution phase only 6-311G** basis set was used. The calculated values showing basis set effects are not listed in tables.

The results of structural parameters for these molecules are shown in Table 4.5. It may be noted that as we move towards a better basis set, the difference between the calculated and experimental results narrow down due to the fact that polarization functions are found to be very effective. For the luteolin, quercetin, rutin and genistein molecule, we found that all the calculated bond lengths are very close to the present NMR experimental results and also compare reasonably well with the X-ray measurements reported in literature (Berton et al. 1975; Rossi et al., 1986; Jin et al., 1990; Mazurek et al., 1998; Cox et al. 2003); the difference lies within a few hundredth of an angstrom. But this trend is not seen in case of bond angles, the calculated bond angles are close to the X-ray measurements but differ with the present experimental results. The maximum variation in the calculated and measured values is less than 7° (gas phase), 2° (solvent); 8.9° (gas phase), 2.5° (solvent); 4.9° (gas phase), 0.9° (solvent) and 3.2° (gas phase), 2.5° (solvent) for luteolin, quercetin, rutin and genistein, respectively (Table 4.5a,b). From the bond length and bond angle analysis, we notice that such differences between calculated and measured values arise due to the fact that structurally the molecule is in dynamic state in solution phase (i.e. Ring B attached to

142

benzopyran ring) as compared to the gas phase optimized structure of the molecule. During restrained Molecular Dynamics simulation of these molecules, it is observed that the side chain phenyl ring (B) attached with a single bond is more flexible and rotate to go upside down. Other A and C ring of these molecule is planar and rigid during simulations (Fig. 4.9 i). In the conformation of minimum energy of luteolin, quercetin, rutin and genistein (Fig. 4.9 i, ii), the hydroxyl groups are oriented in such a way to maximize inter molecular hydrogen bond type interactions which play an important role in DNA binding. Luteolin has two intra molecular hydrogen bonds established between H5 of A-ring and the 4-keto group of C-ring and between the ortho-dihydroxyls in the B- ring, respectively while quercetin has one extra hydrogen bond between the 4-keto group of C-ring and H3. There are several reports which resolved the crystal structure of flavonoids and their derivatives (Cox *et al.* 2003; Jin *et al.* 1990; Cody and Luft, 1994). An X-ray structure determination of luteolin (Cox *et al.* 2003) and another flavonoid quercetin (Jin *et al.* 1990), showed that the benzopyran and phenyl ring are essentially planar. The dihedral angle between the two rings is 9º and that between the annellated rings is 6º (Wallet *et al.* 1988). However, from our study we assume that A and C annellated rings are planar while B ring is non planar as it rotate around the C2-C1' bond with torsional angle C1'-C2-O1-C9 in the solution - 157.6º, 179.6º and 173.5 and in gas phase 179.5º, 179.9º and 179.0 for luteolin, quercetin and rutin, respectively while for genistein the torsional angle C1'-C3-C2-O1 was found 177.0 º in gas phase and -179.4 º in solvent . Further, the rMD results based on the torsional angle C6'-C1'-C3-C4 for genistein and C2'-C1'-C2 -O1 for others depicts that these flavonoids exist in two major conformation *anti* and *syn* of almost
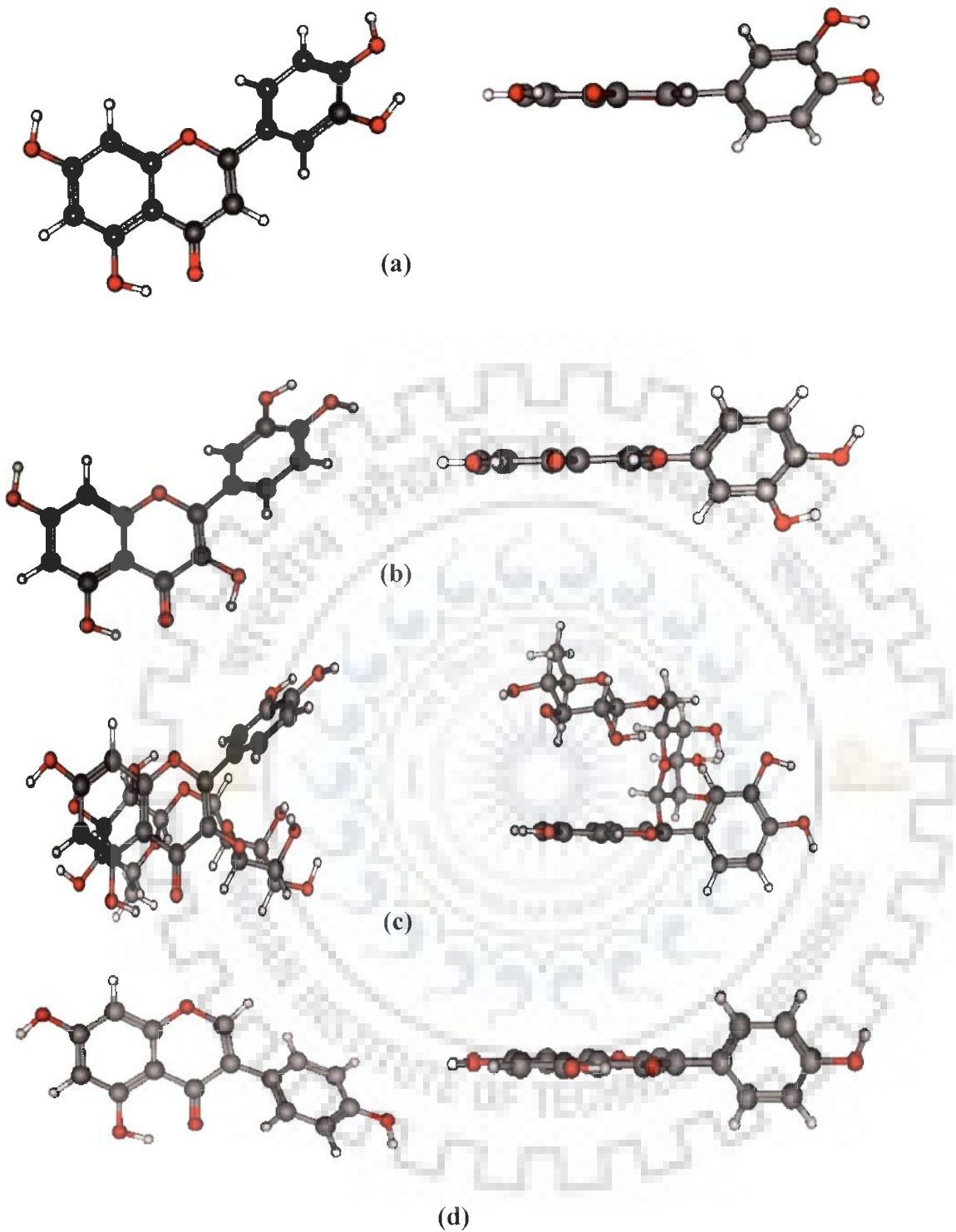
Fig. 4.9(i): Minimized solution structure of (a) luteolin, (b) quercetin and (c) rutin (d) genistein by rMD.

144

(a)

(b)

(c)

(d)
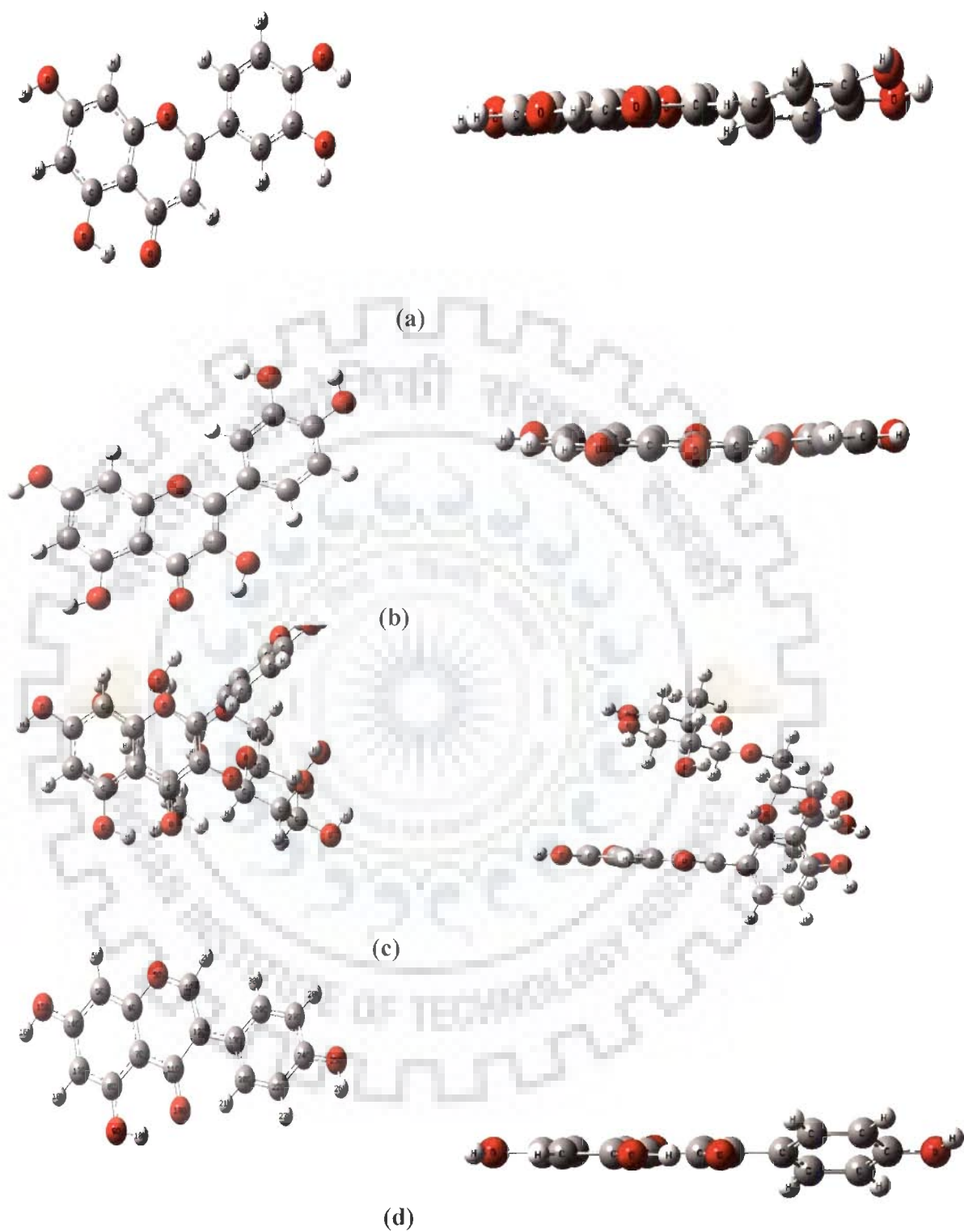
Fig. 4.9(ii): Gaussian optimized structure of (a) luteolin (b)quercetin (c)rutin and (d)

genistein using B3LYP/6-311G** in solvent DMSO.

Table 4.5a: Comparison of experimental structure (in solution), X-ray structure and calculated optimized structure with 6-311G for luteolin, quercetin, rutin and genistein using DFT method.**

Bond Length (Å)	Luteolin				Quercetin							Rutin			
	Theoretical		Experimental		Theoretical				Experimental			Theoretical		Experimental	
	B3LYP/6-311G** Gas Phase	B3LYP/6-311G** DMSO	Present solution structure	X-ray Cox et al. 2003	B3LYP/6-311G** Gas Phase	B3LYP/6-311G** DMSO	B3LYP/6-311++G** Leopoldini et al. 2004 Gas Phase	B3LYP/6-311++G** Leopoldini et al. 2004 DMSO	Present solution structure	X-ray Jin et al. 1990	X-ray Rossi et al. 1986	B3LYP/6-311G**	B3LYP/6-311G** DMSO	Present solution structure	X-ray Jin et al. 1990
O4'-H4'	0.96	0.95	0.97	-	0.95	0.97	-	-	0.97	-	0.97	0.967	0.98	0.98	-
O4'-C4'	1.35	1.36	1.37	1.36	1.42	1.35	1.35	1.35	1.37	1.37	1.40	1.356	1.36	1.37	1.40
C1'-C2	1.46	1.44	1.47	1.45	1.53	1.46	1.41	1.46	1.48	1.47	1.48	1.469	1.47	1.48	1.54
C10-C5	1.42	1.42	1.40	-	1.40	1.42	1.42	1.42	1.39	1.42	1.42	1.423	1.40	1.40	1.45
C2-O1	1.36	1.37	1.38	-	1.39	1.37	1.37	0.98	1.39	1.37	1.36	1.409	1.39	1.39	1.37
C6'-C5'	1.38	1.40	1.40	-	1.40	1.39	1.39	1.45	1.40	1.38	1.39	1.389	1.40	1.40	1.40
C3'-O3'	1.37	1.36	1.37	1.37	1.42	1.36	1.37	1.36	1.37	1.37	1.37	1.376	1.36	1.37	1.33
O3'-H3'	0.96	0.96	0.97	-	0.96	0.98	-	-	0.98	-	0.99	0.963	0.97	0.97	-
O1-C9	1.37	1.37	1.37	-	1.40	1.35	-	-	1.37	1.37	1.37	1.364	1.36	1.37	1.39
O5-C5	1.33	1.36	1.37	1.35	1.42	1.34	1.34	1.34	1.37	1.35	1.37	1.336	1.37	1.37	1.38
O5-H5	0.99	0.95	0.97	-	0.96	0.98	-	-	0.99	-	0.95	0.993	0.99	0.99	-
O7-C7	1.35	1.36	1.37	1.34	1.42	1.35	1.35	1.35	1.36	1.36	1.36	1.359	1.36	1.36	1.38
C4-O4	1.24	1.22	1.22	1.26	1.22	1.24	1.26	1.26	1.23	1.24	1.26	1.247	1.22	1.23	1.26
C3-H3	1.08	1.08	1.08	-	-	-	-	-	-	-	-	-	-	-	-
C6-H6	1.08	1.08	1.09	-	1.08	1.08	-	-	1.09	-	1.00	1.084	1.09	1.09	-

Bond Length (Å)	Genistein				
	Theoretical		Experimental		
	B3LYP/ 6-311G** (Gas Phase)	B3LYP/ 6-311G** (DMSO)	Present solution structure	X-ray * (Mazurek et al.1998)	X-ray (Breton et al. 1975)
O4'-H4'	0.96	0.99	0.97	-	-
O4'-C4'	1.36	1.32	1.36	1.36	-
C1'-C3	1.48	1.47	1.47	1.48	-
C10-C5	1.43	1.43	1.40	1.42	-
C2-O1	1.35	1.32	1.38	1.34	-
C6'-C5'	1.38	1.37	1.40	1.37	-
O1-C9	1.37	1.38	1.37	1.37	-
O5-C5	1.33	1.33	1.37	1.36	-
O5-H5	0.99	0.99	0.99	-	-
O7-C7	1.35	1.34	1.37	1.31	-
C4-O4	1.24	1.24	1.23	1.26	-
C6-H6	1.08	1.08	1.09	-	-

* Genistein complexes with amines

Table 4.5b (i): Comparison of experimental structure (in solution), X-ray structure and calculated optimized structure with 6-311G** for luteolin, quercetin and rutin using DFT method.

Bond Angle	Luteolin				Quercetin							Rutin			
	Theoretical		Experimental		Theoretical				Experimental			Theoretical		Experimental	
	B3LYP/ 6-311G** Gas Phase	B3LYP/ 6-311G** DMSO	Present solution structure	X-ray (Cox et al. 2003)	B3LYP/ 6-311G** Gas Phase	B3LYP/ 6-311G** DMSO	B3LYP/ 6-311++G** Leopoldini et al. 2004 Gas Phase	B3LYP/ 6-311++G** Leopoldini et al. 2004 DMSO	Present solution structure	X-ray Jin et al. 1990	X-ray Rossi et al. 1986	B3LYP/ 6-311G**	B3LYP/ 6-311G** DMSO	Present solution structure	X-ray Jin et al. 1990
C4`-O4`-H4`	108.03	107.12	107.9	-	109.5	110.5	-	-	108.2	-	101.87	107.7259	105.1	104.0	-
C2`-C1`-C2	120.80	121.81	120.4	-	119.9	119.4	121.3	121.3	121.3	120.4	119.34	121.8848	120.9	120.7	-121.6
C2-C1`-C6`	120.63	119.46	120.4	-	122.4	122.4	120.3	120.3	119.9	120.1	121.34	119.6857	120.2	120.4	116.3
C1`-C2-O1	112.21	113.59	114.0	111.1	112.4	112.3	112.4	112.7	110.6	111.0	110.97	111.5221	112.9	112.7	-106.1
C1`-C2-C3	126.34	119.61	121.4	127.4	128.9	129.0	-	-	126.2	128.1	127.75	127.8083	123.1	122.9	-132.4
C3`-O3`-H3`	110.49	103.37	103.9	-	109.9	111.2	-	-	108.0	-	112.59	110.0314	108.6	108.3	-
C2-O1-C9	120.91	116.96	118.0	-	120.0	122.8	122.8	122.7	120.7	120.5	120.90	121.8571	119.1	118.7	-123.1
C9-C10-C4	120.31	117.05	118.9	-	120.0	118.4	119.2	119.6	118.6	119.9	120.17	120.4672	119.7	118.7	-121.7
C5-O5-H5	106.40	107.65	107.0	-	109.4	110.3	-	-	107.5	-	101.93	106.3927	107.6	107.4	-
C7-O7-H7	109.37	110.01		108.5	-	109.7	116.1	-	-	118.6	-	109.3524	1087	108.9	-
Torsional Angle															
O4`-C4`-C3`-O3`	0.37	0.7	-0.3	4.7	0.0	-0.0	-	-	-0.0	-	-	0.4	-0.2	-0.4	-
C6`-C1`-C2-O1	166.9	-24.9	-34.1	-	179.9	175.1	-	-	47.5	-	-	-22.0	-37.9	-47.3	165.5
C1`-C2-O1-C9	179.4	-157.5	-178.4	-	179.9	179.6	-	-	179.2	-	-	179.0	-173.5	-173.5	-
O1-C9-C10-C4	-0.5	20.7	-1.4	-	0.0	-0.1	-	-	0.1	-	-	-0.4	-0.7	-2.7	-
C6-C5-O5-H5	-0.0	153.6	179.4	-	-0.0	-0.0	-	-	179.9	152.0	-	-179.2	-179.0	-180.0	-
C2`-C1`-C2-O1	-13.2	151.0	143.6	-	0.0	-4.6	-	-	-130.5	-	7.0	156.8	138.8	-128.6	-12.9
C2`-C1`-C2-C3	166.1	-36.0	-36.1	-	-179.9	174.8	-	-	58.2	-	7.0	-23.1	-36.9	-59.9	158.9
C6`-C1`-C2-C3	166.1	145.8	146.2	-	0.0	-5.3	-	-	-131.8	-	-	157.9	145.8	134.2	-22.7
Total Energy (a.u)	-1029.2	-1029.0	-	-	-1104.4	-1104.1	-	-	-	-	-	-2251.0	-2251.0	-	-
Diploe moment μ (D)	2.60	2.55	-	-	6.49	6.45	-	-	-	-	-	6.27	6.26	-	-

Table 4.5b (ii):

| Bond Angle	Genistein				
	Theoretical		Experimental		
	B3LYP/ 6-311G** Gas Phase	B3LYP/ 6-311G** DMSO	Present solution structure	X-ray * (Mazurek *et al.*1998)	X-ray (Breton *et al.* 1975)
C4'-O4'-H4'	109.25	112.80	108.5	-	-
C3-C1'-C6'	120.68	120.96	120.9	120.2	-
C1'-C3-C2	120.36	120.98	120.9	122.0	-
C1'-C3-C4	121.86	122.46	122.5	120.0	-
C2'-C1'-C3	121.49	120.32	120.4	122.4	-
C2-O1-C9	119.51	120.80	117.6	119.4	116.3
C9-C10-C4	121.19	121.43	119.0	120.9	-
C5-O5-H5	106.47	107.60	107.1	-	-
C7-O7-H7	109.45	111.58	109.0	-	-
Torsional Angle					
O4'-C4'-C3'-H3'	-0.06	-0.07	-0.2	-	-
C6'-C1'-C3-C2	-39.89	-51.22	-51.0	-	-
C1'-C3-C2-O1	177.02	-179.36	-179.5	-	-
O1-C9-C10-C4	-0.85	-0.41	-0.3	-	-
C6-C5-O5-H5	-179.88	179.40	179.6	-	-
C2'-C1'-C3-C2	139.35	129.19	129.5	-	-
C2'-C1'-C3-C4	-41.14	-49.35	-49.2	-	-
C6'-C1'-C3-C4	139.30	130.21	130.4	-	-
Total Energy (a.u)	-953.99	-953.81	-	-	-
Diploe moment μ (D)	1.29	7.71	-	-	-

* Genistein complexes with amines

isoenergetic state. During dynamics, most of the conformations preference lies at torsional angle 179.5° for luteolin (Fig. 4.10a), while for quercetin, rutin and genistein no such preference was observed and conformations which lie at both torsional angle -130.5° and -57.2° for quercetin and rutin (Fig. 4.10b and 4.10c) and 130.4 and 57.6 ° for genistein. Beside this, the bond length of the C10-C5(1.42A°) and C4-O4 (1.23 A°) for luteolin and bond length of the C10-C5 (1.42 A°) and C4-O4 (1.23 A°) for luteolin and the corresponding values (1.42 A° and 1.24 A°) for quercetin, rutin and genistein are found to be longer and shorter, than the average bond length. This further indicates the formation of similar kind of H-bond between – H5 and –O4 of ring A and C in both the molecules. The information about the orientation of substituents in luteolin and quercetin could be obtained from single crystal X-ray data. Although such structural data are available, but it can not explain much about the dynamic rotation of B ring with respect to A and C ring around C2-C1' bond. It is only NMR studies in combination with theoretical methods that can be used to search for explanation of the observed effects. A variable temperature gradient NMR experiment of flavonols and flavones in organic and aqueous mixtures have also revealed the presence of intramolecular hydrogen bonds in aqueous solution (Exarchou *et al.* 2004). The planarities of these molecules manifest intercalation binding with DNA and allow insertion between two adjacent base pairs in a helix. Furthermore, the formation of inter molecular hydrogen bonding due to the expanded orientation of hydroxyl group maximizes the chance of hydrogen bonding between -NH group of base pairs of DNA helix and stabilizes the binding. Comparison of calculated bond lengths and bond angles clearly show that hydroxyl groups of quercetin expands more than the respective hydroxyl groups of luteolin and rutin which is needed relatively more for better binding with DNA. From the calculated optimized structure of this molecule, we saw that the
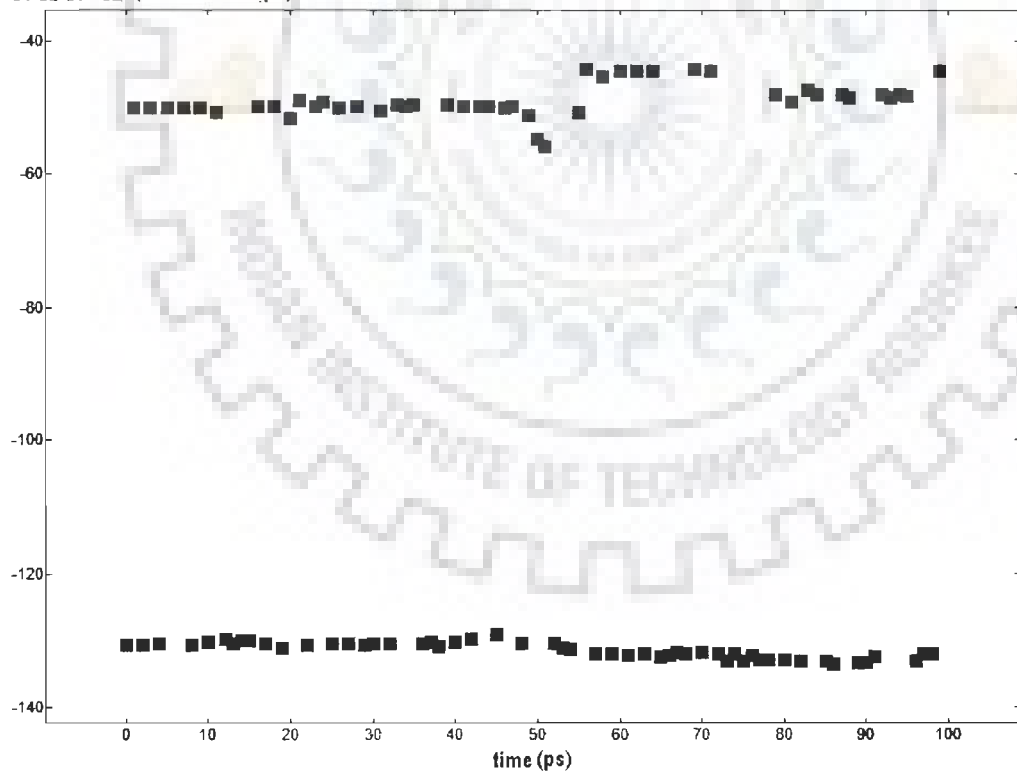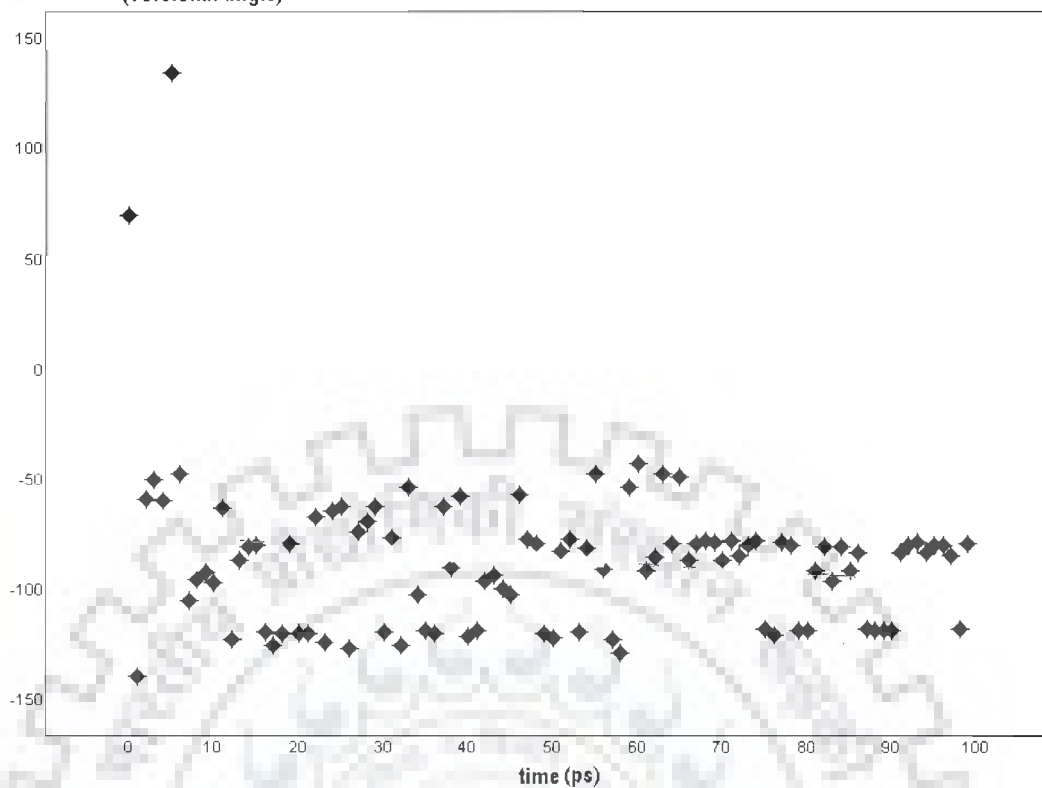
149

C2´-C1´-C2-O1 (Torsional angle)
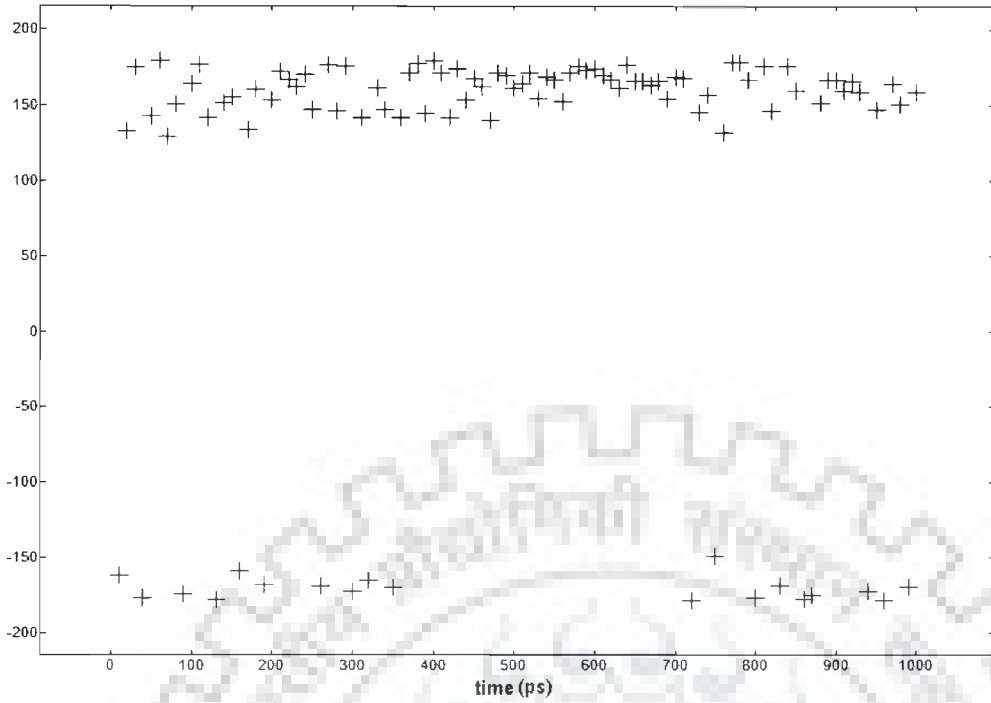
(a)

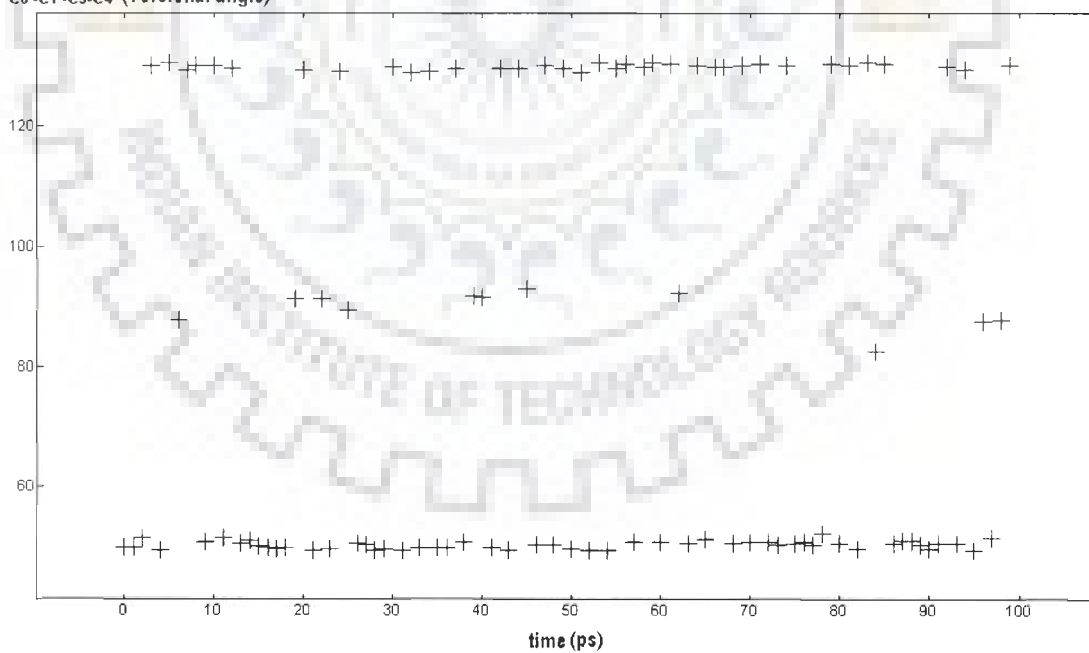O1-C2-C1´-C2´ (Torsional angle)

(b)

150

C2'-C1'-C2-O1 (Torsional angle)

(c)

C6'-C1'-C3-C4 (Torsional angle)

Fig. 4.10: Conformational preference during rMD (a) Luteolin, (b) Quercetin, (c) rutin around torsional angle C1'-C2'-O1-C2 and (d) genistein around torsional angle C6'-C1'-C3-C4 at 100ps.

151

pattern of variation of the bond lengths and bond angles in general are very similar to those of luteolin molecule. Further, we also notice that for quercetin, the difference between the calculated dihedral angles at position C3 position (C2'-C1'-C2-C3; C6'-C1'-C2-C3) and the experimental values are greater than 116°, whereas for luteolin this difference is less than 1° clearly reflects the difference in structure on replacing -H by -OH group.

4.3. Chemical Shift

All the ^1H and ^{13}C chemical shifts were referenced to those of Tetra Methyl Silane (TMS). The absolute ^1H and ^{13}C shielding of TMS based on the B3LYP were calculated at the same level basis set used in the calculation to which they refer. The chemical shifts for each atom (^1H and ^{13}C) were computed by taking the difference between their value and the reference value for TMS. The calculated chemical shift using B3LYP/6-311G** with GIAO method along with the present experimental results are listed in Tables 4.1a-c and 4.2a-b. A quick look at the tables tells us that calculated chemical shift range for ^1H are more sensitive to the variation of basis sets compared to that of ^{13}C. This can be rationalized by the fact that ^1H atoms being the smallest of all atoms and mostly localized on periphery of the molecules, their chemical shifts would be more susceptible to intermolecular interactions in the aqueous solutions compared to that for other heavier atom. From the tabulated data, it can be easily seen that the variation of the difference between measured values and calculated results at B3LYP/6-311G** level of theory are quantitatively good and compare well with the experiment. The largest difference in ^{13}C chemical shifts is observed for the carbon bonded to the hydroxyl group in compound. The value for chemical shifts of four protons of hydroxyl group is excluded during calculation because both in solution and in gas phase the environment is quite different which results in to greater difference in chemical shift for hydroxyl proton.

Beside this, other protons of hydroxyl group may also give several conformations in solvent as well. Further, it is also noticed from the Table 4.1a,b and 4.2a,b that there is a difference in the magnitude between experimental and theoretical chemical shift in solvent, for example 2.19 for proton (H3') and 7.17 for carbon (C7) in luteolin, 4.0 (H7') 6.4 (C9) in quercetin, 2.10 (H3') 9.61 (C7) in rutin and 2.57 (H4') 18.98 (C4') in genistein . The large difference in carbon chemical shift is because the hydroxyl group attached to this carbon is free in the environment. Similar results for the carbon attached to hydroxyl group have been also observed for quercetin. The large difference of the chemical shifts for some atoms in luteolin, quercetin, rutin and genistein, may be due to higher structural flexibility of this part of molecule in solution, whereas C5 atom being rigid in its position, involved in intra molecular hydrogen bonding within the molecule and is not showing such large difference.

Considering the fact that NMR chemical shifts are affected by the chemical environment i.e. molecular conformation and interaction with the solvent molecules, it is seen that the overall agreement between the calculated and measured values both for ^{1}H and ^{13}C chemical shift is satisfactory. It is of interest, however to see, how good the correlation between experimental and calculated results is? We therefore plot our experimental NMR results versus theoretical calculation obtained with 6-311G** basis set as given in Tables 4.1a-c, 4.2a and 4.2b for the luteolin, quercetin, rutin and genistein molecule. A linear correlation between theoretical and experimental both for carbon and proton (excluding hydroxyl proton) chemical shift is clearly seen in Fig. 4.11a-h. In solvent phase, the correlation coefficient for carbon is 0.99 for all these molecules and for proton their value are 0.98, 0.89, 0.95 and 0.84 whereas in gas phase these values for carbon are 0.98 and for protons are 0.81; 0.78; 0.91 and 0.63 for luteolin, quercetin, rutin and genisein, respectively. The correlation in solvent is good

153

and approaching to 1 for carbon but for hydrogen this variation may be due to less number of hydrogen apart from OH groups. Though the difference is expected in proton chemical shift of hydroxyl group (OH7, OH4' and OH3') as these groups are involved in intramolecular and inter molecular hydrogen bonding with solvent. The calculated value for OH5 is same both in solvent and gas phase because it is involved in strong intramolecular hydrogen bonding with O4 and its proton is the least, mobile and accessible to the solvent. On the whole good correlation demonstrates that in general 6-311G** basis set predicts reasonably well all the NMR parameters.

4.4. Structure-Function Relatioship of Luteolin, Quercetin, Rutin and Genistein

Among the natural phenolic antioxidants, the flavonoid family is the most important class. Individual differences within each flavonoid result from the variation in number and arrangement of the hydroxyl groups as well as from the nature and extent of glycosylation of these groups. A number of in vitro studies have established the hierarchy of flavonoids in terms of their antioxidant activities (Cos *et al.* 1998; Rice-Evans *et al.* 1996), topoisomerase poisoning and DNA binding for anti tumor activities. The most commonly occurring flavones and flavonols are those with dihydroxylation in the 3' and 4' position of B ring. The preffered glycosylation site on the flavonoids is the 3 position and less frequent at the 7 position. The glycosylation of quercetin at this site not only make it water soluble but also affects the antioxidant and DNA binding like activities. It has been seen that the glycosylation of flavonoid at 3-C position of C ring reduces their antioxidant (Rice-Evans *et al.* 1996) as well as DNA binding and topoisomerase poisoning activities (Webb and Ebeler, 2004).

4.4.1 Anti oxidant Activity

The mechanism by which phenolic compounds are able to scavenge free radicals is yet

154
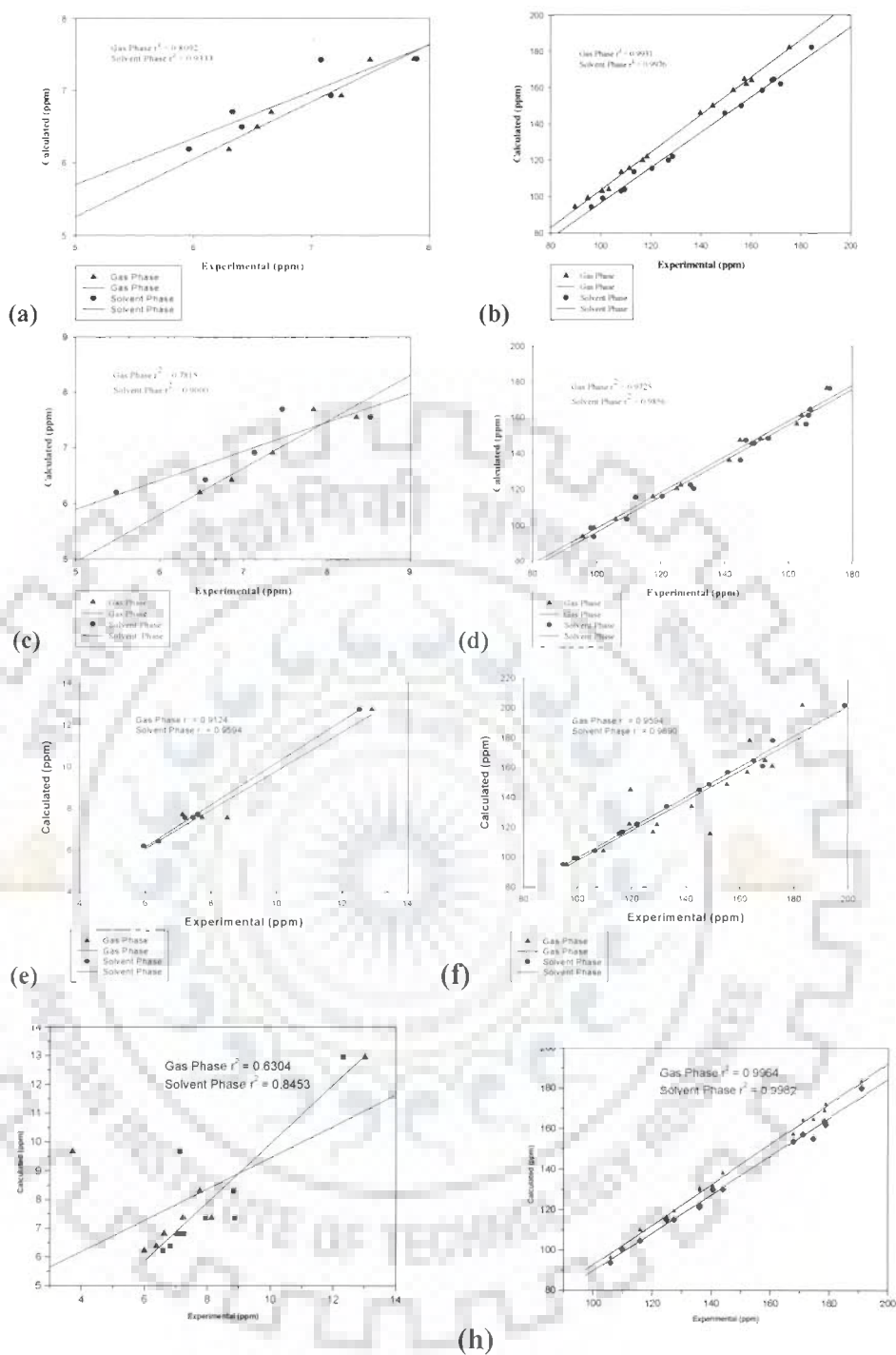
Fig. 4.11: Correlation of experimental and calculated chemical shifts with B3LYP/6-311G**/GIAO method (a) proton of luteolin in gas and solvent phase; (b) carbon of luteolin in gas and solvent phase; (c) proton of quercetin in gas and solvent phase; (d) carbon of quercetin in gas and solvent phase; (e) proton of in gas and solvent phase and (f) carbon of genistein in gas and solvent phase (g) proton of in gas and solvent phase and (h) carbon of genistein in gas and solvent phase

155

to be exactly established. In any case it seems to be clear that the basic structure of compounds and other structural factors are very important in the scavenging mechanism (Choi *et al.* 2002; Sadeghipour *et al.* 2005). As reported by Heijnen *et al.* (Heijnen *et al.* 2001), the aromatic OH groups are the reactive centres, primarily 3',4'-dihydroxy catechol group, and their activity can be enhanced by electron donating effects of other substituents. For flavonoid compounds, *O*-dihydroxy groups in the B-ring, the presence of a C 2-3 double bond in conjunction with 4-oxo in the C-ring, the 3- and 5-hydroxy groups and the 4-oxo function in the A and C-rings are associated with antioxidant activity (Lopez *et al.* 2003).

The Chemistry of the flavonoids is predictive of their free radical scavenging activity because the reduction potential of flavonoid radical are lower than those of alkyl peroxyl radicals and the superoxide radical, which means the flavonoids may inactivate these oxyl species and prevent the deleterious consequences of their reactions (Wardman, 1989; Jovanovic *et al.* 1992). The removal of 3-OH of C ring in flavonoids reduces their activity when compared to the corresponding molecule like quercetin. Removing the 3-hydroxyl group at the C ring of quercetin as in luteolin decreases the antioxidant activity to a value of 2.1 $\pm$ 0.05 (n = 4) (Shahidi and Wanasundara, 1992). Further, blocking the 3–hydroxyl group in the C-ring of quercetin as a glycoside while retaining the 3', 4'-dihydroxy structure in the B ring as in rutin (quercetin rutinoside) decreases the antioxidant activity to a value of 2.4$\pm$ 0.12 mM (n = 7). This could be explained by the steric hindrance created by the saccharides (Lopez *et al.* 2003). In fact, it has also been reported that aglycones are generally stronger antioxidant than their corresponding glycosides, but in some assays rutinose is a unique case in which addition of this disaccharide to aglycone does not consistently decrease antioxidant ability (Heim *et al.* 2002). Thus, the maximum effectiveness for radical scavenging apparently requires the 3-OH

group attached to the 2, 3 –double bond and adjacent to the 4-carbonyl in the C ring. Thus, the maximum effectiveness for radical scavenging apparently requires the 3-OH group attached to the 2,3-double bond and adjacent to the 4-carbonyl in the C ring which is not available in luteolin, rutin and genistein. Retaining the catechol-type structure in the B ring but removing the 2-3 double bond in the C ring, eliminates the means of delocalization of electrons from the aryloxyl radical on the B ring to the A ring, as in taxifolin (dihydroquercetin), giving a trolox equivalent antioxidant activity (TEAC) value of $1.9 + 0.03$ mM (n = 6), of the same order as catechin but more effective than kaempferol. The comparison of quercetin with luteolin and rutin demonstrates the influence of the 3-OH in combination with the adjacent double bond in the C ring, and if one is dispensed with the other apparently loses its impact on the antioxidant activity (Shahidi and Wanasundara, 1992; Rice-Evans *et al.* 1996). Further, 3-OH of quercetin is also believed to be involved in coordination with copper atom which is important for the several enzymes activity (Balogh-Hergovich *et al.* 1997).

4.4.2 DNA binding and Topoisomerase Poisioning Activity

Recently, flavonoids are found to be an inhibitor of tumor growth and there is experimental evidence for a number of mechanisms. It is known that most of the anti tumor drugs target either topoisomerase or DNA for their anti tumor activities. For targeting DNA, it may be a DNA intercalator or groove binder. The planarity and probable hydrophobicity of chromophore limit binding to the DNA as intercalator or groove binder. During structural analysis of luteolin, quercetin, rutin and genistein, it has been found that the benzopyran-4-one ring is planar and this ring stabilizes in to the interior of the DNA helix similar to that of the adjacent planes of the nitrogenous base (Solimani, 1997). Similar mode of DNA binding for both luteolin and quercetin has been ascertained after finding that the existence of luteolin

influences the binding capacity of quercetin with DNA and there is competition between the quercetin and luteolin when they co exist in the system. Further, determination of binding constants for flavonoids–double stranded DNA (dsDNA) or flavonoids–single stranded DNA (ssDNA) followed the trend like kaempferide > quercetin > luteolin for ds-DNA and quercetin > kaempferide > luteolin for ss-DNA. (Bi *et al.* 2006). Removal of 3-OH of C ring in quercetin make slight difference with luteolin and the binding constant has been found to be 3.19 x 10^4 and 2.33 x 10^4 for luteolin and quercetin, respectively. But glycosylated flavonols like rutin which shows conjugation with various saccharides, resulted in loss of topoisomerase poisoning and intercalation activity (Formica and Regelson 1995; Strick *et al.* 2000; Rueff *et al.* 1986). For intercalative binding with DNA, double bond between the 2 and 3 carbons of the C-ring of benzo pyrone moiety is necessary, as this double bond ensures a sufficiently planar structure to allow placement between adjacent bases of the DNA duplex (Snyder and Gillies, 2002). For topoisomerase poisoning activity, essentially equivalent behaviour of luteolin, quercetin and genistein indicates that the 3 position hydroxyl group plays a relatively minor role in this process and also in DNA binding activity (Yamashita *et al.* 1990; Webb and Ebeler, 2004). Further, the loss of intercalative capacity by flavonols which have been glycosylated at the 3 position hydroxy group for rutin suggests that steric constraints on intercalation play a more important role than isomerization, ionization or hydrogen bonding at the 3 position hydroxy group. If intercalation of this active compound involves entry of the fused A- and C-rings along the edge defined by the 4 and 5 position carbons, a bulky moiety attached at the 3-carbon would significantly hinder this process. In our present study, it has been observed that A and C-ring of these three molecules is essentially planar which favors DNA intercalation (Fig. 4.9 i and 4.9 ii). But in case of rutin the sugar moiety orient in such a

fashion in solution structure that it become parallel with A and C-ring of the aglycone moiety. Usually, the planar ring intercalates between the bases of DNA with stacking interaction. Luteolin, quercetin and genistein are found to be a potent intercalator and work in this fashion. In case of rutin, it is expected that when aglycone part tries to fit in between the DNA bases, this glycoside part of rutin causes hinderance in DNA intercalation as this part is oriented parallel to the A and C-ring which can not be fitted in between -1 or +1 nucleotides of DNA due to its bulky size but surplus of hydroxyl group which may involve in hydrogen bonding with oxygen present in the DNA backbone, thus this molecule can work as potent groove binder In future, comparison of structure of these flavonoids with different DNA sequences is expected to provide further knowledge on sequence specificity or selectivity for their binding.

4.5 Summary and Conclusion

Complete ^{1}H and ^{13}C NMR assignments of luteolin, quercetin and rutin were achieved using a combination of 1D and 2D (HSQC, HMBC, and ROESY) experiments in DMSO solvent. An optimized solution structure has been determined by analyzing the 2D NMR data followed by restrained molecular dynamics simulation. The experimental findings were combined with a theoretical investigation using density functional theory (DFT) using B3LYP functional for luteolin, quercetin, rutin and genistein molecule in gaseous phase and in DMSO solvent system. Among all the methods B3LYP functional has shown to produce best results for geometries, energies, and all other NMR parameters both in gas phase and solvent and the same are reported here. In gas phase a variety of basis sets (STO-3G, 6-31G, 6-31G*, 6-31G** and 6-311G**) were used. The effect of increasing size of the basis set slow down the calculation but tends towards to accurate results. An overall analysis shows that B3LYP/6-311G** level of theory predicts results which are quantitatively good and compare well with

159

the experiment. Further, the structural analysis shows the role of inter and intra molecular hydrogen bonding in solution which is important for the flavonoids for their several functions especially DNA binding as anti cancerous activity likely to other intercalating agent, quercetin complexation is stipulated by its planar structure and additional carboxyl group that can be protonated these facilitate intercalation and subsequent π- stacking with base pairs. An optimized solution structure has been obtained by restrained Molecular Dynamics simulations using ROE restraints for luteolin, quercetin, rutin and genistein. These structures are compared with that obtained from quantum mechanical calculations. It is observed that A and C ring are planar in these flavonoids and the B ring of the quercetin and rutin rotate around C2'-C1'-C2 - O1 torsional angle to go in to two different conformation, *anti* and *syn* in rMD structure and in DFT studies (Fig 4.9). The presence of *anti* and *syn* conformers were also confirmed by solid state NMR and DFT studies (Olejniczak and Potrzebowski, 2004). Similar effect has been also observed in case of genistein but around C6'-C1'-C3 –C4 torsional angle. A variation in flexibility of adopting two different conformations in these flavonoids may be related to a differential efficacy in biological activity and hence antioxidant or anticancer action.

Chapter 5

Molecular association of flavonoids luteolin, quercetin, rutin and genistein using Nuclear Magnetic Resonance Spectroscopy supported by other biophysical methods

The study of molecular association is of paramount importance to understand solution structures. Flavonoids are known to have hydroxyl group and individual differences within each flavonoid result from the variation in number and arrangement of these hydroxyl groups. Hydrogen bonds involving hydroxyl group are not only considered as playing a determinant role in all biochemical processes, but are also of crucial importance in solution structures. In this regard, it is expected to observe the molecular association by formation of intermolecular hydrogen bonding. Prior to the determination of the structural and thermo-dynamical characteristics of the intercalative binding of flavonoids to defined DNA sequences by NMR spectroscopy, it is necessary to determine the molecular association of these molecules in solution. This chapter includes:

- Proton 1D NMR spectra as a function of concentration (0.01-10.00 mM) at 298 K and of 10 mM concentration as a function of temperature (275-355 K) in DMSO for these flavonoid luteolin, quercetin, rutin and genistein.

- Restrained molecular dynamics simulations of the dimer model of above flavonoids using inter-proton distances calculated from 2D NOESY spectra at 298 K ($\tau_m = 300$ ms).

- Absorption and fluorescence spectral studies of these flavonoids as a function of concentration.

161

• Calculation of diffusion coefficient from proton DOSY experiment for all the four molecules.

• Electron-Spray Ionization Mass Spectra (ESI-MS) studies of these flavonoids.

5.1 Results and Discussion

5.1.1. NMR Studies

Fig. 5.1 (a-d) shows the proton NMR spectra of luteolin, quercetin, rutin and genistein at 298K in d-DMSO with increasing concentrations. The variation in chemical shifts is shown in Fig. 5.2 (a-d) and the values are given in Table 5.1-5.5. An increase in concentration from 0.01 to 10.0 mM leads to downfield shift in a ring A protons H6 and H8 up to $\Delta\delta$ 0.023 and 0.052 ppm in luteolin (Table 5.1), $\Delta\delta$ 0.006 and 0.004 ppm in quercetin (Table 5.2); 0.011 and 0.006 ppm rutin (Table 5.3), and 0.013 each for genistein (Table 5.4), respectively. The ring B aromatic protons H5' and H6' in luteolin, quercetin, rutin and genistein also show similar kind of meager shifts up to $\Delta\delta$ 0.015 and 0.005 ppm; $\Delta\delta$ 0.003 and 0.001; $\Delta\delta$ 0.001 ppm and 0.000; $\Delta\delta$0.003 and 0.008, respectively. No such studies have been carried out so far for any of the flavonoid molecules to the best of our knowledge. The quercetin differs in their structure with luteolin only by an inversion of the substituents H by OH at C3 position of C-ring and rutin by substituting rutinoside sugar moiety while B ring is placed in genistein at the same position. However, we observed that there are meager differences in $\Delta\delta$ values 0.023 and 0.052 ppm in luteolin; 0.006 and 0.004 ppm in quercetin; 0.011 and 0.006 ppm in rutin and 0.013 each for genistein of downfield shift with increase in concentration of ring A protons H6 and H8 which is likely to pyridinium moiety of porphyrin molecule which show downfield shift with increase in concentration explained by the formation of a partially side slipped face to face dimer (Kano et al. 2000). However, the present spectrum was found to be concentration independent as the
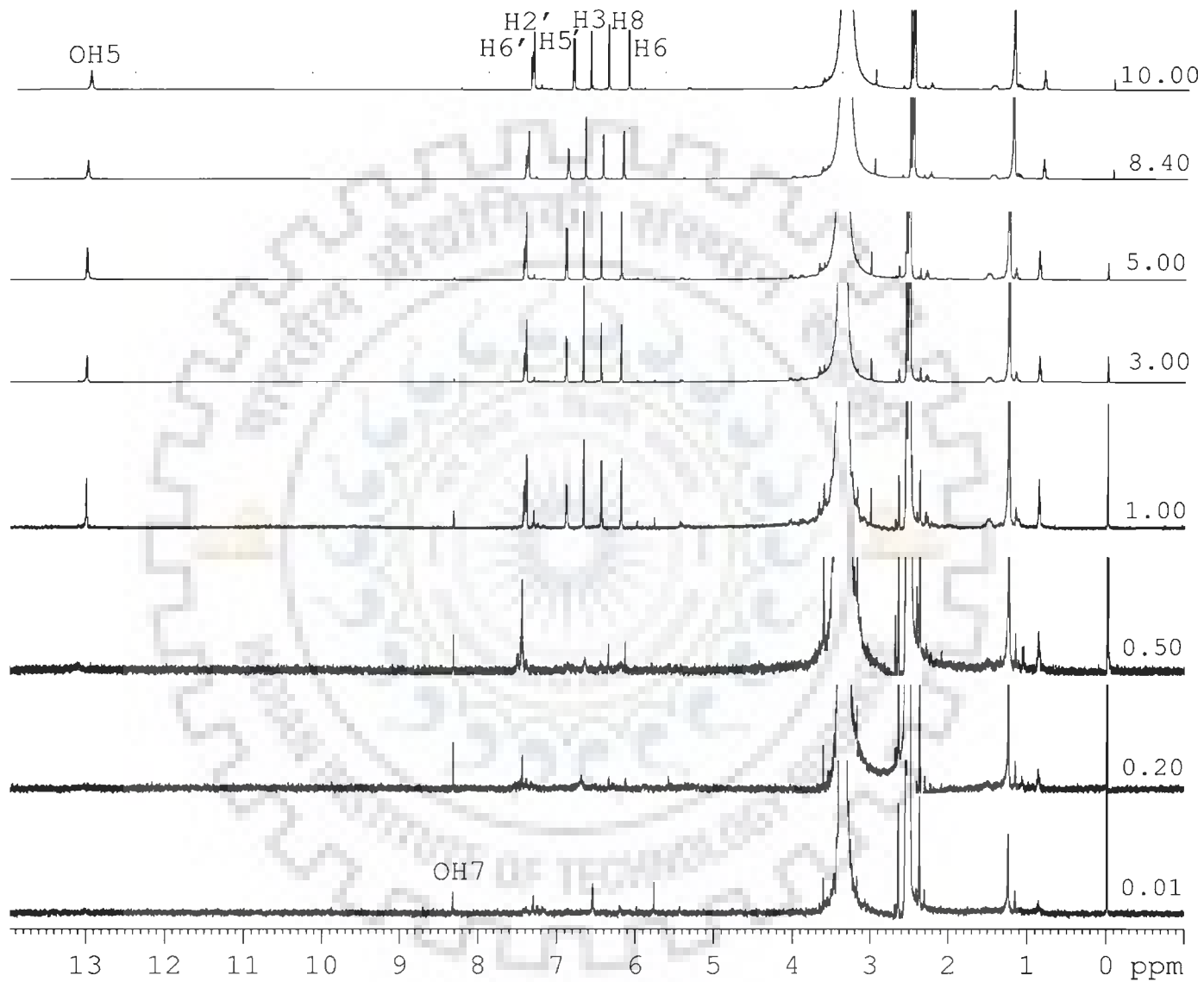
162

Fig. 5.1: (a) One-dimensional proton NMR spectra of luteolin in d-DMSO as a function of concentration (in mM)
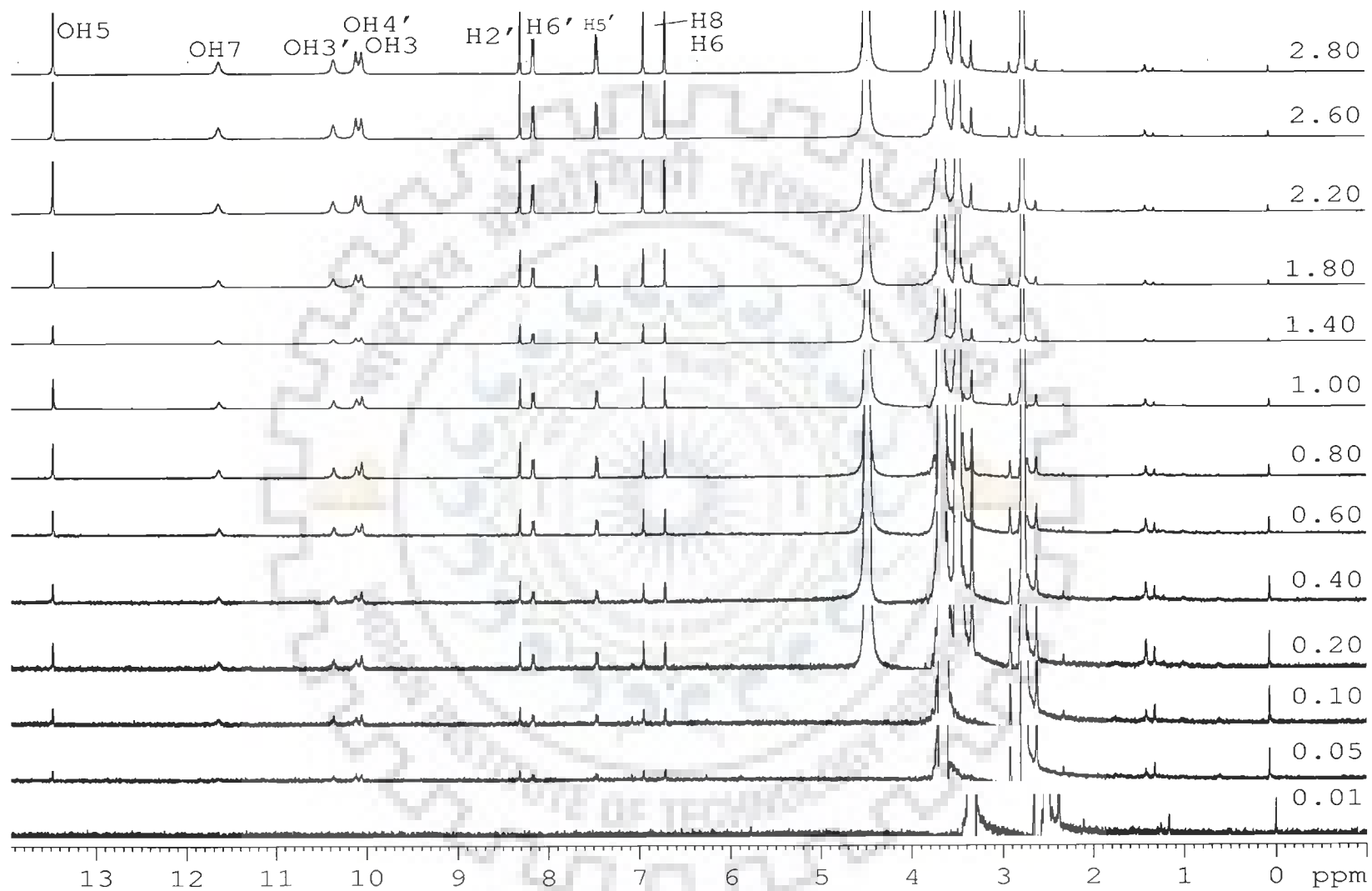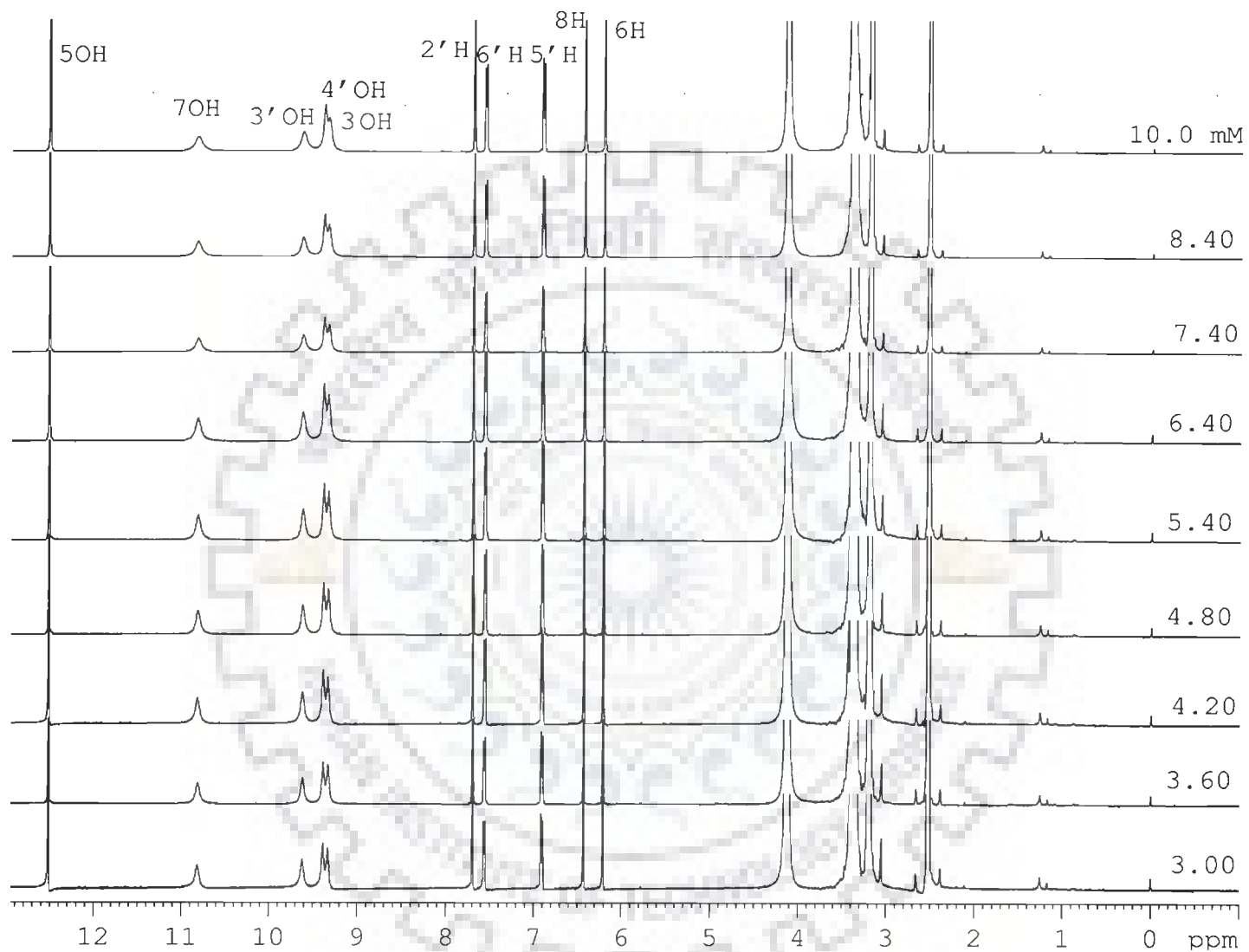
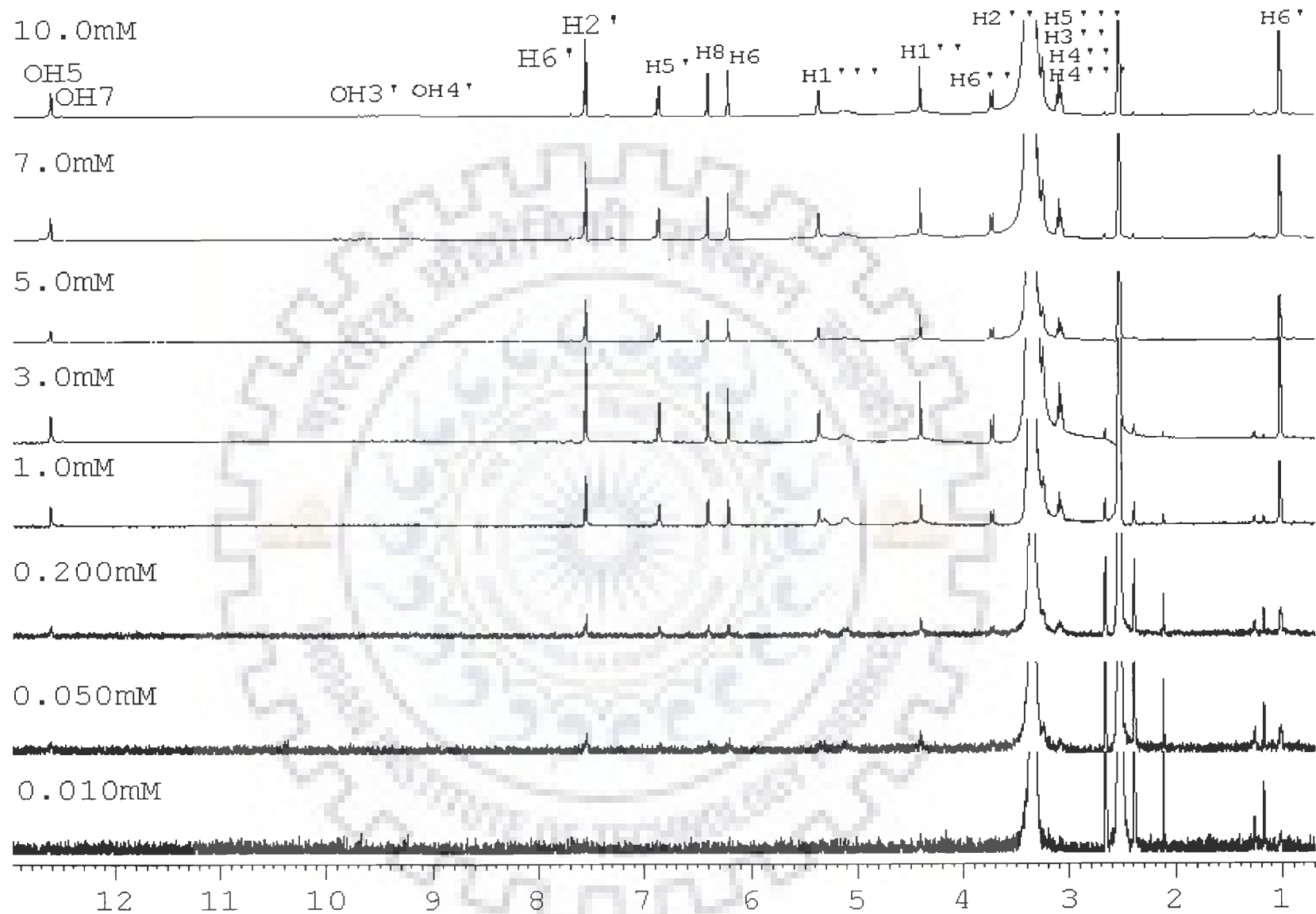**Fig. 5.1: (b) (i) One-dimensional proton NMR spectra of quercetin in d-DMSO as a function of concentration (in mM)**
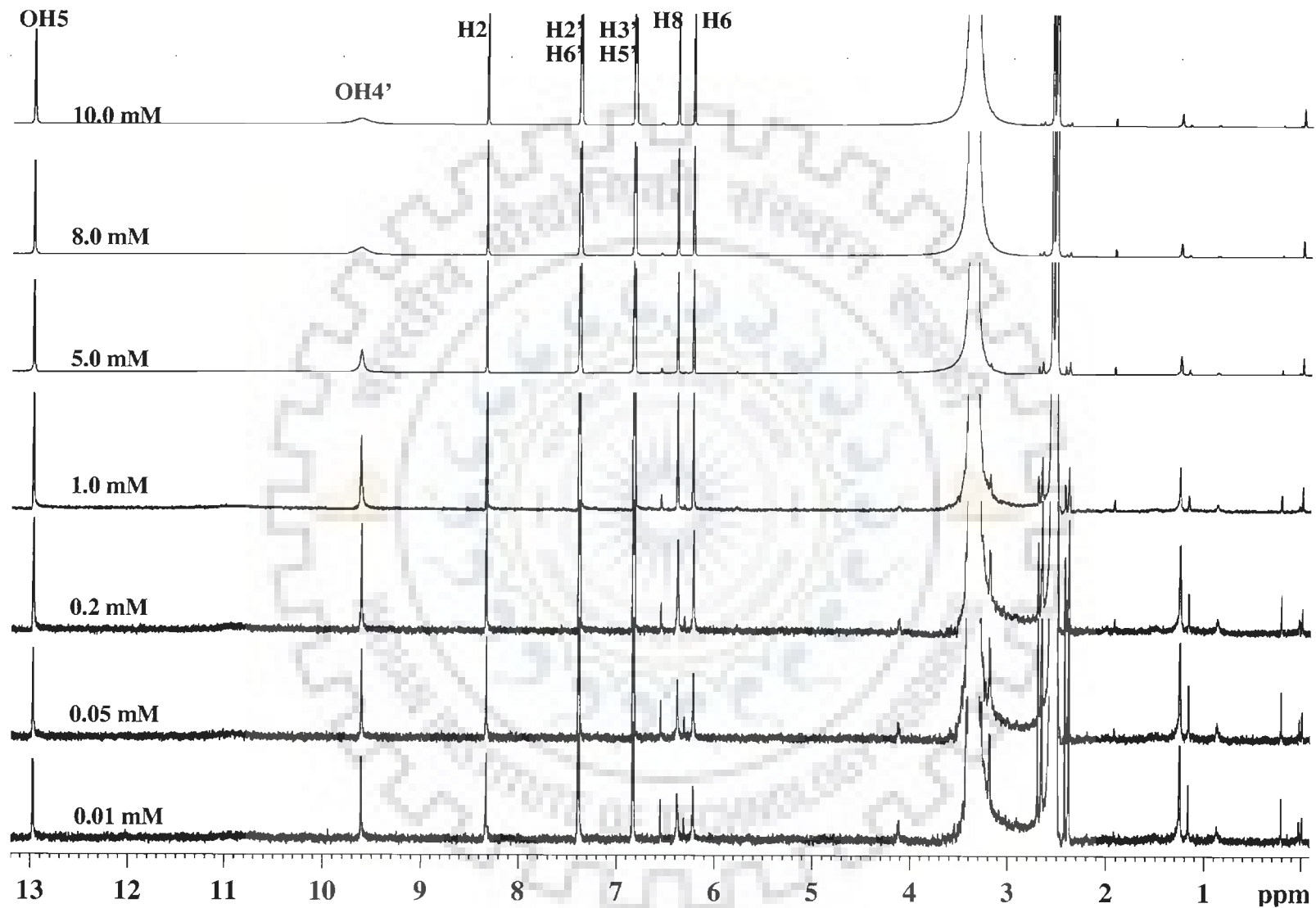
Fig. 5.1: (b) (ii) One-dimensional proton NMR spectra of quercetin in d-DMSO as a function of concentration (in mM)

165

Fig. 5.1: (c) One-dimensional proton NMR spectra of rutin in d-DMSO as a function of concentration (in mM).

166

Fig. 5.1: (d) One-dimensional proton NMR spectra of genistein in d-DMSO as a function of concentration.

Table 5.1: **Proton chemical shifts of luteolin in d-DMSO as a function of concentration at 298 K** $\Delta\delta = \delta_{10\ mM} - \delta_{0.01\ mM}$ **indicates total change in chemical shift.**

Conc. (mM)	H3	H6	H8	H2'	H5'	H6'	OH5	OH7
0.010	6.677	6.182	6.138	7.398	6.891	7.429	13.000	8.332
0.020	6.678	6.187	6.265	7.398	6.892	7.429	13.000	8.330
0.050	6.679	6.192	6.355	7.401	6.894	7.429	13.000	8.329
1.000	6.681	6.196	6.453	7.404	6.895	7.430	13.000	8.329
3.000	6.684	6.200	6.684	7.407	6.899	7.431	12.998	8.329
5.000	6.686	6.201	6.686	7.408	6.890	7.432	12.996	8.328
8.000	6.689	6.203	6.688	7.410	6.904	7.433	12.995	8.328
10.00	6.690	6.205	6.690	7.412	6.906	7.434	12.994	8.328
$\Delta\delta$	+0.223	+0.023	+0.052	+0.014	+0.015	+0.005	-0.006	-0.004

Downfield shift is +ve.
Upfield shift is –ve.

Table 5.2: **Proton chemical shifts of quercetin in d-DMSO as a function of concentration at 298 K.** $\Delta\delta = \delta_{10\text{ mM}} - \delta_{0.01\text{ mM}}$ **Indicates total change in chemical shift.**

Conc. (mM)	OH5	OH7	OH3'	OH4'	OH3	H6'	H2'	H5'	H8	H6
0.010	12.513	10.805	9.605	9.378	9.324	7.697	7.559	6.908	6.428	6.206
0.050	12.513	10.805	9.606	9.378	9.324	7.697	7.560	6.908	6.428	6.206
0.100	12.513	10.805	9.606	9.378	9.324	7.697	7.560	6.908	6.428	6.206
0.200	12.513	10.805	9.606	9.378	9.324	7.697	7.562	6.908	6.428	6.206
0.400	12.513	10.805	9.610	9.378	9.324	7.697	7.562	6.908	6.428	6.207
0.600	12.513	10.805	9.611	9.378	9.324	7.697	7.562	6.908	6.428	6.208
0.800	12.513	10.805	9.611	9.378	9.324	7.697	7.562	6.908	6.429	6.208
1.000	12.513	10.806	9.613	9.378	9.324	7.697	7.562	6.908	6.429	6.208
1.400	12.513	10.807	9.613	9.378	9.324	7.697	7.562	6.908	6.430	6.209
1.800	12.513	10.809	9.613	9.378	9.324	7.697	7.564	6.908	6.430	6.210
2.200	12.514	10.809	9.613	9.378	9.324	7.697	7.564	6.908	6.431	6.210
2.600	12.514	10.810	9.617	9.378	9.324	7.697	7.564	6.908	6.431	6.210
3.000	12.514	10.810	9.617	9.378	9.324	7.697	7.564	6.908	6.431	6.210
3.600	12.514	10.810	9.617	9.378	9.324	7.697	7.564	6.908	6.431	6.210
4.200	12.514	10.811	9.617	9.378	9.324	7.697	7.564	6.908	6.431	6.210
4.800	12.514	10.811	9.617	9.378	9.324	7.697	7.564	6.908	6.432	6.210
5.400	12.514	10.814	9.617	9.378	9.324	7.698	7.564	6.908	6.432	6.210
6.400	12.514	10.814	9.621	9.378	9.324	7.698	7.564	6.911	6.432	6.210
7.400	12.514	10.815	9.622	9.378	9.324	7.698	7.564	6.911	6.432	6.210
8.400	12.514	10.819	9.623	9.377	9.324	7.698	7.564	6.911	6.432	6.212
10.000	12.514	10.822	9.626	9.376	9.329	7.698	7.565	6.911	6.432	6.212
$\Delta\delta$	+0.001	+0.017	+0.021	-0.002	+0.005	+0.001	+0.006	+0.003	+0.004	+0.006

Downfield shift is +ve.
Upfield shift is −ve.

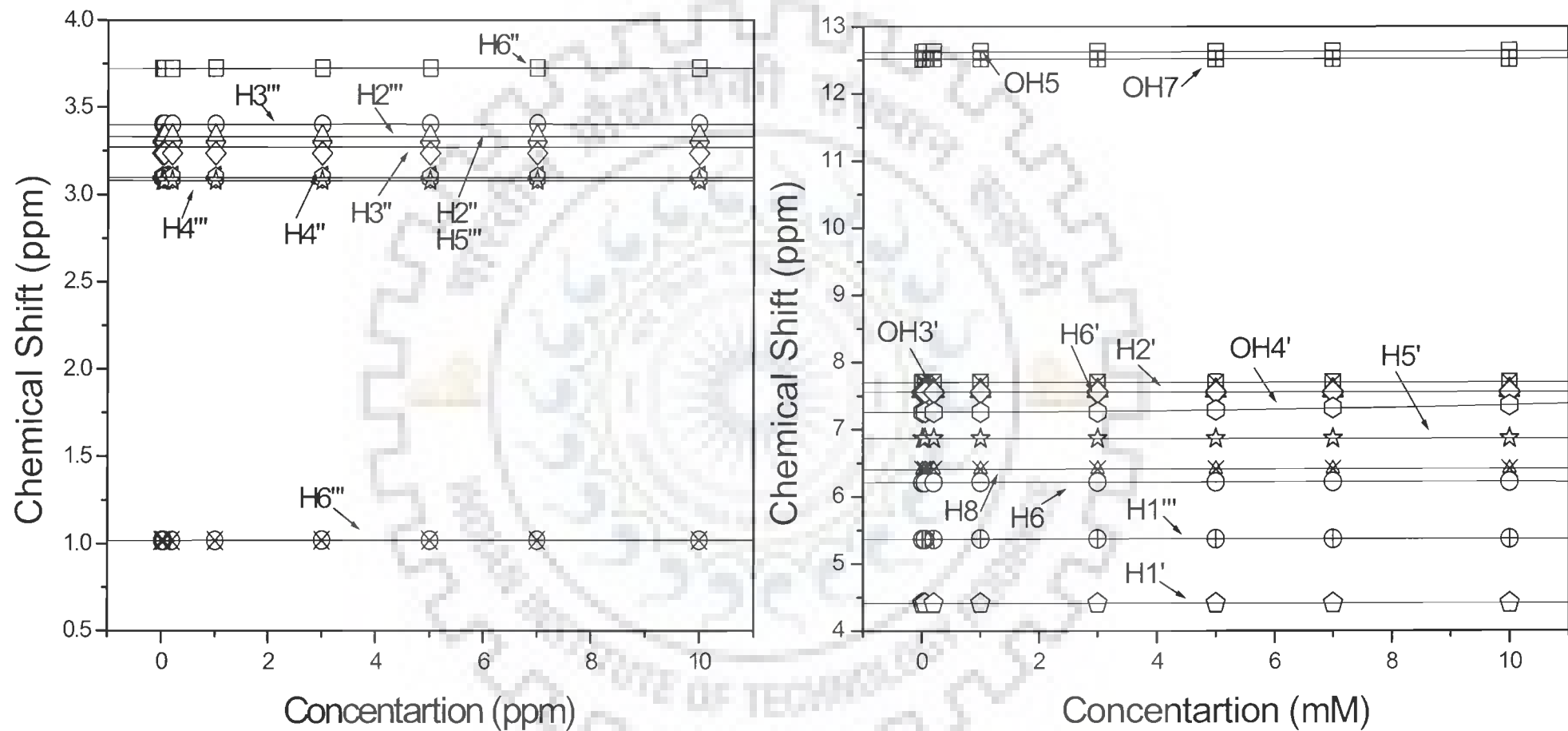**Table 5.3:** (a) Proton chemical shifts of rutin in d-DMSO as a function of concentration at 298 K. $\Delta\delta = \delta_{10\,mM} - \delta_{0.01\,mM}$ indicates total change in chemical shift.

Conc. (mM)	OH5	OH7	OH3'	H6'	H2'	OH4'	H5'	H8	H6	H1'''	H1'
0.010	-	-	-	-	-	-	-	-	-	-	-
0.050	12.616	12.523	9.261	7.576	7.557	-	-	-	6.209	-	4.408
0.200	12.618	12.523	9.261	7.576	7.557	-	-	6.405	6.211	5.362	4.408
1.000	12.623	12.523	9.261	7.576	7.557	-	6.864	6.407	6.216	5.371	4.408
3.000	12.624	12.523	9.261	7.576	7.557	9.742	6.864	6.408	6.217	5.371	4.408
5.000	12.626	12.523	9.261	7.576	7.557	9.805	6.865	6.410	6.218	5.371	4.408
7.000	12.627	12.523	9.261	7.576	7.557	9.820	6.865	6.411	6.219	5.371	4.408
10.000	12.631	12.523	9.261	7.576	7.557	9.839	6.865	6.411	6.220	5.371	4.408
$\Delta\delta$	+0.015	0	0	0	0	+0.097	+0.001	+0.006	+0.011	+0.009	0

Downfield shift is +ve.
Upfield shift is −ve.

Table 5.3: (b) Proton chemical shift of rutinoside part of 10 mM rutin in DMSO as a function of concentration $\Delta\delta = \delta_{10\,mM} - \delta_{0.01\,mM}$ indicates total change in chemical shift due to molecular association.

Conc. (mM)	H6''	H3'''	H5'''	H2'''	H2''	H3''	H4''	H4'''	H6'''
0.010	-	-	-	-	-	-	-	-	-
0.050	3.721	-	-	3.272	-	-	-	-	-
0.200	3.721	3.401	3.330	3.272	3.237	3.098	3.098	3.079	-
1.000	3.723	3.402	3.331	3.272	3.237	3.098	3.098	3.079	1.018
3.000	3.723	3.402	3.331	3.272	3.237	3.098	3.098	3.079	1.019
5.000	3.723	3.404	3.332	3.272	3.237	3.098	3.098	3.079	1.019
7.000	3.723	3.404	3.332	3.272	3.237	3.098	3.098	3.079	1.019
10.000	3.723	3.404	3.332	3.272	3.237	3.098	3.098	3.079	1.019
$\Delta\delta$	+0.002	+0.003	+0.002	0	0	0	0	0	+0.001

Downfield shift is +ve.
Upfield shift is −ve.

Table 5.4: Proton chemical shift of 10 mM genistein in DMSO as a function of concentration. $\Delta\delta = \delta_{10\ mM} - \delta_{0.01\ mM}$ **indicates total change in chemical shift due to molecular association.**

Conc. (mM)	H2	H6	H8	OH5	H2'	H3'	OH4'	H5'	H6'
0.010	8.331	6.219	6.382	12.973	7.389	6.832	9.608	6.832	7.389
0.050	8.331	6.219	6.382	12.972	7.389	6.832	9.608	6.832	7.389
0.200	8.331	6.219	6.382	12.971	7.389	6.832	9.609	6.832	7.389
1.000	8.334	6.228	6.390	12.973	7.389	6.835	9.614	6.835	7.389
5.000	8.336	6.231	6.393	12.975	7.381	6.835	9.618	6.835	7.381
8.000	8.336	6.232	6.395	12.975	7.381	6.835	9.623	6.835	7.381
10.000	8.336	6.232	6.395	12.973	7.381	6.835	9.624	6.835	7.381
$\Delta\delta$	+0.005	+0.013	+0.013	0	-0.008	+0.003	+0.018	+0.003	-0.008

Downfield shift is +ve.
Upfield shift is −ve.

Table 5.5: Changes in chemical shift $\Delta\delta$ (in ppm) as a function of concentration of various flavonoids protons in d-DMSO.

	Present Work $\Delta\delta = \delta_{10mM} - \delta_{0.01mM}$ 298K				
	Luteolin	Quercetin	Rutin		Genistein
H3	+0.223	-	-	H2	+0.005
H6	+0.023	+0.006	+0.011	H6	+0.013
H8	+0.052	+0.004	+0.006	H8	+0.013
OH5	-0.006	+0.001	+0.015	OH5	0
OH7	-0.004	+0.017	0.000	-	-
H2'	+0.014	+0.006	0.000	H2'	-0.008
OH3'	-	-0.002	0.000	H3'	+0.003
OH4'	-	+0.021	-0.004	OH4'	+0.018
H5'	+0.015	+0.003	-0.005	H5'	+0.003
H6'	+0.005	-0.003	0.000	H6'	-0.008

Downfield shift is +ve.
Upfield shift is –ve.
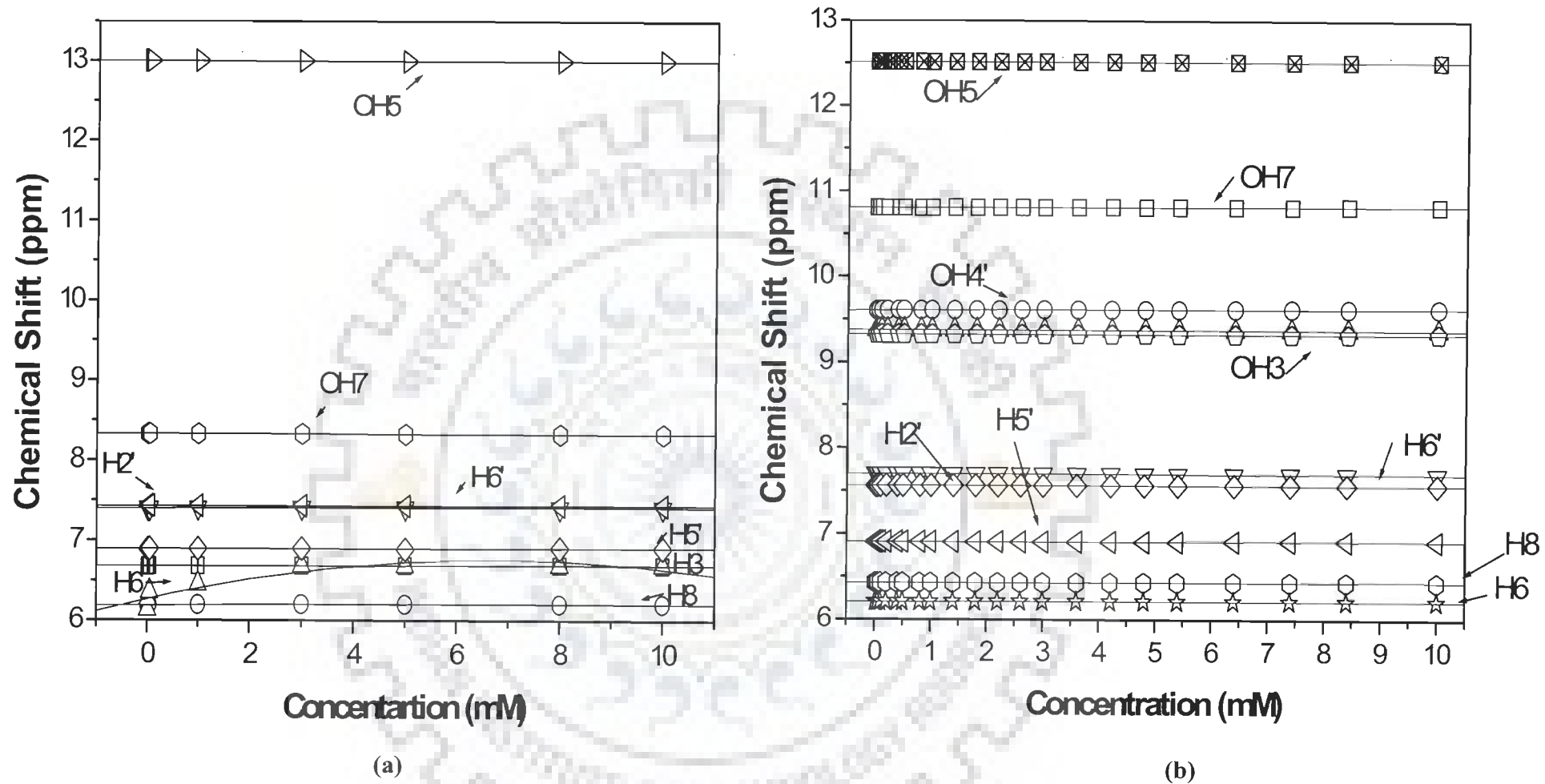
Fig. 5.2: One-dimensional proton chemical shift of (a) luteolin and (b) quercetin in d-DMSO as a function of concentration

Fig. 5.2: (c) One-dimensional proton chemical shift of rutin in d-DMSO as a function of concentration
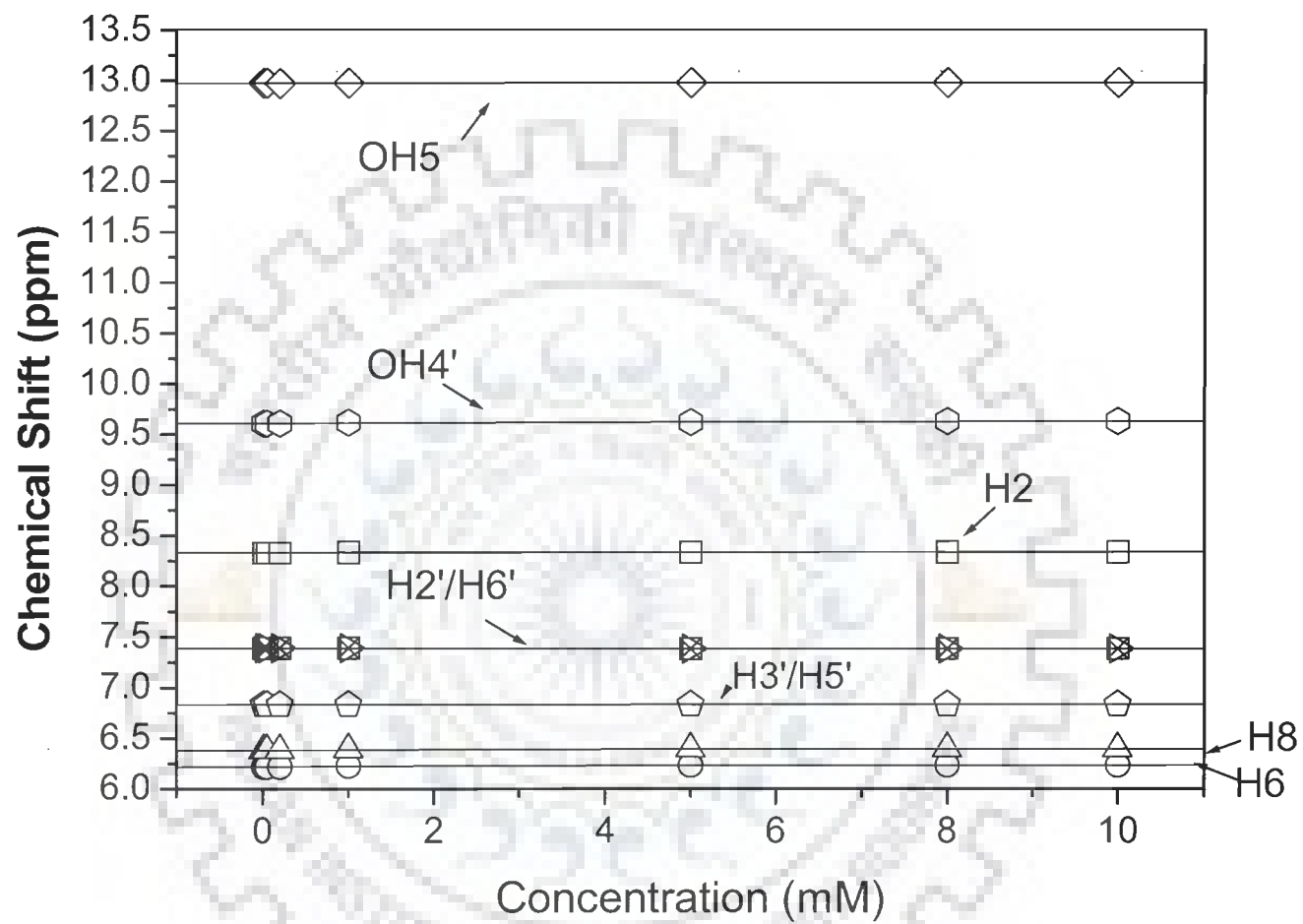
Fig. 5.2: (d) One-dimensional proton chemical shift of genistein in d-DMSO as a function of concentration

change in chemical shift is very little. This clearly shows that inter or intramolecular association through hydrogen bonding has taken place in the solution. This also reduces the chances of the availability of stacking interactions between planar benzopyran rings at 0.36 nm distance as reported in x-ray crystal data (Jin et al. 1990; Cox et al., 2003).

Further, in view to reveal the inter or intra molecular hydrogen bonding, we have also examined the NMR spectra of bioflavonoids at 10 mM concentration as a function of temperature (Fig. 5.3a-d). The variation in chemical shifts with respect to increase in temperature is shown in Fig. 5.4 a-d and the values are given in Table 5.6-5.10. An increase in temperature from 275 K to 355 K leads to significant differences in the proton chemical shift especially for hydorxy protons among these four flavonoids. In case of rutin hydroxyl protons OH7, OH4', OH3' and in genistein OH7 are not observed in NMR spectra at higher temperature as they might be free or may be exchanging fast with the solvent. The ring A and C hydroxy protons OH5, OH7 and OH3', OH4' reflect large upfield shifts up to $\Delta\delta$ 0.181, 0.239 and 0.138, 0.136 ppm in luteolin, $\Delta\delta$ 0.284, 1.970 and 0.478, 0.862 in quercetin, and $\Delta\delta$ 0.10 for OH5 and 0.55 for OH4', respectively with temperature (Fig. 5.4a-c) which may be due to unharmonicity of the low frequency streching vibration of X-H...Y. As the temperature increases the H...Y distance increases due to increased populations of the excited vibrational levels. Therefore, the electric field exerted by Y at H decreases, leading to an upfield shift from 0.2 to 0.8 x 10^{-2} ppm per °C (Schaefer and Kotowycz, 1968). This temperature dependent spectra confirms that inter or intramolecular association through hydrogen bonds has taken place. However, it is not clear here whether this change is due to the intermolecular or intramolecular hydrogen bonding. There are other factors such as change in (i) monomer-dimer equilibrium or, (ii) structural changes, which contribute towards change in chemical
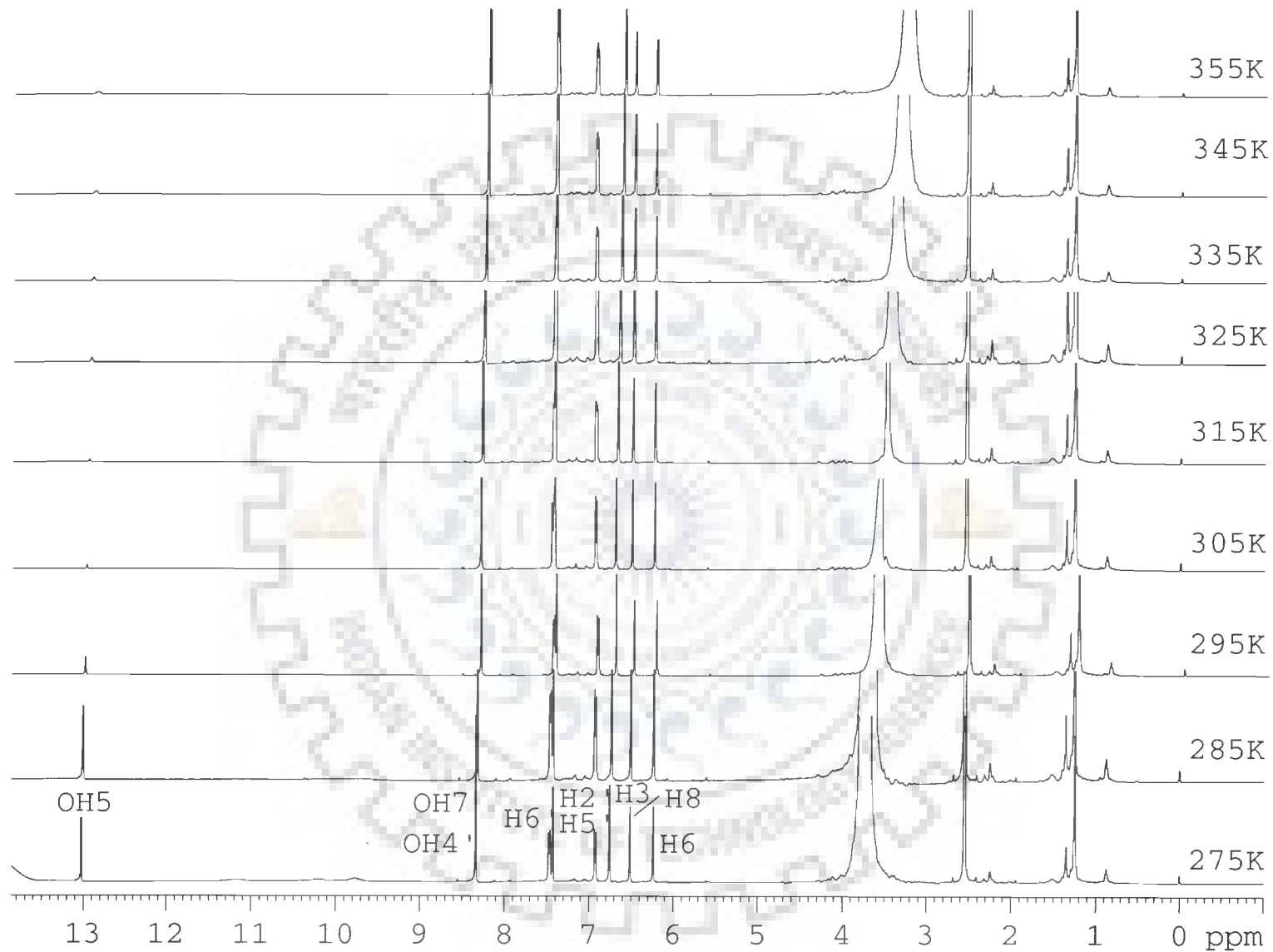
Fig. 5.3: (a) One-dimensional proton NMR spectra of 10 mM luteolin in d-DMSO as a function of temperature

Temperature labels (right side, top to bottom): 355K, 345K, 335K, 325K, 315K, 305K, 295K, 285K, 275K

Peak labels: OH5, OH7, OH3', OH3, OH4', H2', H6', H5', H8, H6

X-axis (ppm): 12, 11, 10, 9, 8, 7, 6, 5, 4, 3, 2, 1 ppm
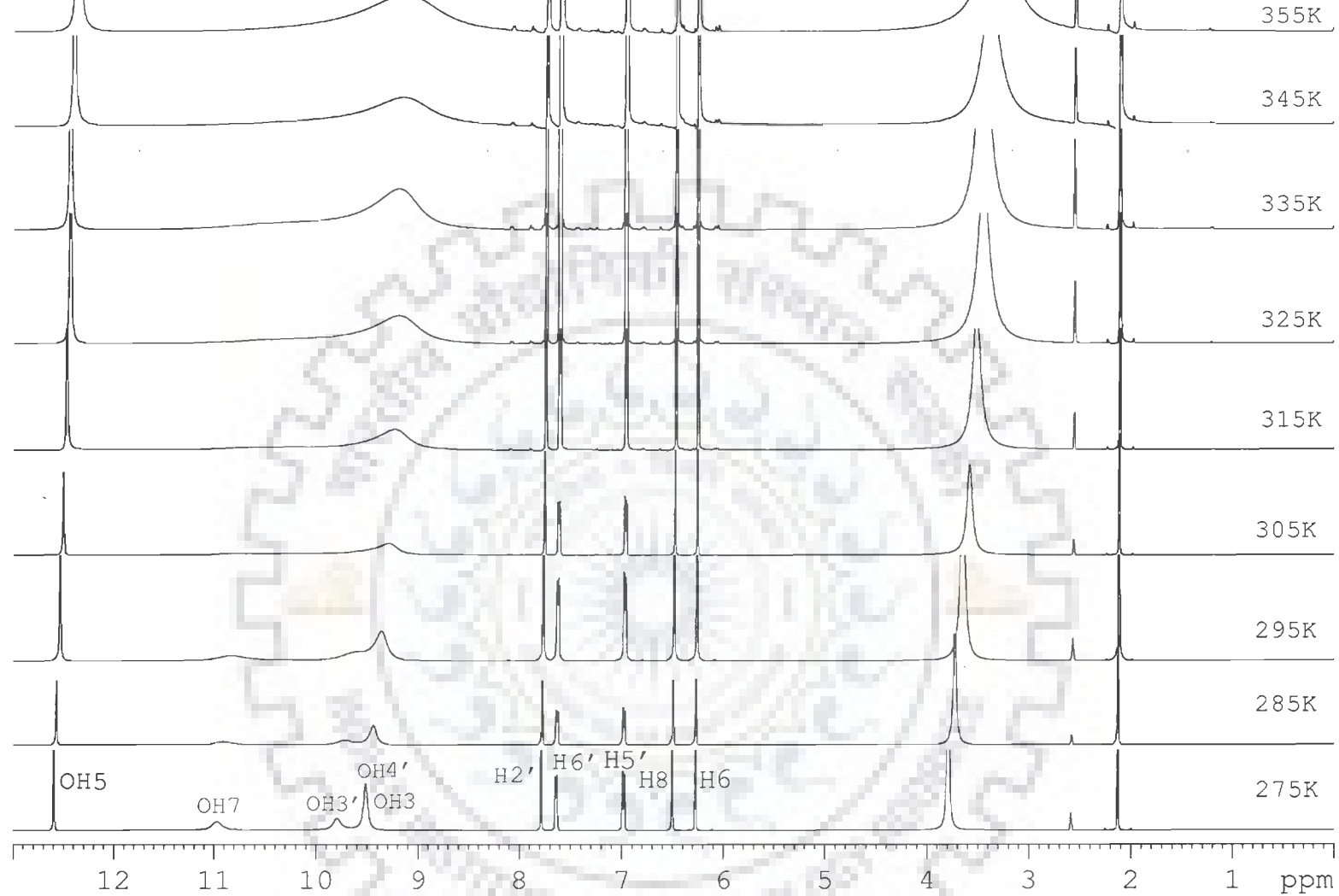
Fig. 5.3: (b) One-dimensional proton NMR spectra of 10 mM quercetin in d-DMSO as a function of temperature
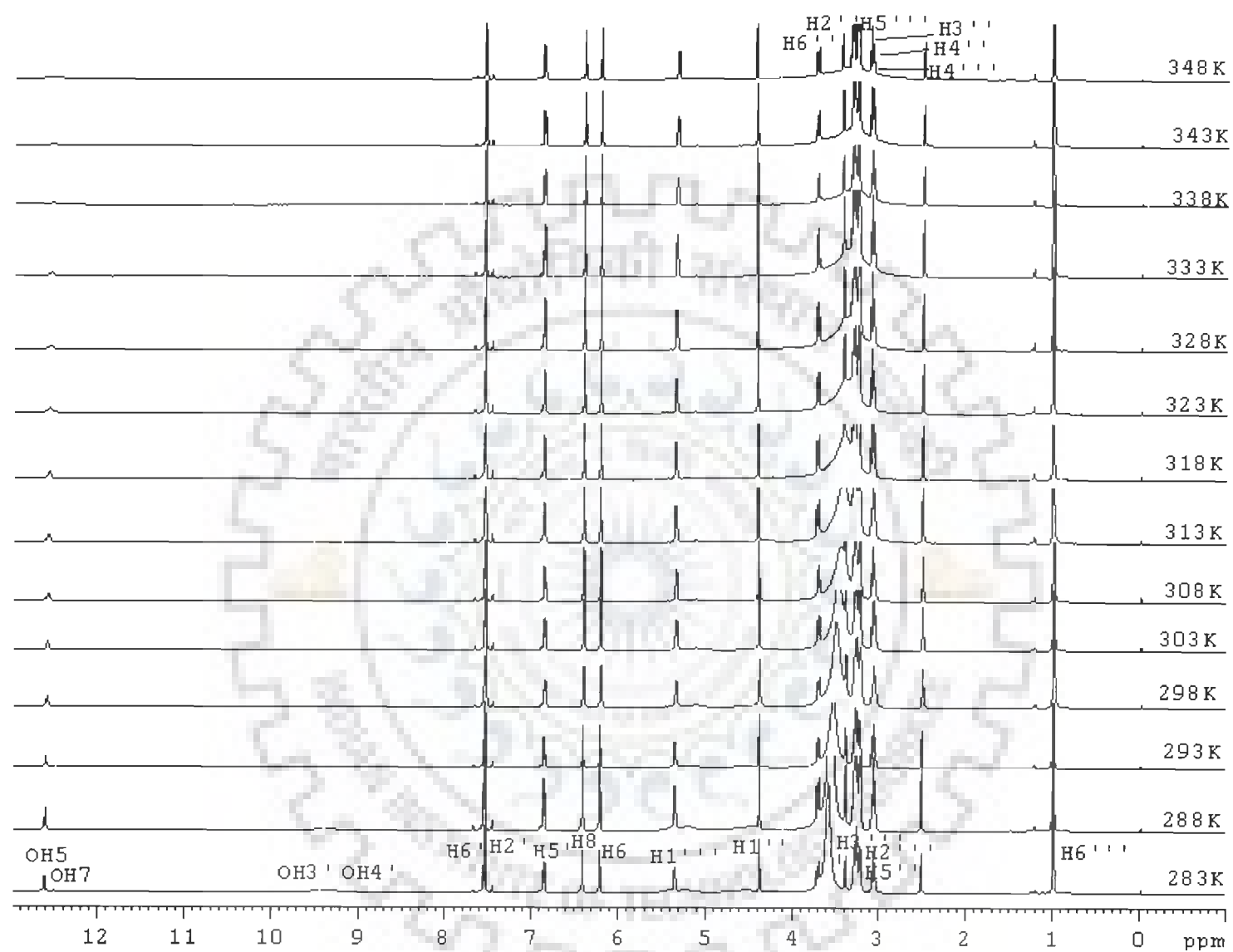
Fig. 5.3: (c) One-dimensional proton NMR spectra of 10 mM rutin in d-DMSO as a function of temperature
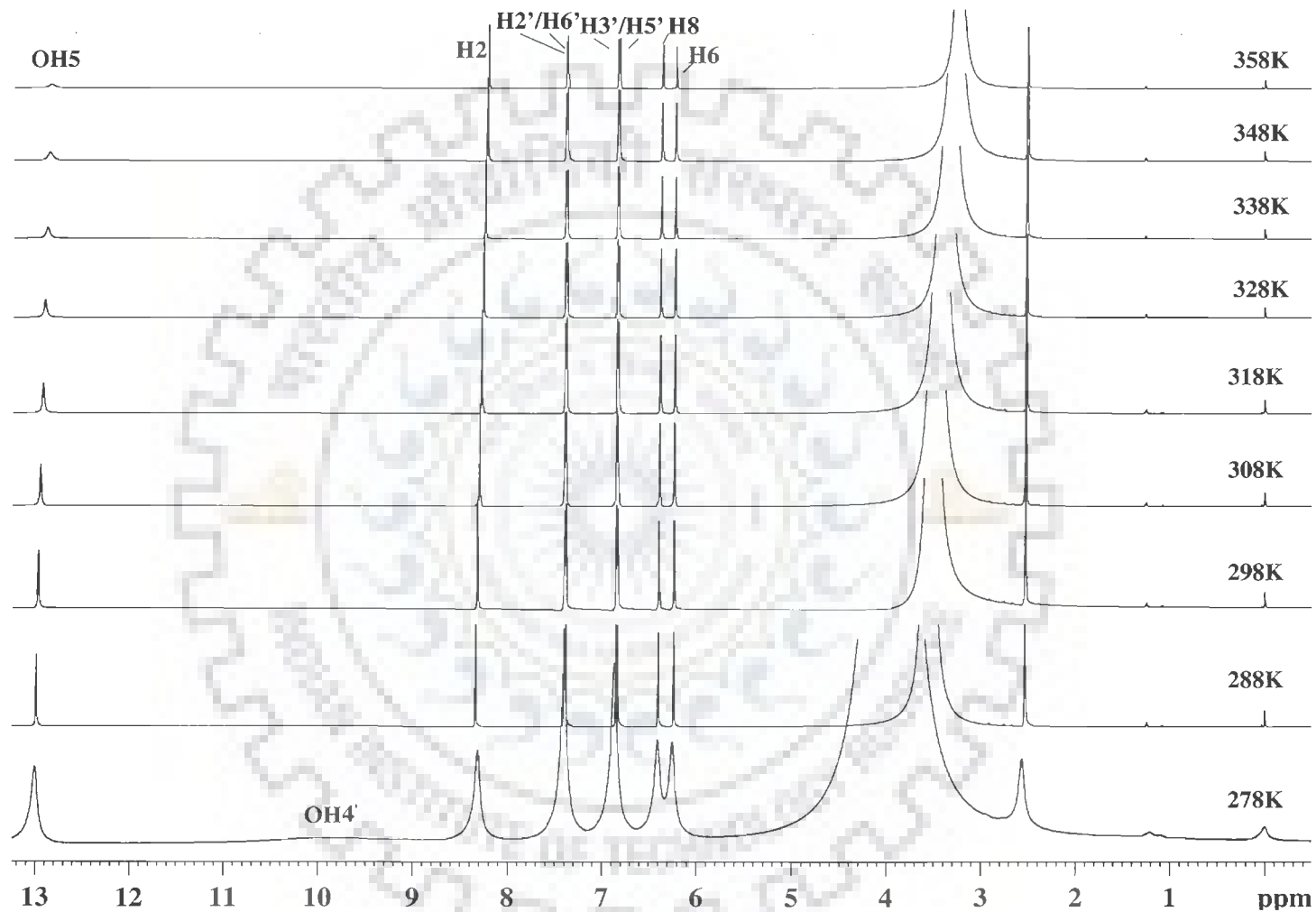
Fig. 5.3: (d) One-dimensional proton NMR spectra of 10 mM genistein in d-DMSO as a function of temperature.

Table 5.6: Proton chemical shift of 10 mM luteolin in d-DMSO as a function of temperature. $\Delta\delta = \delta_{355\,K} - \delta_{275\,K}$ indicates total change in chemical shift.

	H3	H6	H8	OH5	OH7	H2'	OH3'	OH4'	H5'	H6'
275K	6.758	6.234	6.511	13.027	8.339	7.430	8.552	8.118	6.931	7.470
285K	6.733	6.232	6.504	13.000	8.323	7.425	8.536	8.103	6.931	7.459
295K	6.709	6.230	6.499	12.984	8.304	7.420	8.520	8.086	6.931	7.449
305K	6.689	6.228	6.495	12.964	8.270	7.418	8.505	8.069	6.931	7.439
315K	6.668	6.226	6.489	12.940	8.234	7.416	8.486	8.053	6.931	7.432
325K	6.648	6.225	6.484	12.917	8.207	7.412	8.468	8.035	6.931	7.423
335K	6.631	6.224	6.480	12.894	8.176	7.407	8.451	8.016	6.930	7.416
345K	6.616	6.224	6.476	12.870	8.149	7.403	8.433	7.999	6.930	7.412
355K	6.597	6.224	6.472	12.846	8.100	7.398	8.414	7.982	6.930	7.401
$\Delta\delta$	-0.161	-0.010	-0.039	-0.181	-0.239	-0.032	-0.138	-0.136	-0.001	-0.069

Table 5.7: Proton chemical shift of 10 Mm quercetin in DMSO as a function of temperature. $\Delta\delta = \delta_{355\,K} - \delta_{275\,K}$ indicates total change in chemical shift.

	H6	H8	OH5	OH7	H2'	OH4'	OH3'	H5'	H6'
275K	6.280	6.514	12.654	11.08	7.789	9.590	9.974	6.989	7.652
285K	6.275	6.504	12.595	10.975	7.785	9.520	9.813	6.983	7.640
295K	6.269	6.495	12.568	10.914	7.786	9.452	9.740	6.976	7.631
305K	6.261	6.484	12.536	10.831	7.775	9.364	9.623	6.968	7.622
315K	6.256	6.476	12.506	10.740	7.763	9.295	9.574	6.963	7.614
325K	6.250	6.468	12.473	10.600	7.753	9.238	9.275	6.958	7.606
335K	6.247	6.462	12.441	10.410	7.744	9.194	9.224	6.955	7.601
345K	6.243	6.455	12.405	9.150	7.736	9.144	9.150	6.951	7.595
355K	6.240	6.449	12.370	9.110	7.727	9.112	9.112	6.947	7.587
$\Delta\delta$	-0.040	-0.065	-0.284	-1.970	-0.062	-0.478	-0.862	-0.042	-0.065

Downfield shift is +ve.
Upfield shift is –ve.

Table 5.8:(a) Proton chemical shift of 10 Mm rutin in DMSO as a function of temperature. $\Delta\delta = \delta_{355\,K} - \delta_{275\,K}$ indicates total change in chemical shift.

Temp. (K)	OH5	OH7	OH3'	H6'	H2'	OH4'	H5'	H8	H6	H1'''	H1'
283	12.635	11.075	7.692	7.574	7.554	9.398	6.869	6.425	6.227	5.364	4.392
285	12.632	11.052	7.690	7.573	7.553	7.468	6.868	6.422	6.225	5.363	4.396
293	12.618	11.051	7.687	7.570	7.552	7.469	6.867	6.420	6.223	5.361	4.398
298	12.611	12.611	7.684	7.569	7.551	7.471	6.866	6.416	6.221	5.359	4.401
303	12.601	12.601	7.681	7.567	7.550	7.470	6.866	6.413	6.219	5.357	4.404
308	12.592	12.592	7.679	7.565	7.550	7.471	6.866	6.411	6.218	5.355	4.407
313	12.583	12.583	7.676	7.564	7.549	7.470	6.866	6.409	6.217	5.352	4.411
318	12.573	12.573	7.674	7.561	7.548	7.470	6.865	6.406	6.215	5.350	4.413
323	12.564	12.564	7.672	7.560	7.547	7.471	6.865	6.404	6.214	5.348	4.417
328	12.554	12.554	7.669	7.558	7.546	7.472	6.865	6.402	6.213	5.345	4.419
333	12.546	12.546	7.666	7.557	7.545	7.472	6.864	6.400	6.212	5.343	4.422
338	12.535	12.535	7.664	7.556	7.544	7.472	6.864	6.399	6.211	5.340	4.427
343	12.523	12.523	7.662	7.543	7.543	7.471	6.864	6.396	6.210	5.337	4.429
348	12.513	12.513	7.660	7.539	7.542	7.472	6.864	6.395	6.209	5.335	4.431
353	12.504	12.504	7.658	7.538	7.540	7.472	6.864	6.393	6.208	5.332	4.436
$\Delta\delta$	-0.131	-1.405	-0.034	-0.036	-0.014	+0.004	-0.005	-0.032	-0.019	-0.032	+0.044

Downfield shift is +ve.
Upfield shift is –ve.

Table 5.8: (b) Proton chemical shift of rutinoside part of 10 Mm rutin in DMSO as a function of Temperature. $\Delta\delta = \delta_{355\,K} - \delta_{275\,K}$ indicates total change in chemical shift due to molecular association.

Temp. (K)	H6''	H3'''	H5'''	H2'''	H2''	H3''	H4''	H4'''	H6'''
283	3.717	3.398	3.321	3.270	3.230	3.084	3.066	3.103	1.002
285	3.719	3.402	3.324	3.274	3.232	3.086	3.067	3.105	1.003
293	3.720	3.404	3.328	3.275	3.234	3.087	3.070	3.106	1.004
298	3.720	3.407	3.331	3.288	3.238	3.088	3.071	3.107	1.004
303	3.722	3.409	3.333	3.293	3.238	3.090	3.072	3.109	1.007
308	3.722	3.414	3.335	3.302	3.242	3.093	3.075	3.111	1.008
313	3.723	3.416	3.336	3.305	3.244	3.095	3.078	3.113	1.010
318	3.723	3.419	3.337	3.307	3.245	3.098	3.079	3.115	1.012
323	3.726	3.423	3.341	3.310	3.247	3.100	3.082	3.118	1.013
328	3.726	3.426	3.343	3.312	3.251	3.101	3.083	3.120	1.015
333	3.727	3.430	3.346	3.315	3.252	3.104	3.085	3.123	1.016
338	3.729	3.435	3.348	3.318	3.255	3.106	3.089	3.125	1.018
343	3.729	3.438	3.350	3.321	3.259	3.108	3.090	3.126	1.019
348	3.730	3.443	3.352	3.324	3.264	3.111	3.094	3.129	1.020
353	3.732	3.445	3.355	3.327	3.266	3.113	3.097	3.132	1.022
$\Delta\delta$	+0.015	+0.047	+0.034	+0.057	+0.036	+0.029	+0.031	+0.029	+0.02

Downfield shift is +ve.
Upfield shift is –ve.

Table 5.9: Proton chemical shift of 10 mM genistein in d-DMSO as a function of temperature. $\Delta\delta = \delta_{358\ K} - \delta_{278K}$ indicates total change in chemical shift.

	H2	H6	H8	OH5	H2'	H3'	OH4'	H5'	H6'
278K	8.360	6.246	6.409	13.002	7.404	6.844	9.954	6.844	7.404
288K	8.341	6.239	6.401	12.997	7.396	6.841	9.743	6.841	7.396
298K	8.324	6.236	6.395	12.976	7.393	6.840	9.671	6.840	7.393
308K	8.304	6.233	6.390	12.952	7.392	6.838	9.586	6.838	7.392
318K	8.285	6.230	6.383	12.935	7.391	6.836	9.493	6.836	7.391
328K	8.265	6.227	6.377	12.908	7.389	6.834	9.405	6.834	7.389
338K	8.247	6.224	6.371	12.884	7.387	6.833	b	6.833	7.387
348K	8.229	6.222	6.369	12.862	7.385	6.830	b	6.830	7.385
358K	8.216	6.221	6.363	12.841	7.381	6.828	b	6.828	7.381
$\Delta\delta$	-0.144	-0.025	-0.046	-0.161	-0.023	-0.016	-0.549	-0.016	-0.023

Downfield shift is +ve.
Upfield shift is –ve.
b- Broaden

Table 5.10: Changes in chemical shift $\Delta\delta$ (in ppm) as a function of temperature of various flavonoids protons in d-DMSO.

Protons	Present Work			Protons	10.0 mM
	$\Delta\delta = \delta_{355} - \delta_{275\,K}$ 10.0 mM				
	Luteolin	Quercetin	Rutin		Genistein
H3	-0.161	-	-	H2	-0.144
H6	-0.010	-0.040	-0.019	H6	-0.025
H8	-0.039	-0.065	-0.032	H8	-0.046
OH5	-0.181	-0.284	-0.131	OH5	-0.161
OH7	-0.239	-1.970	-1.405	H2'	-0.023
H2'	-0.032	-0.062	-0.014	H3'	-0.016
OH3'	-0.138	-0.478	-0.034	OH4'	-0.549
OH4'	-0.136	-0.862	-0.004	H5'	-0.016
H5'	-0.001	-0.042	-0.005	H6'	-0.023
H6'	-0.069	-0.065	-0.036	-	-

Downfield shift is +ve.
Upfield shift is –ve.
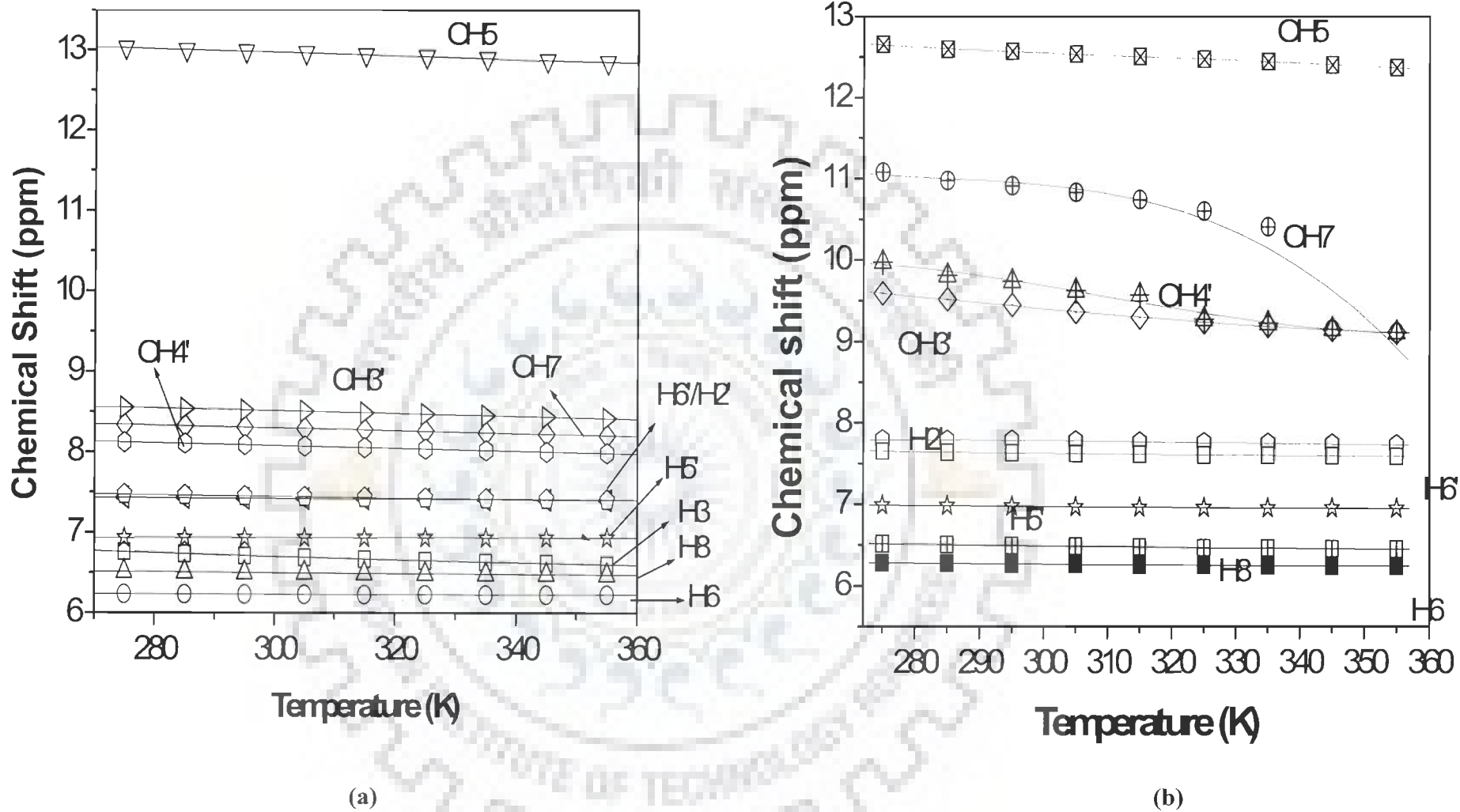
Fig. 5.4: Proton chemical shift of 10 mM (a) luteolin (b) quercetin in d-DMSO as a function of Temperature (K).
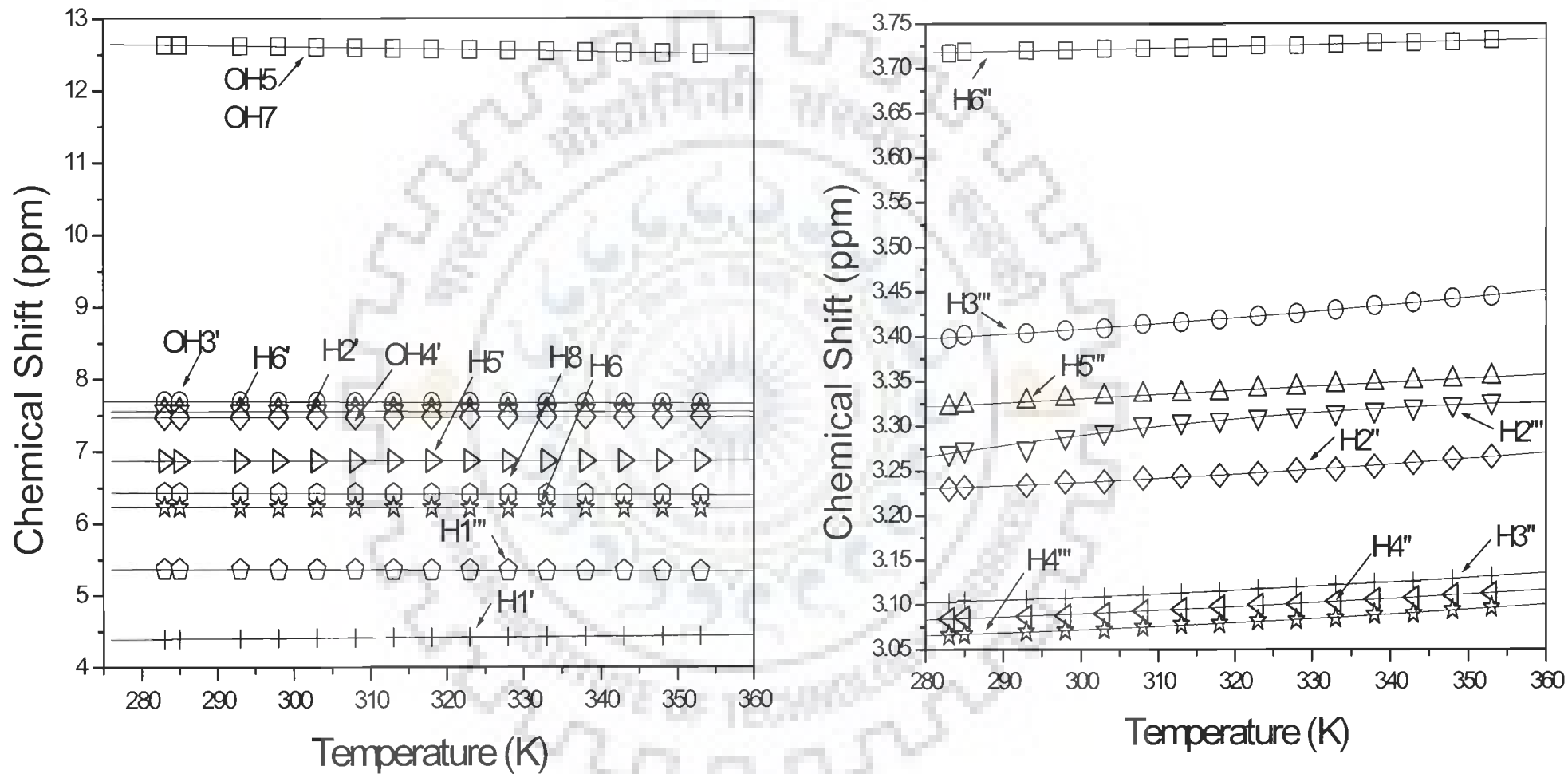
Fig. 5.4: (c) Proton chemical shift of 10 mM rutin in d-DMSO as a function of Temperature (K).

187
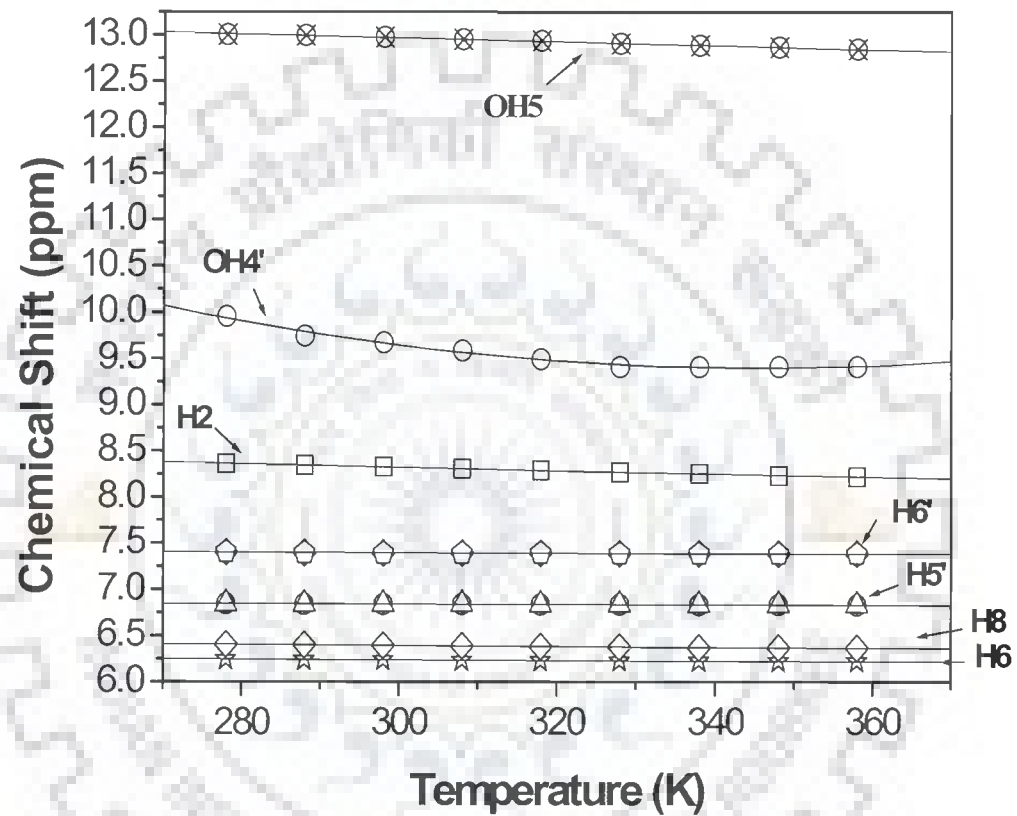
Fig. 5.4: (d) Proton chemical shift of 10 mM genistein in d-DMSO as a function of Temperature (K).

shift with temperature. It is noteworthy that there are significant differences in $\Delta\delta_{355-275\ K}$ of hydroxy protons OH5, OH7 and OH3', OH4' in luteolin and quercetin and meager difference in aromatic rings proton. Analysis of the induced proton chemical shifts for a dimer ($\Delta\delta = \delta m - \delta d$, Table 5.10) reveals a remarkable difference in the magnitude of shielding for hydroxyl protons OH7 of luteolin (0.24 ppm), quercetin (1.97 ppm) and rutin (1.41 ppm), which can be correlated for the different structures of the dimer molecules. From the crystal structural data (Jin et al., 1990; Cox et al. 2003) and our NMR and DFT data (in chapter 4), it has already been reported that OH3', OH4' and OH5 are involved in strong intramolecular hydrogen bonding as hydrogen bond donor and acceptor are available in close proximity, so at higher temperature the hydrogen bond must be destroyed and induced the upfield shift $\Delta\delta$ 0.181, 0.284, 0.131 and 0.161 for OH5 proton in luteolin, quercetin, rutin and genistein, respectively. But OH7 is free and not involved in any intramolecular hydrogen bonding, showed the maximum upfield shift among other protons up to $\Delta\delta$ 0.24 in luteolin, $\Delta\delta$ 1.970 in quercetin and $\Delta\delta$1.41 in rutin. In case of genistein, OH4' is free which is expected to involve in inter molecular hydrogen bonding and shows upfield shift of $\Delta\delta$ 0.55. So, OH7 in luteolin, quercetin, rutin and in genistein OH4'must be involved in some other kind of hydrogen bond like interaction apart from intra molecular one. Strong intramolecular hydrogen bond C-5–OH...O$=$C-4 in these flavonoids were reported and confirmed several times, similar for the crystalline genistein–morpholine complex which probably appears also in the pure solid genistein (measured by MAS NMR) and persists in its solution. Other interactions in the solid phase may involve intermolecular hydrogen bonds formed by OH7 (Zielinska et al. 2008). We also expected the involvement of OH7 in luteolin, quercetin, rutin and genistein (OH4' also) in self association forced by intermolecular hydrogen bonding. The change in chemical shift for

189

these protons i. e OH7 and OH4' (for genistein) from temperature dependent studies clearly supports the above mentioned views. It is suggested that the OH groups located at ring B and the C-7—OH can form intermolecular hydrogen bonds, whereas C-5—OH and C-3—OH form mainly intramolecular ones (Zielinska et al. 2008).

For further analysis, we did two dimensional NOESY experiments with the same concentration of luteolin, quercetin, rutin and genistein in the same solvent DMSO at 298K. Analysis of NOESY spectra (Fig. 5.12a-d) shows presence of not only several intra molecular inter-proton contacts but also few important inters molecular NOE (Table 5.11), for which the distances have been calculated. The corresponding distances in the rMD simulated structures are close to experimental restraints (Table 5.11) and hence are true representative of the experimental results. Several NOE connectivities, e.g. H5'-H6', H5'-H3, H6-H8 in luteolin, H5'-H6', H2'-OH4', OH7-H8, OH5-OH7, OH5-OH3 in quercetin; H5'-H6', H6-OH5, H6'-H1''', H6-H5''' in rutin and H2'-H3', H2-H8, OH5-H6, H2-H2', H2-H6' show proximity of protons within ring A and within ring B as well as proximity of ring B protons to rutinoside sugar in case of rutin. These intramolecular connectivities characterize specific conformation of benzopyran and phenol ring in each flavonoids. Intermolecular NOE contacts such as H3-H5' / H8 in luteolin; OH5-OH3'/OH4', OH7-OH3/OH3'/OH4' in quercetin; OH5-OH3'/OH4'/H1'', H8-H6', H1''- H1''' in rutin and H2-H6, OH5-H8 in genistein are possible only if aromatic chromophores of two flavonoid molecules associate or overlap and form homo dimer.

5.1.1.1 Restrained Molecular Dynamics (rMD) studies

The initial structure of dimer models of luteolin, quercetin and rutin have been built using builder module in MOE (Moleculoar Operating Environment), version 2006.08

Fig. 5.5: (a) 2D NOESY spectra of 10 mM luteolin in DMSO at 298 K. The figure shows expansions of specific regions to highlight connectivities.
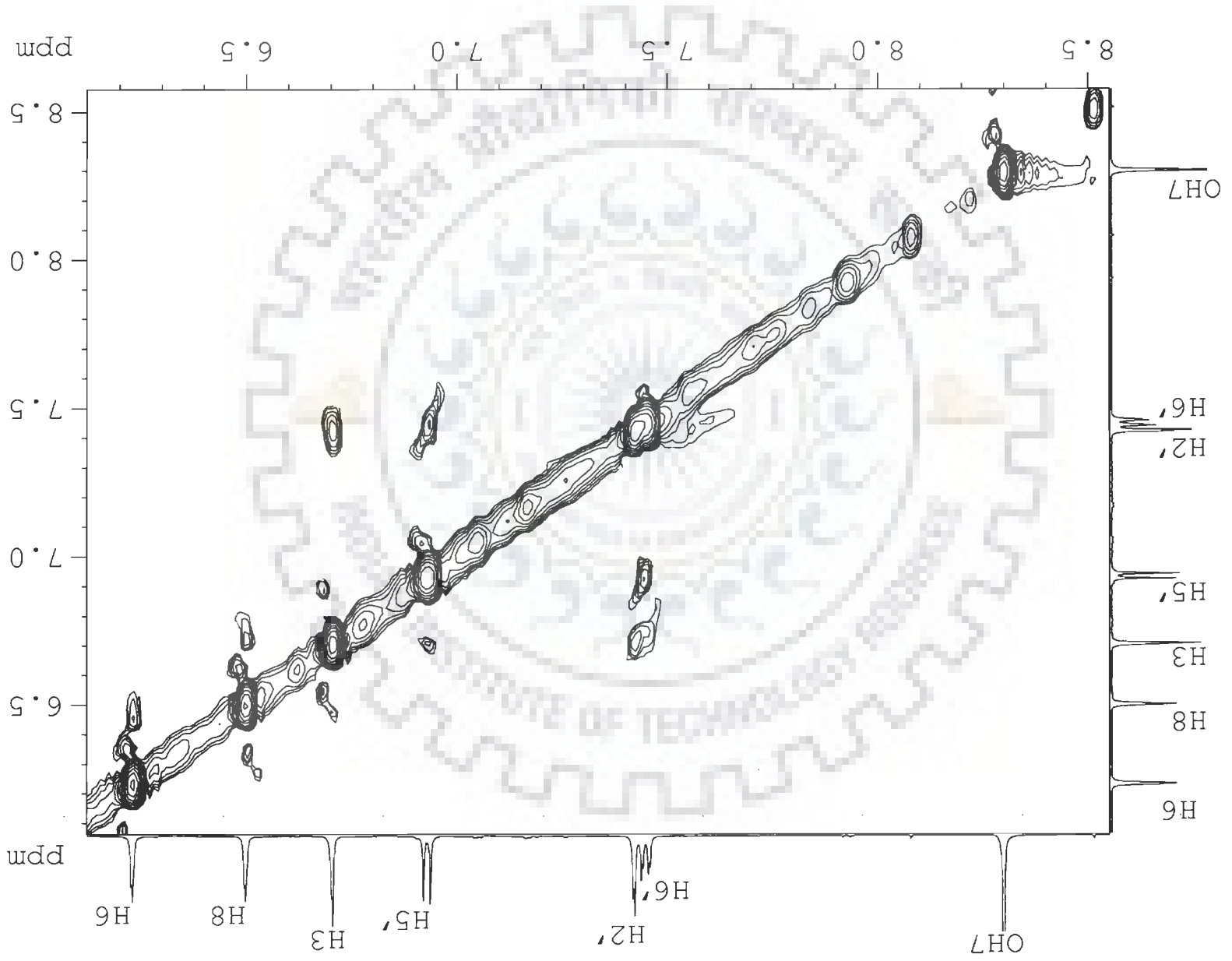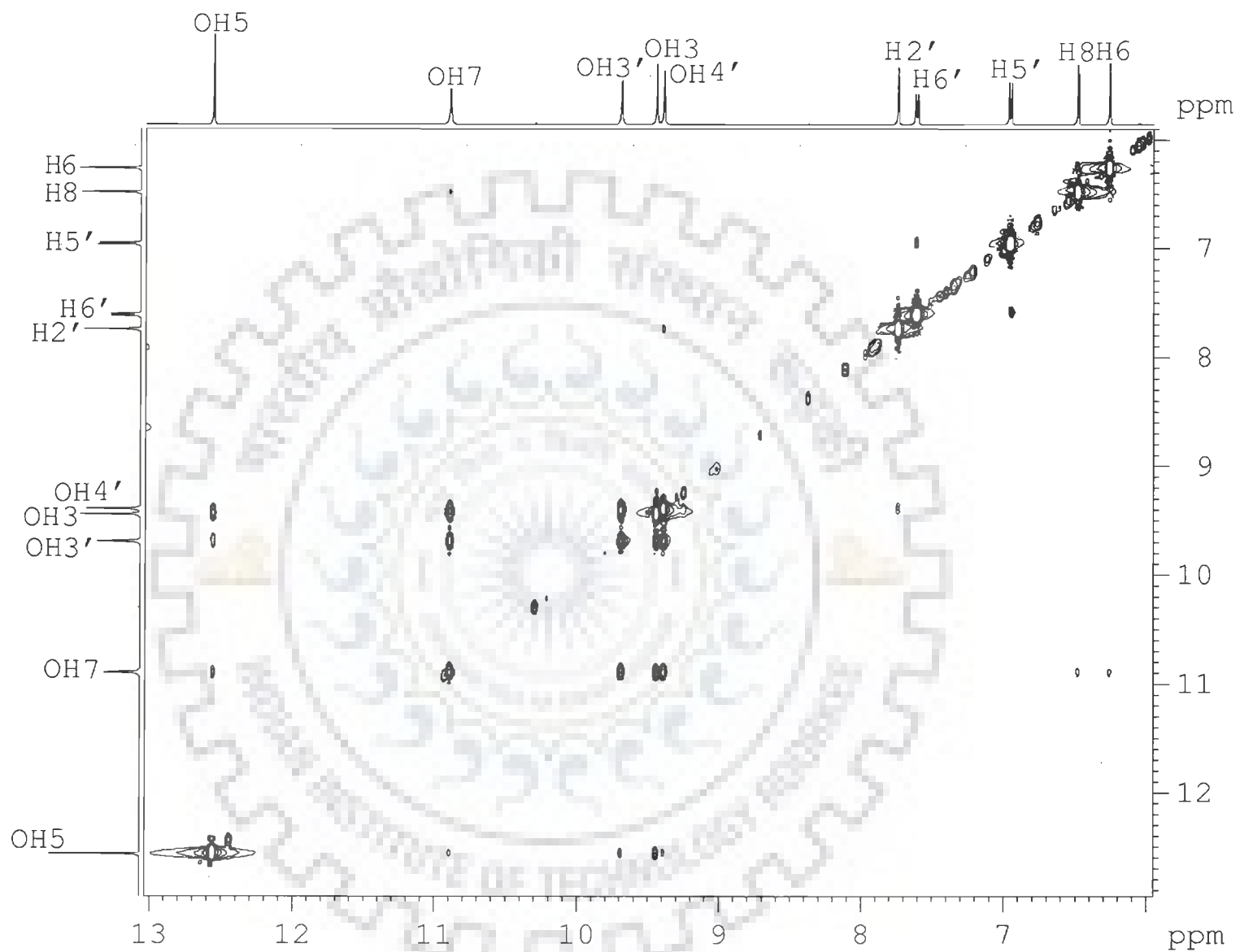
Fig. 5.5: (b) 2D NOESY spectra of 10 mM quercetin in DMSO at 298 K. The figure shows expansions of specific regions to highlight connectivities.
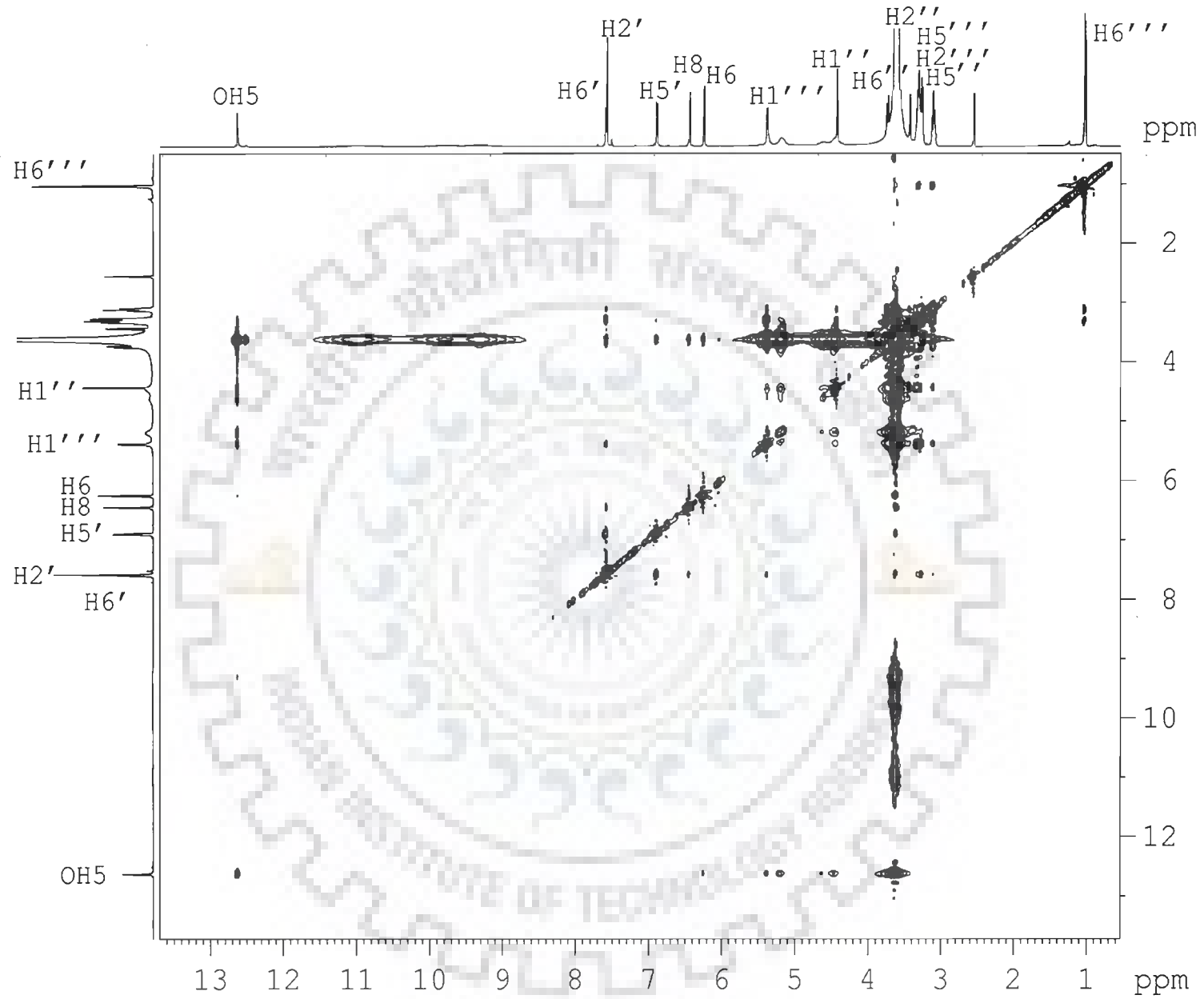
Fig. 5.5: (c) 2D NOESY spectra of 10 mM rutin in DMSO at 298 K. The figure shows expansions of specific regions to highlight connectivities.
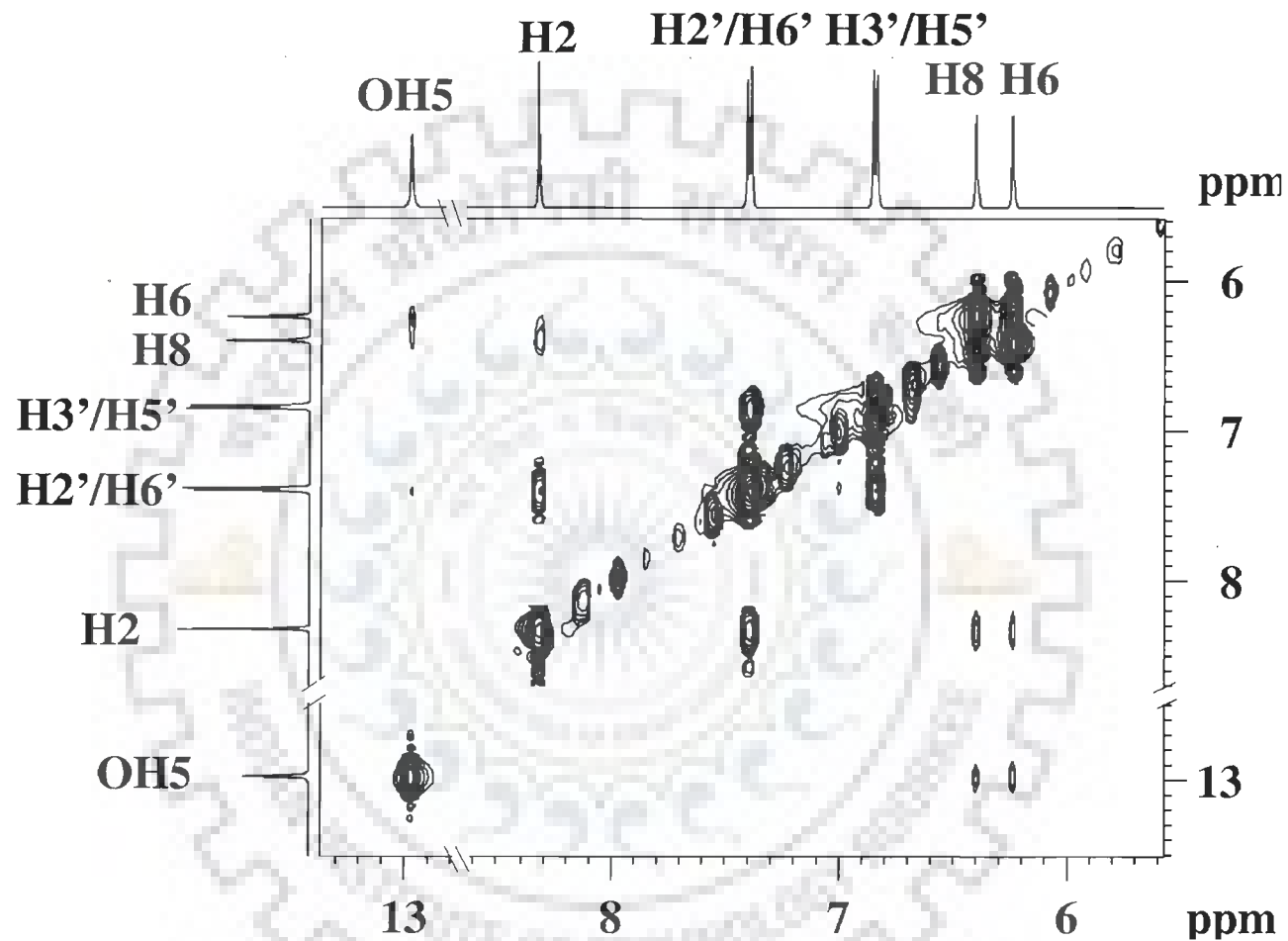
Fig. 5.5: (d) 2D NOESY spectra of 10 mM genistein in DMSO at 298 K. The figure shows expansions of specific regions to highlight connectivities.
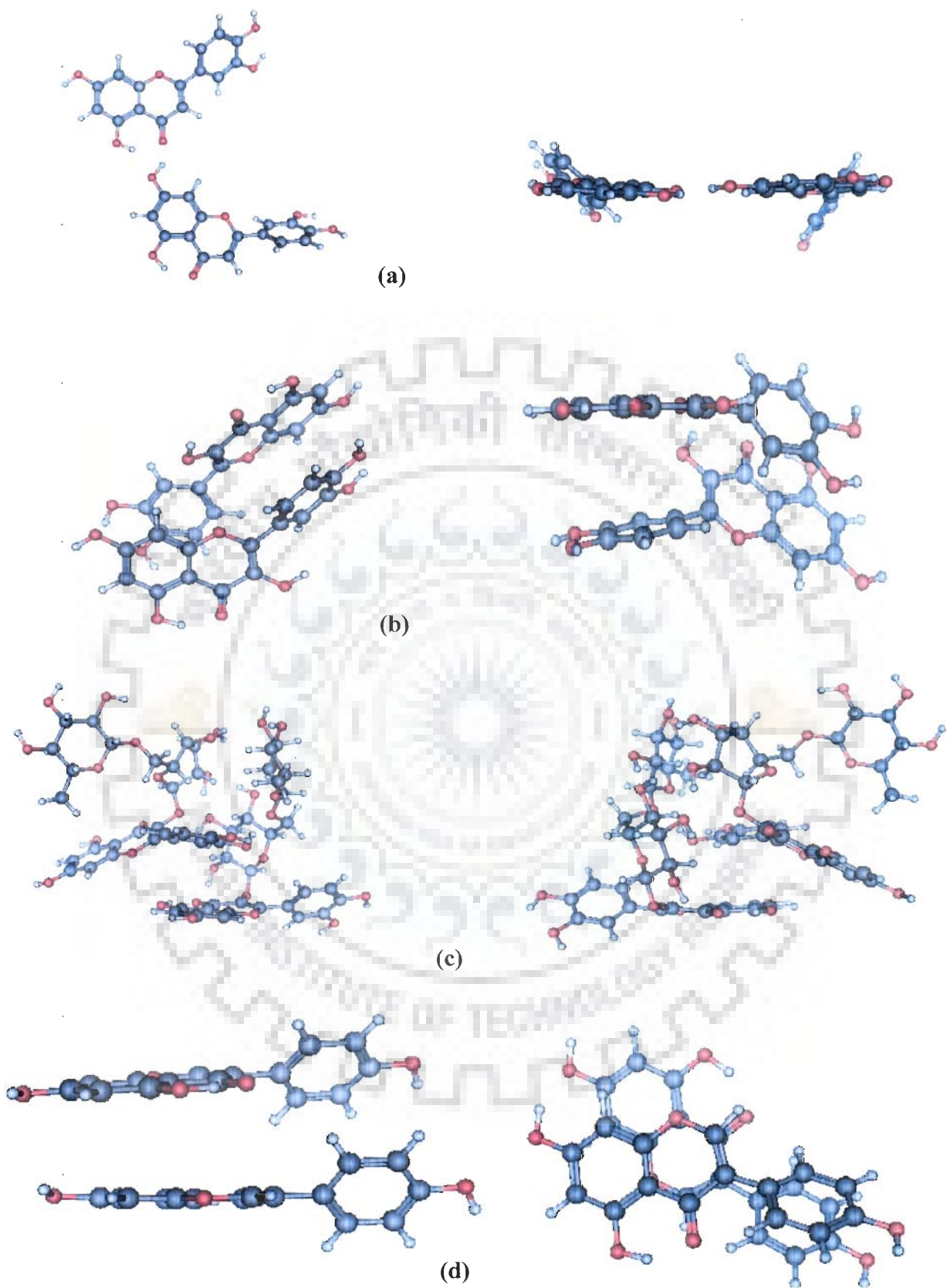
Fig. 5.6: Minimized dimer models of the flavonoids (a) luteolin, (b) quercetin, (c) rutin and (d) genistein obtained from rMD simulations.

Table 5.11: Connectivities and inter-proton distances (Å) of (a) luteolin and quercetin, (b) rutin and (c) genistein obtained from NOESY spectra (τ_m=300 ms) at 298 K. The corresponding distances obtained from optimized rMD structure are also shown. Overlap of peak is shown by 'o' and '-' indicates absence of peak.

Table 5.11(a):

Connectivities	Luteolin		Quercetin	
	Distance obtained from NMR (Å)	Distance in rMD structure (Å)	Distance obtained from NMR (Å)	Distance in rMD structure (Å)
INTRAMOLECULAR CONNECTIVITIES				
H5'-H6'	2.45	2.47	2.45	2.47
H2'-H3	3.16	3.18	-	-
H5'-H3	3.75	3.65	-	-
H6-H8	4.24	4.24	-	-
H2'-OH4'	-	-	3.80	4.37
OH7-H8	-	-	4.18	3.53
OH5-OH7	-	-	4.78	4.98
OH5-OH3	-	-	3.07	3.65
INTERMOLECULAR CONNECTIVITIES				
H8-H3	3.18		-	-
OH5-OH4'	-	-	4.49	5.67
OH5-OH3'	-	-	4.20	4.01
OH7-OH3'	-	-	3.50	4.10
OH7-OH3	-	-	3.83	6.22*
OH7-OH4'	-	-	2.87	3.44

Table 5.11(b):

Rutin		
Connectivities	Distance obtained from NMR (Å)	Distance in rMD structure(Å)
INTRAMOLECULAR CONNECTIVITIES		
H5'-H6'	2.45	2.46
OH5-H6	5.13	4.47
H2'-H1''	5.32 (o)	3.69(*anti* conformer)
H6'-H1''	5.32 (o)	5.46(*anti* conformer)
H2'-H1'''	3.85(o)	3.78(*anti* conformer)
H6'-H1'''	3.85(o)	5.79(*anti* conformer)
H6-H5'''	2.82	3.42
INETRMOLECULAR CONNECTIVITIES		
H8-H2'	3.89	4.12(*anti* conformer)
H8-H6'	3.89	5.92(*anti* conformer)
OH5-OH4'	4.21	4.05
OH5-OH3'	5.44	5.43
OH5-H1''	2.73	3.41
H1'''-H1''	3.31	4.12

Table 5.11(c):

Genistein		
Connectivities	Distance obtained from NMR (Å)	Distance in rMD structure(Å)
INTRAMOLECULAR CONNECTIVITIES		
H5'-H6'	2.45(o)	2.45
H2'-H3'	2.45(o)	2.46
H2-H8	4.82	4.50
OH5-H6	5.39	3.53
H2-H2'	2.92(o)	2.62 (*syn* conformer) 4.42 (*anti* conformer)
H2-H6'	2.92(o)	4.38 (*syn* conformer) 2.61 (*anti* conformer)
INETRMOLECULAR CONNECTIVITIES		
H2-H6	5.30	5.29
OH5-H8	5.78	5.83

(Chemical Computing Group, Canada) software. The energy of the molecule was minimized using 1000 steps each of Steepest Descent and Conjugate Gradient to remove any internal strain due to short contacts in starting structure using MMFF94x force field. Dielectric constant was fixed as 1.0 for calculation of electrostatic interactions. Conformational search was performed by using the following simulated annealing restrained Molecular Dynamics protocol. The molecule was heated to a temperature of 800 K in steps of 100 K so that the chances of molecule being trapped in local minima become least and it can reach global minima. Molecular Dynamics was carried out for 100 ps up to 800 K during which 100 structures were saved at regular intervals of 1 ps. Each of them was then slowly cooled at 300 K in steps of 100 K. At the end of simulated annealing all the structures are minimized by 1000 steps of Conjugate Gradient until a predefined convergence limit of root mean square derivative of < 0.001 Kcal mole^{-1} Å^{-1} is reached. Same protocol was repeated for quercetin and rutin to see the difference due to their slight variation in structures.

The dimer models of the flavonoids obtained from rMD simulations (Figs. 16-18) show that there is significant overlap of the aromatic rings in luteolin, quercetin, genistein and the rutinoside sugar in rutin. The rutinoside sugar moiety of one molecule of rutin interacts with the chromophore of the other molecule, thus there is possibility of H-bond formation between the OH3' or OH4' group of aromatic ring C of the chromophore of one molecule and the OH group of rutinosides. Such bond are absent in other flavonoids luteolin, quercetin and genistein. From rMD studies it can be seen that the aromatic ring of one molecule partially overlap on the other. This can be correlated to meager change in chemical shift. Though the association of aromatic molecules is known to be driven but the stacking force involved is not ascertained. During rMD studies hydrogen bond formation was observed between OH7 of one molecule of luteolin and OH5 of other molecule. There may be probability of stacking

interactions also, as quercetin and genistein prefer the stack formation due to to planarity of their rings. But concentration dependent meager change in chemical shift abolish the idea of stacking interaction while temperature dependent study support hydrogen bond based dimer formation. There is need to find out whether self association is available in flavonoids or not. In this regards, further other physico-chemical methods have been used to explain this phenomena in flavonoids.

5.1.2 Absorption and Emission studies

Visible absorbance spectra are recorded in CARY 100 Bio spectrophotometer. The concentration of flavonoids in DMSO solution were determined spectro photometrically at the λ_{max} of 349 nm (ε = 20,417 $M^{-1}cm^{-1}$), 380 nm (ε = 14,920 $M^{-1}cm^{-1}$), 368 nm (ε = 19,700 $M^{-1}cm^{-1}$) and 260 nm (ε = 37,260 $M^{-1}cm^{-1}$) for luteolin, quercetin, rutin and genistein, respectively. All experiments were performed in the HPLC grade DMSO at 25°C. Absorbance and emission scans are done from 1, 3, 5, 6, 7, 8, 9, 10, 11, 12 µM concentration. The dimerization constant is calculated by using least square fitting curve (Kapuscinski et al., 1985; Lee, et al., 1989) in MATLAB 7.0 version software. The ligand dimerization constants (K_D) were calculated according to the method described by von Tscharner and Schwarz, 1979:

$$K_D = C_T\text{-}C_M / 2C_M^2$$

Where C_T is the total flavonoid concentration and C_M is the monomer concentration. The absorption spectrum of flavonoids shows one band near the visible region (350 nm) and one in the ultraviolet region (260 nm) for luteolin and genistein. Quercetin gives these two bands at 380 nm and 260 nm while rutin at 365nm and 265 nm, respectively (Fig.5.7). The one visible region bands are characteristic of the conjugated benzopyran ring; in the ultraviolet region, one at 260-265 nm is for aromatic phenyl ring of these flavonoids. As the concentration of drug increases, there are weak but definite changes in the shape of their

spectra. The maxima located at 260 and 380 nm at which absorption increases with increases in concentration. For any concentration (~ 1-12 μM), the absorption did not follow the Beer-Lambert law. The more deviation was observed in the case of quercetin while slight deviations were observed in luteolin and quercetin. In dilute solution (1 μM) the 260 and 349 nm bands are of equal intensity at all the concentration of luteolin, while in case of quercetin and rutin, the ultraviolet band intensity increases with increase in concentration (12 μM). It is found that the absorption maximum of the soret region at 348 nm for dimer exhibits a slight blue shift of about 2 nm compared to that at 350 nm of monomer, indicating a weak coupling between the transitions in the benzopyran moieties adopting the arrangements as H-type aggregate which is similar result as in case of porphyrin dimer (Kanoet al. 2000; Gong et al. 2007). The benzopyran chromophores of the flavonoids are planar and have free hydroxyl groups for intermolecular hydrogen bonding. Further, due to planar structure, there is uneven electronic charge distribution and such a charge distribution could favor the formation of dimers. Using excitation wavelength (λ_{ex}) as 349, 380 and 368 nm and emission wavelength (λ_{em}) as 425 nm for luteolin, quercettn and rutin, the emission scans were done in spectrofluorimeter (make HORIBA Jobin, Horiba model Fluorolog -3). Fluorescence intensity gets quenched when the drugs start forming dimer. Since the dipole moment of the monomer–dimer transition is zero, observed fluorescence is mainly contributed by the monomer species (Fig. 5.8).and there is no contribution from the dimer species. Also, there is no shift in the emission maxima with increase in concentration. The dimerization constant (K_D) is calculated by computer-aided extrapolation of the spectral changes to high dilution of the drugs, that is, least square fitting curve using software MATLAB 7.0 version. The concentration of monomer, dimer and the dimerization constant is calculated (Fig. 5.8) and the values are 6500 M^{-1} for luteolin; 58100

200
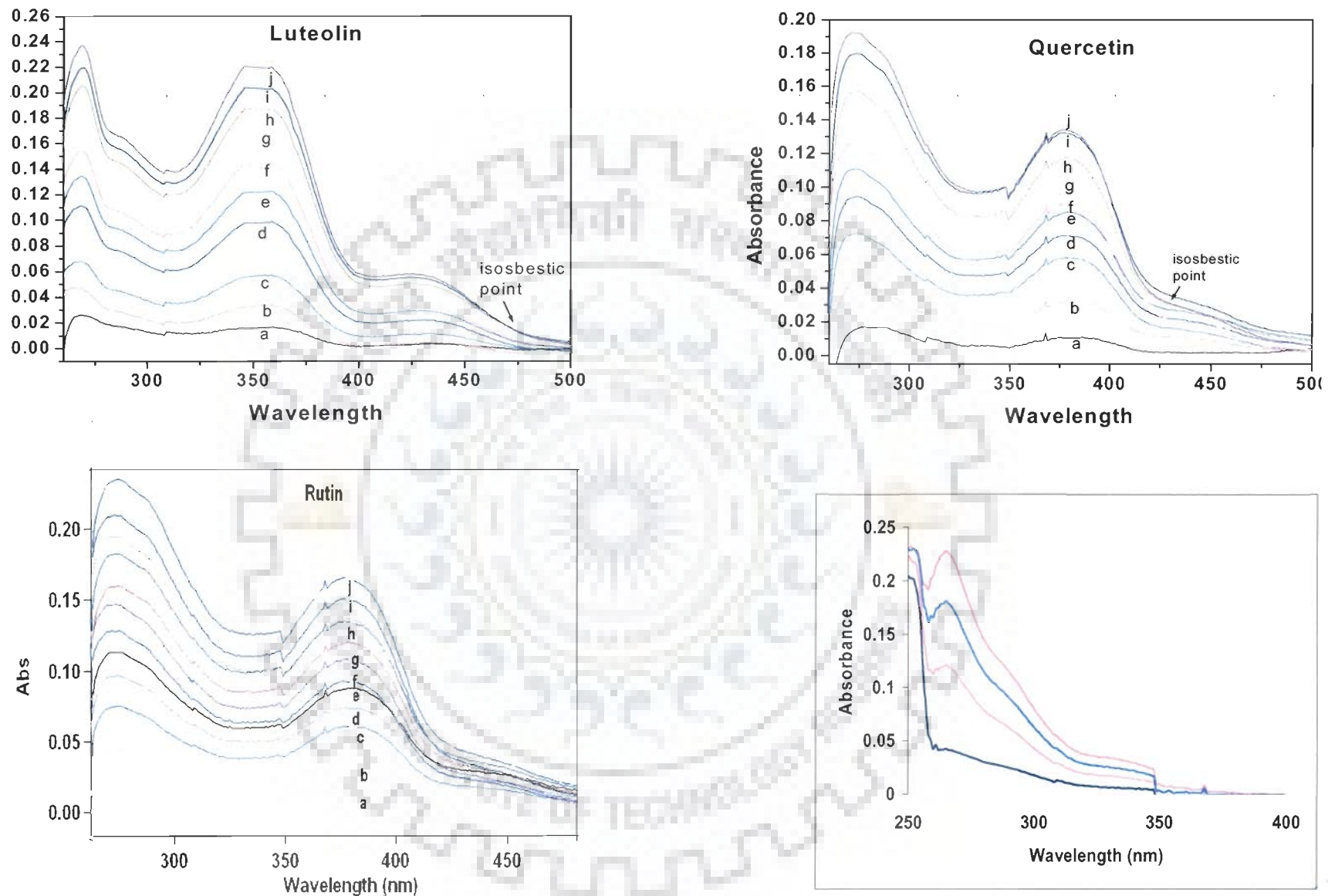
Fig. 5.7: Absorption Spectra of luteolin, quercetin, rutin and genistein as a function of concentration (a, b, c, d, e, f, g, h, i, j denotes 1, 3, 5, 6, 7, 8, 9, 10, 11 and 12 µM concentration) in DMSO.
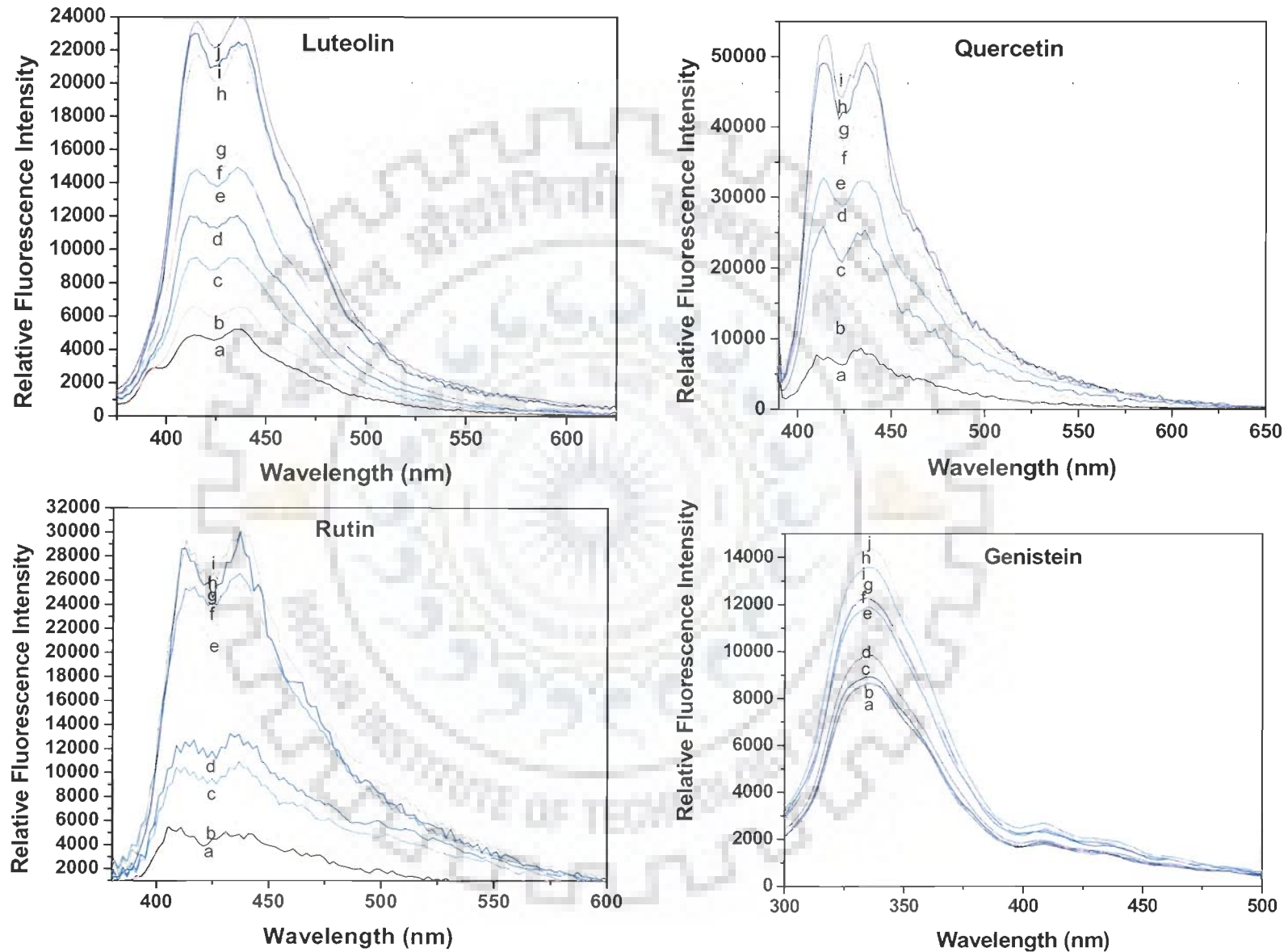
Fig. 5.8: Fluorescence Spectra of luteolin, quercetin, rutin and genistein as a function of concentration (a, b, c, d, e, f, g, h, i, j denotes 1, 3, 5, 6, 7, 8, 9, 10, 11 and 12 μM concentration) in DMSO.

M^{-1} for quercetin, 6500 M^{-1} for rutin and 17300 for genistein (Table 5.12). It is found that the magnitude of the self-association constant for quercetin is higher than that of luteolin, rutin and genistein, indicating that quercetin has higher degree of self-aggregation than luteolin and quercetin. It may be noted that there is a possibility of the existence of higher aggregates at higher concentration.

Table 5.12: Dimerization Constant calculations for luteolin, quercetin and rutin using fluorescence data.

Luteolin Conc (µM)	Monomer (µM)	Dimer (µM)	Dimerization constant 'K' (x 10^6 M^{-1})
1.00	0.92	0.08	0.047259
3.00	2.79	0.21	0.013489
5.00	4.84	0.16	0.003415
6.00	5.97	0.13	0.000421
7.00	6.96	0.04	0.000201
8.00	8.01	0.01	0.000078
9.00	9.02	0.02	0.00012
10.00	9.99	0.01	0.0000501
11.00	10.97	0.03	0.000125
12.00	11.98	0.02	0.0000697
		Mean	0.0065
Quercetin Conc (µM)	Monomer (µM)	Dimer (µM)	Dimerization constant 'K' (x 10^6 M^{-1})
1.00	0.70	0.30	0.306122
3.00	2.14	0.86	0.093895
5.00	3.82	1.18	0.040432
6.00	4.75	1.25	0.027701
7.00	5.69	1.31	0.020231
8.00	6.16	1.84	0.024245
9.00	7.10	1.9	0.018845
10.00	7.91	2.09	0.016702
11.00	8.85	2.15	0.013725
12.00	8.98	3.02	0.018725
		Mean	0.0581
Rutin Conc (µM)	Monomer (µM)	Dimer (µM)	Dimerization constant 'K' (x 10^6 M^{-1})
1.00	0.90	0.1	0.061728
3.00	2.89	0.11	0.006585

5.00	5.07	0.07	0.00136
6.00	6.03	0.03	0.00041
7.00	7.04	0.04	0.0004
8.00	8.03	0.03	0.00023
9.00	8.90	0.1	0.000631
10.00	10.21	0.21	0.00101
11.00	11.09	0.09	0.00037
12.00	12.08	0.08	0.00027
		Mean	0.0065
Genistein Conc (μM)	Monomer (μM)	Dimer (μM)	Dimerization constant 'K' ($\times 10^6 \text{ M}^{-1}$)
1.00	0.82	0.18	0.133849
3.00	2.67	0.43	0.030159
5.00	4.77	0.23	0.005054
6.00	5.87	0.13	0.001886
7.00	6.94	0.04	0.000415
8.00	8.15	0.15	0.001129
9.00	9.08	0.02	0.000121
10.00	9.99	0.01	0.000005
11.00	10.96	0.04	0.000166
12.00	11.94	0.06	0.00021
			0.0173

5.1.3. Diffusion Ordered Spectroscopy (DOSY) studies

NMR-based techniques have been in use for many years to characterise hydrogen bonding (Konrat et al. 1999). Using NMR spectroscopic techniques, the hydrogen bonding is mostly manifested such as characteristic downfield shift of the proton resonance (Cordier et al. 1990). Other NMR techniques include the observation of deuterium isotope effects (Timmerman et al. 2000), solution measurement of the chemical shift anisotropy (Kapur et al. 2000), dynamic NMR studies (Johnson, 1996), the studies of intermolecular NOE effects (Fielding, 2000), and very recently the observation of spin–spin coupling constants across the hydrogen bond in proteins (Keresztes and Williard, 2000). We want to show here that diffusion-ordered spectroscopy (DOSY) can be another useful probe to qualitatively understand the relative strength of hydrogen bonding between a common ligand, and various

other components present as a mixture in non-aqueous solutions. In diffusion-ordered spectroscopy (DOSY)(Johnson, 1999), which was introduced only a few years ago (Pelta, 1998), the results are displayed as 2D spectra with the NMR chemical shift on the horizontal axis and the derived diffusion coefficients on the vertical axis. Such DOSY plots are obtained by effective data inversion of the pulsed field gradient (PFG) spin echo NMR data obtained by incrementing the gradient strength. PFG NMR is a very effective tool to study the translational motion of molecules, and is used for studying molecular associations (Rogers-Sanders et al. 2001). However, DOSY has the advantage of immediately visualising the effects even in more complex mixtures. The diffusion coefficient of the molecule is inversely proportional to the molecular radius. If the molecule is aggregating, their global size and molecular weight should be greater than the uncomplexed ones, and consequently they should exhibit different diffusion coefficient values. The observed diffusion is an average of the populations of the diffusion of the complexed and uncomplexed forms in equilibrium. A change in the chemical shift does not provide a sufficient indication about the strength of interaction between the components, which could be due to other effects influencing the chemical shift but the DOSY plots provide a better insight about the strength of such interactions which are clearly manifested in the diffusion dimension. The molecules are known to exhibit self association at the concentration used. Our results show that the rate of exchange between monomer and dimer is apparently fast; but instead of two distinct separate peaks, less separated peaks are observed for flavonoid protons, which is averaged value of each weighted by its relative concentration. Rutin shows the least diffusion rate than that of quercetin, while genistein shows lesser than quercetin and luteolin shows the fastest diffusion (Fig. 5.9a-d). The average diffusion coefficient of the molecule is 5.18 x 10^{-10} m^2/s for luteolin, 1.14 x 10^{-10} m^2/s for quercetin, 9.65 x 10^{-11} m^2/s for

rutin and 2.32 x 10^{-10} for genistein at 298 K (Table 5.13). The apparent diffusion rate is fastest for luteolin and least for rutin. The bulky rutinoside moiety in rutin could be one of the reasons for its least diffusion than luteolin and quercetin. Further, the rates are weighted by the relative concentrations of monomer and aggregated forms, it may be inferred that greater extent of self association exists in rutin. As discussed in chapter 4, genistein has one while luteolin has two intra molecular hydrogen bonds established between H5 of A-ring and the 4-keto group of C-ring and between the ortho-dihydroxyls in the B- ring, respectively while quercetin has one extra hydrogen bond between the 4-keto group of C-ring and H3. while H-O3 group lacks in rutin so no hydrogen bond persists between the 4-keto group of C-ring, between H-O3 of C-ring but rutin has two other hydrogen bonds, one between the 4-keto group of C-ring of quercetin part and H-O2'' of glucose moiety and H3, the other between H6' at B ring and the oxygen O1'' of glucose moiety of rutinoside. More number of hydroxyl group present in rutin manifest inter/intermolecular interaction leading to self molecular association. This may be the reason for the least diffusion of rutin while luteolin, quercetin and genistein has relatively less number of free hydroxyl group than rutin and hence it can be expected that hydrogen bonding is responsible for molecular association.

5.1.4 Electron Spray Ionization-Mass spectrometry Studies (ESI-MS)

Negative-ion ESI-MS spectra are obtained on Esquire 4000 (Bruker Daltonics, Germany) with the normal ESI source. The 5-50 µM concentration solutions of drugs are prepared in the solvent DMSO. The solutions are infused directly into the mass spectrometer at 250 µl/hr rate. The parameters selected are: cone voltage 4.0 KV, nebulizer pressure 15 psi, dry gas flow rate 6 l/min and the capillary temperature 60°C. Data is collected for approximately 10 scans. The maximum accumulation time is 200 ms and scan range is 200-
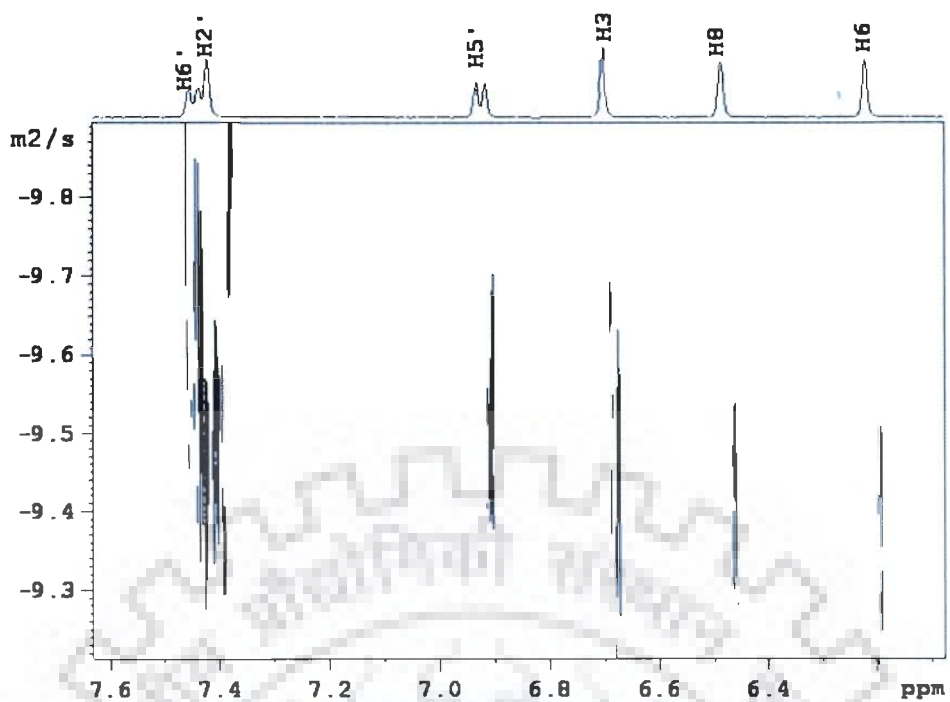
Fig. 5.9 a: DOSY spectra of 10mM luteolin in d-DMSO at 298K
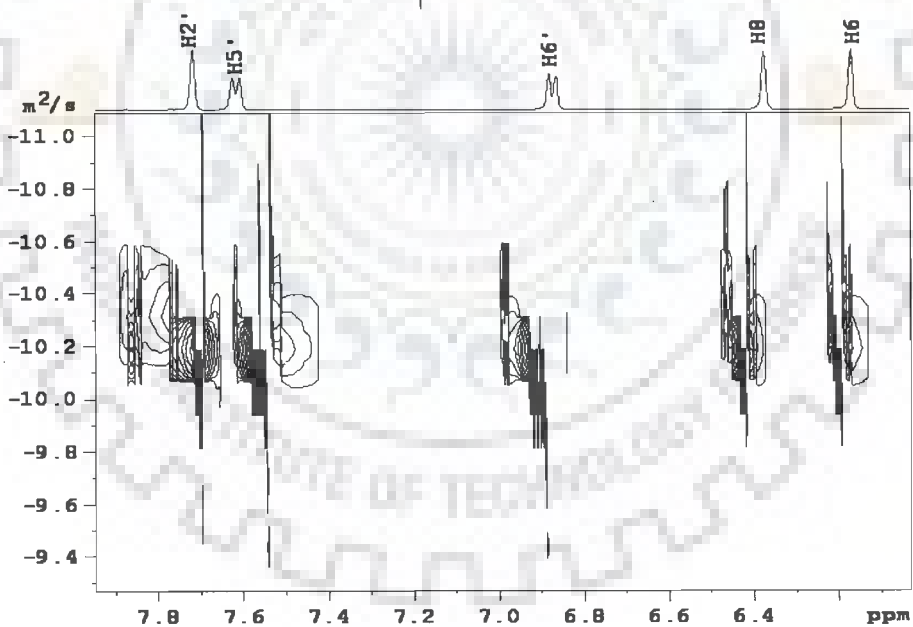
Fig. 5.9 b: DOSY spectra of 10mM quercetin in d-DMSO at 298K
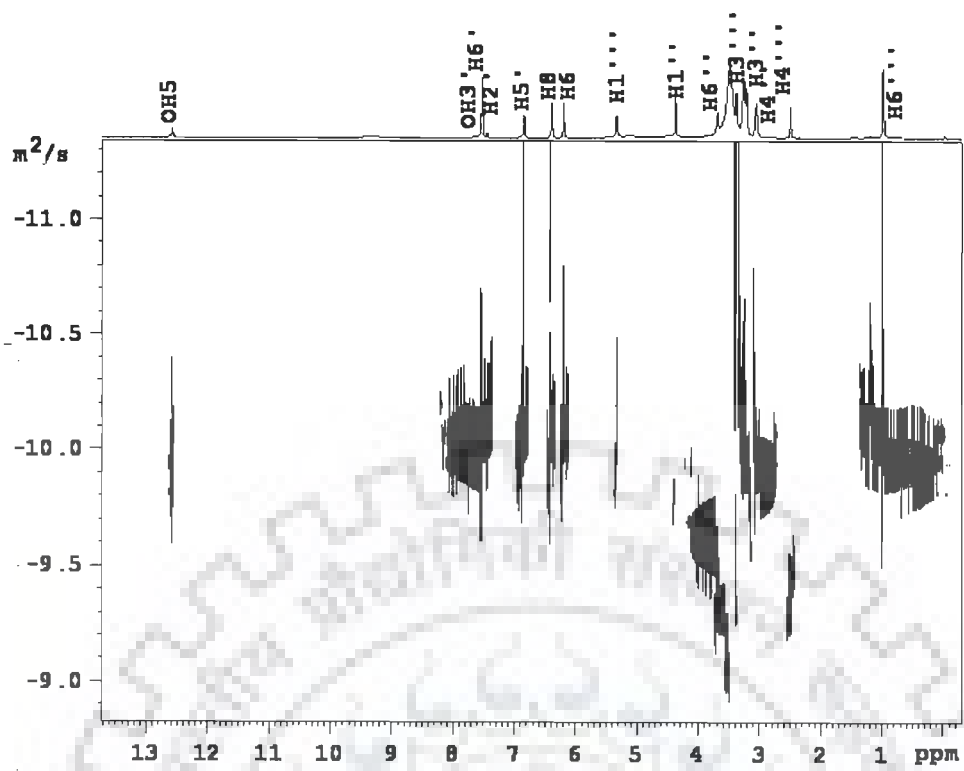
Fig. 5.9 c: DOSY spectra of 10mM rutin in d-DMSO at 298K
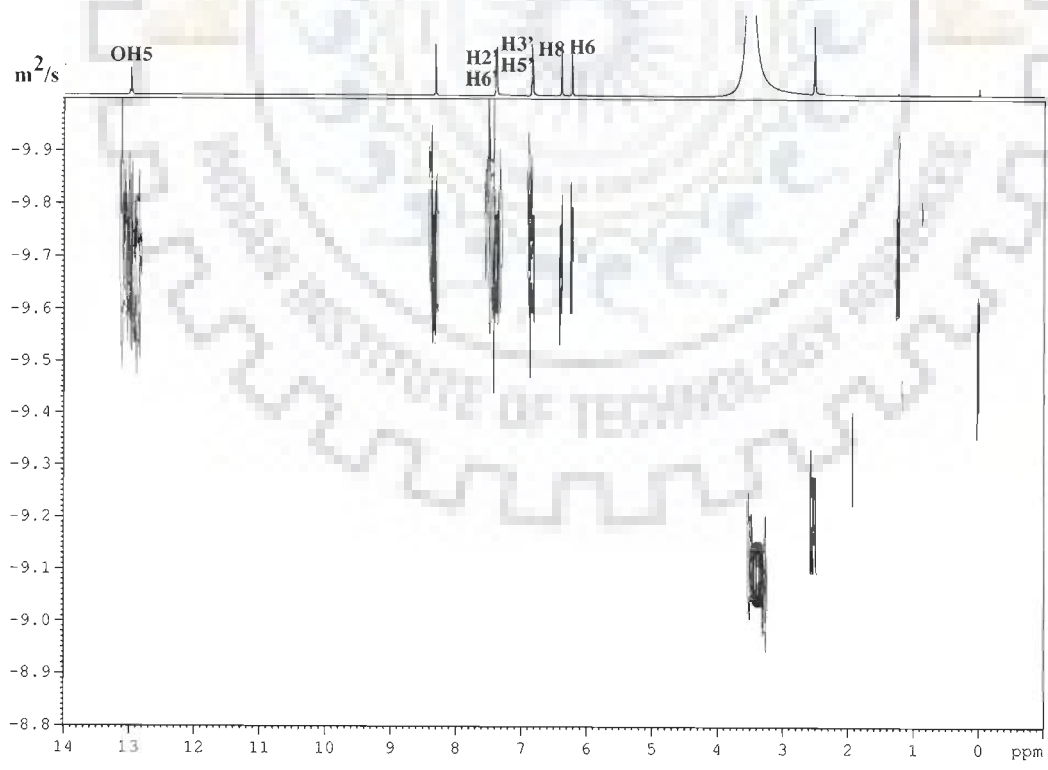
Fig. 5.9 d: DOSY spectra of 10mM genistein in d-DMSO at 298K

208

Table 5.13: **Diffusion constant of protons of 10mM luteolin, quercetin, rutin and genistein in d-DMSO at 298K**

Diffusion Constant (m^2/s)					
Proton	Luteolin	Quercetin	Rutin	Proton	genistein
H3	1.11×10^{-9}	-	-	H2	2.30×10^{-10}
H6	4.38×10^{-10}	1.12×10^{-10}	9.14×10^{-11}	H6	2.32×10^{-10}
H8	7.86×10^{-10}	1.12×10^{-10}	8.59×10^{-11}	H8	2.28×10^{-10}
H2'	3.39×10^{-10}	1.12×10^{-10}	9.98×10^{-11}	H2'	2.28×10^{-10}
H5'	4.70×10^{-10}	1.12×10^{-10}	9.52×10^{-11}	H5'	2.29×10^{-10}
H6'	3.88×10^{-10}	1.14×10^{-10}	9.19×10^{-11}	H6'	2.28×10^{-10}
OH5	1.00×10^{-10}	1.19×10^{-10}	1.15×10^{-10}	OH5	2.52×10^{-10}

1500 m/z. The Electron Spray Ionization Mass Spectrometric studies of these four bioflavonoids viz. luteolin, quercetin, rutin and genistein (Fig. 4.1, Chapter 4) show that these molecules exist in monomeric as well as dimeric or trimeric state at 5-50 µM concentration. Quercetin differs with luteolin in having –OH group at C3 position by replacing –H atom and their intense peaks appear at 300.96 and 283.0 m/z ratio, respectively. Rutin which is a sugar derivative of quercetin differs by replacing –OH group at C3 position with a rutinoside moiety. Similarly, substitution of phenyl ring B at position C3 yield in to an isoflavone genistein and peak appear at 269 m/z. The monomer form of this quercetin glycoside peaks appears at 609.18 m/z ratio corresponding to the molecular weight with single charge. The dimer form of these flavonoids luteolin, quercetin, rutin and genistein are observed at 567.30, 602.90, 1020.32 and 538 m/z ratio corresponding to the molecular weight with single/double charge, respectively (Fig.5.10 a-d). We also observed peaks corresponding to trimer with single / double charge. But the intensity was very less. Further, MS-MS fragmentation of their dimer signals at 567.30, 602.90 and 1020.32 m/z ratio cleaved in to their corresponding monomer m/z ratio at 283.0, 300.96 and 609.18 (Fig. 5.11a-d). The mass spectrum gives a direct proof of the existence of dimer and trimer or may be higher aggregates species due to self association.

However it may be noted that this method cannot be used to give a quantitative estimate of the relative amount of monomer and dimer since the process of electron spray ionization in gaseous phase may cleave the dimers or higher aggregates, if present. We observe a peak at $m/z = 1039.87$ in mass spectra of rutin. This mass number corresponds to dimer ($m/z = 1169.02$) without glucoside sugar moiety ($m/z = 129.15$). No such corresponding peak is observed in luteolin, quercetin and genistein. This shows that cleavage is higher in rutin as compared to luteolin, quercetin and genistein due its bulky rutinoside ring.

5.2 Biological relevance

5.2.1 Bioavailability and metabolism

Molecular association plays an important role in many chemical and biological systems. It can be correlated with the physiological activities and bioavailability of these flavonoids. A large number of studies focus on the bioavailability and absorption of bioflavonoids in vivo are cited in literature (Manach et al., 2005; Williams et al., 2004; Kroon et al., 2004; Manach et al., 2004). Many pharmacologically active polyphenols are hydrophobic molecules, which may undergo different kinds of homo and hetero association, and whose site of action in the organism frequently is through the plasma membrane for their intracellular activities. Many studies attribute their poor gastrointestinal membrane absorption to reduced dissolution rate (Arcari et al., 1992; Liu et al., 2006) or degradation by enzymes (from bacteria and host) in the gastrointestinal tract and liver (Scalbert and Williamson, 2000; Stahl et al., 2002). In most of cases, complexation of many hydrophobic substances using β-CD can improve oral bioavailability by increasing both the dissolution rate (Arcari et al., 1992; Tommasini et al., 2004; Loftsson and Duchene, 2007) and/or protecting against biodegradation (Salmaso et al., 2007). The resultant complex obtained from the inclusion of flavonoids in β-

210
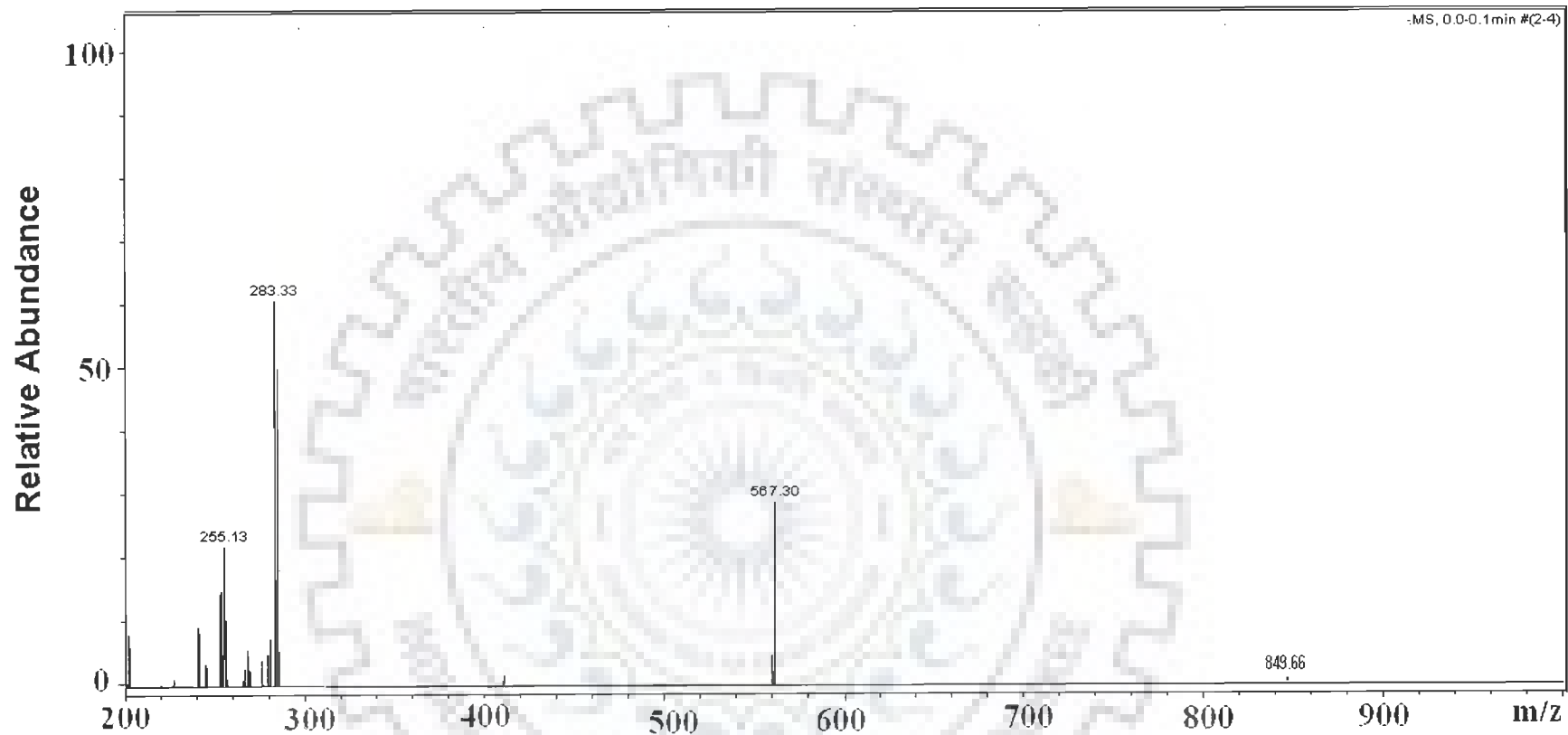
Fig. 5.10(a): Electron-Spray Ionization Mass Spectra (ESI-MS) of showing their monomeric and dimeric state of luteolin with single/double charge.
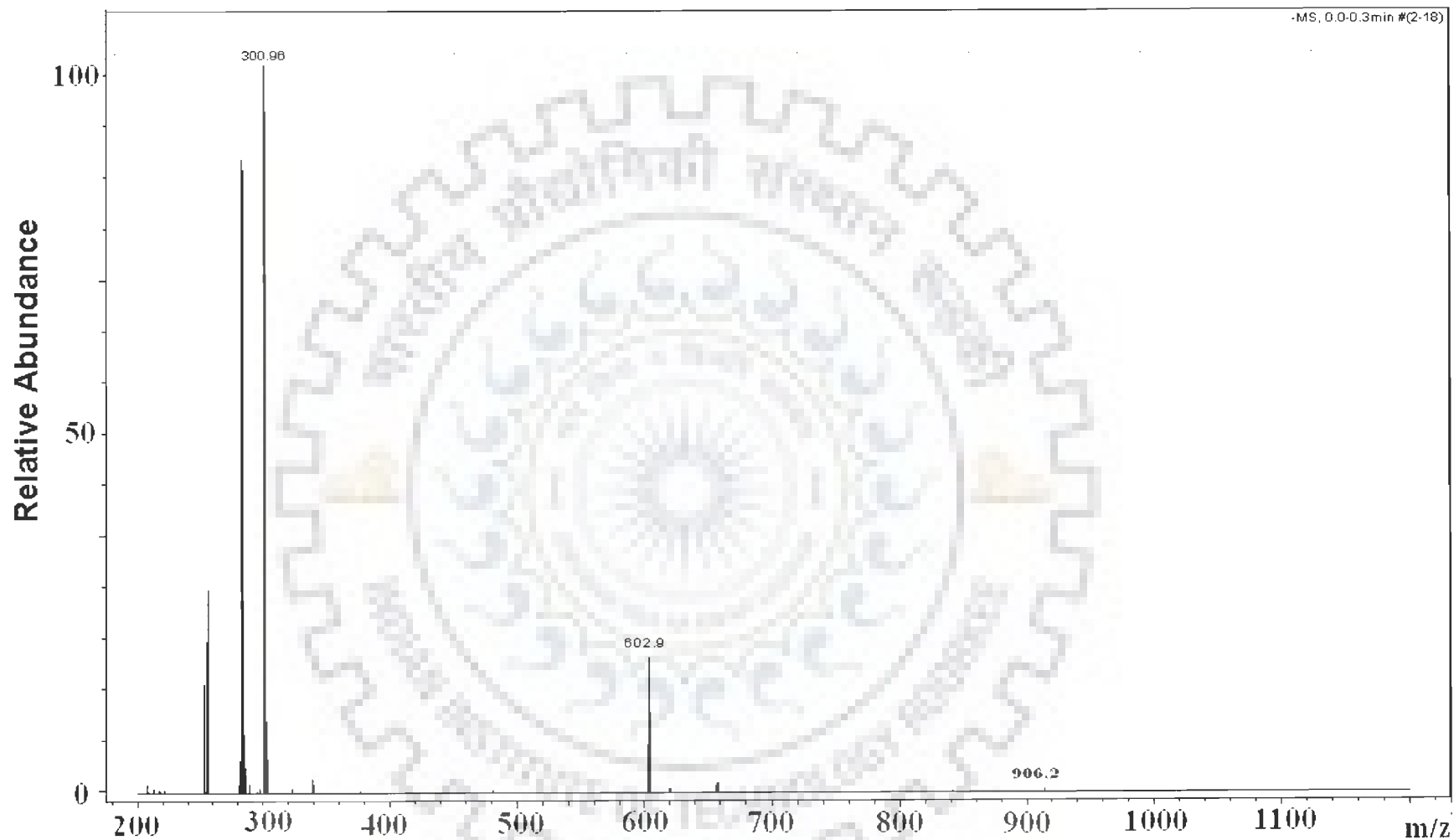
Fig. 5.10(b): Electron-Spray Ionization Mass Spectra (ESI-MS) of   showing their monomeric, dimeric and higher state of quercetin with single/double charge.
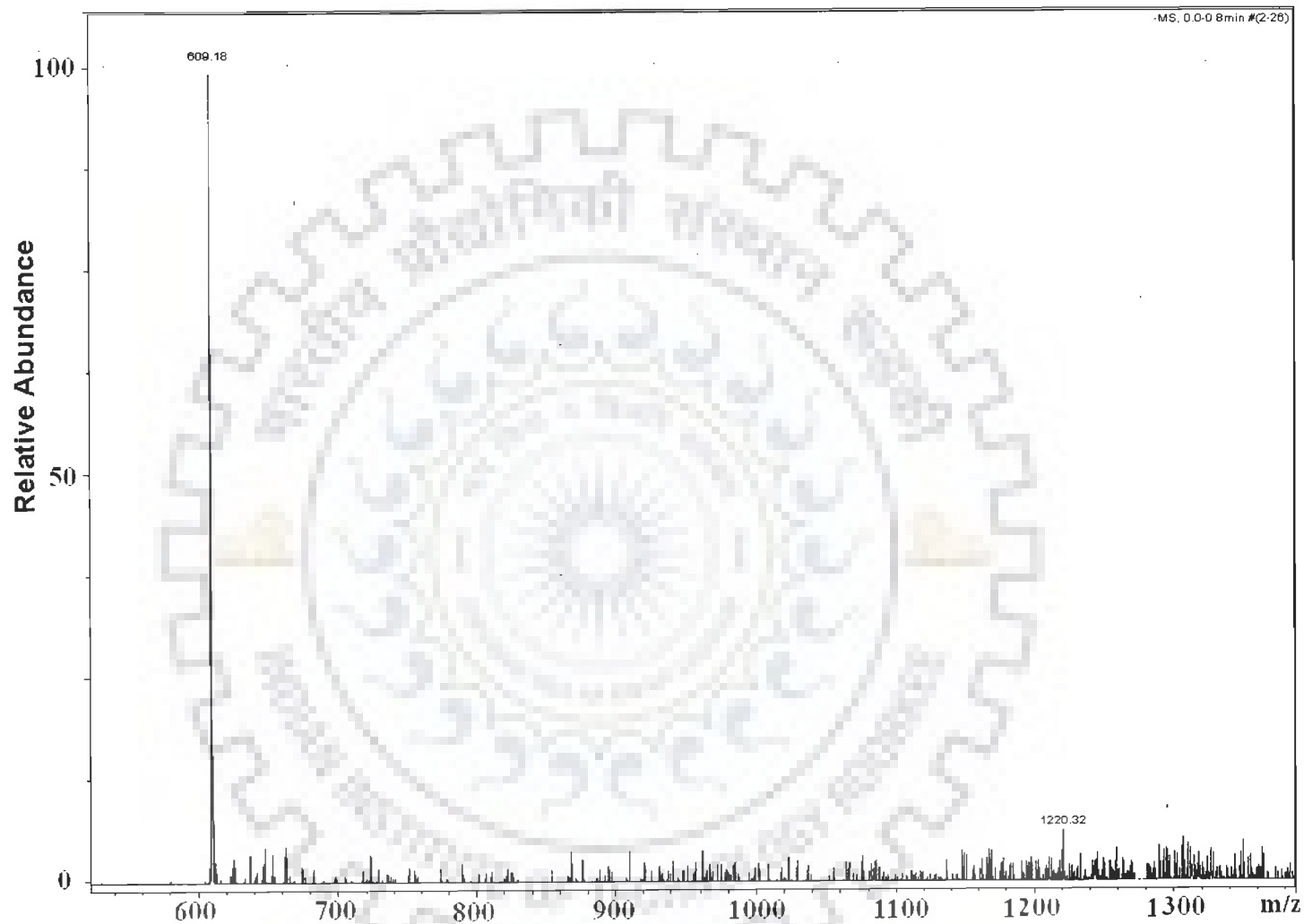
Fig. 5.10 (c): Electron-Spray Ionization Mass Spectra (ESI-MS) of showing their monomeric, dimeric and higher state of rutin with single/double charge.
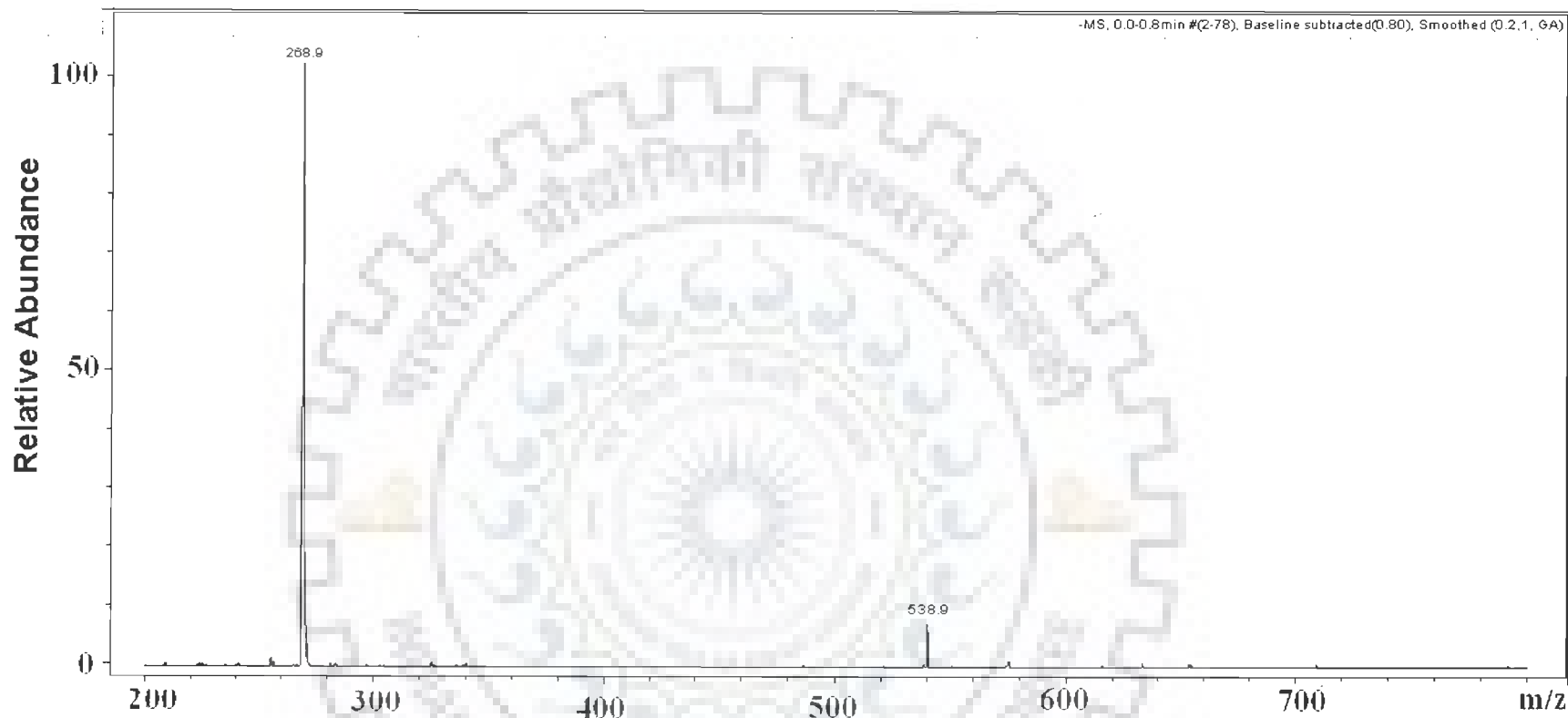
Fig. 5.10 (d): Electron-Spray Ionization Mass Spectra (ESI-MS) of showing their monomeric, dimeric and higher state of genistein with single/double charge.

Fig. 5.11(a): Electron-Spray Ionization/ MS-MS (ESI/MS-MS) of showing fragmentation of dimeric state of luteolin yielding monomeric form with single/double charge.
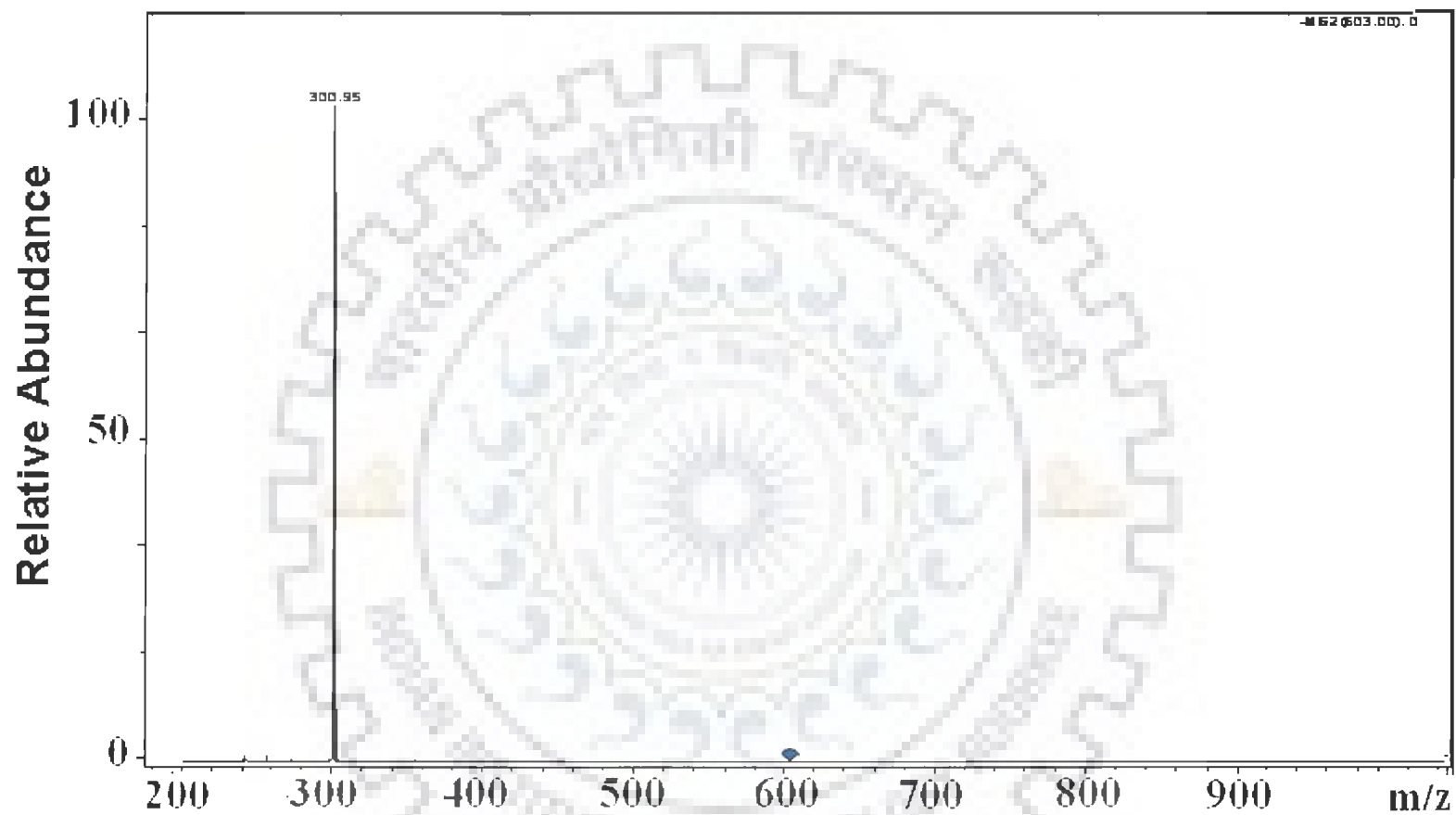
Fig. 5.12 (b): Electron-Spray Ionization/ MS-MS (ESI/MS-MS) of showing fragmentation of dimeric state of quercetin yielding monomeric form with single/double charge.
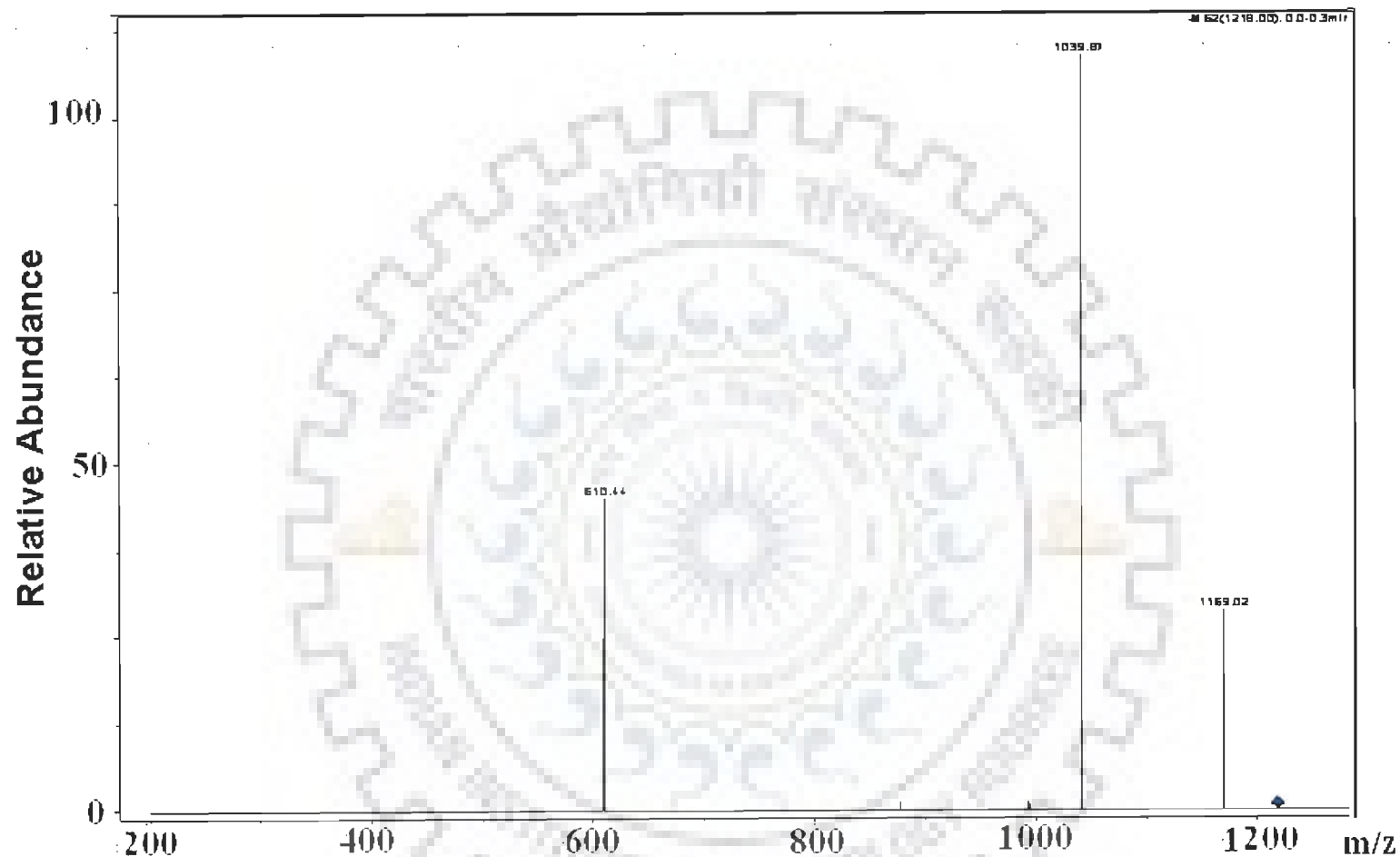
Fig. 5.12 (c): Electron-Spray Ionization/ MS-MS (ESI/MS-MS) of showing fragmentation of dimeric state of rutin yielding monomeric form with single/double charge.
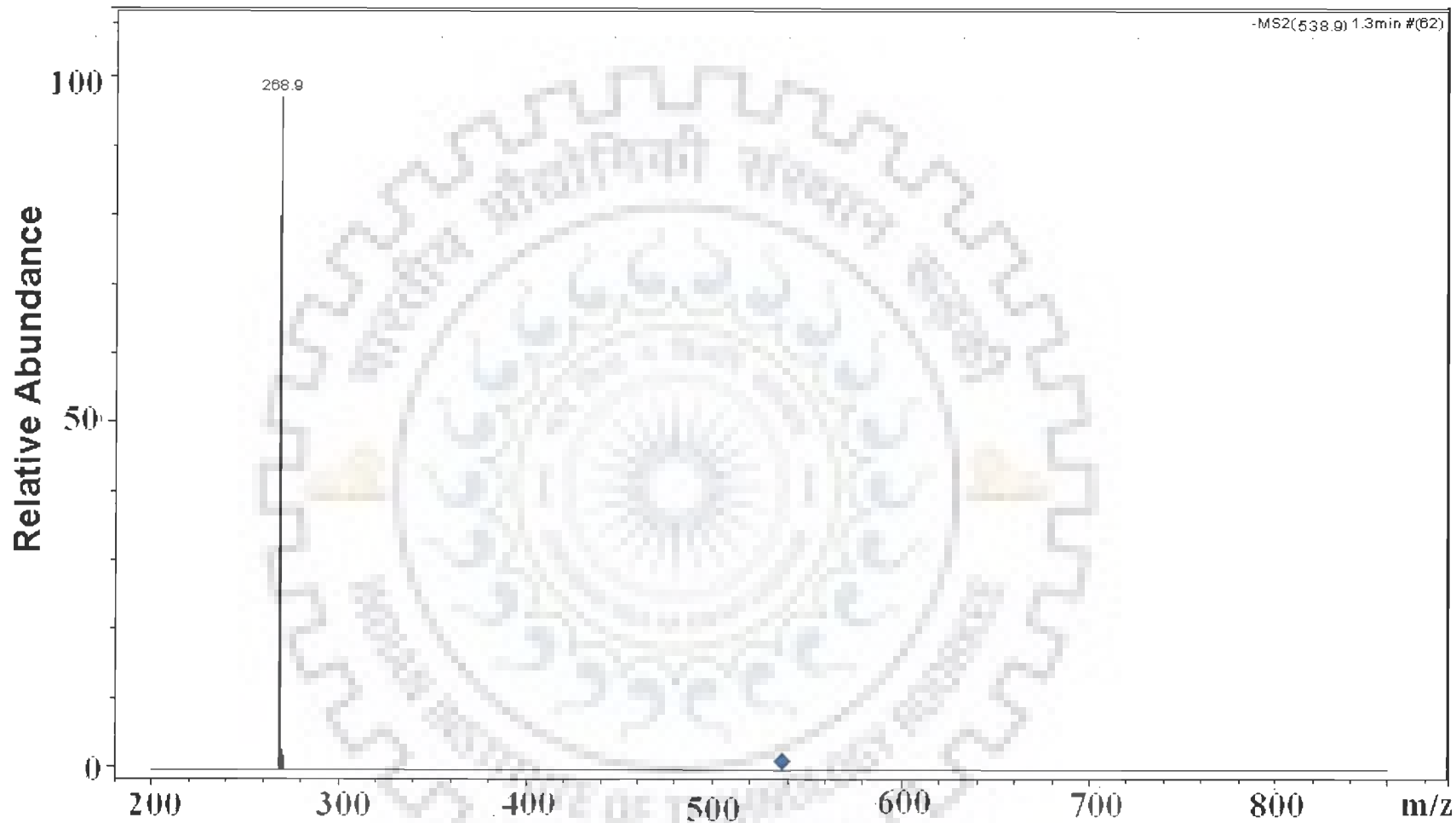
Fig. 5.12(d): Electron-Spray Ionization/ MS-MS (ESI/MS-MS) of showing fragmentation of dimeric state of genistein yielding monomeric form with single/double charge

Fig. 5.12 (e): Electron-Spray Ionization/ MS-MS (ESI/MS-MS) of   showing fragmentation of trimeric state of genistein yielding monomeric form with single/double charge

CD has greater pharmacological effectiveness compared to flavonoids alone probably due to changes in solubilization properties or/and biodegradation that enable complexed flavonoids to be active by oral route.

Our results from NMR and other physico-chemical techniques describes about the role of hydroxyl group present at different position in flavonoids in molecular association. This may be correlated for the molecular complexation and their solubilization properties. Among these flavonoids stable dimer may initially slow down their uptake through the cell membrane. However once absorbed, it may not let the drug get ejected out through channel across membrane, increasing thereby the efficacy of these molecules in their therapeutic application.

5.2.2 Anticancer action and drug toxicity mitigation

Several naturally occurring aromatic molecules consumed as a part of food (e.g. methyl xanthines, polyphenols) associate with anticancer drugs. It has been shown that caffeine (present in tea, coffee, coca, chocolate) forms homo association with itself and hetero-association complexes with number of anticancer aromatic drugs. It is suggested that caffeine, which is non-toxic up to the millimolar range (Ambrosio et al., 1994) and is known to form stacking complexes with both riboflavin (Evstigneev et al. 2005) and doxorubicin (Piosik et al., 2002; Davies et al., 2001) and may be used to modify the complexation among several types of human neoplastic diseases (Young et al.1981). However, clinical use of some drugs is limited by its severe cumulative dose-related cardiotoxicity (Keefe, 2001) by generation of reactive oxygen species (ROS) due to the catalytic quinone moiety of doxorubicin and inducing cardiomyocyte apoptosis (Keizer et al., 1990; Takemura and Fujiwara, 2007). Similarly, daunorubicin, mitoxantrone, bleomycin, epirubicin and cisplatin induce oxidative stress by generation of oxygen free

220

radicals (Carmody et al. 1999; Hagiwara et al. 2000; Novak et al. 1985) and induce cardio and hepato toxicity as side effects. Flavonoids, having cardioprotective efficacy (Chlopcíková et al., 2004; Kaiserová et al., 2007) exhibit protective effects against doxorubicin-induced cardiactoxicity (Bast et al., 2007; Du et al., 2007; Yen et al., 1996; Kang et al., 1996). Further, flavonoids like genistein and resveratrol provide protective effect against mutagen (ethidium bromide, acridine orange) induced DNA damage or toxicity by deintercalation at their maximum concentration (Usha et al. 2006). The thermodynamical and structural analysis of intercalative binding of these flavonoids to DNA sequence therefore requires a precise pre-knowledge of self association. The self aggregation of such molecules also plays a biological role in influencing the selective transport of these substances through cell membrane as well as multiple drug resistance caused by proteins forming channels in bilayer lipid membrane (Evstigneev et al., 2006, Davies et al., 2001). Besides, several other naturally occurring aromatic molecules consumed as a part of food (e.g. methyl xanthines, polyphenols) associate with these drugs. Alternately these drugs are used in combination with some aromatic molecules (Alberts et al., 1981; Adel et al., 1993). It has been shown that caffeine forms hetero association complexes with number of anticancer aromatic drugs, which effectively lowers the concentration of free ligands and thereby reduces the pharmacological activity of drugs. The major mechanism responsible for marked reduction in toxicity of adriamycin in cultured cell lines treated with caffeine (Piosik et al., 2002; Traganos et al., 1991) was found to be formation of adriamycin-caffeine complex. Caffeine is also able to block potential DNA binding site or remove the antibiotic already complexed with DNA, particularly in case of daunomycin. The relative importance of each process, hetero-association or competition for binding site on DNA, depends upon several factors. The

221

specific conjugated aromatic ring system of anthracycline / anthraquinone and the side chains will influence van der Waal's dispersive forces responsible for overlap of aromatic rings, intermolecular interactions with side chains attached to aromatic ring, steric factors, hydrophobicity and intermolecular hydrogen bonding. It has been suggested (Evstigneev et al., 2006) that the scavenging effect of cell detoxification can be used as a potential strategy of regulation of medico-biological activity of these drugs in clinical practice, say for example in reduction of the consequences of drug's overdosing during chemotherapy or in production of anti mutagenic effects in vivo.

5.3 Summary and Conclusions

1D Proton NMR of various flvonoids show downfield shift in a ring A protons H6 and H8 up to $\Delta\delta$ 0.023 and 0.052 ppm in luteolin; $\Delta\delta$ 0.006 and 0.004 ppm in quercetin; 0.011 and 0.006 ppm rutin and 0.013 each for genistein, respectively on increasing concentration from 0.01 mM to 10.00 mM. This meager shift in chemical shift may be attributed to the poor stacking of the chromophore rings and involved in other mode of association. The temperature dependence studies show downfield shift upto 1.97 ppm with temperature for the hydroxyl protons OH7 in luteolin, quercetin, rutin and OH4' in genistein indicating that these flavonoids exist in aggregated form which is forced by the hydrogen bonding. 2D NOESY spectra at 298 K show various inter-molecular and intra-molecular cross peaks which are evolved due to the association of aromatic chromophores of drug molecules. Restrained Molecular Dynamics studies show the existence of hydrogen bonds between two aromatic rings in the dimer. To date no such structure of dimer has been reported for any of the flavonoids. Absorption and fluorescence studies show that aggregation of these flavonoids are their inherent property due to intermolecular hydrogen bonding which starts at very low concentration and the observed isobestic point

222

for absorption spectra is 475 nm. The DOSY studies indicate that the rate of diffusion increases in the following manner rutin < quercetin < genistein < luteolin. ESI-MS experiments clearly demonstrate the existence of dimer and also the higher aggregates. The mass spectra of rutin also show presence of rutinoside resulting from cleavage of glycosidic bond. Absence of cleaved moiety in rutin gives direct proof of how easily it can convert in to quercetin after the cleavage of glycosidic bond. The structural difference between different levels of intermolecular association of these four flavonoids may be related to their competitive binding with DNA and hence different in their pharmacological action.
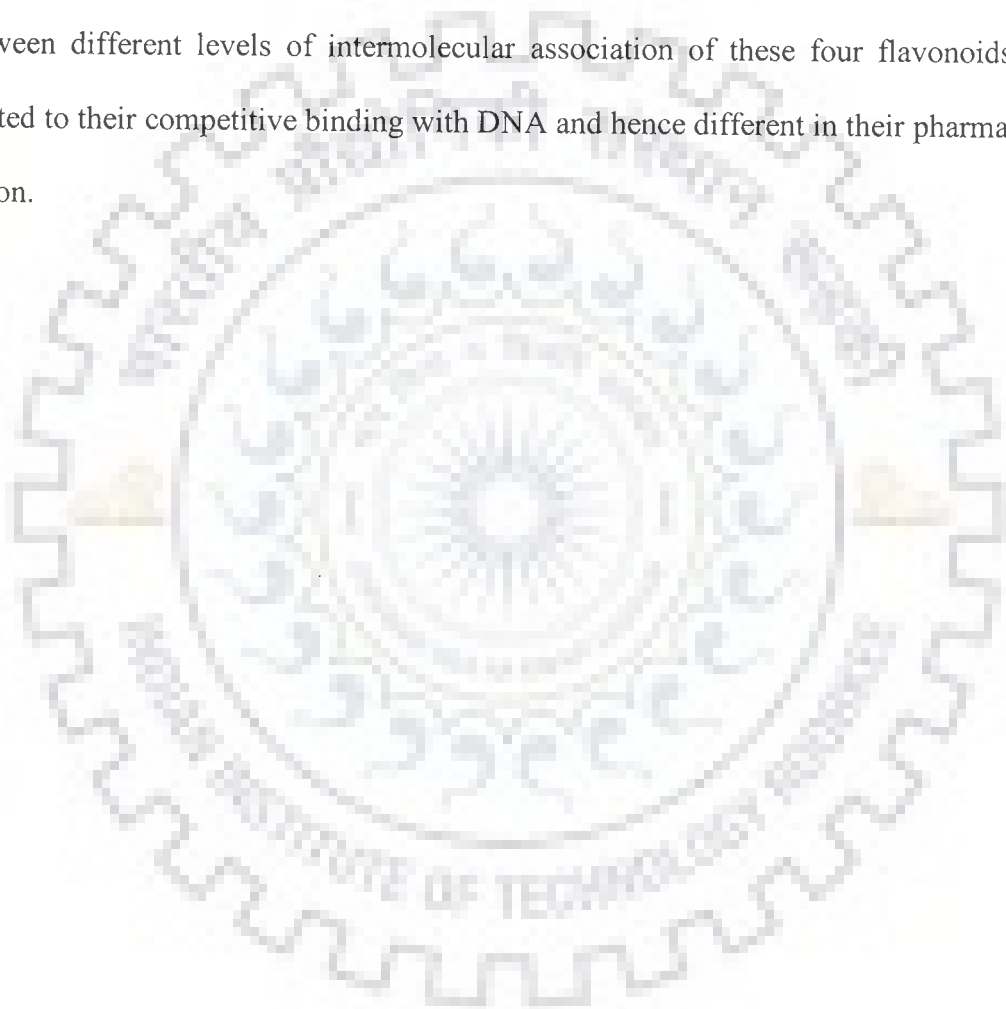
Study of Interaction of Flavonoids with Various Duplex
Polynucleotide and Telomeric G-Quadruplex Oligonucleotide
DNA Sequences using Biophysical Methods

The G-quadruplex structure plays a role in interfering with telomerase action suggesting it as a potential therapeutic target for telomerase inhibition in cancer therapy. The basic unit of the G-quadruplex is the G-tetrad, which consists of a square planar arrangement of guanines hydrogen-bonded through their Watson-Crick and Hoogsteen edges. Therefore, molecules which could stabilize this conformation are thought to be effective telomerase inhibitors. Recently, flavonoids a bioactive molecule, available in our daily diets, found to be a potent anticancer drug *in vitro* and in cohort studies. Further, due to planarity of these molecules one may expect it could intercalate in to G-quadruplexes and can exhibits anti telomerase activity. The present work reports the attempt to investigate the interaction of four flavonoids, viz. Quercetin, Luteolin, Genistein and Rutin which have a similar structure differing only in a number and /or distribution of OH groups, with various duplex DNA and G-quadruplex forming oligonucleotides. This chapter includes:

• Competition dialysis assay for structural selectivity and relative binding preference of luteolin, quercetin, rutin and genistein with different duplex and quadruplex DNA.

• Absorption, fluorescence and circular dichroism spectral studies of these flavonoids for binding with above mentioned DNA.

• Electron-Spray Ionization Mass Spectra (ESI-MS) studies of these flavonoids with telomeric G-quadruplex sequences.

6.1 Results and Discussion

6.1.1. Competitive Dialysis Assay

The competition dialysis assay is a new, powerful and effective tool based on the fundamental thermodynamic principle of equilibrium dialysis for the discovery of ligands that can bind to nucleic acids with structural and sequence selectivity (Ren and Chaires, 2001; Chaires, 2002). Fig. 6.1 shows the result from the competition dialysis assay of the five polynucleotide and three G-quadruplex forming oligonucleotide samples (at identical concentration of 75 µM base pair unit) dialyzed against 1 µM luteolin, quercetin, rutin and genistein presented as a bar graph in which the concentration of these flavonoids bound to each of the DNA sample is plotted. The striking result that emerges from this experiment is the pronounced binding of these flavonoids to the calf thymus DNA followed by herring sperm DNA. These flavonoids show their preference for binding with poly(dA-dT).poly(dA-dT) followed by poly(dG-dC).poly(dG-dC) and least for poly(dI-dC).poly(dI-dC) among duplex DNA sequences. Recently this method was also utilized in screening of G-quadruplex selective ligands (Ragazzon and Chaires, 2007). Thus, binding of these flavonoids with telomeric G-quadruplex DNA sequences d(TTAGGG)$_4$, d(TTAGGGT)$_4$, d(TTGGGGT)$_4$ can also be determined. In our results, these flavonoids show binding with G-quadruplex DNA sequences and no preference among these three G-quadruplex sequences was observed. These flavonoids show more binding to the d(TTAGGG)$_4$. This may be expected as d(TTAGGG)$_4$ sequence exist as dimeric G-quadruplexes that formed through end-to-end stacking of 3′-terminal G-tetrads in phosphate buffer with KCl (Kato et al. 2005) and hence provide more number of ligand binding sites (Fig. 6.2). From competition binding assay data, K_{app} were calculated for the binding of different flavonoids
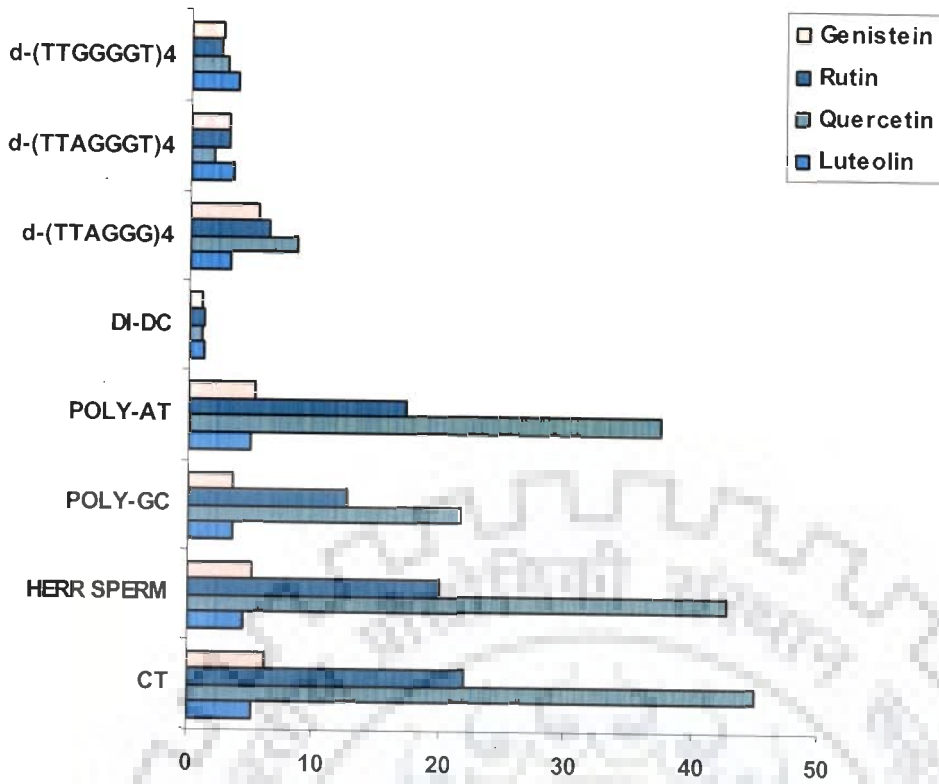
Fig. 6.1: Competition dialysis experiment after equilibration for 24 h showing preferential binding of luteolin, quercetin, rutin and genistein with respective DNA sequences.
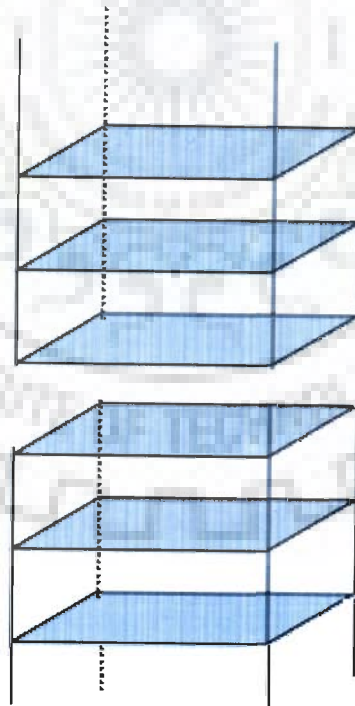
Fig. 6.2: Schematic diagram of dimeric G-quadruplexes that formed through end-to-end stacking of 3′-terminal G-tetrads.

to these duplex and quadruplex DNA and these values are shown in Table 6.1. This result indicates that the affinity of binding of flavonoids to poly d-(A-T) is stronger than the poly d-(G-C) and among these flavonoids quercetin serves the best binder. Competition dialysis data may be used to derive a number of quantitative parameters that characterize binding affinity and selectivity (Ren and Chaires, 2001; Chaires, 2002; Chaires, 2005 [a,b]). The apparent binding constant, K_{app}, can be obtained from the equation

$$K_{app} = C_b / \{C_f \text{ x } ([DNA]_{total} - C_b)\}$$

Where C_b and C_f are the bound and free flavonoids concentrations, respectively; $[DNA]_{total}$ is the total nucleic acid concentration. This treatment assumes that potential binding sites are in excess. Binding free energies can then be calculated by using the standard equation:

$$\Delta G_{app} = -RT \ln K_{app}$$

Binding constants and free energy parameters obtained in this way are only an indication as they are derived from a single set of reactant concentrations and would correspond only to a single point on a more complete binding isotherm. Nonetheless, binding constants obtained in the way correlate well with more complete binding constants determined by spectrophotometric analysis (Chaires, 2005 [a,b]) which is described in next section.

6.1.2. UV-Visible Spectrophotometric Studies

The binding of these flavonoids to duplex and quadruplex DNA is further examined more rigorously by absorbance and fluorescence titration measurements. UV-Visible absorbance spectra were recorded in CARY 100 Bio spectrophotometer. The concentration of flavonoids in DMSO solution were determined spectro photometrically at the λ_{max} of 349 nm ($\varepsilon = 20,417$ M^{-1}cm^{-1}), 380 nm ($\varepsilon = 14,920$ M^{-1}cm^{-1}), 368 nm ($\varepsilon = $

Table 6.1: Binding parameters for flavanoid with duplex and quadruplex DNA complexation obtained from competition dialysis assay.

DNA	Binding Constant (x 10^4)			
	Luteolin	Quercetin	Rutin	Genistein
Calf Thymus	0.072	1.51	0.42	0.090
Herring sperm	0.063	1.33	0.37	0.073
Poly d-(A-T)	0.069	1.00	0.30	0.076
Poly d-(G-C)	0.049	0.41	0.20	0.049
Poly d-(I-C)	0.017	0.01	0.01	0.014
d-(TTAGGG)$_4$	0.044	0.13	9.3	0.077
d-(TTAGGGT)$_4$	0.048	0.06	4.2	0.043
d-(TTGGGGT)$_4$	0.052	0.034	3.3	0.034

19,700 $M^{-1}cm^{-1}$) and 260 nm ($\varepsilon = 37,260$ $M^{-1}cm^{-1}$) for luteolin, quercetin, rutin and genistein, respectively. The absorption spectrum of flavonoids shows one band near the visible region (350 nm) and one in the ultraviolet region (260 nm) for luteolin and genistein. Quercetin gives these two bands at 368 nm and 260 nm while rutin at 365 nm and 265 nm, respectively. The one visible region bands are characteristic of the conjugated benzopyran ring and in the ultraviolet region at 260-265 nm; another is for aromatic phenyl ring of these flavonoids. On titration with CT-DNA, hyperchromic effects with no shift were observed in visible region band of luteolin with sharp isobestic points at 387 and 405 nm while in quercetin, hypochromicity with bathochromic shift were observed in visible region band with isobestic point at 389 nm indicating clearly equilibrium between free and bound flavonoid molecules. On titration with CT-DNA, marginal hyperchromicity was observed in rutin while maximum hyperchromicity equivalent to luteolin was observed in genistein but with no isobestic point was determined. Similar effects were also observed for the three other polynucleotide studied (Fig. 6.3 and Table 6.2). The titration studies with different polynucleotide like poly d-(A.T), poly d-(A-T) and poly d-(G-C) show hypochromic or hyperchromic and bathochromic or hypsochromic effects essentially indicate strong intermolecular interaction involving effective overlap of the π electron cloud of these flavonoids with the polynucleotide bases and are speculative of intercalative ligand–DNA complexation. These results are in accordance with the literature available for standard intercalator like ethidium bromide and acridine orange (Usha et al. 2006). Further, the titration studies with G-quadruplex sequences depict better binding of these flavonoids with d-(TTAGGG)$_4$ due to end stacking of this sequence enable it into dimeric form (as mentioned in section 6.1.1). Adding solution mainly containing monomeric d-(TTAGGGT)$_4$, d-(TTGGGGT)$_4$ or dimeric d-(TTAGGG)$_4$ form of G-quadruplexes, band at 368 nm red-shifts to 381 and 383 nm

for quercetin, respectively, and the absorbance of both bands is enhanced, indicating the formation of complex between quercetin and G-quadruplex. This result is in accordance with the previous report (Sun et al., 2006, Sun et al., 2007). Based on the binding constant (K_b), no preference for G-quadruplex sequences has been observed (Table 6.2) which is similar to the apparent binding constant (K_{app}) obtained from competition dialysis assay. From this titration, the change in molar extinction coefficient $\Delta\varepsilon$ was calculated (see Table 6.2). The extinction coefficients of the fully bound flavonoids at their wavelength maxima and the respective isobestic points were determined. Further, the intrinsic binding constant 'K_b' for flavonoid-DNA complex was calculated according to the equation (1):

$$[DNA] / (\varepsilon_a - \varepsilon_f) = [DNA] / (\varepsilon_b - \varepsilon_f) + 1/ K_b (\varepsilon_b - \varepsilon_f) \quad \text{------------} (1)$$

where [DNA] is the total concentration of DNA at each step of titration. ε_a, ε_f and ε_b are the extinction coefficients of flavonoid-DNA complex at each step, free and bound flavonoids at saturation, respectively. In plots of [DNA] / (ε_a-ε_f) versus [DNA], K_b is given by the ratio of slope to the intercept.

Fig. 6.3 and 6.4 showing absorption spectra denote the binding of flavonoids with different DNA and the upward and downward direction of arrow shows hyperchromicity and hypochromicity with addition increasing concentration of DNA, respectively. From spectrophotometric data, it was observed that different flavonoids which differs in the number and position of their hydroxyl group show preference to the sequence base pair differently. The observed basepair-dependent differences in the UV-Visible spectra of flavonoids are most likely the consequence of different electronic properties of G-C and A-T basepair. Among only few compounds known to exhibit significantly different spectroscopic changes upon addition of sequences with G-C and A-T base pairs. It should be stressed that efficient impact of basepair can be
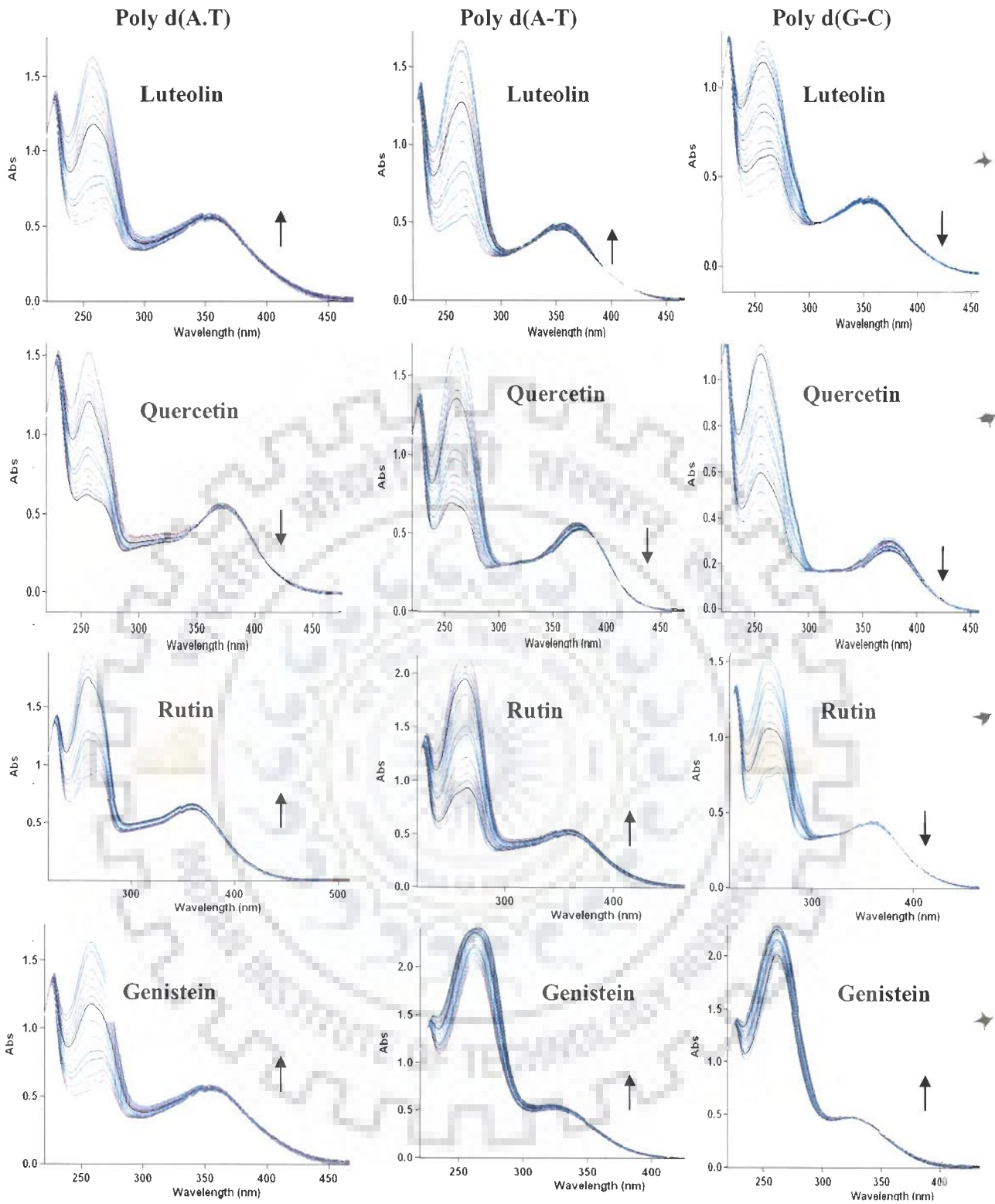
Fig. 6.3: UV-Visible spectra showing interaction of different flavonoids (22 µM each) with increasing concentration of duplex DNA sequences (7 µM).
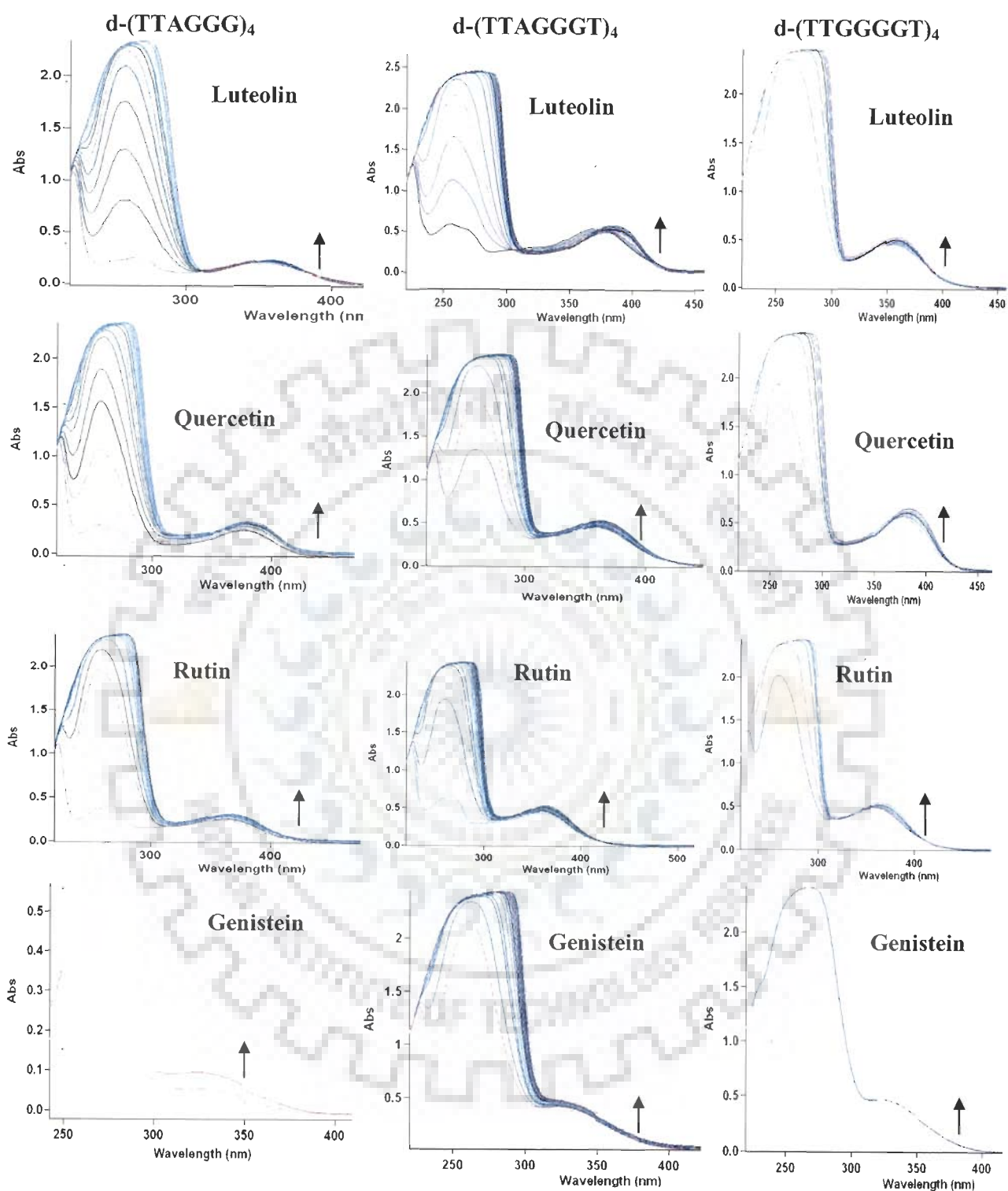
Fig. 6.4: UV-Visible spectra showing interaction of different flavonoids (22 µM each) with increasing concentration of quadruplex DNA sequences (7 µM).

Table 6.2: Absorption spectral characteristics of luteolin, quercetin, rutin and genistein with various duplex polynucleotide and quadruplex DNA oligonucleotides.

DNA	ε_{free} DNA	ε_{bound} Drug	$\Delta\varepsilon$ drug = $(\varepsilon_{free}- \varepsilon_{bound})$	λ_{final}	$\Delta\lambda*$	Isobestic Point	% Chromicity[#]	Binding Constant (K_b) M^{-1}
LUTEOLIN								
CT DNA	6600	28633	-8216	355	0	387; 405	+27.84	5.4 x 10^2
Poly d(A-T)	6000	23662	-3245	355	0	399; 410	+10.96	4.2 x 10^2
Poly d(A.T)	6000	23520	-3103	355	0	-	+9.29	2.4 x 10^4
Poly d(G-C)	7400	18882	1534	348	0	457	-11.63	6 x 10^2
d-(TTAGGG)$_4$	61300	23275	-2858	359	-11	389	+13.27	5.1 x 10^4
d-(TTAGGGT)$_4$	69800	26488	-6071	359	-11	391; 428	+28.70	1.3 x 10^5
d-(TTGGGGT)$_4$	65900	23937	-3520	358	-10	389; 428	+15.95	7.5 x 10^4
QUERCETIN								
CT DNA	6600	14252	667	375	-7	389	-9.25	1.7 x 10^4
Poly d(A-T)	6000	14026	893	376	-8	311; 389	-9.79	1.4 x 10^4
Poly d(A.T)	6000	15006	-86	368	0	356; 406	-3.37	1.0 x 10^4
Poly d(G-C)	7400	12269	2650	375	-3	431	-21.27	4.3 x 10^2
d-(TTAGGG)$_4$	61300	18711	-3791	381	-13	415, 428	+24.16	7.9 x 10^4
d-(TTAGGGT)$_4$	69800	16552	-1632	383	-15	415	+9.67	6.0 x 10^4
d-(TTGGGGT)$_4$	65900	16875	-1955	383	-15	428; 435	+11.85	6.0 x 10^4
RUTIN								
CT DNA	6600	19840	-1040	359	+2	-	+1.43	3.4 x 10^3
Poly d(A-T)	6000	21844	-3044	358	+3	-	+11.70	1.9 x 10^3
Poly d(A.T)	6000	21308	0.88	359	+2	-	+9.67	9.6 x 10^2
Poly d(G-C)	7400	18738	61	357	+4	399	-4.68	2.4 x 10^2
d-(TTAGGG)$_4$	61300	23953	-4253	368	-9	420	+28.21	4.0 x 10^4
d-(TTAGGGT)$_4$	69800	23290	-4490	361	-3	-	+22.15	2.7 x 10^4
d-(TTGGGGT)$_4$	65900	22079	-3279	368	-9	420	+16.05	1.4 x 10^4
GENISTEIN								
CT DNA	6600	49512	-12252	324	-1	-	+27.36	8.2 x 10^2
Poly d(A-T)	6000	43627	-6367	321	+1	-	+12.70	6.4 x 10^2
Poly d(A.T)	6000	46800	-9540	323	0	352	+17.65	2.3 x 10^2
Poly d(G-C)	7400	41012	-3752	322	+1	-	+5.62	1.8 x 10^2
d-(TTAGGG)$_4$	61300	-	-	-	-	-	-	ND
d-(TTAGGGT)$_4$	69800	43096	-5836	321	+2	ND	+16.60	4.6 x 10^4
d-(TTGGGGT)$_4$	65900	43822	-4342	322	+1	323; 325	+14.40	ND

*$\Delta\lambda = \lambda_{initial} - \lambda_{final}$ [(+) sign shows hypsochromic shift; (-) sign shows bathochromic shift]

[#] (+) sign shows hyperchromicity and (-) sign shows hypochromicity.

ND- not determined due to merging of genistein band at 269 nm with the DNA at 260 nm.
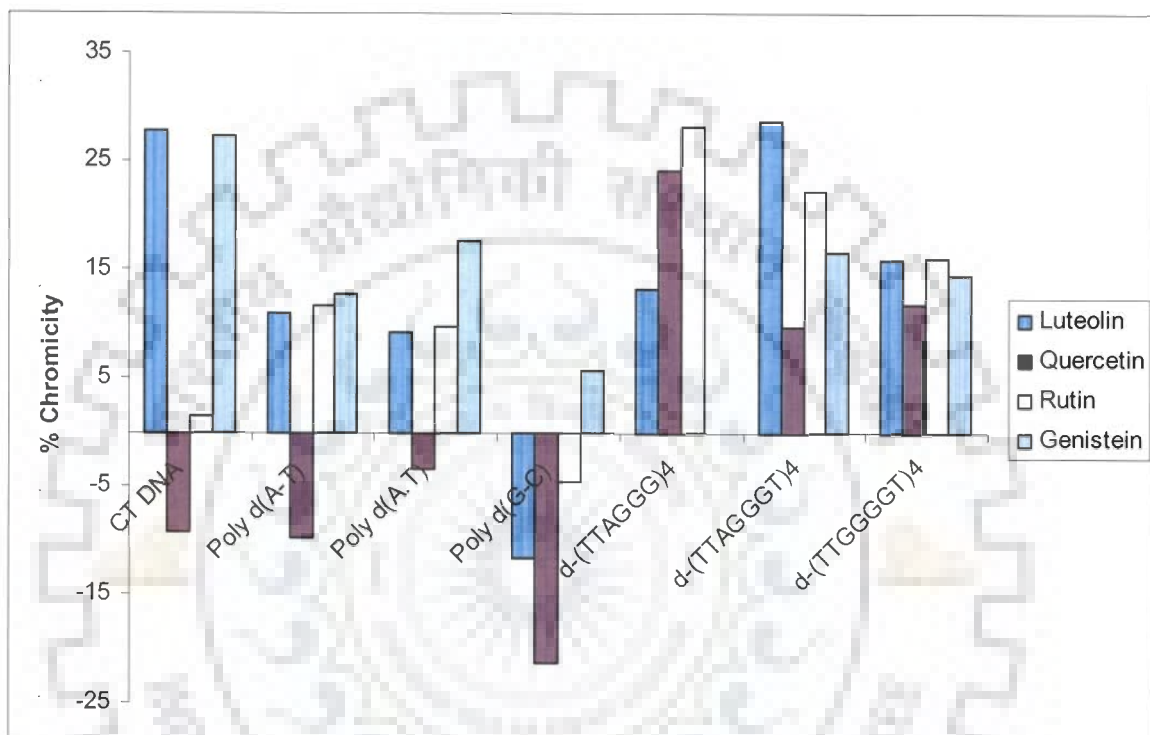
Fig. 6.5: Observed % chromicity of luteolin, quercetin, rutin and genistein with different duplex and quadruplex DNA. % Chromicity in (+) shows hyperchromicity and (−) shows hypochromicity.

234

reflected on the UV-vis spectrum of phenyl benzopyrane core of flavonoids through aromatic π–π stacking interactions either by direct aromatic stacking interactions with adenine or by thymine sites over the electron-transfer mechanism through the π-stacked DNA helix when the aromatic compound (in this case flavonoid) is efficiently stacked within the DNA double helix (Kelley and Barton, 1999; Marras et al., 2002). Both mechanisms presume strong aromatic stacking interactions of flavonoid with ds-polynucleotide and therefore suggest intercalation into polynucleotide as a dominant binding mode for all studied compounds which is also supported by the report showing quercetin, rutin and morin binding with CT-DNA (Solimani, 1997). Aromatic surface of these flavonoids which provide planarity and it is more than large enough to satisfy requirements of concept of minimal DNA intercalator (Demeunynck et al., 2002). The intercalation mode of binding of these flavonoids is further supported by ethidium bromide displacement experiment (Ahmed et al., 1994; Bi et al., 2006). Since these flavonoids do not posses positive charges at pH 7, it can not form any electrostatic interaction with negatively charged polynucleotides. Hence the mode of binding does not involves electrostatic interactions and prefers to bind with A-T specific sequence in DNA.

6.1.3 Fluorescence Spectroscopic Studies

6.1.3.1 Steady State Fluorescence Studies

Fluorescence spectra can reflect the information about the changes of the local environment of the chromophore and therefore can probe the interaction of the fluorophore with its surrounding environment. Here, we examined the interactions of four different flavonoids with duplex polynucleotide and quadruplex DNA oligonucleotide sequences by fluorescence spectroscopy.

The fluorescence intensities were monitored at the emission maximum for these free flavonoids (22 μM each) luteolin, quercetin, rutin and genistein flavonoids
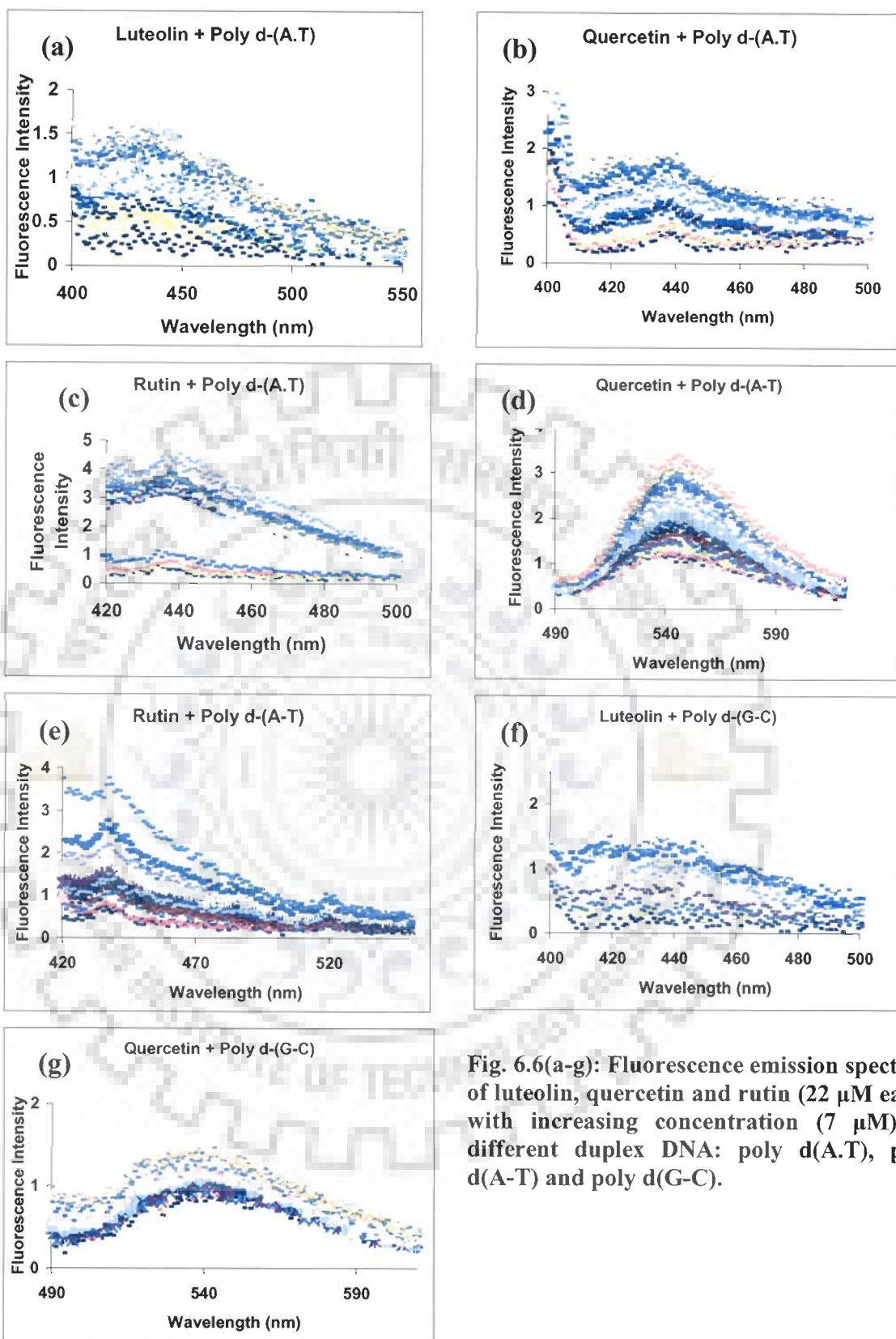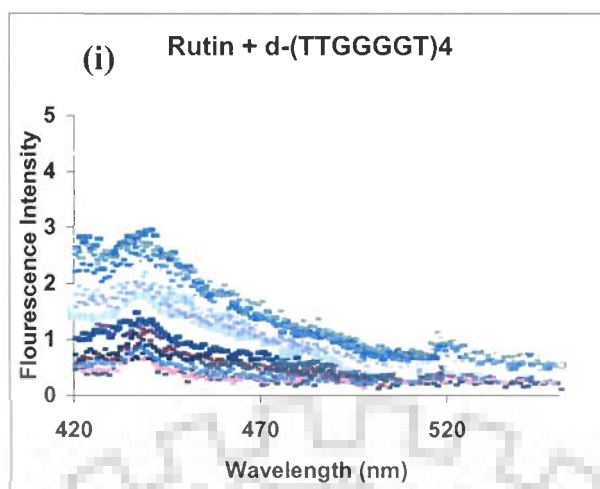
Fig. 6.6(a-g): Fluorescence emission spectra of luteolin, quercetin and rutin (22 µM each) with increasing concentration (7 µM) of different duplex DNA: poly d(A.T), poly d(A-T) and poly d(G-C).

complexed with different duplex and quadruplex DNA. Fig. 6.6(a-g) and 6.7(a-i) show the fluorescence emission spectra of flavonoids in presence of increasing concentration of these DNA. The titration studies with G-quadruplex sequences were not determined for genistein due to merging of genistein band at 269 nm with the DNA at 260 nm, when concentration of DNA is increased. In an aqueous buffer, flavonoids alone exhibit weak fluorescence due to a radiationless process involving an internal molecular motion, most probably due to the torsional motion of the phenyl and c-pyrone rings (Woolfe and Thistlethwaite, 1981). These flavonoids have an emission spectrum with a λ_{max} centered around 435 nm for luteolin, 550 nm for quercetin, 429 nm for rutin and 405 nm for genistein, when excited at 269 nm for genistein and 360 nm for the rest of flavonoids. Addition of DNA causes a slight shift of the maximum peak with a concomitant increase in fluorescence intensity suggesting the binding with DNA and limited the torsional motion of the phenyl and c-pyrone rings (Sun et al., 2007). A progressive change in the fluorescence spectra of these flavonoids on addition of increasing concentration of duplex and quadruplex DNA indicated association between them (Fig. 6.6, 6.7, 6.8 and Table 6.3). Results obtained show that relative fluorescence enhancement was found maximum for quercetin when bound to CT DNA while luteolin show slightly more than other flavonoids when bound to poly d-(A.T), poly d-(A-T) and G-quadruplex DNA sequences d-(TTAGGG)$_4$, d-(TTAGGGT)$_4$ and d-(TTGGGGT)$_4$. The plot of relative fluorescence intensity versus concentration of G-quadruplex DNA sequences was found to be hyperbolic, indicating the formation of a saturable complex (Fig. 6.9). Our results are in line with the previous literature available on binding of different flavonoids with calf thymus DNA (Choudhary et al., 2002; Sengupta et al., 2005; Usha et al., 2006). For sequence selectivity studies, no fluorometric data are available
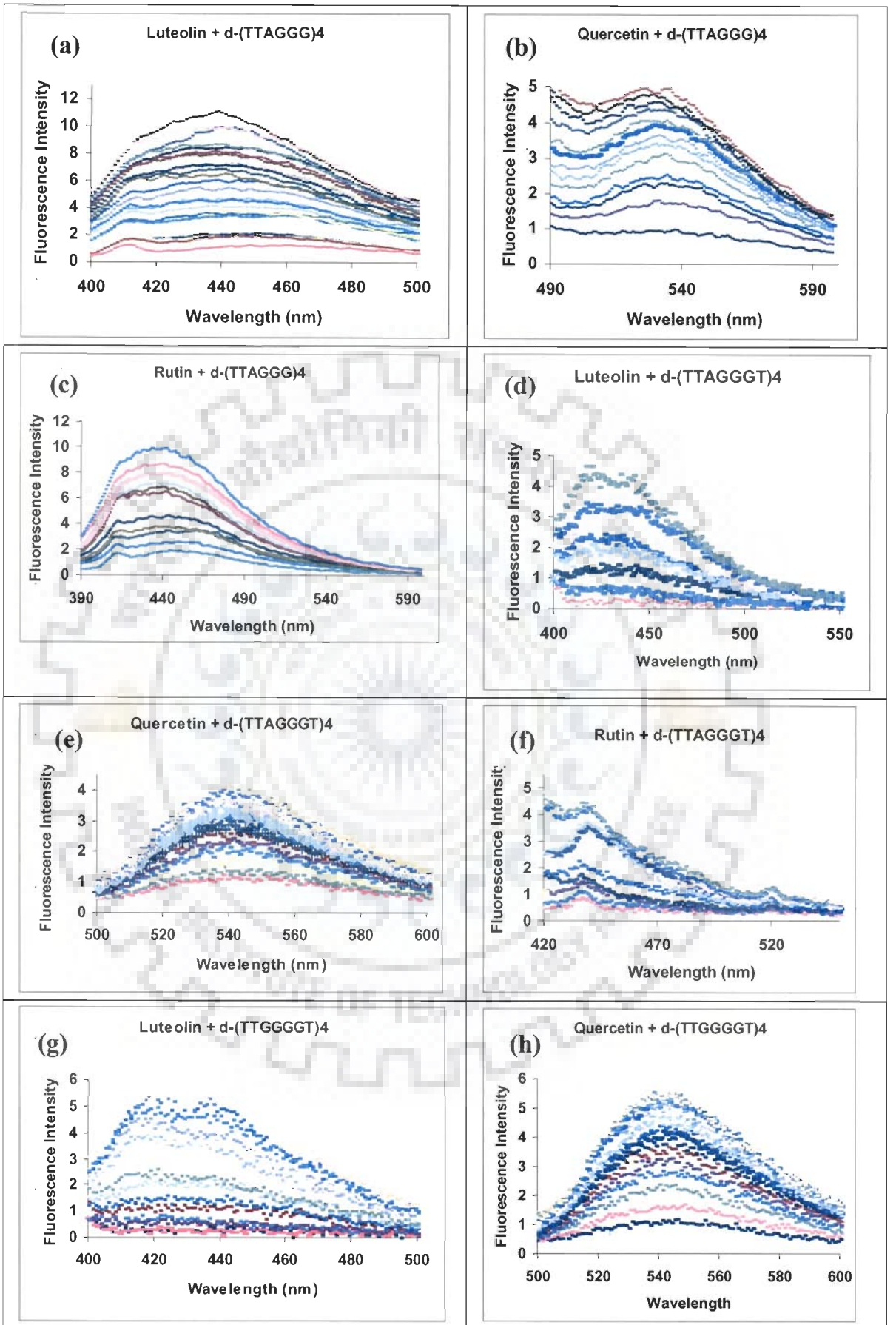
Fig. 6.7(a-i): Fluorescence emission spectra of luteolin, quercetin and rutin (22 μM each) with increasing concentration (7 μM each) of different G-quadruplex DNA sequences d-(TTAGGG)$_4$, d-(TTAGGGT)$_4$, d-(TTGGGGT)$_4$

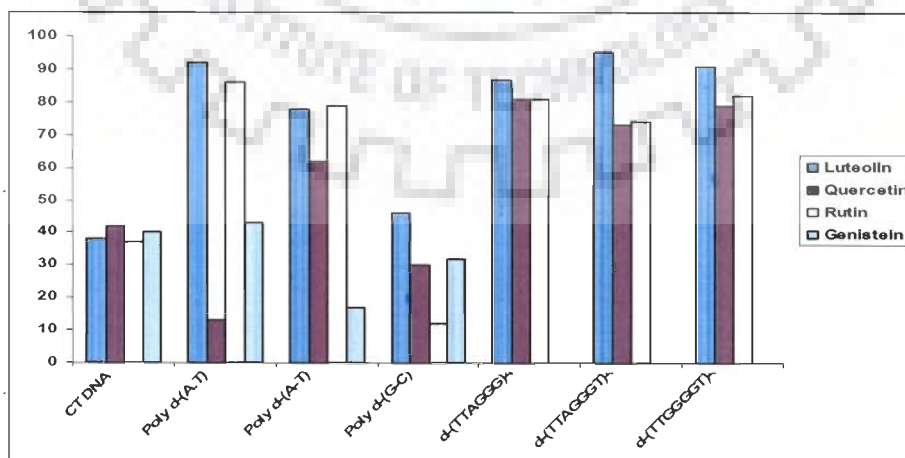Table 6.3: Enhancement of fluorescence intensity of flavonoids after addition of duplex and G-quadruplex DNA.

Sr. No.	DNA	% Increase in fluorescence			
		Luteolin	Quercetin	Rutin	Genistein
1.	CT DNA	38	42	37	40
2.	Poly d-(A.T)	92	13	86	43
3.	Poly d-(A-T)	78	62	79	17
4.	Poly d-(G-C)	46	30	12	32
5.	d-(TTAGGG)$_4$	87	81	81	ND
6.	d-(TTAGGGT)$_4$	95	73	74	ND
7.	d-(TTGGGGT)$_4$	91	79	82	ND

Fig. 6.8: Enhancement of fluorescence intensity of flavonoids after addition of duplex and G-quadruplex DNA.

(a)

Luteolin

(b)

Quercetin

(c)
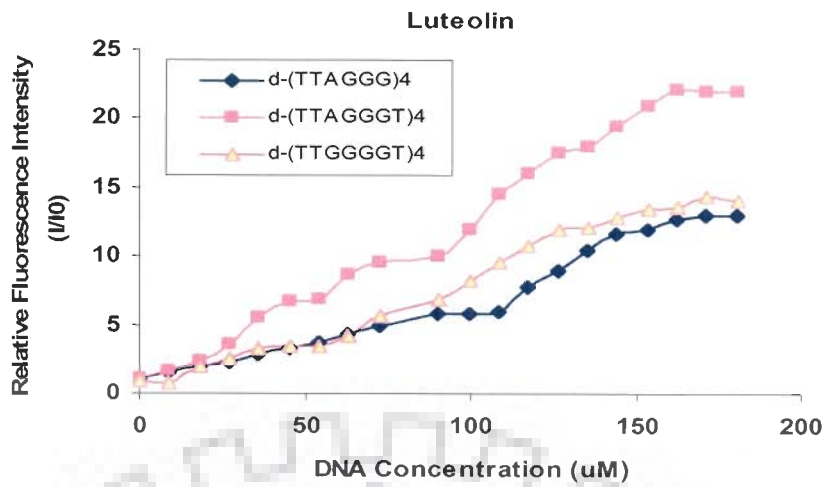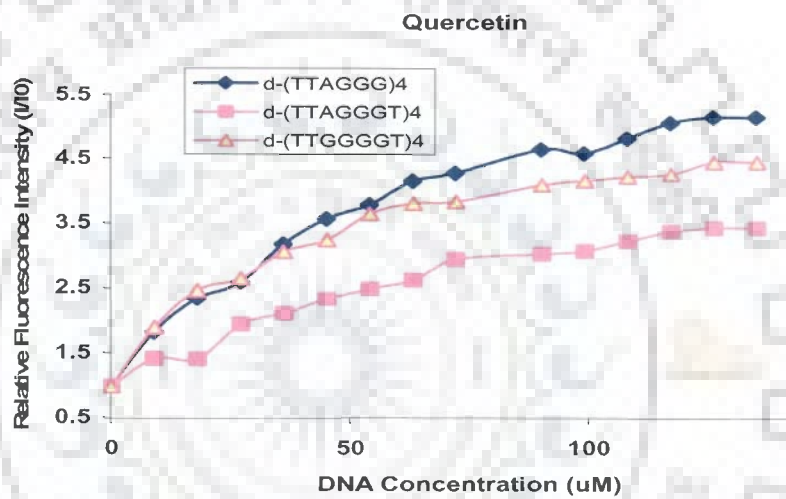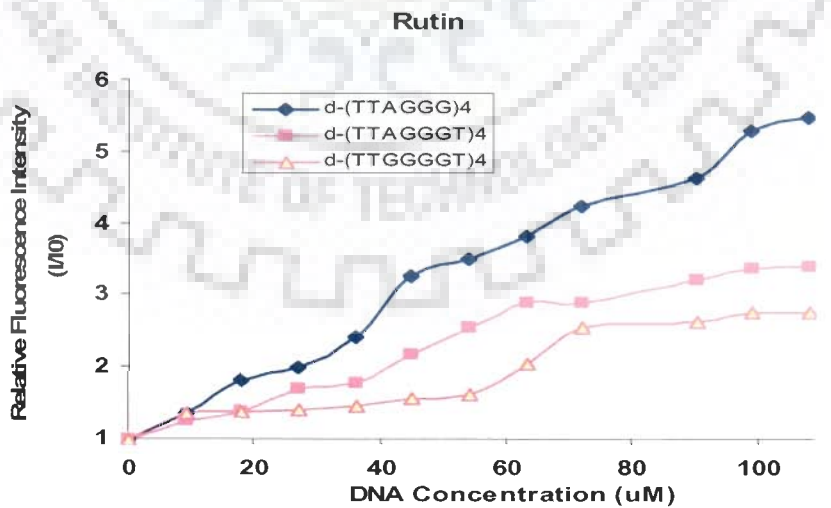
Rutin

Fig. 6.9: Relative fluorescence intensity of (a) luteolin, (b) quercetin and (c) rutin with different G-quadruplex DNA sequences d-(TTAGGG)₄, d-(TTAGGGT)₄ and d-(TTGGGGT)₄.

yet. Presently, spectrofluorometric studies of flavanoid with G-quadruplex sequences show that d-$(TTAGGG)_4$ enhanced the fluorescence intensity of all the flavonoids much stronger than that of the other quadruplexes d-$(TTAGGGT)_4$ and d-$(TTGGGGT)_4$, suggesting stronger interaction between flavanoid. The reason behind the better binding with the former is due to the end stacking of d-$(TTAGGG)_4$. The results were similar to that of absorption spectra (mentioned in section 6.1.2) and further supported by the previous reports (Sun et al., 2006, Sun et al., 2007). The binding of flavonoids with these quadruplex DNA sequences are further studied by CD, mentioned in next section.

6.1.3.2 TCSPC Analysis: Time-Resolved Fluorescence Measurements

In order to provide further insight into the binding sites of each G-quadruplex for these flavonoids, the time-resolved fluorescence spectra were measured, which gives the more detailed information of environment around a fluorophore (Lenz et al., 2007). Fluorescence excited state lifetimes are very sensitive to the structure and dynamics of a fluorescent molecule. Time resolved fluorescence decays were obtained by the Time-Correlated Single-Photon Counting method on the Spectrofluorimeter (model Fluoro Log-TCSPC, make HORIBA Jobin Yvon Spex), used for the life time measurement study of flavonoids and their complex with telomeric G-quadruplex sequences d-$(TTAGGG)_4$, d-$(TTAGGGT)_4$ and d-$(TTGGGGT)_4$. The excitation source, $\lambda_{ex} = 360$ nm was a fixed-wavelength NanoLED. The emission was detected at the emission wavelength, $\lambda_{em} = 550$ nm. The fluorescence emission of these flavonoids and its complex with d-$(TTAGGG)_4$, d-$(TTAGGGT)_4$ and d-$(TTGGGGT)_4$ were counted by a micro channel plate photo multiplier tube, after passing through the monochromator and processed through constant fraction discriminator (CFD), time-to-amplitude converter (TAC) and multi channel analyzer (MCA). All measurements were performed at 298 K in 10 mM phosphopate buffer with 100mM KCl. The

fluorescence decay was obtained and all the parameters were systematically analysed and processed by the software program DAS provided by FluoroLog-TCSPC instrument.

Global analysis was performed on each set of fluorescence decays and found that complexity of the model is well calculated with a tri exponential decay function which fits with an excellent statistical quality having global χ^2 value ~1.2 for flavonoids and their complexes with - d-(TTAGGG)$_4$, d-(TTAGGGT)$_4$ and d-(TTGGGGT)$_4$ (Table 6.4). The low global values for χ^2 indicate that the tri exponential decay function is an excellent statistical description of both the systems (Byrne and de Mello, 1998). The exponential function with three lifetimes ($\tau1$, $\tau2$ and $\tau3$) and three amplitudes (B1, B2 and B3) indicate the presence of three conformations of flavonoids, correspondingly. This is because flavonoids have one benzopyran ring attached through a single bond with a phenyl ring having rotation around this bond and can have more than one conformer in solution (discussed in chapter 4). For uncomplexed and complexed flavonoids with different G-quadruplexes, the values of life time decay $\tau1$, $\tau2$ and $\tau3$ with their corresponding amplitude B1, B2 and B3 are listed in Table 6.4

Fig. 6.10 shows the fluorescence decays of flavonoids in free form and G-quadruplexes-flavonoids complexes at 2:1 molar ratio of flavonoids to G-quadruplexes. For free flavonoids, the fluorescence decay lifetime was lesser and upon binding to DNA the contribution of the long life time component increased (Table 6.4). However, the fluorescence decays for G-quadruplex-flavonoids complexes are three exponential, requiring three lifetime components to give a satisfactory fit, which indicates the existence of three binding states of flavonoids, in which flavonoids experiences different interactions and environments and hence has different quenching rates. From the data it has been found that genistein have lower
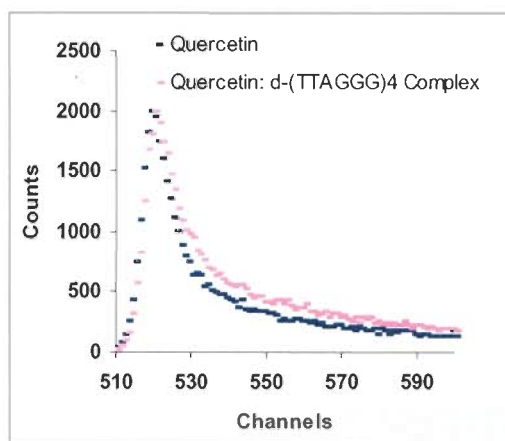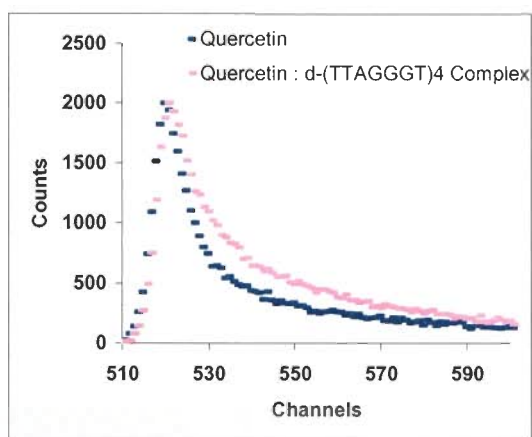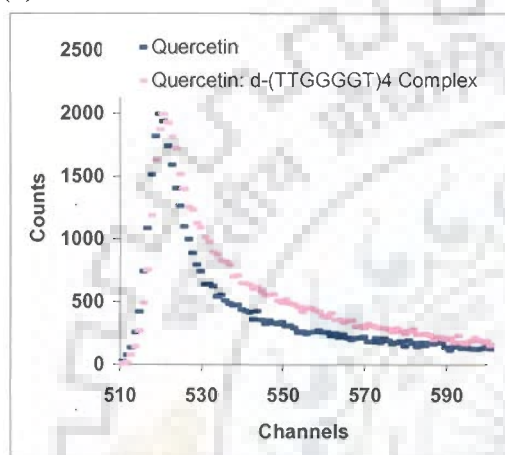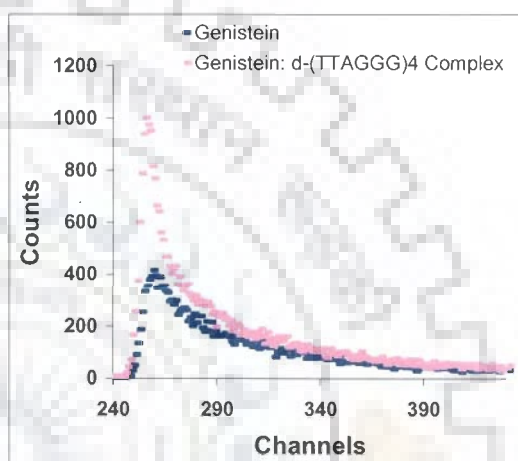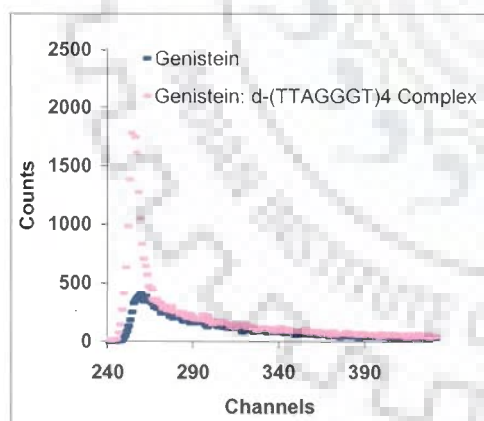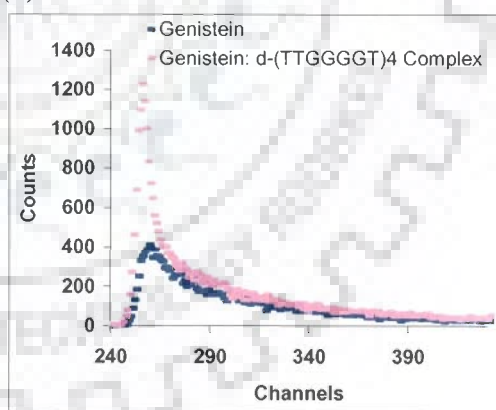
Fig. 6.10: Fluorescence lifetime decay measurement profile of selected flavonoids (a-c) Quercetin and (d-f) Genistein and their complex with d-(TTAGGG)$_4$, d-(TTAGGGT)$_4$ and d-(TTGGGGT)$_4$.

: **Table 6.4: Life time fluorescence decay parameters for flavonoids and their 2:1 complex with d-(TTAGGG)₄, d-(TTAGGGT)₄ and d-(TTGGGGT)₄ at 298 K.**

Flavonoids	Uncomplexed Flavonoids							d-(TTAGGG)$_4$						
	Decay (ns)			Amplitude				Life Time Decay (ns)			Amplitude			
	$\tau 1$	$\tau 2$	$\tau 3$	B1	B2	B3	χ^2	$\tau 1$	$\tau 2$	$\tau 3$	B1	B2	B3	χ^2
Luteolin	3.2	1.4	7.5	64.4	19.5	16.1	1.36	2.8	5.1	6.18	24.1	28.0	47.8	1.18
Quercetin	0.03	2.4	9.3	79.5	7.9	12.5	1.34	0.25	5.1	27.7	26.7	47.7	25.5	1.27
Rutin	1.4	2.7	7.5	81.4	9.7	8.9	1.21	0.5	4.9	5.4	27.7	46.7	31.5	1.16
Genistein	5.6	21.9	0.5	59.5	29.0	11.5	1.44	0.01	5.0	25.0	99.4	0.36	0.15	1.14

Flavonoids	d-(TTAGGGT)$_4$							d-(TTGGGGT)$_4$						
	Decay (ns)			Amplitude				Life Time Decay (ns)			Amplitude			
	$\tau 1$	$\tau 2$	$\tau 3$	B1	B2	B3	χ^2	$\tau 1$	$\tau 2$	$\tau 3$	B1	B2	B3	χ^2
Luteolin	4.5	14.8	0.16	43.4	21.0	35.6	1.32	4.21	0.82	9.21	32.5	28.7	38.8	1.34
Quercetin	3.8	13.1	0.12	34.1	18.0	47.8	1.20	2.41	0.08	7.35	23.6	37.5	38.9	1.18
Rutin	4.9	12.8	0.54	64.5	19.3	16.2	1.14	6.14	1.51	8.56	32.5	42.6	24.9	1.21
Genistein	5.9	38.3	0.007	0.0	0.0	100.0	1.16	5.9	37	0.048	32.4	9.9	57.6	1.16

decay rate (in range of ps) with highest amplitude value when complexed with d-$(TTAGGG)_4$, d-$(TTAGGGT)_4$ and d-$(TTGGGGT)_4$ (Table 6.4). This may indicate the existence of single binding pattern of genistein in which the major population complex can exist. Unlikely to genistein, other flavonoids luteolin, quercetin and rutin have shorter and longer lifetime with roughly similar amplitudes. These results further support the existence of different pattern of complex formation. The shorter and longer lifetimes for different components suggest binding at more than one site. In summary, different pattern of distinct nonequivalent binding sites of flavonoids to d-$(TTAGGG)_4$, d-$(TTAGGGT)_4$ and d-$(TTGGGGT)_4$ in the presence of K^+ were confirmed by the fluorescence lifetime measurement. The earlier results show that flavonoids interact with G-quadruplexes by end-stacking and outside binding (Sun *et al.*, 2007). The lifetimes of flavonoids in the end-stacking mode are larger than those in the outside binding mode for G -quadruplexes. Similar kind of results were reported for TPrPyP4 binding to two different G-quadruplex (Chunying *et al.*, 2008). The analysis of fluorescence decay time of flavonoids and their d-$(TTAGGG)_4$, d-$(TTAGGGT)_4$ and d-$(TTGGGGT)_4$ complex clearly elucidate the binding. The significant change in the values of both the decay components and their relative contributions of flavonoids upon binding with d-$(TTAGGG)_4$, d-$(TTAGGGT)_4$ and d-$(TTGGGGT)_4$ indicate the change in their microenvironment. Further, the binding of these flavonoids are ascertained by other biophysical methods like circular dichromism as described in next section.

6.1.4 Circular Dichroic Measurement Studies

Luteolin, quercetin, rutin and genistein are optically inactive and hence do not have any circular dichroism (CD) spectrum. The interaction of these flavonoids to several telomeric G-quadruplex sequences was followed in the ultraviolet region. CD of d-$(TTAGGG)_4$, d-$(TTAGGGT)_4$ and d-$(TTGGGGT)_4$ display clean spectra with a

positive CD band near 260 nm and a negative CD band near 240 nm are characteristic of parallel stranded G-quadruplexes (Fig. 6.11 and 6.12) (Keniry, 2001). The CD spectra of these sequences were perturbed after the addition of flavonoids at twice the concentration of G-quadruplex sequences. The change in CD spectra of DNA due to complexation of flavonoids is clearly depicted in Fig. 6.11 and 6.12 Addition of flavonoids perturbs maximum in d-$(TTAGGG)_4$ sequence (Fig. 6.11 a, d and 6.12 a, d). This may be attributed to its feature of d-$(TTAGGG)_4$ to form the dimer structure by end to end stacking and providing more binding site to the ligand. On the other hand, The CD spectrum of other sequences d-$(TTAGGGT)_4$ and d-$(TTGGGGT)_4$ was marginally affected with addition of luteolin (Fig. 6.12 b, c), quercetin (Fig. 6.12 e, f), rutin (Fig. 6.12 b, c) and genistein (Fig. 6.12 e, f). Such change in CD spectrum of different G-quadruplex sequences can be correlated with the binding of flavonoids which causes some alternation in their G- quadruplex structure after binding. Hence, CD spectra of alone and complex G-quadruplex sequences confirms the binding of flavonoids. Further, it is interesting to know the stoichiometry and the position of flavonoids in binding to these sequences. In this context, we did ESI-MS studies for these complexes which are discussed in the next section.

6.1.5 Mass Spectrometric Studies

Electro Spray Ionization-Mass Spectrometry (ESI-MS) is a highly sensitive method to study the interactions of drugs with DNA duplex, triplex and quadruplex structures (Gabelica et al., 1999; Rosu et al., 2002; Carraso et al., 2002). The interactions between flavonoids and DNA duplexes or quadruplex have been widely investigated by solution-phase methods in previous sections of this chapter. The noncovalent interactions between members of flavonoid family viz. luteolin,
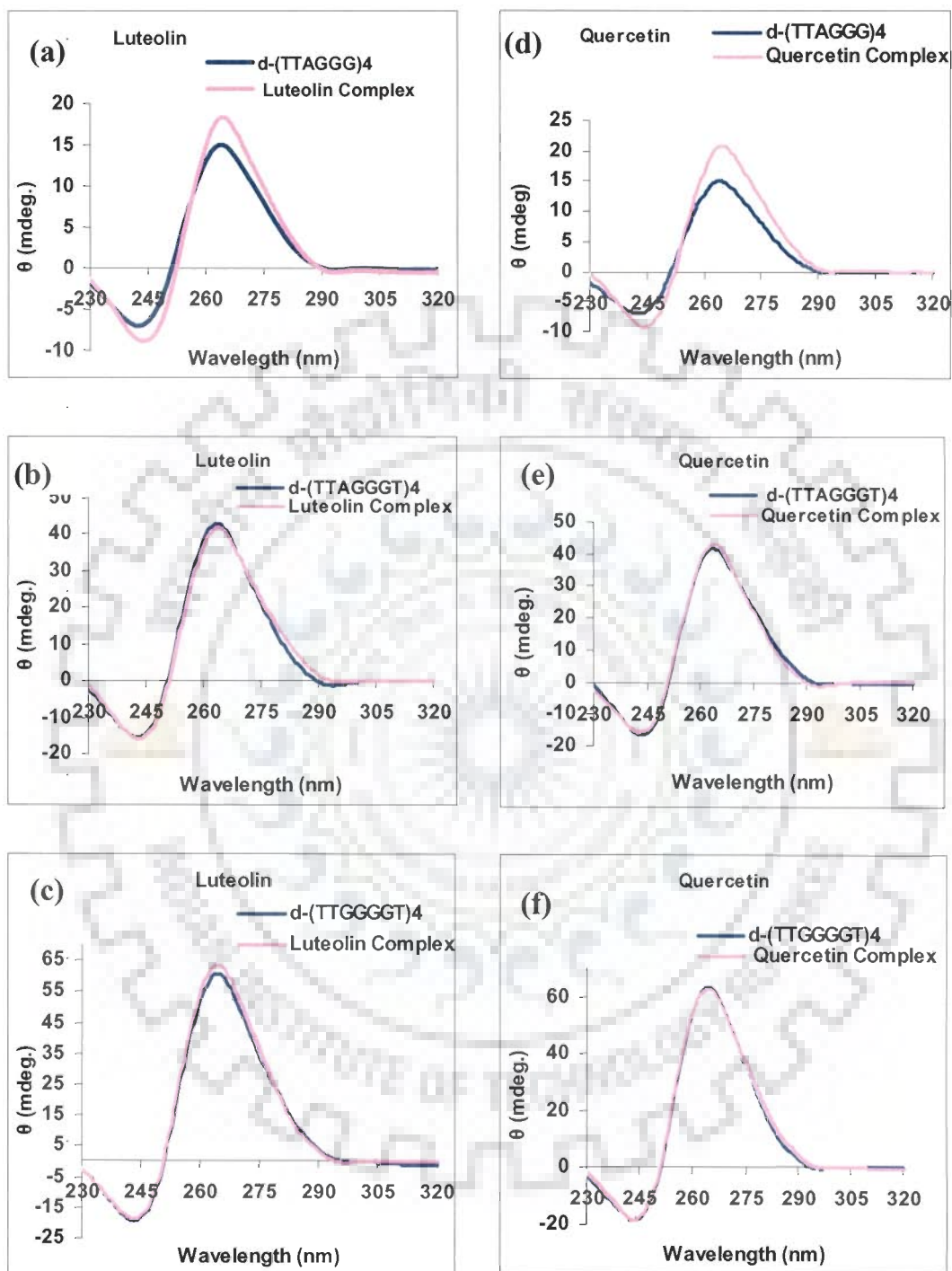
Fig. 6.11: CD spectra of different G-quadruplex sequences d-(TTAGGG)₄, d-(TTAGGGT)₄ and d-(TTGGGGT)₄ alone and complexed with luteolin and quercetin at ratio 2:1 (Flavonoid:DNA).
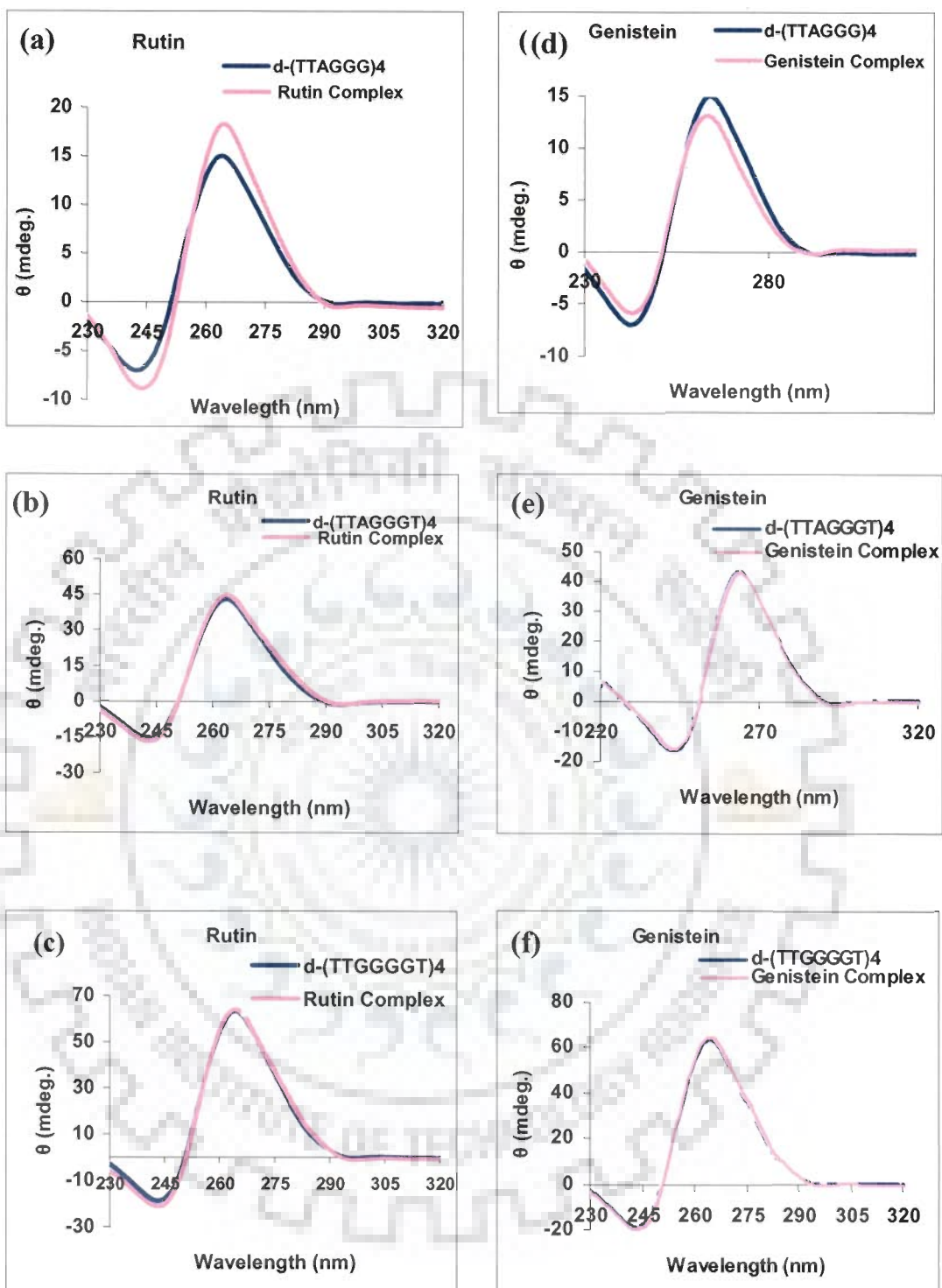
Fig. 6.12: CD spectra of different G-quadruplex sequences d-(TTAGGG)₄, d-(TTAGGGT)₄ and d-(TTGGGGT)₄ alone and complexed with rutin and genistein at ratio 2:1 (Flavonoid:DNA).

quercetin, genistein, rutin and DNA quadruplex sequences d-(TTAGGG)$_4$, d-(TTAGGGT)$_4$, d-(TTGGGGT)$_4$ are further evaluated for their binding abilities by using negative ion mode ESI-MS. The respective molecular weight for single strand of these quadruplex sequences d-(TTAGGG)$_4$, d-(TTAGGGT)$_4$, d-(TTGGGGT)$_4$ were 1847.5, 2151.5 and 2167.5, respectively. The quadruplex structure of these sequences require potassium ion between the guaning base pairs for their stabilization of G-tetrad. The mass of potassium (38.1) is also included in the calculation. Similarly, the mass of luteolin, quercetin, rutin and genistein were taken 289.0, 300.1, 609.3 and 269.7, respectively. Mixtures of one flavonoid and one G-quadruplex sequence at a 4:1 molar ratio (80 and 20 µM, respectively) were analyzed using ESI-MS and selected mass spectra are shown in Fig. 6.13-6.15.

6.1.5.1 Binding of flavonoid to DNA quadruplexes

In mass spectra, intact DNA in the form of quadruplex, triplex, duplex and single strand with different charges range of -4 to -7 were observed. The telomeric G-quadruplex sequence d-(TTAGGG)$_4$ exist in another form of dimer due to end to end stacking of 3`-terminal G-tetrads and show peaks with negative charge range beyond seven also. The respective mass peaks were observed which confirms the coexistence of dimer state of d-(TTAGGG)$_4$ sequence. Peaks at m/z 1493 with negative charge of five and 2127 with negative charge seven were correlated with monomer and dimer form, respectively. Other peaks were also observed at different m/z ratio with different charges for monomer and dimer forms. This is the reason for better binding of flavonoids with d-(TTAGGG)$_4$ sequence, as shown in our Uv-vis, fluorimetry and CD studies. Further, 1:1, 1:2 and 1:3 stoichiometries for luteolin, querectin, rutin and genistein were observed and correlated with their complex formation with d-(TTAGGG)$_4$ (Fig. 6.13a-d).

Similarly, Peaks corresponding to the 1:1 and 1:2 flavonoid/quadruplex complexes of luteolin and quercetin with d-(TTAGGGT)$_4$ were clearly observed (Fig. 6.14a, b). The same binding stoichiometries were observed for the other flavonoid rutin and genistein but with a peak of an extra stoichiometry of 1:3 complex ion with 50% relative intensities was observed at m/z 1575 with negative charges of six in genistein and 1490 m/z with seven negative charge in rutin complexed with d-(TTAGGGT)$_4$ (Fig. 6.14c, d). In contrast, the complex of luteolin and quercetin, peaks corresponding to the flavonoid/DNA complexes stoichiometry of 1:3 complex ion were not detected (Fig. 6.14a,b), indicating rather weak interactions of stoichiometry 1:3 between the d-(TTAGGGT)$_4$ quadruplex and luteolin or quercetin. The peaks corresponding to 1:1 and 1:2 complex were observed at1282 m/z with negative charge of seven and 1546 with negative charge of six for luteolin complexed with d-(TTAGGGT)$_4$, respectively. Similarly, for quercetin peaks at 1489 m/z with negative charge six and at 1856 m/z with negative charge five corresponds to 1:1 and 1:2 complex, respectively.

Another G-quadruplex sequence d-(TTGGGGT)$_4$ and its complex with quercetin, rutin and genistein exhibit all stoichiometry of 1:1, 1:2 and 1:3 unlikely to luteolin. In the mass spectra of luteolin: d-(TTGGGGT)$_4$, the 1:1 species was located as 1299 m/z with the negative charge of seven and 1500 m/z with the negative charge of six Similarly, for 1:2 complex peak was found at 1545 m/z with the negative charge of six. The flavonoids quercetin, rutin and genistein complexed with d-(TTGGGGT)$_4$, show 1:3 stoichiometry in addition to 1:1 and 1:2. The peaks observed were 1290 m/z with charge seven, 1866 m/z with charge five, 1605.3 m/z with charge six, for 1:1, 1:2 and 1:3 stochiometry for luteolin complex, respectively (Fig. 6.15 a). For genistein, 1:1, 1:2, 1:3 stochiometry peaks observed were 1285 m/z with charge seven, 1545 m/z with charge six, 1908 m/z with charge five, respectively (Fig.6.15d).
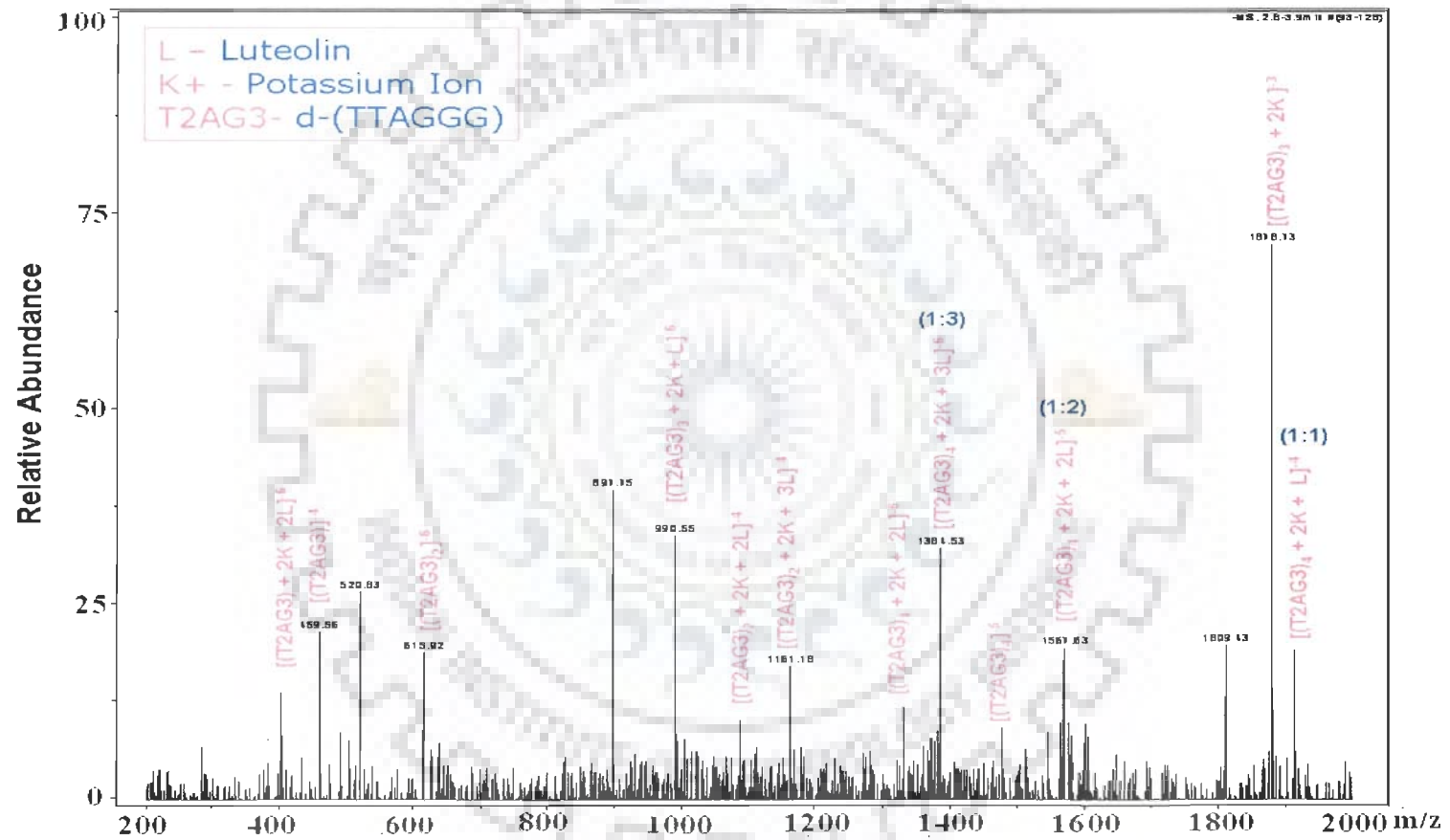
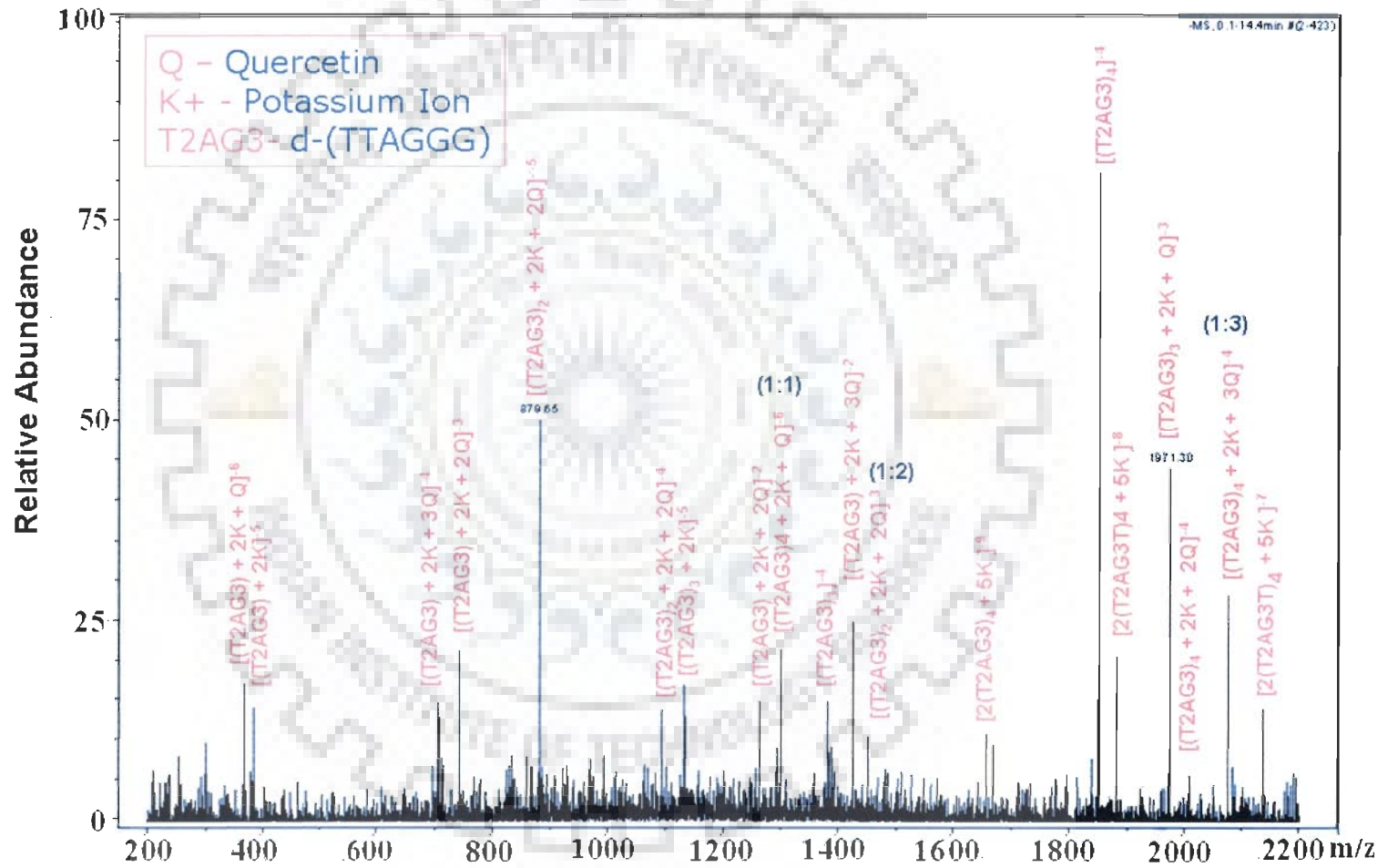Fig. 6.13: ESI-MS spectra of d-(TTAGGG)₄ complexed with (a) Luteolin, (b) Quercetin, (c) Rutin and (d) Genistein
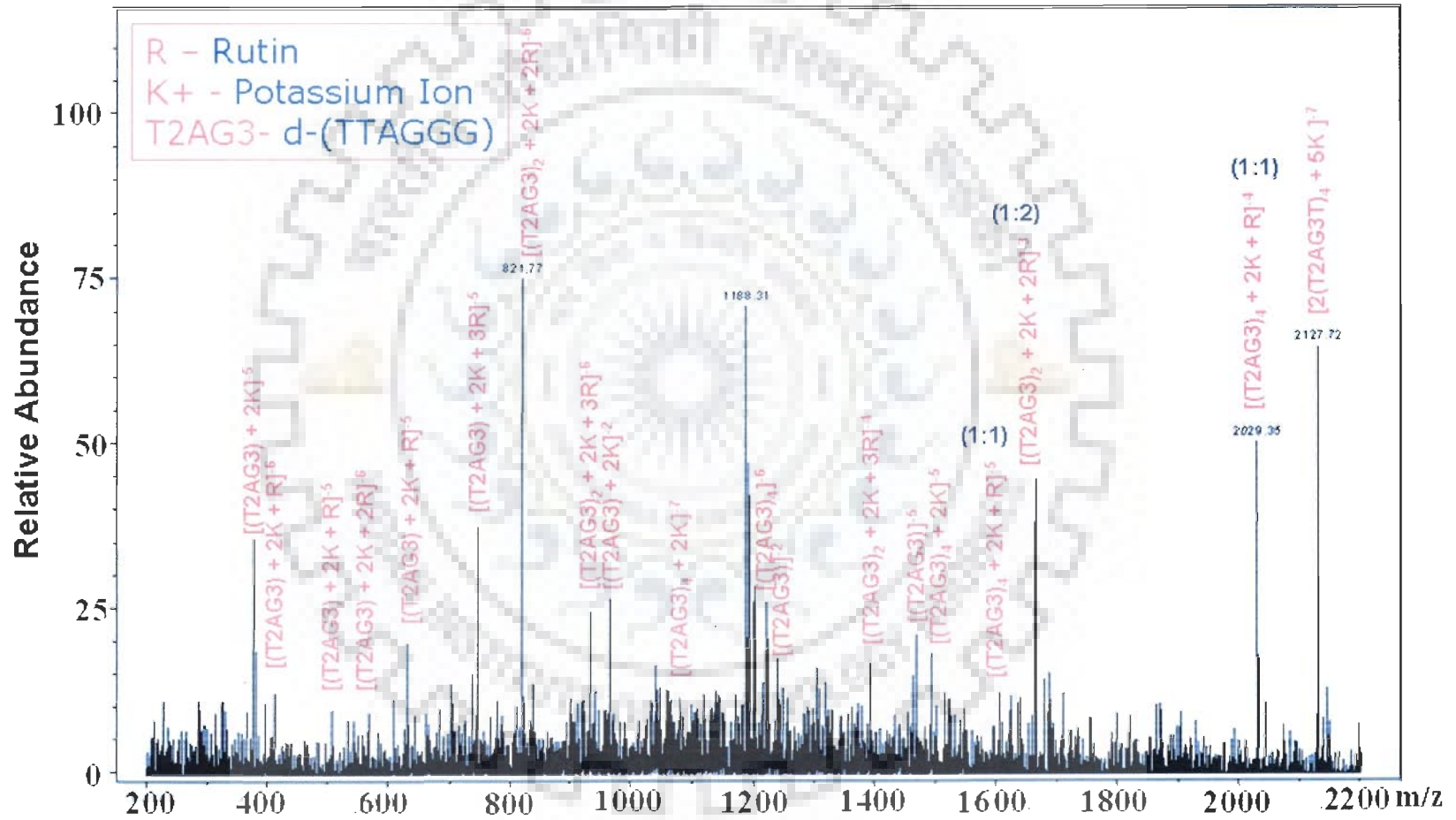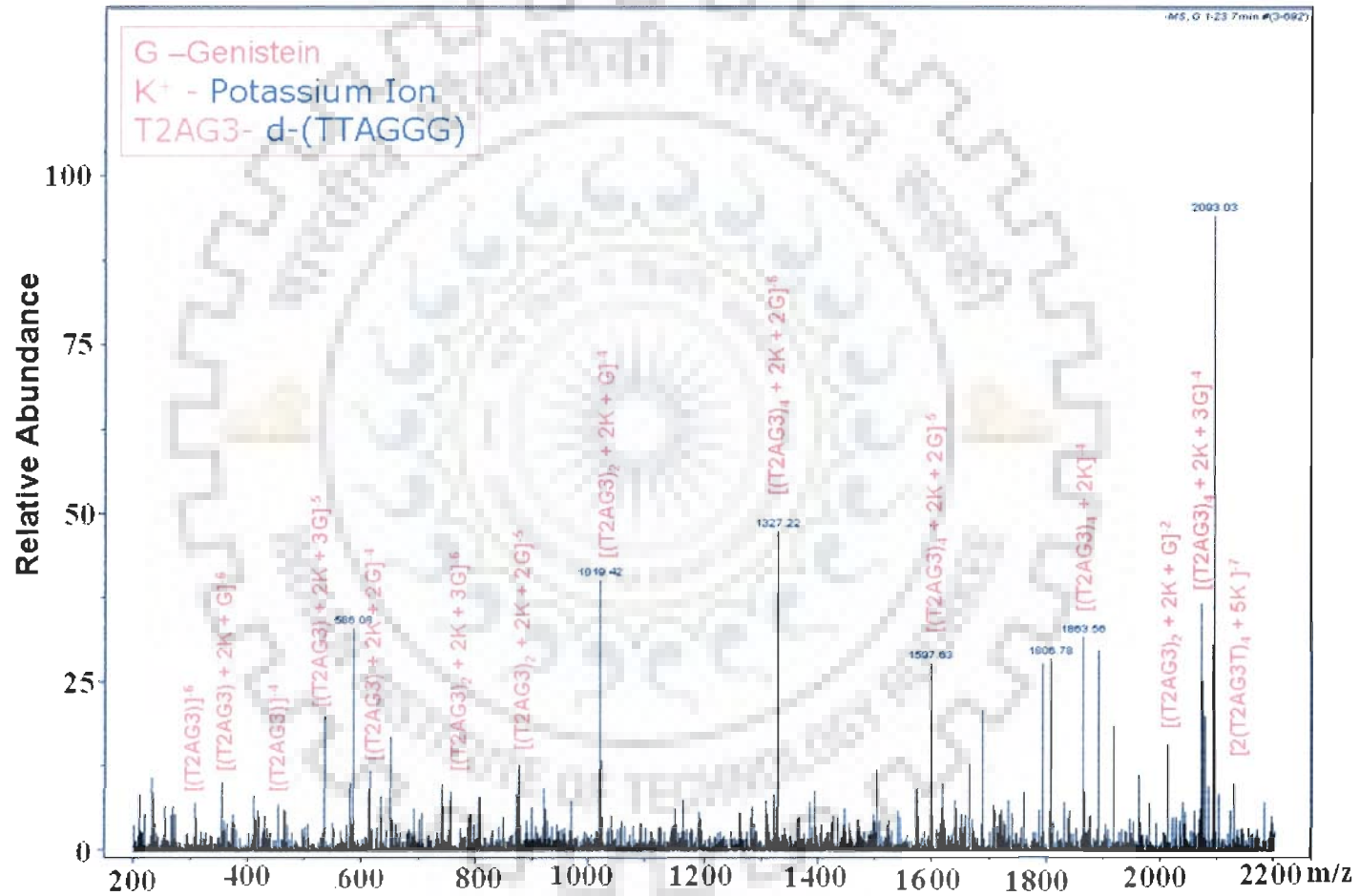
Fig. 6.13 (b):
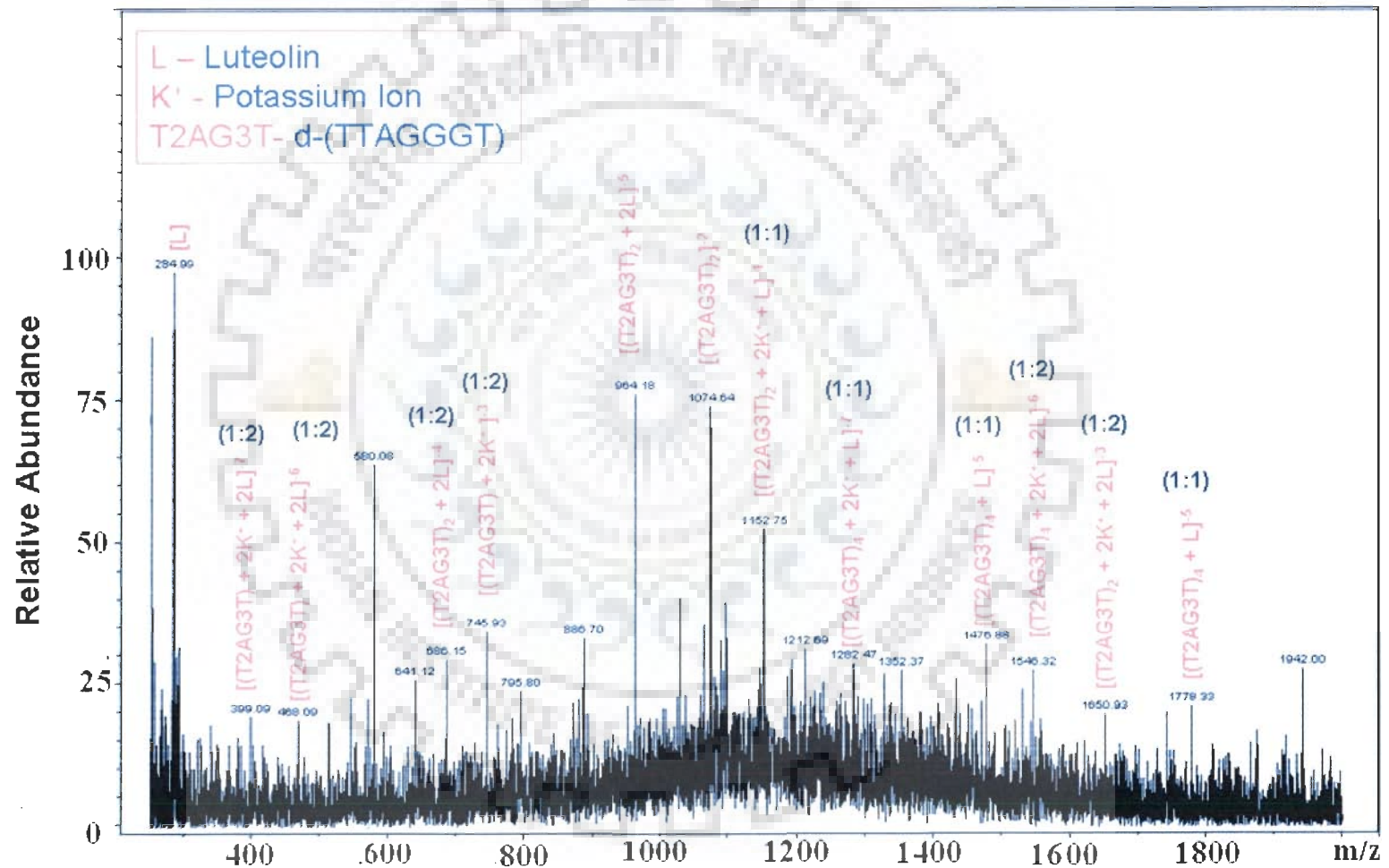
Fig. 6.13(c):

Fig. 6.13(d):

Fig. 6.14: ESI-MS spectra of d-(TTAGGGT)$_4$ complexed with (a) Luteolin, (b) Quercetin, (c) Rutin and (d) Genistein
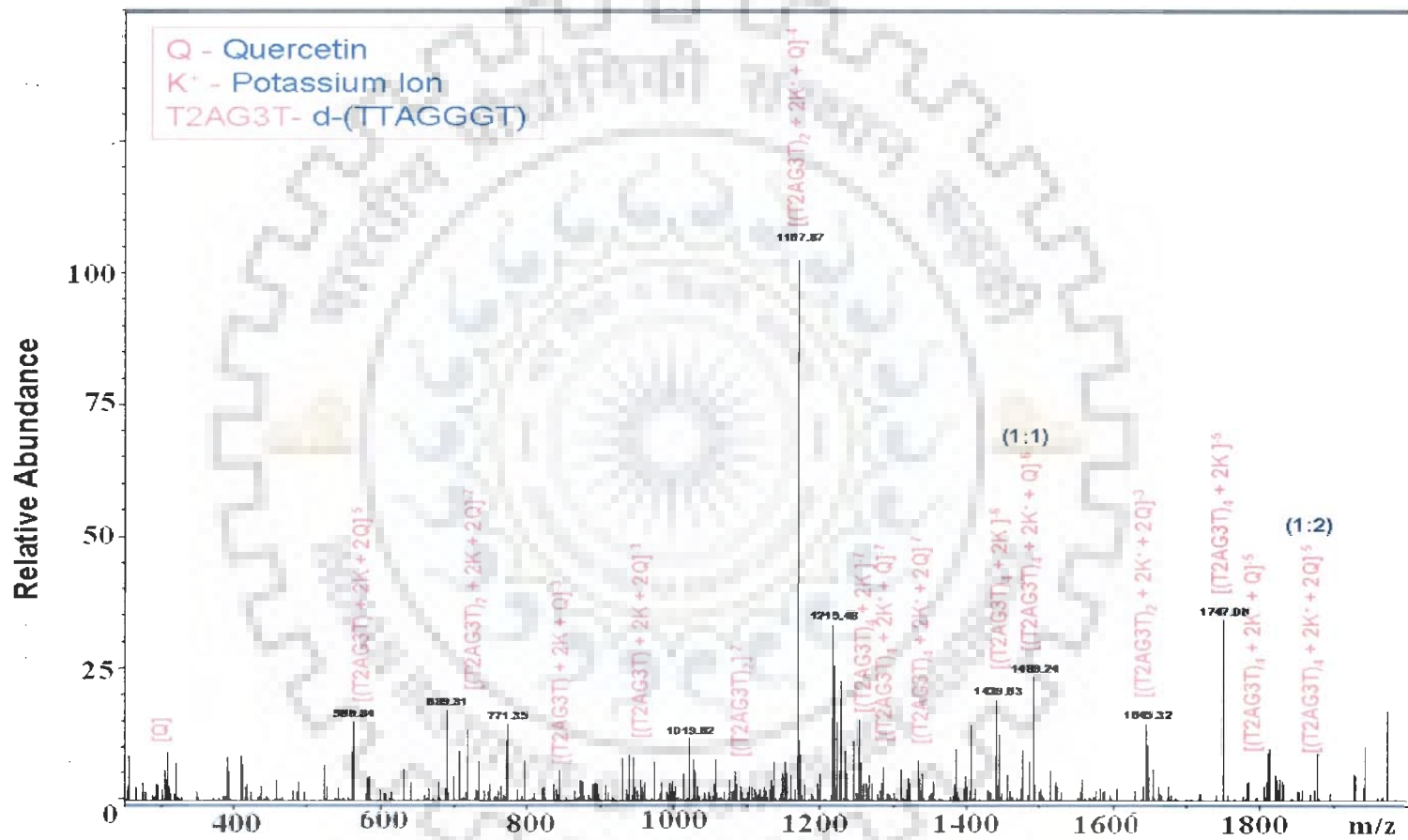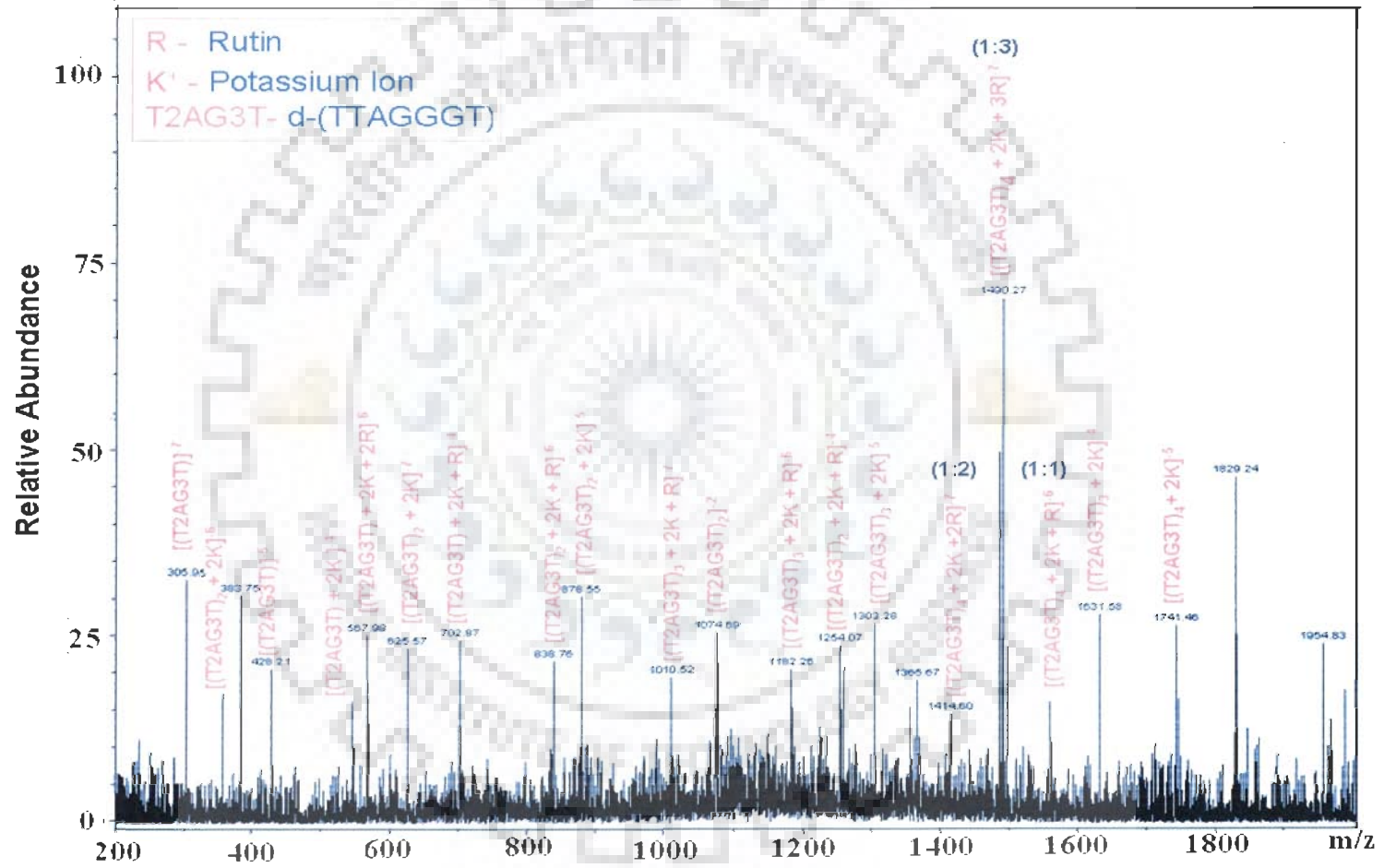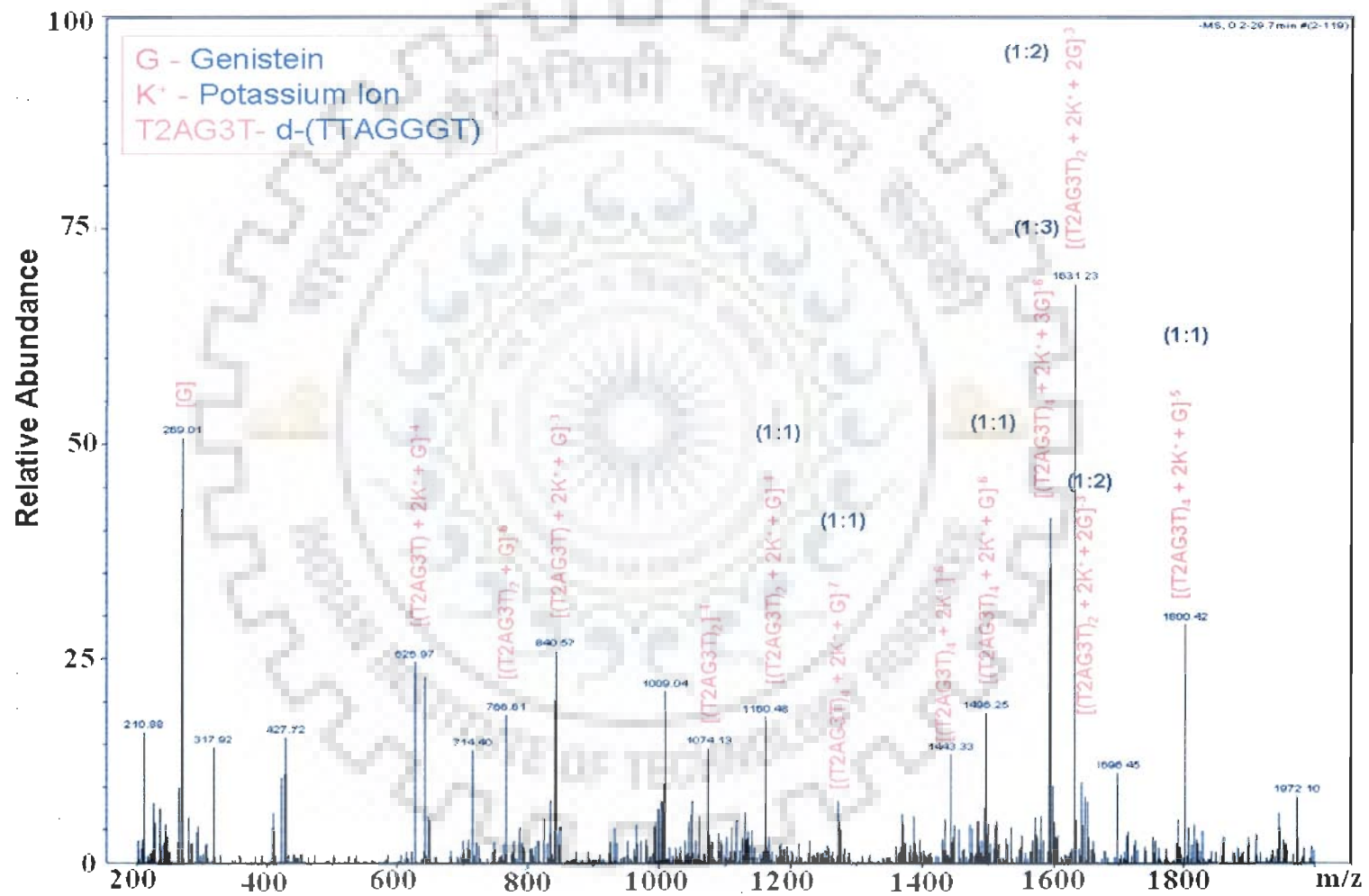
Fig. 6.14 (b):
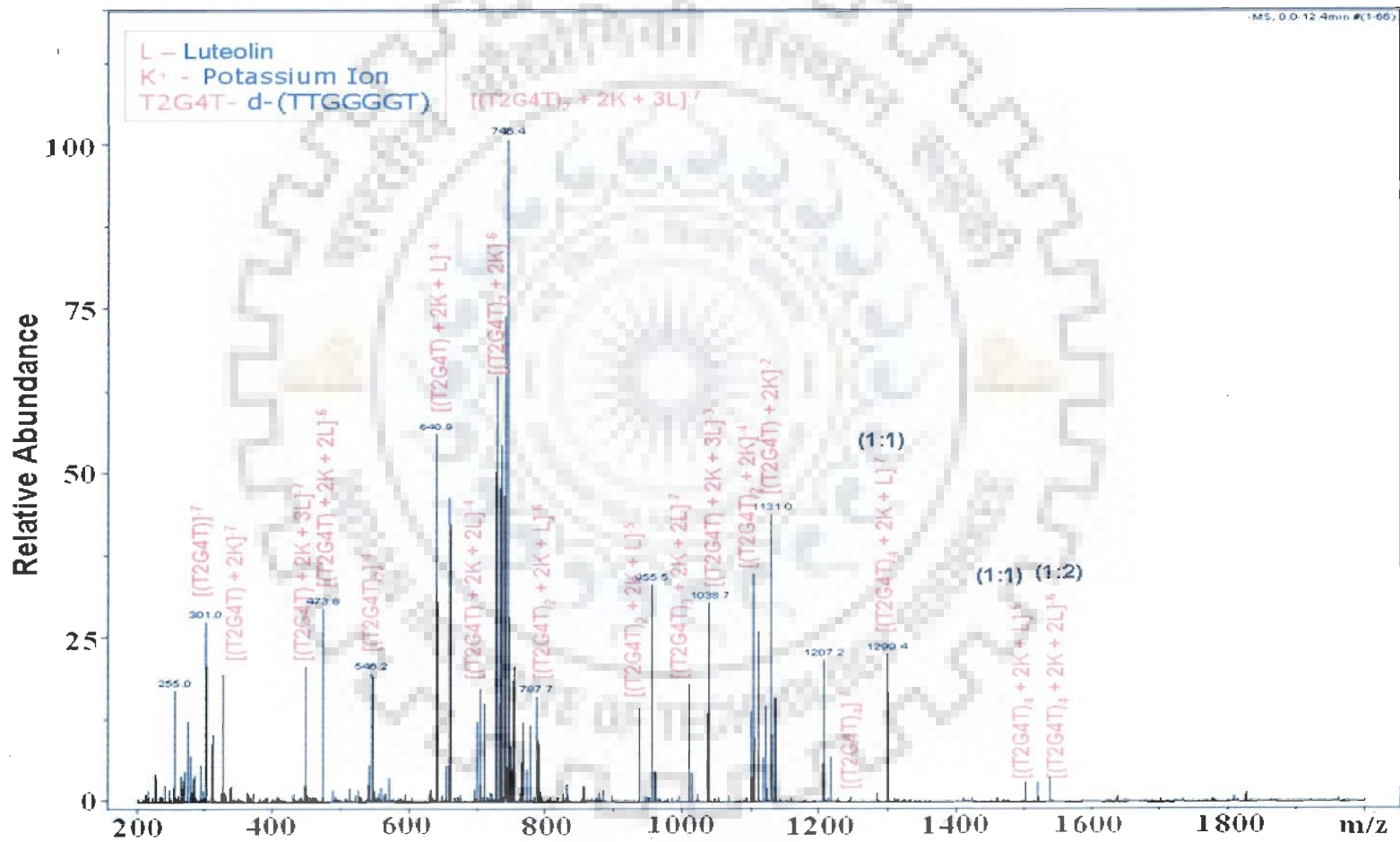
Fig. 6.14 (c):

Fig. 6.14 (d):

Fig. 6.15: ESI-MS spectra of d-(TTGGGGT)₄ complexed with (a) Luteolin, (b) Quercetin, (c) Rutin and (d) Genistein
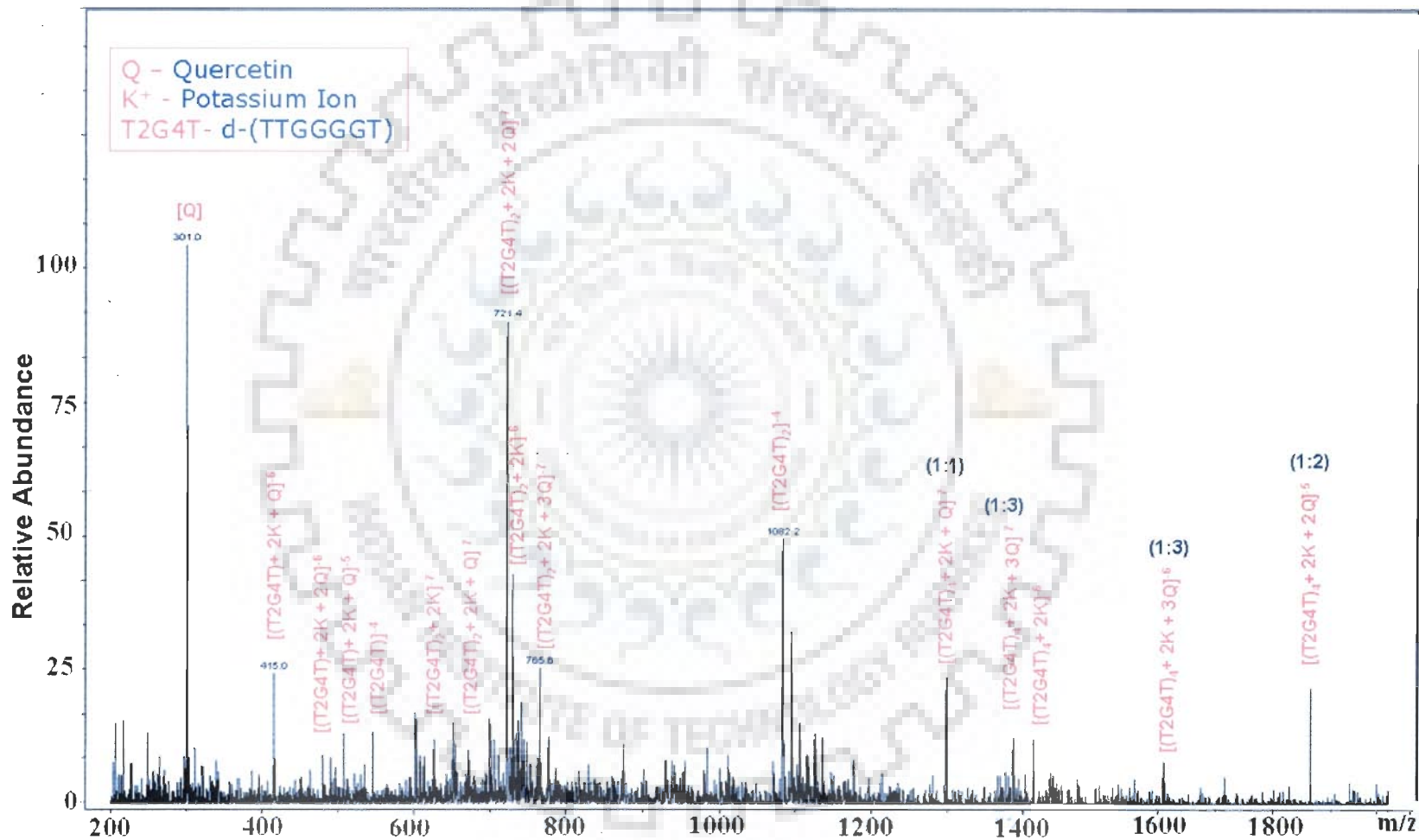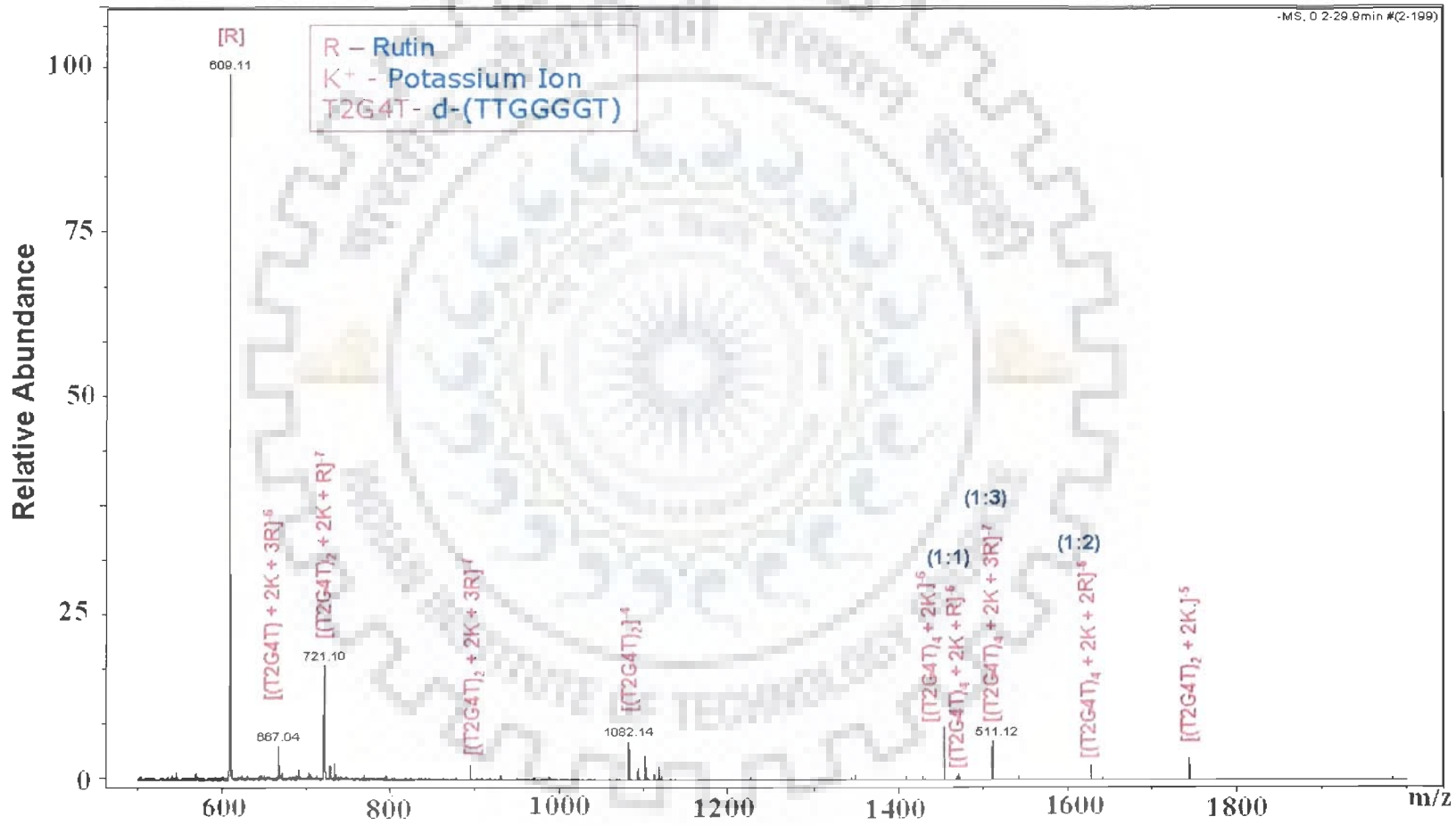
Fig. 6.15 (b):

Fig. 6.15(c):

6.2 Summary and Conclusion

The present work explores the interaction of luteolin, quercetin, rutin and genistein with duplex DNA and telomeric quadruplex forming oligonucleotides which were extensively investigated using competition dialysis, spectrophotometric, fluorometric steady as well as life time, CD and ESI-MS techniques. Different flavonoids showed change in absorption spectrum differently after addition of DNA. Luteolin, rutin and genistein showed hyperchromicity with little bathochromic effect unlikely to quercetin which showed hypochromicity and significant bathochromic shift on addition of duplex DNA. Interaction study with different polynucleotides revealed that these flavonoids do not show any specificity to the DNA sequences but prefer to bind to -AT rich sequences. Further, addition of quadruplex DNA sequences shows hyperchromicity with significant bathochromic effect in all the four flavonoids indicates their intercalative mode of binding. These results are also supported by fluorometric studies which shows enhancement in fluorescence intensity. CD studies confirm the binding of these flavonoids to different G-quadruplex sequences. Life time fluorescence decay and mass spectrometric studies clearly indicated the different stoichiometries of the complex formation. Three different life time decay which is attributed to three different binding complexes, can be correlated to the results obtained from MS data showing 1:1, 1:2 and 1:3 stoichiometries. In view of getting further information about the mode of binding of these flavonoids to G-quadruplex seuquences, structural studies are warranted. Next chapter may give more light on the structural studies and information about the binding of the representative flavonoids quercetin with the G-quadruplex sequence (d-TTAGGGT)$_4$.

Study of Interaction of quercetin with Telomeric G-Quadruplex Sequence d-(TTAGGGT)₄ Using Nuclear Magnetic Resonance Spectroscopy and restrained molecular dynamic approach.

. Recently, the G–quadruplex structure is found to plays an important role in interfering with telomerase action suggesting it as a potential therapeutic target for telomerase inhibition in cancer therapy. The basic unit of the G-quadruplex is the G-tetrad. Based on these structural features of quercetin, one may expect the usage of this model flavonoid in recognizing and stabilizing the G-quadruplexes structure to target cancer. Thus, apart from proton NMR data, knowledge of detailed conformational changes at each phosphate site is important to understand the quercetin-G- quadruplex interaction. This chapter contains the following studies of the complex of quercetin-d-(TTAGGGT)$_4$ by one- and two-dimensional ^{31}P and ^{1}H NMR followed by restrained molecular dynamics simulations:

- 1D ^{1}H and ^{31}P NMR titration studies of quercetin-d-(TTAGGGT)$_4$ complex at various drug (D)/DNA duplex (N) ratios of 0.2, 0.5, 0.75 and 1.0 at 298 K and 318 K in 90% water and 10% D$_2$O.

- The temperature dependence of ^{31}P and ^{1}H chemical shift of 2.41 mM d-(TTAGGGT)$_4$ quadruplex in the range of 278 - 328 K.

- Temperature dependence of ^{31}P and ^{1}H NMR of the quercetin- d-(TTAGGGT)$_4$ complex having D/N = 1.0 in the range of 278 - 328 K.

- 2D ^{31}P - ^{31}P exchange spectra of drug-DNA complex by a phase-sensitive NOESY using mixing time of 200 ms, for D/N = 0.5 at 298 K and 1.0, at 298 K, 308 K and 318 K.

- 2D NOESY ^{1}H - ^{1}H at D/N = 1.0, 1.5, 2.0 using mixing time τ_m = 100, 200, 250, 300 ms at 298 K in 90% H_2O and 10% D_2O.

- Diffusion Ordered Spectroscopy (DOSY) experiments of complex of quercetin-d-(TTAGGGT)$_4$ and uncomplexed quercetin.

- Restrained molecular dynamics studies on the solution structure for the complex of quercetin with d-(TTAGGGT)$_4$ using inter-proton distances obtained from 2D NOESY as restraints.

7.1 Results and Discussion

7.1.1   Phosphorous-31 NMR Studies of quercetin-d-(TTAGGGT)$_4$ Complex

For the purposes of this discussion, the positions of the bases in the heptamer are designated as follows: d–(T1pT2pA3pG4pG5pG6pT7)$_4$. The assignment of phosphate resonances of heptamer d-(TTAGGGT)$_4$ were done using ^{31}P - ^{1}H Heteronuclear Multiple Bond Correlation (HMBC) 2D NMR at 298K (Fig. 7.1). Three bond scalar coupling of ^{31}P with (H3')$_n$ and (H5'/H5")$_{n+1}$ protons as well as four bond coupling with (H4')$_n$ and (H4')$_{n+1}$ protons are expected to manifest as cross peaks in the 2D ^{31}P - ^{1}H correlation map. Based on the proton assignments of the d-(TTAGGGT)$_4$ (Gavathiotis and Searle, 2003), the assignment of ^{31}P nucleotide resonances were quite straight forward using the three bond scalar coupling of ^{31}P with (H3')$_n$ of the sugar residue. Accordingly the phosphate resonances at -2.26, -2.50, -2.56, -2.62, 2.61 and -2.66 were assigned as A3pG4, T2pA3, T1pT2, G6pT7, G4pG5 and G5pG6, respectively at 298K.

7.1.1.1. Chemical Shift

The binding of quercetin to d-(TTAGGGT)$_4$ was investigated by titrating a known concentration of quercetin (200mM) successively to a fixed heptanucleotide concentration of 2.41 mM (quadruplex) to arrive at Drug to Nucleotide (D/N) stoichiometric ratios from 0 to 1.0. Fig. 7.2 (a-c), Table 7.1 and 7.2 show the change in ^{31}P chemical shift due to binding as a function of added quercetin at 298K, 308K and 318K. There are only six resonances observed on the formation of the DNA-drug complex and they show a moderate shift with appearance of new set of resonances as compared to the resonances from free d-(TTAGGGT)$_4$, but broaden severely with increase in D/N ratio to 1.0, thus indicates that there is a chemical exchange on the NMR time scale. It is observed that the T1pT2, G4pG5, G5pG6 and A3pG4 resonances shift ($\Delta\delta = \delta^b - \delta^f$) downfield by 0.02, 0.009, 0.021 and 0.023 ppm, respectively for the complexes of D/N 0.5 at 298K and broadens at higher ratio upto 1.0. T2pA3 and A3pG4 resonance shift further beyond D/N ratio 0.5 to an extent by 0.09 and 0.139 ppm. All six phosphate resonances showed downfield shift in the titration experiments performed at 298K and 318 while upfield shift at 308 K. Maximum shift were observed for T1pT2 resonance in all the temperatures. This shows that T1pT2 is more involved in binding to quercetin than other bases on the heptamer and since T2pA3 is adjacent to T1pT2 thus got affected more than succeeding phosphate. Other resonances show marginal shift, but comparatively in lesser extent than observed for T1pT2 and T2pA3 resonances. This shows that the quercetin is interacting with d-(TTAGGGT)$_4$ at the T1pT2 site and hence other sites are least affected.

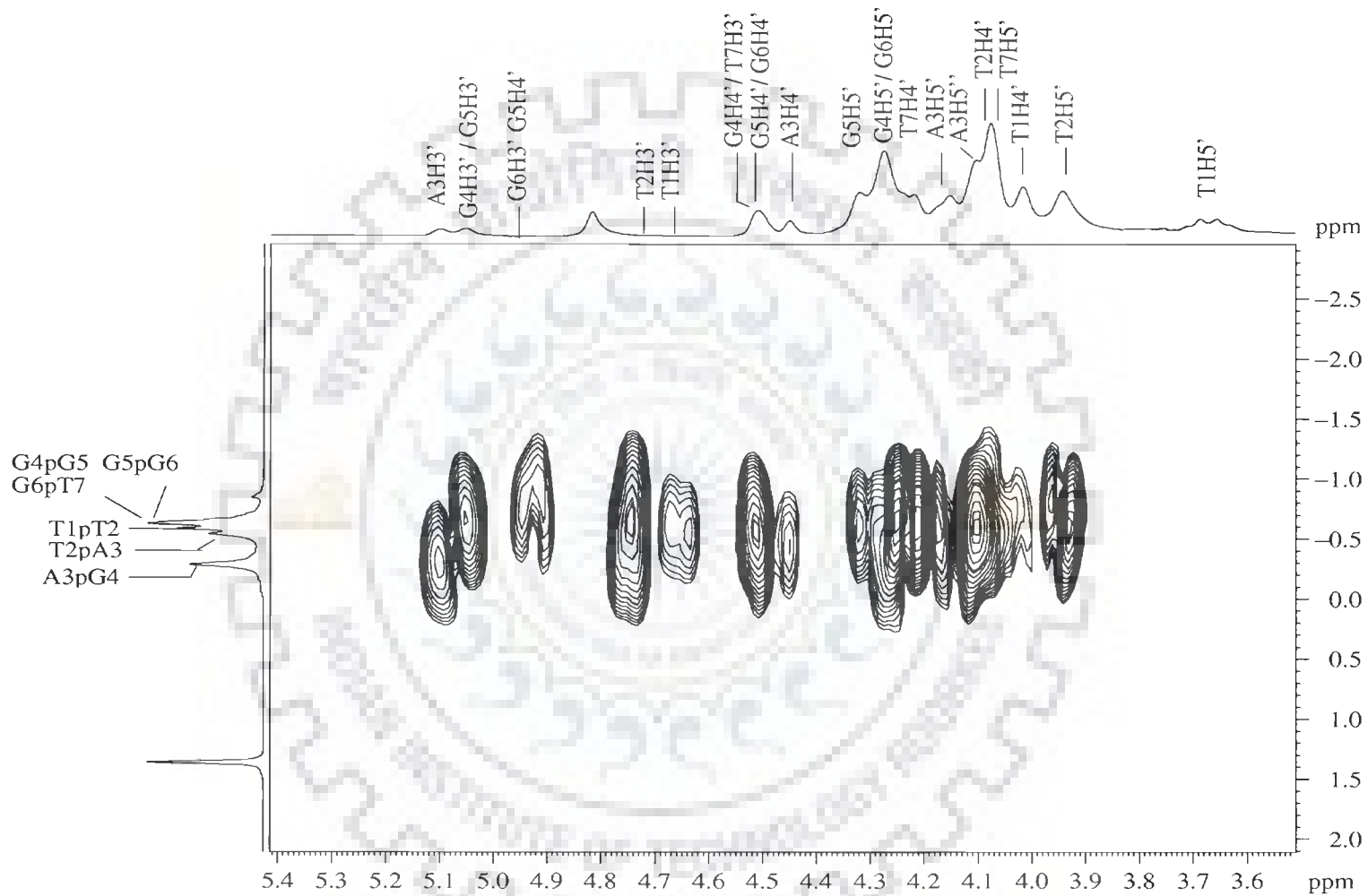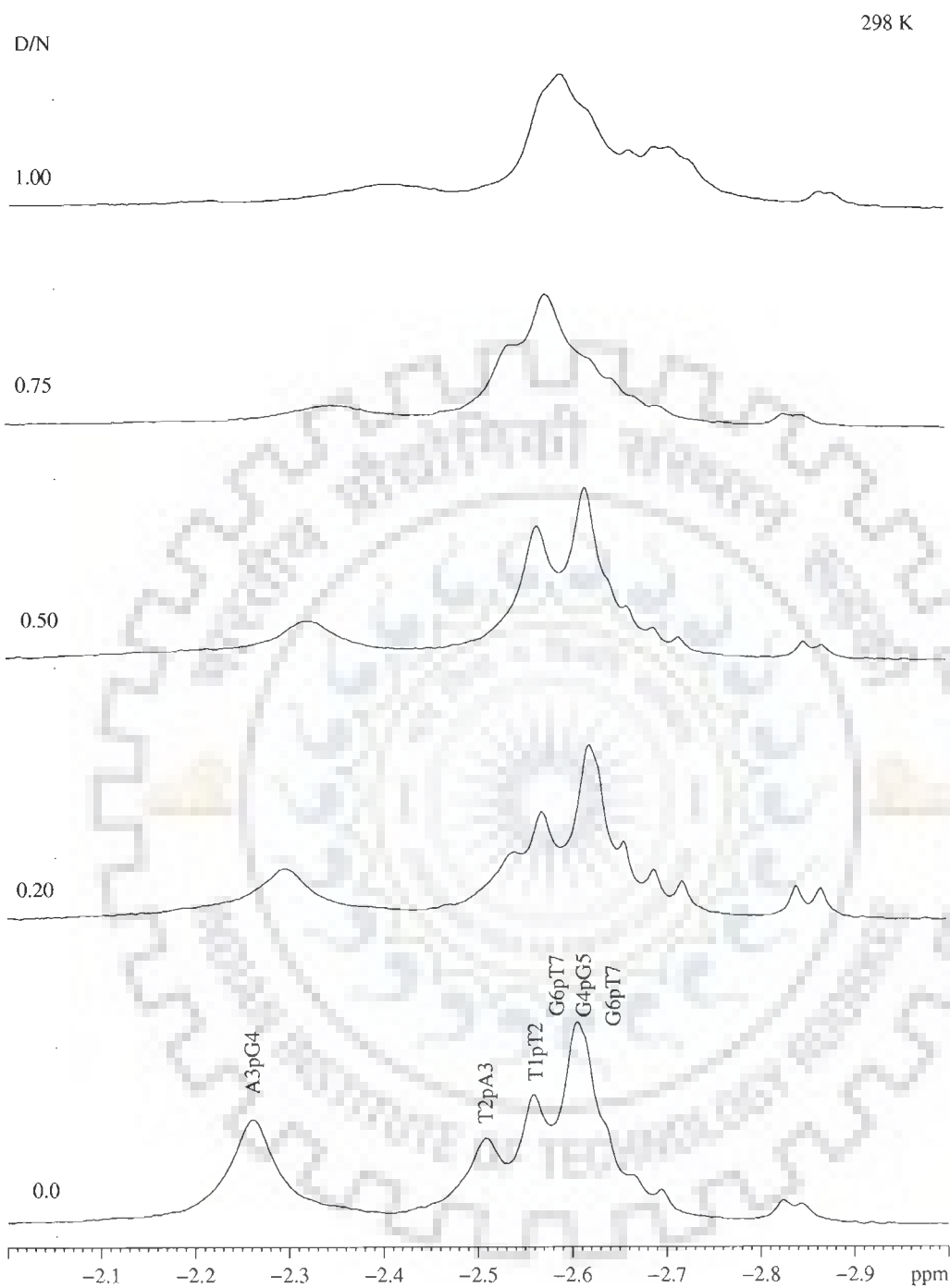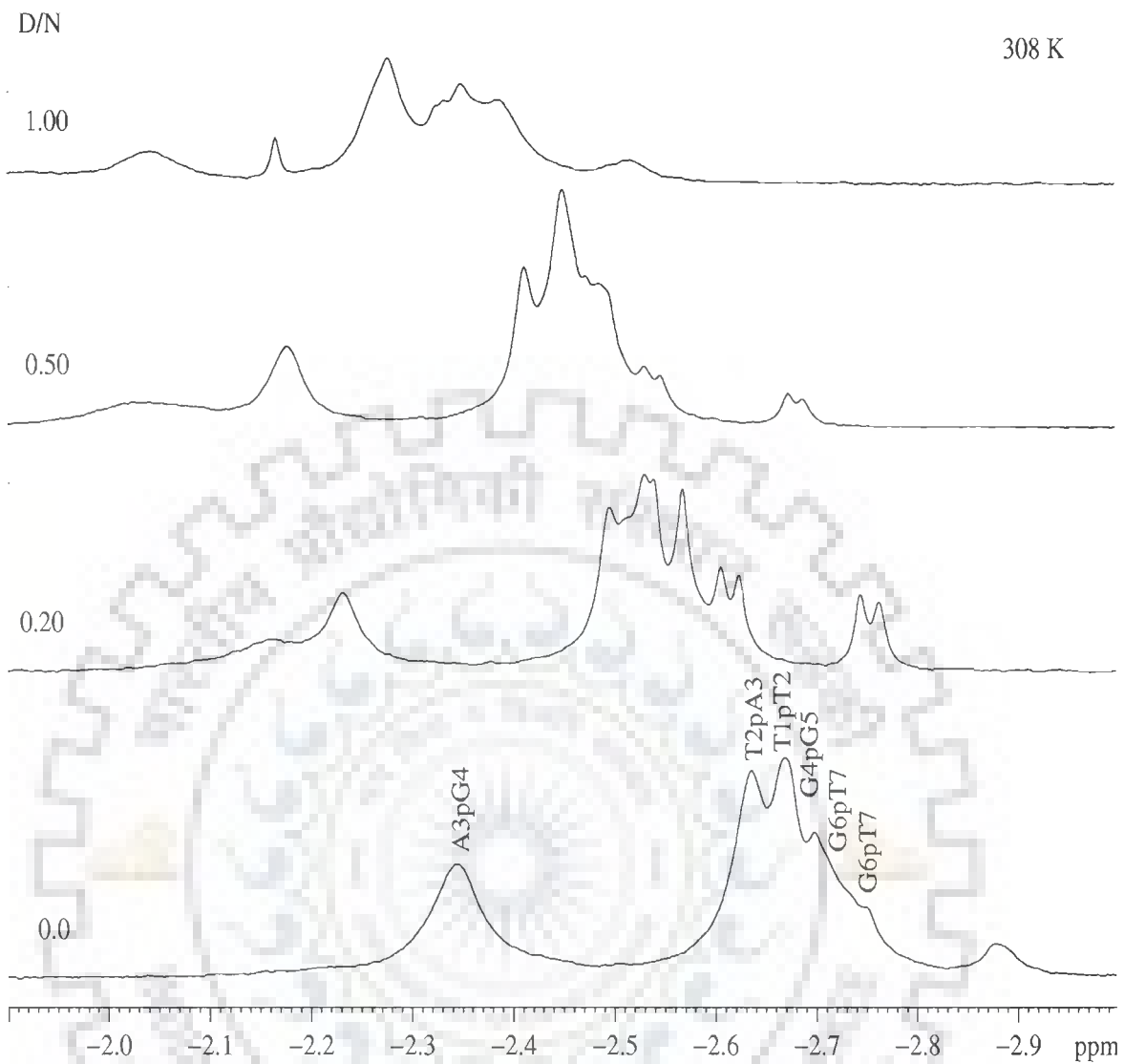Fig. 7.1: Two Dimensional $^{31}P - ^1H$ Heteronuclear Multiple Bond Correlation (HMBC) spectra of d-(TTAGGGT)$_4$ at 298 K.

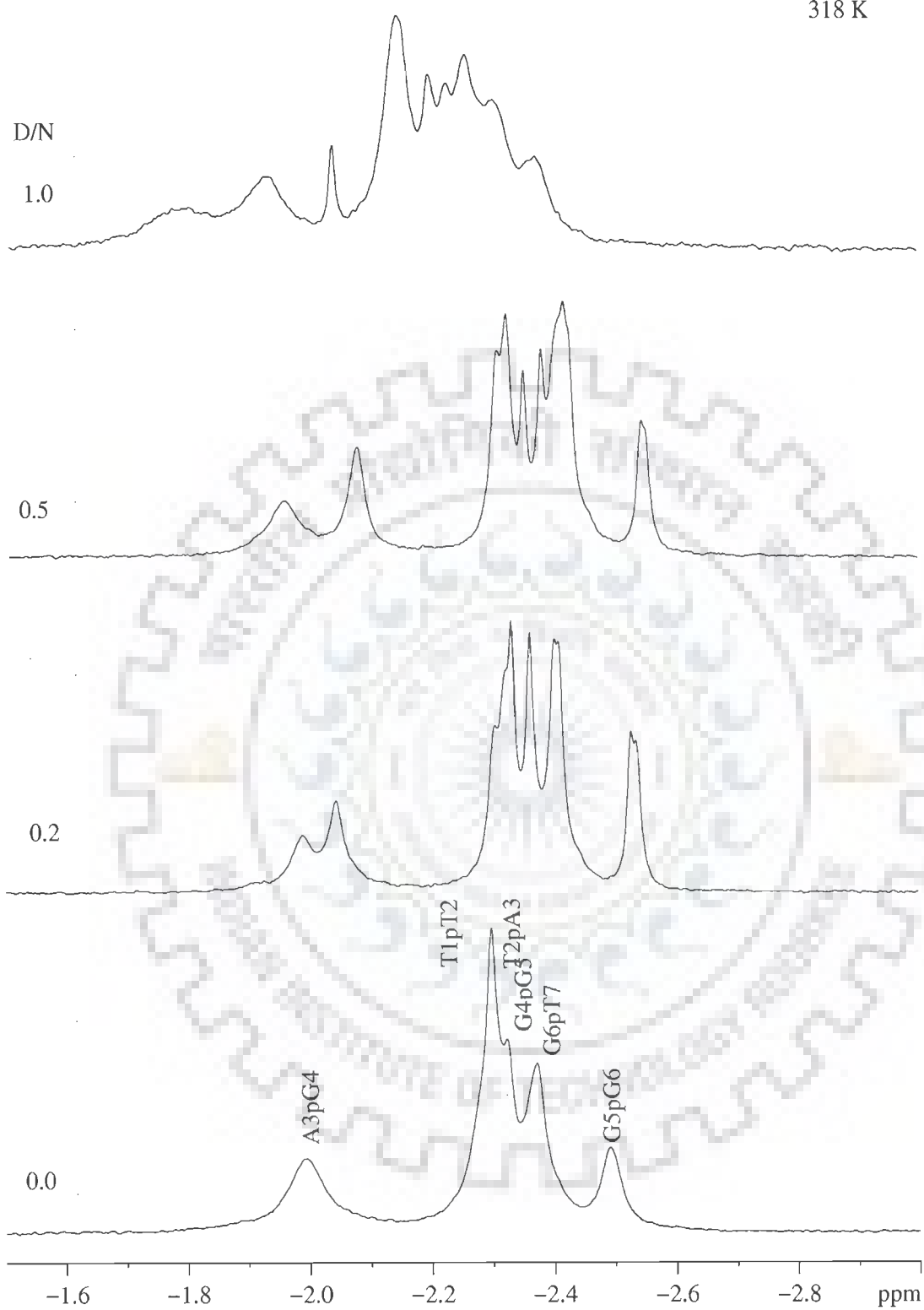**(Fig. 7.2a)**

Fig. 7.2 (a-c): Proton decoupled ^{31}P NMR spectra of 2.41 mM d-(TTAGGGT)$_4$ in uncomplexed state and complexed with quercetin with increasing drug (D) to nucleic acid duplex (N) ratio, D/N, at (a) 298 K, (b) 308K and (c) 318K.

(Fig. 7.2b)

(Fig. 7.2c)

Table 7.1: Chemical shift of ^{31}P resonances of the phosphate groups of DNA heptamer, in complex of quercetin with d-(TTAGGGT)$_4$ at 298 K, 308 K, 318 K with different drug (D) to nucleic acid duplex (N) ratios (D / N). +ve $\Delta\delta$ indicates downfield shift whereas -ve $\Delta\delta$ indicates upfield shift. $\Delta\delta = (\delta_{D/N=1.0} - \delta_{D/N=0})$.

298 K						
D/N	T1pT2	T2pA3	A3pG4	G4pG5	G5pG6	G6pT7
0.00	-2.558	-2.507	-2.261	-2.604	-2.667	2.693
0.20	-2.566	-2.536	-2.297	-2.611	-2.684	2.716
0.50	-2.585	-2.562	-2.321	-2.613	-2.688	2.716
0.75	b	-2.574	-2.350	b	b	b
1.00	b	-2.590	-2.400	b	b	b
$\Delta\delta$	0.027	0.09	0.139	0.009	0.021	0.023
308 K						
0.00	-2.666	-2.634	-2.343	-2.697	-2.875	-2.745
0.20	-2.533	-2.497	-2.235	-2.569	-2.762	-2.622
0.50	-2.466	-2.408	-2.174	-2.485	-2.685	-2.528
1.00	-2.276	-2.276	-2.04	-2.345	-2.514	-2.384
$\Delta\delta$	-0.39	-0.358	-0.303	-0.352	-0.361	-0.356
318 K						
0.00	-2.296	-2.322	-1.984	-2.321	-2.491	-2.372
0.20	-2.334	-2.364	-2.047	-2.366	-2.537	-2.412
0.50	-2.407	-2.407	-2.067	-2.373	-2.543	-2.417
1.00	b	b	b	b	b	b
$\Delta\delta$	0.111	0.085	0.083	0.052	0.052	0.045

Table 7.2: ^{31}P chemical shift of phosphate groups in the quercetin with d–(TTAGGGT)$_4$ complex at drug (D) to nucleic acid duplex (N) ratio, D/N = 0, 0.2, 0.5 and 1.0 at 298K, 308K and 318K. The change in chemical shift, due to Drug-DNA complex formation is also indicated for the three complexes.

298K

Phosphate Group	Uncomplexed DNA $\delta_{D/N=0}$	Drug-DNA Complex					
		$\delta_{D/N=0.2}$	$\delta_{D/N=0.2}-\delta_{D/N=0}$	$\delta_{D/N=0.5}$	$\delta_{D/N=0.5}-\delta_{D/N=0}$	$\delta_{D/N=1}$	$\delta_{D/N=1}-\delta_{D/N=0}$
T1pT2	2.557	-2.569	0.012	-2.616	0.059	b	0.027
T2pA3	-2.506	-2.520	0.014	-2.565	0.059	2.579	0.090
A3pG4	-2.260	-2.296	0.034	-2.319	0.059	-2.339	0.139
G4pG5	-2.606	-2.631	0.025	-2.631	0.025	b	0.009
G5pG6	-2.659	-2.682	0.023	-2.682	0.023	-2.689	0.021
G6pT7	-2.624	-2.644	0.020	-2.649	0.025	-2.649	0.023

308K

Phosphate Group	Uncomplexed DNA $\delta_{D/N=0}$	Drug-DNA Complex					
		$\delta_{D/N=0.2}$	$\delta_{D/N=0.2}-\delta_{D/N=0}$	$\delta_{D/N=0.5}$	$\delta_{D/N=0.5}-\delta_{D/N=0}$	$\delta_{D/N=1}$	$\delta_{D/N=1}-\delta_{D/N=0}$
T1pT2	-2.666	0.200	-2.466	-2.466	-0.200	-2.276	-0.390
T2pA3	-2.634	-2.533	-0.101	-2.408	-0.266	-2.276	-0.358
A3pG4	-2.343	-2.497	0.154	-2.174	-0.169	-2.040	-0.303
G4pG5	-2.697	-2.235	-0.462	-2.485	-0.212	-2.345	-0.352
G5pG6	-2.875	-2.569	-0.306	-2.685	-0.190	-2.514	-0.361
G6pT7	-2.745	-2.762	0.017	-2.528	-0.217	-2.384	-0.356

318K

Phosphate Group	Uncomplexed DNA $\delta_{D/N=0}$	Drug-DNA Complex					
		$\delta_{D/N=0.2}$	$\delta_{D/N=0.2}-\delta_{D/N=0}$	$\delta_{D/N=0.5}$	$\delta_{D/N=0.5}-\delta_{D/N=0}$	$\delta_{D/N=1}$	$\delta_{D/N=1}-\delta_{D/N=0}$
T1pT2	-2.296	-2.334	0.038	-2.407	0.111	b	-
T2pA3	-2.322	-2.364	0.042	-2.407	0.111	b	-
A3pG4	-1.984	-2.047	0.063	-2.067	0.083	b	-
G4pG5	-2.321	-2.366	0.045	-2.373	0.007	b	-
G5pG6	-2.491	-2.537	0.046	-2.543	0.052	b	-
G6pT7	-2.372	-2.412	0.040	-2.417	0.045	b	-

+ve $\Delta\delta$ indicates downfield shift

-ve $\Delta\delta$ indicates up field shift
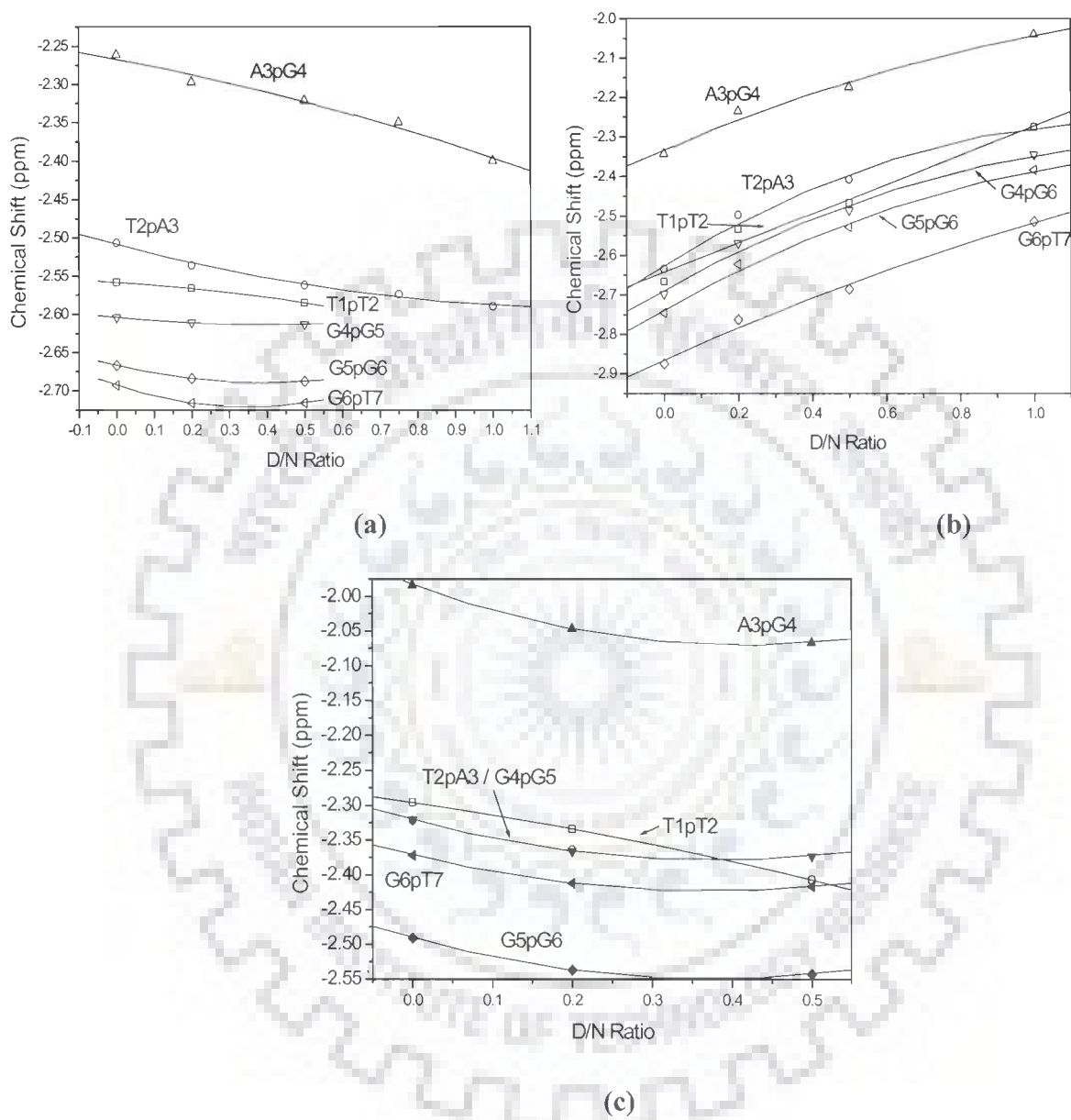
Fig. 7.3 (a-c): ^{31}P Chemical shift variation of d–(TTAGGGT)$_4$ in complex with quercetin, as a function D/N ratio (a) at 298K (b) at 308K (c) at 318K.

However, generally it is unable to provide information on the conformation of the phosphate ester backbone since no direct inter-proton distance constraints are available though NOESY spectra. [31]P chemical shifts vary in response to local, sequence specific and induced environmental distortions in the duplex geometry (Schroeder et al, 1989). Theoretical studies have shown that variation in conformation of two of the six torsional angles (α: O3'-P-O5'-C5' and ζ: C3'-O3'-P-O5') can cause perturbations in ^{31}P shifts. A switching from energetically more favorable B_I conformation ($\zeta = g^-$, $\alpha = g^-$) to the more flexible B_{II} conformation ($\zeta = t$, $\alpha = g^-$) having energy 1 Kcal/mol higher than B_I, introduces a downfield shift of about 1.5 ppm (Gorenstein et al, 1977). The dispersion in ^{31}P chemical shifts of oligonucleotides has also been attributed to different populations of B_I and B_{II} states (Gorenstein, 1992). [31]P chemical shift has also been correlated with degree of unwinding of duplex DNA resulting from increase in the length of the sugar phosphate backbone to accommodate intercalation of drug chromophore. Besides, the ester O-P-O bond angle distortions in drug-duplex DNA complexes also affect the chemical shift. Widening of ester O-P-O angle is expected to produce an upfield shift (Gorenstein, 1984; Gorenstein, 1975) while narrowing of this bond angle causes a downfield shift. Purely electrostatic associations between drug and nucleic acid on the other hand produce only small and generally upfield ^{31}P chemical shifts (Patel, 1979; Wilson et al., 1982).

The change in chemical shifts obtained for the ^{31}P resonances of quercetin-d-(TTAGGGT)$_4$ complex can be compared with corresponding $\Delta\delta$ values reported in literature (Table 7.3a–b) for binding of mitoxantrone with d–(CGCG)$_2$ (Lown et al, 1985b), d–(CGATCG)$_2$ (Kotovych et al, 1986), 2-pyrido[1, 2–e]purine–4–yl)amino–

274

ethanol with d–(CGATCG)$_2$ (Favier et al, 2001), berberine with d–(AAGAATTCTT)$_2$ (Mazzini et al, 2003), nogalamycin with d–(GCATGC)$_2$ (Searle et al, 1988), adriamycin and methoxy–morpholinodoxorubicin with d–(CGATCG)$_2$ and d–(CGTACG)$_2$ (Mazzini et al, 1998). In case of external binding drugs, pyridopurine (Favier et al, 2001) and berberine (Mazzini et al, 2003), downfield shift in the range 0–0.17 ppm have been reported. On the other hand adriamycin, morpholinyldoxorubicin, daunorubicin and nogalamycin (Mazzini et al, 1998; Ragg et al, 1988; Searle et al, 1988), which intercalate between two base pairs of DNA oligomer, lead to downfield shifts up to 1.57 ppm of phosphorus resonances at the intercalation site or at site adjacent to it. Earlier shifts ~2.6 ppm has been reported on intercalation of aromatic chromophores in DNA (Gorenstein et al, 1992; Patel et al, 1976; Patel et al, 1974; Patel et al, 1982). Similarly, studies on mitoxantrone show downfield field shift up to 0.15–0.34 ppm (Lown et al, 1985b; Kotovych et al, 1986).

^{31}P chemical shift variations in nucleotides reflect the conformation of the phosphodiester groups at the level of the P–O5' and O3'–P bonds i.e. the values of torsion angles α = O3'–P—O5'–C5'and ζ = C3'–O3'–P–O5'. For a nucleotide in a B–DNA type conformation, the phosphate groups are normally found in gauche$^-$, gauche$^-$ (g$^-$, g$^-$) conformation with α and ζ angles of -60° and -90°, respectively whereas the gauche$^-$, trans (g$^-$, t) conformation (α = -60°, ζ = 180°) is generally associated with a deshielding of 1.5 ppm. Such transition from g$^-$, g$^-$ to g$^-$, t on intercalation of drug chromophore by opening of adjacent base pairs at intercalation site from a distance of 3.4 to 6.8 Å have been reported in X–ray crystallographic structure of adriamycin and daunomycin to d–CGATCG, d–TGATCA, d–CGTACG sequences (Frederick et al, 1990) as well in similar

NMR structures (Mazzini et al, 1998). The pyridopurine (Favier at al, 2001) and berberine (Mazzini et al, 2003), which does not show such large shifts in phosphorus resonances on binding to DNA, have been shown to bind externally in the restrained molecular dynamics structures obtained by using experimental intermolecular inter proton distances from NOESY spectra. Thus it may be inferred that binding of quercetin to d–(TTAGGGT)$_4$ does not lead to opening of base pairs, which is generally associated with large down field shifts of ^{31}P resonance, of the order of 1.6–2.6 ppm (Gorenstein et al, 1992; Patel et al, 1976; Patel et al, 1974; Patel et al, 1982). However, apart from chemical shift change, a new set of resonance starts appearing at downfield position as quercetin concentration was increased but shows broadening at D/N ratio 1.0. These resonances may be correlated to the coexistence of two populations i. e bound and free phosphate backbone indicating that the exchange between intercalated and free DNA sites is slow on the ^{31}P-NMR time scale for these ligands. At lower temperature all free and bound peaks were merged but at higher temperature of 318 K peaks separates and become sharp. The best resolved spectrum was observed at D/N ratio 0.2 at 318 K (Fig. 7.2c). Similar kind of pattern of having another peak at downfield position were reported in A-85226 and also in potent intercalator ethidium bromide with d(G-C)$_5$ presumably due to conformational changes on the DNA phosphate backbone induced by their intercalation (Frederick and Hurley 1999).

7.1.1.2. Temperature Dependence Studies

^{1}H decoupled ^{31}P NMR spectra of d-(TTAGGGT)$_4$ were obtained over the temperature range from 288 K to 318 K. At ambient temperatures, the ^{31}P resonances resolve into six distinct signals corresponding to six phosphate groups in d-(TTAGGGT)$_4$

Table 7.3a: Chemical shift of free (δ^f) bound (δ^b), and change in chemical shift due to binding, $\Delta\delta = \delta^b - \delta^f$ in phosphate groups of some of the drug–DNA complexes taken from literature.

Phosphate Group	Mazzini et al., 1998 d-(CGATCG)$_2$ + Adriamycin			Mazzini et al., 1998 d-(CGTACG)$_2$ + Adriamycin			Searle et al., 1988 d-(GCATGC)$_2$ + Nogalamycin		
	δ^f	δ^b	$\Delta\delta$	δ^f	δ^b	$\Delta\delta$	δ^f	δ^b*	$\Delta\delta$
C1pG2/ G1pC2	-0.91	-0.48	+0.43	-1.03	-0.58	+0.45	-3.30	-2.90	+0.20
G2pA3/ C2pA3	-0.86	0.67	+1.53	-1.40	-0.56	+0.84	-3.00	-2.50	+0.50
A3pT4/ T3pA4	-1.26	-1.28	≤0.2	-1.12	-1.26	-0.14	-3.40	-3.20	+0.20
T4pC5/ T4pG6	-1.06	-1.12	-0.06	-1.20	-1.34	-0.14	-3.10	-1.60	+1.50
C5pG6/ G5pC6	-0.73	0.84	+1.57	-0.90	+0.63	+1.53	-3.00	-3.00	+0.00
	Mazzini et al., 1988 d-(CGATCG)$_2$ + Morpholinodoxorubicin			Mazzini et al., 1988 d-(CGTACG)$_2$ + Morpholinodoxorubicin			Ragg et al., 1988 d-(CGTACG)$_2$ + Daunorubicin		
	δ^f	δ^b	$\Delta\delta$	δ^f	δ^b	$\Delta\delta$	δ^f	δ^b	$\Delta\delta$
C1pG2	-0.91	-0.32	+0.59	-1.03	-0.56	+0.47	-1.02	-1.45	-0.43
G2pA3 / G2pT3	-0.86	0.19	+1.05	-1.40	-0.50	+0.90	-1.42	-1.95	-0.53
A3pT4/ T3pA4	-1.26	-1.36	-0.10	-1.12	-1.45	-0.33	-1.08	-1.28	-0.20
T4pC5/ A4pC5	-1.06	-1.11	-0.05	-1.20	-1.46	-0.26	-1.28	-1.48	-0.20
C5pG6	-0.73	0.52	+1.25	-0.90	+0.22	+1.12	-0.88	+0.44	+1.32

+ve $\Delta\delta$ indicates downfield shift.

-ve $\Delta\delta$ indicates upfield shift.

* Tentative assignment

Table 7.3b: Chemical shift of free (δ^f), bound (δ^b), and the change in chemical shift due to binding, $\Delta\delta = \delta^b - \delta^f$ in phosphate resonances of some of the drug–DNA complexes taken from literature.
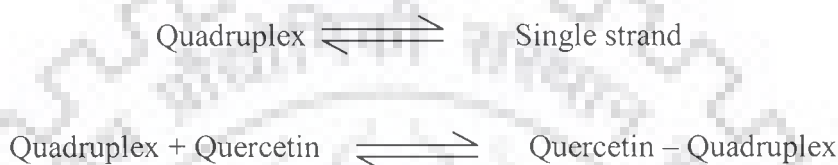
Phosphate Group	Lown et al., 1985b d-(CGCG)$_2$ + mitoxantrone			Kotovych et al., 1986 d-(CGATCG)$_2$ + mitoxantrone				Favier et al., 2001 d-(CGATCG)$_2$ + pyridopurine				Mazinni et al., 2003 d-(AAGAATTCTT)$_2$ + berberine			
	δ^f	δ^b	$\Delta\delta$		δ^f	δ^b	$\Delta\delta$		δ^f	δ^b	$\Delta\delta$		δ^f	δ^b	$\Delta\delta$
C1pG2	-3.46	-3.31	+0.15	C1pG2	-1.71	-1.70	+ 0.01	C1pG2	1.2	1.1	-0.1	A1pA2	-1.31	-1.19	+0.12
G2pA3	-3.30	-3.40	-0.10	G2pA3	-1.71	-1.70	+ 0.01	G2pA3	1.1	1.1	0.0	A2pG3	-1.00	-0.98	+0.02
C3pG4	-3.46	-3.31	+0.15	A3pT4	-2.19	-2.21	-0.02	A3pT4	0.7	0.8	-0.1	G3pA4	-1.14	-1.12	+0.02
				T4pC5	-1.95	-1.97	-0.02	T4pC5	0.4	0.5	-0.1	A4pA5	-1.40	-1.23	+0.17
				C5pG6	-1.59	-1..25	+0.34	C5pG6	1.2	1.2	0.0	A5pT6	-1.37	-1.40	+0.03

Mazzini et al., 2004 Topotecan+d(CGTACG)$_2$				Mazzini et al., 2004 Camptothecin+d(CGTACG)$_2$				Mazzini et al., 2004 Camptothecin+d(CGTATACG)$_2$				Mazinni et al., 2003 d-(AAGAATTCTT)$_2$ + berberine			
												T6pT7	-1.18	-1.10	+0.08
C1pG2	-1.00	-1.00	0.00	C1pG2	-0.88	-0.95	+0.07	C1pG2	-0.94	-0.96	+0.02	T7pC8	-1.11	-1.07	+0.04
G2pT3	-1.29	-1.35	-0.06	G2pT3	-1.32	-1.33	+0.01	G2pT3	-1.33	-1.33	+0.00	C8pT9	-1.14	-1.10	+0.04
T3pA4	-1.08	-1.10	-0.02	T3pA4	-1.14	-1.17	-0.03	T3pA4	-1.03	-1.03	+0.00	T9pT10	-1.04	-1.07	+0.03
A4pC5	-1.12	-1.20	-0.08	A4pC5	-1.14	-1.17	-0.03	A4pC5	-1.33	-1.33	+0.00				
C5pG6	-0.90	-1.00	-0.10	C5pG6	-0.78	-0.85	+0.07	T5pA6	-1.10	-1.13	-0.03				
								A6pC7	-1.09	-1.11	+0.02				
								C7pG8	-0.82	-0.84	-0.02				

+ve $\Delta\delta$ indicates downfield shift   -ve $\Delta\delta$ indicates upfield shift

(Fig. 7.4a). Temperatures lower and higher than the ambient cause some of the signals to shift towards each other and to overlap.

The variation of ^{31}P NMR spectra of d-(TTAGGGT)$_4$ and its complex with quercetin at D/N ratios of 0.5 and 1.0 in the temperature range 288 K to 328 K was examined (Fig. 7.4b,c), it shows the variation of chemical shift as a function of temperature. The signals are found to be shifted with temperature, which may be due to shift in the following equilibrium:

$$\text{Quadruplex} \rightleftharpoons \text{Single strand}$$

$$\text{Quadruplex + Quercetin} \rightleftharpoons \text{Quercetin – Quadruplex}$$

These reactions correspond to single strand transition and drug–DNA complexation (Davies\ et al, 2001b). It is observed that shift in ^{31}P resonances in uncomplexed d-(TTAGGGT)$_4$ are very gradual and not abrupt with increase in temperature (Fig. 7.4a). This is consistent with the earlier observations in oligonucleotides (Patel, 1977) on change in chemical shift with temperature due to helix to coil transition.

7.1.1.3. 2D ^{31}P - ^{31}P Exchange Spectra

Fig. 7.5 (a-b) show 2D ^{31}P NMR exchange spectrum of the complex of quercetin with d-(TTAGGGT)$_4$ at drug to DNA (D/N) ratio of 1.0 at 275K. The one dimensional ^{31}P spectra are shown along both axes. In 2D ^{31}P NMR exchange spectrum, each of the 6 phosphorus signals seen in uncomplexed DNA is expected to give cross peak due to chemical exchange with its respective bound resonance. On binding of quercetin to d-(TTAGGGT)$_4$, as the drug is progressively added to the nucleotide, additional cross peaks observed due to very slow

279
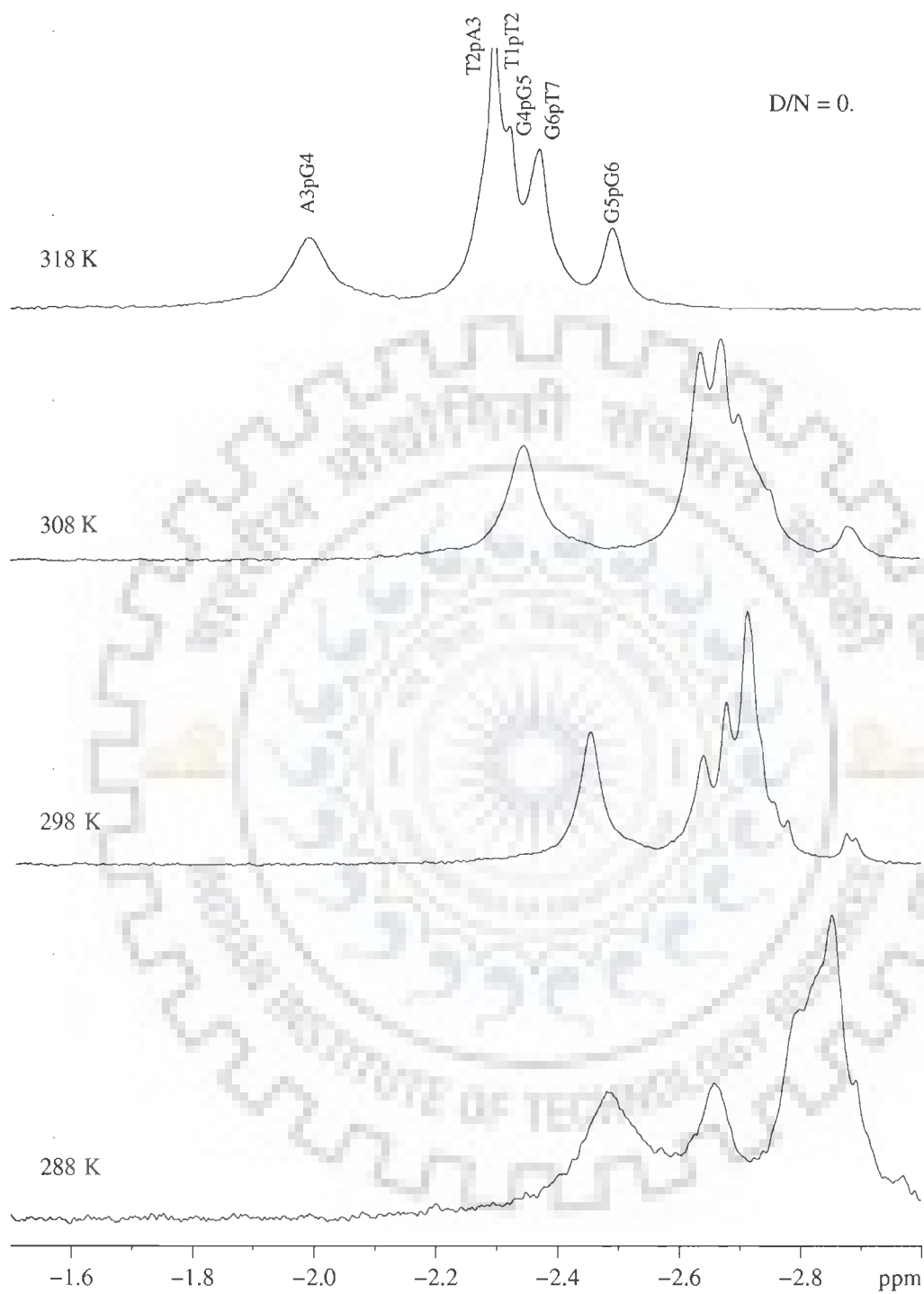
Fig. 7.4a: Proton decoupled ^{31}P NMR spectra of uncomplexed d–(TTAGGGT)$_4$ as a function of temperature.
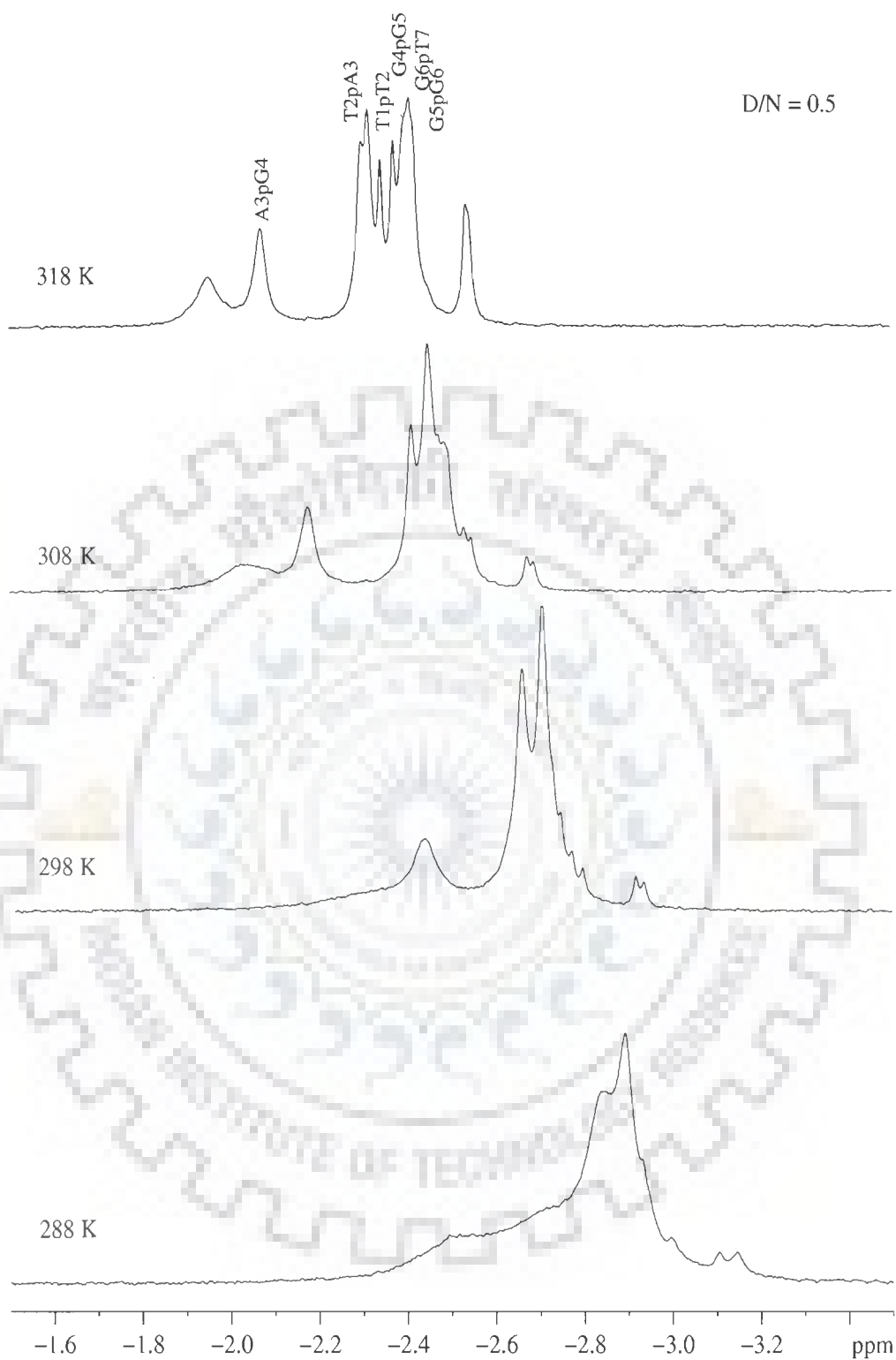
Fig. 7.4b: Proton decoupled ^{31}P NMR spectra of d–(TTAGGGT)$_4$ complexed with quercetin as a function of temperature at D/N ratio 0.5.

281
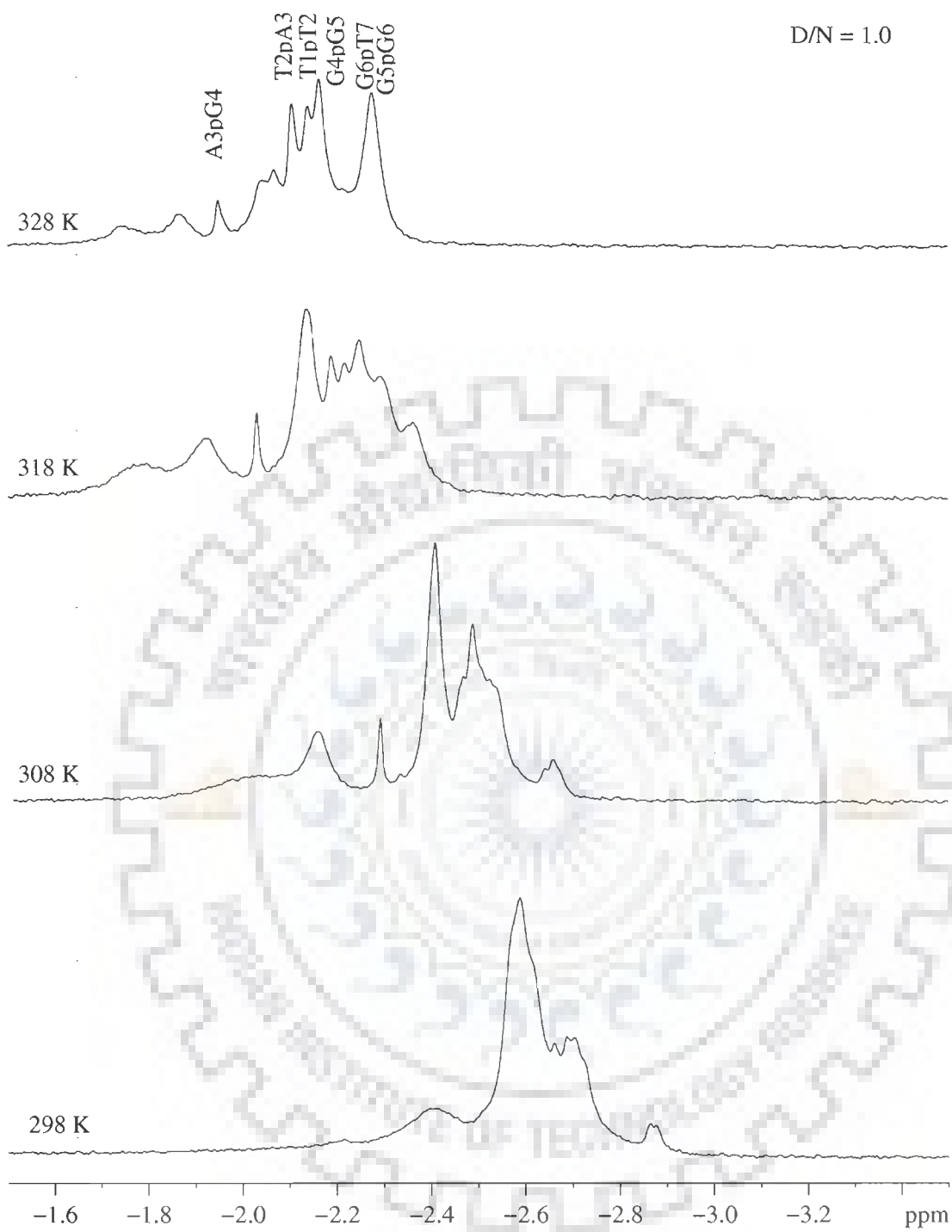
Fig. 7.4c: Proton decoupled ^{31}P NMR spectra of d–(TTAGGGT)$_4$ complexed with quercetin as a function of temperature at D/N ratio 1.0
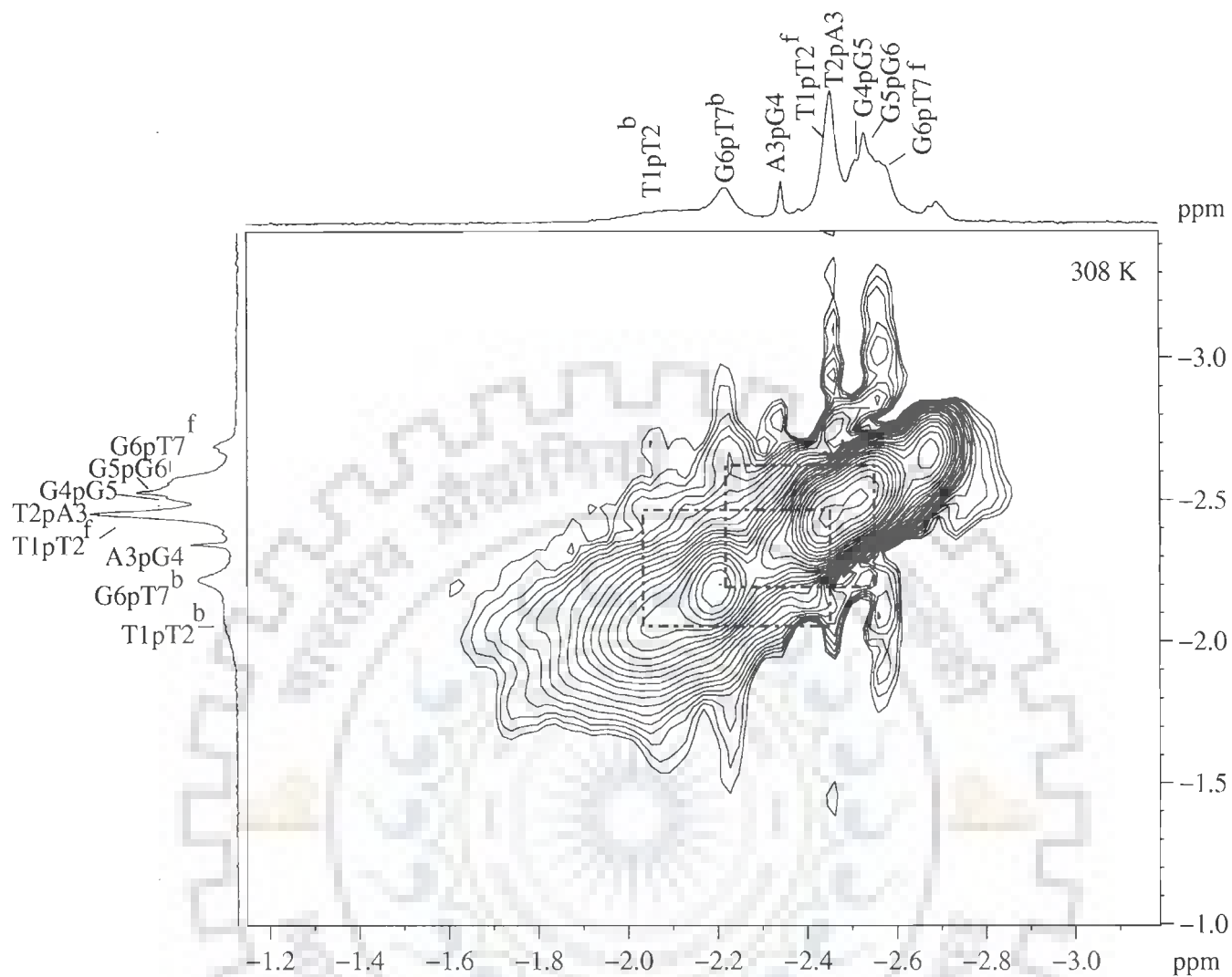
Figure 7.5(a-b): ³¹P NMR exchange spectrum of the complex of d–(TTAGGGT)₄ - quercetin complex at drug (D) to nucleic acid duplex (N) ratio, D/N of 1.0 at (a) 308 K (b) 318 K.

(Fig. 7.5b)

exchange between the bound and free phosphate resonances. Since new set of resonances are observed for the complexes at different D/N ratios for free d-(TTAGGGT)$_4$ and d-(TTAGGGT)$_4$ bound to quercetin, it is expected that ^{31}P signals from the bound DNA are in slow exchange with the corresponding signals from free DNA to be followed individually at 318 K on NMR time scale.

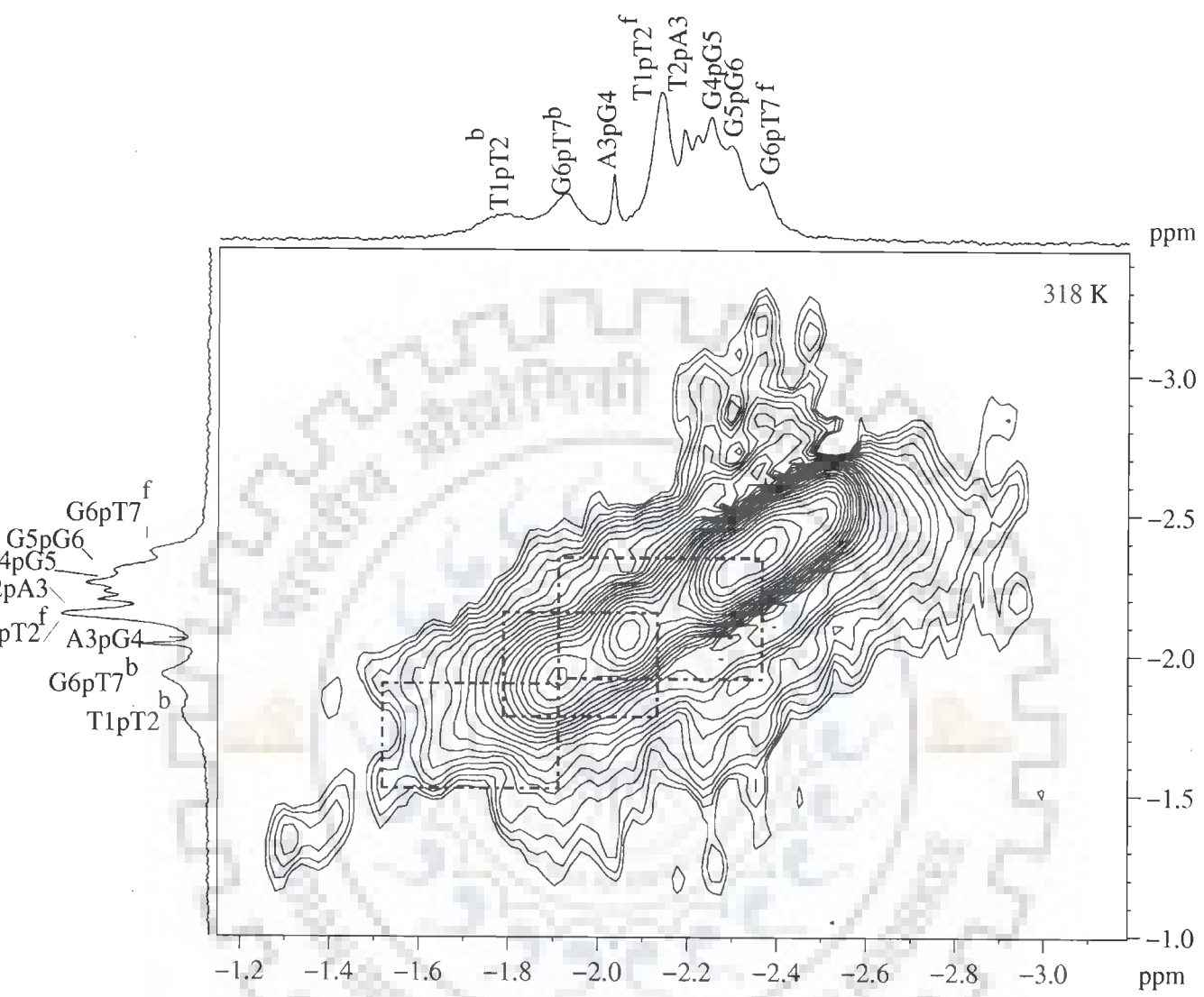The study on ^{31}P NMR of the drug-DNA complex provide an independent proof of the intercalation mode of binding of quercetin to d-(TTAGGGT)$_4$ and it is supported by the cross peaks observed between the bound and free T1pT2 and G6pT7 in ^{31}P - ^{31}P exchange spectra (Fig. 7.5 a,b). Although the ^{31}P NMR studies provide information on the conformation of the phosphate ester backbone, it is unable to provide detailed information on the overall conformation of the sugar rings and bases of oligonucleotides. Direct inter-proton distance (NOE) that is available through ^{1}H NMR studies is discussed further in this chapter and we have found the ^{31}P NMR results are consistent with proton NMR studies.

7.1.2. Proton NMR Studies of Quercetin-d-(TTAGGGT)$_4$ Complex

Fig. 7.6(a-d) and 7.7 (a-e) show the ^{1}H 1D NMR spectra of d–(TTAGGGT)$_4$ and change in chemical shift on successive addition of quercetin to DNA at 298 K. Fig. 7.8 shows the change in quercetin protons chemical shift as a function of D/N ratio. ^{1}H NMR spectra of the drug–DNA complex at D/N=1.0, as a function of temperature are shown in Fig. 7.9(a-d), 7.10 (a-d) and 7.11. The 2D NMR experiments are carried out at 298 K as quadruplex protons are sharpened and intensified at this temperature. DNA is expected to be present in quadruplex state at this temperature. The assignment of spectral lines to specific protons of quercetin has been made by following the strategies used for assignment in

NMR spectra of uncomplexed drug as mentioned in chapter 4. The assignment of nucleotide protons has been carried out by following the strategies adopted for standard B–DNA structures that is, sequential NOEs (base H8/H6)$_n$–sugar (H1')$_{n-1}$, (base H8/H6)$_n$–sugar(H2")$_{n-1}$, (base H8/H6)$_n$–sugar(H2')$_{n-1}$; expected NOEs due to several short intra nucleotide distances (Wuthrich, 1986) as well as NMR data of uncomplexed d–(TTAGGGT)$_4$ (Gavathiotis and Searle, 2003). NOEs between adjacent guanine imino protons in the sequence, G4NH–G5NH and G5NH–G6NH, are evident in Fig. 7.15 a,b. The present oligonucleotide exists as G-quadruplex structure which can be evident from connectivities between the base protons of G4-G5-G6 (Fig. 7.16). The position of each and every resonance was thus ascertained and unambiguous assignment was done. The chemical shift positions of uncomplexed drug and DNA, drug–DNA complex (D/N =1.0) and the change in chemical shift due to binding are given in Tables 7.4, 7.5 and 7.6. The observed intra molecular and intermolecular NOE contacts are listed in Tables 7.9-7.12 Fig. 7.17(a-j) show expansions of specific regions of 2D NOESY spectra of quercetin complexed to d–(TTAGGGT)$_4$ in the stoichiometric ratio of D/N = 1.0.

7.1.2.1. Effects of Titrimetric Addition of quercetin

On addition of quercetin (drug) to DNA, new resonance peaks pertaining to protons start appearing, with increase in intensity as D/N ratio increases. The spectral lines start broadening uniformly at higher ratios indicating binding of drug to DNA. The change in chemical shift ($\Delta\delta$) of base and H1' protons with increasing D/N ratio are gradual and small in magnitude (Fig. 7.6a-d). The $\Delta\delta$ increases with D/N ratio as more and more DNA oligomer binds to the drug and a 0.04 ppm upfield shift was observed for T1H1' and 0.05 ppm for G4H1' protons at D/N =1.0. The downfield shift of 0.07 ppm

was observed in T7H1'. In uncomplexed d–(TTAGGGT)$_4$, G4NH, G5NH and G6NH resonances appear at 11.64, 11.26 and 11.05 ppm, respectively. While the thymine imino resonances were not observed presumably due to exchange with water solvent. The resonance of G4NH, G5NH and G6NH broaden considerably with increasing ratio of quercetin. The thymine imino protons were not observed even at DN ratio 1.0 at 283 K, indicating that drug binding does not induce T-tetrad formation. Further, the broadening in the case of G4NH is more significant with the resonance being slightly elevated from the base line at D/N ratio of 1.00. These imino protons show considerable shift of ~0.1 ppm for G4NH or G5NH and ~0.2 ppm for G6NH on increasing the D/N upto 1.0. The same trend was almost observed for change in chemical shift when the titration was followed through at 308 K and 318 K. At 318 K, other resonances start appearing at the downfield of each guanine imino protons which clearly indicates the presence of two populations having bound and free DNA at D/N ratio 1.0. Further, in the H1' protons T1H1' and G4H1' showed maximum upfield shift than other protons while only T7H1' showed the downfield shift and G5H1', G6H1' protons were least affected. A significant broadening was observed in T1H6 resonance after D/N ratio 0.75 while Guanine base protons shows upfield up to 0.16 ppm and rest other base protons showed downfield shift maximum up to 0.11 for T7H6 at D/N ratio 1.0. Similarly, A3H2 and T1CH$_3$ started broaden after D/N ratio 0.50 while T2CH$_3$ and T7CH$_3$ showed the downfield shift of 0.08 ppm at D/N ratio 1.0 at 298K(Fig. 7.6 a, 7.6 c and Table 7.4 and 7.6).
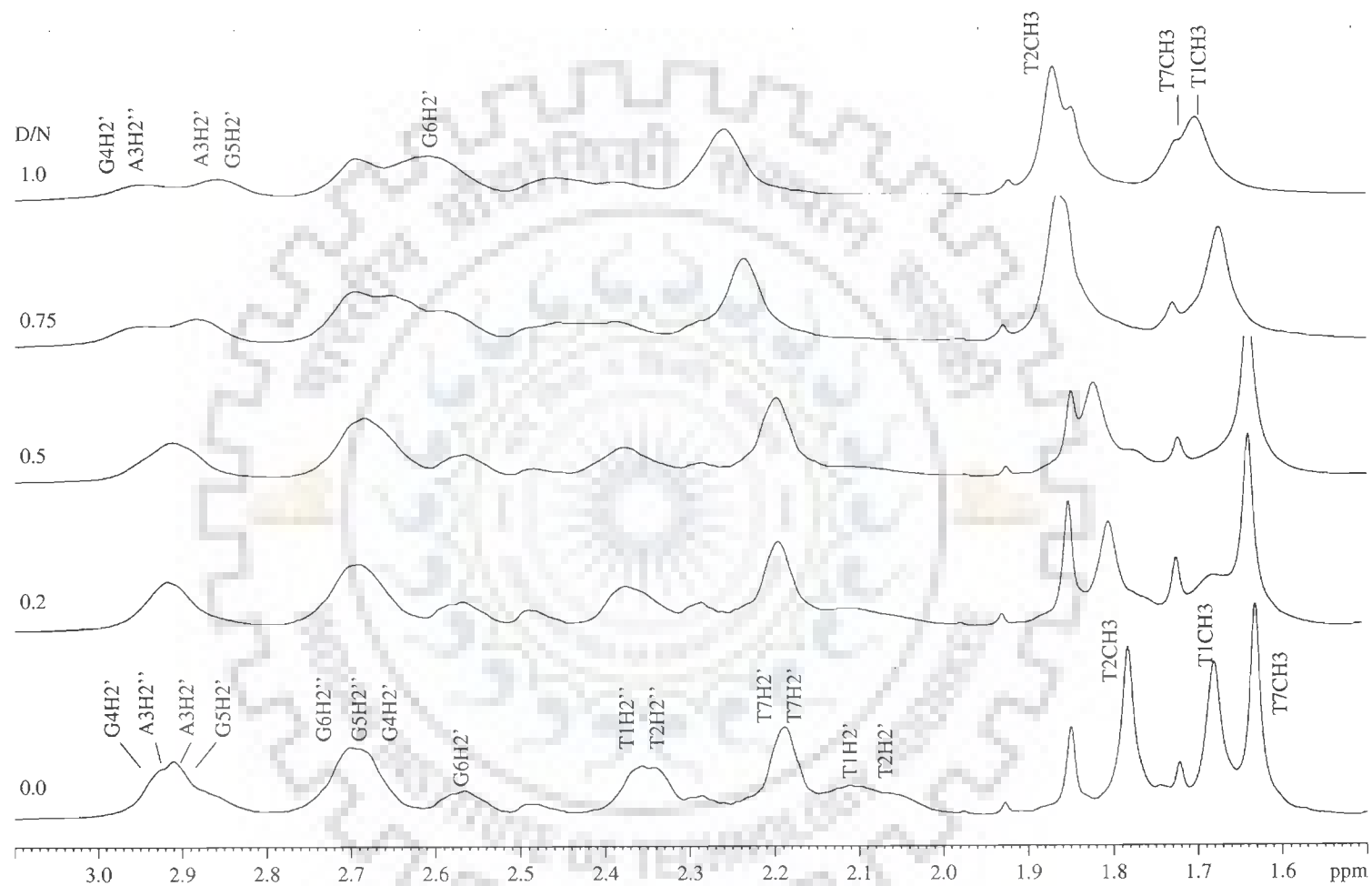
The shift in quercetin protons on binding are expected to be maximum at low D/N ratio when maximum amount of drug is present in the bound state. The benzopyrone ring protons, H2' and H6' shift upfield 0.74 and 0.68 ppm while phenyl ring protons H6 and

287

H8 shift upfield by 0.89 and 0.73 ppm substantially with respect to the chemical shift position of uncomplexed quercetin in 1:1 quercetin to DNA complex at 298 K (Fig. 7.8 and Table 7.5). The proton chemical shift of quercetin alone was measured in the same buffer and DMSO ratio which were used for the study of the complex. Though there was no change in chemical shift of these protons were observed when compared with the spectra recorded in the DMSO solvent. Further in quercetin DNA complex, the change in chemical shift is almost similar in all these drug protons which indicate that these protons experience the similar kind of environment during complexation with DNA. Anticancer drugs like camptothecin and topotecon which are proved as binder of DNA by stacking at the terminal end of oligonucleoiteds also shows a chemical shift variation of ~0.50 ppm for several oligonucleotides (Mazzini et al., 2004).

All the spectral lines are somewhat uniformly broadened on binding, as the internal motions are affected and the protons are getting immobilized. The imino protons of DNA, G4NH and G6NH broaden considerably with temperature at 298 K but at 318 K, other resonances start appearing at the position downfield to each guanine imino protons which clearly indicates the presence of two populations bound and free DNA (Fig. 7.9 a and 7.15). Futher, the substantial upfield shift of ~0.8 ppm in H6, H8, H2' and H6' of quercetin, respectively on binding is indicative of stacking of quercetin aromatic chromophore with base pair of DNA (Table 7.5 and Fig. 7.8). Such stacking interaction is shown by an upfield shift of the resonance signals induced by the ring current effect of the associating molecules.

This Stacking interaction can also be supported by temperature dependent studies of 1:1 D/N ratio complex. Similar to concentration dependent studies of DNA complex, a

Figure 7.6 (a-d): Proton NMR spectra of complex of quercetin with d–(TTAGGGT)₄ as a function of D/N ratio at 298 K
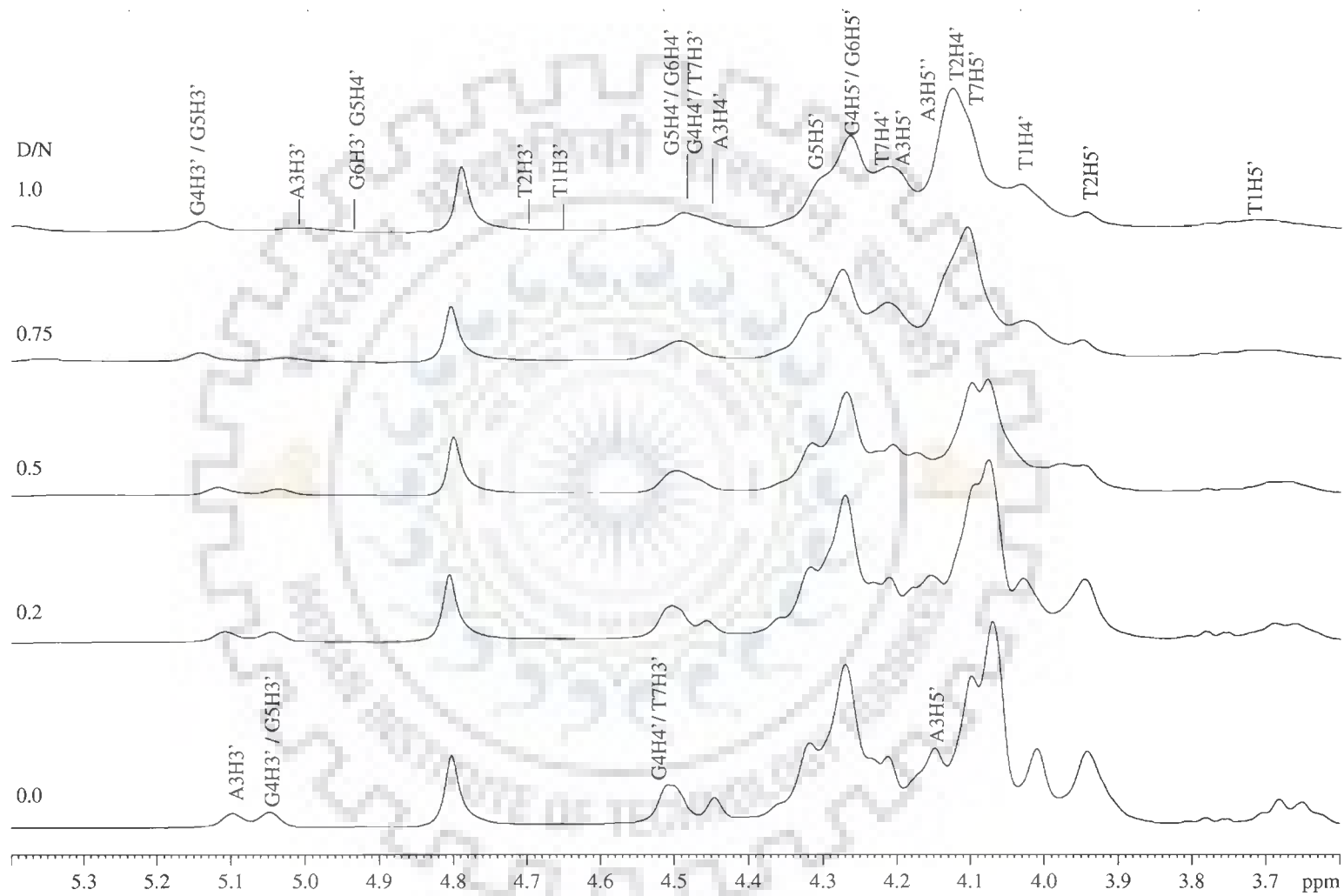
(Fig. 7.6b)

(Fig. 7.6c)

* i -Peaks

(Fig. 7.6d)

Table 7.4: Chemical shift (ppm) of nucleotide, d-(TTAGGGT)$_4$, protons as a function of drug (D) to nucleic acid duplex (N) ratio, D/N, at 298 K. Also shown here is the change in chemical shift on binding, $\Delta\delta = \delta_{D/N=1.0} - \delta_{D/N=0.0}$.

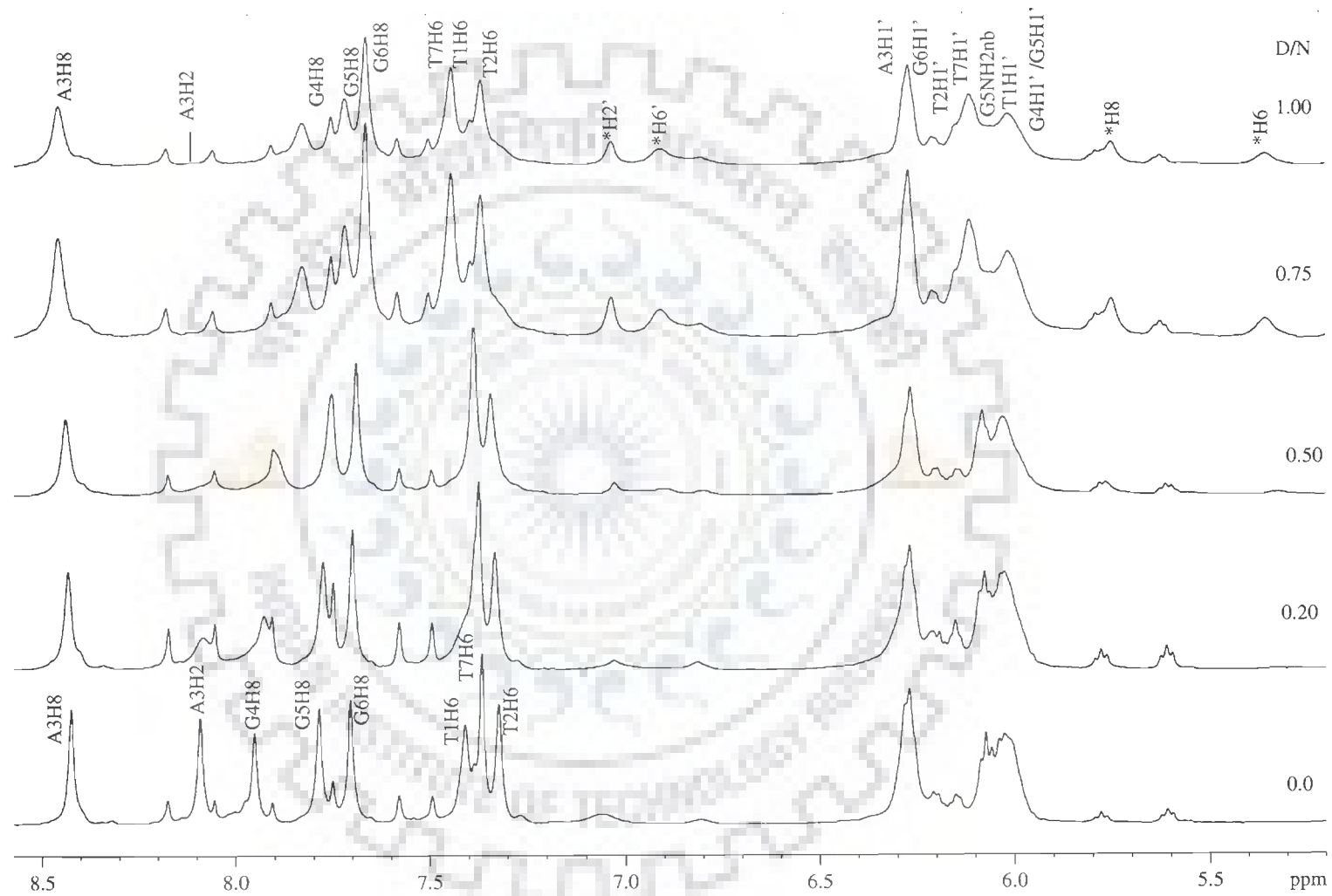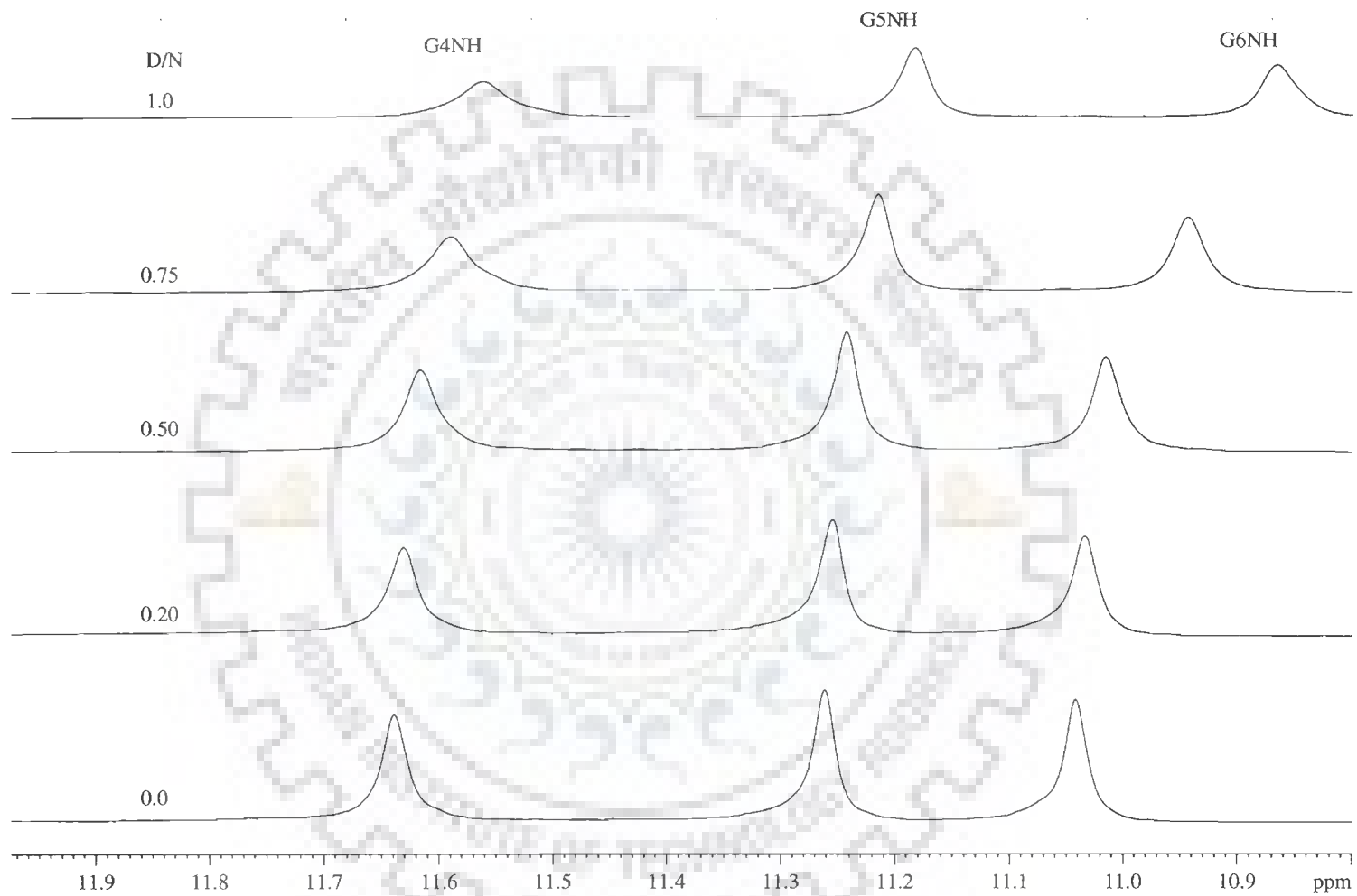| D/N Ratio	T1H1'	T2H1'	A3H1'	G4H1'	G5H1'	G6H1'	T7H1'
0.00	6.031	6.154	6.283	6.046	6.05	6.270	6.074
0.20	6.031	6.151	6.281	6.045	6.05	6.270	6.078
0.50	6.031	6.146	6.279	6.034	6.05	6.270	6.085
0.75	6.015	6.154	6.273	6.013	6.05	6.268	6.117
1.00	5.990	6.144	6.265	5.991	6.05	6.265	6.143
$\Delta\delta$	-0.041	-0.01	-0.018	-0.055	0.0	-0.005	0.069

D/N Ratio	T1H2'	T2H2'	A3H2'	G4H2'	G5H2'	G6H2'	T7H2'
0.00	2.115	2.06	2.874	2.686	2.874	2.574	2.190
0.20	2.115	2.06	2.903	2.686	2.903	2.574	2.194
0.50	2.115	2.06	2.914	2.686	2.914	2.574	2.200
0.75	B	b	2.947	2.686	2.947	2.592	2.238
1.00	B	b	2.947	2.686	2.947	2.609	2.261
$\Delta\delta$	0	0	0.073	0	0.073	0.035	0.071

D/N Ratio	T1H2"	T2H2"	A3H2"	G4H2"	G5H2"	G6H2"	T7H2"
0.00	2.359	2.344	2.912	2.912	2.686	2.703	2.190
0.20	2.378	2.365	2.912	2.912	2.686	2.693	2.194
0.50	2.378	2.375	2.912	2.912	2.686	2.684	2.200
0.75	B	b	2.884	2.884	2.653	2.653	2.238
1.00	B	b	2.861	2.861	2.624	2.622	2.261
$\Delta\delta$	-	-	-0.051	-0.051	-0.062	-0.081	0.071

D/N Ratio	T1H6	T2H6	A3H8	G4H8	G5H8	G6H8	T7H6
0.00	7.410	7.324	8.426	7.955	7.788	7.707	7.367
0.20	7.356	7.334	8.434	7.931	7.777	7.703	7.375
0.50	7.356	7.345	8.442	7.906	7.756	7.693	7.388
0.75	B	7.371	8.461	7.832	7.721	7.668	7.447
1.00	B	7.375	8.463	7.791	7.686	7.638	7.484
$\Delta\delta$	-	0.051	0.037	-0.164	-0.102	-0.069	0.117

D/N Ratio	T1 CH$_3$	T2 CH$_3$	A3H2	G4NH	G5NH	G6NH	T7 CH$_3$
0.00	1.681	1.784	8.093	11.641	11.264	11.045	1.633
0.20	1.680	1.802	8.087	11.632	11.257	11.036	1.635
0.50	B	1.824	b	11.618	11.244	11.018	1.640
0.75	B	1.864	b	11.592	11.216	10.945	1.674
1.00	B	1.871	b	11.563	11.185	10.868	1.702
$\Delta\delta$	-	0.087	-	-0.078	-0.079	-0.177	0.069

-ve $\Delta\delta$ indicates upfield shift
+ve $\Delta\delta$ indicates downfield shift.
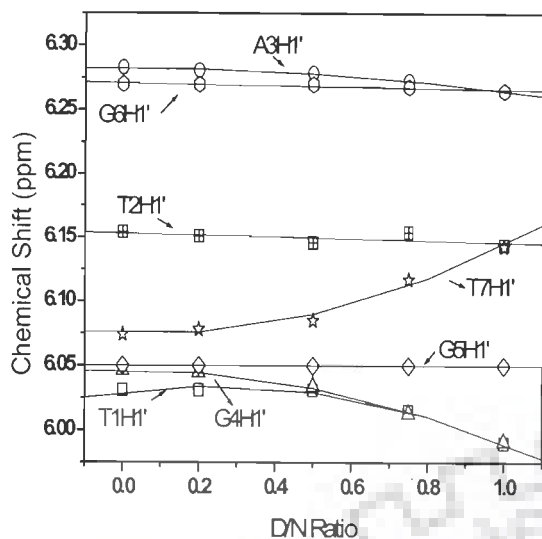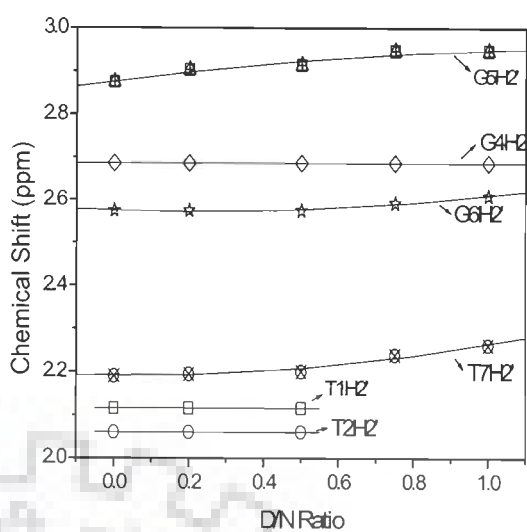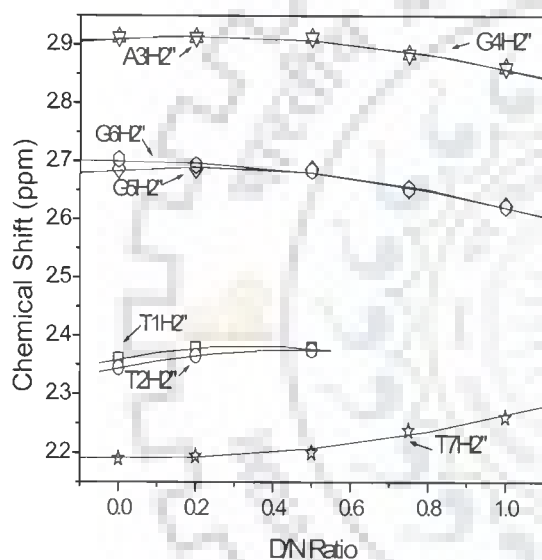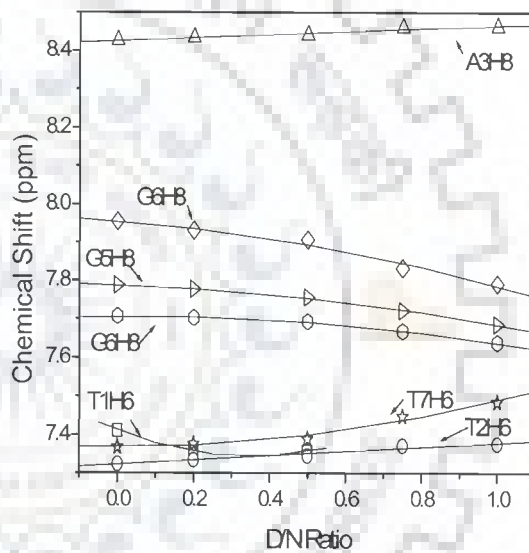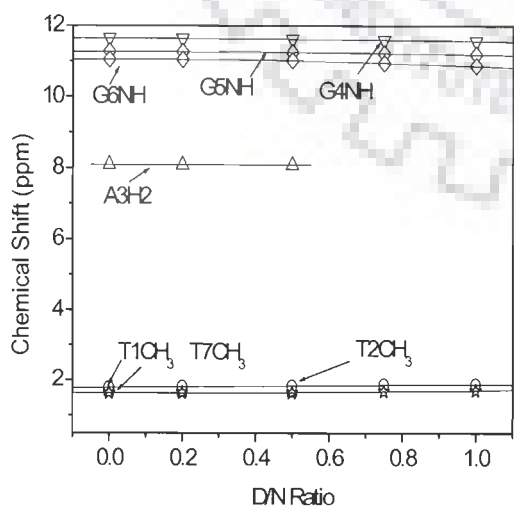
Fig. 7.7 (a-e): Change in chemical shift of d-(TTAGGGT)₄ protons complexed with quercetin as a function of drug to DNA (D/N) ratio, 298 K

294

Table 7.5: Chemical shift (ppm), δ^b, of quercetin protons bound to nucleic acid quadruplex at drug (D) to nucleic acid (N) as a function of D/N ratio, at 298 K. Change in chemical shift, due to binding, that is, $\Delta\delta = \delta^b - \delta^f$ with respect to free drug is also shown.

Protons	$\delta^f_{(D/N=0)}$	$\delta^b_{(D/N=0.2)}$	$\delta^b_{(D/N=0.5)}$	$\delta^b_{(D/N=0.75)}$	$\delta^b_{(D/N=1.0)}$	$\Delta\delta = \delta^b_{(D/N=1)} - \delta^f$
H6	6.251	5.331	5.331	5.352	5.357	-0.894
H8	6.480	5.730	5.744	5.749	5.749	-0.731
H2'	7.652	6.899	6.903	6.907	6.908	-0.744
H6'	7.708	7.032	7.030	7.033	7.027	-0.681

-ve $\Delta\delta$ indicates upfield shift on binding

+ve $\Delta\delta$ indicates downfield shift on binding
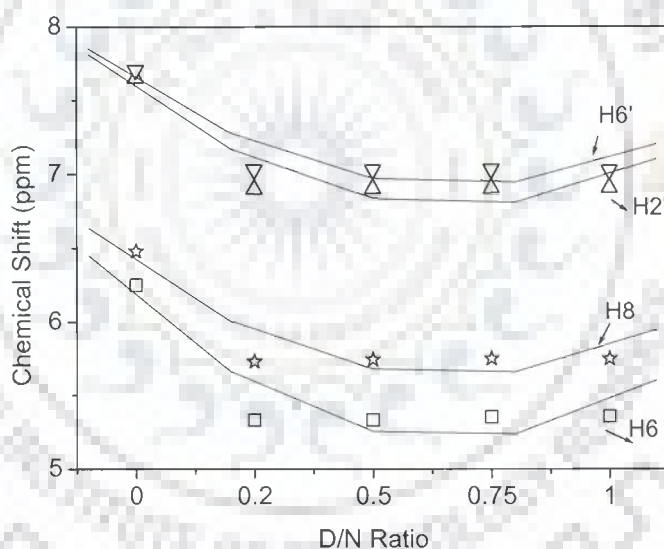
Fig. 7.8: Change in ^{1}H chemical shift of quercetin protons complexed with d-(TTAGGGT)$_4$ at various D/N ratio, 298 K.

Table 7.6: Chemical shift (ppm) of nucleic acid, d-(TTAGGGT)$_4$, protons in uncomplexed state (δ_f) and that bound to drug (δ_b) at drug (D) to nucleic acid duplex (N) ratio D/N=1.0 at 298 K. Also shown here is the change in chemical shift on binding,

$$\Delta\delta = \delta_{b(D/N=1.0)} - \delta_f$$

Proton	T1			T2			A3			G4			G5			G6			T7		
	δ_b	δ_f	$\Delta\delta$	δ_b	δ_f	$\Delta\delta$	δ_b	δ_f	$\Delta\delta$	δ_b	δ_f	$\Delta\delta$	δ_b	δ_f	$\Delta\delta$	δ_b	δ_f	$\Delta\delta$	δ_b	δ_f	$\Delta\delta$
H8/H6	b	7.41	-	7.37	7.32	0.05	8.46	8.42	0.04	7.79	7.95	-0.16	7.68	7.78	-0.10	7.63	7.71	-0.08	7.48	7.37	0.11
H1'	5.99	6.03	-0.04	6.14	6.15	-0.01	6.26	6.28	-0.02	5.99	6.04	-0.05	6.05	6.05	0	6.27	6.27	0	6.14	6.07	0.07
H2'	b	2.11	-	b	2.06	-	2.94	2.87	0.07	2.69	2.69	0	2.98	2.87	0.11	2.61	2.57	0.04	2.26	2.19	0.07
H2"	b	2.35	-	b	2.34	-	2.86	2.91	-0.05	2.86	2.91	-0.05	2.62	2.69	-0.07	2.62	2.70	-0.08	2.26	2.19	0.07
H3'	b	4.66	-	b	4.72	-	5.02	5.09	-0.07	5.14	5.04	0.10	5.14	5.04	0.10	4.88	4.91	-0.03	4.48	4.51	-0.03
H4'	4.04	4.01	0.03	4.12	4.06	0.06	4.49	4.44	0.05	4.48	4.51	-0.03	4.48	4.51	-0.03	4.48	4.50	-0.02	4.27	4.24	0.03
H5'	3.71	3.65	0.06	3.94	3.94	0	4.21	4.15	0.06	4.26	4.27	-0.01	4.30	4.32	-0.02	4.26	4.27	-0.01	4.12	4.06	0.06
H5"	3.71	3.65	0.06	3.94	3.94	0	4.12	4.06	0.06	4.26	4.27	-0.01	4.30	4.32	-0.02	4.26	4.27	-0.01	4.12	4.06	0.06
H5/H2/CH	b	1.68	-	1.87	1.78	0.10	b	8.09	-										1.70	1.63	0.07
NH										11.5	11.6	0.10	11.2	11.3	0.10	10.9	11.0	0.10			

-ve $\Delta\delta$ indicates upfield shift
+ve $\Delta\delta$ indicates downfield shift

significant change in chemical shift with temperature for quercetin protons was observed. These protons were shifted downfield by ~0.2 ppm with increase in temperature clearly indicating destacking of quercetin chromophore from the quercetin-DNA complex (Table 7.8 and Fig. 7.11). In fact the change in chemical shift is not a sufficient indicator of the interaction; instead the observed intermolecular short contacts are a direct proof of the structure of a specific drug–DNA complex.

7.1.2.2 Temperature dependence studies

Binding of quercetin to d-(TTAGGGT)$_4$ gradually became weak with increase in temperature. Therefore, to spot the changes in resonances of drug and DNA protons due to dissociation of bound quercetin from d-(TTAGGGT)$_4$, ^{1}H NMR spectra of the quercetin to d-(TTAGGGT)$_4$ complex at D/N=1.0, was observed for the temperature range of 278 to 328 K (Figure 7.9 a-d and 7.10). The observation of the shifts as a function of temperature further helped to resolve the overlapping resonance peaks.

Quercetin resonances, which were broad and tough to identify in 1D ^{1}H spectrum of complex were identified at higher temperature due to signal sharpening with increased temperature. It can be clearly seen from Figure 7.9b that quercetin resonances H6, H8, H2' and H6' in quercetin-d-(TTAGGGT)$_4$ complex were broad at low temperature, whereas at high temperature destacking takes place and the binding of quercetin with d-(TTAGGGT)$_4$ weaken and thus the resonances become sharp.

Resonances of quercetin protons in quercetin-d-(TTAGGGT)$_4$ complex shift downfield with the increase in temperature (Table 7.5 and Fig. 7.8) which is in contrast to free quercetin where no significant change in chemical shift was observed with enhanced temperature (see chapter 5: Table 5.7).This clearly indicates that these protons

were involved in binding with the G-quadruplex sequence d-(TTAGGGT)$_4$. Chemical shift value for these quercetin protons at different temperatures at D/N 1.0 is tabulated in Table 7.12. Figure 6.13 shows the difference in chemical shift $\Delta\delta = \delta$ (328 K) - δ (278 K) at D/N 1.0. It was found that $\Delta\delta$ values for H6, H8, H2' and H6' at the entire D/N ratio were found to be almost same. It may be credited to the concentration independent tight binding of quercetin to d-(TTAGGGT)$_4$. Consequently, as we found that even on 328 K chemical shift value for these protons of quercetin in the complex was found to keep on shifting downfield then at 328 K. These results clearly indicate that quercetin binds tightly with d-(TTAGGGT)$_4$ at even at higher temperature (328 K). The chemical shift for d-(TTAGGGT)$_4$ protons showed a linear dependence on temperature in the range of 278- 328 K (Fig. 7.9a-d and Fig. 7.10). It was observed that chemical shift of G-quadruplex DNA sequence varied with temperature. All the DNA protons chemical shift values at different temperatures for D/N ratio 1.0 are listed in Table 7.7. At higher temperature, a small subset of signals was apparent that arise from single strands of DNA (< 10%). In –NH region one set of new resonances start appearing downfield to the original one at 308 K and it also persist at higher temperature which can be attributed to free and bound conformation of d-(TTAGGGT)$_4$. Thus, it can be clearly seen from these changes in chemical shift due to titrimetric and temperature dependent studies showed that quercetin binds to d-(TTAGGGT)$_4$.

7.1.2.3 Diffusion Ordered Spectroscopy (DOSY) studies on quercetin-d-(TTAGGGT)$_4$ complex

Complexed and noncomplexed forms in a mixture can be distinguished using Diffusion Ordered Spectroscopy (DOSY) due to differences in their relative diffusion

coefficient values. Diffusion observed for any interacting molecule in complexed state orms is an average of the populations of the diffusion of the molecule in free and complexed forms in equilibrium. A change in the chemical shift does not provide sufficient indication about the strength of interaction between the components which could be due to other effects influencing the chemical shift but DOSY plots can provide a better insight about the strength of such interactions which are clearly manifested in the diffusion dimension. The NMR diffusion measurements for quercetin (5 mM) and quercetin-d-(TTAGGGT)$_4$ complex of D/N ratio 1.0 were done at 298 K according to the following conditions: 16 spectra were acquired using stimulated echo sequence incorporating bipolar gradients. The gradient strengths were incremented as a square dependence in the range of 1 to 16 G cm^{-1}. The diffusion time (Δ) and the length of diffusion gradient (δ) used were 100ms and 6 ms respectively. The data were processed by fitting the diffusion decays using the SimFit algorithm provided with Bruker processing software- Topspin (version 1.3) and verified by plotting -ln(I/Io) versus $\gamma_H^2\delta^2G_z^2(\Delta-\delta/3)$. The slope of the line provides the Diffusion coefficient according to the equation:

$$I / Io = -exp[D\gamma_H^2\delta^2G_z^2(\Delta-\delta/3]$$

DOSY spectra of quercetin and quercetin-d-(TTAGGGT)$_4$ complex of 1:1 D/N ratio is shown in Fig. 7.12 a,b and 7.13. We found that quercetin alone has a diffusion coefficient (D) ~0.8 x 10^{-10} m^2/s at D/N ratio 1.0, indicating a strong interaction. Accurate measurement of the diffusion was not possible for other protons except for H2'in the complex because of their broadened signals. Since, H2' was found well separated with

299

D/N = 1.0

G4NH^f G5NH^f G6NH^f

G4NH^b G5NH^b G6NH^b

328K

318 K

308 K

298 K

288 K

278 K

12.8   12.6   12.4   12.2   12.0   11.8   11.6   11.4   11.2   11.0   10.8   10.6   10.4   10.2   ppm
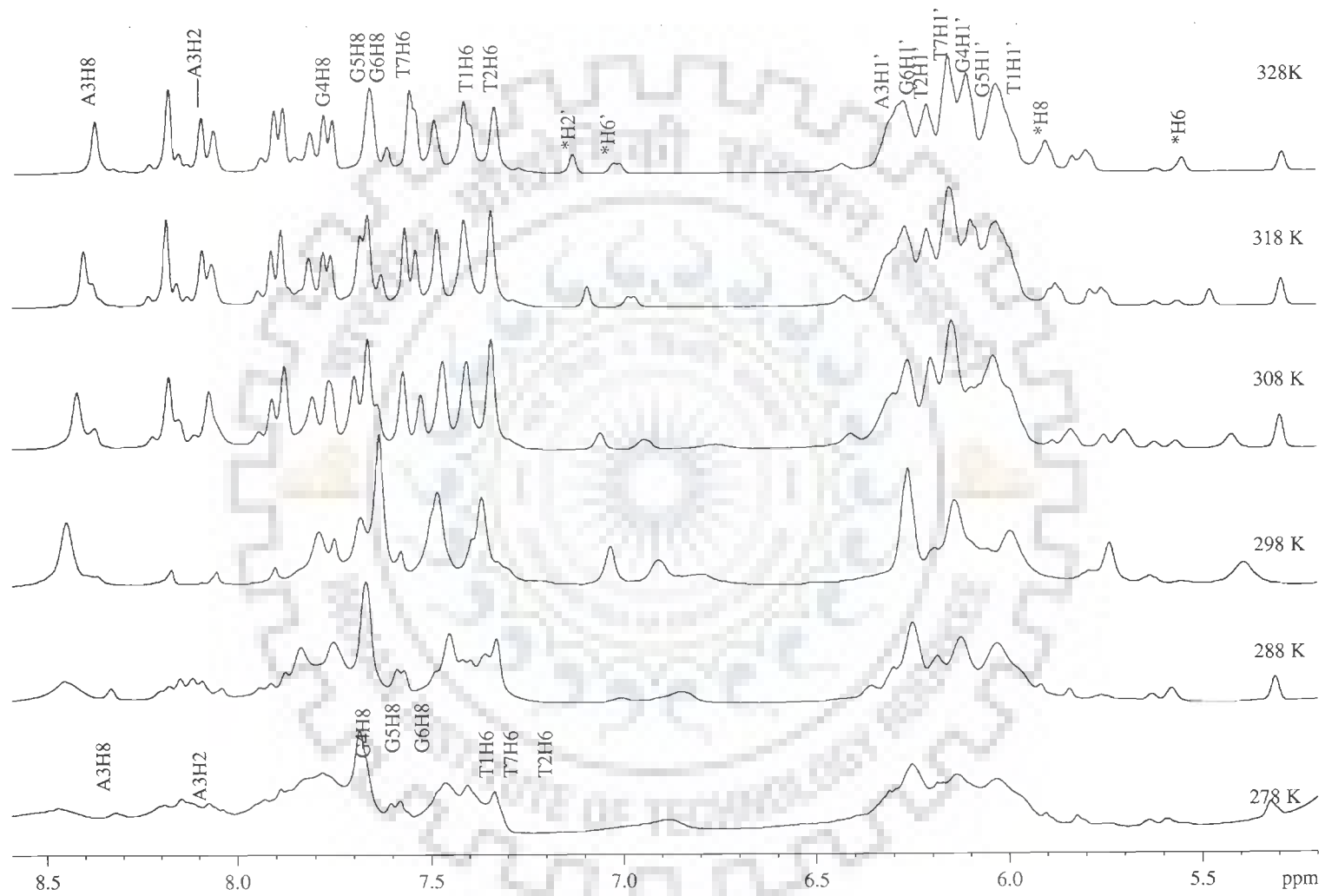
Fig. 7.9 (a-d)
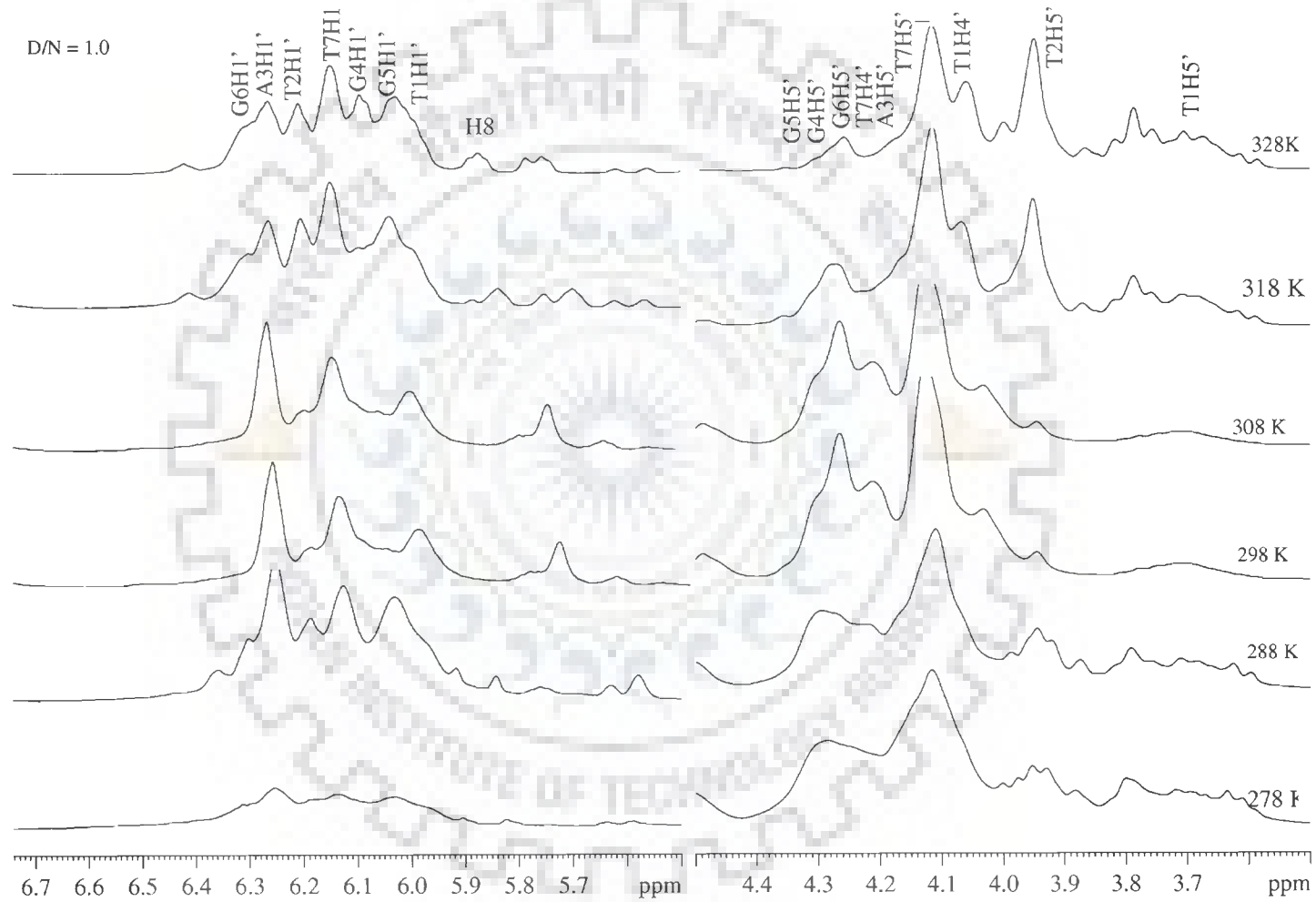
300
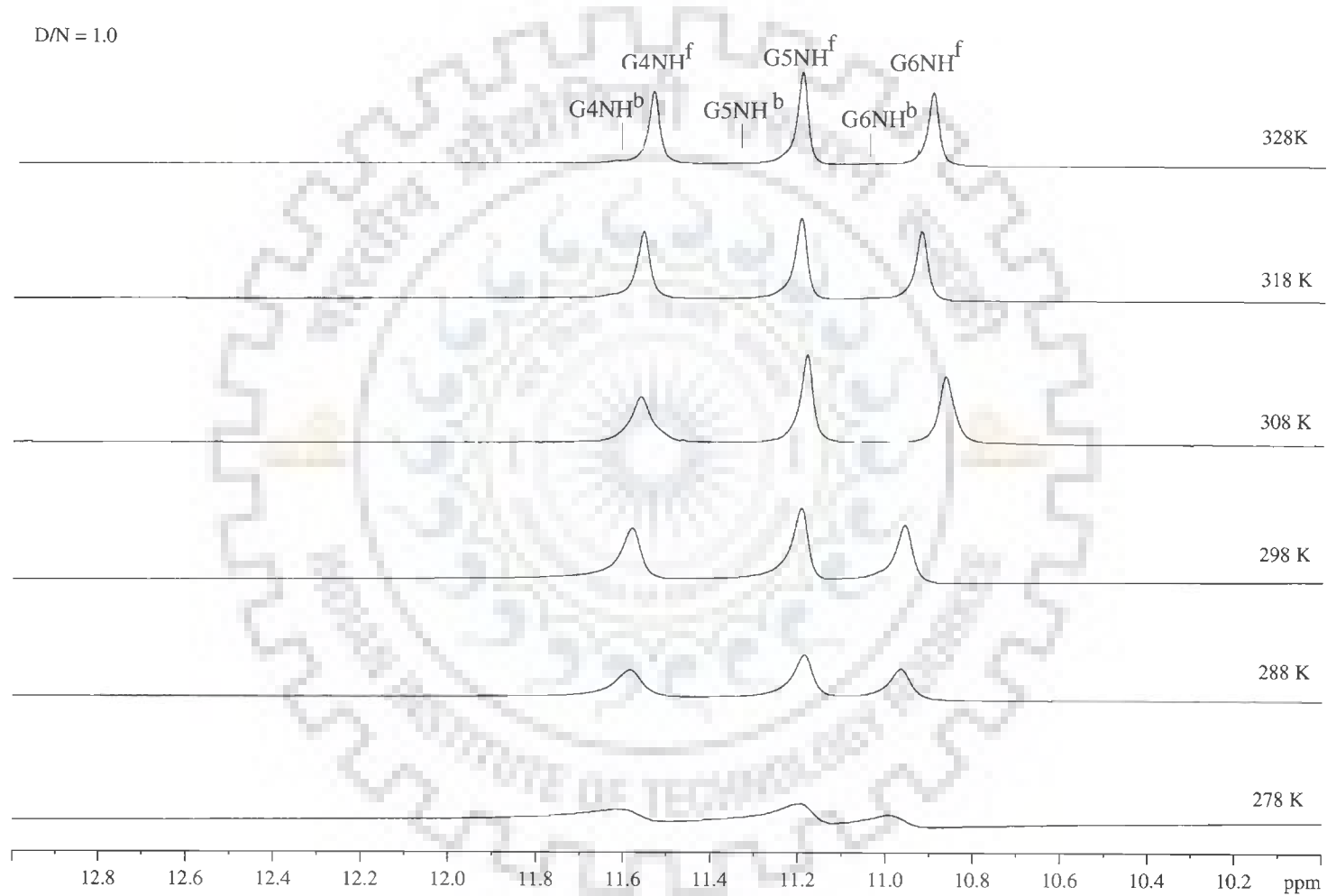
Fig. 7.9 (b)

Fig. 7.9 (c)

Fig. 7.9 (d)

Table 7.7 : Chemical shift (ppm) of DNA d-(TTAGGGT)$_4$ as a function of temperature at drug (D) to nucleic acid duplex (N) ratio, D / N= 1

Temperature	T1H1'	T2H1'	A3H1'	G4H1'	G5H1'	G6H1'	T7H1'
278	6.034	6.187	6.255	6.034	6.034	6.255	6.136
288	6.034	6.190	6.255	6.034	6.034	6.255	6.136
298	6.034	6.20	6.263	6.034	6.034	6.263	6.142
308	6.034	6.205	6.263	6.034	6.034	6.263	6.148
318	6.034	6.216	6.272	6.034	6.034	6.272	6.156
328	6.034	6.218	6.278	6.034	6.034	6.278	6.161
Δδ	0	0.031	0.023	0	0	0.023	0.025

Temperature	T1H2'	T2H2'	A3H2'	G4H2'	G5H2'	G6H2'	T7H2'
278	2.113	2.042	2.874	2.684	2.874	2.569	2.190
288	2.114	2.065	2.911	2.686	2.903	2.570	2.193
298	2.115	2.068	2.914	2.686	2.914	2.574	2.197
308	2.117	2.089	2.928	2.688	2.947	2.580	2.221
318	2.117	2.092	2.947	2.690	2.947	2.608	2.341
328	2.118	2.110	2.978	2.693	2.948	2.718	2.370
Δδ	0.005	0.068	0.104	0.009	0.074	0.149	0180

Temperature	T1H2"	T2H2"	A3H2"	G4H2"	G5H2"	G6H2"	T7H2"
278	2.369	2.344	2.914	2.918	2.689	2.703	2.190
288	2.378	2.365	2.916	2.916	2.689	2.691	2.194
298	2.401	2.375	2.918	2.914	2.689	2.672	2.200
308	2.435	2.404	2.920	2.913	2.664	2.653	2.238
318	2.468	2.426	2.920	2.861	2.661	2.642	2.261
328	2.491	2.431	2.941	2.841	2.659	2.640	2.190
Δδ	0.122	0.087	0.027	-0.077	-0.03	-0.063	0

Temperature	T1H6	T2H6	A3H8	G4H8	G5H8	G6H8	T7H6
278	7.335	7.409	8.477	7.889	7.781	7.690	7.406
288	7.335	7.409	8.453	7.839	7.754	7.673	7.453
298	7.342	7.409	8.453	7.795	7.690	7.669	7.487
308	7.342	7.409	8.426	7.768	7.683	7.666	7.487
318	7.342	7.409	8.406	7.61	7.680	7.666	7.501
328	7.342	7.409	8.389	7.760	7.678	7.666	7.501
Δδ	0.007	0	-0.088	-0.129	-0.103	-0.024	0.095

Temperature	T1 CH$_3$	T2 CH$_3$	A3H2	G4NH	G5NH	G6NH	T7 CH$_3$
278	1.709	1.822	8.143	11.608	11.192	10.991	1.669
288	1.709	1.822	8.122	11.568	11.189	10.966	1.669
298	1.710	1.832	8.119	11.565	11.186	10.961	1.697
308	1.748	1.861	8.116	11.559	11.182	10.924	1.709
318	1.748	1.863	8.095	11.543	11.182	10.901	1.709
328	1.748	1.864	8.085	11.527	11.181	10.877	1.709
Δδ	0.039	0.042	-0.058	-0.081	-0.011	-0.114	0.040

-ve Δδ indicates upfield shift

+ve Δδ indicates downfield shift.
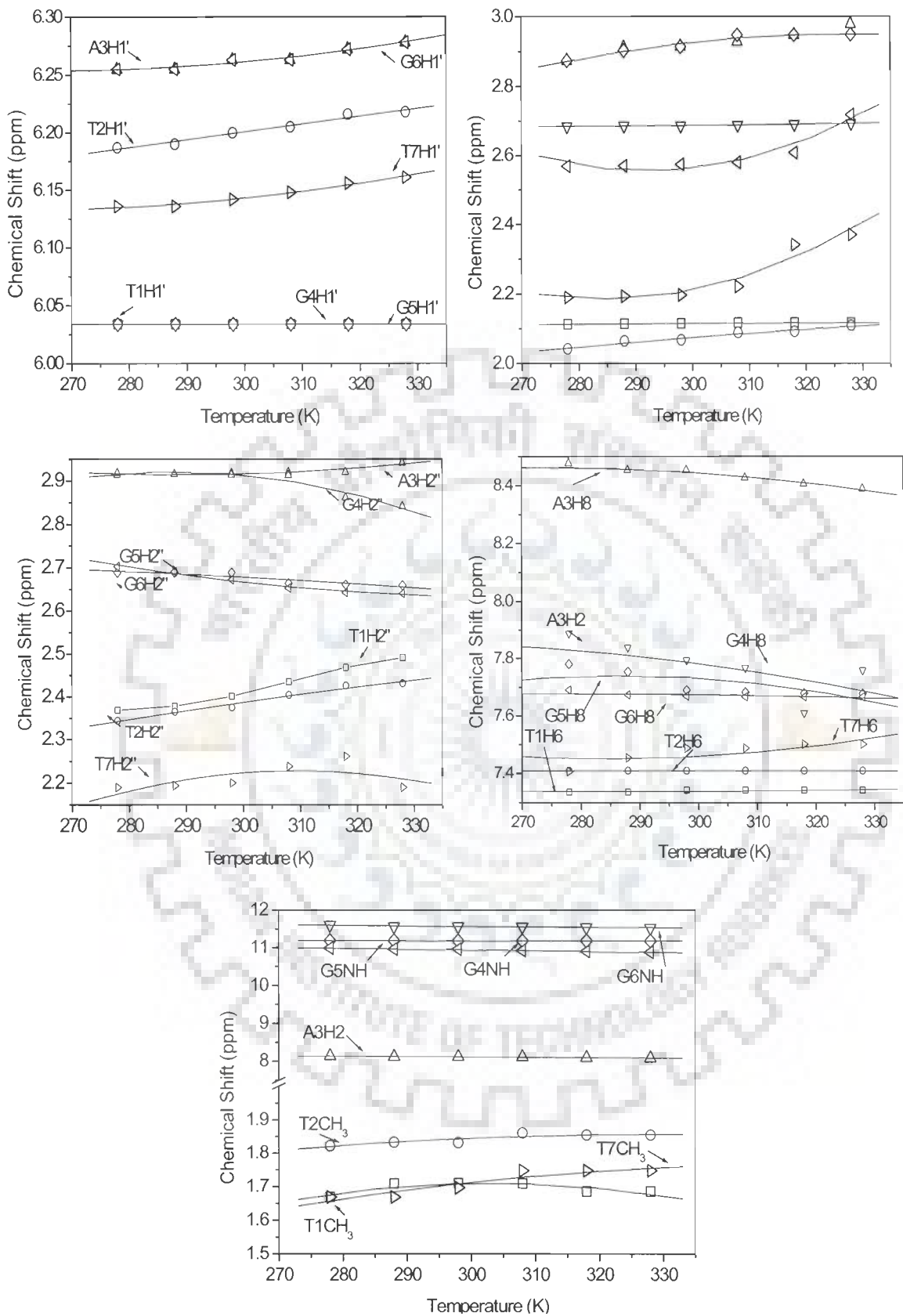
Fig. 7.10: Change in chemical shift of d-(TTAGGGT)$_4$ protons complexed with quercetin as a function of drug to DNA (D/N) ratio, 298 K

Table 7.8: Chemical shift (ppm) of some of the quercetin protons as a function of temperature. Also shown here is the net change in chemical shift with temperature, that is, $\Delta\delta = \delta$ (328 K) - δ (278 K).

Temperature	H6	H8	H2'	H6'
278	5.303	5.634	6.891	6.875
288	5.313	5.634	7.015	6.899
298	5.390	5.742	7.063	6.907
308	5.424	5.839	7.063	6.951
318	5.480	5.880	7.099	6.983
328	5.552	5.906	7.139	7.027
$\Delta\delta$	0.249	0.272	0.248	0.152

-ve $\Delta\delta$ indicates upfield shift
+ve $\Delta\delta$ indicates downfield shift.
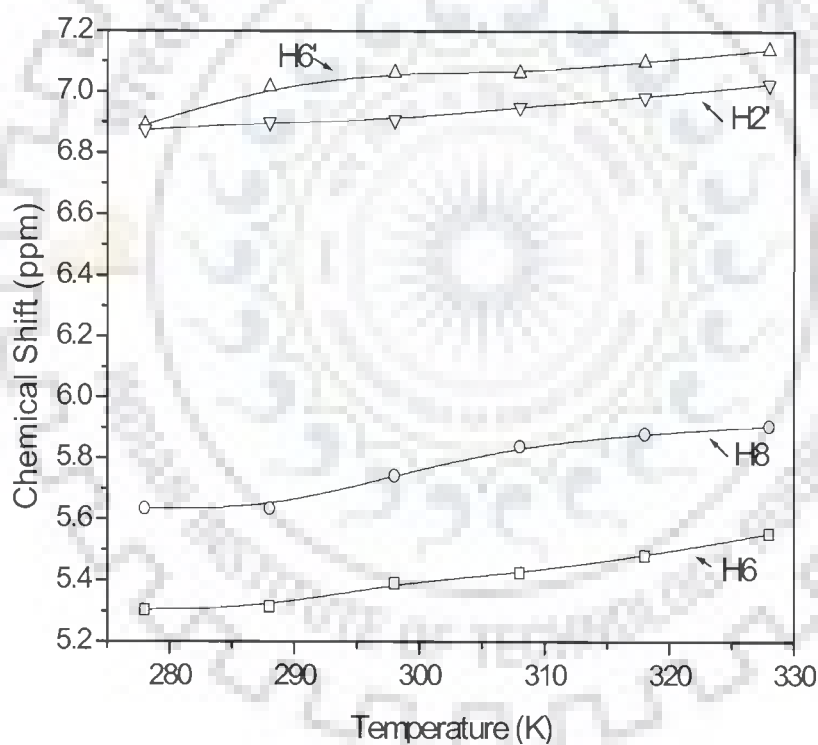
Fig. 7.11: Change in ^{1}H chemical shift of quercetin protons complexed with d-(TTAGGGT)$_4$ at various D/N ratio, 298 K.
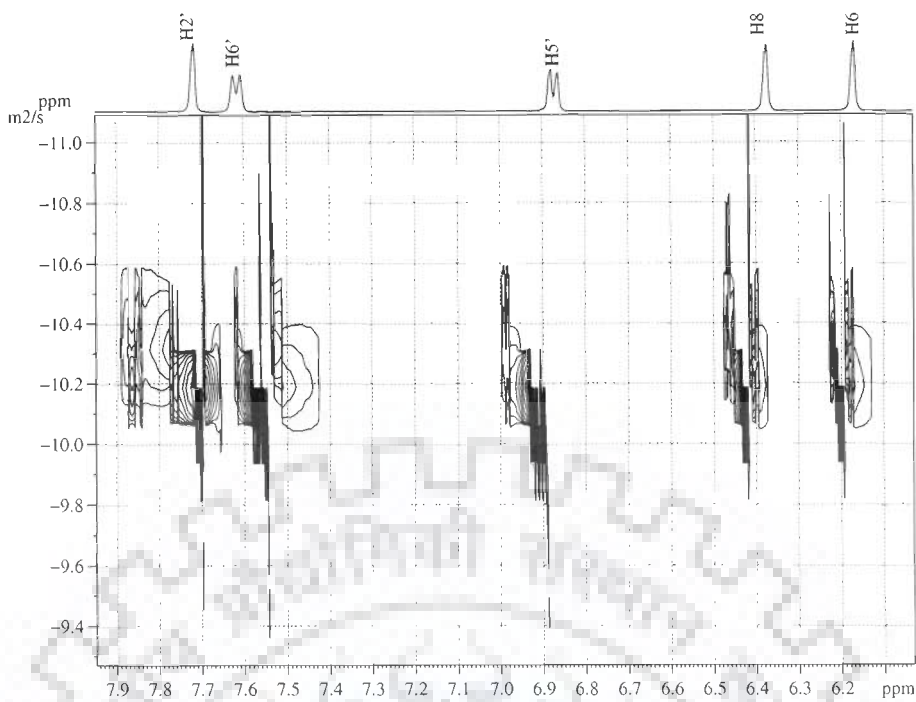
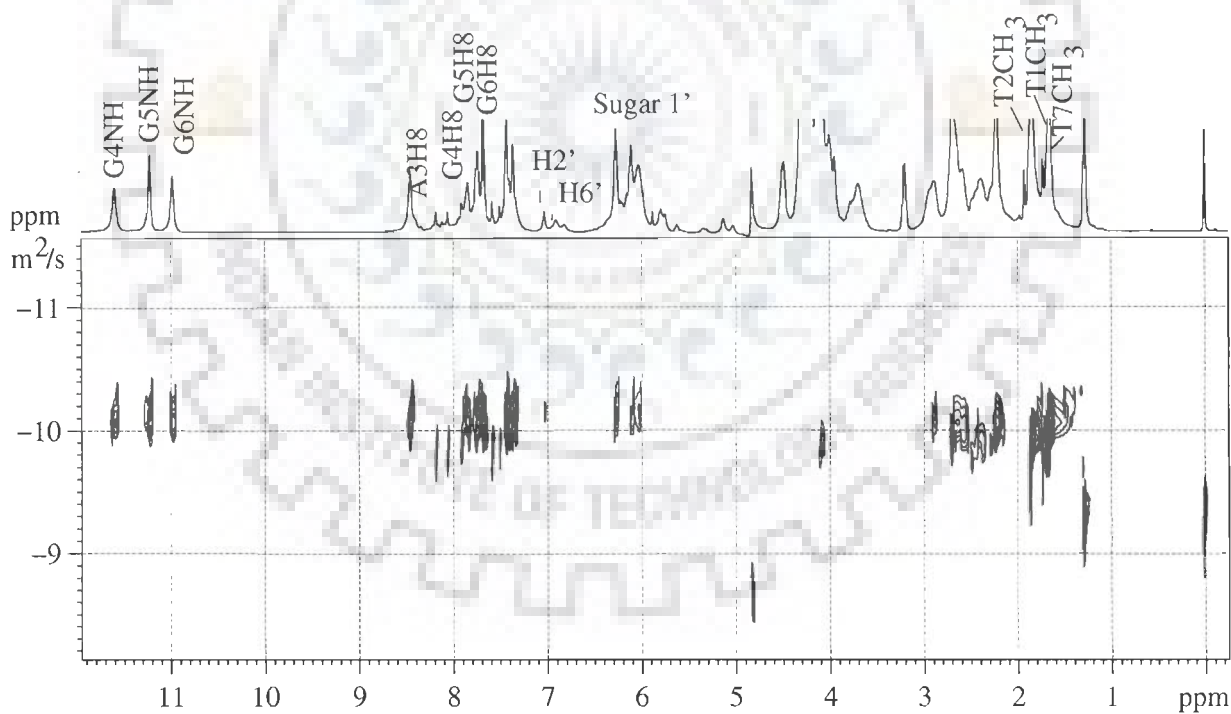**Fig. 7.12: DOSY of (a) quercetin and (b) quercetin- d-(TTAGGGT)₄ complex at 298 K.**
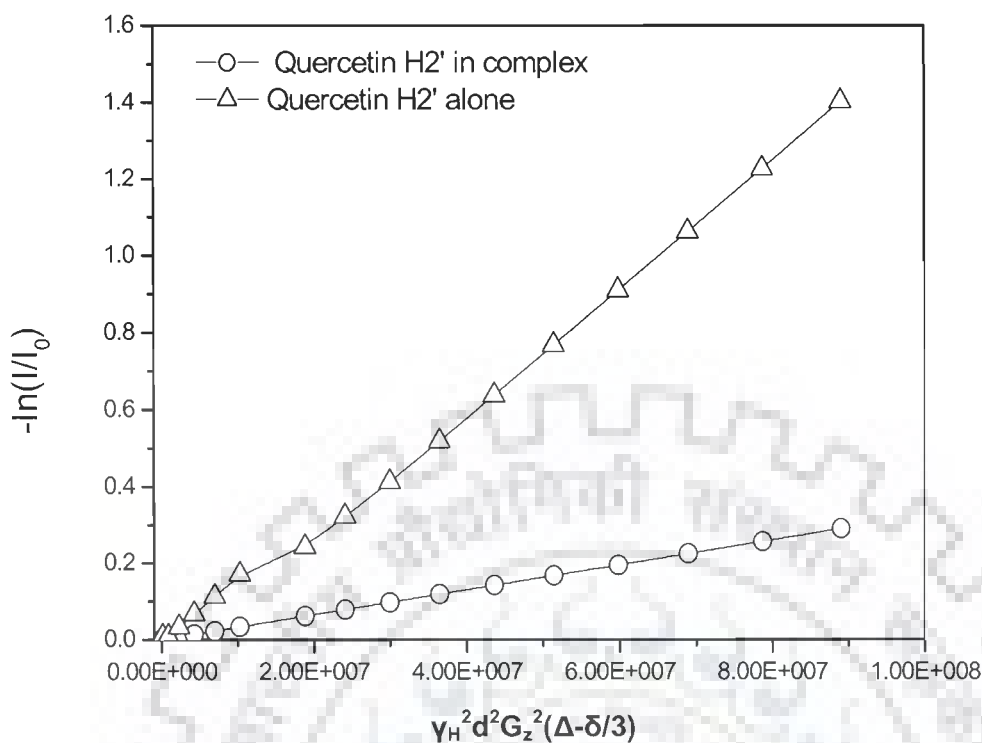
Fig. 7.13: NMR diffusion measurements at 298 K for quercetin proton H2' (Δ) without d-(TTAGGGT)$_4$ and in complex with d-(TTAGGGT)$_4$ (O). The diffusion coefficient is the slope of the plot -ln(I/Io) versus $\gamma_H^2\delta^2G_z^2(\Delta-\delta/3)$ in D$_2$O

good intensity from other proton resonances and thus values for all the 16 gradients used were calculated, of ~ 1.1 x 10^{-10} m^2/s. However, in the presence of d- d-(TTAGGGT)$_4$, quercetin diffused with diffusion plot for H2' in free quercetin as well as in complex with d-(TTAGGGT)$_4$ was made. The result clearly shows that on complex formation, the value of diffusion coefficient of the quercetin resonances decreased in the complex compared to that in the quercetin alone (Fig. 7.13). This is because of the interaction of the quercetin with d-(TTAGGGT)$_4$ which slows down the rate of diffusion. However, only one set of peaks was present, which is due to averaging of the diffusion coefficients for complexed and non-complexed resonances of quercetin.

308

7.1.2.4 Structure of the quercetin- d-(TTAGGGT)$_4$ complex

The 2D NOESY spectra of quercetin-d-(TTAGGGT)$_4$ complex at D/N=1.0 was investigated extensively at mixing time (τ_m) of 350, 300, 200, 150 and 100ms at 298 K and 318 K. The intensities of cross peaks were estimated qualitatively as strong intense (ss), strong (s) medium (m) weakly (w) and very weakly (vw) for distances of about 1.8 - 2.5, 2.5 - 3.0, 3.0 - 3.5, 3.5 - 4.0, and 4.0 - 5.0 Å respectively from the spectra recorded at τ_m = 200 ms (Figure 7.17a-g). The observed NOEs for intranucleotide connectivities, sequential connectivities, and connectivities involving imino protons of base pairs are given in Table 7.9and 7.10, respectively.

NOEs between adjacent guanine imino protons in the sequence, G4NH–G5NH and G5NH–G6NH, are evident in Fig. 7.15a,b. In addition, guanine imino protons show NOEs with their own base protons and also to their 5'- flanking base protons in the A3–G4–G5–G6 part of the d(TTAGGGT)$_4$ quadruplex structure (Fig. 7.16a,b). The G6NH at 10.9 ppm exhibits NOEs to the base protons of G6H8 and G5H8, and the 11.2 ppm imino proton of the G5 exhibits NOEs with the base protons of G5H8 and G4H8. These NOEs are evidence of the interstrand interactions between the guanine residues that are involved in G-tetrad formation, as they cannot be accounted for by NOEs within the same strand. Importantly, we also observe NOEs from the base protons A3H8 and A3H2 to the imino proton of G4 at 11.67 ppm, providing evidence for good stacking interactions across the A3pG4 step in uncomplexed d(TTAGGGT)$_4$ quadruplex structure but after quercetin complexation this stacking interaction is slightly perturbed as G4NH-A3H2 NOE disappear and one new NOE contact appears for G5NH-G6H8 which clearly indicates the binding of two quercetin molecules, one near A3 and

another near G6 base of the d(TTAGGGT)$_4$ quadruplex structure (Figure 7.16b). Similarly, another set of –NH resonance start appearing which clearly separated and become sharp at 318 K. When compared with uncomplexed d(TTAGGGT)$_4$ –NH resonance at this temperature, no other set of peak were observed. Thus in quercetin-d(TTAGGGT)$_4$ complex, this may account for the bound and free –NH peak which can also be seen in NOESY spectra (Fig.7.15b). In addition, a total of 31 drug-DNA intermolecular NOEs were identified in the 1:1 complex representing the time averaged interaction of the bound drug at the two sites(Table 7.11). By far the largest number of NOEs involves the base and sugar protons of T1pT2 and G6pT7. In contrast, no NOE to G4 and G5 were identified at the centre of the stack of G-tetrads. The absence of NOEs to G4 and G5 excludes any possibility of quercetin molecules intercalated at the A3-G4 or G4-G5 step. Majority of the NOEs are detected at the T1-T2 and T7 step and involve both pyrimidine nucleotides, indicating that the TpT step is a primary intercalation site. A number of NOEs to T7 show that the drug inserts also at the G6–T7 step. Two strong NOEs from the quercetin H2' to T7H1' and T1/T2 H2', T1/T2 H2'', show that end stacking on the G-quadruplex is energetically very favourable. Majority of NOEs came from quercetin H2', H6', H8 and H6 protons to T1, T2 and T7 of DNA base and sugar protons position the edges of the benzopyran ring of ligand in between the base. Other NOE cross-peaks between quercetin and protons of A3 and G6 are evident in the portion of the NOESY spectrum shown in Fig.7.18. The list of total intermolecular peaks for quercetin- d-(TTAGGGT)$_4$ complex has been mention in Table 7.11. The data strongly support binding to the ends of the G-quadruplex stacking primarily between T1pT2 and G6pT7 (Fig. 7.14). A detailed analysis of the unbound

quadruplex showed clear evidence from guanine imino and adenine base proton NOE data that both guanine and adenine nucleotides form hydrogen-bonded tetrads. NOEs from adenine H2 are consistent with intermolecular A-tetrad formation and stabilising stacking interactions with the adjacent G-tetrad of G4 (Gavanthiotis and Searle, 2003) This is evident from strong NOEs from the G4 imino to A3H2 and H8. MD refinement of d(TTAGGGT)$_4$ shows that the A-tetrad persists over long dynamics simulations.
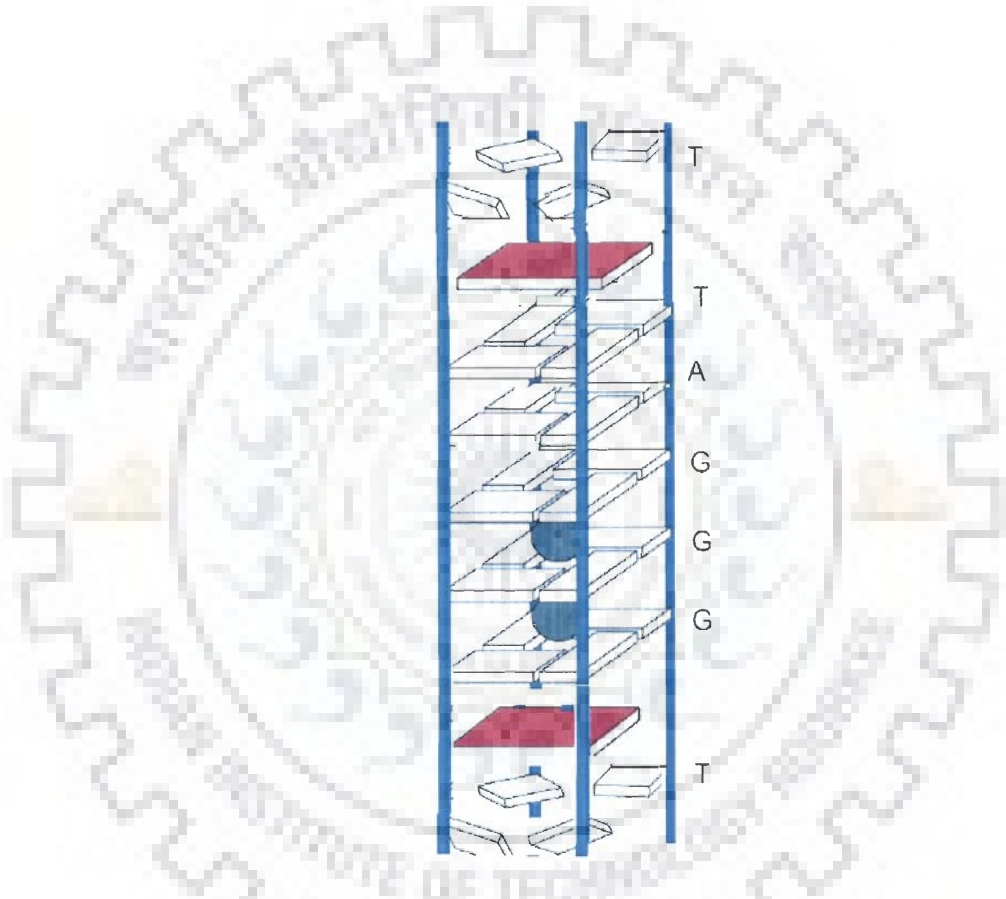
Fig. 7.14 Schematic Representation of quercetin - d-(TTAGGGT)$_4$ complex.

However, because of the significant line-broadening effects of the quercetin on A3H2, analogous NOEs to those described above could not be identified to confirm the integrity of a hydrogen bonded A-tetrad. NOEs between A3 and G4, which were

311
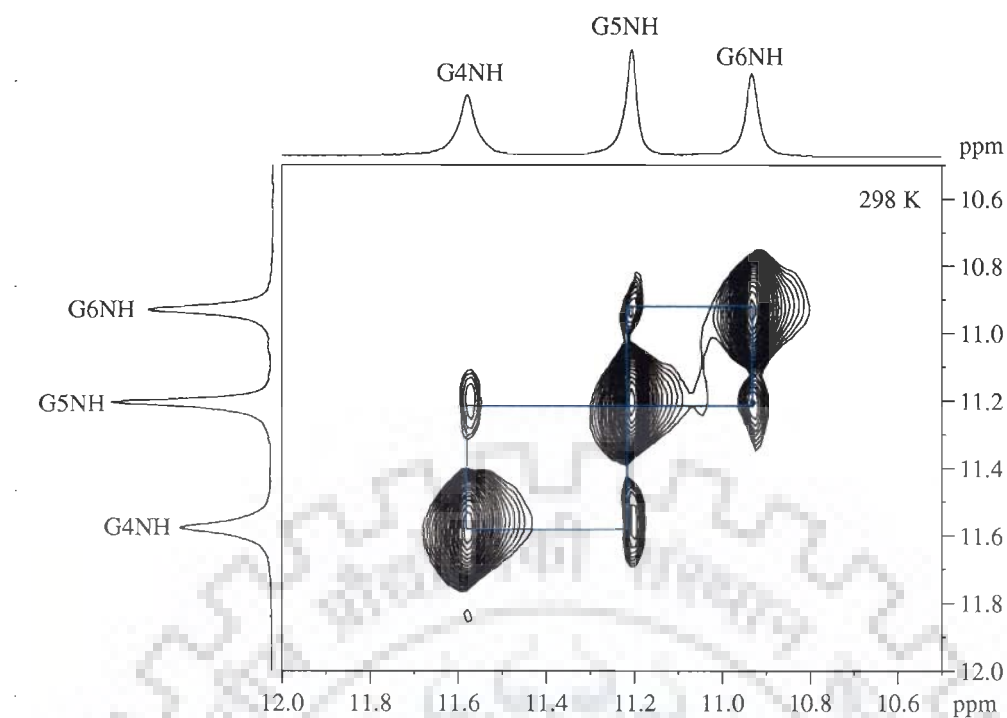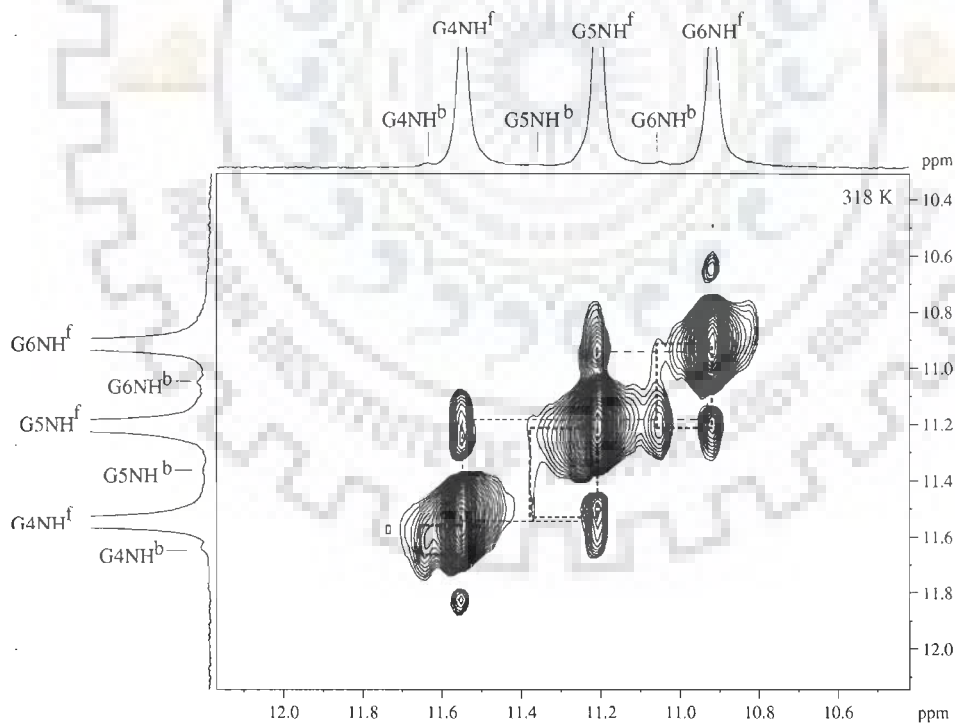
Fig. 7.15: Expansion of the NOESY spectrum of quercetin - d-(TTAGGGT)$_4$ complex showing (a) NH-NH NOEs between adjacent G-tetrads at 298 K. (b) Free and bound –NH signals due to quercetin complexation at 318 K.
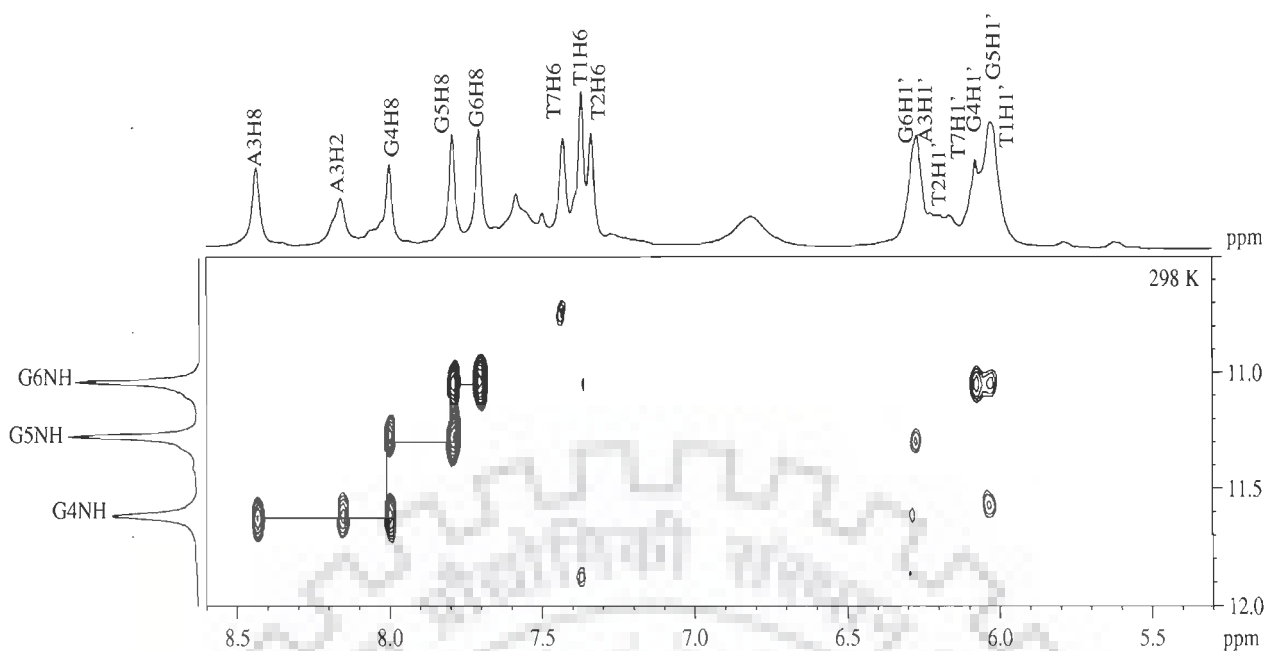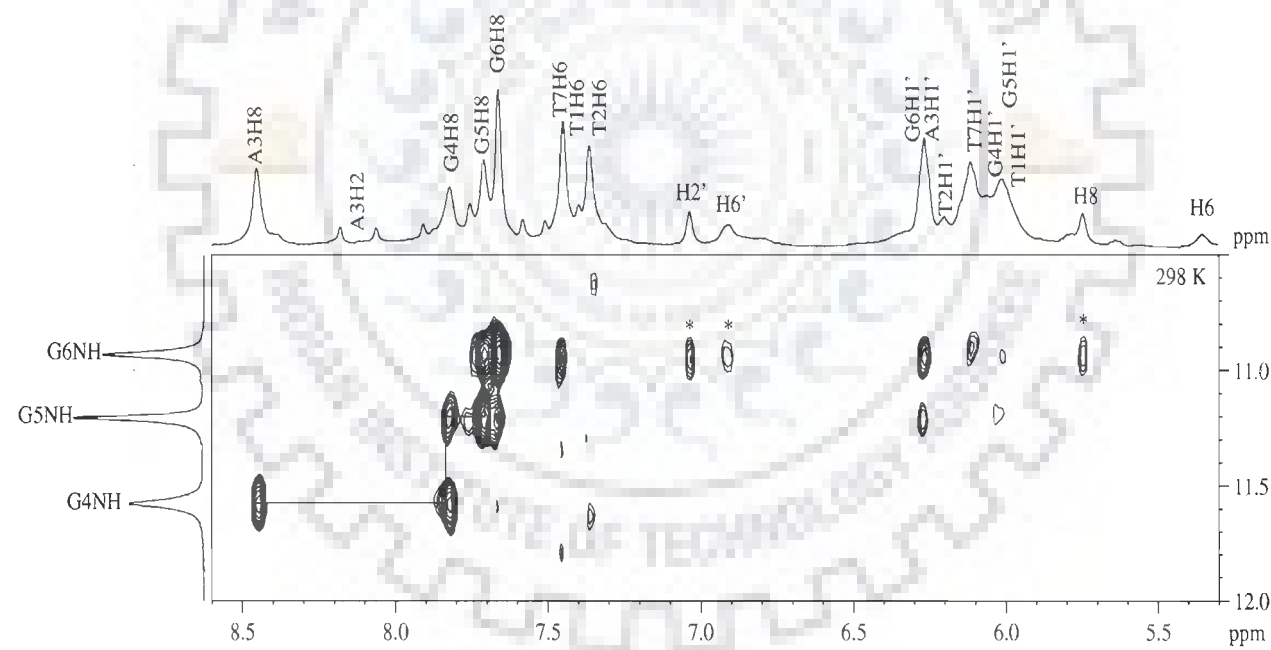
Fig. 7.16: Expansion of NOESY spectrum of (a) uncomplexed d-(TTAGGGT)₄ showing G-N1-H NOEs to own base and 5'-flanking base H6/H8 illustrating base stacking between G and A-tetrads. G4NH-A3H2 NOE shows good stacking interaction (b) quercetin complexed d-(TTAGGGT)₄ showing absence of G4NH-A3H2 NOE and presence of G5NH-G6H8 NOE illustrating perturbations in stacking interaction of G and A-tetrads.
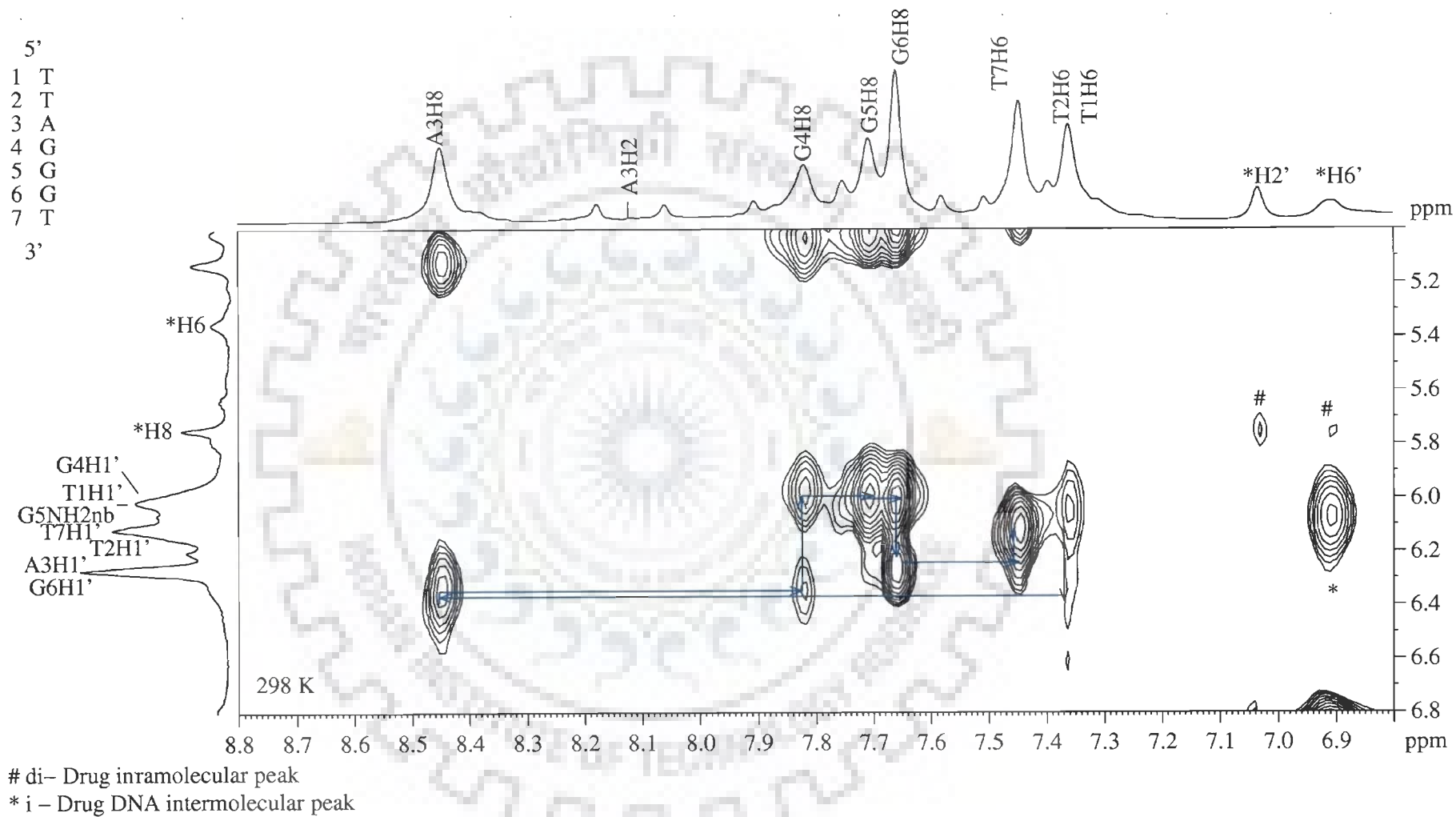
Fig. 7.17(a–g): Expansions of the specific regions of NOESY spectra of quercetin complexed with d–(TTAGGGT)$_4$ to highlight specific connectivities.

di– Drug inramolecular peak

* i – Drug DNA intermolecular peak

Fig. 7.17(b):

Top axis labels (left to right): A3H8, A3H2, G4H8, G5H8, G6H8, T7H6, T1H6, T2H6, H2', H6', ppm

Right axis (ppm): 1.6, 1.8, 2.0, 2.2, 2.4, 2.6, 2.8, 3.0, 3.2

Bottom axis (ppm): 8.8, 8.7, 8.6, 8.5, 8.4, 8.3, 8.2, 8.1, 8.0, 7.9, 7.8, 7.7, 7.6, 7.5, 7.4, 7.3, 7.2, 7.1, 7.0, 6.9, ppm

Left axis labels: T1CH3, T7CH3, T2CH3, T2H2', T1H2', T7H2', T7H2'', T2H2'', T1H2'', G6H2', G4H2'', G5H2'', G6H2'', G5H2', A3H2', A3H2'', G4H2'

298 K

* i –Peak

315
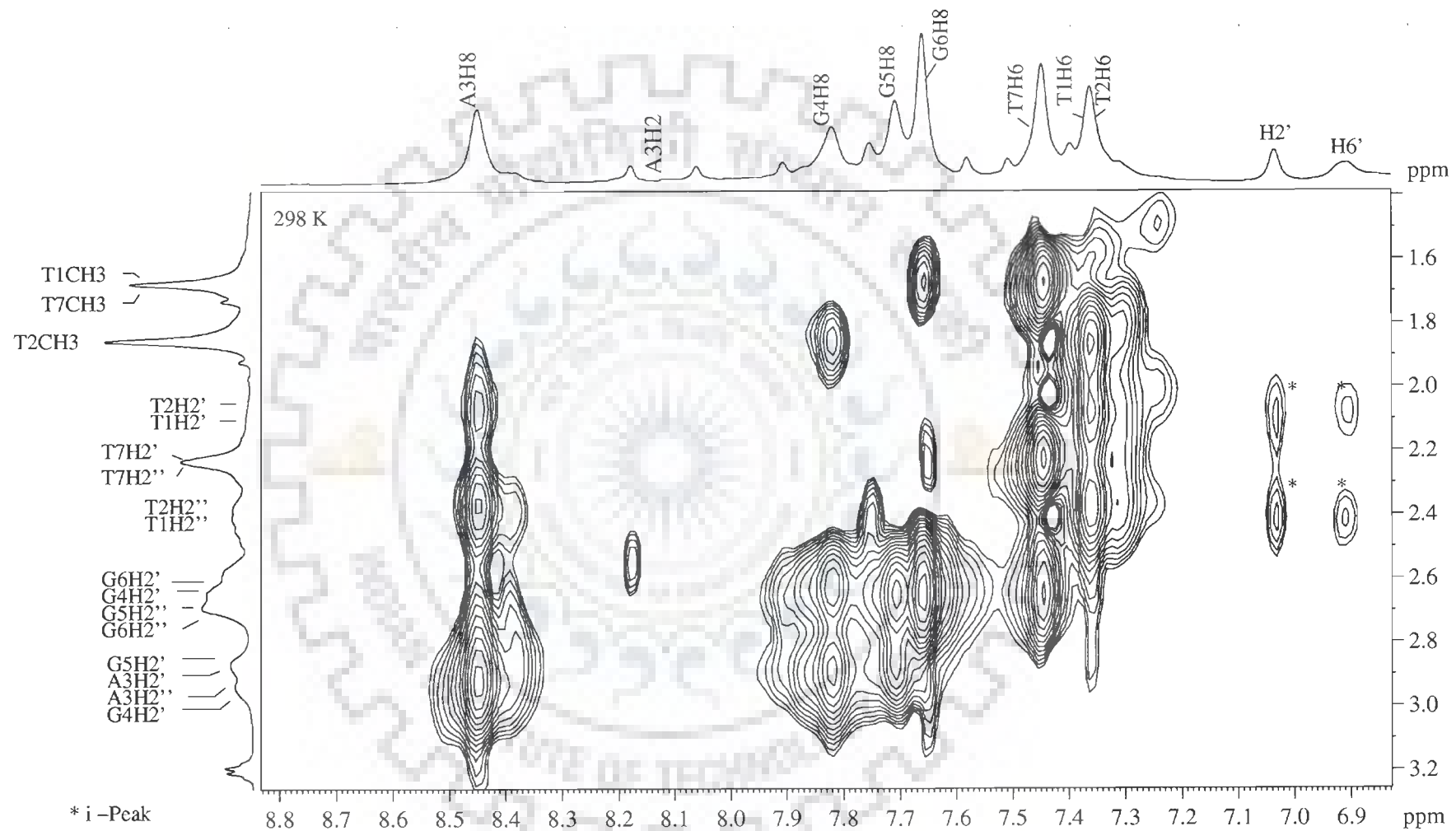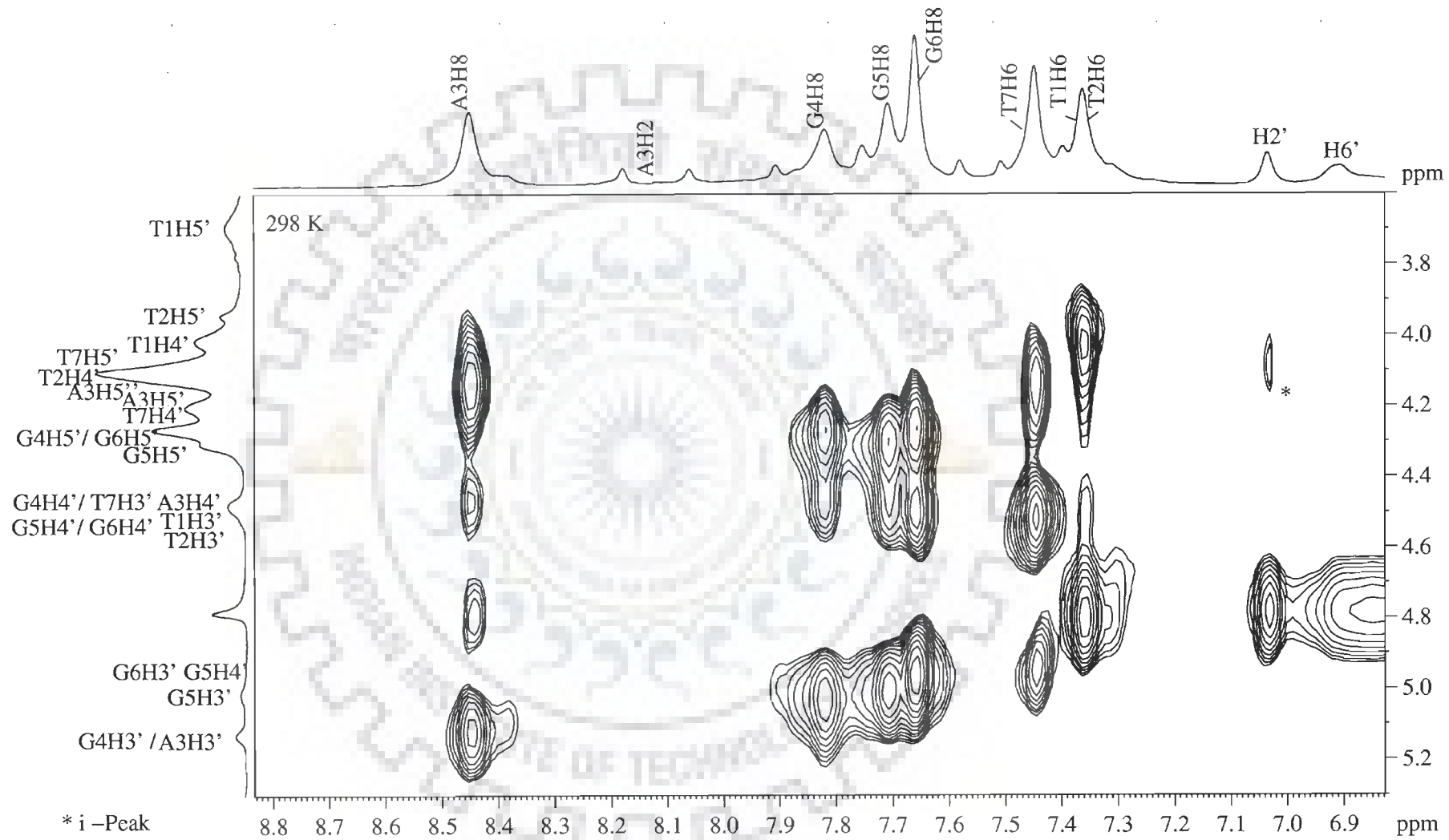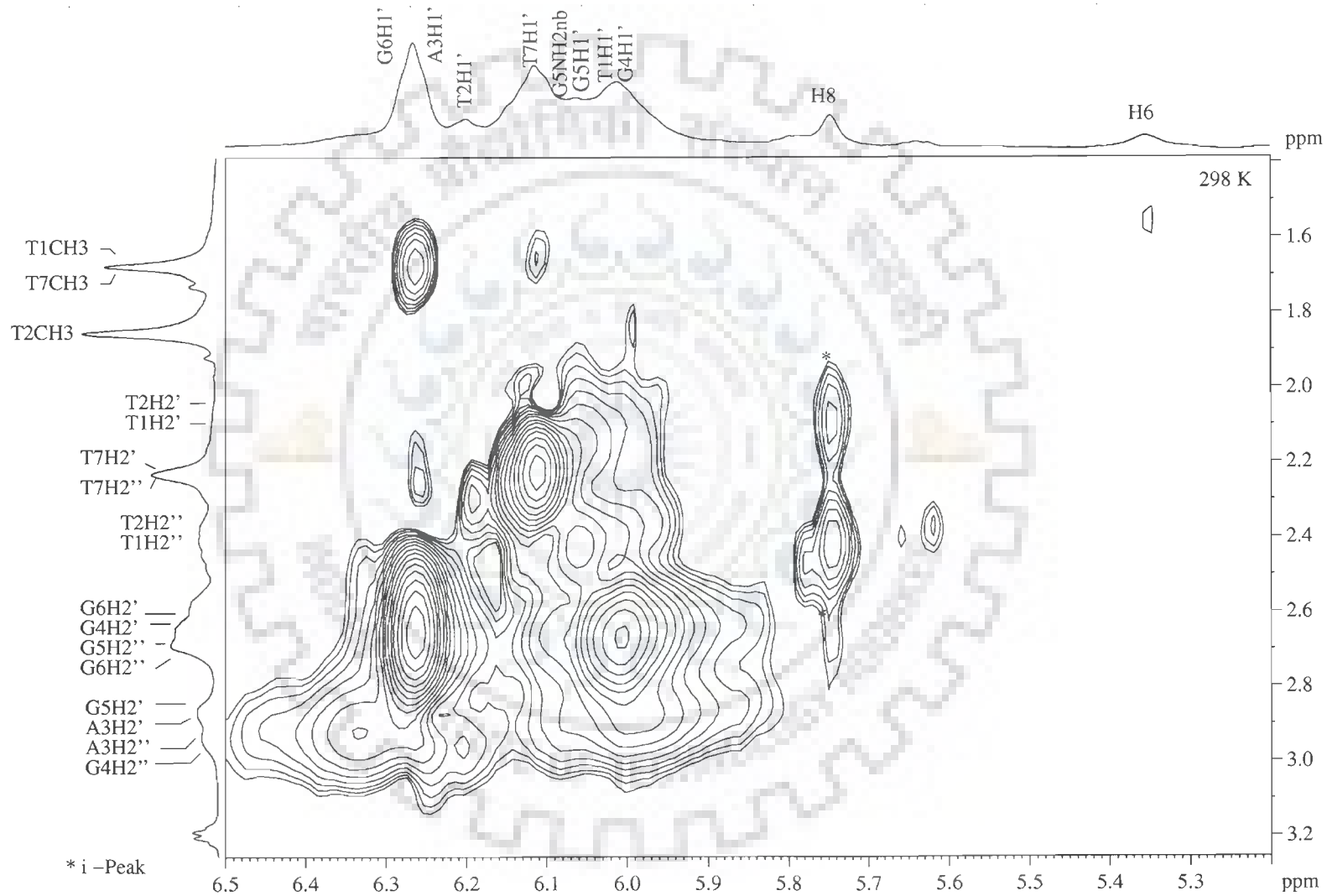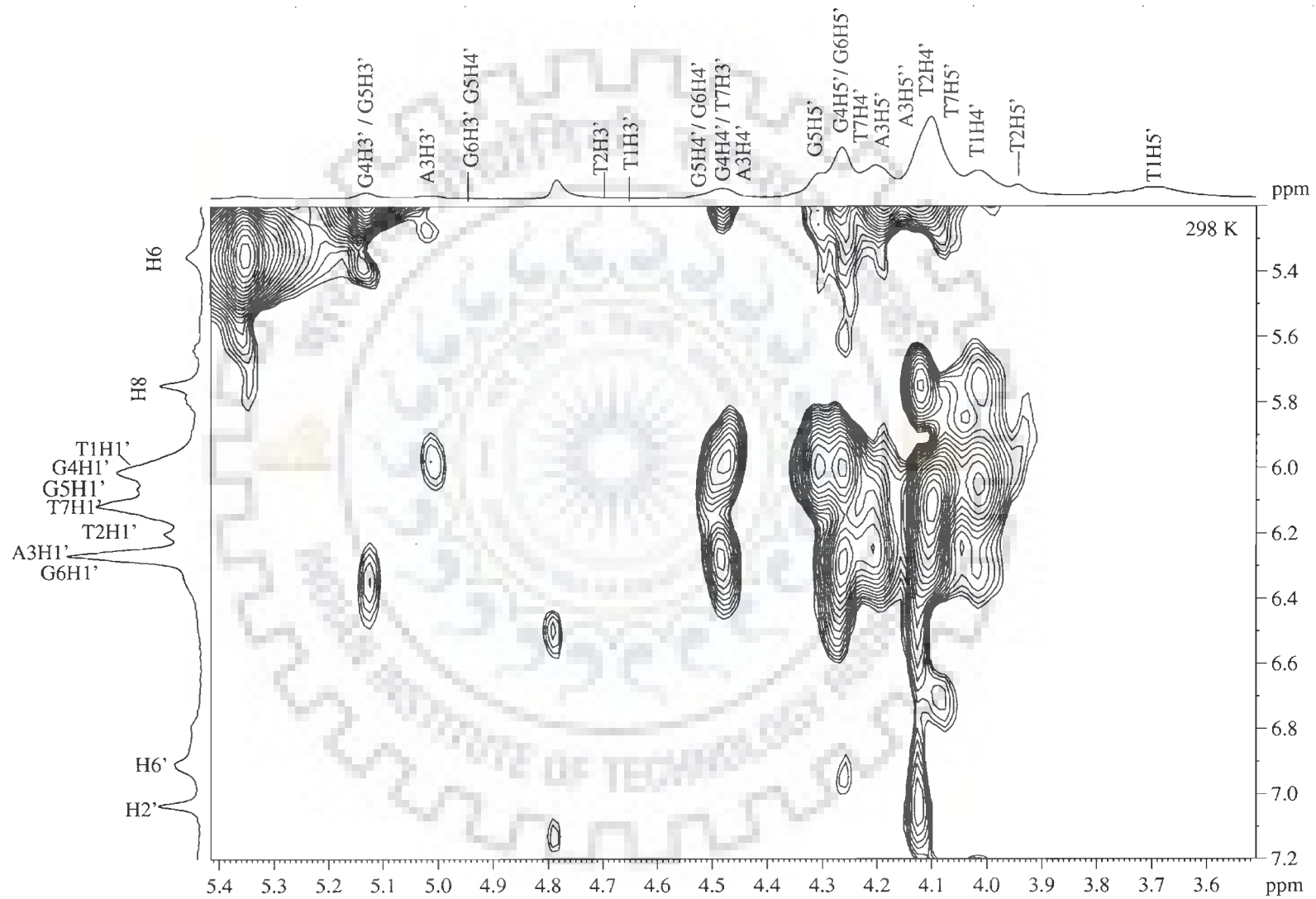
Fig. 7.17(c):

Fig. 7.17(d):

Fig. 7.17(e):
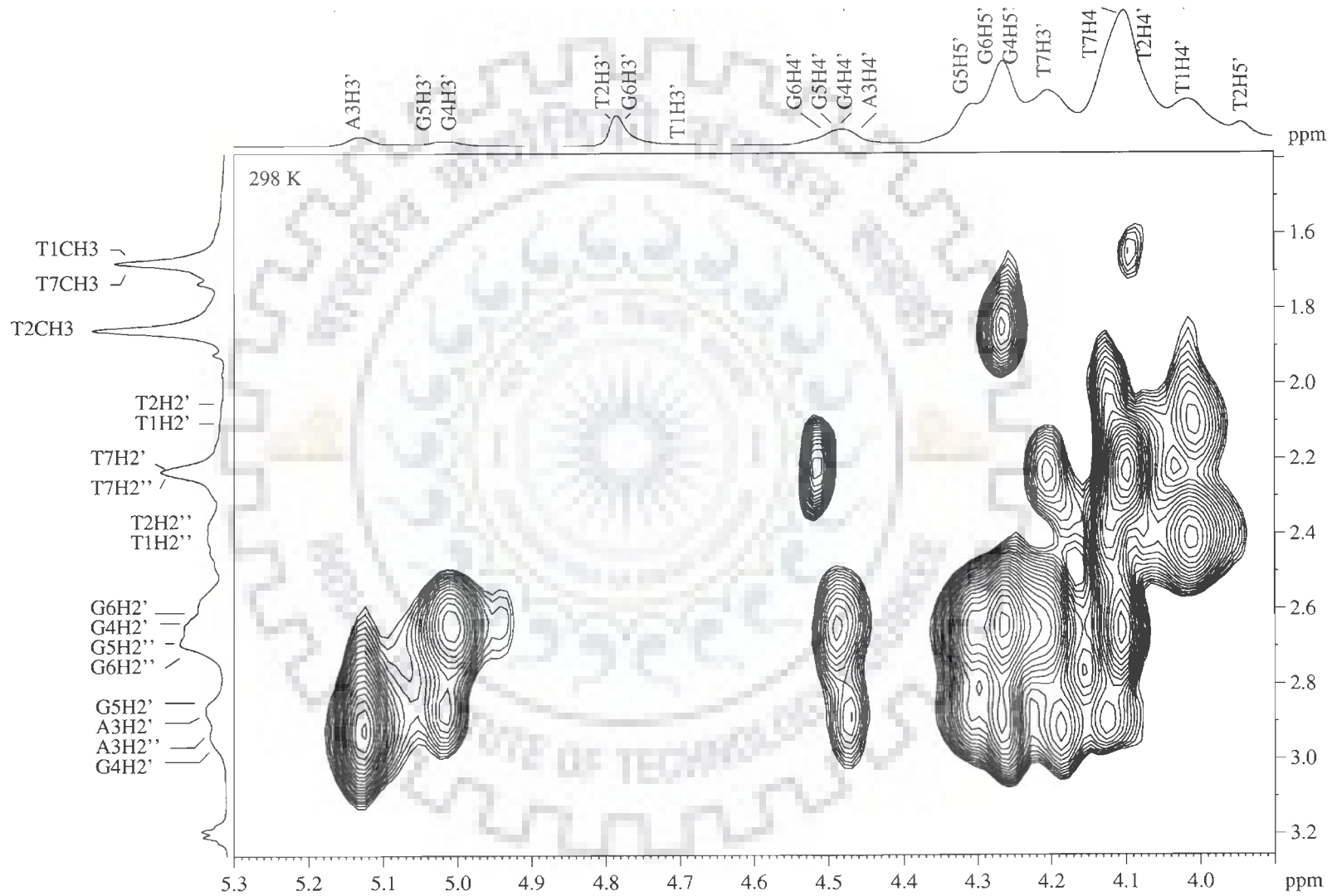
Fig. 7.17(f):
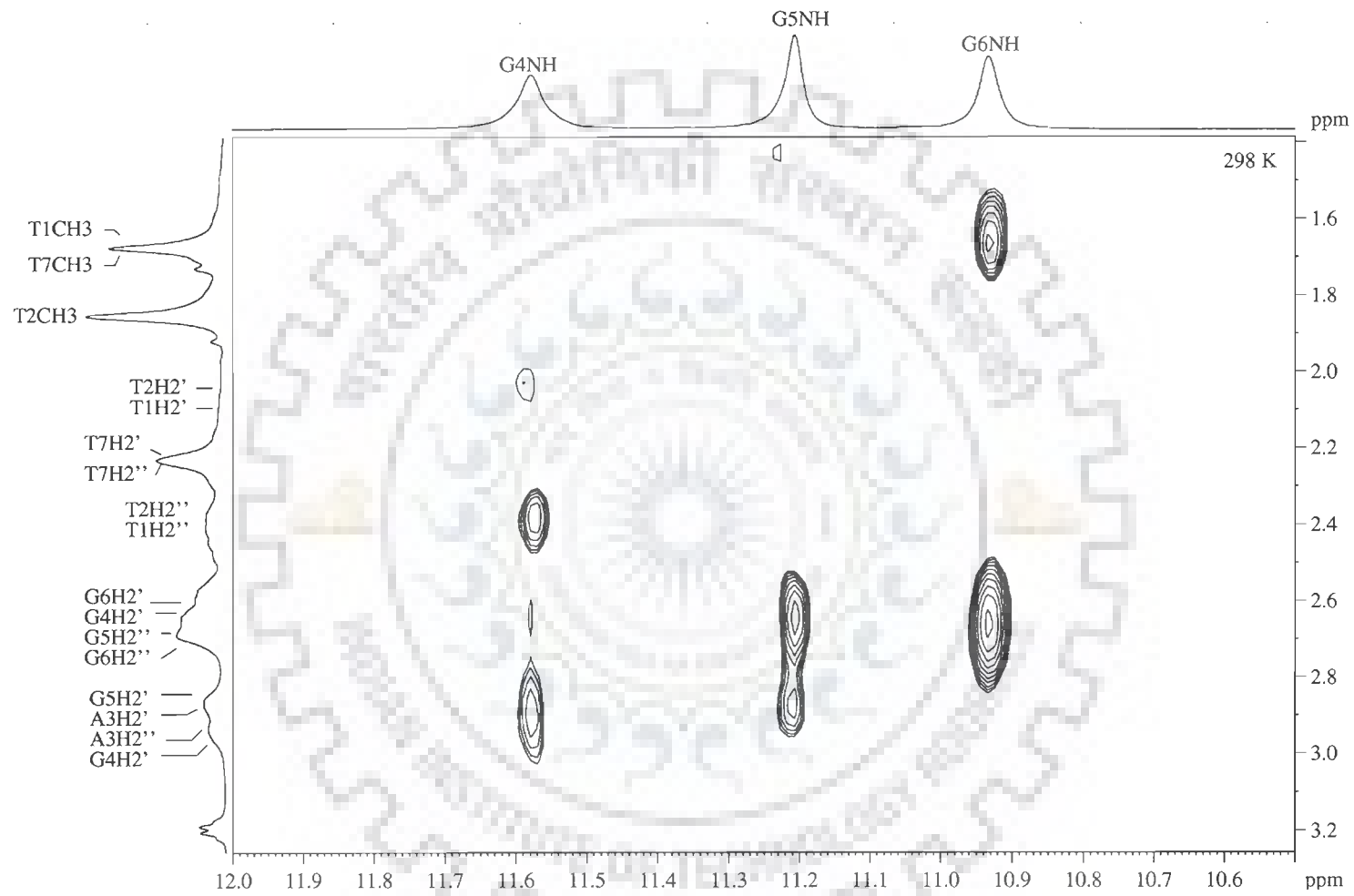
Fig. 7.17(g):

Table 7.9: Interproton distance (Å) obtained from intra nucleotide NOE connectivities (di) of base to sugar protons, sugar-sugar protons, and base to base protons of d-(TTAGGGT)$_4$ in quercetin- d-(TTAGGGT)$_4$ complex estimated from NOESY spectra. The strong intense (ss), strong (s), medium (m), weak (w), very weakly (vw) intense cross peaks correspond to distances in the range ss 1.8 - 2.5 Å, s 2.5 - 3.0 Å, m 3.0 - 3.5 Å, w 3.5 - 4.0 Å, vw 4.0 - 5.0 Å, respectively.

	H8/H6- H1'		H8/H6-H2'		H8/H6-H2"		H8/H6-H3'	
	Intensity	Strand	Intensity	Strand	Intensity	Strand	Intensity	
T1	w (o)	4.9	m (o)	3.4	m	3.4	vw(o)	4.7
T2	vw (o)	4.5	m (o)	3.2	m(o)	3.4	vw(o)	4.5
A3	s	2.0	s	2.4	s(o)	2.6	s	3.4
G4	m	3.2	m	3.4	m	3.9	s	2.8
G5	s	2.6	m	3.6	m(o)	3.2	s	2.9
G6	s	2.7	m	3.4	m(o)	3.5	s(o)	2.9
T7	s	2.5	s (o)	2.6	s(o)	2.6	s	3.2

	H8/H6-H4'		H1'- H2'		H1'- H2"		H1'- H3'	
	Intensity	Strand	Intensity	Strand	Intensity	Strand	Intensity	Strand
T1	s(o)	2.6	w(o)	3.6	m(o)	3.9	m	3.9
T2	s(o)	2.7	-	5.4	-	5.2	m	3.2
A3	s	2.5	m(o)	3.6	m(o)	3.5	-	5.5
G4	s	2.6	m(o)	3.5	m(o)	3.9	m(o)	3.9
G5	s(o)	2.7	s(o)	2.6	m(o)	3.2	m(o)	3.2
G6	s(o)	2.5	s(o)	2.7	s(o)	3.5	s(o)	2.9
T7	s	2.6	s(o)	2.9	s(o)	3.9	s(o)	2.9

	H1'- H4'		2.5		H2"-H4'		CH$_3$-H6	
	Intensity	Strand	Intensity	Strand	Intensity	Strand	Intensity	Strand
T1	w(o)	4.2	s(o)		ss(o)	3.5	w(o)	4.5
T2	-	4.9	-		s(o)	3.9	m	2.9
A3	ss(o)	3.9	m(o)	3.4	m(o)	3.2		
G4	ss(o)	3.2	m(o)	3.6	m(o)	3.5		
G5	ss(o)	3.5	m(o)	3.4	m(o)	3.9	ss	2.1
G6	ss(o)	3.9	m(o)	3.9	s(o)	3.5		
T7	m(o)	3.2	s(o)	2.6				

Table 7.10: NOE connnectivities observed in NOESY spectra for exchangeable protons of the quercetin - d-(TTAGGGT)$_4$ complex at Drug/DNA ratio (D/N) = 1.0 at 298 K. The strong intense (ss), strong (s), medium (m), weak (w), very weakly (ww) intense cross peaks correspond to distances in the range ss 1.8 - 2.5 Å, s 2.5 - 3.0 Å, m 3.0 - 3.5 Å, w 3.5 - 4.0 Å, vw 4.0 - 5.0 Å, respectively.

Cross peak	NOE Intensity	Cross peak	NOE Intensity
G4NH^f – G5NH^f	s	G6NH^f -T7H6	m
G5NH^f – G6NH^f	s	G6NH^f -G6H8	s
G4NH^f – G4NH^b	m	G6NH^f -G5H8	s
G5NH^f – G5NH^b	m	G5NH^f – G6H8	s
G6NH^f – G6NH^b	m	G5NH^f – G5H8	s
G4NH^b – G5NH^b	-	G5NH^f -G4H8	s
G5NH^b – G6NH^b	-	G4NH^f – G4H8	s
		G4NH^f – A3H8	s
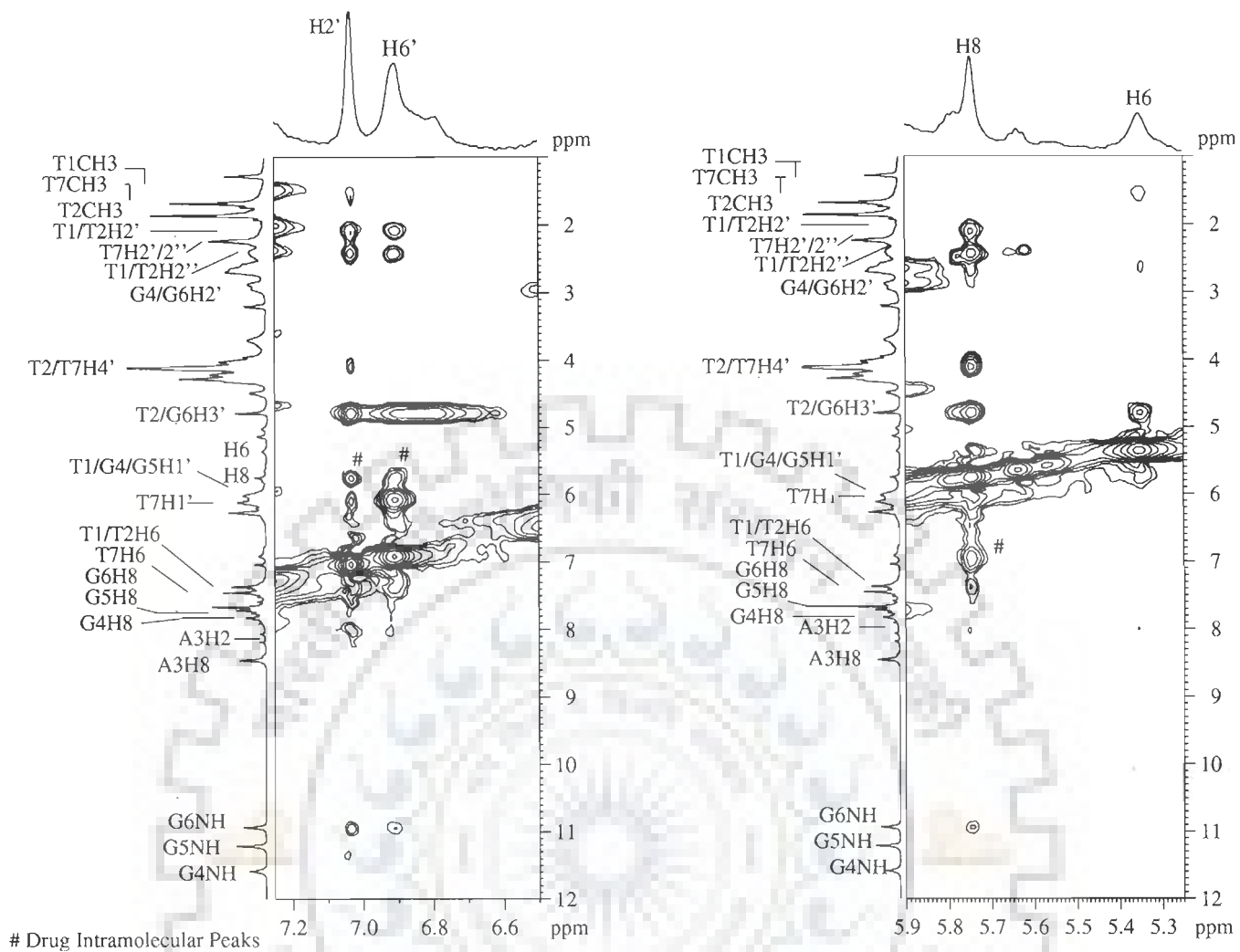
Fig. 7.18: Expansion of the specific regions of NOESY spectra of quercetin complexed with d-(TTAGGGT)₄ to highlight specific intramolcular connectivities (#) within quercetin and Intermolecular peaks of (a) quercetin H2', H6' and (b) quercetin H8, H6 with -(TTAGGGT)₄.

323

Table 7.11: Relative intensities of intermolecular NOE connectivities between d-(TTAGGGT)₄ and the quercetin molecule in the quercetin-d-(TTAGGGT)₄ complex at drug to DNA ratio D / N =1.0 from NOESY spectra at 298 K.

Sequence connectivity	Intensity	Distances obtained by rMD	Sequence connectivity	Intensity	Distances obtained by rMD
T1/T2H2'- H2'	s	2.6	T1/T7CH₃- H6	vw	5.2
T1/T2H2'-H6'	s	2.9	T1/T2H2'-H8	s	2.4
T1/T2H2''-H2'	s	2.7	T1/T2H2''-H8	ss	1.9
T1/T2H2''-H6'	s	3.1	G6H2'-H8	vw	5.3
T2/T7H4'-H2'	w	3.8	G6H2'-H6	vw	5.6
T7H1'-H2'	w	3.9	T2/T7H4'-H8	ss	1.5
T7H1'-H6'	ss	2.1	T2/G6H3'-H8	ss	1.7
A3/G6H1'-H2'	vw	4.7	T2/G6H3'-H6	ss	1.6
G6H8-H2'	s	3.1	T1H1'-H8	s	2.8
T7H6-H2'	s	2.7	T2H1'-H8	s	2.9
T7H6-H6'	vw	4.8	T2H1'-H6	s	2.5
A3H2-H2'	w	4.5	T1/T2H6-H8	s	3.1
A3H2-H6'	w	4.8	A3H2-H8	vw	5.1
G6NH-H2'	vw	4.9	A3H2-H6	vw	4.9
G6NH-H6'	s	2.7	G6NH-H8	vw	5.1
G5NH-H2'	m	4.2			

strong intense (ss), strong (s) medium (m) weakly (w) and very weakly (vw) for distances of about 1.8 - 2.5, 2.5 - 3.0, 3.0 - 3.5, 3.5 - 4.0, and 4.0 - 5.0 Å respectively

relatively strong for the unbound quadruplex, are weaker, reflecting the structural distortions caused by drug intercalation at the T1pT2 step. We investigate further the stability of the complex and its contribution to drug binding in MD simulations

7.1.3 Restrained Molecular Dynamics Studies

Restrained Molecular Dynamics (rMD) permits the system to undergo conformational and momentum change so that different parts of the phase space accessible to the molecule can be explored and stable conformations identified by energy minimization. Based on the observed intermolecular and intramolecular NOE data an initial model with quercetin located at the two place in d-(TTAGGGT)₄ was considered (Fig. 7.19 a). The relative strengths of the cross peaks were used only in qualitative

manner. Distances used were about 1.8 - 2.5, 2.5 - 3.0, 3.0 - 3.5, 3.5 - 4.0, and 4.0 - 5.0 Å for strong intense (ss), strong (s) medium (m) and weakly (w) and very weakly (vw) intense peaks, respectively. The best-fit refined structure showing all atoms of the front view of the complex is shown in Fig. 7.19a and the π- stacking of quercetin with G7 tetrad. The quercetin -d-(TTAGGGT)$_4$ complex was stabilized via π- stacking and hydrogen bonding were imposed in the structure calculations based on the experimental evidence from NOESY spectra. All other restraints for the intramolecular and intermolecular connectivities were also given. The final structure obtained after rMD is shown in Fig. 7.19a Table 7.12 a,b indicates an assessment of refined structures after equilibration (at the end of 100 ps) in terms of energetics including restraint violations energies and root mean square derivative of energy w.r.t atomic coordinates. The total potential energy of the final structure was 2627 kcal mol^1, which was lower than the corresponding energy of initial model structure (3984 kcal mol^{-1}).

The forcing potential, which indicates contribution to potential energy due to violations of both experimental distances data, exhibited a decrease from 954 to 727 kcal mol^{-1} after restrained energy minimization and restrained molecular dynamics simulations. Close contacts which involved specific vander Waal's and electrostatic interactions and which is clearly shown in Figure 7.20. Therefore it is established with the help of rMD that quercetin binds to d-(TTAGGGT)$_4$ in intercalation binding mode. Model obtained through rMD supports the results from the ^{31}P NMR, proton chemical shift analysis, DOSY and intramolecular and intermolecular interaction obtained from 2D NOESY spectrum.

(a)

(b)
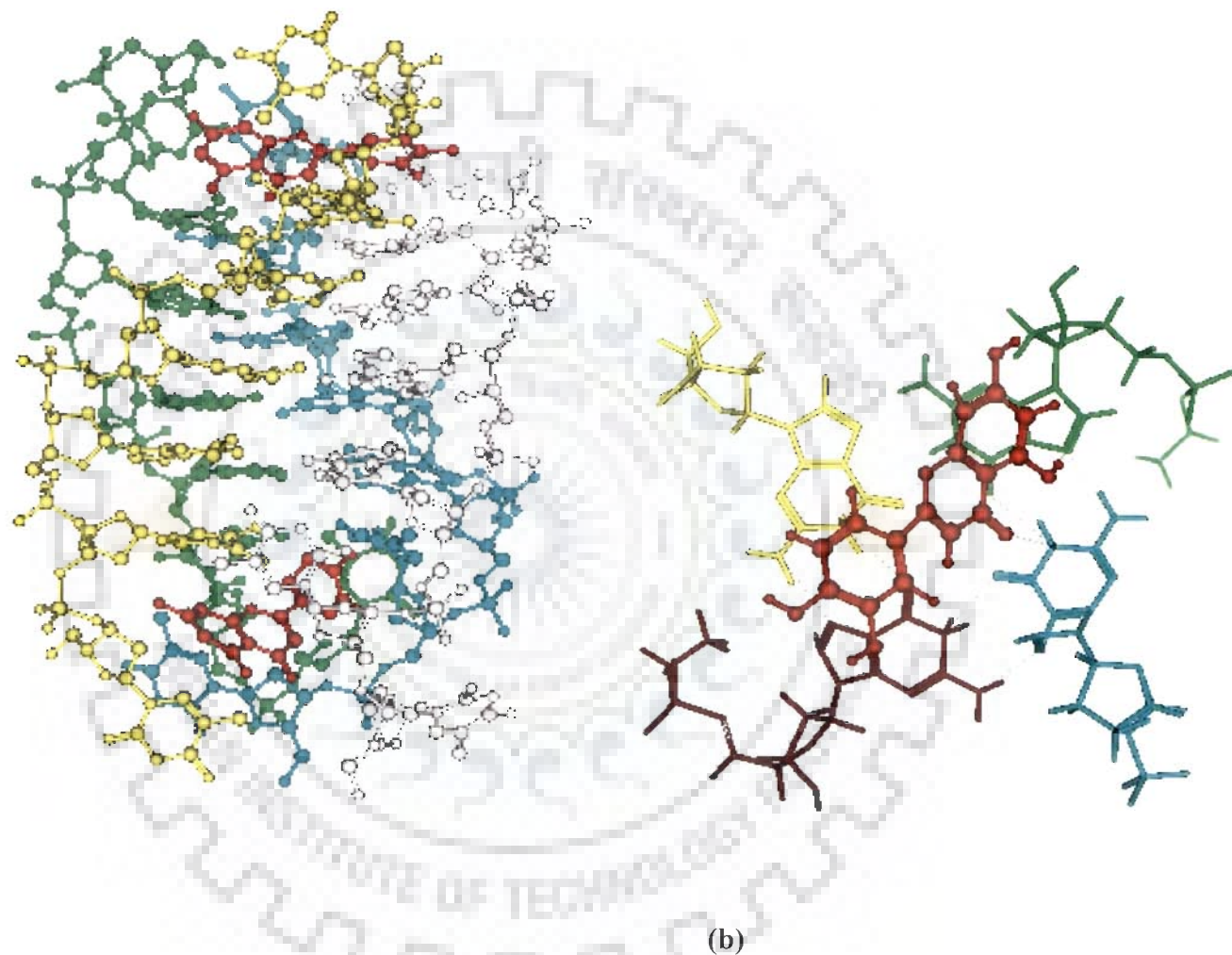
Fig. 7.19: (a) Front view of the final structure of quercetin-d-(TTAGGGT)$_4$ complex obtained by restrained molecular dynamics simulations and (b) Offset π-stacking of quercetin with G7 tetrad.

Table7.12a: Energy terms (Kcal mol^{-1}) for starting structure and final rMD structure.

Structure	Total	Bond	Angle	Dihedral
Initial	3984	519	1152	789
Final	2627	340	1099	610
	Vdw	Electrostatic	Restraint	Out of plane
Initial	992	-1595	954	340
Final	982	-1568	727	265

Table 7.12b: Summary of experimental restraints and statistical analysis of final structure generated by restrained molecular dynamics (rMD)

Parameter	
	No. of Distance Restraints
Intra residue	175
Inter residue	84
Inter molecular	31
Average pairwise RMSD	Initial = 0 Final = 0.51

327
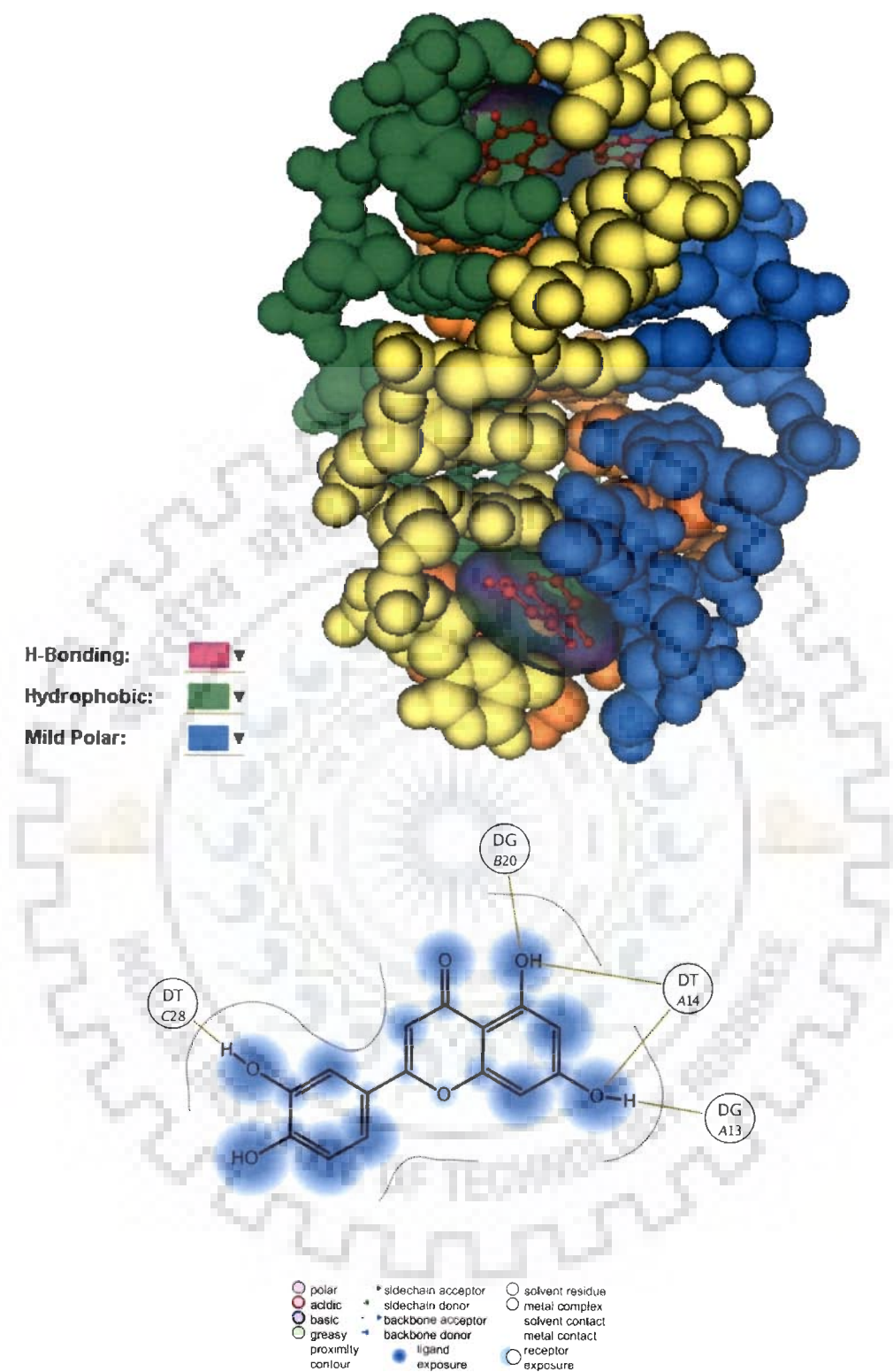
Fig. 7.20: (a) overall symmetry of the quercetin-d-(TTAGGGT)₄ complex showing different forces and (b)Various Interactions present in 1:1 quercetin-d-(TTAGGGT)₄ complex

7.2. Summary and Conclusions

Even at higher quercetin concentration the variation of chemical shift with D/N ratio is small and did not show any saturation behavior as would be expected if chromophore of quercetin was to intercalate between base pairs. However, there was absence of a large downfield shift ~1.5 ppm in ^{31}P chemical shifts, as observed with intercalators. But appearance of new set of in ^{31}P spectra after concomitant addition of quercetin can be attributed to the intercalation mode likely to ethidium bromide which showed similar pattern with ([G-C]$_5$)$_2$ (Frederick and Hurley 1999). These observations rule out the interaction mode other than the intercalation.. ^{31}P-^{31}P exchange spectrum of the d-(TTAGGGT)$_4$ - quercetin complex at various D/N ratios showed exchange peaks for free and bound resonances. Shift in ^{31}P resonances versus temperature in the bound complexes were gradual and the total change, $\Delta\delta = \delta_{328\ K} - \delta_{298\ K}$, was higher for D/N 1.0 as compared to D/N 0.5. These results suggest that quercetin binding involves T1pT2, T2pA3 and G6pT7 bases. Proton chemical shift was also observed through titration and it was found that one more set of –NH protons appeared with increasing concentration of quercetin. It is suggested that the signals were in slow exchange regime and the observed resonance was considered to be of free and bound proton. It was proved by titrimataric analysis of ^{1}H chemical shift and temperature dependence studies at D/N 1.0 that the central aromatic chromophore of the quercetin was involved in the interaction with d-(TTAGGGT)$_4$. Binding was also proved by DOSY which showed majority of the quercetin binding to DNA even at D/N ratio 1.0, which was further supported by NOESY data analysis. Presence of all internucleotide sequential connectivities suggests that the G-tetrad did not open up to accommodate the quercetin chromophore. All the quadruplex

pair peaks, sequential intra and inter-strand peaks exist. The sequential peak of T2H6-T1H1' for T1pT2 is lost which may be due to intercalation of quercetin at this site. Intermolecular peaks obtained from NOESY spectra recorded at D/N 1.0 suggested that the drug protons, H2', H6' and H6, H8 located at ring B and ring A were giving cross peaks with sugar protons of DNA at T1, T2 and T7 region in majority. This supports significantly that quercetin binds at two places in quadruplex d-(TTAGGGT)$_4$ with intercalation mode involving stacking interaction with A3 and G6. Hence ^{31}P and ^{1}H NMR studies also support this mode of binding. Major participation of stacking interaction and hydrogen bonding interaction in the complex formation was also observed in the final rMD model.

CHAPTER 8

Summary and Conclusions

DNA, the genetic material in living cells, can interact with certain classes of drugs, carcinogens, mutagens; dyes all of which are characterized by planar or extended (hetero)-cyclic aromatic chromophores. A variety of biochemical evidence suggests that DNA is the principal cell target for many antitumor agents. Owing to the central role of DNA in biological replication and protein biosynthesis, modification by such interaction greatly alters cell metabolism, diminishing and in some cases terminating cell growth. The cancer chemotherapy relies on inhibition of nucleic acid synthesis or interference with mitosis as a means of discriminating selectively against fast growing tumor cells. Recently, telomeric DNA which forms G-quadruplex has become very hot target for anticancer therapy. The telomeric end is maintained and stabilized by an enzyme telomerase which is found only in cancerous cell. The high anti-tumour chemotherapeutic potential of ligands with the capability to stabilize G-quadruplex has focused several research groups on structure-based design approaches to the development of molecules that interact with G-quadruplexes. A number of synthetic compounds with an extended aromatic ring system capable of π-stacking with G-tetrads have shown the ability to inhibit telomerase activity through the stabilisation of G-quadruplexes. Many synthetic compounds have been added to this list in the search for more potent drugs for use in chemotherapy but also exhibit toxic side effects, such as cardiotoxicity, nausea, vomiting etc. which limits their further application in targeting telomere for cancer therapy. Looking for non toxic or less toxic compounds with similar property is necessary to reveal. One may expect that natural compounds which are usually available in our diets would be an ideal goal. In

this regard, flavonoids can solve our problem for not only the reason that these compounds are equally effective as their synthetic counterparts but for not posing problems like synthetic drugs. Thus, flavonoids are found to be less toxic to normal cells than conventional chemotherapeutic agents and therefore offer an opportunity for more successful treatment of cancer. So, it is of prime importance to unravel their efficacy in targeting telomere or stabilizing G-quadruplex structure to prevent the activity of telomerase in cancerous cells. Thus, the present work will allow us to enter into a new era of cancer therapy using drugs of the natural origin, available in our daily diets. Experiments on different cancerous cell lines showed that flavonoids acts as anticancer agent by inducing apoptosis. But still their action on molecular target like duplex or quadruplex DNA is not clear. Further, flavonoids are a large family which includes more than 3000 members. All members vary on the basis of substitution of functional groups and it has been found that the functional activities of flavonoids are changed by means of various degrees of functional group substitution and the number of hydroxyl groups. So, there is great possibility to find out the most potent anticancer drugs with least side effects and whose action should be on both kinds of DNA duplex as well as quadruplex. Keeping above points in view the present work has been contemplated with several objectives.

We have demonstrated the use of DFT method in the theoretical studies on molecular properties and electronic structure of representative molecules of flavone, flavanol and flavanone of flavonoid group to find out the best optimized conformer. An overall analysis shows that B3LYP/6-311G** level of theory in solvent DMSO predicts sound results which are quantitatively good and compare well with the experimental data. Further, the structural analysis shows the role of inter and intra molecular hydrogen bonding in solution which is important for the flavonoids for

their several functions like antioxidant properties and especially DNA binding for anti cancerous activity. Due to difficulties in growing a crystal for X -ray diffraction studies, the optimized molecular structure obtained from DFT method can pave the way for structure function studies. The DFT studies yields enough information about the chemical shift and structural parameters of their best optimized conformation. Theoretical calculation of NMR parameter like chemical shift for different class of flavanoids compare well with the experimental data available in the literature. As the totality of the available evidence on different position of hydroxyl group and structural parameters for these flavonoids suggests a role in the prevention of cancer and for antioxidant properties.

Further, complete ^{1}H and ^{13}C NMR assignments of member of each group of flavone, flavonol and isoflavone viz. luteolin, quercetin, rutin (flavonol glycosides) and genistein were achieved using a combination of 1D and 2D (HSQC, HMBC, and ROESY) experiments in DMSO solvent. An optimized solution structure has been determined by analyzing the 2D NMR data followed by restrained molecular dynamics simulation. The experimental findings were combined with a theoretical investigation using density functional theory (DFT) using B3LYP functional for luteolin, quercetin, rutin and genistein molecule in gaseous phase and in DMSO solvent system. Among all the methods B3LYP functional has shown to produce best results for geometries, energies, and all other NMR parameters both in gas phase and solvent and the same are reported here. In gas phase a variety of basis sets (STO-3G, 6-31G, 6-31G*, 6-31G** and 6-311G**) were used. The effect of increasing size of the basis set slow down the calculation but tends towards to accurate results. An overall analysis shows that B3LYP/6-311G** level of theory predicts results which are quantitatively good and compare well with the experiment. Further, the structural

analysis shows the role of inter and intra molecular hydrogen bonding in solution which is important for the flavonoids for their several functions especially DNA binding as anti cancerous activity likely to other intercalating agent, quercetin complexation is stipulated by its planar structure and additional carboxyl group that can be protonated these facilitate intercalation and subsequent π- stacking with base pairs. An optimized solution structure has been obtained by restrained Molecular Dynamics simulations using ROE restraints for luteolin, quercetin, rutin and genistein. These structures are compared with that obtained from quantum mechanical calculations. It is observed that A and C ring are planar in these flavonoids and the B ring of the quercetin and rutin rotate around C2'-C1'-C2 -O1 torsional angle to go in to two different conformation, *anti* and *syn* in rMD structure and in DFT studies. The presence of *anti* and *syn* conformers were also confirmed by solid state NMR and DFT studies (Olejniczak and Potrzebowski, 2004). Similar effect has been also observed in case of genistein but around C6'-C1'-C3 -C4 torsional angle. A variation in flexibility of adopting two different conformations in these flavonoids may be related to a differential efficacy in biological activity and hence antioxidant or anticancer action.

Flavonoids are known to have hydroxyl group and individual differences within each flavonoid result from the variation in number and arrangement of these hydroxyl groups. Hydrogen bonds involving hydroxyl group are not only considered as playing a determinant role in all biochemical processes, but are also of crucial importance in solution structures. In this regard, it is expected to observe the molecular association by formation of intermolecular hydrogen bonding. Prior to the determination of the structural and thermo-dynamical characteristics of the

intercalative binding of flavonoids to defined DNA sequences, it is necessary to determine the molecular association of these molecules in solution.

1D Proton NMR of various flvonoids show downfield shift in a ring A protons H6 and H8 on increasing concentration from 0.01 mM to 10.00 mM. This meager shift in chemical shift may be attributed to the poor stacking of the chromophore rings and involved in other mode of association. The temperature dependence studies show downfield shift upto 1.97 ppm with temperature for the hydroxyl protons OH7 in luteolin, quercetin, rutin and OH4' in genistein indicating that these flavonoids exist in aggregated form which is forced by the hydrogen bonding. 2D NOESY spectra at 298 K show various inter-molecular and intra-molecular cross peaks which are evolved due to the association of aromatic chromophores of drug molecules. Restrained Molecular Dynamics studies show the existence of hydrogen bonds between two aromatic rings in the dimer. To date no such structure of dimer has been reported for any of the flavonoids. Absorption and fluorescence studies also support the results for self association. The DOSY studies indicate that the rate of diffusion increases in the following manner rutin < quercetin < genistein < luteolin. ESI-MS experiments clearly demonstrate the existence of dimer and also the higher aggregates. The mass spectra of rutin also show presence of rutinoside resulting from cleavage of glycosidic bond. Absence of cleaved moiety in rutin gives direct proof of how easily it can convert in to quercetin after the cleavage of glycosidic bond. The structural difference between different levels of intermolecular association of these four flavonoids may be related to their competitive binding with DNA and hence different in their pharmacological action. Further their interaction with different types of DNA is worth important to reveal their efficacy for anticancer activity.

335

The effort has been taken to explore the interaction of luteolin, quercetin, rutin and genistein with duplex DNA and telomeric quadruplex forming oligonucleotides which were extensively investigated using competition dialysis, spectrophotometric, fluorometric steady as well as life time, CD and ESI-MS techniques. Different flavonoids showed change in absorption spectrum differently after addition of DNA. Luteolin, rutin and genistein showed hyperchromicity with little bathochromic effect unlikely to quercetin which showed hypochromicity and significant bathochromic shift on addition of duplex DNA. Interaction study with different polynucleotides revealed that these flavonoids do not show any specificity to the DNA sequences but prefer to bind to -AT rich sequences. Further, addition of quadruplex DNA sequences shows hyperchromicity with significant bathochromic effect in all the four flavonoids indicates their intercalative mode of binding. These results are also supported by fluorometric studies which shows enhancement in fluorescence intensity. CD studies confirm the binding of these flavonoids to different G-quadruplex sequences. Life time fluorescence decay and mass spectrometric studies clearly indicated the different stoichiometries of the complex formation. Three different life time decay which is attributed to three different binding complexes, can be correlated to the results obtained from MS data showing 1:1, 1:2 and 1:3 stoichiometries. In view of getting further information about the mode of binding of these flavonoids to G-quadruplex seuquences, further structural studies are warranted. In view of this model flavonoids quercetin has been considered for the study regarding interaction with telomeric G quadruplex sequence d-(TTAGGGT)$_4$ by NMR and rMD approach.

In this study, at higher quercetin concentration the variation of chemical shift with D/N ratio is small and did not show any saturation behavior as would be expected if chromophore of quercetin was to intercalate between base pairs. However,

there was absence of a large downfield shift ~1.5 ppm in ^{31}P chemical shifts, as observed with intercalators. But appearance of new set of in ^{31}P spectra after concomitant addition of quercetin can be attributed to the intercalation mode likely to ethidium bromide which showed similar pattern with $([G-C]_5)_2$ (Frederick and Hurley 1999).These observations rule out the interaction mode other than the intercalation.. ^{31}P-^{31}P exchange spectrum of the d-$(TTAGGGT)_4$ - quercetin complex at various D/N ratios showed exchange peaks for free and bound resonances. Shift in ^{31}P resonances versus temperature in the bound complexes were gradual and the total change, $\Delta\delta = \delta_{328\ K} - \delta_{298\ K}$, was higher for D/N 1.0 as compared to D/N 0.5. These results suggest that quercetin binding involves T1pT2, T2pA3 and G6pT7 bases. Proton chemical shift was also observed through titration and it was found that one more set of –NH protons appeared with increasing concentration of quercetin. It is suggested that the signals were in slow exchange regime and the observed resonance was considered to be of free and bound proton. It was proved by titrimataric analysis of ^{1}H chemical shift and temperature dependence studies at D/N 1.0 that the central aromatic chromophore of the quercetin was involved in the interaction with d-$(TTAGGGT)_4$. Binding was also proved by DOSY which showed majority of the quercetin binding to DNA even at D/N ratio 1.0, which was further supported by NOESY data analysis. Presence of all internucleotide sequential connectivities suggests that the G-tetrad did not open up to accommodate the quercetin chromophore. All the quadruplex pair peaks, sequential intra and inter-strand peaks exist. The sequential peak of T2H6-T1H1' for T1pT2 is lost which may be due to intercalation of quercetin at this site. Intermolecular peaks obtained from NOESY spectra recorded at D/N 1.0 suggested that the drug protons, H2', H6' and H6, H8 located at ring B and ring A were giving cross peaks with sugar protons of DNA at T1, T2 and T7 region in majority. This

supports significantly that quercetin binds at two places in quadruplex d-(TTAGGGT)$_4$ with intercalation mode involving stacking interaction with A3 and G6. Hence ^{31}P and ^{1}H NMR studies also support this mode of binding. Major participation of stacking interaction and hydrogen bonding interaction in the complex formation was also observed in the final rMD model.

Thus present thesis explored the structure–activity basis for direct anticancer activity by targeting different duplex and quadruplex DNA.

REFERENCES

1. Aboulela F., Murchie A.I.H., Norman D.G. and Lilley D.M. J. J. Mol. Biol., 1994, 243, 458–471

2. Abraham, R.J., Mobil, M. and Smith, R.J. 1H chemical shifts in NMR. Part 20--anisotropic and steric effects in halogen substituent chemical shifts (SCS), a modelling and *ab initio* investigation, Magn. Reson. Chem., 2004, 42, 436-444.

3. Adel A. L., Dorr R. T. and Liddil J. D. The effect of anticancer drug sequence in experimental combination chemotherapy. Cancer Invest. 1993, 11, 15-24.

4. Ahmed, M.S., Ramesh, V., Nagaraja, V., Parish, J.H. and Hadi, S.M. Mode of binding of quercetin to DNA Mutagenesis, 1994, 9(3) 193-197.

5. Alberts D. S., Salmon S. E., Surit E. A., Chen H. S. G., Moon T. E. and Meyskens F. L. Combination chemotherapy (CRX) in vitro with the human – tumor stem-cell assay. Proc Am Assoc Cancer Res. 1981, 23, 153.

6. Ambrus A., Chen D., Dai J., Jones R.A. and Yang D. Solution structure of the biologically relevant G-Quadruplex element in the human c-MYC promoter. Implications for G-quadruplex stabilization. Biochemistry, 2005, 44, 2048 - 2058.

7. American Cancer Society (December 2007). "Report sees 7.6 million global 2007 cancer deaths. http.//www.reuters.com/article/healthNews/idUSN1633064920071217

8. Anter E., Thomas S.R., Schulz E., Shapira O.M., Vita J.A. and Keaney J.F., Jr. Activation of endothelial nitric-oxide synthase by the p38 MAPK in response to black tea polyphenols. J Biol Chem. 2004, 279(45), 46637-46643.

9. Arcari., M., Brambilla., A., Brandt., A., Caponi., R., Corsi., G., Di Rella., M., Solinas, F. and Wachter, W.P.A., New inclusion complex of silibinin and betacyclodextrins:

in vitro dissolution kinetics and in vivo absorption in comparison with traditional formulations. Boll. Chim. Farm., 1992, 131, 205–209.

10. Arora, A., Nair, M.G. and Strasburg, G.M. Structure-activity relationships for antioxidant activities of a series of flavonoids in a liposomal system, Free Radic. Biol. Med., 1998, 24, 1355-1363.

11. Arts I.C, Jacobs D.R, Jr., Gross M, Harnack L.J. and Folsom A.R. Dietary catechins and cancer incidence among postmenopausal women, the Iowa Women's Health Study (United States). Cancer Causes Control. 2002, 13(4), 373-382.

12. Arts I.C., Hollman P.C., Bueno De Mesquita H.B., Feskens E.J. and Kromhout D. Dietary catechins and epithelial cancer incidence, the Zutphen elderly study. Int J Cancer. 2001, 92(2), 298-302.

13. Bagli E., Stefaniotou M. and Morbidelli L., et al. Luteolin inhibits vascular endothelial growth factor-induced angiogenesis, inhibition of endothelial cell survival and proliferation by targeting phosphatidylinositol 3'-kinase activity. Cancer Res. 2004, 64(21), 7936-7946.

14. Bailey D.G. and Dresser G.K., Interactions between grapefruit juice and cardiovascular drugs. Am J Cardiovasc Drugs. 2004, 4(5), 281-297.

15. Balasubramanian S. and Govindasamy S., Inhibitory effect of dietary flavonol quercetin on 7, 12-dimethylbenz[a]anthracene-induced hamster buccal pouch carcinogenesis. Carcinogenesis. 1996, 17(4), 877-879.

16. Balogh-Hergovich, E., Kaiser, J., and Speier, G. Synthesis and characterization of copper (I) and copper (II) flavonolate complexes with phthalazine, and their oxygenation and relevance to quercetinase. Inorg. Chim. Acta, 1997, 256, 9–14.

17. Balzer J., Rassaf T., Heiss C., et al. Sustained benefits in vascular function through flavanol-containing cocoa in medicated diabetic patients a double-masked, randomized, controlled trial. J Am Coll Cardiol. 2008, 51(22), 2141-2149.

18. Barthwal R., Prashansa A., Tripathi A. N., Sharma U., Jagannathan N. R. and Govil G. Structural elucidation of 4'-epiadriamycin by nuclear magnetic resonance spectroscopy and comparison with adriamycin and daunomycin using quantum mechanical and restrained molecular dynamics approach. Arch Biochem Biophys. 2008, 474, 48-64.

19. Becke, A.D. Density-functional thermochemistry. III. The role of exact exchange, J. Chem. Phys., 1993, 98, 5648-5652.

20. Beecher G.R. Overview of dietary flavonoids, nomenclature, occurrence and intake. J Nutr. 2003, 133(10), 3248S-3254S.

21. Bi, S., Qiao, C., Song, D., Tian, Y., Gao, D., Sun, Y. and Zhang, H., Study of interactions of flavonoids with DNA using acridine orange as a fluorescence probe. Sensors and Actuators B, 2006, 119, 199–208

22. Blake G.J. and Ridker P.M., C-reactive protein and other inflammatory risk markers in acute coronary syndromes. J Am Coll Cardiol., 2003, 41(4 Suppl S), 37S-42S.

23. Block G. Role of antioxidants in reducing cancer risk. Nutr. Rev. 1992, 50, 207–213.

24. Bocian, W., Kawecki, R., Bednarek, E., Sitkowski, J., Ulkowskab, A. and Kozerski, L. Interaction of flavonoid topoisomerase I and II inhibitors with DNA oligomers. New J. Chem., 2006, 30, 467–472.

25. Bonkovsky H.L. Hepatotoxicity associated with supplements containing Chinese green tea (Camellia sinensis). Ann Intern Med. 2006, 144(1), 68-71.

26. Bouaziz S., Kettani A. and Patel D.J. A K cation-induced conformational switch within a loop spanning segment of a DNA quadruplex containing G-G-G-C repeats. J.Mol.Biol. 1998, 282, 637 - 652.

27. Buchler P., Gukovskaya A.S., Mouria M., Buchler M.C., Buchler M.W., Friess H., Pandol S.J., Reber H.A. and Hines O.J. Prevention of metastatic pancreatic cancer growth in vivo by induction of apoptosis with genistein, a naturally occurring isoflavonoid. Pancreas. 2003, 26, 264–273.

28. Bucki R., Pastore J.J., Giraud F., Sulpice J.C. and Janmey P.A. Flavonoid inhibition of platelet procoagulant activity and phosphoinositide synthesis. J Thromb Haemost. 2003, 1(8), 1820-1828.

29. Buhl, M., Kaupp, M., Malkina, O. L. and Malkin, V. G. The DFT route to NMR chemical shifts, J. Comput. Chem., 1999, 20, 91-105.

30. Burda, S., and Oleszek, W. Antioxidant and antiradical activities of flavonoids, J. Agric. Food Chem., 2001, 49, 2774-2779.

31. Burns, D.C., Ellis. D.A. and March. R.E. A predictive tool for assessing $^{(13)}$C NMR chemical shifts of flavonoids, Mag. Res. Chem., 2007, 45, 835-845.

32. Caceres C., Wright G., Gouyette C., Parkinson G. and Subirana J.A. A Thymine tetrad in d(TGGGGT) quadruplexes stabilized with Tl+1/Na+1 ions Nucleic Acids Res. 2004, 32, 1097 -1102.

33. Campbell N.H., Parkinson G.N., Reszka A.P. and Neidle S. Structural basis of DNA quadruplex recognition by an acridine drug. J.Am.Chem.Soc., 2008, 130, 6722 – 6724

34. Campbell N.H., Parkinson, G. and Neidle, S. Selective ligand recognition of G-quadruplex loops. To be Published.

35. Cao, G., Sofic, E. and Prior RL. Antioxidant and prooxidant behavior of flavonoids: structure-activity relationships, Free Radic Biol Med., 1997, 22, 749-760.

36. Cao, Y. and He, X.W. Studies of interaction between safranine T and double helix DNA by spectral methods, Spectrochim. Acta A, 1998, 54, 883–892.

37. Cao, Y., He, X.W., Gao, Z. and Peng, L. Fluorescence energy transfer between acridine orange and safranine T and its application in the determination of DNA, Talanta, 1999, 49, 377–383.

38. Carmody, R.J., McGowan, A.J. and Cotter, T.G. Reactive oxygen species as mediators of photoreceptor apoptosis in vitro, Exp. Cell Res., 1999, 248, 520-530.

39. Casanovas, J., Namba, A.M., da Silva, R., Aleman, C. DFT-GIAO study of aryltetralin lignan lactones: conformational analyses and chemical shifts calculations, Bioorg. Chem., 2005, 33, 484-492.

40. Casanovas, J., Namba, A.M., Leon, S., Aquino, G.L., da Silva, G.V. and Aleman,C. Calculated and experimental NMR chemical shifts of p-menthane-3,9-diols. A combination of molecular dynamics and quantum mechanics to determine the structure and the solvent effects, J. Org. Chem., 2001, 66, 3775-3782.

41. Casini M.L., Marelli G., Papaleo E., Ferrari A., D'Ambrosio F. and Unfer V. Psychological assessment of the effects of treatment with phytoestrogens on postmenopausal women, a randomized, double-blind, crossover, placebo-controlled study. Fertil Steril. 2006, 85(4), 972-978.

42. Castillo, M.H., Perkins, E., Campbell, J.H., Doerr, R., Hassett, J.M., Collins, A.R. Antioxidant intervention as a route to cancer prevention. Eur. J. Cancer, 2005, 41, 1923–1930.

43. Chakraborty T.K., Srinivasa K., Udaya Kiran M. and Jagadeesh B. Nucleation of the β-hairpin structure in a linear hybrid peptide containing α-, β- and γ-amino acids. Tetrahedron Letters, 2008, 2228-2231

44. Chaoudhary, A.R. Sharma, S., Mandal, S., Goswami, A., Sibabrata, Mukhopadhyay, S. and Majumdar, H.K. Luteolin. An emerging anti-cancer flavonoid, poisons eukaryotic DNA topoisomerase I. Biochem. J., 2002, 366, 653-661

45. Chen J.J., Ye Z.Q. and Koo M.W. Growth inhibition and cell cycle arrest effects of epigallocatechin gallate in the NBT-II bladder tumour cell line. BJU Int. 2004, 93(7), 1082-1086.

46. Chen, D., Chen, M.S., Cui, Q.C., Yang H. and Dou, Q.P. Structure–proteasome-inhibitory activity relationships of dietary flavonoids in human cancer cells, Front. Biosci., 2007, 12, 1935-1945.

47. Chen, Q.Y., Li, D.H., Yang, H.H., Zhu, Q.Z., Xu, J.G. and Zhao, Y. Interaction of a novel red-region fluorescent probe, Nile Blue, withDNAand its application to nucleic acids assay, Analyst, 1999, 124, 901–906.

48. Cheng I.F. and Breen K. On the ability of four flavonoids, baicilein, luteolin, naringenin, and quercetin, to suppress the Fenton reaction of the iron-ATP complex. Biometals. 2000, 13(1), 77-83.

49. Cheong C. and Moore P.B. Solution structure of an unusually stable RNA tetraplex containing G- and U-quartet structures. Biochemistry. 1992, 31, 8406 - 8414.

50. Cho S.Y., Park S.J., Kwon M.J., et al. Quercetin suppresses proinflammatory cytokines production through MAP kinases andNF-kappaB pathway in lipopolysaccharide-stimulated macrophage. Mol Cell Biochem. 2003, 243(1-2), 153-160.

51. Choi J.S., Choi Y.J, Park S.H, Kang J.S. and Kang Y.H. Flavones mitigate tumor necrosis factor-alpha-induced adhesion molecule upregulation in cultured human endothelial cells, role of nuclear factor-kappa B. J Nutr. 2004, 134(5), 1013-1019.

52. Chow H.H., Cai Y., Hakim I.A., et al. Pharmacokinetics and safety of green tea polyphenols after multiple-dose administration of epigallocatechin gallate and polyphenon E in healthy individuals. Clin Cancer Res. 2003, 9(9), 3312-3319.

53. Chun O.K., Kim D.O. and Lee C.Y. Superoxide radical scavenging activity of the major polyphenols in fresh plums. J Agric Food Chem. 2003, 51(27), 8067-8072.

54. Chunying W., Gaoyi H., Guoqing J., Jun Z., Can L. Study on the interaction of porphyrin with G-quadruplex DNAs. Biophysial Chemistry, 2008, 137, 19-23

55. Clark G.R., Pytel P.D., Squire C.J. and Neidle S. Structure of the First Parallel DNA Quadruplex-drug Complex. J.Am.Chem.Soc. 2003, 125, 4066 - 4067.

56. Cody V. and Luft J.R. Conformational analysis of flavonoids:. crystal and molecular structures of morin hydrate and myricetin (1:2) triphenylphosphine oxide complex, J. Mol. Struct., 1994, 317, 89-97.

57. Commenges D., Scotet V., Renaud S., Jacqmin-Gadda H., Barberger-Gateau P. and Dartigues J.F. Intake of flavonoids and risk of dementia. Eur J Epidemiol. 2000, 16(4), 357-363

58. Cordier., F. and Grzesiek., S. Direct observation of hydrogen bonds in proteins by interresidue $^3J_{NC'}$ scalar couplings, J. Am. Chem. Soc., 1999, 121, 1601-1602.

59. Cos, P., Ying, L., Calomme, M., Hu, J.P., Cimanga, K., Van Poel, B., et al., Structure-Activity Relationship and Classification of Flavonoids as Inhibitors of Xanthine Oxidase and Superoxide Scavengers, J. Natural Products, 1998, 61, 71-76.

60. Cox, P.J., Kumarasamy, Y., Nahar, L., Sarker, S.D. and Shoeb, M. Luteolin, Acta cryst. 2003, E59, o975-o977.

61. Creze C., Rinaldi B., Haser R., Bouvet P. and Gouet P. Structure of a d(TGGGGT) quadruplex crystallized in the presence of Li^{+} ions Acta Crystallogr., Sect.D , 2007, 63, 682 - 688.

62. Crnugelj M., Hud N.V. and Plavec J. The solution structure of d(G(4)T(4)G(3))(2), a bimolecular G-quadruplex with a novel fold. J.Mol.Biol. 2002, 320, 911 - 924.

63. D'Ambrosio., S.M. Evaluation of the genotoxicity data on caffeine, Reg. Toxicol. Pharmacol., 1994, 19, 243-281.

64. Dahan A. and Altman H. Food-drug interaction, grapefruit juice augments drug bioavailability--mechanism, extent and relevance. Eur J Clin Nutr. 2004, 58(1), 1-9.

65. Dai J., Carver M., Punchihewa C., Jones R.A. and Yang D. Structure of the Hybrid-2 type intramolecular human telomeric G-quadruplex in K+ solution, insights into structure polymorphism of the human telomeric sequence Nucleic Acids Res., 2007, 35, 4927 - 4940.

66. Dai J., Chen D., Jones R.A., Hurley L.H. and Yang D. NMR solution structure of the major G-quadruplex structure formed in the human BCL2 promoter region. Nucleic Acids Res., 2006, 34, 5133 - 5144.

67. Dai J., Punchihewa C., Ambrus A., Chen D., Jones R.A. and Yang D. Structure of the intramolecular human telomeric G-quadruplex in potassium solution, a novel adenine triple formation. Nucleic Acids Res., 2007, 35, 2440 - 2450.

68. Dai, J., Carver, M., Punchihewa, C., Jones, R.A. and Yang, D. Structure of the Hybrid-2 type intramolecular human telomeric G-quadruplex in K+ solution, insights

into structure polymorphism of the human telomeric sequence Nucleic Acids Res., 2007, 35, 4927 - 4940.

69. Davies., D.B., Veselkov., D.A., Djimant., L.N. and Veselkov, A.N. Heteroassociation of caffeine and aromatic drugs and their competitive binding with a DNA oligomer Eur. Biophys. J., 2001, 30, 354-366.

70. De Rijk M.C., Breteler M.M., den Breeijen J.H., et al. Dietary antioxidants and Parkinson disease. The Rotterdam Study. Arch Neurol. 1997, 54(6), 762-765

71. De Stefani E, Ronco A, Mendilaharsu M. and Deneo-Pellegrini H. Diet and risk of cancer of the upper aerodigestive tract--II. Nutrients. Oral Oncol. 1999, 35(1), 22-26

72. Dean, J.A., LANGE'S Handbook of Chemistry (15th ed.), McGraw-Hill, USA (1999).

73. Deana R., Turetta L., Donella-Deana A., et al. Green tea epigallocatechin-3-gallate inhibits platelet signalling pathways triggered by both proteolytic and non-proteolytic agonists. Thromb Haemost. 2003, 89(5), 866-874.

74. Deng J. and Xiong Y. Sundaralingam M. X-ray analysis of an RNA tetraplex (UGGGGU)(4) with divalent Sr(2+) ions at subatomic resolution (0.61 A). Proc.Natl.Acad.Sci.USA 2001, 98, 13665 - 13670.

75. Ditchfield, R. Self-consistent perturbation theory of diamagnetism. I. A gage-invariant LCAO (linear combination of atomic orbitals) method for NMR chemical shifts, Mol. Physics., 1974, 27, 789-807.

76. Duffy S.J. and Keaney J.F, Jr., Holbrook M., et al. Short- and long-term black tea consumption reverses endothelial dysfunction in patients with coronary artery disease. Circulation. 2001, 104(2), 151-156.

77. Duffy S.J. and Vita J.A. Effects of phenolics on vascular endothelial function. Curr Opin Lipidol. 2003, 14(1), 21-27.

78. Duffy S.J., Vita J.A., Holbrook M., Swerdloff P.L. and Keaney J.F., Jr. Effect of acute and chronic tea consumption on platelet aggregation in patients with coronary artery disease. Arterioscler Thromb Vasc Biol. 2001, 21(6), 1084-1089.

79. Dugas, A.J., Jr, Castaneda-Acosta, J., Bonin, G.C., Price, K.L., Fischer N.H. and Winston, G.W. Evaluation of the total peroxyl radical-scavenging capacity of flavonoids: structure-activity relationships, J. Nat. Products, 2000, 63, 327-331.

80. Engelhart M.J., Geerlings M.I., Ruitenberg A., et al. Dietary intake of antioxidants and risk of Alzheimer disease. JAMA. 2002, 287(24), 3223-3229

81. Engler M.B., Engler M.M., Chen C.Y., et al. Flavonoid-rich dark chocolate improves endothelial function and increases plasma epicatechin concentrations in healthy adults. J Am Coll Nutr. 2004, 23(3), 197-204.

82. Evstigneev, M.P., Khomich, V.V., and Davies, D.B. Complexation of anthracycline drugs with DNA in the presence of caffeine. Eur. Biophys. J., 2006b, 36, 1.

83. Evstigneev, M.P., Khomich, V.V., and Davies, D.B. Self-Association of Daunomycin Antibiotic in Various Buffer Solutions. Russ. J. Phys. Chem., 2006a, 80, 741.

84. Evstigneev., M.P., Rozvadovskaya., A.O., Hernandez Santiago., A.A., Mukhina., Yu.V., Veselkov., K.A., Rogova., O.V., Davies., D.B. et al. ^{1}H NMR study of the association of caffeine with flavine mononucleotide in aqueous solutions, Russ. J. Phys. Chem., 2005, 79, 573-578.

85. Exarchou, V., Troganis, A., Gerothanassis, I.P., Tsimidou, M. and Boskou, D. Do strong intramolecular hydrogen bonds persist in aqueous solution? Variable temperature gradient ^{1}H, ^{1}H-^{13}C GE-HSQC and GE-HMBC NMR studies of

flavonols and flavones in organic and aqueous mixtures, Tetrahedron, 2002, 58, 7423-7429.

86. Faska, N., Auhmani, A. and Esseffar, M. Solvent effects on 13C and 1H NMR shielding of cyclic ketones: An experimental and theoretical study, J. Mol. Struc., 2007, 811, 203-213.

87. Favier A., Blackledge M., Simorre J.P., Crouzy S, Dabouis V., Gueiffier A., Marion D. and Debouzy JC (2001). Solution Structure of 2-(Pyrido [1, 2-e] purin-4-yl) amino-ethanol Intercalated in the DNA Duplex d (CGATCG)$_2$. Biochemistry, 30: 8717-8726.

88. Ferry D.R., Smith A., Malkhandi J., et al. Phase I clinical trial of the flavonoid quercetin, pharmacokinetics and evidence for in vivo tyrosine kinase inhibition. Clin. Cancer Res. 1996, 2(4), 659-668.

89. Fielding., L. Determination of Association Constants (K_a) from Solution NMR Data, Tethrahedron, 2000, 56, 6151-6170.

90. Frederick C.S and Hurley L.H.31P NMR as a probe for drug nucleic acid interactions. Phosphorus, sulfur and silicon, 1999, 144, 297-300.

91. Freedman J.E. and Parker C., 3rd, Li L., et al. Select flavonoids and whole juice from purple grapes inhibit platelet function and enhance nitric oxide release. Circulation. 2001, 103(23), 2792-2798.

92. Freese R., Vaarala O., Turpeinen A.M. and Mutanen M. No difference in platelet activation or inflammation markers after diets rich or poor in vegetables, berries and apple in healthy subjects. Eur J Nutr. 2004, 43(3), 175-182.

93. Frei B. and Higdon J.V. Antioxidant activity of tea polyphenols in vivo, evidence from animal studies. J Nutr., 2003, 133(10), 3275S-3284S.

94. Frisch, M.J., Trucks, G.W., Schlegel, H.B., Scuseria, G.E., Robb, M.A., Cheeseman, J.R., Zakrzewski, V.G., Jr., Montgomery, J.A., Stratmann, R.E., Burant, J.C., Dapprich, S., Millam, J.M., Daniels, A.D., Kudin, K.N., Strain, M.C., Farkas, O., Tomasi, J., Barone, V., Cossi, M., Cammi, R., Mennucci, B., Pomelli, C., Adamo, C., Clifford, Ochterski, S., Petersson, J., Ayala, G.A., Cui, P.Y., Morokuma, Q., Rega, K., Salvador, N.P., Dannenberg, J.J., Malick, D.K., Rabuck, A.D., Raghavachari, K., Foresman, J.B., Cioslowski, J., Ortiz, J.V., Baboul, A.G., Stefanov, A.G., Liu, A.G., Liashenko, G., Piskorz, A., Komaromi, P., Gomperts, I., Martin, R., Fox, R.L., Keith, D.J., Al-Laham, M.A.T., Peng, C.Y., Nanayakkara, A., Challacombe, Gill, M.P.M.W., Johnson, B., Chen, W., Wong, M.W., Andreas, J.L., Gonzalez, C., Head-Gordon, M., Reploge, E.S, Po Lampert, H.J.A., Mikenda, W., Karpfen, A. and Kahlig, H. J. Phys. Chem. A, 1997, 101, 9610-9617.

95. Garcia R, Gonzalez CA, Agudo A and Riboli E. High intake of specific carotenoids and flavonoids does not reduce the risk of bladder cancer. Nutr Cancer. 1999, 35(2), 212-214

96. Garcia-Closas R, Gonzalez CA, Agudo A. and Riboli E. Intake of specific carotenoids and flavonoids and the risk of gastric cancer in Spain. Cancer Causes Control. 1999, 10(1), 71-75.

97. Garcia-Closas R., Agudo A., Gonzalez C.A. and Riboli E. Intake of specific carotenoids and flavonoids and the risk of lung cancer in women in Barcelona, Spain. Nutr Cancer. 1998, 32(3), 154-158.

98. Gavathiotis E. and Searle M.S. Structure of the parallel-stranded DNA quadruplex d(TTAGGGT)4 containing the human telomeric repeat, evidence for A-tetrad

formation from NMR and molecular dynamics simulations. ORG.BIOMOL.CHEM. 2003, 1, 1650 - 1656.

99. Gavathiotis E., Heald R.A., Stevens M.F.G. and Searle M.S. Drug Recognition and Stabilisation of the Parallel-stranded DNA Quadruplex d(TTAGGGT)4 Containing the Human Telomeric Repeat J.Mol.Biol. 2003, 334, 25 – 36.

100. Geleijnse J.M., Launer L.J., Van der Kuip D.A., Hofman A. and Witteman J.C. Inverse association of tea and flavonoid intakes with incident myocardial infarction, the Rotterdam Study. Am J Clin Nutr. 2002, 75(5), 880-886.

101. Gill M.L., Strobel S.A. and Loria J.P. Crystallization and characterization of the thallium form of the Oxytricha nova G-quadruplex. Nucleic Acids Res., 2006, 34, 4506 - 4514.

102. Gill M.L., Strobel S.A. and Loria J.P. Tl NMR methods for the characterization of monovalent cation binding to nucleic acids J.Am.Chem.Soc. 2005, 127, 16723 - 16732.

103. Goldbohm R.A., Hertog M.G., Brants HA, van Poppel G. and van den Brandt P.A. Consumption of black tea and cancer risk, a prospective cohort study. J Natl Cancer Inst. 1996, 88(2), 93-100.

104. Goldbohm R.A., Van den Brandt P.A., Hertog M.G., Brants H.A. and Van Poppel G. Flavonoid intake and risk of cancer, a prospective cohort study. Am J Epidemiol. 1995, 41, 561.

105. Gorenstein DG. ^{31}P NMR of DNA. Methods in enzymology, 1992, 211: 254-286.

106. Goyarzu P., Malin D.H., Lau F.C., et al. Blueberry supplemented diet, effects on object recognition memory and nuclear factor-kappa B levels in aged rats. Nutr Neurosci. 2004, 7(2), 75-83

107. Gu L., Kelm M.A., Hammerstone J. F., et al. Concentrations of proanthocyanidins in common foods and estimations of normal consumption. J Nutr. 2004, 134(3), 613-617

108. Gunther U.L., Ludwig C. and Ruterjans H. NMRLAB-Advanced NMR data processing in MATLAB. J. Magn. Reson., 2000, 145, 201.

109. Guo J.Y., Li X., Browning J. D., Jr., et al. Dietary soy isoflavones and estrone protect ovariectomized ERalphaKO and wild-type mice from carcinogen-induced colon cancer. J Nutr. 2004, 134(1), 179-182. .

110. Gupta G., Garcia A.E., Guo Q., Lu M. and Kallenbach N.R. Biochemistry, 1993, 32, 7098–7103.

111. Gupta S., Hastak K., Ahmad N., Lewin J.S. and Mukhtar H. Inhibition of prostate carcinogenesis in TRAMP mice by oral infusion of green tea polyphenols. Proc Natl Acad Sci U S A. 2001, 98(18), 10350-10355. .

112. Haddad A.Q., Venkateswaran V., Viswanathan L., Teahan S.J., Fleshner N.E. and Klotz L.H. Novel antiproliferative flavonoids induce cell cycle arrest in human prostate cancer cell lines. Prostate Cancer Prostatic Dis. 2006, 9(1), 68-76

113. Haenen, G.R., Paquay, J.B., Korthouwer, R.E. and Bast, A. Peroxynitrite scavenging by flavonoids, Biochem. Biophys. Res. Commun., 1997, 236, 591-593.

114. Hagiwara, S.I., Ishii, Y. and Kitamura, S. Aerosolized administration of N-acetylcysteine attenuates lung fibrosis induced by bleomycin in mice, Am. J. Respir. Crit. Care Med., 2000, 162, 225-231,

115. Haider S., Parkinson G.N. and Neidle S. Crystal structure of the potassium form of an Oxytricha nova G-quadruplex. J.Mol.Biol., 2003, 320, 189 - 200.

116. Haider S.M., Parkinson G.N. and Neidle S. Structure of a G-quadruplex-Ligand Complex J.Mol.Biol., 2003, 326, 117 - 125.

117. Han, F.X.G., Wheelhouse, R.T. and Hurley, L.H. Interactions of TMPyP4 and TMPyP2 with quadruplex DNA. Structural basis for the differential effects on telomerase inhibition. J. Am. Chem. Soc., 1999, 121, 3561–3570.

118. Hazel P., Parkinson G.N. and Neidle S. Topology variation and loop structural homology in crystal and simulated structures of a bimolecular DNA quadruplex. J.Am.Chem.Soc., 2006, 128, 5480 - 5487.

119. Heijnen C.G., Haenen G.R., van Acker F.A., van der Vijgh W.J. and Bast A. Flavonoids as peroxynitrite scavengers, the role of the hydroxyl groups. Toxicol In Vitro. 2001, 15(1), 3-6.

120. Hendler S.S., Rorvik D.R., eds. PDR for Nutritional Supplements. Montvale, Medical Economics Company, Inc, 2001

121. Henning S.M., Fajardo-Lira C., Lee H.W., Youssefian A.A., Go V. L. and Heber D. Catechin content of 18 teas and a green tea extract supplement correlates with the antioxidant capacity. Nutr Cancer. 2003, 45(2), 226-235

122. Hertog M.G, Feskens E.J. and Kromhout D. Antioxidant flavonols and coronary heart disease risk. Lancet. 1997, 349(9053), 699.

123. Hertog M.G., Feskens E.J., Hollman P.C., Katan M.B. and Kromhout D. Dietary flavonoids and cancer risk in the Zutphen Elderly Study. Nutr Cancer. 1994, 22(2), 175-184

124. Hertog M.G., Sweetnam P.M., Fehily A.M., Elwood P.C. and Kromhout D. Antioxidant flavonols and ischemic heart disease in a Welsh population of men, the Caerphilly Study. Am J Clin Nutr. 1997, 65(5), 1489-1494.

125. Higdon J.V and Frei B. Tea catechins and polyphenols, health effects, metabolism, and antioxidant functions. Crit Rev Food Sci Nutr. 2003, 43(1), 89-143.

126. Hirvonen T., Pietinen P., Virtanen M., et al. Intake of flavonols and flavones and risk of coronary heart disease in male smokers. Epidemiology. 2001, 12(1), 62-67.

127. Hirvonen T., Virtamo J., Korhonen P., Albanes D. and Pietinen P. Intake of flavonoids, carotenoids, vitamins C and E, and risk of stroke in male smokers. Stroke. 2000, 31(10), 2301-2306.

128. Hodgson J.M., Puddey I.B., Burke V., Beilin L.J., Mori T.A. and Chan S.Y. Acute effects of ingestion of black tea on postprandial platelet aggregation in human subjects. Br J Nutr. 2002, 87(2), 141-145

129. Hodgson J.M., Puddey I.B., Burke V., Watts G.F. and Beilin L.J. Regular ingestion of black tea improves brachial artery vasodilator function. Clin Sci (Lond). 2002, 102(2), 195-201.

130. Horvath M.P. and Schultz S.C. DNA G-quartets in a 1.86 A resolution structure of an Oxytricha nova telomeric protein-DNA complex. J.Mol.Biol. 2001, 310, 367 - 377.

131. Hosur R.V., Sheth A, Chary K.V.R., Ravikumar M., Govil G., Tan zu-kun and Miles H.T. A novel loop structure observed in d-GAATTCCCGAATTC by 2D NMR., 1986, Biochem. Biophys. Res. Commun. 139, 1224-1232.

132. Hou Z, Lambert J.D., Chin K.V. and Yang C.S. Effects of tea polyphenols on signal transduction pathways related to cancer chemoprevention. Mutat Res. 2004, 555(1-2), 3-19.

133. Hounsou C., Guittat L., Monchaud D., Jourdan M., Saettel N., Mergny J.L. and Teulade-Fichou, M. G-Quadruplex Recognition by Quinacridines, a SAR, NMR, and Biological Study ChemMedChem , 2007, 2, 655 - 666.

134. Huang M.T., Xie J. G., Wang Z.Y., et al. Effects of tea, decaffeinated tea, and caffeine on UVB light-induced complete carcinogenesis in SKH-1 mice, demonstration of caffeine as a biologically important constituent of tea. Cancer Res. 1997, 57(13), 2623-2629

135. Huang, C.Z., Li, Y.F. and Feng, P. A spectrophotometric study on the interaction of neutral red with double-stranded DNA in large excess, Talanta, 2001, 55, 321–328.

136. Hubbard G.P., Wolffram S., Lovegrove J.A. and Gibbins J.M. The role of polyphenolic compounds in the diet as inhibitors of platelet function. Proc Nutr Soc. 2003, 62(2), 469-478.

137. Hurley, L.H. DNA and its associated processes as targets for cancer therapy, Nat. Rev. Cancer, 2002, 2, 188–200.

138. Hurrell R. F., Reddy M. and Cook J. D. Inhibition of non-haem iron absorption in man by polyphenolic-containing beverages. Br. J. Nutr. 1999, 81(4), 289-295

139. Innes A.J., Kennedy G., McLaren M., Bancroft A.J. and Belch J.J. Dark chocolate inhibits platelet aggregation in healthy volunteers. Platelets. 2003, 14(5), 325-327

140. Jangaz, K.H., Saeed, S.A. and Gilani, A.H. Protective effect of rutin on paracetamol- and CCl4-induced hepatotoxicity in rodents, Fitoterapia 2002, 73, 557–563.

141. Janssen K., Mensink R.P., Cox F.J., et al. Effects of the flavonoids quercetin and apigenin on hemostasis in healthy volunteers, results from an in vitro and a dietary supplement study. Am J Clin Nutr. 1998, 67(2), 255-262

142. Jatoi A, Ellison N, Burch P.A., et al. A phase II trial of green tea in the treatment of patients with androgen independent metastatic prostate carcinoma. Cancer. 2003, 97(6), 1442-1446

143. Javaid A. and Bonkovsky H.L. Hepatotoxicity due to extracts of Chinese green tea (Camellia sinensis), a growing concern. J Hepatol. 2006, 45(2), 334-335.

144. Jin, G.-Z., Tomita K.I. and Yamagata, Y. Structure of Rutin Pentamethanol, Chem. Pharm. Bull., 1990, 38, 297-300.

145. Jin, G.Z., Yamagata, Y. and Tomita, K.I., Structure of quercetin dehydrate, Acta Crystallogr., C46, 310-313.

146. Johnson C.S. In *Encyclopedia of Nuclear Magnetic Resonance*, vol. 3, Grant DM, Harris RK (eds). John Wiley & Sons: Chichester, 1996, 1626–1644.

147. Johnson., C.S. Diffusion ordered nuclear magnetic resonance spectroscopy: principles and applications Prog. Nucl. Magn. Reson. Spectrosc., 1999, 34, 203-256.

148. Joseph J.A., Denisova N.A., Arendash G., et al. Blueberry supplementation enhances signaling and prevents behavioral deficits in an Alzheimer disease model. Nutr Neurosci. 2003, 6(3), 153-162

149. Joseph J.A., Shukitt-Hale B., Denisova N.A., et al. Reversals of age-related declines in neuronal signal transduction, cognitive, and motor behavioral deficits with blueberry, spinach, or strawberry dietary supplementation. J Neurosci. 1999, 19(18), 8114-8121

150. Joshi B.S., Singh K.L. and Raja R. An approach for complete assignments of 1H and 13C NMR spectra of pentacyclic triterpene. Magn. Reson. Chem., 1999, 37, 295.

151. Jovanovic, S.V.; Jankovic, I. and Josimovic, L. Electron-transfer reactions of alkyl peroxy radicals. J. Am. Chem. Soc., 1992, 114, 9018-9022.

152. Joyeux, M., Rolland, A., Fleurentin, J., Mortier, F. and Dorfman, P. *tert*-Butyl-hydroperoxide-induced injury in isolated rat hepatocytes: a model for studying anti hepatotoxic crude drugs. Planta Med., 1990, 56, 171–174.

154. Kanakis *et al.,* J. Biomol. Struct. Dyn., 2005, 22, 719–724.

155. Kanakis, C.D., Tarantilis, P.A., Pollisiou, M.G. and Tajmir-Riahi. H. Interaction of Antioxidant Flavonoids with tRNA, Intercalation or External Binding and Comparison with Flavonoid-DNA Adducts. DNA and Cell Biology., 2006, 25(2), 116–123.

156. Kandaswami, C. and Middleton Jr, E. The effects of the bioflavonoid quercetin on squamous cell carcinoma of head and neck origin, Am. J. Surg., 1989, 158, 361- 366.

157. Kapur., G.S., Cabrita., E.J. and Berger., S. The qualitative probing of hydrogen bond strength by diffusion-ordered NMR spectroscopy, Tetrahedron Lett., 2000, 41, 7181-7185.

158. Kavanagh K.T., Hafer L.J., Kim D.W., et al. Green tea extracts decrease carcinogen-induced mammary tumor burden in rats and rate of breast cancer cell proliferation in culture. J Cell Biochem. 2001, 82(3), 387-398.

159. Keefe., D.L. Anthracycline-induced cardiomyopathy, Semin. Oncol., 2001, 4, 2–7.

160. Keevil J.G., Osman H.E., Reed J.D. and Folts J.D. Grape juice, but not orange juice or grapefruit juice, inhibits human platelet aggregation. J Nutr. 2000, 130(1), 53-56

161. Keizer et al., 1990 H.G. Keizer, H.M. Pinedo, G.J. Schuurhuis and H. Joenje, Doxorubicin (adriamycin): a critical review of free radical-dependent mechanisms of cytotoxicity, Pharmacol. Ther., 1990, 47, 219–231.

162. Keli S.O., Hertog M.G., Feskens E.J. and Kromhout D. Dietary flavonoids, antioxidant vitamins, and incidence of stroke, the Zutphen study. Arch Intern Med. 1996, 156(6), 637-642.

163. Kellis Jr., J.T. and Vickery, L.E. Inhibition of human estrogen synthetase (aromatase) by flavones. Science. 1984, 225, 1032–1034

164. Keniry M.A., Strahan G.D., Owen E.A. and Shafer R.H. Solution structure of the Na+ form of the dimeric guanine quadruplex [d(G3T4G3)]2. Eur.J.Biochem. 1995, 233, 631 - 643

165. Keniry., M.A. Quadruplex structures in nucleic acids, Biopolymers, 2001, 56, 123–146

166. Keresztes., I. and Williard, P.G. Diffusion-Ordered NMR Spectroscopy (DOSY) of THF Solvated *n*-Butyllithium Aggregates, J. Am. Chem. Soc., 2000, 122, 10228-10229.

167. Kettani A., Basu G., Gorin A., Majumdar A., Skripkin E., Patel D.J. A two-stranded template-based approach to G.(C-A) triad formation, designing novel structural elements into an existing DNA framework. J.Mol.Biol. 2000, 301, 129 - 134.

168. Kettani A., Bouaziz S., Gorin A., Zhao H., Jones R.A. Patel D.J. Solution structure of a Na cation stabilized DNA quadruplex containing G.G.G.G and G.C.G.C tetrads formed by G-G-G-C repeats observed in adeno-associated viral DNA. J.Mol.Biol. 1998, 282, 619 - 636.

169. Kettani A., Bouaziz S., Wang W., Jones R.A. and Patel D.J. Bombyx mori single repeat telomeric DNA sequence forms a G-quadruplex capped by base triads. Nat.Struct.Biol. 1997, 4, 382 - 389.

170. Kettani A., Gorin A., Majumdar A., Hermann T., Skripkin E., Zhao H., Jones R., Patel D.J. A dimeric DNA interface stabilized by stacked A.(G.G.G.G).A hexads and coordinated monovalent cations. J.Mol.Biol. 2000, 297, 627 - 644.

171. Kettani A., Kumar A. and Patel D. J. J. Mol. Biol., 1995, 254, 638–656.

172. Khetrapal, C.L., Kunwar, A.C., Tracey, A.S. and Diehl P.; Nuclear Magnetic Resonance Studies in Lyotropic Liquid Crystals, NMR: Basic Principles and Progress, 9, 1975, Berlin-Heidelberg-New York, Springer.

173. Kim M. H. Flavonoids inhibit VEGF/bFGF-induced angiogenesis in vitro by inhibiting the matrix-degrading proteases. J Cell Biochem. 2003, 89(3), 529-538.

174. Knekt P., Isotupa S., Rissanen H., et al. Quercetin intake and the incidence of cerebrovascular disease. Eur J Clin Nutr. 2000, 54(5), 415-417.

175. Knekt P., Kumpulainen J., Jarvinen R., et al. Flavonoid intake and risk of chronic diseases. Am J Clin Nutr. 2002, 76(3), 560-568.

176. Kohno H., Tanaka T., Kawabata K., Hirose Y., Sugie S., Tsuda H. and Mori H. Silymarin, a naturally occurring polyphenolic antioxidant flavonoid, inhibits azoxymethane-induced colon carcinogenesis in male F344 rats. International Journal of Cancer. 2002, 101, 461–468.

177. Kondo J., Adachi W., Umeda S., Sunami T. and Takenaka A. Crystal structures of a DNA octaplex with I-motif of G-quartets and its splitting into two quadruplexes suggest a folding mechanism of eight tandem repeats Nucleic Acids Res. 2004, 32, 2541 - 2549.

178. Kong A.N., Owuor E., Yu R., et al. Induction of xenobiotic enzymes by the MAP kinase pathway and the antioxidant or electrophile response element (ARE/EpRE). Drug Metab Rev. 2001, 33(3-4), 255-271.

179. Konrat., R.; Tollinger., M.; Kontaxis., G. and Kräutler., B. NMR Techniques to Study Hydrogen Bonding in Aqueous Solution, Monatsh. Chem., 1999, 130, 961-982.

180. Kotovych, J.W. Lown, J and P.K. Tong, High field ^{1}H and ^{31}P NMR studies on the binding of the anticancer agent mitoxantrone to d–(CpGpApTpCpG)$_2$, J. Biomol. Struct. Dyn., 1986, 4, 111–125.

181. Kreijkamp-Kaspers S., Kok L., Grobbee D.E., et al. Effect of soy protein containing isoflavones on cognitive function, bone mineral density, and plasma lipids in postmenopausal women, a randomized controlled trial. JAMA. 2004, 292(1), 65-74

182. Krishna, A.G., Kumar, D.V., Khan, B.M., Rawal, S.K. and Ganesh, K.N. Taxol–DNA interactions, fluorescence and CD studies of DNA groove binding properties of taxol, Biochim. Biophys. Acta, 1998, 1381, 104–112.

183. Kroon P.A., Clifford M.N., Crozier A, et al. How should we assess the effects of exposure to dietary polyphenols in vitro? Am J Clin Nutr., 2004, 80(1),15-21.

184. Kumari G.N.K. Rao L.J.M.and Rao N.S.P.Chem. Sci.1986, 97, 171.

185. Kupka, T.; Pasterna, G.; Jaworska, M.; Karali, A. and Photis, D. GIAO NMR calculations for carbazole and its N-methyl and N-ethyl derivatives. Comparison of theoretical and experimental 13C chemical shifts, Magn. Reson. Chem., 2000, 38, 149-155.

186. Kupka, T.; Pasterna, G.; Lodowski, P. and Szeja, W. GIAO-DFT prediction of accurate NMR parameters in selected glucose derivatives, Magn. Reson. Chem., 1999, 37, 421-426.

187. Kuryavyi V., Majumdar A., Shallop A., Chernichenko N., Skripkin E., Jones R. Patel D.J. A double chain reversal loop and two diagonal loops define the architecture of a unimolecular DNA quadruplex containing a pair of stacked G(syn)-G(syn)-G(anti)-G(anti) tetrads flanked by a G-(T-T) Triad and a T-T-T triple. J.Mol.Biol. 2001, 310, 181 - 194.

188. Lambert J.D and Yang C.S. Mechanisms of cancer prevention by tea constituents. J Nutr. 2003, 133(10), 3262S-3267S.

189. Lagiou P, Samoli E, Lagiou A, et al. Flavonoids, vitamin C and adenocarcinoma of the stomach. Cancer Causes Control. 2004, 15(1), 67-72. :

190. Lallemand J.Y. and Duteil M. Organic Magnetic Resonance, 1977, 9, 179.

191. Lancker, M.V. and Gheyssens, L.C. A comparison of 4 frequently used assays for quantitative-determination of DNA, Anal. Lett., 1986, 19, 615– 623.

192. Laughlan G., Murchie A.I., Norman D.G., Moore M.H., Moody P.C., Lilley D.M. and Luisi, B. The high-resolution crystal structure of a parallel-stranded guanine tetraplex. Science. 1994, 265, 520 - 524.

193. Laurin D., Masaki K.H., Foley D.J., White L.R. and Launer L.J. Midlife dietary intake of antioxidants and risk of late-life incident dementia, the Honolulu-Asia Aging Study. Am J Epidemiol. 2004, 159(10), 959-967

194. Lee H. S. Characterization of major anthocyanins and the color of red-fleshed Budd Blood orange (Citrus sinensis). J Agric Food Chem. 2002, 50(5), 1243-1246

195. Lee M. P. H., Haider, S., Parkinson, G. N., Neidle, S. Crystal structure of D(G4T4G4) with four and six quadruplexes in the asymmetric unit. To be Published.

196. Lee M.P., Parkinson G.N., Hazel P. and Neidle S. Observation of the coexistence of sodium and calcium ions in a DNA G-quadruplex ion channel. J. Am. Chem. Soc., 2007, 129, 10106 - 10107.

197. Lee, W.Y. and Parr, R.G. Development of the Colle-Salvetti correlation-energy formula into a functional of the electron density, Phys. Rev. B. 37 (1988) 785-789.

198. Lenz T., Bonnist E.Y.M., Pljevaljčić G. Neely R.K, Dryden D.T.F., Scheidig A.J., Jones A.C., Weinhold E. 2-Aminopurine flipped into the active site of the adenine-

specific DNA methyltransferase M. Taq I: crystal structures and time-resolved fluorescence, J. Am. Soc., 2007, 129, 6240–6248.

199. Leopoldini M., Marino T., Russo N. and Toscano M. Theor. Chem. Acc., 2004, 111, 210.

200. Leopoldini M., Pitarch I.P., Russo N. and Toscano M. J. Phys. Chem. A, 2004, 108, 92.

201. Letenneur L., Proust-Lima C., Le Gouge A., Dartigues J.F. and Barberger-Gateau P. Flavonoid intake and cognitive decline over a 10-year period. Am J Epidemiol. 2007, 165(12), 1364-1371

202. Li Z. G., Shimada Y., Sato F., et al. Inhibitory effects of epigallocatechin-3-gallate on N-nitrosomethylbenzylamine-induced esophageal tumorigenesis in F344 rats. Int J Oncol. 2002, 21(6), 1275-1283

203. Li, W., Zhang, M., Zhang, J., Li, H., Zhang, X., Sun, Q. and Qiu, C. Interactions of diadzin with intramolecular G-quadruplex. FEBS Letters, 2006, 580, 4905-4910.

204. Lin J., Rexrode K.M., Hu F., et al. Dietary intakes of flavonols and flavones and coronary heart disease in US women. Am J Epidemiol. 2007, 165(11),1305-1313.

205. Lin, C.H. and Patel, D. Solution structure of the covalent duocarmycin A–DNA duplex complex, J. Mol. Biol., 1995, 248, 162–179.

206. Liu H., Matsugami A., Katahira M. and Uesugi, S. A Dimeric RNA Quadruplex Architecture Comprised of Two G,G(,A),G,G(,A) Hexads, G,G,G,G Tetrads and UUUU Loops J.Mol.Biol., 2002, 322, 955 - 970.

207. Liu R.H. Health benefits of fruit and vegetables are from additive and synergistic combinations of phytochemicals. Am J Clin Nutr. 2003, 78(3 Suppl), 517S-520S.

208. Liu, J., Qui, L., Gao, J., Jin, Y.,. Preparation, characterization and in vivo evaluation of formulation of baicalein with hydroxypropyl-_-cyclodextrin. Int. J. Pharm. 2006, 312, 137–143

209. Loftsson, T. and Duchene, D. Cyclodextrins and their pharmaceutical applications, Int. J. Pharm., 2007, 329, 1–11.

210. Lotito S.B. and Frei B. Consumption of flavonoid-rich foods and increased plasma antioxidant capacity in humans, cause, consequence, or epiphenomenon? Free Radic Biol Med. 2006, 41(12), 1727-1746.

211. Lown J.W. and Hanstock C.C. (1985). High field 1H-NMR analysis of the 1: 1 intercalation complex of the antitumor agent mitoxantrone and the DNA duplex [d (CpGpCpG)]. J Biomol Struct Dyn 2, 6: 1097.

212. Ludwig A, Lorenz M, Grimbo N, et al. The tea flavonoid epigallocatechin-3-gallate reduces cytokine-induced VCAM-1 expression and monocyte adhesion to endothelial cells. Biochem Biophys Res Commun. 2004, 316(3), 659-665.

213. Lupu, R. and Menendez, J.A. Pharmacological inhibitors of Fatty Acid Synthase (FASN)--catalyzed endogenous fatty acid biogenesis: a new family of anti-cancer agents, Curr. Pharm. Biotechnol. 2006, 7, 483-493.

214. Luu K.N., Phan A.T., Kuryavyi V.V., Lacroix L. and Patel D.J. Structure of the human telomere in k(+) solution, an intramolecular (3 + 1) g-quadruplex scaffold. J.Am.Chem.Soc., 2006, 128, 9963 - 9970.

215. Manach C, Scalbert A, Morand C,. Remesy C. and Jimenez L. Polyphenols, food sources and bioavailability. Am J Clin Nutr., 2004, 79(5),727-747.

216. Manach C, Williamson G, Morand C, Scalbert A and Remesy C. Bioavailability and bioefficacy of polyphenols in humans. I. Review of 97 bioavailability studies. Am J Clin Nutr., 2005, 81(1 Suppl), 230S-242S.

217. Mao X., Marky L.A. and Gmeiner W.H. NMR structure of the thrombin-binding DNA aptamer stabilized by Sr2+. J.Biomol.Struct.Dyn., 2004, 22, 25 - 33.

218. Marathias V.M. and Bolton P.H. Structures of the potassium-saturated, 2,1, and intermediate, 1,1, forms of a quadruplex DNA. Nucleic Acids Res. 2000, 28, 1969 - 1977.

219. Marathias V.M., Wang K.Y., Kumar S., Pham T.Q., Swaminathan S. and Bolton P.H. Determination of the number and location of the manganese binding sites of DNA quadruplexes in solution by EPR and NMR in the presence and absence of thrombin. J.Mol.Biol. 1996, 260, 378 - 394.

220. Marinic, M., Piantanida, I., Rusak, G. and Zinic, M. Interactions of quercetin and its lanthane complex with double stranded DNA/RNA and single stranded RNA, Spectrophotometric sensing of poly G. J. Inorg. Biochem., 2006, 100, 288–298.

221. Markham K.R. and Chari V.M. In, Harborne, J.B., Mabry, T.J. (Eds.), Chapman and Hall, London, UK, 1982, pp. 19–134.

222. Markham K.R. ^{13}C NMR of flavonoids Tetrahedron, 1977, 34, 1389-1397.

223. Martin-Arag´on, S., De Las Heras, B., Sanchez-Reus, M.I. and Benedi, J. Pharmacological modification of endogenous antioxidant enzymes by ursolic acid on tetrachloride-induced liver damage in rats and primary cultures of rat hepatocytes, Exp. Toxicol. Pathol., 2001, 53, 199–206.

224. Martino L., Virno A., Pagano B., Virgilio A., Di Micco S., Galeone A., Giancola C., Bifulco G., Mayol L. and Randazzo A. Structural and thermodynamic studies of the

interaction of distamycin A with the parallel quadruplex structure [d(TGGGGT)]4 J.Am.Chem.Soc. , 2007, 129, 16048 - 16056.

225. Martino L., Virno A., Randazzo A., Virgilio A., Esposito V., Giancola C., Bucci M., Cirino G. and Mayol L. A new modified thrombin binding aptamer containing a 5'-5' inversion of polarity site. Nucleic Acids Res., 2006, 34, 6653 - 6662.

226. Marzolini C., Paus E., Buclin T. and Kim R. B. Polymorphisms in human MDR1 (P-glycoprotein), recent advances and clinical relevance. Clin. Pharmacol. Ther. 2004, 75(1), 13-33

227. Matsugami A., Okuizumi T., Uesugi S. and Katahira M. Intramolecular Higher Order Packing of Parallel Quadruplexes Comprising a G,G,G,G Tetrad and a G(,A),G(,A),G(,A),G Heptad of GGA Triplet Repeat DNA J.BIOL.CHEM. 2003, 278, 28147 - 28153.

228. Matsugami A., Ouhashi K., Kanagawa M., Liu H., Kanagawa S., Uesugi S. and Katahira, M. An intramolecular quadruplex of (GGA)(4) triplet repeat DNA with a G,G,G,G tetrad and a G(,A),G(,A),G(,A),G heptad, and its dimeric interaction. J.Mol.Biol. 2001, 313, 255 - 269.

229. Matsugami A., Xu Y., Noguchi Y., Sugiyama H. and Katahira M. Structure of a human telomeric DNA sequence stabilized by 8-bromoguanosine substitutions, as determined by NMR in a K+ solution Febs J., 2007, 274, 3545 - 3556.

230. Mazzini S, Bellucci MC and Mondelli R. Mode of binding of the cytotoxic alkaloid berberine with the double helix oligonucleotide d-(AAGAATTCTT)$_2$. Bioorg Med Chem, 2003, 11, 4: 505-514.

231. Mazzini S, Mondelli R and Ragg E. Structure and dynamics of intercalation complexes of anthracyclines with d $(CGATCG)_2$ and d $(CGTACG)_2$. 2D-^{1}H and ^{31}P NMR investigations. J Chem Soc Pak 2 1998, 9: 1983-1992.

232. Middleton Jr., E., Kandaswami, C., Theoharides, T.C. The effects of plant flavonoids on mammalian cells, implications for inflammation, heart disease, and cancer. Pharmacological Reviews. 2000, 52, 673–751.

233. Mink P.J., Scrafford C.G., Barraj L.M., et al. Flavonoid intake and cardiovascular disease mortality, a prospective study in postmenopausal women. Am J Clin Nutr. 2007, 85(3), 895-909.

234. Mira L, Fernandez M.T., Santos M, Rocha R, Florencio M.H. and Jennings KR. Interactions of flavonoids with iron and copper ions, a mechanism for their antioxidant activity. Free Radic Res., 2002, 36(11), 1199-1208.

235. Mora, A., Paya, M., Rios, J.L. and Alcaraz, M.J. Structure-activity relationships of polymethoxyflavones and other flavonoids as inhibitors of nonenzymic lipid Peroxidation, Biochem. Pharmacol. 1990, 40, 793-797.

236. Moyer R. A., Hummer K. E., Finn C. E., Frei B. and Wrolstad R. E. Anthocyanins, phenolics, and antioxidant capacity in diverse small fruits, vaccinium, rubus, and ribes. J Agric Food Chem. 2002, 50(3), 519-525

237. Murphy K.J., Chronopoulos A.K., Singh I., et al. Dietary flavanols and procyanidin oligomers from cocoa (Theobroma cacao) inhibit platelet function. Am J Clin Nutr. 2003, 77(6), 1466-1473

238. Nickavar B., Amin G. and Mehregan N. Iranian Journal of Pharmaceutical Research, 2003, 249.

239. Nielsen J.T., Arar K. and Petersen M. NMR solution structures of LNA (locked nucleic acid) modified quadruplexes. Nucleic Acids Res., 2006, 34, 2006 - 2014.

240. Nissler, L.; Gebhardt, R. and Berger, S. Flavonoid binding to a multi-drug-resistance transporter protein: an STD-NMR study Anal. Bioanal. Chem., 2004, 379, 1045-1049.

241. Novak, R.F. and Kharasch, E.D. Mitoxantrone: Propensity for free radical formation and lipid peroxidation-implications for cardiotoxicity. Invest. New Drugs, 1985, 3, 95-99.

242. O'Leary K.A, de Pascual-Tereasa S, Needs P.W., Bao Y.P., O'Brien N. M. and Williamson G. Effect of flavonoids and vitamin E on cyclooxygenase-2 (COX-2) transcription. Mutat Res. 2004, 551(1-2), 245-254.

243. Olejniczak S. and Potrzebowski M.J. Solid state NMR studies and densiy functional theory (DFT) calculations of conformers of quercetin. Org. Biomol. Chem. 2004, 2, 2315.

244. Owen, R.W., Haubner, R., Mier, W., Giacosa, A., Hull, W.E., Spiegelhalder, B. and Bartsch, H. Isolation, structure elucidation and antioxidant potential of the major phenolic and flavonoid compounds in brined olive drupes, Food Chem. Toxicol., 2003, 41, 703-717.

245. Padmanabhan K. and Tulinsky A. An ambiguous structure of a DNA 15-mer thrombin complex. Acta Crystallogr.,Sect.D 1996, 52, 272 - 282,.

246. Pan B., Shi K. and Sundaralingam, M. Crystal structure of an RNA quadruplex containing inosine tetrad, implications for the roles of NH_2 group in purine tetrads. J.Mol.Biol., 2006, 363, 451 - 459.

247. Pan B., Xiong Y., Shi K. and Sundaralingam M. Crystal Structure of a Bulged RNA Tetraplex at 1.1 A Resolution, Implications for a Novel Binding Site in RNA Tetraplex STRUCTURE, 2003, 11, 1423 - 1430.

248. Pan B., Xiong Y., Shi K., Deng J. and Sundaralingam M. Crystal structure of an RNA purine-rich tetraplex containing adenine tetrads, implications for specific binding in RNA tetraplexes Structure. 2003, 11, 815 – 823.

249. Pan B.C., Xiong Y., Shi K. and Sundaralingam M. An Eight-Stranded Helical Fragment in RNA Crystal Structure, Implications for Tetraplex Interaction Structure. 2003, 11, 825 - 831.

250. Pannala, A.S., Chan, T.S., O'Brien, P.J. and Rice-Evans, C.A. Flavonoid B-ring chemistry and antioxidant activity: fast reaction kinetics, Biochem. Biophys. Res. Commun., 2001, 282, 1161-1168.

251. Papas A. Diet and Antioxidants Status, In Antioxidant Status, Diet, Nutrition and Health. ed. Andreas M. Papas. CRC Press, New York. 1999, pp. 89-106.

252. Park Y.B., Moon E., Lee Y., Lee Y., Yoon J. and Ahn Y. Mag. Res. Chem. 45 (2007) 674.

253. Parkinson G. N., Cuenca F. and Neidle S., Topology Conservation and Loop Flexibility in Quadruplex-drug Recognition, Crystal Structures of Inter- and Intramolecular Telomeric DNA Quadruplex-drug Complexes, J. Mol. Biol., 2008, 381(5), 1145-1156

254. Parkinson G.N., Ghosh R. and Neidle S. Structural basis for binding of porphyrin to human telomeres, Biochemistry, 2007, 46, 2390 - 2397.

255. Parkinson G.N., Lee M.P. and Neidle S. Crystal structure of parallel quadruplexes from human telomeric DNA. Nature, 2002, 417, 876 - 880.

256. Patel DJ. d-CpCpGpG and d-GpGpCpC self-complementary duplexes: Nmr studies of the helix-coil transition. Biopolymers, 1977, 8, 1635-1656.

257. Patel DJ. Helix-coil transition of the dG-dC-dG-dC self-complementary duplex and complex formation with daunomycin in solution. Biopolymers, 1979, 3, 553-569.

258. Patel DJ. Peptide antibiotic-dinucleotide interactions. Nuclear magnetic resonance investigations of complex formation between actinomycin D and d-pGpC in aqueous solution. Biochemistry, 1974, 11, 2388-2395.

259. Patel P.K. and Hosur R.V. NMR observation of T-tetrads in a parallel stranded DNA quadruplex formed by Saccharomyces cerevisiae telomere repeats. Nucleic Acids Res. 1999, 27, 2457 - 2464.

260. Patel P.K., Bhavesh N.S. and Hosur R.V. NMR observation of a novel C-tetrad in the structure of the SV40 repeat sequence GGGCGG. Biochem.Biophys.Res.Commun. 2000, 270, 967 - 971.

261. Patel P.K., Koti A.S. and Hosur R.V. NMR studies on truncated sequences of human telomeric DNA, observation of a novel A-tetrad. Nucleic Acids Res. 1999, 27, 3836 - 3843.

262. Patel, P.K. and Hosur, R.V. NMR observation of T-tetrads in a parallel stranded DNA quadruplex formed by Saccharomyces cerevisiae telomere repeats. Nucleic Acids Res., 1999, 27, 2457 - 2464.

263. Patel, P.K., Bhavesh, N.S. and Hosur, R.V. NMR observation of a novel C-tetrad in the structure of the SV40 repeat sequence GGGCGG. Biochem.Biophys.Res.Commun., 2000, 270, 967 - 971.

264. Patil C.S., Singh V.P., Satyanarayan P.S., Jain N.K., Singh A. and Kulkarni S.K. Protective effect of flavonoids against aging- and lipopolysaccharide-induced cognitive impairment in mice. Pharmacology. 2003, 69(2), 59-67

265. Pelta., M.D., Barjat., H., Morris., G.A., Davis., A.L. and Hammond, S.J. Pulse sequences for high-resolution diffusion-ordered spectroscopy, (HR-DOSY), Magn. Reson. Chem., 1998, 36, 706-714.

266. Peterson J, Lagiou P, Samoli E, et al. Flavonoid intake and breast cancer risk, a case-control study in Greece. Br J Cancer. 2003, 89(7), 1255-1259. .

267. Peterson, G. and Barnes, S. Genistein inhibition of the growth of human breast cancer cells: independence from estrogen receptors and the multi-drug resistance gene, Biochem. Biophys. Res. Commun., 1991, 179, 661-667.

268. Phan A.T., Kuryavyi V. Gaw, H.Y. and Patel, D.J. Small-molecule interaction with a five-guanine-tract G-quadruplex structure from the human MYC promoter. Nat.Chem.Biol. 2005, 1, 167 - 173.

269. Phan A.T., Kuryavyi V.V., Burge S., Neidle S. and Patel D.J. Structure of an unprecedented G-quadruplex scaffold in the human c-kit promoter. J.Am.Chem.Soc., 2007,129, 4386 - 4392.

270. Phan A.T., Kuryavyi V.V., Ma J.B., Faure A., Andreola M.L. and Patel D.J. An interlocked dimeric parallel-stranded DNA quadruplex, A potent inhibitor of HIV-1 integrase Proc. Natl.Acad.Sci.USA, 2005, 102, 634 - 639.

271. Phillips, K., Dauter, Z., Murchie, A.I., Lilley, D.M. and Luisi, B. The crystal structure of a parallel-stranded guanine tetraplex at 0.95 A resolution. J.Mol.Biol., 1997, 273, 171 - 182.

272. Piantanida I., Mašic L. and Rusak G. Structure-spectrophotometric selectivity relationship in interactions of quercetin related flavonoids with double stranded and single stranded RNA. Journal of Molecular Structure. 2009, 924, 138–143

273. Piosik., J., Zdunek.., M. and Kapuscinski., J. The modulation by xanthines of the DNA-damaging effect of polycyclic aromatic agents. Part II. The stacking complexes of caffeine with doxorubicin and mitoxantrone, Biochem. Pharmacol., 2002, 63, 635-646.

274. Pisters K.M., Newman R.A., Coldman B., et al. Phase I trial of oral green tea extract in adult patients with solid tumors. J Clin Oncol. 2001, 19(6), 1830-1838

275. Polagruto J.A., Schramm D.D, Wang-Polagruto J.F., Lee L. and Keen C.L. Effects of flavonoid-rich beverages on prostacyclin synthesis in humans and human aortic endothelial cells, association with ex vivo platelet function. J Med Food. 2003, 6(4), 301-308

276. Pullay, P. and Hinton, J. F. Encyclopedia of Nuclear Magnetic Resonance. Willey: New York, 1995.

277. Rablen, P.R., Pearlman, S.A. and Finkbiner, J. A Comparison of Density Functional Methods for the Estimation of Proton Chemical Shifts with Chemical Accuracy, J. Phys. Chem. A., 1999, 103, 7357-7363.

278. Radi, A., Ries, M.A.E. and Kandil, S. Electrochemical study of the interaction of levofloxacin with DNA, Anal. Chim. Acta, 2003, 495, 61–67.

279. Ragg E, Mondelli R, Battistini C, Garbesi A and Colonna FP. ^{31}P NMR study of daunorubicin-d (CGTACG) complex in solution. Evidence of the intercalation sites. FEBS letters, 1988, 236, 1: 231.

280. Rajeshwari, M. R. Tryptophan Intercalation in G, C containing Polynucleotides: Z to B conversion of Poly [d(G-5MC)] in low salt induced by a tetrapeptide. J. Biomol. Struct. & Dyn., 1996, 14, 25-30.

281. Ramassamy C. Emerging role of polyphenolic compounds in the treatment of neurodegenerative diseases, a review of their intracellular targets. Eur J Pharmacol. 2006, 545(1), 51-64

282. Ramos S. Effects of dietary flavonoids on apoptotic pathways related to cancer chemoprevention. J Nutr Biochem. 2007, 18(7), 427-442.

283. Randazzo A., Esposito V., Ohlenschlager O., Ramachandran R. and Mayola L. NMR solution structure of a parallel LNA quadruplex. Nucleic Acids Res. 2004, 32, 3083 - 3092.

284. Ratty, A.K. and Das, N.P. Effects of flavonoids on nonenzymic lipid peroxidation: structure-activity relationship, Biochem. Med. Metab. Biol., 1988, 39, 69-79.

285. Rein D, Paglieroni T.G, Wun T, et al. Cocoa inhibits platelet activation and function. Am J Clin Nutr. 2000, 72(1), 30-35

286. Rein D., Paglieroni T.G., Pearson D.A., et al. Cocoa and wine polyphenols modulate platelet activation and function. J Nutr. 2000, 130 (8S Suppl), 2120S-2126S

287. Reinhardt, C.G. and Krugh, T.R. A comparative study of ethidium bromide complexes with dinucleotides and DNA, direct evidence for intercalation and nucleic acid sequence preferences, Biochemistry, 1978, 17, 4845–4854.

288. Rice L., Samedi V.G., Medrano T.A., Sweeney C.A., Baker H.V., Stenstrom A., Furman J. and Shiverick K.T. Mechanisms of the growth inhibitory effects of the isoflavonoid biochanin A on LNCaP cells and xenografts. Prostate. 2002, 52, 201–212.

289. Rice-Evans, C.A., Miller, N.J. and Paganga, G. Structure antioxidant-activity relationships of flavonoids and phenolic acids, Free Radic Biol Med., 1996, 20, 933-956.

290. Rimm E.B., Katan M.B., Ascherio A., Stampfer M.J. and Willett W.C. Relation between intake of flavonoids and risk for coronary heart disease in male health professionals. Ann Intern Med. 1996, 125(5), 384-389.

291. Robinson, H., Priebe, W., Chaires, J.B. and Wang, A.H.J. Binding of two novel bisdaunorubicins to DNA studied by NMR spectroscopy, Biochemistry, 1997, 36, 8663–8670.

292. Rogers-Sanders., S.A., Velde., D.V. and Larive., C.K. Evaluation of NMR diffusion measurements for the conformational analysis of flexible peptides, Fresenius' J. Anal. Chem,. 2001, 369, 308-312.

293. Ross J.A. and Kasum C.M. Dietary flavonoids, bioavailability, metabolic effects, and safety. Annu Rev Nutr. 2002, 22, 19-34

294. Rossi, M., Rickels, L.F. and Halpin, W.A. The crystal and molecular structure of quercetin: a biologically active and naturally occurring flavonoids, Bioorg. Chem., 1986, 14, 55-69.

295. Ryan J.M. and Revilla E. Anthocyanin composition of Cabernet Sauvignon and Tempranillo grapes at different stages of ripening. J Agric Food Chem. 2003, 51(11), 3372-3378

296. Rye, H.S., Dabora, J.M., Quesada, M.A., Mathies, R.A. and Glazer, A.N. Fluorometric assay using dimeric dyes for double- and single-stranded DNA and RNA with picogram sensitivity, Anal. Biochem., 1993, 208, 144–150.

297. Sah J. F., Balasubramanian S., Eckert R.L. and Rorke E.A. Epigallocatechin-3-gallate inhibits epidermal growth factor receptor signaling pathway. Evidence for direct inhibition of ERK1/2 and AKT kinases. J Biol Chem. 2004, 279(13), 12755-12762.

298. Sakata K, Hirose Y, Qiao Z, Tanaka T. and Mori H. Inhibition of inducible isoforms of cyclooxygenase and nitric oxide synthase by flavonoid hesperidin in mouse macrophage cell line. Cancer Lett. 2003, 199(2), 139-145.

299. Salmaso, S., Bersani, S., Semenzato, A., Caliceti, P. New cyclodextrin bioconjugates for active tumor targeting. J. Drug Target, 2007, 15, 379–390.

300. Salvayre A.N, Dousset N., Ferretti G., Bacchetti T., Curatola G. and Salvayre R., Antioxidant and cytoprotective properties of high-density lipoproteins in vascular cells Free Radical Biology and Medicine, 2006, 7, 1031-1040.

301. Scalbert, A., Williamson, G. Dietary intake and bioavailability of polyphenols. J. Nutr. 2000, 130, 2073S–2085S.

302. Scambia, G., Panici, P.B., Ranelletti, F.O., Fenandina, G., De Vincenzo, R., Piantelli, M., Masciullo, V., Bonamro, G., Isola, G. and Mancuso, S. Quercetin enhances transforming growth factor /31 secretion by human ovarian cancer cells, Int. J. Cancer, 1994, 67, 21 I-216.

303. Schmitt-Schillig S., Schaffer S., Weber C.C., Eckert G. P. and Muller W. E. Flavonoids and the aging brain. J Physiol Pharmacol. 2005, 56 Suppl 1, 23-36.

304. Schroeder SA, Roongta V, Fu JM, Jones CR and Gorenstein DG (1989). Sequence-dependent variations in the phosphorus-31 NMR spectra and backbone torsional angles of wild-type and mutant lac operator fragments. Biochemistry, 21: 8292-8303.

305. Schroeter H., Heiss C., Balzer J., et al. (-)-Epicatechin mediates beneficial effects of flavanol-rich cocoa on vascular function in humans. Proc Natl Acad Sci U S A. 2006, 103(4), 1024-1029.

306. Schultze P., Hud N.V., Smith F.W. Feigon J. The effect of sodium, potassium and ammonium ions on the conformation of the dimeric quadruplex formed by the Oxytricha nova telomere repeat oligonucleotide d(G(4)T(4)G(4)). Nucleic Acids Res. 1999, 27, 3018 - 3028.

307. Schultze P., Macaya R.F. Feigon J. Three-dimensional solution structure of the thrombin-binding DNA aptamer d(GGTTGGTGTGGTTGG). J.Mol.Biol. 1994, 235, 1532 - 1547.

308. Schultze P., Smith F.W. Feigon J. Refined solution structure of the dimeric quadruplex formed from the Oxytricha telomeric oligonucleotide d(GGGGTTTTGGGG). Structure. 1994, 2, 221 - 233.

309. Searle MS, Hall JG, Denny WA and Wakelin LPG (1988). NMR studies of the interaction of the antibiotic nogalamycin with the hexadeoxyribonucleotide duplex d (5'-GCATGC)$_2$. Biochemistry, 1988, 12: 4340-4349.

310. Sengupta, B., Uematsu, T., Jacobsson, P. and Swenson, J. Exploring the antioxidant property of bioflavonoid quercetin in preventing DNA glycation, A calorimetric and spectroscopic study. Biochem. Biophys. Res. Commun., 2006, 339, 355–361.

311. Sesso H.D., Gaziano J.M., Liu S. and Buring J.E. Flavonoid intake and the risk of cardiovascular disease in women. Am J Clin Nutr. 2003, 77(6), 1400-1408.

312. Setchell K.D., Brown N.M. and Lydeking-Olsen E. The clinical importance of the metabolite equol-a clue to the effectiveness of soy and its isoflavones. J Nutr. 2002, 132 (12), 3577-3584.

313. Shafer R.H. Spectroscopic studies of the interaction of daunomycin with transfer RNA. Biochem. Pharmacol., 1977, 26, 1729.

314. Shahidi, F. and Wanasundara, P.K.J. Phenolic antioxidants. Crit. Rev. Food Sci. Nutr., 1992, 32, 67-103.

315. Shoskes D.A., Zeitlin S.I., Shahed A. and Rajfer J. Quercetin in men with category III chronic prostatitis, a preliminary prospective, double-blind, placebo-controlled trial. Urology. 1999, 54(6), 960-963

316. Singh M.P., Joseph, T., Kumar S., Bathini, Y. and Lown, J.W. Synthesis and Sequence –Specific DNA binding of a Topoisomerase Inhibitory Analog of Hoechst 33258 designed for altered base and sequence recognition. Chem. Res. Toxicol. 1992, 5, 597-607.

317. Sket P., Crnugelj M. and Plavec J. d(G3T4G4) forms unusual dimeric G-quadruplex structure with the same general fold in the presence of K+, Na+ or NH4+ ions. Bioorg.Med.Chem. 2004, 12, 5735 - 5744.

318. Smith, F.W., Schultze, P. and Feigon, J. Solution structures of unimolecular quadruplexes formed by oligonucleotides containing Oxytricha telomere repeats. Structure, 1995, 3, 997 - 1008.

319. Snyder, R.D. and Gillies, P.J. Evaluation of the clastogenic, DNA intercalative and topoisomerase II-interactive properties of bioflavonoids in Chinese hamster V79 cells, Environ. Mol. Mutagen., 2002, 40, 266–276.

320. Solimani, R. Quercetin and DNA in solution, analysis of the dynamics of their interaction with a linear dichroism study. Internat. J. Biol. Macromol., 1996, 18, 287-295.

321. Solimani, R. The flavonols quercetin, rutin and morin in DNA solution: UV-vis dichroic (and mid-infrared) analysis explain the possible association between the biopolymer and a nucleophilic vegetable-dye, Biochimica et Biophysica Acta, 1997, 1336, 281-294.

322. Solimani, R., Bayon, F., Domini, I., Pifferi, P.G., Todesco, P.E., Marconi T.G. and Samori, B. Flavonoid-DNA interaction studied with flow linear dichroism technique. *J. Agric. Food Chem.* 1995, 43, 876-882.

323. Song J., Kwon O., Chen S., et al. Flavonoid inhibition of sodium-dependent vitamin C transporter 1 (SVCT1) and glucose transporter isoform 2 (GLUT2), intestinal transporters for vitamin C and Glucose. J Biol. Chem. 2002, 277(18), 15252-15260

324. Spencer J. P., Schroeter H., Crossthwaithe A. J., Kuhnle G., Williams R. J. and Rice-Evans C. Contrasting influences of glucuronidation and O-methylation of epicatechin on hydrogen peroxide-induced cell death in neurons and fibroblasts. Free Radic Biol Med. 2001, 31(9), 1139-1146.

325. Spencer J.P., Rice-Evans C. and Williams R. J. Modulation of pro-survival Akt/protein kinase B and ERK1/2 signaling cascades by quercetin and its in vivo metabolites underlie their action on neuronal viability. J Biol Chem. 2003, 278(37), 34783-34793.

326. Spencer J.P.E., Khunle G.G.C., Williams R. J. and Rice Evans C. Biochem. J. 2003, 372, 173.

327. Spinozzi, F., Pagliacci, MC. and Migliorati, G. The natural tyrosine kinase inhibitor genistein produces cell cycle arrest and apoptosis in Jurkat T-leukemia cells, Leukemia Res., 1994, 18, 431-439.

328. Stahl,W., Van den Berg, H., Bast, A., Faulks, J.R.M., Gartner, C., Haenen, G., Hollman, P., Holst, B., Kelly, F.J., Polidori, M.C., Rice-Evans, C., Southon, S., Van Vliet, T., Vina- Ribes, J., Williamson, G., Astley, S.B., 2002. Bioavailability and metabolism. Mol. Aspects Med., 2002, 23, 39–100.

329. Steele V.E., Hawk E.T., Viner J.L. and Lubet R.A. Mechanisms and applications of non-steroidal anti-inflammatory drugs in the chemoprevention of cancer. Mutat Res. 2003, 523-524, 137-144.

330. Stein J.H., Keevil J.G., Wiebe D.A., Aeschlimann S and Folts J. D. Purple grape juice improves endothelial function and reduces the susceptibility of LDL cholesterol to oxidation in patients with coronary artery disease. Circulation. 1999, 100(10), 1050-1055.

331. Stewart Z.A., Westfall M.D. and Pietenpol J. A. Cell-cycle dysregulation and anticancer therapy. Trends Pharmacol Sci. 2003 24(3), 139-145.

332. Stocker R. and Keaney J.F. Jr. Role of oxidative modifications in atherosclerosis. Physiol Rev. 2004, 84(4), 1381-1478.

333. Sun, H., Tang, Y., Xiang, J., Xu, G., Zhang, Y., Zhang, H. and Xu. L. Spectroscopic studies of the interaction between quercetin and G-quadruplex DNA, Bioorg. Med. Chem. Lett., 2006, 16, 3586-3589.

334. Sun, H., Xiang, J., Tang, Y. and Xu, G. Regulation and recognization of the extended G-quadruplex by rutin. Biochem. Biophys. Res. Commun., 2007, 352, 942–946.

335. Sung-Won Ha, Tetsuo A. and Raghuvansh K. Distinctive influence of two hexafluoro solvents on the structural stabilization of Bombyx mori silk fibroin protein and its derived peptides: 13C NMR and CD studies. Biomacromolecules 2006, 7(1):18-23.

xl

336. Sutherla, J.C. and Sutherla, B.M. Ethidium bromide–DNA complex—wavelength dependence of pyrimidine dimer inhibition and sensitized fluorescence as probes of excited States, Biopolymer, 1970, 9, 639–654.

337. Tajmir-Riahi, H.A., Diamantoglou, S., Kanakis, C.D., Tarantilis, P.A. and Polissiou, M.G. Flavonoids interactions with DNA and RNA, Binding modes and anti oxidative effects International Symposium on Human Health Effects of Fruits and Vegetables ISHS Acta Horticulturae 744, I

338. Takemura., G. and Fujiwara, H. Doxorubicin-induced cardiomyopathy from the cardiotoxic mechanisms to management, Prog. Cardiovasc. Dis., 2007, 49, 330–352.

339. Tan, J., Wang, B. and Zhu Liancai. Hydrolytic cleavage of DNA by quercetin zinc (II) complex. Bioorg. Medicinal Chem. Letters., 2007, 17(5), 1197-1199.

340. Taubert D., Roesen R., Lehmann C., Jung N., Schomig E. Effects of low habitual cocoa intake on blood pressure and bioactive nitric oxide, a randomized controlled trial. JAMA. 2007, 298(1), 49-60

341. Theobald D.L. and Schultz S.C. Nucleotide Shuffling and ssDNA Recognition in Oxytricha Nova Telomere End-Binding Protein Complexes Embo J. 2003, 22, 4314 - 4324.

342. Timmerman., P, Weidmann, J.L., Jolliffe., K.A., Prins., L.J., Reinhoudt., D.N., Shinkai., S., Frish., L. and Cohen, Y. NMR diffusion spectroscopy for the characterization of multicomponent hydrogen-bonded assemblies in solution, J. Chem. Soc., Perkin Trans., 2000, 2, 2077-2089.

343. Tommasini., S. Raneri., D.; Ficarra., R., Calabro., M.L., Stancanelli, R. and Ficarra, P. Improvement in solubility and dissolution rate of flavonoids by complexation with cyclodextrin, J. Pharm. Biomed. Anal., 2004, 35, 379–387.

344. Traganos F., Kapuscinski J. and Darzynkiewicz Z. Caffeine modulate the effects of DNA-intercalating drug in vitro: a flow cytometric and spectrophotometric analysis of caffeine interaction with novatrone, doxorubicin, ellipticine and doxorubicin analogue AD198. Cancer Res. 1991, 51, 3682-3689.

345. Trouillas, P., Marsal, P., Siri, D., Lazzaroni, R. and Duroux, J-L. A DFT study of the reactivity of OH groups in quercetin and taxifolin antioxidants: The specificity of the3-OH site, Food Chem., 2006, 97, 679-688.

346. U.S. Department of Agriculture. USDA database for the flavonoid content of selected foods. March 2003. Available at, http://www.nal.usda.gov/fnic/foodcomp/Data/Flav/flav.html.

347. U.S. Department of Agriculture. USDA database for the proanthocyanidin content of selected foods. August, 2004. Available at, http://www.nal.usda.gov/fnic/foodcomp/Data/PA/PA.html.

348. Usha, S., Johnson, M.I, and Malathi, R. Interaction of Resveratrol and Genistein with Nucleic Acids. J. Biochem. Mol. Biol., 2005, 38(2), 198-205.

349.

350. Van Acker, S.A.B.E., De Groot, M.J., van den Berg, D.J., Tromp, M.N.J.L., den Kelder, G.D.O., van der Vijgh, W.J.F. and Bast, A. A quantum chemical explanation of the antioxidant activity of flavonoids, Chem. Res. Toxicol., 1996, 9, 1305-1312.

351. Vergani, L., Mascetti, G., Gavazzo, P. and Nicolini, C. Ethidium bromide intercalation and chromatin structure, A thermal analysis, Thermochim. Acta, 1997, 294, 193–204.

352. Vita J.A. Tea consumption and cardiovascular disease, effects on endothelial function. J Nutr. 2003, 133(10), 3293S-3297S.

353. Vrhovsek U., Rigo A., Tonon D. and Mattivi F. Quantitation of polyphenols in different apple varieties. J Agric Food Chem. 2004, 52(21), 6532-6538

354. Wadkins R.M.m Vladu B. and Tung C.S. Actinomycin D binds to metastable hairpins in single-stranded DNA, Biochemistry 37, 998, 11915–11923.

355. Walle U.K. and Walle T. Induction of human UDP-glucuronosyltransferase UGT1A1 by flavonoids-structural requirements. Drug Metab Dispos. 2002, 30(5), 564-569.

356. Wallet, J.C., Gaydou, E.M., Fadlane, A. and Baldy, A. Structure of 3-methoxy-2-phenyl-4*H*-1-benzopyran-4-one (3-methoxyflavone), Acta Crystallogr., 1988, C44, 357-359.

357. Wang W, VanAlstyne P.C, Irons K. A., Chen S., Stewart J.W. and Birt D. F. Individual and interactive effects of apigenin analogs on G2/M cell-cycle arrest in human colon carcinoma cell lines. Nutr Cancer. 2004, 48(1), 106-114.

358. Wang Y. and Patel D.J. Solution structure of the human telomeric repeat d[AG3(T2AG3)3] G-tetraplex. Structure, 1994, 2, 1141–1156.

359. Wang Y. Patel D.J. Solution structure of a parallel-stranded G-quadruplex DNA. J.Mol.Biol. 1993, 234, 1171 - 1183.

360. Wang Y. and Patel D.J. Solution structure of the human telomeric repeat d[AG3(T2AG3)3] G-tetraplex. Structure.1993, 1, 263 - 282.

361. Wang-Polagruto J.F., Villablanca A.C., Polagruto J.A., et al. Chronic consumption of flavanol-rich cocoa improves endothelial function and decreases vascular cell adhesion molecule in hypercholesterolemic postmenopausal women. J Cardiovasc Pharmacol. 2006, 47 Suppl 2, S177-186, S206-179.

362. Wardman, P. Reduction potentials of one-electron couples involving free radicals in aqueous solution, J. Phys. Chem. Ref Data Ser., 1989, 18, 1637-1755.

363. Wawer I. and Zielinska A., ^{13}C CP/MAS NMR studies of flavonoids Magn. Reson. Chem. 2001, 39, 374.

364. Webb M.R. and Ebeler S.E., Comparative analysis of topoisomerase IB inhibition and DNA intercalation by flavonoids and similar compounds: structural determinates of activity, Biochem J., 2004, 384, 527-541.

365. Webba da Silva M. Association of DNA quadruplexes through G,C,G,C tetrads. Solution structure of d(GCGGTGGAT). Biochemistry , 2003, 42, 14356 - 14365.

366. Webba da Silva M. Experimental Demonstration of T,(G,G,G),T Hexad and T,A,A,T Tetrad Alignments within a DNA Quadruplex Stem. Biochemistry , 2005, 44, 3754 - 3764,.

367. White L.R, Petrovitch H., Ross G.W., et al. Brain aging and midlife tofu consumption. J Am Coll Nutr. 2000, 19(2), 242-255

368. WHO (February 2006). "Cancer". World Health Organization. http.//www.who.int/mediacentre/factsheets/fs297/en/

369. Williams R.J., Spencer J.P. and Rice-Evans C. Flavonoids, antioxidants or signalling molecules? Free Radic Biol Med. 2004, 36(7),838-849

370. Williamson G. Common features in the pathways of absorption and metabolism of flavonoids. In, Meskin MS, R. BW, Davies AJ, Lewis DS, Randolph RK, eds. Phytochemicals, Mechanisms of Action. Boca Raton, CRC Press, 2004, 21-33.

371. Wilson, W.D. and Jones, R.L. Interaction of actinomycin D, ethidium quinacrine daunorubicin, and tetralysine with DNA: ^{31}P NMR chemical shift and relaxation investigation. Nucleic Acids. Res. 1982, 10, 1399-1410.

372. Wu D. and Meydini S.N. Antioxidants and Immune Function, In Antioxidant Status, Diet, Nutrition and Health. ed. Andreas M. Papas. CRC Press, New York. 1999, pp. 371 - 400.

373. Xiao, Hendler S.S., Rorvik D.R., eds. PDR for Nutritional Supplements. Montvale, Medical Economics Company, Inc, 2001

374. Yamagishi M., Natsume M., Osakabe N., et al. Effects of cacao liquor proanthocyanidins on PhIP-induced mutagenesis in vitro, and in vivo mammary and pancreatic tumorigenesis in female Sprague-Dawley rats. Cancer Lett. 2002, 185(2), 123-130

375. Yamane T., Nakatani H., Kikuoka N., et al. Inhibitory effects and toxicity of green tea polyphenols for gastrointestinal carcinogenesis. Cancer. 1996, 77(8 Suppl), 1662-1667.

376. Yamashita, Y., Kawada S. and Nakano H. Induction of mammalian topoisomerase II dependent DNA cleavage by nonintercalative flavonoids, genistein and orobol, Biochem. Pharmacol. 1990, 39(4), 737-44.

377. Yanagihara, K., Ito, A. Toge, T. and Numoto, M. Antiproliferative effects of isoflavones on human cancer cell lines established from the gastrointestinal tract, Cancer Res., 1993, 63, 6816-6821.

378. Yang C. S., Yang G.Y., Landau J.M., Kim S. and Liao J. Tea and tea polyphenols inhibit cell hyperproliferation, lung tumorigenesis, and tumor progression. Exp Lung Res. 1998, 24(4), 629-639

379. Ying G., Jie X., Andong X. Xuebin S., Zhanting L. Spectroscopic properties of hydrogen-bond-modulated porphyrin dimer in different polar solvents Journal of Luminescence 2007, 250-252

380. Yochum L, Kushi LH, Meyer K. and Folsom AR. Dietary flavonoid intake and risk of cardiovascular disease in postmenopausal women. Am J Epidemiol. 1999, 149(10), 943-949.

381. Youdim K.A., Qaiser M.Z., Begley D.J., Rice-Evans C.A. and Abbott N. J. Flavonoid permeability across an in situ model of the blood-brain barrier. Free Radic Biol Med. 2004, 36(5), 592-604

382. Yuan J.P., Wang J.H. and Liu X. Metabolism of dietary soy isoflavones to equol by human intestinal microflora--implications for health. Mol Nutr Food Res., 2007, 51(7), 765-781.

383. Zhang N., Gorin A., Majumdar A., Kettani A., Chernichenko N., Skripkin E. and Patel D.J. Dimeric DNA quadruplex containing major groove-aligned A-T-A-T and G-C-G-C tetrads stabilized by inter-subunit Watson-Crick A-T and G-C pairs. J.Mol.Biol. 2001, 312, 1073 - 1088.

384. Zhang N., Phan A.T. and Patel, D.J. (3 + 1) Assembly of three human telomeric repeats into an asymmetric dimeric G-quadruplex. J.Am.Chem.Soc. 2005, 127, 17277 - 17285.

385. Zhang, N., Gorin, A., Majumdar, A., Kettani, A., Chernichenko, N., Skripkin, E. and Patel, D.J. V-shaped scaffold, a new architectural motif identified in an A x (G x G x G x G) pentad-containing dimeric DNA quadruplex involving stacked G(anti) x G(anti) x G(anti) x G(syn) tetrads. J.Mol.Biol., 2001, 311, 1063 - 1079.

386. Zhou S., Lim L. Y. and Chowbay B. Herbal modulation of P-glycoprotein. Drug Metab Rev. 2004, 36(1), 57-104

387. Zijp I. M., Korver O. and Tijburg L.B. Effect of tea and other dietary factors on iron absorption. Crit. Rev. Food Sci. Nutr. 2000, 40(5), 371-398.